Structural Studies on Hydrophobins from *Neurospora*

Robert Douglas Winefield

Institute of Technology and Engineering

Massey University

Palmerston North

New Zealand

A thesis submitted in partial fulfilment
of the requirements for the degree of
Doctor of Philosophy
2004

ABSTRACT.

Background:

Hydrophobins are a group of low molecular weight, cysteine-rich, fungal cell-wall proteins with unique biophysical properties. Principal among these is the ability of hydrophobin monomers to self-assemble into insoluble, chemically resistant amphipathic films at the interface between hydrophobic and hydrophilic surfaces. This enables fungi to coat their hyphae and fruiting bodies with a hydrophobic layer that prevents these structures from becoming waterlogged. Proposed industrial and medical applications have sought to exploit these protein's polymeric hydrophobins to reverse the wettability of a surface upon binding.

The hydrophobin protein EAS (product of the gene *eas*) coats macroconidia produced by the model ascomycete *Neurospora crassa*, making this species an ideal subject for structural studies on hydrophobins.

Results:

(1) Genes homologous to *eas* were detected in each of the *Neurospora* species examined. EAS proteins isolated from each of the conidiating species proved to be identical to that known in *N. crassa.* The aconidiate homothallic *Neurospora* species also possess copies of *eas,* essentially identical to that from *N. crassa*, but transcription studies implied that the gene is inactive in these species.

(2) I attempted to express EAS in its native form and I succeeded in generating recombinant *Pichia pastoris* and *Escherichia coli* as isolates. However, I did not detect the expression of EAS in any of these isolates. This was despite the fact that the *Pichia* isolates were actively transcribing the recombinant gene.

(3) EAS was chemically digested according to Wu and Watson (1997). Mass spectrometric analysis of these digests revealed that the four intramolecular disulfide bridges in EAS exist between Cys_9-Cys_{60}, Cys_{18}-Cys_{54}, Cys_{19}-Cys_{45}, and Cys_{61}-Cys_{80}. This arrangement is identical to that recently determined for the class II hydrophobin HFB2.

(4) Atomic force microscopic analysis of rodlet films deposited on hydrophilic mica and hydrophobic graphite revealed the presence of a central cleft in the hydrophobic and hydrophilic sides of individual rodlets. This cleft is believed to be the boundary between the long protofilaments that are bundled together to form polymeric rodlets. Also seen were shorter oval structures, consistent with short protofilaments detected during real-time analysis of amyloid polymerisation.

ACKNOWLEDGEMENTS.

This research was supported with funding from The Marsden Fund and The Horticulture and Food Research Institute of New Zealand (Hort Research).

I would like to thank my supervisors, Dr. Matthew Templeton (Hort Research) and Associate Professor Richard Haverkamp (ITE, Massey University), for their guidance, sage advice, and support. I would also like to thank Dr Ross Beever and Stephanie Parkes (Landcare Research) for their help with all things mycological including providing the strains used in this study. I am grateful for the help given to me by many people at Hort Research. In particular I would like to thank Dr David Greenwood, Dr Joe Win, Dr Agnieszka Mudge, Dr Kim Plummer, Dr Wei Cui, Dr Janine Cooney, Dwayne Jenson, Anna Fitzgerald, Carolyn Moore, Peter Murphy, and Anthony Thrush for their help, advice, friendship, technical assistance and even excusing my occasional pilfering of their marker pens... At Massey University I would especially like to thank Mike Sahayam, Mike Stevens, and Joan Brookes, for their help in navigating the obstacles I encountered while moving to Massey University to complete this degree.

Thank you to my brothers (Peter and Chris) and my parents for their support throughout my university career. I am sure my mother and father will be especially glad to read this because it means that the last of their sons finally has his PhD and they can finally start saving for a Caribbean cruise. Of course saving would not be necessary if only one of us had become a dentist instead of biologists and geologists but that is another story. My girl friend, Maria, deserves a special mention, not just, for being a delightful lass who is very dear to me, but because her comprehensive disinterest in all things scientific is a refreshing tonic after a frustrating day in the laboratory.

Finally this PhD cost me most of my hair and a significant proportion of my youth but the following friends helped me to retain my sanity (most of it anyway). Stefan Fairweather, Aaron Clarke, Graeme and Pam Fell, Peter Cresswell and Carol Potts, Lindsay Perigo, Greg Jacobson, John Holmes, the crew from Riddet Building Post-Grad room, the indoor cricketers who represented Western though three Northern Region Super league campaigns and finally the gentlemen and players from Auckland's Grafton United and Palmerston North's Marist (Outdoor) Cricket Clubs.

TABLE OF CONTENTS.

LIST OF FIGURES.

LIST OF TABLES.

1

GENERAL INTRODUCTION.

1.0 INTRODUCTION TO THE *NEUROSPORA* GENUS.

1.0.1 *NEUROSPORA CRASSA* – A MODEL EUKARYOTE.

Fungi from the genus *Neurospora* have been known to science since the nineteenth century when they were investigated as the cause of a fungal infestation in French bakeries (Davis, 2000). Since then one member of the genus, *N. crassa*, has served as an eukaryotic model organism for a diverse array of genetic and biochemical research culminating in the sequencing of the *N. crassa* genome (Galagan *et al.*, 2003).

Currently the *Neurospora* genus is taxonomically sub-divided according to sexual phenotype (see Table 1). *Neurospora* are either heterothallic (self-sterile and out-breeding), or homothallic (self-fertile and in-breeding) or pseudohomothallic (an in-breeding species that occasionally out-breeds). The non-homothallic species (heterothallic and pseudohomothallic) can produce two forms of asexual spore: microconidia and macroconidia (Perkins and Turner, 1988). By contrast, the homothallic *Neurospora* are aconidiate; they have not been reported to produce conidia of any kind.

1.0.2 REPRODUCTION AND GROWTH.

1.0.2.1 THE ASSEXUAL LIFE CYCLE.

Figure 1A depicts the life cycle of typical heterothallic *Neurospora* species, the inner cycle of this diagram illustrates the asexual life cycle. The macroconidia produced by the non-homothallic species are easily dispersed by air perturbation and, when mature, are covered with a proteinaceous rodlet film derived from the hydrophobin EAS.

Desiccation, nitrogen and carbon starvation, and the action of the circadian clock induce macroconidiation; while light or lowered CO_2 concentrations can either induce macroconidiation or enhance its intensity (see review by Springer, 1993). Macroconidiation begins when minor constrictions develop on juvenile aerial hyphae. The process continues as arrays of proconidia develop at each tip and finishes when the mature macroconidia separate as the constrictions evolve into full cross-walls (Figure 1B). The result is a profusion of bright-orange coloured, multinucleate, asexual-propagules that are connected by a delicate, collar-like, chitin-based, constriction at the nearest septum (Figure 1C and 1D, Springer and Yanofsky, 1992; Davis, 2000).

TABLE 1: SPECIES OF THE GENUS *NEUROSPORA*.

CONIDIA PRODUCING (CONIDIATING) SPECIES.

Species	Mating Phenotype	MAT idiomorphs	Spores per asci	Carotenoid Colour	Total strains
N. crassa. (Shear and Dodge, 1927)	*het*	*A or a*	*8*	*Orange*	*524*
N. discreta. (Perkins and Raju, 1986)	*het*	*A or a*	*8*	*Orange*	*143*
N. intermedia. (Tai, 1935)	*het*	*A or a*	*8*	*Orange (typically)*	*3020*
N. sitophila. (Shear and Dodge, 1927)	*het*	*A or a*	*8*	*Orange*	*568*
N. tetrasperma. (Nelson *et al.*, 1964)	*phom*	*A + a (A or a)*	*4 (typically)*	*Orange*	*411*

ACONIDIATE SPECIES.

Species Name & Discoverer	Mating Phenotype	MAT idiomorphs	Spores per asci	Carotenoids	Total strains
N. africana. (Mahoney *et al.*, 1969)	*hom*	*A*	*8*	*None*	*1*
N. dodgei. (Nelson *et al.*, 1964)	*hom*	*A*	*8*	*None*	*1*
N. galapagosensis. (Mahoney *et al.*, 1969)	*hom*	*A*	*8*	*None*	*2*
N. lineolata. (Frederick *et al.*, 1969)	*hom*	*A*	*8*	*None*	*1*
N. pannonica. (Krug and Khan, 1991)	*hom*	*A + a*	*8*	*None*	*1*
N. sublineolata. (von Arx, 1981; Perkins and Turner, 1988)	*hom*	*A + a*	*8*	*None*	*1*
N. terricola. (Nelson *et al.*, 1964)	*hom*	*A + a*	*8*	*None*	*1*

Table 1 lists the mating phenotypes present in *Neurospora*. These are heterothallic (het), pseudohomothallic (phom) and homothallic (hom). Pseudohomothallic *N. tetrasperma* normally produces heterokaryotic ascospores, with nuclei from both parents present, occasionally homokaryotic spores are produced increasing the number of ascospores per asci and giving rise to heterothallic progeny (Perkins and Turner, 1988). The "Total strains" column refers to the number of strains from each species held by the Fungal Genetics Stock Centre (Turner *et al.*, 2001; FGSC website: http://www.fgsc.net). The MAT idiomorph data was obtained from Beatty *et al.* (1994), Glass *et al.* (1990), and Dettman *et al.* (2001). The carotenoid and ascospore data was obtained from Perkins and Turner (1988).

Microconidia are a second type of asexual cell produced by the heterothallic species. Compared to macroconidia, microconidia are smaller, less robust, and slower to germinate. The production of microconidia is triggered by environmental cues different from those that induce macroconidiation (microconidiation is triggered by cool, humid conditions as well as nitrogen or carbon starvation) and the microconidia's hydrophilic surfaces appear bereft of hydrophobins (see review by Maheshwari, 1999). Both microconidia and macroconidia can act as fertilizing agents during sexual reproduction (Davis, 2000).

FIGURE 1: THE LIFE CYCLE OF *NEUROSPORA*.

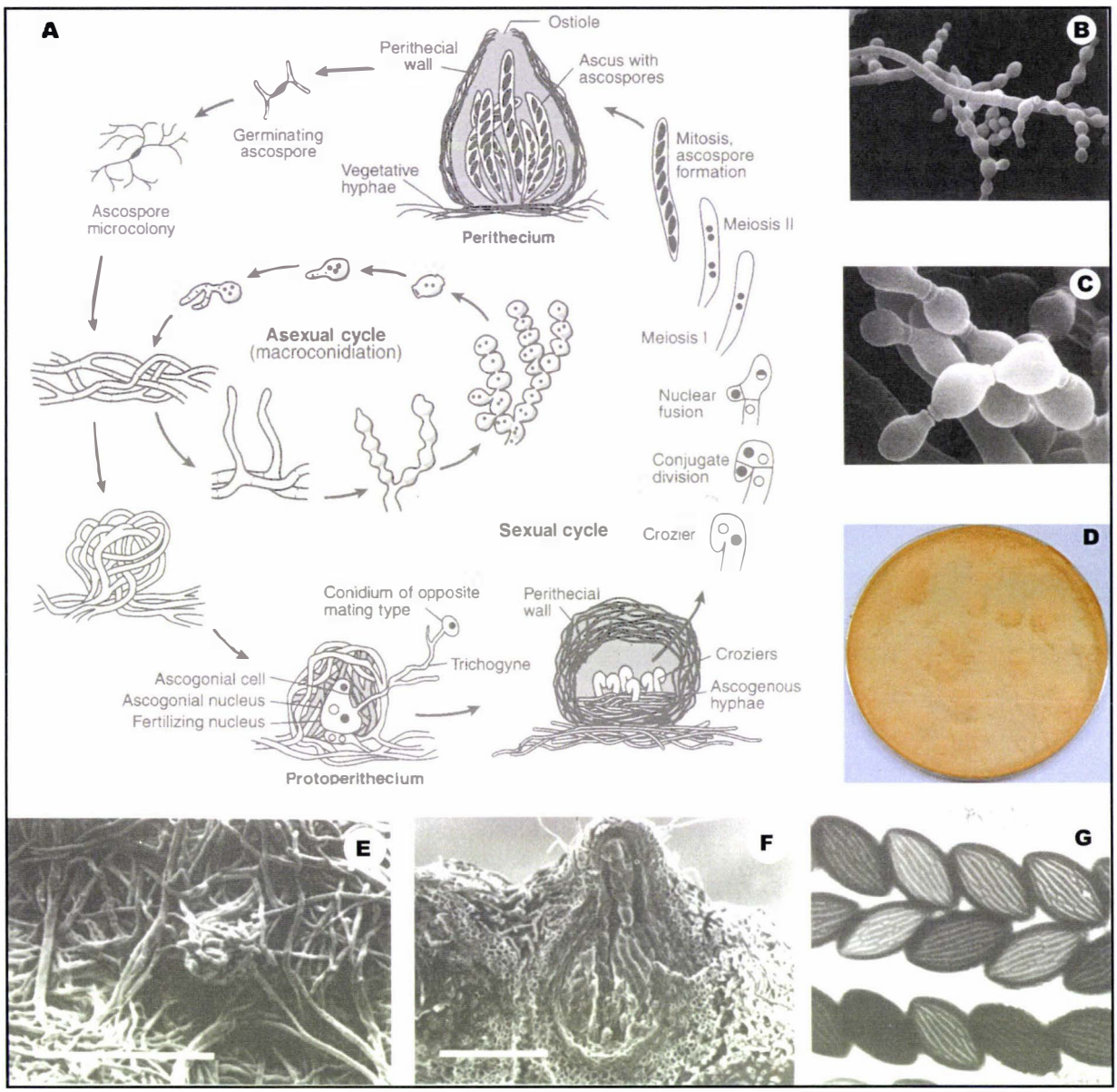

Figure 1A diagrammatically depicts the life cycle of *Neurospora* (Davis, 2000). The inner sequence represents the asexual cycle showing the production of macroconidia and their germination to form new mycelium. Microconidia can also be formed during this stage of life but are not illustrated here. The outer sequence depicts the sexual cycle starting with the formation of protoperithecium (left) and progressing through to the fertilisation of the female gamete. Fertilisation occurs as the trichogyne fuses with a cell of opposite mating-type (in this case a conidium). Figure 1B shows scanning electron micrographs that depict the budding and constriction process in the aerial hyphae that later leads to the formation of chains of macroconidia. Figure 1C depicts almost mature macroconidia showing the delicate connections joining neighbouring macroconidia in the chain. The diameter of mature *N. crassa* conidia is between 5 and 9 µm (Lowry *et al.*, 1967). Figure 1D is a photograph of a vegetatively grown *N. crassa* culture in the producing profuse amounts of orange coloured macroconidia. Figure 1E: A scanning electron micrograph of a protoperithecium. Figure 1F: Perithecium after 12 days of development. Figure 1F: Ascospores visualised before they become completely melanized, note the characteristic ribbing that formed the morphological criterion for membership of the genus *Neurospora* (Glass *et al.*, 1990). All images except Figure 1D were obtained from pages 13-17 Davis (2000). Figure 1D was taken by the author.

1.0.2.2 THE SEXUAL LIFE CYCLE.

Sexual reproduction in the heterothallic (out-breeding) *Neurospora* is mating-type dependent: only individuals of opposite mating-types can mate. An individual's mating-type is dependent on which of the two genetic mating elements (also called "idiomorphs"), *mat A* or *mat a* (for *mat*ing-type A or a), is present in its genome.

These loci are also some of a number of genes responsible for the *het* (for vegetative *het*erokaryon incompatibility) reaction: a form of self/non-self recognition between somatic cells.

The self-fertile homothallic *Neurospora* species have no definable mating-type but do possess homologues of the *mat* idiomorphs. This has permitted the *mat* idiomorphs to be used the genus-wide phylogenetic studies that are discussed below (section 1.0.4.2). Because homothallic *Neurospora* do not conidiate they are harder to identify and isolate, hence little is known of their genetic, biochemical or ecological disposition. For example, the FGSC stores over 4,700 heterothallic *Neurospora strains,* but it stores fewer than 20 homothallic *Neurospora* strains (Turner *et al.,* 2001; FGSC website: http://www.fgsc.net).

N. tetrasperma is the only pseudohomothallic *Neurospora* species. During sexual reproduction *N. tetrasperma* produces four binucleic, dual-mating-type (*A+a*), ascospores per ascus instead of the eight uninucleate single-mating-type ascospores produced by heterothallic *Neurospora* (Dodge, 1927; Shear and Dodge, 1927; Perkins *et al.,* 1976; Raju and Perkins, 1994). The progeny of these ascospores are haploid and homothallic. However, around 10% of ascospores *N. tetrasperma* produces are uninucleate and possess only one mating-type idiomorph; when this happens, the number of ascospores per asci increases and fungi derived from these spores will be both haploid and heterothallic (Raju, 1992; Raju and Perkins, 1994).

1.0.3 *Neurospora* – Habitat.

The global distribution, habitat, and life-style of the heterothallic *Neurospora* have been the subject of a thirty-year study carried out by David Perkins and his associates (Perkins *et al.,* 1976; Perkins and Turner, 1988; Turner *et al.,* 2001). They concluded that *Neurospora* species are saprophytic filamentous fungi growing on plant remains, especially species with pithy stems and sugary sap such the succulent and monocotyledonous species. *Neurospora* ascospores are activated by heat, which explains why isolates from freshly burnt vegetation dominate Perkins' study (Perkins and Turner, 1988). *Neurospora* species are non-pathogenic, and form the basis for local culinary delicacies in West Java and parts of Brazil (Perkins and Turner, 1988; Perkins and Davis, 2000; Turner *et al.,* 2001).

Globally, the genus is naturally ubiquitous in humid tropical and subtropical regions, although the composition of species in the *Neurospora* population varies according to the geographic region. For instance, *N. intermedia* is the most commonly isolated

species overall, while *N. tetrasperma* is the predominant species isolated from cooler latitudes - perhaps because of adaptations allowing it to tolerate a wide ranges of both temperature and moisture. *N. crassa* itself appears restricted to sub-tropical and tropical regions areas of the Western Hemisphere (including the Caribbean, coastal regions of the south-eastern USA, as well as northern Brazil), Africa, India, and Asia.

1.0.4 The Taxonomy of the Genus *Neurospora*.

1.0.4.1 The Species of *Neurospora*.

The twelve species of *Neurospora* currently recognised are described in Table 1. Two previously recognised species, *N. erthraea* and *N. toroi* (Shear and Dodge, 1927; Tai, 1935), are considered to be indistinguishable from *N. tetrasperma* (Nelson *et al.,* 1964; Metzenberg and Ahlgren, 1971; Perkins *et al.,* 1976).

At first, *Neurospora* species were delineated according to the unique variations in the grooves and longitudinal ribs decorating the surfaces of ascospores (see Figure 1G). This system has largely been discarded because the intra-species variation in ascospore ornamentation was determined to be larger than was originally thought. Currently heterothallic species are identified according to their mating compatibility with type- or tester-strains from each of the five established heterothallic species (Perkins and Turner, 1988).

1.0.4.2 The Phylogeny of *Neurospora*.

Several phylogenetic investigations have been conducted on *Neurospora*, the general aim being to identify the evolutionary origin of both the mating-type idiomorphs and the three sexual life-styles (Natvig *et al.,* 1987; Taylor and Natvig, 1989; Randall and Metzenberg, 1995; Skupski *et al.,* 1997; Pöggeler, 1999). Recently the genus was analysed as part of an effort to develop phylogenetic techniques sensitive enough to identify individual species (Taylor *et al.,* 2000; Dettman *et al.,* 2001).

The conclusions from these studies are that the heterothallic *Neurospora* species are closely related – each shares a common ancestor, but *N. discreta* is the most divergent species in this group – while the homothallic species do not form a single monophyletic grouping (Dettman *et al.,* 2001). Instead, three monophyletic groupings could be identified: (1) *N. sublineolata* is grouped with a homothallic and a pseudohomothallic *Gelasinospora* species. (2) *N. terricola* and *N. pannonica* group with a heterothallic *Gelasinospora* species. (3) A homothallic *Gelasinospora* species

groups with *N. lineolata* and the closely related trio of *N. africana*, *N. dodgei,* and *N. galapagosensis*.

These final three species are so closely related that Dettman *et al.* suggested they were individual strains of the same species possessing unimportant morphological variations (Dettman *et al.,* 2001). It has been noted previously that, morphologically speaking, *N. galapagosensis, N. africana,* and *N. dodgei* are almost identical (Mahoney *et al.,* 1969).

The genus *Gelasinospora*, like *Neurospora*, is a member of the Sordariaceae and is considered distinct because of unique pit-like decorations present on the ascospores. The investigation by Dettman *et al.* (2001) indicated that *Neurospora* and *Gelasinospora* did not form two distinct monophyletic genera. Instead, they segregated into one polyphyletic grouping of taxa whose members are similar both morphologically and phylogenetically. As yet, there has not been a formal reorganisation of these genera to account for these incongruities because more research must be conducted before firm conclusions can be reached (Dettman *et al.,* 2001).

1.1 The Hydrophobin Protein Family.

1.1.1 Introduction.

While investigating some highly-expressed genes in the basidiomycete *Schizophyllum commune*, Joseph Wessels and colleagues isolated four genes that each encoded a cysteine-rich, low molecular-weight protein found on the exterior surfaces of *S. commune's* fruiting bodies and aerial hyphae and rendered these air-exposed structures hydrophobic (reviewed by Wessels, 1997). Wessels *et al.* named these novel proteins hydrophobins because of the number of hydrophobic amino acids they contained (Wessels, 1997). Since then, 47 more hydrophobins (listed in Figure 2 and in Appendix I) have been identified in a wide range of filamentous fungal species. The evolutionary diversity of the fungal species producing hydrophobin species indicates that this protein family is ubiquitous in the basidiomycete and ascomycete fungal families (Wessels, 1996, 1997).

Research described in this thesis concentrates on the hydrophobin EAS which coats the macroconidia (hereafter referred to as conidia) of *N. crassa.*

Wild-type *N. crassa* conidia are hydrophobic; water rapidly beads off them. By contrast, conidia from the mutant strain *N. crassa eas* (*eas*ily wettable) do not resist wetting, and water droplets are rapidly absorbed causing the conidia to clump together reducing their ability to disperse in air (Selitrennikoff, 1976; Beever and

Dempsey, 1978). A hydrophobic coating has been seen as advantageous in allowing spores to adhere to the chitinous exoskeleton of insects (Bowden *et al.*, 1996) and this coupled with bright colouration (see Figure 1D) may explain why honeybees have been observed with pollen-sacs full of *Neurospora* conidia (Perkins and Turner, 1988).

Biochemical and electron microscope studies by Beever and Dempsey (1978, 1979) and Beever *et al.* (1979) established that the *eas* mutants lacked the chemically resistant, proteinaceous film of rodlets that coats the surface of wild-type conidia. Later, two research groups independently characterised the *eas* gene and showed that it was capable of restoring this hydrophobic rodlet layer to conidia from the *N. crassa eas* mutants. The sequence of *eas* revealed that it is a member of the hydrophobin gene family (Sommer *et al.*, 1989; Lauter and Russo, 1991; Loros *et al.*, 1989; Loros and Dunlap, 1991; Bell-Pedersen *et al.*, 1992; Eberle and Russo, 1992; Lauter *et al.*, 1992).

The rest of this chapter is devoted to describing the unique properties of hydrophobins and the roles they play in the physiology of the basidiomycetes and ascomycetes, and concludes by describing recent advances in elucidating the tertiary and quaternary structure of hydrophobin proteins.

1.1.2 Hydrophobin Primary Structure.

Hydrophobin proteins appear to be unique to the basidiomycetes and ascomycetes because they have yet to be discovered in the more primitive zygomycetes and chytridiomycetes (chitrids) (personal communication with H.A.B. Wösten). This observation implies that the hydrophobins arose in the ancestral species common to both basidiomycetes and ascomycetes (fungal phylogeny is discussed in Bruns *et al.* 1991, 1993). However analysing the phylogenetic relationships between hydrophobins is difficult because the sequences of hydrophobin genes and proteins are extremely diverse (see Figure 2). Despite the low overall sequence homology within this protein family, the hydrophobins share common physiochemical properties; in fact, several studies have shown that hydrophobins produced by one species can partially compensate for the loss of the endogenous hydrophobin in another species (Lugones *et al.*, 1998; Kershaw *et al.*, 1998a; van Wetter *et al.*, 2000a). The evidence supporting such conclusions is comprehensively reviewed in Wessels (1997), Wösten and de Vocht (2000), Wösten and Willey (2000), and Wösten (2001). The general characteristics shared by all hydrophobins are listed below. Note that while the gross chemical and physical properties of hydrophobins are similar, the finer properties may differ.

(1) Hydrophobins have been defined as small proteins (120 ± 30 amino acids) that are moderately hydrophobic, but this level of hydrophobicity varies between hydrophobins (Wessels, 1997).

(2) The presence of signal sequences within hydrophobin genes implies that every hydrophobin is secreted to the cell-wall. In the case of EAS, the evidence of this includes phenotype rescue experiments, N-terminal amino acid sequencing data, and DNA sequencing data (Bell-Pedersen *et al.,* 1992; Lauter *et al.,* 1992; Templeton *et al.,* 1995).

(3) Experiments on SC3 (produced by *S. commune*) led Wösten *et al.* (1994a, 1994b) to conclude that hydrophobins are able to spontaneously polymerise into a film when confronted by the interface between water and any substance (solid, liquid, or gas) with minimal hydrophobicity. Subsequent investigation has confirmed this hypothesis (*e.g.* EAS: Mackay *et al.,* 2001; SC4: Lugones *et al.,* 1999a; and ABH1: Lugones *et al.,* 1996, 1999a). Polymeric hydrophobin films possess two main properties:

   (a) They are extremely surface-active. For example, adding 50 μg mL^{-1} of SC3 to water lowers the surface tension of the water from 72 mJ m^{-2} to <24 mJ m^{-2} when the protein polymerises at the waters surface (cf. the detergent SDS lowers the surface tension of water to 32 mJ m^{-2}). This means that SC3 the one of the most powerful biosurfactants known (van der Vegt *et al.,* 1996; Wösten *et al.,* 1999a). Similar results have been obtained with purified solutions of other hydrophobins (Wösten and de Vocht, 2000). However, unlike SC3, some of those hydrophobins (ABH2, SC4) are unglycosylated (de Vocht *et al.,* 1998; Asgeirsdóttir *et al.,* 1998). This implies that the hydrophobins surface activity is attributable to the protein's unique amino acid sequence or the structural changes that accompany its polymerisation or both (de Vocht *et al.,* 1998; de Vocht, 2001).

   (b) Experiments that measure the contact-angles of water-droplets deposited on hydrophobin films show that these films are amphipathic. Hydrophilic surfaces cause droplets to spread across a surface and to yield contact angles of 0° while non-wettable surfaces will yield droplets with contact angles greater than 90° because the droplet beads and will slide off the surface (Noordmans and Busscher, 1991). The wettability of the hydrophilic side of a hydrophobin film (which is exposed when the

hydrophobin self-assembles on a hydrophobic substance) is variable, yielding water-droplets with a contact angle between 22° and 63° (Wösten and de Vocht, 2000). The wettability of the hydrophobic side is always about 110°. Similar contact angles are obtained from the surface of Teflon® (Wösten and de Vocht, 2000). Thus, hydrophobins can reverse the wettability of the surfaces on which they self-assemble.

(4) The amino acid sequences of hydrophobins are dissimilar, there are no amino-acid signature-sequences associated with hydrophobin proteins, other than the presence of eight cysteine residues (see Figure 2 and Figure 3).. However, similarities between the cysteine spacing and hydropathy patterns exist, each hydrophobin possesses eight cysteine residues whose spacing is roughly conserved thus:

$$X_{2\text{-}38}\text{-}C\text{-}X_{5\text{-}9}\text{-}C\text{-}C\text{-}X_{11\text{-}39}\text{-}C\text{-}X_{8\text{-}23}\text{-}C\text{-}X_{5\text{-}9}\text{-}C\text{-}C\text{-}X_{6\text{-}18}\text{-}C\text{-}X_{2\text{-}13}.$$

where X denotes any non-aromatic amino acid (phenylalanine, tryptophan, and tyrosine occur infrequently in hydrophobins). The symmetry of this consensus sequence has led some to suggest that hydrophobins consist of two linked domains, each containing four cysteine residues (Wessels, 1997). A single exception to this rule has been identified: QID3 is a hydrophobin produced by *Trichoderma harzianum* in which a serine substitutes for the second cysteine residue (Lora *et al.,* 1994; Wessels, 1996).

(5) Hydrophobin films can aid in the adhesion of fungal structures to hydrophobic surfaces like Teflon (Wösten *et al.,* 1994a). Class I films adhere very tightly to hydrophobic surfaces and resist treatments with 2 %(w/v) SDS at 100 °C, but not concentrated TFA at 0 °C. The fact that only neat, ice-cold TFA (or formic acid) can de-polymerise hydrophobins, suggests that hydrophobin polymers are held together by hydrophobic interactions only (Wösten *et al.,* 1994a; de Vocht *et al.,* 1998).

(6) Hydrophobins can also adsorb to some hydrophilic surfaces. The adsorption is believed to be enhanced either by lectin activity or by some N-terminally located structural motifs.

(a) When ABH1, ABH3, SC3, and SC4 assemble on filter-paper, they resist attempts to remove them using 2 %(w/v) SDS at 100 °C (Lugones *et al.,* 1996, 1998, 1999a).

(b) QID3, HCF-6, and CFTH1 are called bimodular hydrophobins because their N-termini contain lengthy stretches of hydrophilic residues (mainly proline, glycine, and asparagine) that are predicted to enable these hydrophobins to bind to the fungal cell wall (Lora *et al.,* 1995; de Vries *et al.,* 1999; Nielsen *et al.,* 2001; Whiteford and Spanu, 2002). SC3, EAS, and other hydrophobins lacking this domain only adhere to submerged hyphae after the hyphae breaches the liquid surface (Wösten *et al.,* 1994a, and 1999a).

(c) Lectin-activity has been found in SC3, SC4, and cryparin; at present, these are the only hydrophobins that have been tested (Wösten and de Vocht, 2000; van Wetter *et al.,* 2000a; McCabe and Van Alfen, 1999). Wösten and de Vocht (2000) suggest that this ability to agglutinate animal cells could be related to binding to hydrophilic surfaces. This property of lectin-activity must be due solely to the hydrophobin's unique amino-acid sequence or structure; because this is the only thing that these proteins have in common – mature SC4 and cryparin are neither glycosylated nor are they endowed with a long hydrophilic N-terminus (McCabe and Van Alfen, 1999, van Wetter *et al.,* 2000a).

(d) Three hydrophobins SC3, POH2, and VMH3 are known to contain glycosylated residues near their N-termini (Asgeirsdóttir, 1994; de Vocht *et al.,* 1998; Asgeirsdóttir *et al.,* 1998; Peñas *et al.,* 2002). Van Wetter *et al.* (2000a) observed that films of SC3 adhere more tightly to the *S. commune* cell walls than do films of the unglycosylated SC4. De Vocht *et al.* (1998) found that they could increase the hydrophobicity of the hydrophilic side of an SC3 film by deglycosylating the protein (de Vocht *et al.,* 1998). These findings suggest that the glycosylated residues serve to anchor the hydrophobin to the hydrophilic cell wall (Whiteford and Spanu, 2002). As yet, no one has investigated how glycosylated residue might be exploited to augment a hydrophobin's ability to adsorb to a surface.

1.1.3 Classification of Hydrophobins.

Wessels (1994) identified divergent physical properties and hydropathy patterns within two groups of hydrophobins and he subdivided the family into two classes (classes I and II) on this basis; recent phylogenetic investigations have supported this distinction (see Figure 2 and Figure 3, Wessels, 1997; Wösten, 2001).

1.1.3.1 Physiochemical Properties of Class I Hydrophobin Films.

Of the 48 hydrophobins genetically identified only a handful, all of them class I, have had the identity and morphology of their polymeric protein form confirmed (reviewed in Wessels, 1997). The single concordant theme arising from these studies is that the class I hydrophobin polymer films consist of rodlets – with a diameter between 5-12 nm – bundled into fascicles. The fascicles are arranged in random mosaics that completely cover the surfaces upon which they assemble. Chemically, the films are very robust: they are insoluble in water and treatment with 1 %(w/v) SDS or 1 M NaOH at 100 ºC does not disrupt them (*e.g.* EAS: Beever *et al.,* 1979. SC3: de Vries *et al.,* 1993). Only treatment with ice cold, concentrated TFA, or formic acid can disassociate the films by disrupting the short-range intermolecular hydrophobic interactions. This leaves the hydrophobin monomers intact and biologically active (de Vries *et al.,* 1993; Wösten *et al.,* 1993, 1994b; Templeton *et al.,* 1995). The dissociated hydrophobin must remain unaffected by these aggressive agents because the dissociation and assembly cycle can be repeated many times (Wösten *et al.,* 1993).

1.1.3.2 Physiochemical Properties of Class II Hydrophobin Films.

The films formed by class II hydrophobins do not contain rodlets and, compared with their class I counterparts; they are less chemically resistant (Wösten and de Vocht, 2000). The polymeric films formed by cerato-ulmin and other class II hydrophobins are soluble both in 60 %(v/v) ethanol and 2 %(w/v) SDS, but they must be unstable in water because the films de-polymerise when subjected to increased pressure (Richards, 1993; Carpenter *et al.,* 1992; de Vries *et al.,* 1999).

1.1.3.3 Phylogenetic Protein Sequence Analysis.

Hydrophobins native to a particular genus have similar sequence and function and have been successfully phylogenetically compared (*e.g.* Geiser *et al.,* 1998). However, phylogenetic analysis of the entire family has done little more than highlight the futility of attempting to identify hydrophobins based on protein-sequence homology alone (Wessels, 1997; Wösten and Wessels, 1997). Nevertheless the general observations made by Wösten, Whiteford and Spanu are noteworthy (Wösten, 2001; Whiteford and Spanu, 2002). Figure 2 and Figure 3 were constructed according to their methods and they show that class I and II hydrophobins are indeed distinct from each other. Further, the class I hydrophobins found in the basidiomycetes are distinct from those found in the ascomycetes.

FIGURE 2: COMPARISON OF AMINO-ACID SEQUENCES FROM CLASS I AND II HYDROPHOBINS.

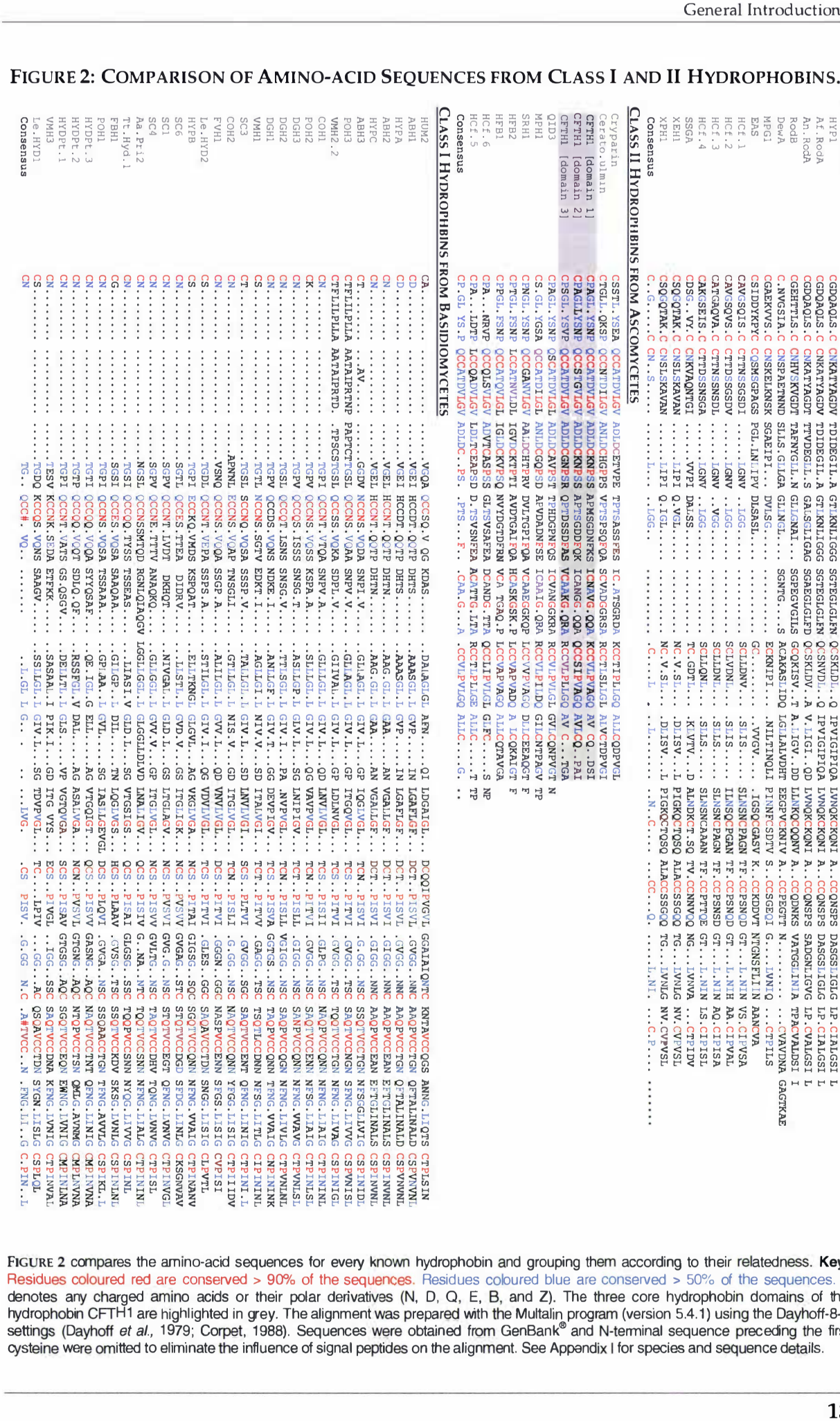

FIGURE 2 compares the amino-acid sequences for every known hydrophobin and grouping them according to their relatedness. **Key:** Residues coloured red are conserved > 90% of the sequences. Residues coloured blue are conserved > 50% of the sequences. # denotes any charged amino acids or their polar derivatives (N, D, Q, E, B, and Z). The three core hydrophobin domains of the hydrophobin CFTH1 are highlighted in grey. The alignment was prepared with the Multalin program (version 5.4.1) using the Dayhoff-8-0 settings (Dayhoff *et al.*, 1979; Corpet, 1988). Sequences were obtained from GenBank® and N-terminal sequence preceding the first cysteine were omitted to eliminate the influence of signal peptides on the alignment. See Appendix I for species and sequence details.

FIGURE 3: PHYLOGENETIC TREE DEPICTING THE RELATEDNESS OF KNOWN HYDROPHOBINS.

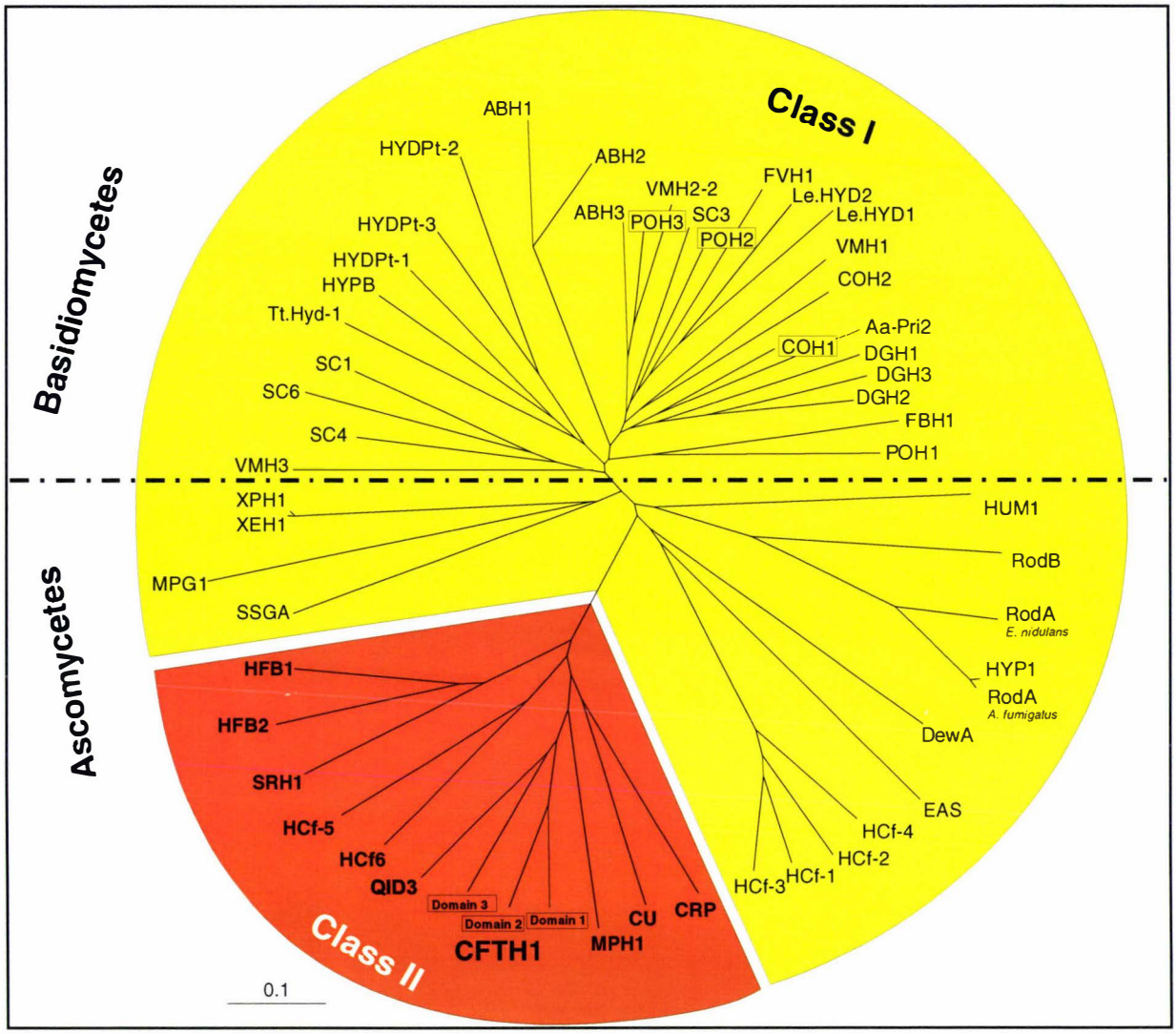

Figure 3 shows an unrooted tree-diagram depicting the degree of similarity between known hydrophobins. The scale bar indicates the distance on each branch equivalent to 0.1 amino acid substitutions per site. The three hydrophobin domains of CFTH1 are labelled Domain 1, 2 and 3. Le.HYD1 and Le.HYD2 refer to the hydrophobins found in *Lentinula edodes* (Ng *et al.*, 2000) to avoid confusion with Tt.Hyd-1 the hydrophobin from *Tricholoma terreum* (Mankel *et al.*, 2002). The tree was constructed as follows: every sequence shown in Figure 2 was aligned with the Multalin program (version 5.4.1) using Dayhoff-8-0 settings (Corpet, 1988). The unrooted tree was constructed with the Neighbour Joining method using the Clustal X (version 1.8) and TreeView (version 1.6.6) packages (Thompson *et al.*, 1997; Page, 1996).

Notice that the protein sequences of the class II hydrophobins are less heterogeneous than those of the class I hydrophobins. As Whiteford and Spanu (2002) have suggested, this may indicate that the class I hydrophobins were present in filamentous fungi prior to the separation of the basidiomycetes and the ascomycetes; afterwards the class II hydrophobins are believed to have evolved independently within the ascomycetes.

1.2 Biological Functions of Hydrophobins.

The polymeric form of hydrophobins imparts hydrophobic and surface-active properties to the air-exposed surfaces of fungal-structures. As is discussed below these coatings serve fungi in more ways than just repelling water.

1.2.1 The Production of Aerial Reproductive Structures.

1.2.1.1 Hydrophobins Impart Hydrophobic Coatings.

As described previously, class I hydrophobins provide a hydrophobic, water-repellent layer to fungal propagules and they are believed to be virtually ubiquitous in the basidiomycetes and ascomycetes (reviewed by Wessels, 1997).This hydrophobic coating plays a key role in the production of aerial hyphae and later in the dissemination of spores and conidia. By preventing the spores from clumping together when wetted, the coating enhances the scattering of propagules by air currents or rain splashes. Hydrophobin deficient mutants have been isolated from several species and these strains exhibit an *eas*ily wettable phenotype, that is their propagules are bereft of any hydrophobic coating (*e.g. N. crassa*: Selitrennikoff, 1976; Dempsey and Beever, 1979. *Cladosporium fulvum*: Whiteford and Spanu, 2001; *Aspergillus nidulans*: Stringer *et al.,* 1991).

In a variation on this theme the hydrophobic hydrophobin-coatings imparted to spores from *Ophiostoma ulmi* and *Metarhizium anisopliae* are believed to enhance the adhesion of spores to the chitinous exoskeleton of the insects which act as vector and host for these pathogens respectively (Temple *et al.,* 1997; St Leger *et al.,* 1992).

1.2.1.2 A Rodlet Does Not a Hydrophobin Make...

Fibrous or rodlet-laden films have been detected many times during freeze-etching investigations of spore surfaces (see review by Wessels, 1997). These films have often been shown to consist of class I hydrophobins - but not always.

Rodlet-layers cover both the exterior surfaces of spores produced by aerobic bacteria and the hyphae and spores formed by filamentous bacteria (see Figure 4, Holt and Leadbetter, 1969; Wildermuth *et al.,* 1971; Wildermuth, 1972a, 1972b; Aronson and Fitz-James, 1976; Wösten *et al.,* 1999b; Wösten and Willey, 2000). In the case of *Streptomyces coelicolor*, two different groups of proteins – unrelated to the hydrophobins – are responsible. The "chaplins" are a family of highly surfactive proteins that enable the *S. coelicolor* hyphae to breach the air-water interface and grow into the air. *In vitro*, chaplins form hydrophobic films containing rodlets of similar dimensions to those formed by the hydrophobins (Claessen *et al.*, 2003). The

"rodlin" proteins also play a role in the formation of the rodlet films that coat the air-exposed structures formed by *S. coelicolor* (Claessen *et al.*, 2002). Claessen *et al.* believe that the chaplins form a hydrophobic rodlet-layer that is anchored to the bacterial cell wall by covalent bonds. After this layer has been formed, it is believed to trigger the formation of a second rodlin-containing rodlet-film that covers the first (Claessen *et al.*, 2003). Interestingly, the biological activity of the chaplin-proteins is believed to derive from the amyloid-like structure of their polymeric form – in other words, they are functional amyloids (Claessen *et al.*, 2003), this is a property they share with the hydrophobins (see section 1.3.6).

FIGURE 4: A COMPARISON OF RODLET-FILMS SEEN IN NATURE.

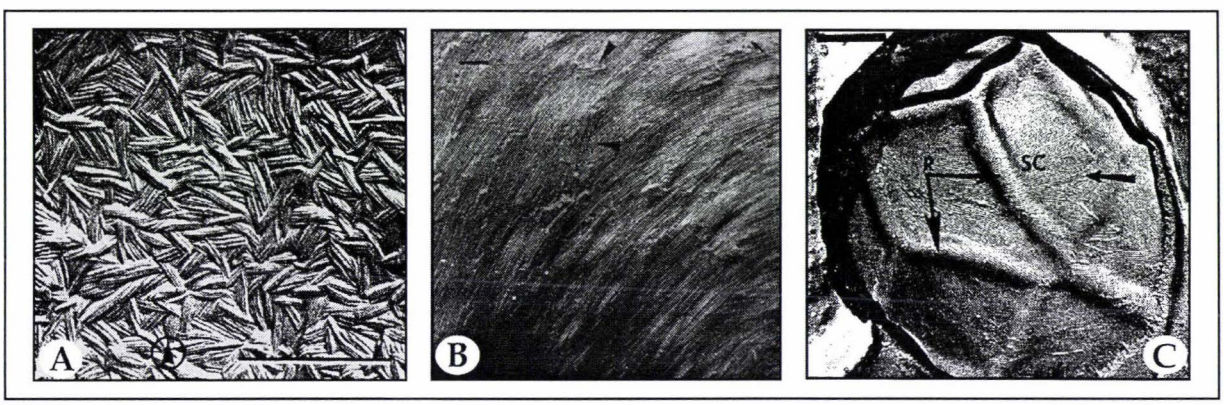

Figure 4 compares the electron micrographs of rodlet layers from three species. In **A**, the hydrophobic rodlet layer coating the surface of a *N. crassa* conidium is shown. The scale bar denotes 0.5 µm (image from Beever and Dempsey, 1978, page 609). In **B**, the hydrophilic rodlets from the surface of a *Phanerochaete chrysosporium* conidiospore are shown. Scale bar denotes 0.1 µm (image from Gerin *et al.*, 1994, page 413). **C** depicts spores from *Bacillus fastidiosus*. "R" indicates the ridges of the spore "SC" the different layers of the laminated spore coat. Scale bar denotes 0.25 µm (image from Holt and Leadbetter, 1969 page 352).

Dufrêne (2000) used functionalized Atomic Force Microscope (AFM) probes to show that the surface of individual *Phanerochaete chrysosporium* spores are covered with a rodlet-film imparting a *hydrophilic* coating to it's exterior. *If* the rodlet-layer originates from an unknown hydrophobin, this finding contradicts studies that have concluded that the *hydrophobin* rodlet-film presents its hydrophobic side to the atmosphere (*e.g.* ABH1 Lugones *et al.,* 1996; ABH3 Lugones *et al.,* 1998; RodA: Stringer *et al.,* 1991). There are three possible explanations for this result:

(1) That previous measurements, obtained with macroscopic techniques, may have given the false impression that hydrophobins are wholly responsible for the hydrophobic properties of spores (Dufrêne, 2000).

(2) That multiple layers of hydrophobins may be present and orientated to present a hydrophilic external surface (*e.g.* Wösten *et al.,* 1994a, 1995; van der Vegt *et al.,* 1996).

(3) That a hydrophilic rodlet-forming protein, lipid, or carbohydrate unrelated to hydrophobins is responsible.

Ultimately, only biochemical characterisation of the substance forming the rodlet-film in this species will solve this possible incongruity.

1.2.2 Hydrophobins Involved in the Formation of Aerial Hyphae and Air-Channels.

1.2.2.1 Hydrophobins Prevent Water-Logging of Air Channels.

In basidiomycetes, gas exchange is carried out in air channels incorporated into the aerial structures that these fungi form. Fungi must endure frequent cycles of wetting in nature. Hydrophobins, secreted to the air-exposed surfaces of the fungi's air-channels, provide a hydrophobic and gas-permeable barrier that prevents the fungi from suffocation by keeping these surfaces clear of water (van Wetter *et al.,* 2000a; Wösten, 2001). Hydrophobins play a similar role in lichens; they preserve channels crucial to gas *and* nutrient exchange between the mycobiont (fungi like *Xanthoria* species) and the cyanobacterial photobiont (Honneger, 1991; Scherrer *et al.,* 2000, 2002).

Often in mushrooms, unique hydrophobins are produced to shelter different structures. For instance, in *Agaricus bisporus* ABH1/hypA coats the air channels and external surfaces of dikaryotic fruiting bodies (Lugones *et al.,* 1996, 1999a; de Groot *et al.,* 1996). ABH3 is produced in the homokaryon, where it plays a role in the formation and coating of aerial mycelium (de Vries *et al.,* 1993; Lugones *et al.,* 1998). Finally, while *hypC* is expressed in dikaryotic tissues like ABH1/*hypA*, it is expressed in separate localities and at different times (de Groot *et al.,* 1999).

1.2.2.2 Hydrophobins as Determinants of Aerial Growth.

Unless firmly attached to a surface, hyphae are unable to exert enough force to penetrate that surface. Instead, they are deflected, and the hyphae continue growing along the course of least resistance (Wösten, 2001). The surface-activity of hydrophobins that are secreted and self-assemble in aqueous environments is such that they permit profuse aerial growth to occur. But the nutritional burden of supporting aerial growth is so great that fungi like *S. commune* only release hydrophobins when the culture has reached a size sufficient to support it (Wösten *et al.,* 1994a, 1999a).

Hydrophobins are one of several classes of surface-active compounds produced by filamentous microorganisms. Both *Ustilago maydis* and filamentous bacteria excrete surface-active compounds unrelated to hydrophobins, despite *U. maydis* possessing a hydrophobin called *Hum-2* (Bohlmann, 1996). Interestingly, when surface-active proteins from *Streptomyces coelicolor* (SapB and Streptofactin) were added to the

growth medium of SC3-deficient *Schizophyllum commune* mutants, they restored their ability to form aerial hyphae. Similarly, SC3 can complement the loss of SapB and Streptofactin in *S. coelicolor* (Tillotson *et al.*, 1998; Wösten *et al.*, 1999b).

1.2.3 Hydrophobins Involved in Fungal-Pathogenesis.

Pathogenic filamentous fungi produce hydrophobins that help with the emergence of aerial hyphae, and impart protective or adhesive hydrophobic coatings - or both - to hyphae and spores (*e.g.* cerato-ulmin: Svircev *et al.*, 1987; ssgA: St Leger *et al.*, 1992; MPG1: Talbot *et al.*, 1996). Disrupting hydrophobin production therefore reduces the infectivity of the pathogen (*e.g. Magnaporthe grisea*: Talbot *et al.*, 1996; Temple *et al.*, 1997). Hydrophobins can also play direct roles in pathogenesis (see reviews by Wösten, 2001; Tucker and Talbot, 2001; Whiteford and Spanu, 2002).

1.2.3.1 Hydrophobins Protect Against Immunological Attack.

Given the hydrophobins ability to resist chemical attack, Wösten and Wessels (1997) suggested that hydrophobins play a role in protecting non-pathogenic fungi from bacterial infection and environmental abuse. Interestingly, Paris *et al.* (2003) showed that conidia from *Aspergillus fumigatus* mutants, deficient in *both* of its hydrophobins (RodA/Hyp1 and RodB), were more susceptible to attack by alveolar macrophages.

1.2.3.2 Toxic Hydrophobins.

Cerato-ulmin is a hydrophobin secreted by the Dutch elm disease causing pathogens *Ophiostoma ulmi* and *Ophiostoma novo ulmi.* Pure cerato-ulmin is a species-specific phytotoxin (the evidence is reviewed in Richards, 1993; Wösten *et al.*, 1993; Temple and Horgen, 2000). Like SC3, cerato-ulmin assembles around and stabilises air bubbles, which have the potential to cause embolisms in plant vascular tissues (Wösten *et al.*, 1993; Temple and Horgen, 2000). However, this does not explain the species-specificity of the toxin nor why cerato-ulmin is the only known phytotoxic hydrophobin (Wösten, 2001). Other phytotoxic hydrophobins may exist; one possible candidate is magnaporin/MPH1, which was recently discovered by Kim *et al.* (2001). MPH1 is a class II hydrophobin that is only excreted *in planta* by *Magnaporthe grisea.* The properties of this protein are currently under investigation (see unpublished data by Kim, S. O., Park, S. G. and Lee, Y. -H. at the Seoul National University, South Korea).

Curiously, neither the over-expression of nor the deletion of the cerato-ulmin gene has any detectable effect on the pathogenicity of these fungi. But if the cerato-ulmin gene is expressed in *Ophiostoma quercus*, the recombinant organism becomes an

elm pathogen capable of inflicting symptoms similar to Dutch elm disease on its victims (Bowden *et al.,* 1994; Brasier *et al.,* 1995; Temple *et al.,* 1997; Del Sorbo *et al.,* 2000).

Only one mechanism for species-specific toxicity has been suggested: cerato-ulmin may interfere with the permeability of the plasma membrane, leading to a loss of electrolytes in affected cells (Richards, 1993).

Together, the evidence suggests that cerato-ulmin plays a dual role. It is a parasitic fitness factor that enhances the dispersal of the parasite, and it is one of several phytotoxic compounds secreted during infection (Temple and Horgen, 2000; Wösten, 2001).

1.2.3.3 Hydrophobins that Initiate Pathogenesis.

The multifarious tasks performed by MPG1 form the basis for a general model describing the roles that hydrophobins play in plant pathogens (see Tucker and Talbot, 2001). Firstly, MPG1 helps to initiate conidiogenesis in *Magnaporthe grisea* (Talbot *et al.,* 1993; Talbot *et al.,* 1996). Secondly, MPG1 aids in the pathogenesis of *M. grisea*, because mutants unable to produce it are less efficient in forming appressorium and cannot bind to the hydrophobic surfaces of plants. MPG1 could support appressorium function in two ways:

(1) MPG1 is excreted from germinating hyphae to change the wettability of the hydrophobic leaf surface, priming it for the mucilaginous glues secreted to firmly attach the fungus to the leaf.

(2) MPG1 is also associated with a cyclic AMP-dependent signalling pathway that triggers appressorium differentiation (Beckerman and Ebbole, 1996). It is possible that MPG1 is part of the sensor for this signalling pathway (Wösten, 2001). If so the mechanism is likely to involve the interfacial assembly of MPG1 because cross-species complementation experiments show that SC1, SC4, *ssgA*, *eas*, *dewA* and *rodA* can all partly substitute for MPG1 by weakly triggering appressorium formation (Kershaw *et al.,* 1998).

1.2.3.4 Are Hydrophobins Responsible for Species-Specific Recognition?

The cell-wall location of hydrophobins and their involvement in fungal morphogenesis implies that they may be involved in host-pathogen recognition, perhaps by "camouflaging" the elicitor-rich fungal cell wall from the host immune system (Templeton *et al.,* 1994; Whiteford and Spanu, 2002). Wösten (2001) suggested that that hydrophobins have evolved to fulfil discrete roles and cited the

existence of multi-domain hydrophobins, the sequence variation in the N-termini of hydrophobins, and the species-specific toxicity of pure cerato-ulmin as evidence. It is interesting to note that in ectomycorrhiza (fungi that live symbiotically with vascular plants), the hydrophobins expressed by *Pisolithus tinctorius* and *Tricholoma terreum* are up-regulated *in planta.* In addition, in ectomycorrhiza involving *T. terreum* the level of Hyd-1 expression varies in a host-specific manner (Mankel *et al.,* 2002; Duplessis *et al.,* 2001).

However, any investigations of host-pathogen recognition *in vitro* must overcome the attendant difficulties of successfully mimicking the growth conditions *in planta*, and of eliminating the effects of any additional hydrophobins produced by the fungus. Recent technological advances have addressed the first problem and have allowed Kim *et al.* (2001) to identify MPH1 expression *in planta* after infection by *M. grisea.* However, the second difficulty remains intractable. For example, while Spanu *et al.* saw no change in pathogenicity after two of the six hydrophobins produced by *Cladosporium fulvum* were knocked out, they could not discount the possibility that the other four had compensated for the knocked out hydrophobins in some way (Spanu, 1997, Whiteford and Spanu, 2002).

1.2.4 Multi-Domain Hydrophobins.

CFTH1 from *Claviceps fusiformis* and CPPH1 from *Claviceps purpurea* are two recently discovered genes expressing multi-domain proteins (Arntz and Tudzynski, 1997; de Vries *et al.,* 1999; Mey, G., Correia, T., Oeser, B., Garre, V. and Tudzynski, P., unpublished results). CFTH1 contains three domains whose sequence resembles a class II hydrophobin while CPPH1 contains five such domains. In each protein, the hydrophobin domains are separated by a region of glycine and asparagine repeats that may serve to anchor these proteins to the cell wall (Nielsen *et al.,* 2001). All that is known about the mature forms of these proteins is that CFTH1 has a mass of 36.5 kDa and that it is found both on the organism's aerial hyphae, and within the mucilaginous coat that surrounds the organism's submerged hyphae (de Vries *et al.,* 1999). Other than an undefined role in differentiation of aerial hyphae, no other function has been proposed for these proteins. Their inclusion in the hydrophobin family is based solely on sequence homology.

1.3 Hydrophobin Structural Investigations.

Initially the most intense structural studies on hydrophobins were conducted on cerato-ulmin. Then, and until very recently, the bulk of structural studies

concentrated on the class I hydrophobins SC3 and EAS (Mackay *et al.,* 2001; de Vocht, 2001), however Hakanpää *et al.* (2004) became the first to solve the crystal structure of a hydrophobin when they solved HFB2, a class II hydrophobin from *Trichoderma reesei*, to 1.0 Å resolution. Nevertheless a question remains, do the disulfide and the structural motifs identified in this class II hydrophobin exist in class I hydrophobins?

1.3.1 Variation in Hydrophobin N-Termini.

In addition to glycosylation, other post-translational modifications are known to occur in hydrophobins. In EAS the effect of these post-translational modifications is to create, as the product of single gene, a mature protein expressed as two pairs of isoforms.

These isoforms exist because two signal-peptide cleavage sites are present in the amino-acid sequence (see Figure 5 and Mackay *et al.,* 2001). The first site is located at the $Arg_{(-1)}$–Ala_1 peptide bond, giving rise to the Ia and Ib pair of isoforms; these differ because of an undetermined 16 Da addition to isoform Ib.

The second cleavage site, located at the Thr_3-Ile_4 peptide bond, produces the IIa and IIb pair of isoforms, which co-purify as a single peak during RP-HPLC (Figure 5) despite the fact that they too differ by an undetermined 16 Da addition. The N-terminus of mature hydrophobins are often several amino acid residues down stream of the predicted site of signal-peptide cleavage - presumably due to the pro-proteins undergoing further proteolytic cleavage prior to the formation of the mature protein (Segers *et al.,* 1999; Whiteford and Spanu, 2002). The post-translational modifications present in EAS have no discernible effect on either the structure or the self-assembly of each isoform (Mackay *et al.,* 2001). Versions of SC3, bereft of their N-terminal glycosylated residues, retain the structural and self-assembly properties of the unaltered form at a cost of reducing the wettability of the hydrophilic side of its polymer film (de Vocht *et al.,* 1998; de Vocht, 2001).

This evidence, together with observations on the natural variation in hydrophobin N-termini, implies that their role the in self-assembly and the structure of hydrophobins is insignificant (Scholtmeijer *et al.,* 2001a), enabling this region to be genetically altered (*e.g.* to create a fusion protein) without effecting the properties of the hydrophobin (Scholtmeijer *et al.,* 2002).

Yaguchi *et al.* (1993) published an account of experiments that established the identity of the cysteine residues in each of cerato-ulmin's four intramolecular

disulfide bonds. Unfortunately, the two-dimensional NMR evidence corroborating their assignment remains to be published (Mackay *et al.*, 2001). Yaguchi *et al.* believed that the first cysteine in cerato-ulmin is bound to the second cysteine; the third is bound to the fourth and so on, as can be seen in Figure 6. In hindsight, their published data suggests that the first cysteine in cerato-ulmin is bound to the *second or the third* cysteine; the *second or third* is bound to the fourth and so on (Yaguchi *et al.*, 1993; Wösten and de Vocht, 2000).

FIGURE 5: THE PURIFICATION AND AMINO ACID SEQUENCE OF EAS.

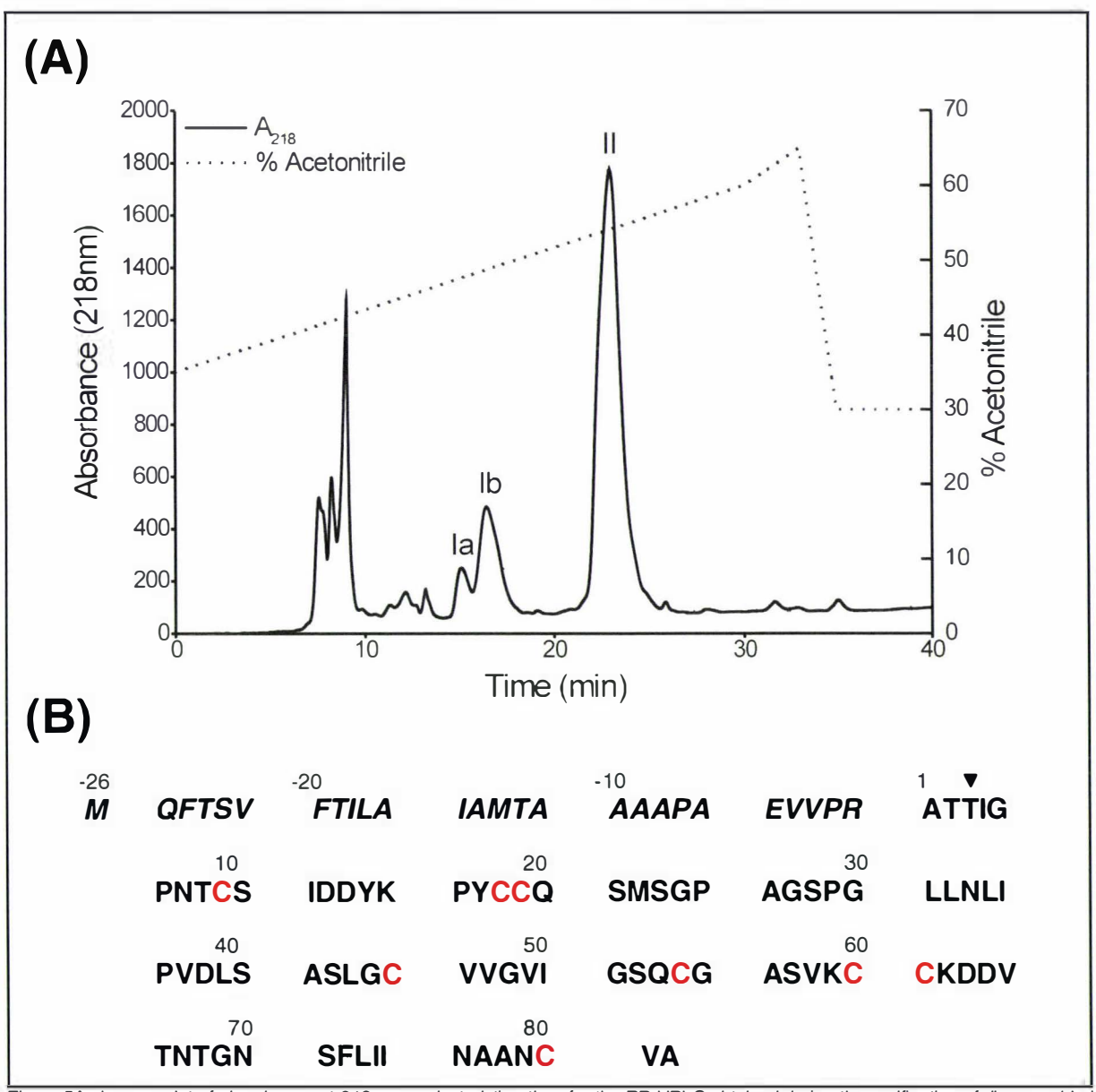

Figure 5A shows a plot of absorbance at 218 nm against elution time for the RP-HPLC obtained during the purification of disassembled *N. crassa* rodlets. Peaks corresponding to isoforms Ia, Ib and II are labelled. Figure 5B depicts the amino acid sequence of EAS: the leader sequence is shown in italics, a black triangle indicates the alternate cleavage site for the signal sequence that generates both isoform IIa and IIb (which co-purify in the peak marked II in Figure 5A). The cysteine residues are highlighted in red.

Until Hakanpää *et al.* (2004) solved the crystal structure of HFB2, the pattern proposed by Yaguchi *et al.* stood as the only map of the disulfide bridges within a

hydrophobin. Their proposal was the basis for a good deal of speculation about how the disulfide bonds might contribute to the unique structural and physical properties of hydrophobins. Essentially the pattern established for cerato-ulmin created four looped domains, roughly equal in size. Each loop consisted mostly of hydrophobic residues and this model implies that the monomer's structure will be flexible (Wösten and Wessels, 1997; Kershaw and Talbot, 1998; Wösten and de Vocht, 2000). If the same pattern is superimposed onto class I hydrophobin sequences then four looped, relatively hydrophobic domains of varying sizes would result.

FIGURE 6: DISULFIDE BOND LINKAGES IN CERATO-ULMIN AND HFB2.

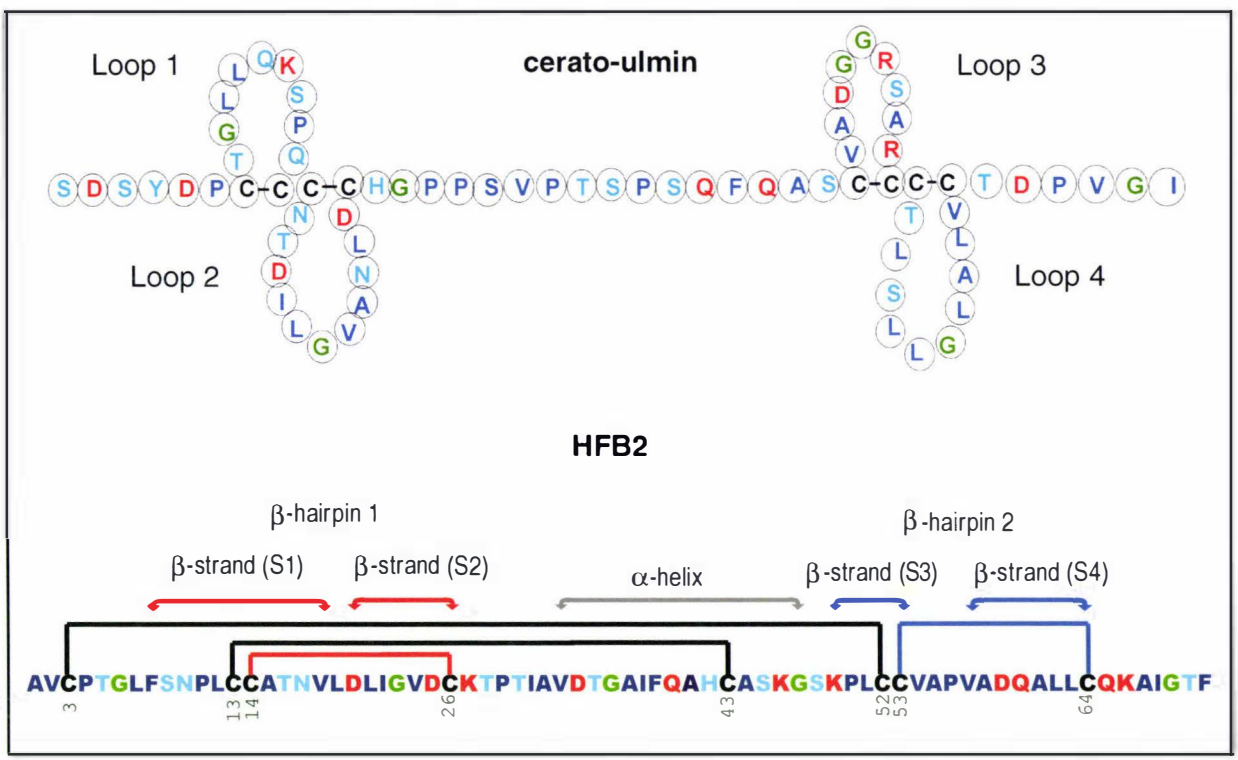

The upper diagram in Figure 6 depicts the amino acid sequence of mature cerato-ulmin shaped to emphasise the disulfide bond linkage-pattern derived by Yaguchi *et al.* (1993) The diagram adapted from Wessels (1997) using the MDL® ISIS/Draw program. The lower diagram of Figure 6 depicts the amino acid sequence of mature HFB2 with lines connecting cysteine residues depicting the disulfide bond linkage-pattern and structural motifs derived by Hakanpää *et al.* (2004). **Key:** arrowed lines indicate the position of structural motifs. HFB2 has two separate β-hairpins consisting of a pair of β-strands each linked by one disulfide. The components of each β-hairpin are colour coded red or blue. A single α-helix (indicated by the grey arrowed line) separates the two β-hairpins. Amino acids are colour coded as follows: Green = glycine, Black = cysteine, Red = charged residues, Light blue = polar residues, Dark blue = hydrophobic residues.

Hakanpää *et al.* (2004) established a different disulfide linkage pattern for HFB2 (see Figure 6), one where the N- and C- terminal domains of the protein are covalently constrained contributing to the rigid globular structure described in section 1.3.3. Hakanpää *et al.* (2004) argue that the disulfide linkage pattern and structural motif they established for HFB2 is common to all class II hydrophobins. The sequence homology between class II hydrophobins, evident in Figure 2, supports the hypothesis that a common structure prevails. But without the two-dimensional NMR data referred to by Yaguchi *et al.* (1993), the only way to be sure

is to solve the crystal structure of other class II hydrophobins, including cerato-ulmin.

1.3.2 The Intracellular Disulfide Bonds.

1.3.2.1 Disrupting the Disulfides Doesn't Inhibit the Self-Assembly of Class I Hydrophobins.

When the disulfide bonds in SC3 were disrupted (reducing them and blocking the nascent sulfhydryls with either iodoacetic acid or iodoacetamide) SC3, with all of it's cysteines carrying a carboxyamide group, was still able to self-assemble spontaneously in water; but this time, the presence of an interface wasn't required (de Vocht *et al.,* 2000). SC3, when reduced and acetylated (thus carrying additional negative charges) could not assemble unless a hydrophobic surface was introduced or the water removed by drying. Once assembled, the film did adhere to hydrophobic surfaces, but the strength of the adhesion was adversely affected by the additional charges. De Vocht *et al.* (2000) suggested that the disulfide bonds exist to stabilise the monomeric form of the protein, and to prevent premature self-assembly without a hydrophobic-hydrophilic interface.

Whether HFB2, bereft of its disulfide bonds, can self-assemble into an amphipathic-film has yet to be determined. The juxtaposition of disulfide bonds within HFB2 appear to hold the molecule rigid, and allow the formation of a hydrophobic region located at the protein's surface. Hakanpää *et al.* (2004) believe that the presence of this region accounts for the protein's amphipathic properties. Essentially, each pair of, β-hairpin-forming β-strands is linked by one disulfide bond (Figure 6). The other disulfide bonds link the β-hairpins to distal regions of the molecule (Hakanpää *et al.,* 2004).

As a result, HFB2 has a compact globular structure (described below) that is (presumably) inflexible even in solution prior to self-assembly. This is in direct contrast to published data on class I hydrophobins, which are mostly unstructured and flexible in solution and become progressively more organised during the self-assembly process (Mackay *et al.,* 2001; de Vocht *et al.,* 2002.)

1.3.3 The Structure of Crystalline HFB2.

Hakanpää *et al.* (2004) determined that crystalline HFB2 forms a single domain protein folded into two β-hairpin motifs (each consisting of two anti-parallel β-strands) linked by an α-helix (see Figure 7). The β-hairpins are arranged in a similar manner in which, quoting Hakanpää *et al.* (2004), "two leather pieces of a baseball are sewn together." This fold is unique to HFB2, and gives the protein a compact,

globular, and rigid structure that is stabilised by four intramolecular disulfide bonds arranged as described above. A large portion of the molecule (12 % of the total surface area of the protein) is devoted to forming a relatively flat, surface region where the aliphatic side-chains of 10 hydrophobic amino acids are exposed to the environment.

FIGURE 7: THE STRUCTURE OF CRYSTALLINE HFB2.

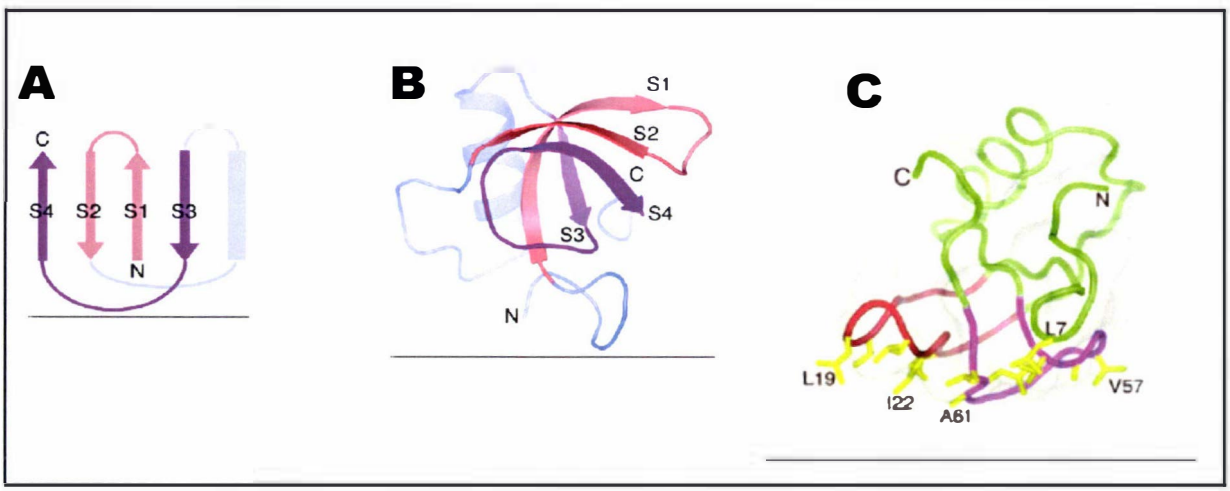

Figure 7A diagrammatically depicts the topology of HFB2. Arrows represent the antiparallel β-strands (labelled S1-S4) and the barrel represents the α-helix. The letters C and N represent the proteins C- and N-terminal residues. Figure 7B is a three-dimensional representation of the structure of HFB2, the central β-barrel constructed from both β-hairpins is in the foreground. Figure 7C is a second representation of HFB2, highlighting the spatial location of aliphatic residues that, according to Hakanpää *et al.* (2004), contribute to the aliphatic nature of this hydrophobin. **Colour key for all images:** the first hairpin containing the hydrophobic residues is coloured red, the second is purple. All images were taken from Hakanpää *et al.* (2004, pages 535-537).

These 10 amino acids are located in both β-hairpins and are thought to be the origin of both the hydrophobin's hydrophobic and self-assembly properties. When the hydrophobin self-assembles, Hakanpää *et al.* (2004) believe that the molecules pack together as dimers so that their hydrophobic regions can face each other. Only the residues on the first β-hairpin are involved in the dimer interface; the residues on the second β-hairpin are thought to be exposed to the solvent. This corresponds to the observation that HFB2 can form dimers or tetramers in solution (depending on the HFB2 concentration) (Torkkeli *et al.,* 2002). Hakanpää *et al.* (2004) argue that the molecule orientates itself in order to bury the solvent-exposed area of the hydrophobic "patch" in any hydrophobic environment such as the water-free environment that exists at a hydrophobic-hydrophilic interface. In so doing, the protein would acquire a lower energy structural-state than would exist in solution alone. Paananen *et al.* (2003) and Hakanpää *et al.* (2004) suggest that this is why HFB2 self-assembles into a rodlet-less, ordered, two-dimensional, amphipathic film.

Interestingly, the SC3 structure predictions indicate that the region between residues Leu_{76} and Cys_{86} are likely to form an α-helix (de Vocht *et al.*, 1998). This region roughly coincides with the α-helical region in HFB2. It is preceded in both proteins

by a proline residue (Pro_{29} in HFB2 and Pro_{75} in SC3) whose presence and position in both class II and basidiomycete class I hydrophobins is tightly conserved (see Figure 2).

In class II hydrophobins, the hydrophobic residues in the hydrophobic patch region are strictly conserved - along with a phenylalanine residue (Phe_{39} in HFB2) which is located in the α-helix and packs against the β-barrel (see Hakanpää *et al.*, 2004 and Figure 2). This fact strongly suggests that the HFB2 structure is common to all class II hydrophobins, and the following quote from Yaguchi *et al.* (1993) suggests that the two-dimensional NMR data they referred to supports this hypothesis:

"Two-dimensional NMR studies show that [sic] presence of two anti-parallel β-sheets. One sheet involves the strands made of residues 16-20 and 28-32. The other is made up of residues 56-61 and 65-71 with a bulge at residues 67-68. A helical structure is indicated in the region of residues 43-49... [and is] confirmed by NMR data (R. Muhandiram, H. Hunter, and E. O. Purisima (unpublished results) from [the] Biotechnology Research Institute, Montreal)."

When the cerato-ulmin sequence is aligned with HFB2, the locations of the β-strands and α-helix roughly coincide.

1.3.4 The Structure of Class I Hydrophobin Monomers.

The starting point for the hydrophobin self-assembly process is the soluble monomer. The ultra-structure of these molecules has been examined in cerato-ulmin, EAS, and SC3. The results are broadly similar in that a small portion of each protein is known to assume β-sheet conformation (Yaguchi *et al.*, 1993; de Vocht *et al.*, 1998; Mackay *et al.*, 2001). In EAS and cerato-ulmin, the β-sheet (anti-parallel in the case of the latter) was localised around the regions containing the cysteines (Yaguchi *et al.*, 1993; Mackay *et al.*, 2001). The rest of EAS was unstructured in solution, while a small amount of α-helix was detected in cerato-ulmin (Yaguchi *et al.*, 1993; Mackay *et al.*, 2001). On the other hand, the conformation of the soluble form of SC3 consisted of ~20% α-helix and ~40% β-sheet (de Vocht *et al.*, 1998). This might be explained by the fact that soluble SC3 was recently shown to form multimeric complexes in water (Wang *et al.*, 2002; Stroud *et al.* 2003).

Because hydrophobins are highly surfactive molecules with a significant number of hydrophobic amino acids, it is not surprising that monomeric hydrophobin molecules aggregate or even self-assemble into rodletless aggregates in the absence of an interface. Stroud *et al.* (2003) believe that freshly dissolved monomeric SC3 exists as a mixture of free, unassembled SC3, and loosely assembled and possibly

micelle-like SDS-soluble multimers whose size seems concentration-dependent (Martin *et al.*, 2000; Stroud *et al.*, 2003). The addition of the polysaccharide schizophyllan (co-secreted with SC3 *in vivo*) is believed to stabilise the monomeric form of SC3. It is thought that schizophyllan stabilises SC3 by associating with single or multiple SC3 molecules and sterically inhibiting the protein from aggregating at least until the SC3/schizophyllan-solution is agitated (Martin *et al.*, 2000; Stroud *et al.*, 2003). Stroud *et al.* (2003) determined that dissolved SC3 would, if left undisturbed at room temperature in the absence of an interface, slowly assemble into large irregularly shaped SDS-insoluble complexes (Stroud *et al.*, 2003). Vortexing these assemblies caused them to irreversibly convert into rodlets.

1.3.5 The Mechanism of Self-Assembly in SC3.

De Vocht *et al.* (2002) devised a model to explain the conformational changes they observed while monitoring the self-assembly of SC3 (Figure 8). Starting at the soluble state, the self-assembly SC3 passes through two different intermediate states before arriving at the final, stable, rodlet-conformation rich in β-sheet. The first transition-state is characterised by a 10% increase in α-helical content in a region of hydrophobic residues between Thr_{52} and Ser_{63} (de Vocht, 2001). If SC3 forms on a hydrophobic solid the self-assembly of SC3 remains in this α-helix-rich state and self-assembly is arrested unless the surface of the hydrophobic material is treated with hot detergent.

In the absence of a hydrophobic surface, hydrophobin self-assembly progresses rapidly through to a second amorphous transition-state with ~65% β-sheet content. After an overnight incubation, the final – rodlet-forming state that also contains ~65% β-sheet – was reached (de Vocht *et al.*, 2002; Wang *et al.* 2002). These results agree with those of Mackay *et al.* (2001), who detected a substantial increase in β-sheet content after EAS had completely self-assembled; unfortunately, they undertook no studies that would have detected either the α-helical or the β-sheet transition states.

De Vocht (2001) determined that self-assembly occurs only when the concentration of hydrophobin in solution exceeds a critical level. This concentration threshold is modulated neither by pH nor by ionic-strength, but is reduced with heat; thus, the self-assembly process is independent of electrostatic interactions but the initial stages are endothermic. The self-assembly process is also irreversible (unless ice-cold TFA is used), because dilution does not dissociate the complexes. De Vocht (2001) explained these observations by concluding that hydrophobin self-assembly is dependent on nucleation, as well as the presence of an interface.

FIGURE 8: MODEL FOR THE SELF-ASSEMBLY OF SC3.

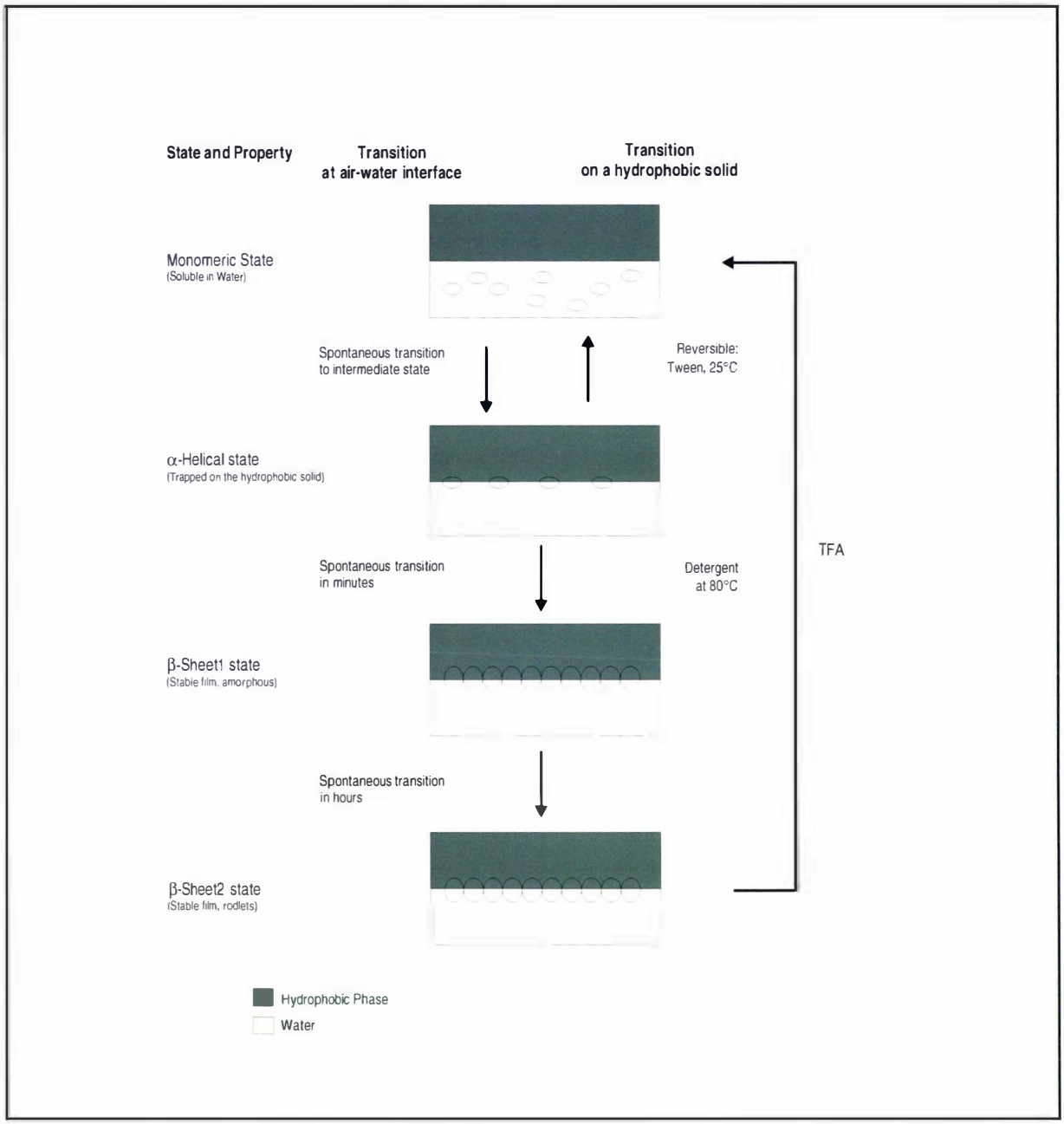

Figure 8 depicts a hypothetical model that explains the self-assembly mechanism of SC3. The diagram was taken from de Vocht (2001, page 50). **Key:** The hydrophobic phase (dark area) represents any hydrophobic substance. Circles represent molecules of SC3.

1.3.6 CLASS I HYDROPHOBINS AND AMYLOIDS.

Alzheimer's disease, Bovine Spongiform Encephalopathy (BSE), and some forms of diabetes are among the more than 20 human diseases whose symptoms include the formation of insoluble plaques of fibrous proteins. In each case, the aggregates are formed from innocuous proteins or peptides (collectively referred to as being amyloidogenic), unrelated by native structural motifs or amino-acid sequences. In fact, the only property these proteins share is the ability to form the fibrillar

structures seen in amyloid-plaques (hereafter referred to as amyloid-fibrils) (reviewed by Gorman and Chakrabartty, 2001).

FIGURE 9: CROSS β-SCAFFOLD.

Figure 9 is a diagram from Jiménez *et al.* (2002, page 9199). This is a model depicting the β-scaffold structure of insulin amyloid fibrils, clearly illustrating the parallel β-sheets (arrows) forming a β-strand. The β-sheets are aligned perpendicular to the longitudinal axis of each strand. Further, several strands form protofibrils (transparent blue surface) from which the amyloid fibril is made. In this diagram the fibrils has a slight helical twist.

Proteins whose biological activity is intrinsic to their ability to form amyloid-like-fibrils *in vivo* are beginning to be identified: e.g. Chorion, URE3, HET-s and the chaplins (Wickner 1994; Iconomidou *et al.,* 2000; Maddelein *et al.,* 2002; Claessen *et al.,* 2003). These proteins along with the hydrophobins have been called "functional amyloids" because the dyes Congo Red and Thioflavin T bind to EAS and SC3 films to produce birefringence and fluorescence spectrum-shift effects that are diagnostic for fibrils with the same structure as amyloid fibrils (Mackay *et al.,* 2001; Butko *et al.,* 2001; de Vocht, 2001). By contrast, neither the monomeric form nor the aggregated-form that Stroud *et al.* (2003) created (which was both rodletless and SDS-insoluble) could react with Thioflavin T as an amyloid plaque would. This suggests that only the rodlet-form of a hydrophobin possesses same structure as amyloid-fibrils.

Hydrophobin-rodlets and amyloid-fibrils are both too refractory for high-resolution structural investigations and such studies are currently impracticable. Instead, low-resolution investigations have been undertaken; the results simultaneously strengthen the perception that these proteins are related while providing some interesting insights on the structure within hydrophobin rodlets.

(1) Hydrophobin self-assembly and amyloid aggregation occur by nucleation dependent polymerisation (Dobson, 1999; de Vocht, 2001)

(2) Both hydrophobins and amyloidogenic proteins (hereafter referred to as amyloids) have diverse and seemingly unrelated amino acid sequences (compare Figure 2 with Gorman and Chakrabartty, 2001); some are known to form at the air–water interface (Schladitz *et al.,* 1999), on hydrophobic solids (Kowalewski and Holtzman, 1999), or when agitated (Ramirez-Alvarado *et al.,* 2000).

(3) The dimensions of amyloid-fibrils and hydrophobin rodlets are similar: the rodlets are often several micrometres long, with unbranched fibres with a diameter of approximately 10 nm (review by Wessels, 1997). By comparison, fibrils of amyloid fibrils are relatively straight, unbranched strands with a diameter of 8-12 nm and a length up to several microns.

(4) The substructure of amyloid fibrils consists of a bundle of protofibrils; each protofibril has a diameter of 2-3 nm. Low resolution X-ray diffractograms and cryo-electron microscopy show that the protofilaments all contain a cross- β-scaffold with β-strands perpendicular to and β-sheets parallel to the axis of each fibril (see Figure 9 and reviews by Wetzel, 2002; Sipe and Cohen, 2000; Dobson, 1999, 2001). PM-IRRAS data from studies on SC3 suggest that a similar orientation of β-sheets is present in hydrophobins (de Vocht *et al.,* 2002).

Recently, proteins unrelated to any human disease have been induced to form amyloid fibrils – *in vitro* – after being exposed to mild denaturing conditions (reviews by Dobson, 1999, 2001). These discoveries have fuelled speculation that the amyloid fibril formation is an inherent, if not a primordial, protein property (Dobson, 1999; Pickersgill, 2003).

1.3.6.1 Are The Polymers of Class II Hydrophobins Amyloid-Like?

Class I hydrophobins may be "functional amyloids" but the same cannot be said for the class II hydrophobins because their polymeric form does not contain rodlets:

(1) TEM studies have shown that cryparin, HFB1 and HFB2 form polymer films are bereft of rodlets (Wösten and de Vocht, 2000; Paananen *et al.,* 2003).

(2) Low-resolution studies on HFB1 and HFB2 films formed using the Langmuir-Blodgett technique indicate that both of these hydrophobins polymerise into tetrameric molecules which then pack into a two-dimensional crystalline monolayer without forming rodlets (Paananen *et al.,* 2003).

However, cerato-ulmin, HFB1, and HFB2 are able to form crystalline fibrillar aggregates that are large enough to be seen with a light-microscope (Takai, 1974; Torkkeli *et al.,* 2002). These crystalline structures arise in HFB1 and HFB2 when relatively concentrated (7.5 mg/mL) aqueous solutions are agitated but they are not amyloid fibrils as they fail to react with Thioflavin T (Torkkeli *et al.,* 2002). Undried HFB2 crystalline fibrils are formed from tetrameric aggregates (Paananen *et al.,* 2003).

1.3.6.2 CONCLUSIONS.

It is clear, then, that fundamental structural differences exist between the structure of both the monomeric and polymeric forms in both classes of hydrophobin proteins. Low-resolution structural data indicates that the class I hydrophobins are unstructured and flexible in solution, They remain in this state unless confronted by a hydrophobic interface whereupon the monomer spontaneously undergoes a transition from a disordered monomer state into an ordered polymeric state in which an undetermined number of monomers form rodlets rich in β-sheet structure. This may be similar to the cross β-sheet structure proposed to exist in amyloidogenic fibrils.

By contrast, for HFB2 - and by extension all class II hydrophobins - the juxtaposition of the protein's intramolecular disulfide bonds appears to lock the monomer into a rigid, amphipathic globular structure that persists both in solution and at the hydrophobic interface. In solution, HFB2 forms dimers and tetramers to bury the hydrophobic region within the interface between the oligomers. Self-assembly in this instance does not involve a change in structural conformation; rather it involves a reorientation of the monomer to hide its hydrophobic face in the water-free environment provided by any hydrophobic interface present.

1.4 APPLICATIONS OF HYDROPHOBINS.

Wessels (1997) and Scholtmeijer *et al.* (2001a) have shown that the opportunity exists to develop many hydrophobin-based biotechnological applications because these proteins combine surface-active, adhesive, and chemically-resistant physiochemical properties with a benign nature. They foresaw hydrophobins being adapted for use in the medical, molecular-biochemical, horticultural and the mycological fields. Indeed, after establishing reliable protocols for expressing hydrophobins in filamentous fungi, researchers at the Universities of Groningen and Helsinki have now begun research directed at developing hydrophobin-based technologies. For example:

(1) Scholtmeijer *et al.* (2002) confirmed that the N-termini of SC3 could be altered, or the first 25 residues removed, without effecting the self-assembly of SC3 – although the absence of the glycosylated residues from the N-terminus did lower the wettability of the hydrophilic side of the films. Further, the fibronectin cell-binding domain (a tri-peptide known as RGD) has been successfully added to the N-terminus of SC3. Both the RGD-fusion *and* the truncated version of SC3 were shown to simultaneously alter the wettability of

Teflon® and improve the ability of fibroblasts to grow on both this surface and in growth media. Neither modification affected the benign nature of SC3 (Scholtmeijer *et al.* 2002; Janssen *et al.*, 2002). Interestingly, fewer fibroblasts grew on Teflon® covered with SC3 in the intermediate α-helix-rich state than grew on bare Teflon®. However, if the SC3 film was treated with detergent prior to the experiment – ensuring the protein entered its β-sheet rich polymer form – the cell numbers returned to normal (Janssen *et al.*, 2004). This result implies that consideration of the conformation of the hydrophobin polymer is critical to the task of developing technologies around hydrophobins.

(2) Linder *et al.* (2001) replaced the C-terminal cellulose-binding domain of the *T. reesei* hydrolytic enzyme endoglucanase I with HFB1 and hence showed that the active enzyme could be strongly bound to hydrophobic surfaces. The same experiment with HFB2 failed; possibly, because the N-terminally linked enzyme interfered with its ability to polymerise in solution. These researchers exploited the amphipathic properties of the hydrophobin domain when they purified the recombinant protein using either detergent/aqueous or a detergent/polymer two-phase purification systems, thus demonstrating another application of hydrophobins — as fusion partners to simplify the purification of heterologous proteins (Collén *et al.*, 2001, 2002).

(3) Nakari-Setälä *et al.* (2002) replaced the lectin domain of the membrane bound flocculin protein from *Saccharomyces cerevisiae* with HFB1 and expressed the recombinant protein back in the membrane of *S. cerevisiae*. As was anticipated, Nakari-Setälä *et al.* detected a two-fold increase in binding affinity between the recombinant yeast cells and the hydrophobic supports. Interestingly the hydrophobin retained its absorption capability despite being spliced between two domains of the flocculin protein.

(4) Palomo *et al.* (2003) have developed a method to non-covalently immobilize lipases to hydrophilic matrices using the *Pleurotus ostreatus* hydrophobins vmh1, vmh2, and vmh3. They believe this offers new possibilities for studying lipases and their chemical activity.

(5) Fundamental scientific questions may also be answered using hydrophobins as a model or by studying them *in* vivo. For instance, Mackay *et al.* (2001) suggest that they might be useful in investigating amyloidosis and any related phenomena. In addition, much has yet to be learned about how hydrophobins and similar proteins influence fungal- and bacterial-development and

reproduction. This is illustrated by the discovery that rodlet fibrils contribute to the surface properties of bacterial spores and that SC3 actively participates in the formation of the fungal cell wall (see section 1.2.1.2 and van Wetter *et al.*, 2000b).

Such applied- and fundamental-scientific efforts would benefit from a better fundamental understanding of the structure of hydrophobins and the means by which they spontaneously self-assemble.

2
METHODS AND MATERIALS.

2.0 General Methods.

2.0.1 Use of Product-Line and Brand Names in this Work.

Prior to the completion of this work, several of the manufacturers supplying equipment and consumables for this project underwent sales or mergers. For clarity and brevity, the origin of manufactured products used in this work is indicated by the appropriate brand-name or product-name because these have remained constant. In Appendix VII, the manufacturers and New Zealand distributors for all manufactured goods (current at the time of printing) are tabulated against the brand- or product-name of the goods they produce. In the text, these brand- and product-names are easily identified by the associated registered trademark (®) and trademark symbols (™). Note also that a list of all abbreviations used in this thesis is presented in Appendix VIII.

2.0.2 Chemicals and Enzymes.

Unless otherwise stated only analytical grade chemicals were used. Chemicals were selected from the Sigma-Aldrich® or BDH AnalR® product-lines. Enzymes were supplied by NEB® or Invitrogen™ but only Roche® *Taq* DNA polymerase was used. Tris(2-carboxyethyl) phosphine was obtained exclusively from the Pierce® Chemical Company, Rockford, IL, USA.

2.0.2.1 Milli-Q® Water.

Water used in every solution was purified with the Millipore® Milli-Q PF-plus water purification system until the water had a resistivity of 18.2 MΩ. Water so treated will be referred to as Milli-Q® water in the text.

2.0.3 Sterile Manipulations and Solutions.

All manipulations involving sterile media, substrates, chemicals or equipment were performed in either a Class-I Airpure® sterile laminar airflow cabinet or, where indicated, in a Class-II Nuaire™ sterile laminar airflow cabinet (Model NU425-400E Series 20).

2.0.3.1 Sterilisation Techniques.

I sterilised chemicals and equipment using one of two methods. Solutions able to withstand heating were autoclaved at 121 °C, 205 kPa (15 lb/sq·in) for 15 min and allowed to cool before use. Solutions that are more delicate were filter sterilised, providing that they were compatible with the filter-membranes used. Solutions less than 50 mL in volume were sterilised by passage through a 0.2 µm Acrodisc® 32 GS syringe filter into a sterile container. Filter sterilisation of larger solutions volumes

took place in a laminar airflow cabinet. The liquid was sterilised, under vacuum, by passage through a 0.22 µm Millipore® GSWP type filter in a Millipore® Pyrex filter-holder attached to a sterilised sidearm flask.

TABLE 2: HAZARDOUS CHEMICALS USED UNSTERILISED.

Acetonitrile	*Formaldehyde*
Chloroform	*Formamide*
Concentrated ethanol (> 50 %v/v)	*Methanol (> 50%v/v)*
Concentrated inorganic acids (> 2 %v/v)	*Phenol*
Concentrated inorganic alkalis (> 2 %v/v)	*PMSF*
Concentrated isopropyl alcohol (> 50 %v/v)	*TFA*
Dimethylformamide	

Table 2 lists the chemicals used in this study which could not be sterilised before use. Aqueous solutions containing acids, alkalis, ethanol and isopropanol at concentrations less than those listed in were sterilised by filtration. According to manufacturer's instructions aqueous solutions containing these chemicals in lesser concentration were compatible with the filter membranes.

The chemicals listed in Table 2 are toxic, or volatile, or flammable, or corrosive and as such were chemically incompatible with the filter-membranes and too dangerous to sterilise in the autoclave. I made the solutions containing these chemicals without the hazardous components and then sterilised them using the one of the methods described above. Prior to use, I completed the solution by adding the hazardous chemical at the appropriate concentration to an aliquot of the sterilised components.

2.0.4 COMPUTING.

2.0.4.1 DATA MANIPULATION AND PRESENTATION.

Photographic results presented in this thesis were prepared from digitised photographs using Corel® Draw Version 7-Select Edition. The fidelity of these data was maintained by limiting the software manipulations to resizing, rotation, cropping, and labelling of images. The resolution of some images was increased (by resampling) to 600 dots per inch to improve the print-quality of the image.

2.0.4.2 NUCLEOTIDE AND PROTEIN SEQUENCE ANALYSIS.

"Proof-reading" DNA Sequencing Results.

DNA-sequencing results were "proof-read" with elements of the *Staden* software package (Staden *et al.*, 1999). Electrophoretogram and sequence-data gathered from the forward-primed and reverse-primed DNA-sequencing reactions were edited to remove vector sequences with *Pregap4* prior to being shotgun-aligned with *gap4* and *Trev*. Once aligned the electrophoretograms from each DNA-sample were compared to enable the 'base-calling' errors (introduced during the automated results-collection phase) to be removed. The consensus DNA-sequences resulting from this process were used for the analysis presented in this work.

Blast® Searches.

If required, nucleotide sequences derived in this study were compared with those stored in GenBank® (Benson *et al.*, 2002) and in the *Neurospora* Sequencing Project Database (located at the Whitehead Institute/MIT Centre for Genome Research). The sequences were compared using the BlastN algorithm (Altschul *et al.*, 1990, 1997).

Miscellaneous DNA and Protein Sequence Analysis.

Computer programs within the Accelrys® *Wisconsin Package* (Version 10.3) and InforMax® *Vector NTI* software packages (versions 4 to 8), were used for expression-vector construction, restriction-digest mapping, vector-map creation, and the comparison and translation of DNA or protein sequences. Preliminary multiple-sequence alignments were prepared using the *Clustal X* version 1.64B (Thompson *et al.*, 1997) software package.

2.1 Microbiological Manipulations.

2.1.1 *Neurospora* Cultivation.

For long-term storage, *Neurospora* spores were adsorbed to silica-gel beads (Perkins, 1977). When cultivating *Neurospora*, cultures were inoculated by the addition of a few silica gel beads onto solid 1x Vogel's media and incubated at 25 °C. All *Neurospora* cultures required to express EAS were grown with a 12 h on 12 h off cycle of either fluorescent or long wave ultra-violet light. *Neurospora* grown in static-liquid culture were incubated at 25 °C after being inoculated with material from cultures freshly grown on solid media. If required, liquid cultures were shaken at 150 rpm during incubation but this precluded the use of the programmed lighting regimen.

2.1.1.1 Cultivation of *Neurospora* for DNA Extraction.

Liquid cultures were grown according to the method of Braithwaite *et al.* (1990), modified by growing *Neurospora* cultures in 250 mL flasks, to which Vogel's medium N (Vogel, 1964) supplemented with 2 %(w/v) sucrose was added. The cultures were incubated in a shaking incubator (250 rpm) at 25 °C until late log-phase growth had occurred. Mycelia was separated from the media by filtration, resuspended in fresh media, and blended for 30 seconds using a VirTis™ homogenizer with an open blade, set to medium speed. A small portion of this slurry was used to inoculate fresh Vogel's liquid media and grown for a further 2-3 days before being used for DNA extraction.

2.1.1.2 CULTIVATION OF *N. LINEOLATA* FOR DNA EXTRACTION.

Pure cultures of *N. lineolata* were grown from activated ascospores prepared as follows: an aqueous suspension of *N. lineolata* ascospores was obtained by scraping the wetted surface of a *N. lineolata* colony cultured on solid media. The suspended ascospores were heat activated according to Murray and Perkins (1963), and the suspension was used to inoculate 15 mL aliquots of sucrose-supplemented Vogel's N media in Petri dishes. The cultures were incubated unshaken at 25 ºC for between four and seven days.

The identity of this culture was confirmed by comparing the sequence of its ITS/5.8S rRNA gene to the *N. lineolata* ITS-sequence obtained by obtained by Dettman *et al.* (2001) (GenBank® accession number: AF388924) as described in section 2.0.4.2. The ITS/5.8S rRNA gene was PCR-amplified from genomic DNA extracted from *N. lineolata* as described in section 2.2.3. The comparison of the two sequences is reproduced in Appendix IIIA.

2.1.1.3 VOGEL'S MEDIA.

All species were grown in 1x Vogel's media diluted from the 50x stock solution as described in Davis (2000). Sucrose (2 %w/v) was added to act as a carbon source in addition to 2 %(w/v) Difco® Bacteriological agar to produce solid media for the harvesting of protein. Liquid Vogel's media was utilised when growing *Neurospora* for the extraction of nucleic acids. The media was dispensed and sterilised by autoclaving before inoculation.

2.1.2 *PICHIA* CULTIVATION.

2.1.2.1 *PICHIA* STRAINS USED IN THIS STUDY.

Pichia pastoris strains GS115 and SMD1168 (Invitrogen™) were used in this study. Both strains are histidine mutants (*his4* genotype) whose auxotrophic deficiency is complemented by the histidinol dehydrogenase gene (*HIS4*) carried by pPIC-series expression vectors. The SMD1168 strain is a protease-deficient strain (*his4*, *pep4* genotype). A GS115 strain engineered to secrete albumin (GS115/His^+, Mut^S phenotype) was purchased from Invitrogen™ for use as a positive control for protein expression (Higgins and Cregg, 1998a).

2.1.2.2 MEDIUM/LONG TERM STORAGE OF *PICHIA* STRAINS.

For medium and long term storage of transformant strains, a single colony obtained from selective (histidine deficient) BMD solid media was inoculated in 2 mL of YPD liquid medium, and grown overnight at 30 ºC with shaking. This culture (1.2 mL) was transferred to a 3 mL cryovial containing 0.6 mL of sterile 100 %(v/v) Glycerol. This

solution was mixed and stored at −80 ºC. Strains were resurrected by plunging a sterile inoculating loop into the frozen media, streaking a few microlitres out onto fresh selective BMD solid media and incubating the culture at 30 ºC until colonies appeared. Cryovials were immediately returned to −80 ºC after inoculation.

To preserve the genetic pedigree of the transformant, sub-culturing was kept to a minimum. Cultures were stored at 4 ºC on selective solid media and used as required for a period no longer than 12 days before the cultures were replaced.

2.1.2.3 Nutrient Media Used During *Pichia* Cultivation.

Two types of media were used for *Pichia* culture: the first was yeast peptone dextrose (YPD) media, which is a rich, non-selective nutrient media used for the maintenance of *Pichia* stock cultures (Higgins and Cregg, 1998b). The second type of media was derived from a standard formulation called "yeast nitrogen base without amino acids" (YNB). When YNB is supplemented with phosphate buffer and the appropriate amino acids and carbon supplements, a series of the buffered minimal media (BMD, BMG, and BMM) can be created. These media were used during protein expression experiments, and for the selection of *Pichia* transformants (Higgins and Cregg, 1998b).

Media Derived from YNB (Yeast Nitrogen Base) Solution.

Normally, the buffered minimal media (BMD, BMG and BMM) used in this study are made using a commercially prepared lyophilised concentrate of YNB (Invitrogen™, 2002). To avoid this, I modified the formulae for "YNB without amino acids" given in the Difco® Laboratories (1984), and created a liquid concentrate form of YNB that could substitute for the lyophilised preparation. The formulae for this concentrated YNB solution (1000x YNB) is given in Appendix II.

A complete description of the procedures for making BMD, BMG and BMM media is given in Appendix II. Essentially, concentrated stock solutions were created for every other constituent in BMD, BMG, and BMM besides YNB; the formulae for these stock solutions are reproduced in Appendix II. These solutions were sterilised and stored at 4 ºC until use. BMD, BMG, and BMM media were prepared by diluting appropriate amounts of these stock-solutions in sterile Milli-Q® water. If an experiment called for solid media, the media constituents were diluted in a hot, autoclave-sterilised, aqueous solution of 2 %(w/v) Difco® Bacteriological Agar and then dispensed into Petri-dishes to cool.

2.1.2.4 Inducing Protein Expression in Recombinant *Pichia*.

Protein expression assays with recombinant *P. pastoris* strains were carried out in batch-culture according to the procedures described in Invitrogen™ (2002). Recombinant isolates were grown until late log-phase in BMG media whereupon the cells were harvested by centrifugation and washed twice in aliquots of BMM media before being resuspended in BMM media and cultured at 30 °C in a Gallenkamp® orbital incubator set to 300 rpm. Induction was maintained by daily addition of neat methanol to a final concentration of 3 %(v/v). Samples taken from these cultures were separated into supernatant and cell fractions by microcentrifugation prior to freezing at –80 °C.

2.1.3 *E. coli* Cultivation.

2.1.3.1 Media and Media-Supplements Used During *E. coli* Cultivation.

E. coli strains were cultivated and manipulated according to techniques described in Sambrook and Russell (2001). For most experiments Luria-Bertani (LB) broth was used, supplemented as necessary with the antibiotics indicated in the text (Sambrook and Russell, 2001). Occasionally, 2XL medium (LB broth with the concentration of each solute doubled) or SOC medium supplemented with antibiotics was used (Seidman *et al.,* 1992). *E. coli* cultures were incubated at 37 °C. Liquid cultures were shaken during incubation. If solid media was required – prior to autoclaving – I added sufficient Bacteriological agar to obtain a final concentration of 2 %(w/v).If solid media needed to be supplemented with other chemicals (for example, antibiotics), they were added to the liquefied media (60 °C) as it cooled following autoclaving.

Antibiotic Stock Solutions.

Ampicillin (D(-)-α-aminobenzylpenicillin sodium salt) solution was prepared as a 100 mg/mL aqueous stock solution. Tetracycline (tetracycline hydrochloride) solution was prepared as a 12.5 mg/mL stock solution in 95 %(v/v) ethanol. Kanamycin (kanamycin monosulfate) solution was prepared as a 15 mg/mL aqueous stock solution. Spectinomycin (spectinomycin dihydrochloride hydrate) solution was prepared as a 100 mg/mL aqueous stock solution and used at a final concentration of 100 µg/mL. Aqueous antibiotic stock solutions were made with Milli-Q® water. All antibiotic stock solutions were filter sterilised and stored as 1 mL aliquots at –20 °C.

X-gal and IPTG Stock Solutions.

X-gal (5-bromo-4-chloro-3-indolyl β-D-galactopyranoside) solution was prepared as a 100 mg/mL stock solution in dimethylformide and stored as 1 mL aliquots in darkened containers, at –20 °C until required. X-gal was used at a final concentration of 40 µg/mL by adding it directly to autoclaved media as it cooled. IPTG (isopropyl-β-D-thiogalactopyranoside) solution was made as a 2 %(w/v) aqueous stock solution in Milli-Q® water then filter sterilised and stored as 1 mL aliquots at –20 °C.

2.1.3.2 *E. COLI* STRAINS USED IN THIS STUDY.

E. coli Strain DH5α™.

E. coli strain DH5α™ (Invitrogen™) was used for routine sub-cloning of plasmid vectors for plasmid amplification, maintenance, and storage purposes. *E. coli* strain DH5α ™ was always cultivated on LB broth. The LB broth used when selecting transformants, was supplemented with ampicillin (100 µg/mL) and X-gal (40 µg/mL).

E. coli Strain AD494.

E. coli strain AD494 produced by Novagen® was used in for protein expression. In this strain, the thioredoxin reductase (*trxB*) gene has been knocked out by interruption with the kanamycin resistance (Kan^R) gene. This necessitates supplementing all growth media with kanamycin (15 µg/mL) to maintain the AD494 phenotype. Cultivation of this strain for recombinant selection and protein expression required the addition of ampicillin (100 µg/mL) to kanamycin-containing media to maintain the presence of the expression vector.

E. coli Strain Origami™.

An *E. coli* strain, Origami™ (Novagen®), was used for protein expression. In *E. coli* Origami™ strains, the thioredoxin reductase (*trxB*) and glutathione reductase (*gor*) genes have been knocked out by interruption with the Kan^R and tetracycline resistance (Tet^R) genes respectively. This necessitates supplementing all growth media with kanamycin (15 µg/mL) and tetracycline (12.5 µg/mL) to maintain the Origami™ phenotype. Cultivating this strain for recombinant selection and protein expression required the addition of ampicillin (100 µg/mL) to the media in addition to the other two antibiotics, in order to maintain the presence of the expression vector.

2.1.3.3 PROTEIN EXPRESSION IN *E. COLI*.

LB broth (5 mL) with the appropriate antibiotics (see above) was inoculated with a single recombinant colony and grown overnight at 37 °C without shaking until the culture density had reached an OD_{600} of 0.4–0.5. At this point, IPTG was added to a

final concentration of 1 mM in order to induce protein expression. The induced cultures were grown for 9 h at 37 °C with shaking and were sampled at regular intervals. The bacterial cells in these 1 mL samples were separated from the growth media by microcentrifugation, and frozen at –80 °C prior to SDS-PAGE analyses.

2.2 Nucleic Acid Manipulations.

2.2.1 Precautions Observed when Manipulating RNA.

2.2.1.1 Anti-RNase Pre-treatments.

Manipulations with solutions containing formaldehyde were done in a chemical fume-hood. All other manipulations with RNase-free solutions were carried out in Class-I sterile laminar airflow cabinets. Only new nuclease-free disposable plastic-ware was used for these manipulations, and nuclease-free aerosol-filtering auto-pipette tips (either the Axygen® or ART® tips) were preferred for pipetting.

Pre-treatments of glassware, non-disposable plastic-ware, and electrophoresis apparatus were carried out according to instructions accompanying the RNeasy® Plant Mini Kit.

RNase-Free Organic Solutions.

Phenol, chloroform, and ethanol were obtained fresh from the manufacturer. Aliquots were stored in RNase-free plastic-ware or pre-treated glassware, and then set aside and used only for the manipulation of RNA.

RNase-Free Aqueous Solutions.

Milli-Q® water was treated for RNase contamination as follows: 1 L aliquots of water were incubated overnight at room temperature with 0.1 %(w/v) DEPC in RNase treated glassware. The water was sterilised by autoclaving at 121 °C, at an absolute pressure of 205 kPa for 15 min, and then allowed to cool. Aqueous solutions whose components were chemically compatible with both DEPC and autoclaving were treated as described above. Solutions of MOPS were created in DEPC-treated Milli-Q® water using RNase treated glassware and chloroform treated metal ware. The amount of acid or base required to adjust the pH of DEPC-sensitive solutions was determined empirically prior to making the RNase-free version of the solution so as to eliminate the pH probe as a source of contamination.

2.2.2 Cellular Extraction of Nucleic Acids.

2.2.2.1 DNA Extraction and Purification from *Neurospora*.

The protocol used to extract genomic DNA from *Neurospora* was based on the method of Weeks *et al.* (1986). Mycelia were collected by filtration through

Myracloth (Calbiochem®) and transferred to sterilised pestles that had been pre-chilled with liquid nitrogen. Then the mycelia were snap frozen in liquid nitrogen and ground into a fine powder, after which it was re-suspended in 5 mL of isolation buffer (150 mM EDTA, 50 mM Tris HCl pH 8.0, 1% (w/v) sarkosyl) and then centrifuged (10 min, 2900*g*, 4 °C). The supernatant was treated with Proteinase K (Roche®), added to a final concentration of 50 µg/mL for 1 h at 50 °C. The aqueous phase was extracted once with phenol, and twice with a phenol/chloroform/isoamyl alcohol solution (25:24:1) prior to the DNA being precipitated by the addition of 1 volume of 1 M $NaCl_{(aq)}$ and 2 volumes of neat ethanol as described in Sambrook and Russell (2001). The DNA was collected by centrifugation (10 min, 2900*g*, 4 °C) and re-suspended in TE buffer (10 mM Tris HCl pH 8.0, 1 mM EDTA). This solution was treated with RNase A (Roche®) then added to a final concentration of 2.5 µg/mL and incubated at 37 °C for 1 h. The RNase A was removed by extracting once with phenol and twice with phenol/chloroform/isoamyl alcohol solution (25:24:1) prior to precipitating the DNA with NaCl and ethanol as above. The DNA was collected by centrifugation (10 min, 2900*g*, 4 °C) and resuspended in TE buffer and stored at 4 °C.

Phenol Equilibration.

UltraPURE™ phenol was liquefied at room temperature and treated twice with an equal volume of Milli-Q® water in the manner described by Sambrook and Russell (2001). After equilibration, 8-hydroxyquinoline was added to a final concentration of 0.1 %(w/v). The phenol solution was stored in the dark at 4 °C until required.

2.2.2.2 Total RNA Extraction and Purification from *Neurospora*.

For RNA extraction, cultures were cultivated in static liquid Vogel's N media, without shaking, (as described in section 2.1.1) until late log phase growth had occurred. Mycelium for RNA extraction was prepared as for DNA extraction, re-suspended in RLC buffer from the RNeasy® Plant Mini Kit and RNA purified according to manufacturer's instructions.

2.2.2.3 Genomic DNA Extraction from *Pichia*.

Acid Washed Glass Beads.

In a sterile 250 mL Schott bottle, 100 g of 0.5 mm glass beads (Sigma®) were shaken with 70 %(v/v) nitric acid for 1 h. Most of the nitric acid was separated from the glass beads by gravity-filtration through a borosilicate glass filter held in a Büchner funnel. The Büchner funnel and filter apparatus, containing the glass beads, were transferred on to a sidearm flask and residual nitric acid with several washes of Milli-Q® water under vacuum filtration.

"Smash and Grab" Pichia Genomic DNA Extraction.

The method of Hoffman and Winston (1987) – developed for *Saccharomyces cerevisiae* and *E. coli* – was used to extract DNA from *P. pastoris.* With this method, solutions containing genomic DNA are vortexed. If DNA samples prepared in this manner are to be used for Southern analysis, the vortex-mixing must be kept to a minimum to ensure that DNA fragments no smaller than 12 kb are created (Hoffman and Winston, 1987). Prior to using the extracted DNA, contaminating RNA was removed by incubating the solution with 2 µL of an RNase A solution (10 mg/mL) for 1 h at 37 °C.

2.2.2.4 *Pichia* Total RNA Extraction by the Phenol/Freeze Method.

The method of Schmitt *et al.* (1990), developed for *S. cerevisiae*, was used without modification in order to extract total RNA from *P. pastoris.*

2.2.3 PCR and RT-PCR Methods.

PCR and RT-PCR thermal-cycling reactions were carried out as described below using either a GeneAmp® PCR System 2400 or Genius® (Model FGEN02TD) thermal cycler. All PCR primers were synthesized to order by Invitrogen™ New Zealand Ltd. Auckland, New Zealand. When received all PCR primers were re-suspended in Milli-Q® water and stored as 0.1 mM aqueous stock solution at –20 °C until required.

2.2.3.1 PCR and RT-PCR for *Neurospora* Survey.

Homologues of the *N. crassa eas* gene were PCR-amplified from genomic DNA. Thermal-cycler protocol: initial denaturation at 94 °C for 5 min, 35 cycles of 94 °C for 30 sec, 60 °C for 30 sec, 72 °C for 1 min; 7 min extension at 72 °C; and a final soak at 15 °C. The PCR reaction conditions were as follows: 1 mM dNTPs, 0.1 µM for each primer, 0.05 U/µL Roche® *Taq* DNA polymerase, and 0.1–1 µg/100 µL of the genomic DNA sample. The sequences of the *eas* 5' primer (ATG CAG TTC ACC AGC GTC TTC ACC ATC) and *eas* 3' primer (TTA GGC AAC GCA GTT GGC AGC GTT GAT) were based on the respective regions of the coding sequence of the *eas* gene from *N. crassa* bd A (Bell-Pedersen *et al.,* 1992). Sequences of the ITS/5.8S rRNA regions were obtained according to Dettman *et al.* (2001) using the ITS5 and ITS4 PCR primers described by White *et al.* (1990).

RT-PCR first strand synthesis was carried out using a SuperScript™ kit according to the manufacturer's instructions. The recommended amount of *Neurospora* DNase I (RNase-free) treated total RNA served as the template. The parameters for the

second strand synthesis were identical to those used for genomic *eas* amplification except that the first strand RT-PCR reaction served as the template.

2.2.3.2 Purifying PCR Products.

PCR products were purified with the Concert™ Rapid PCR Purification System following the manufacturer's instructions.

2.2.4 DNA/RNA Quantitation.

The concentration of nucleic acids in solution was estimated either by one of two methods.

(1) Nucleic samples were resolved by electrophoresis and stained with ethidium bromide. The intensity of fluorescence between the sample(s) and a RNA or DNA mass ladder (Invitrogen™) run in a neighbouring lane (Sambrook and Russell, 2001).

(2) Alternatively, a spectroscopic method was used. The absorbance of the DNA/RNA solution was measured at 260 nm using an Agilent® 8453E UV Spectroscopy System and fresh UVettes® brand disposable cuvettes (Sambrook and Russell, 2001).

2.2.5 Agarose Gel Electrophoresis of Nucliec Acids.

2.2.5.1 Electrophoresis of RNA.

Total RNA samples were resolved by gel formaldehyde gel electrophoresis using the protocols suggested in the instructions accompanying the RNeasy® Plant Mini Kit.

2.2.5.2 Electrophresis of DNA.

DNA samples, mixed with 6x gel-loading buffer, were resolved by electrophoresis in 1x TAE (40 mM Tris-acetate, 1 mM EDTA at pH 8.0) through agarose gels. Electrophoresis grade agarose was dissolved in 1x TAE to make gels with an agarose concentration between 0.8 and 1.2 %(w/v) – depending on the size of DNA to be resolved. The gels were stained with ethidium bromide, at a final concentration of 10 µg/mL, for approximately 30 min and then viewed with ultra-violet illumination.

DNA Gel-Loading Buffers.

Six-fold concentrated (6x) gel-loading buffer was made by dissolving 0.25 %(w/v) bromophenol blue, 0.25 %(w/v) xylene cyanol FF, and 40 %(w/v) sucrose in Milli-Q® water. This solution was diluted six-fold with the sample before loading.

An Orange G-based loading buffer was used preferentially when dealing with samples containing DNA molecules under 300 bp in length because – unlike

bromophenol blue – Orange G migrates faster than all detectable DNA fragments (Guttman *et al.*, 1992). Six-fold concentrated (6x) Orange G gel loading buffer was made by 0.25 %(w/v) Orange G, and 40 %(w/v) sucrose in Milli-Q® water. This concentrated solution was diluted six-fold with the sample before loading.

DNA Electrophoresis Running Buffer.

Fifty-fold concentrated (50x) TAE Buffer was made by dissolving 242 g Tris base; 57.1 mL of glacial acetic acid; and 100 mL of 0.5 M EDTA (pH 8.0) in Milli-Q® water. The volume of the solution was adjusted to 1 L with Milli-Q® water and diluted 50-fold with Milli-Q® water before use.

2.2.5.3 Purifying DNA from Agarose Gels.

DNA was purified from agarose gels using the QIAquick® Gel Extraction Kit according to instructions supplied by the manufacturer.

2.2.6 Transformation and Cloning Methods.

2.2.6.1 Preparation of Competent Cells.

Heat-shock transformation of E. coli strain DH5α.

E. coli strain DH5α™ (Invitrogen™) cells were used for the maintenance and amplification of sequencing and expression plasmid vectors. Chemically competent cells were prepared using the calcium chloride transformation protocol described by Seidman *et al.* (1992) modified as follows: (1) 2XL medium replaces LB broth (section 2.1.3) (2) *E. coli* were grown until they had entered mid log phase (indicated by a solution optical density between OD_{600} 0.45 and OD_{600} 0.55). (3) The $CaCl_2$ solution was replaced with a filter sterilised "Transformation Buffer" containing 100 mM $CaCl_2$, 70 mM $MnCl_2.4H_2O$, and 40 mM aqueous sodium acetate, adjusted to pH 5.5 with 0.1 M acetic acid.

Heat shock transformation was carried out essentially as described by Seidman *et al.* (1992) except that the DNA ligation mixture was made to a volume of 60 µL with additional Milli-Q® water before being mixed with 100 µL of thawed chemically competent cells. After a 30 min incubation on ice this solution was heat shocked at 37 °C for 5 min, being diluted with 800 µL of pre-heated LB broth and incubated for 100 min at 37 °C before plating.

2.2.6.2 Electro-Transformation *E. coli.*

In *E. coli* strains AD494 and Origami™ (Novagen®), plasmid vectors were introduced by electroporation. Electrocompetent cells were prepared and stored cryogenically (at –80 °C until required) according to the method of Seidman *et al.* (1992).

TABLE 3 : CELL-PORATOR® ELECTROPORATION SETTINGS FOR TRANSFORMATION OF *E. COLI*

Parameter	Setting
Capacitance	*330 μF*
Resistance	*Low*
Charge Rate	*Fast*
Voltage Booster	*2 kΩ*

Electrotransformation of *E. coli* was carried out with a Cell-Porator® 230 V Electroporation System I device equipped with a Voltage Booster. The microelectroporation chambers used had a gap width of 0.15 cm and were obtained from Invitrogen™. The electroporation parameters used are described in Table 3 and were suggested by Peter Murphy (personal communication).

2.2.6.3 ELECTRO-TRANSFORMATION OF *P. PASTORIS* CELLS.

Electrocompetent *Pichia pastoris* strains GS115 and SMD1168 were prepared according to the protocol of Cregg and Russell (1998).

Electro-transformation of electrocompetent *P. pastoris* cells was carried out using a Gene-Pulser® transformation apparatus equipped with a Bio-Rad® Pulse Controller device. The electroporation chambers used had a gap width of 0.15 cm. The electroporation apparatus was set using the electroporation parameters suggested for this device by Cregg and Russell (1998).

Cells were transformed with pPIC9K based vectors linearised with either *Sst* I or *Bgl* II to help with the integration of or the transplacement by, the recombinant gene at the genomic locus of the *AOX1* gene as described in Invitrogen™ (2002) and Romanos *et al.* (1998). Transformed cells were diluted with 1 mL of cold 1 M sorbitol and aliquots of this solution were plated on BMD agar. The cultures were incubated at 30 °C for 2--4 days before further experimentation.

The recombinant *Pichia* strains were screened to establish methanol utilisation (Mut) phenotype according to procedures stipulated in Romanos *et al.* (1998) and Invitrogen™ (2002).

2.2.6.4 PLASMID PURIFICATION FROM *E. COLI*.

Screening Clones.

The process of screening transformants for the correct plasmid was carried out according to the method of Zhou *et al.* (1990). Plasmids purified in this manner were analysed by restriction digestion. The enzyme and buffer combinations and incubation conditions recommended by the manufacturer were used, but an

additional 1 µL of RNase A (10 mg/mL) was added to each reaction to remove residual RNA. After having been digested, the samples were resolved by agarose gel electrophoresis and then analysed. When analysing pGEM-T® based plasmids, the restriction enzyme(s) used were a combination of either *Bst* XI and *Sst* II or *Nco* I and *Pst* I. 1 U of each enzyme was used per 20 µL of reaction solution. When analysing pGEM-T Easy® plasmids, *Eco* RI (1 U per 20 µL reaction) was used.

Purification of high-copy-number Plasmids.

Plasmid DNA was purified from *E. coli* using a QIAquick® Plasmid Miniprep Kit as described in the manufacturer's instructions.

Purification of low-copy-number Plasmids.

Plasmid DNA that was required for plasmid construction, or enzymatic digests, or transformation experiments was prepared using the alkaline lysis "mini-prep" method (Engebrecht *et al.,* 1992). Plasmid DNA required for sequencing reactions was amplified by inoculating 3.5 mL of LB broth [supplemented with ampicillin (100 µg/mL)] for 16 h at 37 °C with shaking. After 16 h, 100 µg/mL spectinomycin was added and the culture was incubated as before for an additional 16 h. At this point, the plasmid DNA was purified from the host bacteria using a QIAquick® Plasmid Miniprep Kit according to manufacturer's instructions. The identity of pKK223-3 based plasmids was established by double digestion with *Sal* I and *Nde* I after they had been amplified by this method.

2.2.6.5 Ligation Protocols.

Ligating T-Tailed Vectors.

Ligation reactions were carried out on the appropriate linearised or T-tailed vector using T4 Ligase and buffers supplied with the pGEM-T® and pGEM-T Easy® kits. In each reaction, the molar concentration of insert was always three times that of the vector and the reactions were incubated overnight at 10 °C for maximum efficiency. Otherwise, the reactions were carried out according to the manufacturer's instructions.

Construction of p9KEASF1.

The EAS isoform I cDNA was cloned into the pPIC9K expression vector between the *Xho* $I_{1193\ bp}$ site and the *Eco* $RI_{1223\ bp}$ to create a plasmid called pP9KEASF1.

The *Xho* $I_{1193\ bp}$ is not unique in pPIC9K (see Figure 10), making it necessary to carry out a 3-way ligation reaction in order to link the cDNA with the two separate fragments of pPIC9K.

FIGURE 10: PPIC9K.

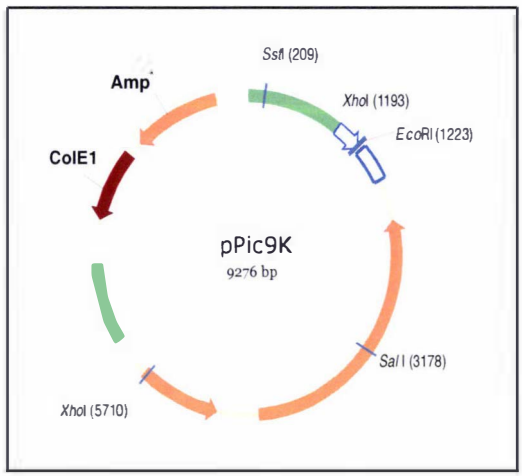

The *eas* cDNA sequence was synthesised by RT-PCR using mRNA extracted from conidiating *N. crassa* StA as the template and oligo-dT as the RT-PCR primer for the 1st strand reaction (sections 2.2.2.2 and 2.2.3.1). The 5'-pPIC9KEASF1 and 3'-pPIC9KEAS PCR primers described in Chapter 4 were to prime the second strand RT-PCR reaction. The final RT-PCR product was ligated into pGEM-T Easy® to simplify amplification (sections 2.1.3 and 2.2.6) and verified by DNA sequencing (section 2.2.7.3).

Concentrated solutions of each plasmid were created by pooling plasmids extracted from three 5 mL bacterial cultures (section 2.2.6) and then passing the resulting solution through DNA-binding columns supplied with the QIAquick® kit. The columns were used according to the manufacturer's recommendations.

The 984 bp (*Sst* $I_{209\ bp}$–*Xho* $I_{1193\ bp}$) and 8,262 bp (*Eco* $RI_{1223\ bp}$–*Sst* $I_{209\ bp}$) arms of pPIC9K and the 261 bp (*Xho* $I_{5\ bp}$–*Eco* $RI_{266\ bp}$) EAS cDNA fragment were excised from their respective plasmids. The plasmid (3 µg) was digested with the appropriate pair of enzymes at 0.1 U/µL. Each fragment was gel purified as described in section 2.2.5.3.

The EAS cDNA fragment and each arm of pPIC9K were ligated together using T4 Ligase and 10X ligation buffer as recommended by the manufacturer (Promega™). The molar ratio of the DNA fragments added to the reaction was 3:1:1 (insert: each arm of pPIC9K). The ligation reaction was incubated overnight at 10 °C to maximise the efficiency of the ligation reaction.

Plasmids extracted from ampicillin resistant *E. coli* recombinants (section 2.2.6), were screened first by *Sal* I digestion (p9KEASF1 is cut twice by *Sal* I) and then by DNA-sequencing with pPIC9K-specific sequencing primers, 5' AOX1 and 3' AOX1, supplied by Invitrogen™ (section 2.2.7.3).

Ligation Reactions Used to Construct pKK223EASF1 and pKK223EASF2.

For reasons outlined in Chapter 4, I cloned the cDNA encoding EAS isoforms I and II into the prokaryotic expression vector pKK223-3 (Figure 11).

FIGURE 11: PKK223-3.

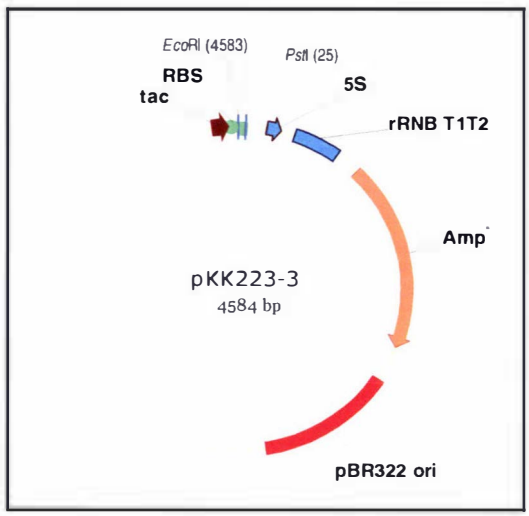

The cDNAs were inserted between the *Eco* RI$_{4583\ bp}$ and *Pst* I$_{25\ bp}$ sites, and two plasmids were created: pPKKEASF1 and pKKEASF2. To created these plasmids, the pKK223-3 plasmid was amplified and purified from *E. coli* (as described in sections 2.1.3 and 2.2.6.4), and then digested with *Eco* RI and *Pst* I.

The digested pKK223-3 plasmid was dephosphorylated with Shrimp Alkaline Phosphatase (Invitrogen™) because this step was found to enhance the efficiency of subsequent ligation reactions. Both digestion and dephosphorylation reactions were carried out according to the enzyme manufacturer's recommendations. The 4,559 bp fragment derived when pKK223-3 was digested was gel-purified and ligated to cDNAs encoding each EAS isoform. These cDNAs had previously been digested with *Eco* RI and *Pst* I and then gel-purified in the same manner as the pKK223-3 fragment. EAS cDNA sequences were amplified and cloned in the same manner described for pPICEASF1, except that different PCR primers – as outlined in Chapter 4 – were used for the second strand RT-PCR reaction. The reaction conditions used to ligate the cDNAs to the pKK223-3 fragment were the same as those used for the T-tailed vector ligation reactions described above.

The fidelity of the pKKEASF1 and pKKEASF2 plasmids constructed in this manner were checked by digesting each with *Pvu* I and *Pvu* II and then comparing the size of the fragments by gel electrophoresis.

2.2.7 NUCLEIC ACID ANALYSIS.

2.2.7.1 SOUTHERN BLOTTING AND HYBRIDISATION.

Genomic DNA was digested with either *Xho* I or *Hin*d III (Invitrogen™) and resolved by TAE/agarose gel electrophoresis. DNA was transferred from agarose gels to Hybond™ N+ Nylon membranes using alkaline capillary transfer (Sambrook and Russell, 2001). For use as a probe, Dr. Agnieszka Mudge (Hort Research) provided a previously prepared copy of the *eas* gene from *N. crassa* StA ligated into the pGEM-T® vector. The *eas* gene was excised from the vector by *Eco*R I (Invitrogen™)

digestion, gel purified using a QIAquick® Gel extraction kit and radioactively labelled with (α-^{32}P) dCTP (Amersham Biosciences®) using the *Redi*prime™ kit as instructed by the manufacturer. Prehybridisation (30 min) and hybridisation (overnight) was carried out in tubes using Church buffer at 65 °C (Church and Gilbert, 1984). The membrane was washed with SSC/SDS buffers of increasing stringency at 65 °C culminating in two or three 10 min washes in either medium stringency (1x SSC, 0.1 %[w/v] SDS) or high stringency (1x SSC, 0.1 %[w/v] SDS) buffers as indicated (Sambrook and Russell, 2001). Autoradiography was carried out using a Storm® 840 Phosphor Imaging™ system.

2.2.7.2 Northern Blotting and Hybridisation.

Total RNA was resolved by gel formaldehyde gel electrophoresis. RNA was capillary transferred from formaldehyde/agarose gels to Hybond™ XL Nylon membranes using 20x SSC as the blotting buffer (Sambrook and Russell, 2001). After blotting, the RNA was bound to the membrane by irradiating it with UV light in a Stratagene® UV Stratalinker 1800. Prehybridisation, hybridisations, preparation, and radio labelling of the probe, washing, and autoradiography methods were identical to those described for Southern blotting.

2.2.7.3 DNA Sequencing and Analysis.

Single-strand sequencing was done with either an ABI Prism® BigDye™ Terminator Cycle Sequencing Kit or a DYEnamic™ ET terminator cycle sequencing pre-mix kit. Unless otherwise stated, M13-forward and -reverse primers at a concentration of 1-2 pmol/µL were used to prime the sequencing reaction. DNA was sequenced using the ABI® 377XL automated DNA Sequencer at the Waikato DNA Sequencing Facility (University of Waikato, Hamilton, New Zealand). Bi-directional sequencing was performed on a Li-Cor® 4000LD IR2 automated sequencer at the Department of Molecular Medicine and Pathology, Auckland University, Auckland, New Zealand.

ITS/5.8S rRNA sequencing discussed in sections 2.1.1 and 2.2.3 was obtained by directly sequencing the PCR-amplified ITS/5.8S rRNA product. The sequencing reactions were carried out as described above by the Waikato DNA Sequencing Facility using the ITS4 and ITS5 primers (White *et al.*, 1990).

2.3 Assessment of Mycelium Hydrophobicity.

The shape of a water droplet on a surface is due in part to the hydrophobicity of that surface (Adamson, 1990). A qualitative assessment of the hydrophobicity of the surface of mycelium from the aconidiate *Neurospora* species was obtained by photographing the shape of water droplets that had been applied to the mycelium.

N. crassa StA cultures were used as a positive control while the hydrophobin deficient *N. crassa eas* strain served as a negative control. *Neurospora* strains were grown in 85 mm plastic Petri-dishes on Vogel's medium N supplemented with 2 %(w/v) sucrose and 2 %(w/v) agar (Vogel, 1964), for 6-8 days at 25 ºC. A 250 µL droplet of water, dyed with 0.00075 %(w/v) Safranin to aid photographic contrast, was applied to the surface of a mycelium agar slice excised from the Petri-dish and photographed from several angles with a Nikon Coolpix 950 digital camera.

2.4 Protein Manipulations.

2.4.1 Hydrophobin Protein Extraction.

Neurospora strains were grown in Pyrex 2 L Beakers and hydrophobins were extracted as described previously (Templeton *et al.*, 1995).

2.4.2 Hydrophobin Purification by RP-HPLC.

All RP-HPLC separations were carried out using a Hewlett Packard® Ti 1050 series instrument equipped with a multi-wavelength detector. Unless otherwise stated the eluent was monitored at 218 nm. Programming of mobile phase gradients was carried out using the Hewlett Packard® ChemStation software (Rev.A.06.03) installed to control and collect data for the Ti 1050 liquid chromatography system. The characteristics of the RP-HPLC columns used in this study are listed in Table 4.

TABLE 4 : RP-HPLC COLUMNS USED IN THIS STUDY

RP-HPLC COLUMNS

Manufacturer	Brand	Dimensions	Particle Size	Pore Size	Solid Phase[1]
Phenomenex®	*Jupiter™*	*250 mm x 10 mm*	*10 µm*	*300 Å*	*Silica: C4*
Phenomenex®	*Jupiter™*	*250 mm x 4.6 mm*	*5 µm*	*300 Å*	*Silica: C4*
Amersham®	*µRPC ST 4.6/100*	*100 mm x 4.6 mm*	*3 µm*	*120 Å*	*Silica: C2/C18*

GUARD COLUMNS

Manufacturer	Brand	Dimensions	Particle Size	Pore Size	Solid Phase[1]
Phenomenex®	*Jupiter™*	*50 mm x 10 mm*	*10 µm*	*300 Å*	*Silica: C4*
Phenomenex®	*Jupiter™*	*20 mm x 0.5 mm*	*5 µm*	*300 Å*	*Silica: C4*

[1]Solid Phase refers to the type of micro-particulate beads used and to the length of alkyl chains bonded to them. C2/C18 indicates that silica beads have been capped with a 2 carbon alkyl capping group (AP-Biotech, 1999).

Preparative purification of hydrophobin extracts from all conidiating *Neurospora* species was carried out as follows: TFA-solvated hydrophobin extracts were resuspended in an aqueous solution containing 30 %(v/v) acetonitrile and 0.1 %(v/v) TFA. This solution was applied to the Jupiter™ 250 mm x 10 mm column protected

with the Jupiter™ 50 mm x 10 mm guard column (see Table 4 for details) and extract was eluted with the gradient profile described by Figure 12.

FIGURE 12: RP-HPLC MOBILE PHASE GRADIENT FOR PURIFYING EAS FROM MACROCONIDIAL EXTRACTS.

CHEMSTATION PROGRAM DETAILS

Time of each Programmed Change.	Solvent components in the mobile phase[1]		
	% A	% C	% D
0 min	*5*	*65*	*30*
30 min	*5*	*30*	*65*
33 min	*5*	*30*	*65*
35 min	*5*	*65*	*30*
40 min	*5*	*65*	*30*
Flow Rate	**Max Pressure Limit**		
2 mL/min	*103 bar*		

GRADIENT PROFILE[2]

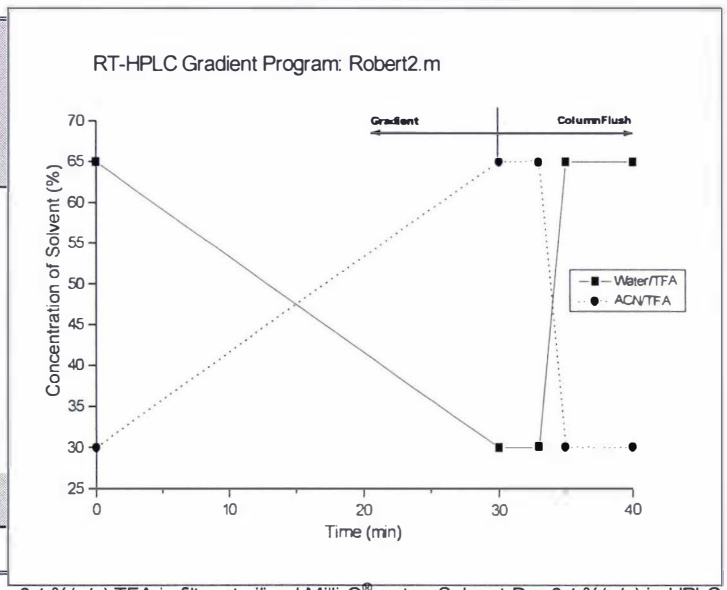

[1] Solvent A = 100% HPLC-grade methanol. Solvent C = 0.1 %(v/v) TFA in filter sterilised Milli-Q® water. Solvent D = 0.1 %(v/v) in HPLC-grade acetonitrile. '%A,' '%C,' and '%D' refer to the concentration of each component as a percentage of the total mobile phase. [2] The gradient profile depicts the RP-HPLC mobile phase gradient resulting from the ChemStation program. This program was used exclusively with the Jupiter™ 250 mm x 10 mm column described in Table 4.

FIGURE 13: RP-HPLC MOBILE PHASE GRADIENT FOR FRACTIONATING *NEUROSPORA* MYCELIUM EXTRACTS.

CHEMSTATION PROGRAM DETAILS

Time of each Programmed Change.	Solvent components in the mobile phase[1]		
	% A	% C	% D
0 min	*5*	*95*	*0*
5 min	*5*	*95*	*0*
45 min	*5*	*30*	*65*
50 min	*5*	*0*	*95*
55 min	*5*	*95*	*0*
Flow Rate	**Max Pressure Limit**		
0.5 mL/min	*120 bar*		

GRADIENT PROFILE[2]

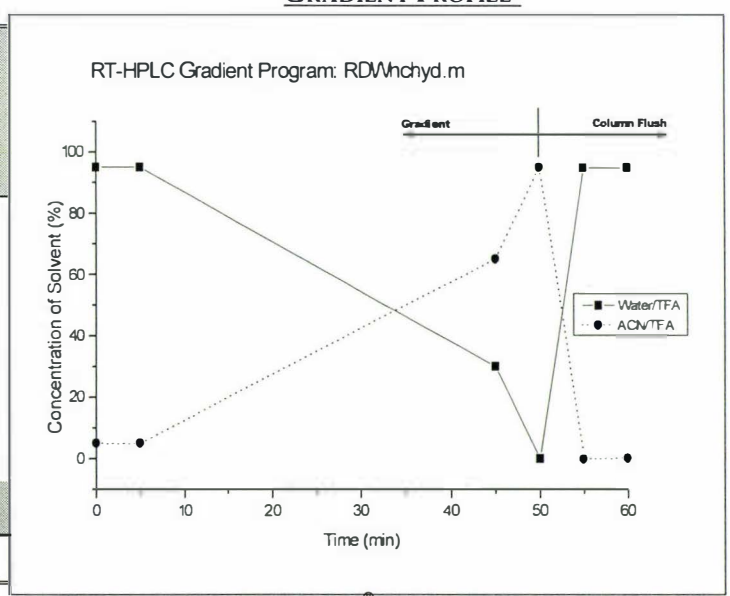

[1] Solvent A = 100% HPLC-grade methanol. Solvent C = 0.1 %(v/v) TFA in filter sterilised Milli-Q® water. Solvent D = 0.1 %(v/v) in HPLC-grade acetonitrile. '%A,' '%C,' and '%D' refer to the concentration of each component as a percentage of the total mobile phase. [2] The gradient profile depicts the RP-HPLC mobile phase gradient resulting from the ChemStation program. This program was used exclusively with the Jupiter™ 250 mm x 4.6 mm column described in Table 4.

Fractionation of the mycelium extracts from aconidiate *Neurospora* species was carried out by as follows: TFA-solvated hydrophobin extracts were re-suspended in an aqueous solution consisting of 5 %(v/v) acetonitrile and 0.1 %(v/v) TFA. This solution was applied to the Jupiter™ 250 mm x 4.6 mm column protected with the Jupiter™ 20 mm x 0.5 mm guard column (see Table 4 for details) and the extract was eluted with the gradient profile described by Figure 13.

2.4.3 Screening Recombinant *P. pastoris* Strains.

Samples of concentrated growth media were obtained from 150 mL *P. pastoris* cultures that had been induced for 5 days (section 2.1.2.4); these samples were prepared as follows. The cultures were sonicated and the yeast cells removed by low speed centrifugation as described by Templeton *et al.* (1995). Insoluble components of the supernatant were isolated by centrifuging at 100,000 *g* for 1 h and then dissolved in 100 %(v/v) TFA at 0 ºC for 15 min. Insoluble material was removed by microcentrifugation and the TFA was removed under a stream of N_2. The remaining residue was either re-suspended in the NuPAGE® LDS sample buffer prior to analysis by SDS-PAGE (Invitrogen™, 2000) or it was re-suspended in an aqueous solution consisting of 5 %(v/v) acetonitrile and 0.1 %(v/v) TFA. The latter solution was applied to the Jupiter™ 250 mm x 4.6 mm column protected with the Jupiter™ 20 mm x 0.5 mm guard column (see Table 4 for details) and the extract was eluted with the gradient profile described by Figure 13. As a positive control for this experiment rodlet extracts from the macroconidia of *N. crassa* StA were purified in the same manner.

2.4.3.1 Screening Proteins Secreted by *P. pastoris* Recombinants.

Frozen growth media supernatant samples were thawed prior to use and mixed with the NuPAGE® SDS sample buffer (section 2.4.5) and then analysed with a combination of SDS-PAGE and silver staining (section 2.4.6) as recommended in Invitrogen™ (2002).

As required, growth media supernatant collected upon the completion of a five-day long methanol-induced batch culture cycle was concentrated 100-fold by lyophilisation. Samples thus treated were prepared for SDS-PAGE analysis as described in section 2.4.6 (but the de-salted step was omitted) and then analysed with a combination of SDS-PAGE and silver staining.

2.4.3.2 SDS-PAGE Analysis of the Internal Proteins Produced by *P. pastoris* Recombinant Strains.

Frozen, pelleted yeast cells obtained from induced batch-cultures were thawed prior to use. The yeast cells were disrupted using the Breaking Buffer/Acid-washed glass-bead method described in Invitrogen™ (2002). The glass beads were prepared as described in section 2.2.2.3.

The protein concentration of each lysate was equalised by diluting with 8 M $urea_{(aq)}$ as described by Appelbaum and Shatzman (1999). The samples were then analysed with a combination of SDS-PAGE and silver-staining as described in section 2.4.6.

2.4.4 Screening Recombinant *E. coli* Strains.

A solution of 1x NuPAGE® SDS sample buffer (section 2.4.5) supplemented with 8 M $urea_{(aq)}$, 1 M Tris HCl (at pH 6.8) and 0.01 M DTT was freshly prepared and *E. coli* cell lysates were prepared for analysis by SDS-PAGE using this solution and the protocol described by Appelbaum and Shatzman (1999).

2.4.5 N-Terminal Sequencing and Hydrophobin ESI-MS measurements.

Lyophilised hydrophobin samples were N-Terminal amino acid sequenced at the School of Biological Sciences, Auckland University, Auckland, New Zealand. Electrospray Ionisation Mass Spectrometry (ESI/MS) measurements were carried out on unmodified, lyophilised hydrophobin samples dissolved in a mixture of acetonitrile and H_2O (1:1) with 0.5 %(v/v) formic acid and analysed by MasSpec Services, Massey University, Palmerston North, New Zealand.

2.4.6 SDS-PAGE.

Proteins were electrophoretically resolved under reducing and denaturing conditions using XCell *SecureLock*™ PAGE apparatus and pre-cast NuPAGE® 4 %(w/v)-12 %(w/v) Bis-Tris gradient SDS-PAGE gels. NuPAGE® electrophoresis protocols recommended for the use of MES-SDS running buffer were followed (Invitrogen™ Corporation, 2000) and a maximum of 30 µL of each sample mixture was loaded per lane. All electrophoresis solutions were according to NuPAGE® recommendations (Invitrogen™ Corporation, 2000). The only alteration made was to substitute SDS for LDS in the NuPAGE® LDS sample-buffer. LDS is used to facilitate the pipetting of this dense solution, thus the substitution of SDS for LDS does not affect electrophoresis performance (Invitrogen™ Corporation, 2000).

Electrophoretically resolved proteins were detected with a combination of the Coommassie® blue staining and the silver-staining techniques. Typically, the resolved proteins would be detected by initially staining with Coommassie® blue and recording the stained gel as a digital image. If a more sensitive detection technique was required, then Coommassie® blue dye was removed by de-staining and the silver staining technique applied. The result of silver-staining was recorded as a digital image and the gel dried for permanent storage.

As a protective measure during photography, the gels were supported between two sheets of wet, A4 sized, OHP transparencies. The stained, water-rinsed, SDS-PAGE gels were digitally photographed through the transparencies with a ScanMaker™ Model 8700 scanner controlled by Photoshop® software. For permanent storage, the gels were dried between sheets of cellophane with a Bio-Rad® Gel-drier (Model 443) as recommended by the manufacturer.

2.4.6.1 Coommassie® Staining.

A rapid Coommassie® staining protocol described by Sasse and Gallagher (2000) was used with two modifications: (1) 40 %(v/v) methanol replaced the isopropanol in the fixing solution. (2) 0.025 %(w/v) Coommassie® brilliant blue R-250 replaced Coommassie® Brilliant blue G-250 in the Rapid Coommassie® staining solution.

2.4.6.2 Silver Staining.

A silver-staining protocol described by Sasse and Gallagher (2000) was used with the following modifications: (1) the formaldehyde-fixing-solution consisted of 50 %(v/v) aqueous methanol, 12 %(v/v) aqueous glacial acetic acid and 0.05 %(v/v) formaldehyde in Milli-Q® water. (2) The 0.1 %(w/v) $AgNO_3$ solution was supplemented with 0.00075 %(v/v) formaldehyde. (3) Development was not halted by adding citric acid to the thiosulfate developer solution; instead the gel was immersed in a "stop" solution [50 %(v/v) methanol, 12% (v/v) glacial acetic acid in Milli-Q® water] for 10 min while being gently agitated. Finally, the residual glacial acetic acid was removed from the gel by immersing it in a in a solution of 30 %(v/v) aqueous methanol for two hours. The methanol solution was changed once during that time.

2.4.7 Disulfide Mapping Protocol.

2.4.7.1 Disulfide Mapping of EAS isoforms.

Predicting the Structure and m/z Ratios of Ionized Fragments.

The disulfide mapping protocol requires that peptides be created from cyanylated protein species by digesting them ammonia and TCEP (Wu and Watson, 1997). It is

necessary to predict both the structure and mass of each peptide that might be created. I used MDL® ISIS Draw (version 2.5) software to draw the structure of each peptide using the amino acid sequence of EAS as a guide (Mackay *et al.,* 2001). The software was then used to calculate the molecular mass of each peptide (equivalent to the m/z value for the molecular ion).

Partial Reduction and Cyanylation of EAS.

The partial reduction and cyanylation reaction was optimised empirically as described in section 5.2.1 (see page 138) and the reaction conditions that gave the best yields of singly-reduced and cyanylated EAS isomers are reported in Table 15 (see page 140). However, the same general procedure (described below) was followed when I performed each partial-reduction and cyanylation reaction; the only parameters I altered were the reaction temperature and the concentration of the reagents.

In order to partially reduce and then cyanylate EAS, between 0.5 - 1 mg (0.07 µmol-0.13 µmol) of a RP-HPLC purified EAS isoform in 50 - 100 µL of a weakly acidic, denaturing-buffer consisting of 6 M guanidine hydrochloride dissolved in 0.1 M citrate buffer, pH 3.0. The citrate buffer solution was made by mixing 82 mL of an aqueous solution 0.1 M citric acid with 18.0 mL of an aqueous solution of 0.1 M trisodium citrate, fine pH adjustments were made with 1 M solutions of either component.

The partial reduction reaction was performed by adding between 0.5 – 5 µL (depending on the experiment) of an 1 M aqueous solution of tris(2-carboxyethyl) phosphine (TCEP, obtained from Pierce®) to the EAS solution and allowing it to react for 15 min at the desired temperature (at either 11 ºC or 25 ºC). Immediately afterward, between 20 µL and 40 µL of a cyanylation solution (1 M 1-cyano-4-dimethylamino-pyridinium tetrafluoroborate (CDAP) dissolved in 0.1 M citrate buffer) was added to the partly reduced EAS solution in order to cyanylate the protein's nascent sulfhydryls. After CDAP was added, the reaction solution was incubated at 25 ºC for 30 min before the reduced and cyanylated EAS species were resolved by RP-HPLC.

Solutions of TCEP and CDAP were freshly prepared just prior to use, and vials containing these chemicals were kept tightly sealed and in the presence of a desiccant at –20 ºC until required. These precautions were necessary because although TCEP is more stable than DTT (Han and Han, 1994; Getz *et al.,* 1999), it is known that TCEP oxidises rapidly in the presence of certain buffering and chelating agents (Getz *et al.,* 1999; Pierce®, 2003). When required, the extent of oxidation in

commercial preparations of TCEP was monitored by spectroscopically measuring its ability to reduce 0.2 mmols of 5,5'-dithiobis(2-nitrobenzoic acid) (DTNB or Ellman's reagent) in a procedure described by Han and Han (1994). During these experiments, equivalent amounts of DTT were used as a control.

RP-HPLC Purification of Cyanylated EAS Isomers.

The RP-HPLC protocol used to fractionate the partially reduced and cyanylated EAS isomers was optimised empirically as described in section 5.2.1.3 (see page 140).

(1) During the initial purification experiments, the reaction solution was de-salted by first diluting with Milli-Q® water as required, applying the solution to an Amersham® pre-packed disposable PD-10 de-salting column (a gravity flow column packed with Sephadex™ G-25 Medium), and then eluting the protein from the column with Milli-Q® water as instructed by the manufacturer. The eluate was freeze-dried and then dissolved in 30 %(v/v) acetonitrile and 0.1 %(v/v) TFA before being applied to the Jupiter™ 250 mm x 10 mm column protected with the Jupiter™ 50 mm x 10 mm guard column (see Table 4 for details). The reduced and cyanylated protein species were eluted using the gradient profile described by Figure 14, except that the flow rate and upper pressure limit was adjusted to 0.5 mL/min and 120 bar respectively.

(2) The parameters of the purification protocol that I used to resolve the singly-reduced and cyanylated EAS isomers that revealed the pattern of disulfide-bonds in EAS were as follows. Reaction solutions prepared according to the "Final optimised protocol" described in Table 15 (page 140), were applied directly to a Amersham® µRPC C2/C18 ST 4.6/100 RP-HPLC column protected with the Jupiter™ 50 mm x 10 mm guard column (see Table 4 for details), and resolved using the RP-HPLC gradient profile described by Figure 15. Each protein fraction was collected manually as it eluted from the column.

Ammonia Catalysed Peptide Cleavage.

The ammonia-catalysed S-cyanylated peptide-cleavage phase of the disulfide mapping protocol methodology was carried out by adding 8 µL of either an ammonium hydroxide (1 M NH_4OH, pH 12) or denaturing ammonium hydroxide solution (6 M guanidine hydrochloride dissolved in 1 M NH_4OH, pH 12) and allowed to react with EAS at 25 °C for 1 hr (Wu and Watson, 1997). In order to achieve complete peptide cleavage in 1 hr, both ammonium hydroxide solutions must be at pH 12: if this wasn't the case then the pH was adjusted with additional NH_4OH (Wu and Watson, 1997).

FIGURE 14: RP-HPLC MOBILE PHASE GRADIENT: USED TO FRACTIONATE REDUCED AND CYANYLATED EAS ISOMERS WITH THE JUPITER 250 mm x 4.6 mm COLUMN.

CHEMSTATION PROGRAM DETAILS

Time of each Programmed Change.	Solvent components in the mobile phase[1]		
	% A	% C	% D
0 min	*0*	*95*	*5*
5 min	*0*	*95*	*5*
45 min	*0*	*30*	*40*
50 min	*0*	*0*	*100*
55 min	*0*	*95*	*5*
Flow Rate	**Max Pressure Limit**		
0.5 mL/min	*300 bar*		

GRADIENT PROFILE[2]

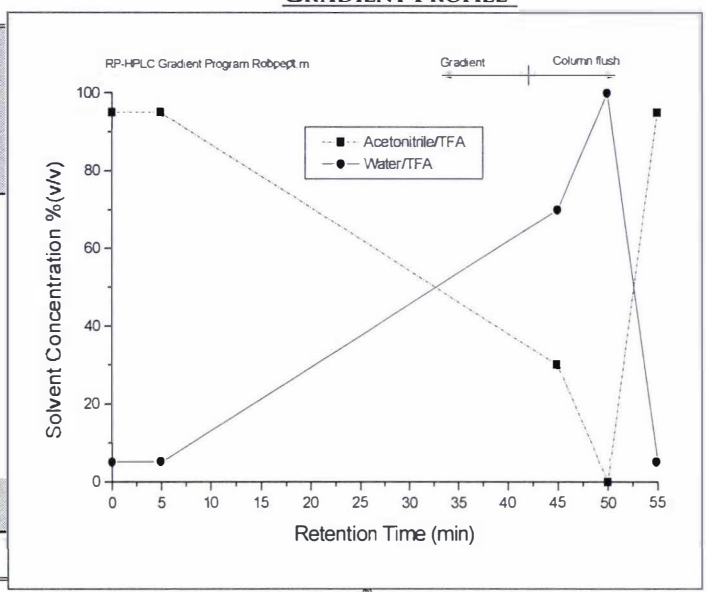

[1] Solvent A = 100% HPLC-grade methanol. Solvent C = 0.1 %(v/v) TFA in filter sterilised Milli-Q® water. Solvent D = 0.1 %(v/v) in HPLC-grade acetonitrile. '%A,' '%C,' and '%D' refer to the concentration of each component as a percentage of the total mobile phase. [2] The gradient profile depicts the RP-HPLC mobile phase gradient resulting from the ChemStation program. This program was used exclusively with the Jupiter™ 250 mm x 10 mm column.This program was used exclusively with the Jupiter™ 250 mm x 4.6 mm column.

FIGURE 15: RP-HPLC MOBILE PHASE GRADIENT USED TO FRACTIONATE REDUCED AND CYANYLATED EAS ISOMERS WITH THE µRPC ST 4.6/100 COLUMN.

CHEMSTATION PROGRAM DETAILS

Time of each Programmed Change.	Solvent components in the mobile phase[1]		
	% A	% C	% D
0 min	*5*	*75*	*20*
5 min	*5*	*75*	*20*
70 min	*5*	*0*	*95*
75 min	*5*	*75*	*20*
70 min	*5*	*75*	*20*
Flow Rate	**Max Pressure Limit**		
0.5mL/min	*300 bar*		

GRADIENT PROFILE[2]

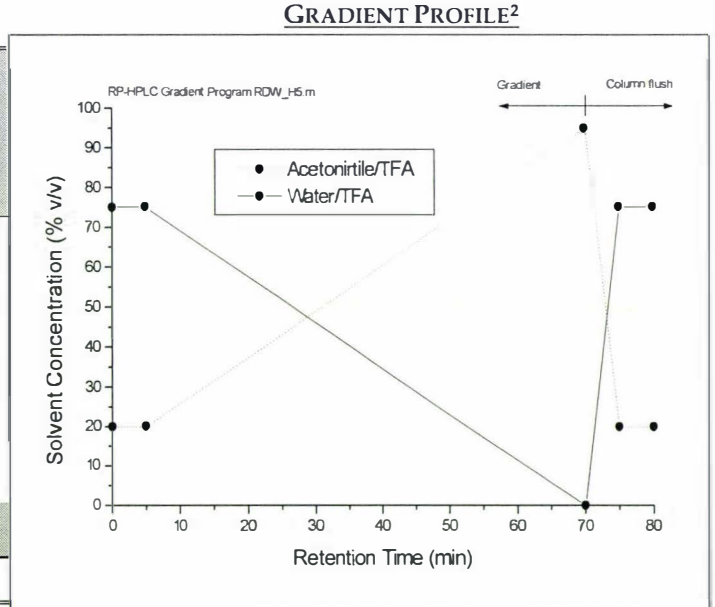

[1] Solvent A = 100% HPLC-grade methanol. Solvent C = 0.1 %(v/v) TFA in filter sterilised Milli-Q® water. Solvent D = 0.1 %(v/v) in HPLC-grade acetonitrile. '%A,' '%C,' and '%D' refer to the concentration of each component as a percentage of the total mobile phase. [2] The gradient profile depicts the RP-HPLC mobile phase gradient resulting from the ChemStation program. This program was used exclusively with the µRPC ST 4.6/100 column described in Table 4.

The ammonia was removed under vacuum and either 2 µL of 0.1 M aqueous TCEP (when the denaturing ammonium hydroxide solution was used) or 2 µL of 0.1 M DTT in 0.1 M Tris HCl buffer (pH 8.0) was mixed with the EAS reaction solution and allowed to reacted at 37 °C for 30 min. Adding these reducing agents had the effect

of removing the residual disulfide bonds that linked the peptides generated during the preceding reactions.

Mass Spectrometry.

The combination of peptide-cleavage and full-reduction reactions produces a mixture of peptide fragments whose composition is dependent on the positions of the cyanylated cysteines in the partly reduced parent-protein. Two mass spectrometry methods, ESI/MS, and Matrix-Assisted Laser Desorption/Ionisation time-of-flight mass spectrometry (MALDI-TOF/MS) were used to analyse these peptide mixtures.

ESI/MS analysis was carried out by Dwayne Jenson (Biological Chemistry, Hort Research) using a Finnigan LCQ™ Deca ion-trap mass spectrometer with a Surveyor® liquid chromatography (LC) system, controlled using the Xcalibur® (version 1.3) software that was also used for signal analysis and de-convolution. Samples analysed by ESI/MS were first diluted in 1:1 mixture of acetonitrile and water with 0.1 %(v/v) acetic acid (added as an ion pairing agent) and applied to a Jupiter™ 5 µm C4 HPLC column (the same model described in Table 4) that had been attached to the Surveyor® LC System. The peptides were then resolved by RP-HPLC. The Finnigan LCQ™ Deca ESI/MS, mounted inline with the LC system, was able to analyse the sample components as they eluted from the column.

MALDI-TOF/MS analysis was performed with a Micromass Systems M@ldi™ LR mass spectrometer equipped with a 337 nm nitrogen UV Laser and was controlled using MassLynx™ software (version 3.5 for Microsoft Windows® NT). This device was based at the Institute of Fundamental Sciences, Massey University, Palmerston North, New Zealand. M@ldi™ LR mass spectrometers are equipped with both linear-mode and reflectron-mode detectors and the time-to-mass conversion in each mode was established by analysing a mixture of protein and peptide standards as described in Table 5.

MALDI-TOF/MS data were acquired in either the positive reflectron or positive linear of operation with the accelerating voltage in the ion source set to 15 KV. Once acquired the data was processed with the background subtraction (parameters: polynumeral = 15, % below curve = 10) algorithms included with MassLynx™.

MALDI-TOF/MS samples were prepared with α-cyano-4-hydroxycinnamic acid (HCCA, obtained from Sigma-Aldrich) as the matrix. Saturated matrix solutions (~10 mg/mL HCCA) were prepared as a 1:1 solution of acetonitrile and Milli-Q® water with 0.1 %(v/v) TFA; this solution was mixed with equal volumes of the sample

solution before an aliquot was applied to the MALDI-TOF/MS sample plate and allowed to air-dry before being introduced into the mass spectrometer.

Where indicated in Chapter 5, protein and peptide samples were de-salted by one of two methods: (1) prior to mixing with the saturated matrix solution, the sample was de-salted by passage through Millipore® Ziptip® µ-C18 pipette tips used according to the manufacturer's instructions. (2) The crystalline sample spots were prepared on the MALDI-TOF/MS sample plate using the fast evaporation method of Vorm *et al* (1994). The water-soluble contaminants within the crystals were removed by treating the spots with cold Milli-Q® water as described by Beavis and Chait (1990).

TABLE 5: STANDARDS USED TO CALIBRATE THE M@LDI LR MASS SPECTROMETER.

Protein/Peptide standard	Monoisotopic Molecular mass (used for Reflectron mode calibration)	Average Molecular mass (used for Linear mode calibration)
Adrenocorticotropic hormone fragment (residues 18-39)	2,465.199 Da	2,466.7 Da
Angiotensinogen (Renin substrate)	1,758.934 Da	1,760.0 Da
Angiotensin II	1,046.542 Da	1047.2 Da
Bovine pancreatic insulin	5730.61 Da	5,734.6 Da
Cytochrome C	Not used	12,385 Da

2.4.7.2 ANALYSING RNASE A.

One milligram of Bovine pancreatic ribonuclease Type III-A (Sigma-Aldrich®) was dissolved in 50 µL in guanidine-citrate buffer (section 2.4.7.1) before 0.5 µL of 1 M TCEP was added. TCEP was allowed to partially reduce the cysteines in RNase A for 15 min at 25 °C before the immediate addition of 40 µL of a 0.5 M CDAP dissolved in 0.1 M citrate buffer. The reaction solution was incubated with CDAP for a further 30 min at 25 °C before the reduced and cyanylated RNase A species were resolved by RP-HPLC.

Reaction solutions containing reduced and cyanylated isomers of RNase A were applied directly to a Amersham® µRPC C2/C18 ST 4.6/100 RP-HPLC column protected with the Jupiter™ 50 mm x 10 mm guard column (see Table 4 for details), and resolved using the RP-HPLC gradient profile described by Figure 16. Each protein fraction was collected manually as it eluted from the column.

The ammonia-catalysed S-cyanylated peptide cleavage reaction was carried out by adding 8 µL of ammonium hydroxide (prepared as described in section 2.4.7.1) and allowing it to react at 25 °C for one hour. The removal of ammonia, the final reduction of disulfide bonds, and the subsequent analysis of the peptide mixture by LC-ESI/MS and MALDI-TOF/MS was performed as described in section 2.4.7.1.

FIGURE 16: RP-HPLC MOBILE PHASE GRADIENT FOR FRACTIONATING REDUCED AND CYANYLATED RNASE A ISOMERS WITH THE µRPC ST 4.6/100 COLUMN.

CHEMSTATION PROGRAM DETAILS

Time of each Programmed Change.	Solvent components in the mobile phase[1]		
	% A	% C	% D
0 min	*5*	*75*	*20*
5 min	*5*	*75*	*20*
60 min	*5*	*65*	*30*
65 min	*5*	*0*	*95*
70 min	*5*	*75*	*20*
Flow Rate	**Max Pressure Limit**		
1.0 mL/min	*300 bar*		

GRADIENT PROFILE[2]

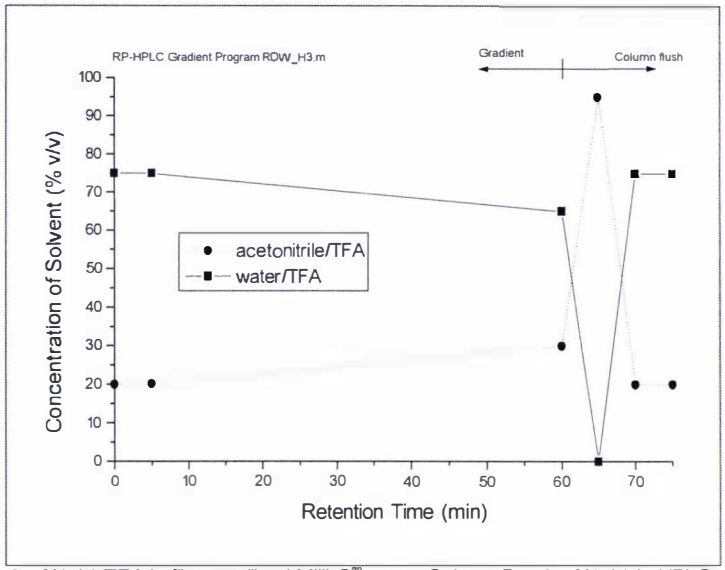

[1] Solvent A = 100% HPLC-grade methanol. Solvent C = 0.1 %(v/v) TFA in filter sterilised Milli-Q® water. Solvent D = 0.1 %(v/v) in HPLC-grade acetonitrile. '%A,' '%C,' and '%D' refer to the concentration of each component as a percentage of the total mobile phase. [2] The gradient profile depicts the RP-HPLC mobile phase gradient resulting from the ChemStation program. This program was used exclusively with the µRPC ST 4.6/100 column described in Table 4.

2.5 AFM TECHNIQUES.

2.5.1 INSTRUMENTATION.

Atomic force microscopy (AF-microscopy) experiments were conducted using one of three different atomic force microscopes (AFMs). Every image captured in Tapping™ mode was obtained with a Veeco® NanoScope® IIIa multimode scanning probe microscope equipped with an AS-130 "J" scanner (125 µm^2 lateral range, 5.0 µm vertical range). This device was controlled using the NanoScope® software (Version 4.23r3), and it was located in the Department of Chemical and Materials Engineering, The University of Auckland, Auckland, New Zealand. Some of the contact mode images were obtained with a Veeco® NanoScope® IIIe multimode scanning probe microscope (model LFM 2.0) equipped with an AS12 "E" scanner (10 µm^2 lateral range, 2.5 µm vertical range). This device was controlled using the NanoScope® E software (Version 5.12b49). All AC mode images and all force measurements were obtained using an Asylum Research Molecular Force Probe 3D Inverted Optical (MFP-3D-IO) atomic force microscope equipped with a Nikon® Eclipse TE2000-U inverted optical microscope and a Nano-K® BM-1 "Biscuit" bench-top vibration isolation platform (minus-k® technology). The MFP3D-IO was controlled with Wavemetrics Igor Pro software (version 4.08) running sub-routines custom designed by Asylum Research (version MFP-3D XOP build 20 up 1). Both the

NanoScope® IIIe and MFP3D-IO were located in the MacDiarmid Institute for Advanced Materials and Nanotechnology at Massey University, Palmerston North.

2.5.1.1 AFM PROBES.

An AFM probe consists of a silicon block known as a "chip" on which one or more flexible "cantilevers" are made from silicon nitride (Si_3N_4) are mounted. A single sharp "tip" (also called a stylus) is mounted on each cantilever. The probes used during this investigation are described in Table 6. Note that the Olympus Bio-lever was used exclusively during contact mode imaging and force measurements under fluid.

TABLE 6: THE CHARACTERISTICS OF AFM PROBES USED.

Probe Manufacturer	Model	AFM Imaging Mode	Nominal Cantilever Spring Constant.[1]	Tip Radius
Olympus®	AC240TS	AC	2 Nm^{-1}	10 nm
NT-MDT®	NSG11	AC	5.5 Nm^{-1}	10 nm
Olympus®	Bio-lever	Contact	0.006 Nm^{-1}	30 nm
Veeco®	NP20	Contact	0.58 Nm^{-1}	20 nm
Veeco®	TESP	Tapping	50–100 Nm^{-1}	5-10 nm

[1] The "Nominal Spring Constants" data was given by the manufacturer as a guide to the stiffness of the each cantilever. The methods the manufacturers use to establish this data are notoriously inaccurate – differing as much as 50% from the advertised figure.

2.5.2 SUBSTRATE PREPARATION.

Muscovite mica (Grade V-4 from SPI® supplies) was used exclusively as the hydrophilic sample support (substrate) during AFM experiments. Highly ordered pyrolytic graphite (HOPG) with a 0.8°± 0.2 mosaic spread (Grade SPI-2 or ZYB from SPI® supplies) was use as a hydrophobic substrate. A fresh flat surface was obtained from substrates by "cleaving" the surface of the material prior to applying any hydrophobin.

Mica and HOPG were "cleaved" by pressing a piece of double sided Sellotape®-brand adhesive tape onto the substrate surface and then pulling it off. The tape removes a thin layer of the substrate and if this is repeated this several times, a chemically-pristine and flat mica or HOPG surface was generated. Substrates were then glued (using Selleys® Araldite Super Strength two-part epoxy resin according to the manufacturer's instructions) to either a magnetic stainless steel puck (when using a NanoScope® device) or a standard light microscope slide (when using the MFP3D-IO device) prior to the substrate being exposed to any hydrophobin solution.

2.5.3 Sample Preparation.

In this study the concentration of aqueous EAS solutions used to preparing AFM specimens is approximately 1000-fold greater than those reported in a pilot study performed by Sertsou (1997). Sertsou's AFM specimens were prepared using aqueous EAS stock solutions whose concentrations were established colourimetrically using the BCA assay (Pierce®) and bovine serum albumin (BSA) as a reference (Sertsou, 1997). A different method was used in this study, the EAS stock solution was prepared by dissolving a weighed amount of lyophilised EAS in water as described below. Prior to conducting the experiments described in Chapter 6, I determined that a 20 µL droplet of a 5 µg/mL to 50 µg/mL (concentration established by weight) aqueous solution of EAS will produce rodlets on a substrate as hydrophilic as mica that allows the droplet to spread (data not shown).

To prepare specimens of EAS for AFM analysis, between 0.5 mL and 1.5 mL of a 1 mg/mL aqueous solution of EAS was prepared by dissolving fresh, lyophilised EAS isoform II in Milli-Q® water. This large quantity of sample is required because lyophilised EAS is a light, fluffy white powder that was difficult to weigh accurately unless quantities of more than 0.5 mg are measured. The 1 mg/mL stock solution was serially diluted in Milli-Q® water as required for the experiments described in Chapter 6 and 20 µL of the appropriate dilution was applied directly to the freshly prepared substrate. The liquid was then left undisturbed to evaporate before anything further was done to the specimen.

In some experiments, EAS was allowed to adsorb onto the surface of a freshly prepared HOPG substrate that had been submerged in a dilute aqueous EAS solution for a particular amount of time. Between 10 mL and 20 mL of an aqueous EAS solution was prepared for these experiments using the serial dilution method described above. The HOPG was then submerged within this solution; the substrate and liquid was contained within a sterile polystyrene screw-capped universal container (Biolab®) that was laid on its side and left undisturbed for the required amount of time.

In some experiments EAS films - freshly deposited on HOPG - were treated by immersing the substrate into a 2 %(w/v) aqueous SDS solution (with silica anti-bumping granules added) for 10 min at 100 °C in order to remove any protein that had not adsorbed to the graphite. The specimens were held stationary in the SDS-solution by fastening the microscope slide (to which the substrate was glued) to a

retort stand. I found that the Selleys® Araldite Super Strength epoxy resin used to glue the substrate to the slide would resist the boiling detergent treatment only if it has been cured for at least 48 h.

After the detergent treatment the SDS was rinsed off the specimen using with about 10 mL of filtered Milli-Q® water delivered from a clean 60 mL syringe equipped with a 0.22 µm Millipore® GSWP type syringe filter and a 25 gauge needle.

2.5.4 AFM Operating Procedures.

When used to image samples in air, each AFM was operated according to the manufacturer's instructions. Images obtained in fluids using the NanoScope® instruments were obtained without the rubber O-ring installed into the NanoScope® Fluid-cell (probe holder) as described in Kindt *et al.* (2002); this same procedure – with allowance for design differences between the devices – was used to image specimens submerged in aqueous fluid using the MFP3D-IO device. Prior to microscopy, the imaging fluid was de-gassed by drawing it into a 5 mL syringe fitted with a narrow bore (22 or 25 gauge) needle; the syringe plunger was held fully extended during this process in order to create a vacuum within the syringe.

In order to perform AFM under fluid the entire cantilever must be fully immersed in liquid; this requires that the probe be pre-wetted with the imaging solution prior to setting up the experiment.

When preparing Olympus® Bio-levers for AFM in fluid some care must be taken because the cantilevers on the Olympus® Bio-lever probes have an exceptionally low spring-constant they are not very rigid. The surface tension of aqueous solutions is such that the Bio-lever cantilevers will not penetrate droplets applied to them. Instead, if they don't break first they bend through 90° and then remain on the surface of the droplet at the interface with any air bubble present or the chip itself. In order to prevent this, the probe holder was wetted with the imaging solution prior to inserting the Bio-lever. After the Bio-lever chip had been inserted into the holder, a droplet of fluid from an 18 gauge syringe needle was placed on the middle of the chip between the retaining spring and the edge bearing the cantilever. Then, using the needle to manipulate the droplet, the droplet was rolled towards and over the front edge of the chip, thereby immersing the cantilevers in fluid. After the probe holder (or scanning head depending on the instrument) was put in place, the probe was allowed to equilibrate in the fluid for at least 30 minutes so as to avoid the effects of mechanical and thermal drift during imaging.

2.5.5 Sectional Analysis.

The dimensions of surface features on specimens imaged with the AFM were obtained using the sectional analysis features of the software package used to control each AFM. During the analysis a thin section of the sample image was manually selected to obtain a height profile of surface features in that region. The dimensions of any surface features were measured from this profile.

Height and width measurements were obtained only from linear sections that intersected the rodlets perpendicular to their longest axis. Width measurements were made at half the height of the surface feature to minimize the effect of probe-broadening on the data; while height measurements were taken at the apex of the feature. The actual height and width of objects detected during AFM experiments were estimated by calculating the mean ($\bar{x}$) height or width while the standard error of each mean ($SE\bar{x}$) was reported to show how the dimensions of those features varied. These statistics were calculated according to Wild and Seber (1993) from samples of more than 15 individual measurements.

2.5.6 Capturing Force Curves.

Force curves – graphs describing the interaction between the probe and the sample as they are brought close to one another then separated – were collected exclusively with the MFP3D-IO device using the software settings described in Table 7.

Table 7: Software Settings Used To Captureg Force Curves.

Software Parameter	Setting
Pull type	*Forward*
Start Distance	*~2 µm*
Force distance	*4 µm*
Scan rate	*1 - 4 Hz*
Trigger Channel	*Deflection*
Trigger Point	*0 nm*
Slope	*Positive*

Table 7 lists the Igor Pro/MFP-3D XOP command software settings used to collect force curves with the MFP-3D-IO. A "forward pull" ensures the probe travels towards the sample before moving away. Start distance refers to the approximate starting separation of tip and sample, Force distance is the approximate distance the piezo-scanner will travel during the force curve, but in this case it was modified by using either an absolute or relative trigger to ensure that the probe did not penetrate the sample. The Trigger and slope settings ensured that the computer monitored the positive deflection of the cantilever and began to retract the piezo when the cantilever deflection exceeded 0 nm.

The procedure for collecting force curves was as follows: (1) the spring constant of the cantilever was determined by fitting the thermal spectrum of the cantilever

motion to a simple harmonic oscillator model (Hutter and Bechhoefer, 1993; Walters *et al.,* 1996). (2) The acquisition and analysis of the cantilever's thermal spectrum were carried out using the Igor Pro/MFP3D-IO XOP command software. The AFM probe was brought into contact with the sample and the feed-back loop was switched off. A single force curve was obtained to determine the "Deflection Inverse Optical Lever Sensitivity." After obtaining an image between 20 and 30 force curves were then acquired using a deflection trigger to prevent the tip from damaging the sample.

The minimum set-point voltage (effectively the minimum force) required to obtain an image in contact mode without damaging the sample was obtained by calculating deflection voltage applied just prior to the tip encountering the extension part of a force curve. The set-point value used was within 0.5 V of this estimated value, and was adjusted during imaging to counteract the effect of thermal drift on the system.

2.5.6.1 Screening Buffers for High Resolution AF-Microscopy.

The aqueous buffers listed below were screened for their ability to compensate for the electrostatic repulsion between the hydrophobic surface of EAS rodlets and a Veeco® NP20 silicon nitrite probe. Those buffers were: (1) Milli-Q® water, (2) 20 mM KCl, 10 mM MOPS (pH 7.0); (3) 50 mM KCl, 10 mM MOPS (pH 7.0); (4) 150 mM KCl, 10 mM MOPS (pH 7.0); (5) 20 mM KCl, 10 mM MOPS (pH 7.0). After each buffer was sterilized by filtration (see section 2.0.3.1) it was dispensed into new, glass bottles that had been sterilized by autoclaving.

Prior to the experiment the probes were treated with Piranha solution to remove any organic contaminants. The Veeco® NP20 silicon nitrite probes were immersed in weak Piranha solution (1-part 98 %(v/v) H_2SO_4, 1-part 30 %(v/v) H_2O_2, 1-part Milli-Q® water) for 20 minutes at 90 °C. The probes were then dipped into fresh Milli-Q® water to remove any residual Piranha solution before being stored in a GelPak® carrier tray (for not longer than 12 h) until use.

The experiment was carried out using an EAS prepared from a 20 µL of a 5 µg/mL EAS solution that had been applied to mica and allowed to dry (section 2.5.3). The probes were prepared for fluid mode imaging as described in section 2.5.4. An image of the film (under liquid) was captured prior to obtaining force curves as described in section 2.5.6. This image served as a map that allowed force curves to be obtained from 15 different locations on the film. When the force curves had been captured, the substrate was rinsed in 20 mL of Milli-Q® water (as described in

section 2.5.3) before repeating the procedure in a buffer with a higher concentration of KCl. A fresh Veeco® NP20 probe was used for each experiment.

3

EAS HOMOLOGUES IN OTHER SPECIES OF *NEUROSPORA*.

3.0 EXPERIMENTAL AIM.

Our intention was to obtain amino acid sequence information from the EAS hydrophobins present in other species of *Neurospora*. We were aiming to identify regions within the protein where the sequence is conserved in the hope of identifying those amino acids that play a role in polymerisation and the properties of the protein. While no specific sequence-motif (except for the number and spacing of cysteines) can explain the common gross physical- and chemical-properties common to all hydrophobins, some individual hydrophobins (e.g. the N-terminally glycosylated SC3) have been shown to have finer, sequence-specific properties. Further, hydrophobins have only been shown to only *partly* compensate the loss of a different hydrophobin (Kershaw *et al.*, 1998). Investigating hydrophobin genes in related species may shed light on the presence and origin of more subtle physical, structural, and chemical properties.

As discussed in section 1.0.4.2, the heterothallic *Neurospora* are closely related and so it was reasonable to expect that rodlet-films that cover the conidia produced by *N. sitophila*, *N. intermedia,* and *N. tetrasperma* (Hallett and Beever, 1981) are the products of endogenous *eas* genes within these species. I could not make such a prediction in relation to the aconidial species of *Neurospora* since they do not produce conidia. These organisms' inability to produce conidia might stem from the lack of a functional version of *eas*. Additionally it was recognised that any information that could be gained from comparing such genes could be useful when it came time to plan mutagenesis experiments.

The fungal strains used in this study are listed in Table 8, accompanied by their mating-types and lineage. Every species recognised in the *Neurospora* genus (except *N. sublineolata*) are represented in this selection. They were supplied by Dr. Ross Beever and Ms Stephanie Parkes (Landcare Research) either as conidia or as ascospores infused on silica-gel-beads. The cultivation of fungi from these silica-gel beads is described in section 2.1.1. For the most part, I obtained luxuriant growth and excellent yields of protein-bearing conidia, or genomic DNA, or total RNA when I cultivated *Neurospora* species these methods. However, my attempts to cultivate *N. galapagosensis* for the purpose of extracting genomic DNA proved problematic; I was unable to extract enough genomic DNA for Southern analysis or DNA-sequencing.

Cultivating *N. tetrasperma* and *N. sitophila* for the purpose of extracting rodlets also proved problematic. I selected Vogel's N media as the growth media for these

experiments because it is known to encourage high levels of conidiogenesis in *Neurospora* (Turian, 1964). Despite this and the fact that this media supported abundant mycelial proliferation in both *N. tetrasperma* and *N. sitophila*, the yields of conidia (and therefore rodlets) – relative to *N. crassa* – from these two species were poor. Lower levels of conidiogenesis may be a trait peculiar to the strains of *N. tetrasperma* and *N. sitophila* examined in this study (personal communication with Dr. Ross Beever).

3.1 Fungal species surveyed for EAS.

TABLE 8 : *NEUROSPORA* ISOLATES USED IN THIS STUDY

Taxa	Mating Phenotype	Strain Designation	Origin
N. africana	Homothallic	Africana N200	FGSC 1740
N. crassa	Heterothallic (*mat a*)	St. Lawrence Sta	J.R.S. Fincham
N. crassa	Heterothallic (*mat A*)	St. Lawrence StA4	J.R.S. Fincham
N. discreta	Heterothallic (*mat A*)	Kirbyville-6	FGSC 3228
N. dodgei	Homothallic	PR300	FGSC 1692
N. galapagosensis	Homothallic	G349	FGSC 1739
N. intermedia	Heterothallic (*mat A*)	Taipei-1c	FGSC 1766
N. lineolata	Homothallic	A-236	FGSC 1910
N. pannonica	Homothallic	TRTC 51327	FGSC 7221
N. sitophila	Heterothallic (*mat A*)	P8085	FGSC 2216
N. terricola	Homothallic	WFS 5000	FGSC 1889
N. tetrasperma	Pseudohomothallic (*mat A*)	85A	FGSC 1270
N. toroi	Pseudohomothallic (*mat A+a*)	259-35	FGSC 2541

The pedigrees of the *Neurospora* strains used in this study are listed in Table 8. Fungal Genetics Stock Centre (FGSC) accession numbers (listed in the Origin column) refer to strains obtained from the FGSC. *N. crassa* strains St. Lawrence Sta and St. Lawrence STA4 were the gift of J. R. S. Fincham.

3.2 Surveying the Genus *Neurospora* for the Gene *eas*.

Genomic DNA extracts were obtained from every *Neurospora* species listed in Table 8, except *N. galapagosensis* (Figure 17). The DNA extraction method described in section 2.2.2.1 yielded several milligrams of genomic DNA from 5-15 g of dried, pulverised mycelium. Genomic DNA was dissolved in TE buffer and stored at 4 °C until required. Prior to using the genomic DNA, each sample was analysed by gel

electrophoresis (section 2.2.5.2) to ensure that no degradation had occurred during the extraction process and subsequent storage.

FIGURE 17: *NEUROSPORA* GENOMIC DNA EXTRACTS.

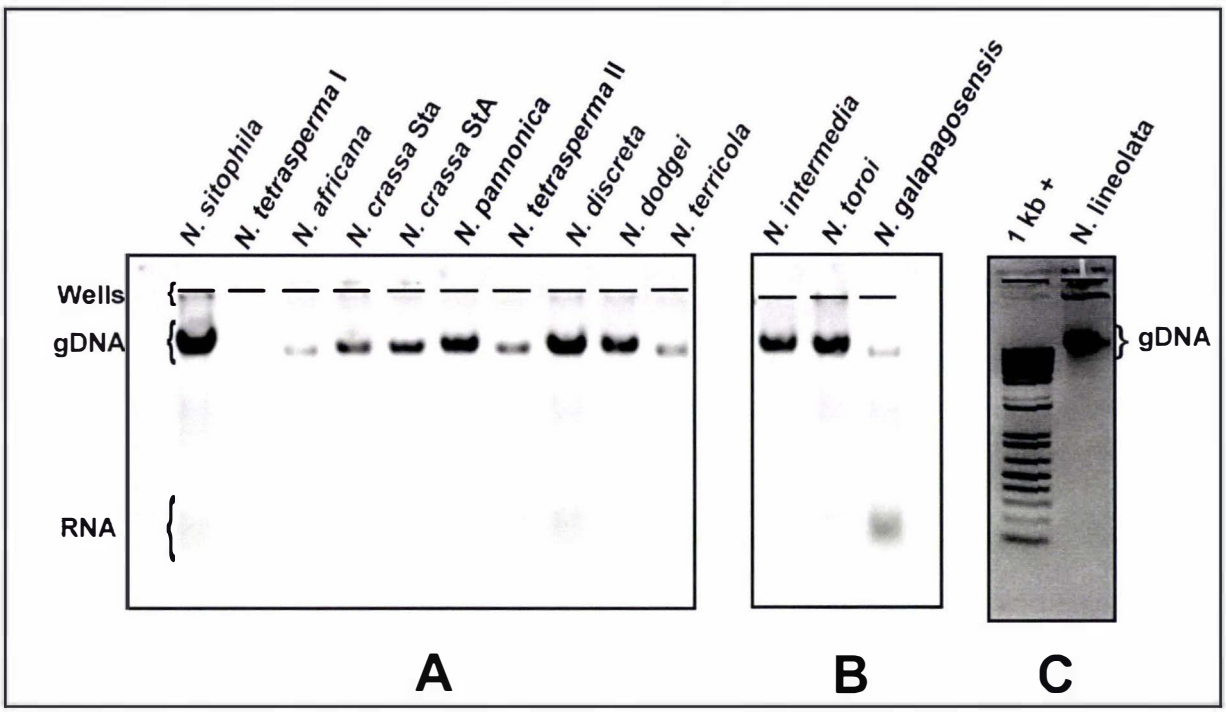

Figure 17 depicts three 0.8 %(w/v) agarose-TAE gels (A, B and C) used to evaluate the condition of *Neurospora* genomic DNA (gDNA) extracts prior to its use. 5 µL of a 1:20 dilution of each extract was mixed with loading buffer and separated electrophoretically as described in section 2.2.5. All of the gDNA bands in this figure are greater than 1.2 kb in size (compare bands in gel C with the upper, 1.2 kb, band in the 1 kb+ lane). Ethidium bromide staining of the walls of the loading wells can be seen (usually the top-most band in the gel). Residual RNA is also present in some samples as indicated.

3.2.1 SOUTHERN BLOTTING ANALYSIS.

The presence – in the other species of *Neurospora* – of genes homologous to *eas* was investigated by Southern hybridisation analysis (described in section 2.2.7.1). A radioactive probe consisting of the *eas* gene from *N. crassa* StA was hybridised to genomic DNA extracted from each *Neurospora* species before the blot containing the DNA was washed in a medium stringency buffer. These results are presented in Figure 18 and Figure 19B.

In Figure 19A, the probe was hybridised to the *N. lineolata* genomic DNA sample before being washed in a low stringency buffer. The fact that a medium stringency wash nearly removed the hybridised-probe from *N. lineolata* genomic DNA (Figure 19B) suggests that the gene in this species is not as closely related to *N. crassa eas* as the genes detected in the other species.

However, it is clear from the results that each species, including *N. lineolata,* contained DNA sequences homologous to *eas*. Experiments were undertaken to amplify and sequence each homologue.

FIGURE 18: SOUTHERN HYBRIDISATION ANALYSIS: PROBING *NEUROSPORA* DNA FOR *EAS*.

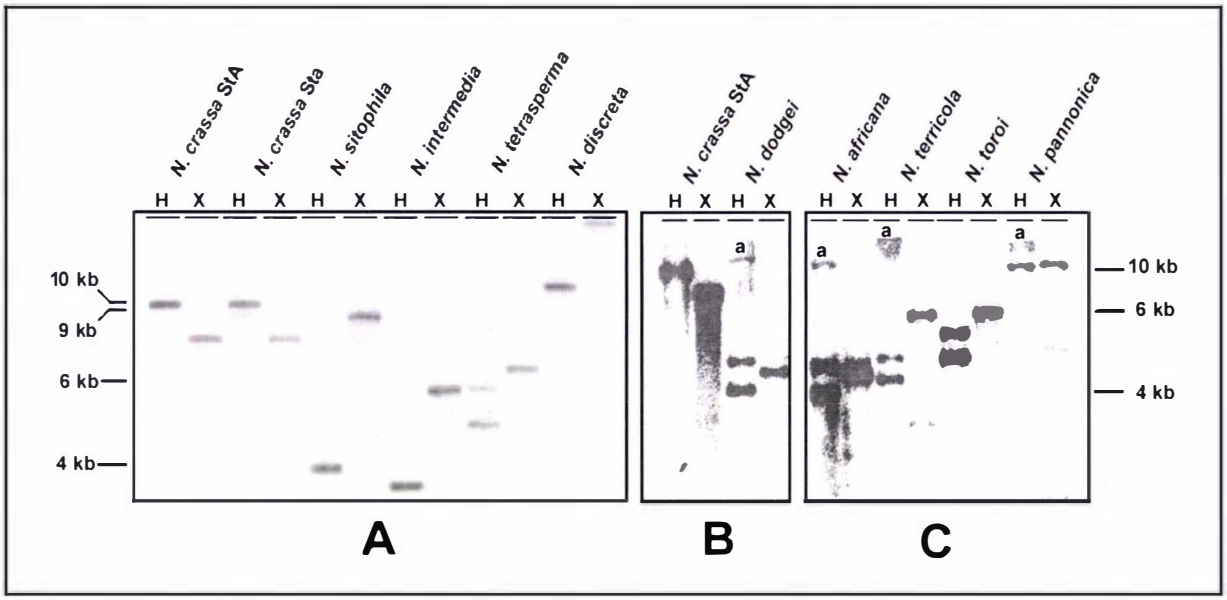

Figure 18 displays the results of two southern hybridisation analysis designed to detect homologues of *eas* gene in *Neurospora*. Figure 18A shows a membrane containing genomic DNA extracts from the conidiating species. A second blot containing genomic DNA extracts from every aconidiate species except for *N. lineolata* is displayed in other the membranes (Figure 18B and Figure 18C). The DNA was digested with *Hind* III (lanes marked H) and *Xho* I (lanes marked X) and hybridised to a radioactive copy of the *eas* gene (section 2.2.7.1). *N. crassa* StA is included in both blots as a positive control. Sizes indicated for each blot indicate the positions of the 1.6 kb and 506 bp markers from a 1 kb Ladder (Invitrogen™). The probe hybridises to these markers and permits a comparison to be made to the ladder run in the corresponding agarose-gel. Bands labelled, "a" is believed to be due to non-specific hybridisation and show up due to the over exposure.

FIGURE 19: SOUTHERN HYBRIDISATION ANALYSIS: PROBING *N. LINEOLATA* DNA FOR *EAS*.

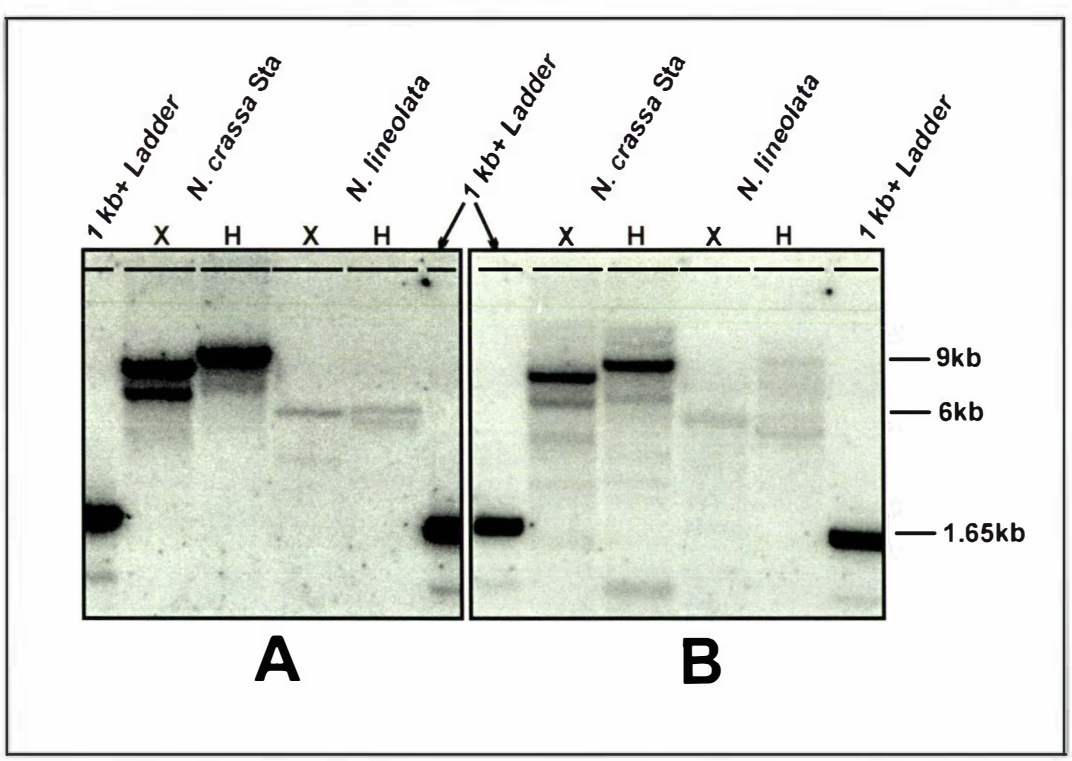

Figure 19 depicts the result of hybridizing *eas* gene-probes to genomic DNA extracted from *N. lineolata*. The DNA was digested with *Hind* III (lanes marked H) and *Xho* I (lanes marked X) and hybridised to a radioactive copy of the *eas* gene from *N. crassa* (section 2.2.7.1). The result of washing the blot with low stringency buffers is seen in membrane A. The result of washing the blot with medium stringency buffers is seen in membrane B. *N. crassa* Sta DNA was used as a positive control to test hybridisation. As can be seen the probe also bound to the 1.6 kb and 506 bp markers from the Invitrogen™ 1 kb Ladder run in the outside lanes. This provides a convenient method of estimating the size of hybridised DNA in the *N. lineolata* and *N. crassa* samples.

3.2.1.1 Gene Copy Numbers.

Southern blot analysis of genomic DNA digested with either *Hin*d III or *Xho* I suggested that there is one copy of *eas* per genome. The fact that the probe hybridised to two sites in *Hin*d III-digested DNA from *N. toroi* and *N. tetrasperma* was explained when sequence analysis identified that in these species, *eas* has a second *Hin*d III site located within the intron. Similarly, a single polymorphism common to the exons of *eas* genes from *N. africana*, *N. dodgei*, *N. lineolata* and *N. terricola* explains why the probe is able to hybridise twice to *Hin*d III-digested DNA samples from these species (Figure 18B and C). The bands greater than 10 kb seen in *Hin*d III samples from *N. africana*, *N. dodgei*, and *N. pannonica* (labelled "a" in Figure 18B and C) were probably caused by the probe hybridising to partially digested genomic DNA.

3.2.2 Amplification and Sequencing of Endogenous *eas* from *Neurospora* Species.

The Southern analysis indicated that an *eas* homologue existed in each of the conidiating and aconidiate *Neurospora* species. I sought to extract enough sequence information from each of these to predict the molecular mass of the *eas* gene-products from all ten *Neurospora* species. The first step was to PCR-amplify each gene.

Figure 20: PCR Amplification of Endogenous *eas*.

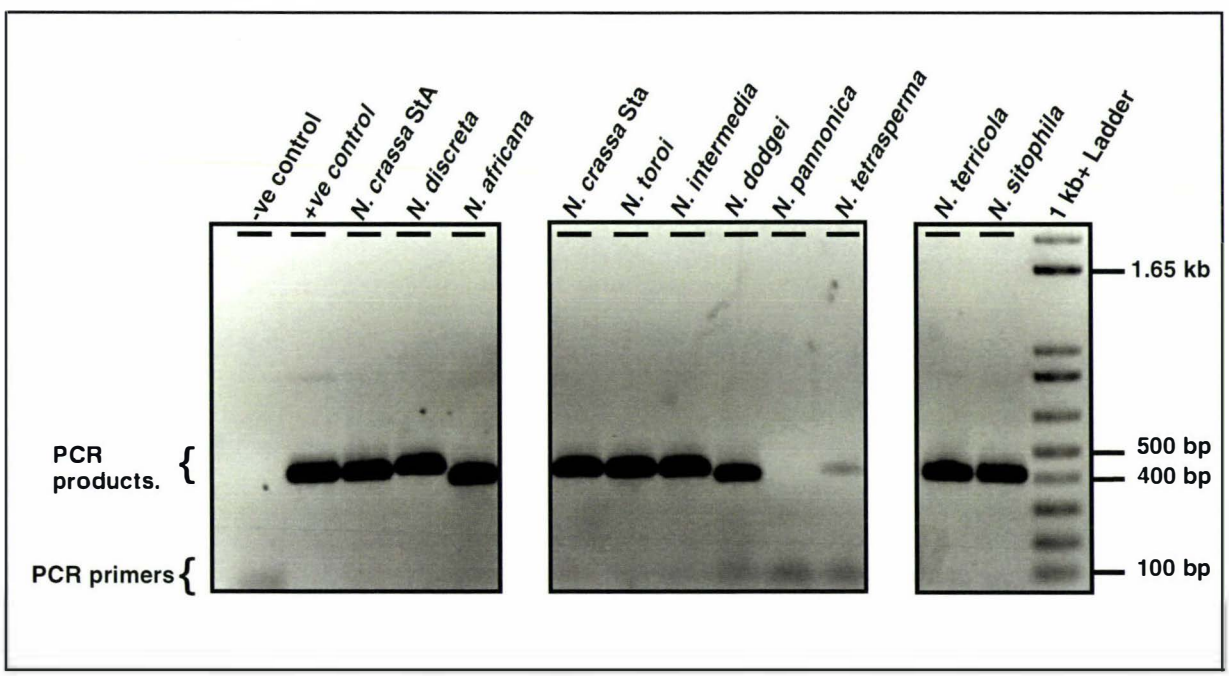

Figure 20 shows an agarose/TAE gel containing electrophoretically-separated *eas* gene PCR products derived from the *Neurospora* genomic DNA extracts indicated. PCR products from the species *N. lineolata*, *N. pannonica*, and *N. tetrasperma* were successfully amplified later (data not shown). The PCR control reactions are displayed included in this gel. The negative (-ve) control consisted on the PCR master mix with water while the positive (+ve) control was a pGEM7 plasmid containing a copy of the *eas* gene from *N. crassa* and was kindly supplied by Dr. Agnieszka Mudge (Hort Research).

FIGURE 21 [A]: ALIGNED ENDOGENOUS *EAS* GENES FROM *NEUROSPORA*.

	▼	5' PCR primer	▼			bp
N. crassa StA	ATGCAGTTCA	CCAGCGTCTT	CACCATCCTC	GCCATTGCCA	TGACCGCCGC	50
N. crassa Sta	ATGCAGTTCA	CCAGCGTCTT	CACCATCCTC	GCCATTGCCA	TGACCGCCGC	50
N. intermedia	ATGCAGTTCA	CCAGCGTCTT	CACCATCCTC	GCCATTGCCA	TGACCGCCGC	50
N. pannonica	ATGCAGTTCA	CCAGCGTCTT	CACCATCCTC	GCCATTGCCA	TGACCGCCGC	50
N. tetrasperma	ATGCAGTTCA	CCAGCGTCTT	CACCATCCTC	GCCATTGCCA	TGACCGCCGC	50
N. toroi	ATGCAGTTCA	CCAGCGTCTT	CACCATCCTC	GCCATTGCCA	TGACCGCCGC	50
N. sitophila	ATGCAGTTCA	CCAGCGTCTT	CACCATCCTC	GCCATTGCCA	TGACCGCCGC	50
N. discreta	ATGCAGTTCA	CCAGCGTCTT	CACCATCCTC	GCCGTCGCCA	TGACCGCCGC	50
N. dodgei	ATGCAGTTCA	CCAGCGTCTT	CACCATCCTC	ACCATCGCCA	TGACCGCCGC	50
N. lineolata	ATGCAGTTCA	CCAGCGTCTT	CACCATCCTT	ACCATCGCCA	TGACCGCCGC	50
N. africana	ATGCAGTTCA	CCAGCGTCTT	CACCATCCTC	ACCATCGCCA	TGACCGCCGC	50
N. terricola	ATGCAGTTCA	CCAGCGTCTT	CACCATCCTC	ACCATCGCCA	TGACCGCCGC	50
N. crassa StA	TGCGGCCCCG	GCTGAGGTTG	TTCCCCGCGC	CACCACCATC	GGCCCCAACA	100
N. crassa Sta	TGCGGCCCCG	GCTGAGGTTG	TTCCCCGCGC	CACCACCATC	GGCCCCAACA	100
N. intermedia	TGCGGCCCCG	GCTGAGGTTG	TTCCCCGTGC	CACCACCATC	GGCCCCAACA	100
N. pannonica	TGCGGCCCCG	GCTGAGGTTG	TTCCCCGTGC	CACCACCATC	GGCCCCAACA	100
N. tetrasperma	TGCGGCCCCG	GCTGAGGTTG	TTCCCCGCGC	CACCACCATC	GGCCCCAACA	100
N. toroi	TGCGGCCCCG	GCTGAGGTTG	TTCCCCGTGC	CACCACCATC	GGCCCCAACA	100
N. sitophila	TGCGGCCCCG	GCTGAGGTTG	TTCCCCGCGC	CACCACCATC	GACGCCAACA	100
N. discreta	TGCCGCCCCG	GCTGAGGTTG	TTCCCCGCGC	CCAGACCATC	GGCCCCAACA	100
N. dodgei	CGCGGCCCCG	GCTGAGGTCG	TTGCCCG···	CACGACCATC	ACTCCCGAGT	97
N. lineolata	CGCGGCCCCG	GCTGAGGTCG	TTGCCCG···	CACGACCATC	ACTCCCGAGT	97
N. africana	CGCGGCCCCG	GCTGAGGTTG	TTGCCCG···	CACGACCATC	ACTCCCGAGT	97
N. terricola	CGCGGCTCCG	GCTGAGGTCG	TTGCCCG···	CACGACCATC	ACTCCCGAGT	97
N. crassa StA	CCTGCTCCAT	CGACGACTAC	AAGCCTTACT	GCTGCCAGTC	TATGTCCGGC	150
N. crassa Sta	CCTGCTCCAT	CGACGACTAC	AAGCCTTACT	GCTGCCAGTC	TATGTCCGGC	150
N. intermedia	CCTGCTCCAT	CGACGACTAC	AAGCCTTACT	GCTGCCAGTC	TATGTCCGGC	150
N. pannonica	CCTGCTCCAT	CGACGACTAC	AAGCCTTACT	GCTGCCAGTC	TATGTCCGGC	150
N. tetrasperma	CCTGCTCCAT	CGACGACTAC	AAGCCTTACT	GCTGCCAGTC	TATGTCCGGC	150
N. toroi	CCTGCTCCAT	CGACGACTAC	AAGCCTTACT	GCTGCCAGTC	TATGTCCGGC	150
N. sitophila	CCTGCTCCAT	CGACGACTAC	AAGCCTTACT	GCTGCCAGTC	TATGTCCGGC	150
N. discreta	CCTGCTCCAT	CGACGACTAC	AAGCCTTACT	GCTGCCAGAG	CATGTCCGGC	150
N. dodgei	CCTGCTCAAT	CCCCAACTAC	AAGCCCTACT	GCTGCCAAAG	CTTGTCCAGC	147
N. lineolata	CCTGCTCAAT	CCCCAACTAC	AAGCCCTACT	GCTGCCAAAG	CTTGTCCAGC	147
N. africana	CCTGCTCAAT	CCCCAACTAC	AAGCCCTACT	GCTGCCAAAG	CTTGTCCAGC	147
N. terricola	CCTGCACCAT	CCCCAACTAC	AAGCCCTACT	GCTGCCAAAG	CTTGTCCGGC	147
				▲		
				***Hind* III site**		
N. crassa StA	CCCGCCGGCT	CCCCTGGTCT	CCTCAAC···	CTCATCCCCG	TCGACCTCAG	197
N. crassa Sta	CCCGCCGGCT	CCCCTGGTCT	CCTCAAC···	CTCATCCCCG	TCGACCTCAG	197
N. intermedia	CCCGCCGGCT	CCCCTGGTCT	CCTCAAC···	CTCATCCCCG	TCGACCTCAG	197
N. pannonica	CCCGCCGGCT	CCCCTGGTCT	CCTCAAC···	CTCATCCCCG	TCGACCTCAG	197
N. tetrasperma	CCCGCCGGCT	CCCCTGGTCT	CCTCAAC···	CTCATCCCCG	TCGACCTCAG	197
N. toroi	CCCGCCGGCT	CCCCTGGTCT	CCTCAAC···	CTCATCCCCG	TCGACCTCAG	197
N. sitophila	CCCGCCGGCT	CCCCTGGTCT	CCTCAAC···	CTCATCCCCG	TCGACCTCAG	197
N. discreta	CCCGCCGGCA	GCCCTGGTCT	CCTCAAC···	CTCATCCCCG	TCGACCTCAG	197
N. dodgei	ACCGGCGG··	····TGGAAT	CCTCGGTGCC	CTTCTCGGCG	TCGACCTCAG	191
N. lineolata	ACCGGCGG··	····TGGAAT	CCTCGGTGCC	CTTCTCGGCG	TCGACCTCAG	191
N. africana	ACCGGCGG··	····TGGAAT	CCTCGGTGCC	CTTCTCGGCG	TCGACCTCAG	191
N. terricola	ACCGGCGG··	····TGGACT	CCTCGGT···	CTTCTCCCCA	TCGACCTCAG	188

Figure 21 shows the aligned sequences of *eas* genes endogenous to each *Neurospora* species aligned as described section 2.0.4. **Key:** The positions of the PCR primers (yellow background), the *Hind* III sites (underlined), the putative intron splice (grey background), and branch (italics) sites, and the exons (bold text) have been highlighted as indicated. Figure 21 continues onto the next two pages.

FIGURE 21 [B]: CONTINUED: ALIGNED ENDOGENOUS *EAS* GENES FROM *NEUROSPORA*.

```
                                                                                                  bp
N. crassa StA     CGCCTCGCTC  GGCTGCGTTG  TCGGTGTCAT  CGGCTCCCAA  TGTGGTGCCA  247
N. crassa Sta     CGCCTCGCTC  GGCTGCGTTG  TCGGTGTCAT  CGGCTCCCAA  TGTGGTGCCA  247
N. intermedia     CGCCTCGCTC  GGCTGCGTTG  TCGGTGTCAT  CGGCTCCCAA  TGTGGTGCCT  247
N. pannonica      CGCCTCGCTC  GGCTGCGTTG  TCGGTGTCAT  CGGCTCCCAA  TGTGGTGCCT  247
N. tetrasperma    CGCCTCGCTC  GGCTGCGTTG  TCGGTGTCAT  CGGCTCCCAA  TGTGGTGCCA  247
N. toroi          CGCCTCGCTC  GGCTGCGTTG  TCGGTGTCAT  CGGCTCCCAA  TGTGGTGCCA  247
N. sitophila      CGCCTCGCTC  GGCTGCGTTG  TCGGTGTCAT  CGGCTCCCAA  TGTGGTGCCA  247
N. discreta       CGCCTCGCTC  GGCTGCGTTG  TCGGTGTCAT  CGGCTCCCAG  TGCGGTGCCA  247
N. dodgei         CGCCACGCTC  GGCTGCGTTG  TCGGTGCCGT  CGGTGGCCAA  TGCAGCGCCA  241
N. lineolata      CGCCACGCTC  GGCTGCGTTG  TCGGTGCCGT  CGGTGGCCAA  TGCAGCGCCA  241
N. africana       CGCCACGCTC  GGCTGCGTTG  TCGGTGCCGT  CGGTGGCCAA  TGCAGCGCCA  241
N. terricola      CGCCACACTC  GGCTGCGTTG  TCGGTGTCAT  CGGTGGCCAA  TGCAGCGCCA  238
                                                     5' splice site
                                                          ▼
N. crassa StA     GCGTCAAGTG  CTGCAAGGAC  GATGTTACCA  ACGTAAGTTT  TTCCTCCTTC  297
N. crassa Sta     GCGTCAAGTG  CTGCAAGGAC  GATGTTACCA  ACGTAAGTTT  TTCCTCCTTC  297
N. intermedia     CCGTCAAGTG  CTGCAAGGAC  GATGTTACCA  ACGTAAGTTT  TTCCTCCTTC  297
N. pannonica      CCGTCAAGTG  CTGCAAGGAC  GATGTTACCA  ACGTAAGTTT  TTCCTCCTTC  297
N. tetrasperma    GCGTCAAGTG  CTGCAAGGAC  GATGTTACCA  ACGTAAGCTT  TTCCTTCTTC  297
N. toroi          GCGTCAAGTG  CTGCAAGGAC  GGTGTTACCA  ACGTAAGCTT  TTCCTCCTTC  297
N. sitophila      GCGTCAAGTG  CTGCAAGGAC  GATGTTACCA  ACGTAAGTTT  TTCCTCCTTC  297
N. discreta       GCGTCAAGTG  CTGCAAGGAC  GACGTTACCA  ACGTAAGTTT  TTCTCCCACT  297
N. dodgei         GCGTCAAGTG  CTGCAAGAGC  GATGCTACCA  ACGTGAGTTT  TTCTTCTAC-  290
N. lineolata      GCGTCAAGTG  CTGCAAGAGC  GATGCTACCA  ACGTGAGTTT  TTCTTCTAC-  290
N. africana       GCGTCAAGTG  CTGCAAGAGC  GATGCTACCA  ACGTGAGTTT  TTCTTCTAC-  290
N. terricola      GCGTCAAGTG  CTGCAAGAGC  GATGTTACCA  ACGTGAATTT  TTCTCCCCCT  288
                                                          ▲
                                                     Hind III site
N. crassa StA     TCCCTC·CAC  ACTA·····C  AGCGCGCTCT  CTTCAGA·AA  CAGTTCCCCT  340
N. crassa Sta     TCCCTC·CAC  ACTA·····C  AGCGCGCTCT  CTTCAGA·AA  CAGTTCCCCT  340
N. intermedia     TCCCTC·CAC  ACTA·····C  AGCGCGCTCT  CTTCAGC·AA  CAGTTCCCCT  340
N. pannonica      TCCCTC·CAC  ACTA·····C  AGCGCGCTCT  CTTCAGC·AA  CAGTTCCCCT  340
N. tetrasperma    TCACTC·CAC  ACTA·····C  AGCGCATTCT  ATTCAGC·AA  CAGTTCCCCT  340
N. toroi          TCACTC·CAC  ACTA·····C  AGCGCACTCT  ATTCAGC·AA  CAGTTCCCCT  340
N. sitophila      TCACTC·TAC  ACTA·····C  AGCGCACTCT  ATTCAGC·AA  CAGTTCCCCT  340
N. discreta       TCACTCTCAC  ATCATTACCC  AATCTGCTCT  ACTCAGC·A·  TAGTTCGTCT  345
N. dodgei         ··········  ·········C  TGCAGATTCT  ACTAAG··CA  CAGTTCGCCT  319
N. lineolata      ··········  ·········C  TGCAGATTCT  TTTAAAAACA  CAGTTCGCCT  321
N. africana       ··········  ·········C  TGCAGATTCT  ACTAAG··CA  CAGTTCGCCT  319
N. terricola      TACTCC··AC  ACCT·····C  TACCTACTCT  ACTAAG··CA  CAGTTCGCCT  329
                  Branch site                                    3' splice site
                  ▼-----▼                                              ▼
N. crassa StA     TGCTAACCTT  CGC·······  ·····TTTTG  TGCCGACGAA  AAAAGACCGG  378
N. crassa Sta     TGCTAACCTT  CGC·······  ·····TTTTG  TGCCGACGAA  AAAAGACCGG  378
N. intermedia     TGCTAACCTT  CGC·······  ·····TTTTG  TGCCGACGAA  AAAAGACCGG  378
N. pannonica      TGCTAACCTT  CGC·······  ·····TTTTG  TGCCGACGAA  AAAAGACCGG  378
N. tetrasperma    TGCTAACCTT  CGC·······  ·····TTTTG  TGCCGACGAA  AAAAGACCGG  378
N. toroi          TGCTAACCTT  CGC·······  ·····TTTTG  TGCCGACGAA  AAAAGACCGG  378
N. sitophila      TGCTAACCTT  CGC·······  ·····TTTTG  TGCCGACGAA  AAAAGACCGG  378
N. discreta       ·GCTAACCTT  TGCCTTTCTT  CTTTCTTTTG  TGCCGACGAA  AAAAGACCGG  394
N. dodgei         TGCTAACCTT  TGCCCTTCTT  CT·····TTT  ··········  CACAGACCGG  357
N. lineolata      TTCTAACCTT  TGCCCTTCTT  CTCCT·····  ··········  CACAGACCGG  362
N. africana       TGCTAACCTT  TGCCCTTCTT  CT·····TTT  ··········  CACAGACGGG  357
N. terricola      TGCTAACTTT  TGCCCTTCTT  CTTCTTCTTC  TTCTTCTCCA  TACAGACCGG  379
```

Figure 21 continues onto the next page.

FIGURE 21 [C]: CONTINUED: ALIGNED ENDOGENOUS *EAS* GENES FROM *NEUROSPORA*.

						bp
N. crassa StA	CAACTCCTTC	CTCATC*ATCA*	ACGCTGCCAA	CTGCGTTGCC	TAA	421
N. crassa Sta	CAACTCCTTC	CTCATC*ATCA*	ACGCTGCCAA	CTGCGTTGCC	TAA	421
N. intermedia	CAACTCCTTC	CTCATC*ATCA*	ACGCTGCCAA	CTGCGTTGCC	TAA	421
N. pannonica	CAACTCCTTC	CTCATC*ATCA*	ACGCTGCCAA	CTGCGTTGCC	TAA	421
N. tetrasperma	CAACTCTTTC	CTCATC*ATCA*	ACGCTGCCAA	CTGCGTTGCC	TAA	421
N. toroi	CAACTCTTTC	CTCATC*ATCA*	ACGCTGCCAA	CTGCGTTGCC	TAA	421
N. sitophila	CAACTCTTTC	CTCATC*ATCA*	ACGCTGCCAA	CTGCGTTGCC	TAA	421
N. discreta	TAACTCTTTC	CTCATC*ATCA*	ACGCTGCCAA	CTGCGTTGCC	TAA	437
N. dodgei	TAACTCCCTC	ATCCTC*ATCA*	ACGCTGCCAA	CTGCGTTGCC	TAA	400
N. lineolata	TAACTCCCTC	ATCCTC*ATCA*	ACGCTGCCAA	CTGCGTTGCC	TAA	405
N. africana	TAACTCCCTC	ATCCTC*ATCA*	ACGCTGCCAA	CTGCGTTGCC	TAA	400
N. terricola	TAACTCCCTC	ATCATC*ATCA*	ACGCTGCCAA	CTGCGTTGCC	TAA	422
		▲	3' PCR primer		▲	

Figure 21 shows the aligned sequences of *eas* genes endogenous to each *Neurospora* species aligned as described section 2.0.4. **Key:** The positions of the PCR primers (yellow background), the *Hind* III sites (underlined), the putative intron splice (grey background), and branch (italics) sites, and the exons (bold text) have been highlighted as indicated. Figure 21 continues from the previous two pages.

I designed PCR primers to anneal to the 5' and 3' ends of the translated region of *eas* from *N. crassa*. The PCR protocol described in section 2.2.3.1 was used to amplify products from each species except *N. galapagosensis* (Figure 20). The PCR products were purified, ligated into the plasmid vector "pGEM-T Easy™" and transformed into *E. coli* strain DH5α (sections 2.2.3.2 and 2.2.6). Plasmid DNA was purified as described in section 2.2.6.4 and sequenced by the commercial DNA sequencing facilities described in section 2.2.7.3. The sequences generated are displayed in Figure 21.

Overall the sequences of each gene are extremely similar, this despite the distinct phenotypic differences between the species. For instance, the *eas*-genes in *N. intermedia* (heterothallic) and *N. pannonica* (homothallic) are identical.

The sequences of the exon-intron junctions in *eas* do not exactly match patterns established by Edelmann and Staben (1994) for *N. crassa* genes. Nevertheless, the predicted position of the intron in *eas* has been confirmed cDNA sequencing (see Appendix IIID; Eberle and Russo, 1992; Bell-Pedersen *et al.*, 1992). This intron appears to be conserved in each of the genes discovered. Most of the species have the same exon-intron junctions and the branch site (where the lariat forms during excision of the intron) known for the *N. crassa* version of *eas* (Figure 21). Sequence variations exist at the 3' intron splice sites of genes from *N. dodgei*, *N. lineolata*, *N. africana,* and *N. terricola* (Figure 21B). However, these changes are still consistent with the conserved 3' splice site-sequence determined by Edelmann and Staben (1994) and these polymorphisms should not significantly affect the ability of these species to accurately excise the intron when they express *eas*.

Relative to the *eas* gene from *N. crassa*, the insertion and deletion polymorphisms present in the first exon of genes from *N. dodgei*, *N. lineolata*, *N. africana*, and *N. terricola* would not cause a reading frame shift because they occur in multiples of three (Figure 21A).

There is nothing, then, in the sequences of *eas* obtained from each aconidiate species indicating that these are pseudo-genes. However, nothing is known of the state of the genetic control regions external to the any of the sequences shown here; additionally the PCR primers (total length of 54 nucleotides) mask ~13% of the total sequence, including the start and stop codons and a portion of the protein-secretion signal.

3.3 Analysis of Hydrophobins From Conidiating *Neurospora* Species.

Given the similarity of each gene, their protein products were predicted to be hydrophobins with physical properties identical to EAS from *N. crassa* (Figure 21). To test this, I undertook experiments to extract hydrophobins from each species using the protocols previously developed to purify EAS (Templeton *et al.,* 1995). Accordingly, rodlet-layers from the macroconidia of the conidiating species listed in Table 8 were extracted, disassembled by treatment with TFA at 0 °C, and purified by RP–HPLC using methods described in section 2.4.1.

3.3.1 RP-HPLC Purification of Hydrophobin Extracts.

As with *N. crassa*, RP-HPLC purification resolved several isoforms of EAS from the rodlet-extracts of each species. The RP-HPLC elution profiles of each rodlet extract are compared to EAS in Figure 22. Note how each profile is similar to that obtained when extracting EAS from *N. crassa*. Both the number of elution peaks and the retention times of those peaks each are similar. This is especially true of the elution peaks for isoforms IIa and IIb (Figure 22A). The profiles of extracts from *N. crassa* StA, *N. crassa* Sta, and *N. discreta* contain produce wider, plateau-topped peaks because the high protein concentration in these extracts overwhelmed the detector attached to the RP-HPLC.

Under identical separation conditions, proteins that elute at similar times during RP-HPLC purification are expected to have similar chemical properties, and be of similar size with similar numbers of charged- and hydrophobic-groups (Dorsey and Cooper, 1994; AP-Biotech, 1999). Thus, I anticipate that proteins resolved from these macroconidial extracts are identical to the isoforms of EAS previously identified by Mackay *et al.* (2001).

FIGURE 22: RP-HPLC ELUTION PROFILES: *NEUROSPORA* MACROCONIDIAL RODLET EXTRACTIONS.

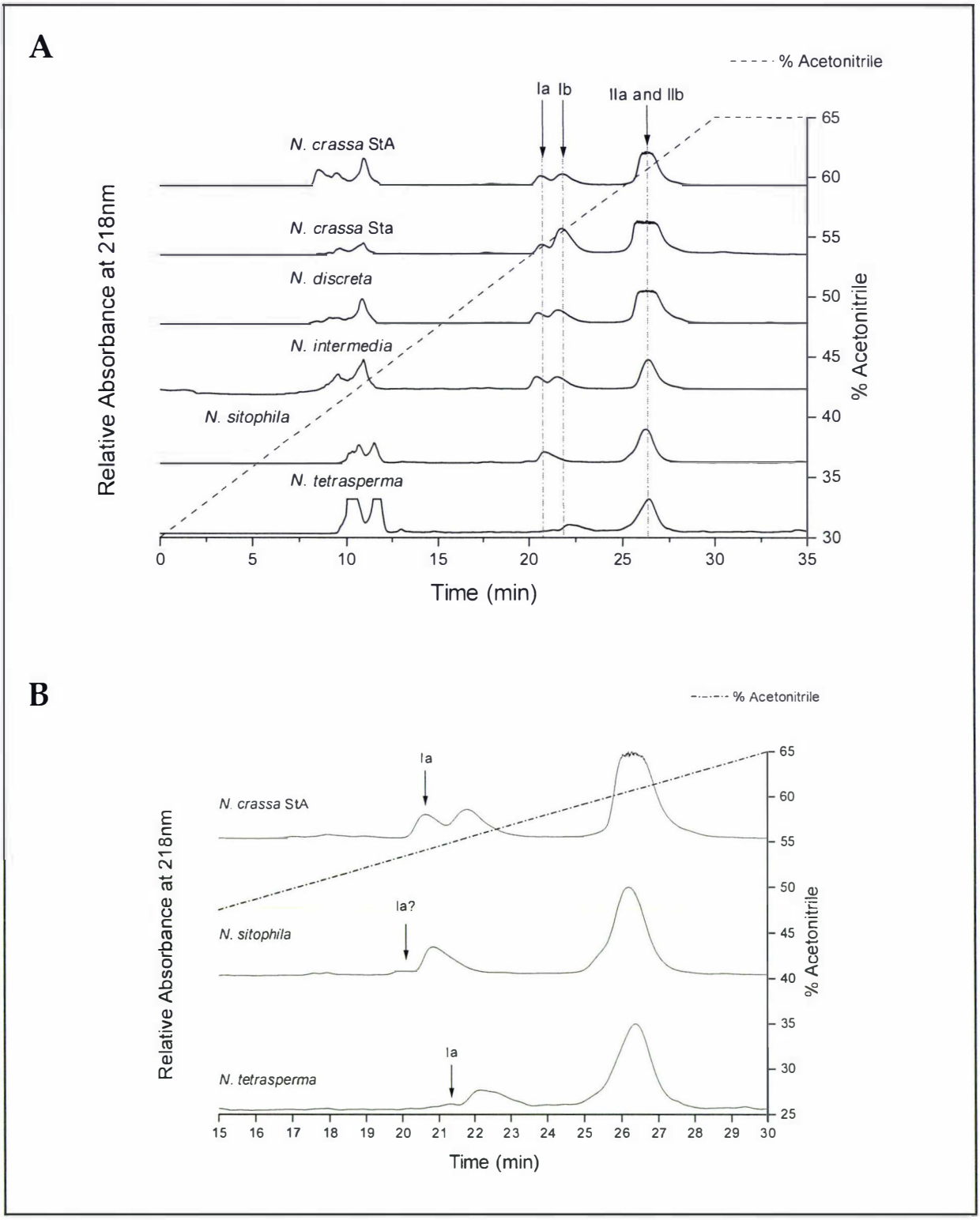

Figure 22A shows the elution profiles derived from the preparative RP-HPLC purification of rodlet extracts. Grey dotted lines indicate approximate retention times for each isoform purified from *N. crassa* StA EAS. Figure 22B shows the final 15 min of the elution profiles from Figure 22A, with *N. sitophila* and *N. tetrasperma* compared to *N. crassa* StA. Arrows indicate putative position of the elution peak containing isoform Ia from each extract. Note that the absorbance data for each profile was transformed to a dimensionless scale between 0 and 1. The absorbance datum at apex of isoform IIa and IIb elution peak was determined and all absorbance data were transformed into a fraction of that value. After this transformation, all data with values >1 were assigned a value of 1. This is why the elution profiles of *N. tetrasperma*, *N. crassa*, and *N. discreta* contain plateaux.

However, RP-HPLC elution profiles reveal nothing about the proteins' secondary or tertiary structure because exposure to concentrated organic solvents at low pH can rapidly denature proteins (Corran, 1998).

3.3.1.1 Isoform Ia in *N. sitophila* and *N. tetrasperma*.

The elution profiles of *N. sitophila* and *N. tetrasperma* extracts are dissimilar to the profile obtained from *N. crassa* EAS. Rodlet-extracts from both species lacked one of *N. crassa's* isoforms. Additionally, other fractions in the *N. sitophila* extract eluted earlier than would have been expected in *N. crassa* EAS extract (Figure 22A). The latter might be caused by the relative differences in the predicted amino acid sequence for the *N. sitophila eas* gene product.

In Figure 22B, a small shoulder can be seen preceding the elution peak labelled isoform Ib (so designated after consideration of ESI/MS data presented below) in rodlet-extracts from both *N. sitophila* and *N. tetrasperma.* This indicates that each species may actually be producing an endogenous EAS isoform Ia, but in much lower concentrations than is normal in *N. crassa.* The cultivation of *N. sitophila* and *N. tetrasperma* was problematic, yielding low amounts of rodlet-bearing macroconidia. To maximise the yield of conidia both *N. tetrasperma* and *N. sitophila* were cultivated for several more days than was used when extracting EAS from *N. crassa.* Potentially the abundance of isoforms seen in *N. crassa* may vary according to culture age; if so, then the extra-long incubation may have contributed to a reduction in production of isoform Ia in both *N. tetrasperma* and *N. sitophila.*

3.3.2 ESI/MS Analysis of Rodlet Extracts.

The sites where the N-terminal peptides in EAS are cleaved were determined by Templeton *et al.* (1995) and Mackay *et al.* (2001). If these modifications are applied to the predicted gene-products of the genes sequenced in section 3.2.2, then the proteins depicted in Figure 23 should be present in each of the rodlet extracts.

The mass of each EAS isoforms isolated by RP-HPLC was measured by ESI/MS as described in section 2.4.5. The results are displayed in Table 9. The molecular mass for each of the predicted-proteins depicted in Figure 23 was calculated is compared to the ESI/MS data (Table 9).

With the exception of *N. sitophila*, the ESI/MS data indicated that the same modifications identified in *N. crassa* EAS are present in the hydrophobins extracted from the other conidiating species (Mackay *et al.,* 2001). In each case, the product of the *eas* gene is post-translationally cleaved at $Arg_{(-1)}$-Ala_1 peptide bond to

generate the first pair of isoforms (Ia and Ib). The second pair of isoforms (IIa and IIb) is generated when the gene-product is post-translationally cleaved at Thr_3–Ile_4 peptide bond. One member of each pair of isoforms (designated "b") differs from the other member by an undetermined 16 Da addition: possibly a hydroxylated residue. The undetermined 16 Da addition known for two isoforms of EAS was not taken into account during calculations yielding the predicted mass of each isoform presented in Table 9.

FIGURE 23: PREDICTED PROTEIN SEQUENCES: CONIDIATING SPECIES OF *NEUROSPORA*.

	-26		-20		-10 ▼		1 ▼		10
N. crassa EAS	*M*	*QFTSV*	*FTILA*	*IAMTA*	*AAAPA*	*EVVPR*	ATTIG	PNTCS	IDDYK
N. tetrasperma	*M*	*QFTSV*	*FTILA*	*IAMTA*	*AAAPA*	*EVVPR*	ATTIG	PNTCS	IDDYK
N. toroi	*M*	*QFTSV*	*FTILA*	*IAMTA*	*AAAPA*	*EVVPR*	ATTIG	PNTCS	IDDYK
N. intermedia	*M*	*QFTSV*	*FTILA*	*IAMTA*	*AAAPA*	*EVVPR*	ATTIG	PNTCS	IDDYK
N. discreta	*M*	*QFTSV*	*FTILA*	*VAMTA*	*AAAPA*	*EVVPR*	AQTIG	PNTCS	IDDYK
N. sitophila	*M*	*QFTSV*	*FTILA*	*IAMTA*	*AAAPA*	*EVVPR*	ATTID	ANTCS	IDDYK
								•	

		20		30		40		50
N. crassa EAS	PYCCQ	SMSGP	AGSPG	LLNLI	PVDLS	ASLGC	VVGVI	GSQCG
N. tetrasperma	PYCCQ	SMSGP	AGSPG	LLNLI	PVDLS	ASLGC	VVGVI	GSQCG
N. toroi	PYCCQ	SMSGP	AGSPG	LLNLI	PVDLS	ASLGC	VVGVI	GSQCG
N. intermedia	PYCCQ	SMSGP	AGSPG	LLNLI	PVDLS	ASLGC	VVGVI	GSQCG
N. discreta	PYCCQ	SMSGP	AGSPG	LLNLI	PVDLS	ASLGC	VVGVI	GSQCG
N. sitophila	PYCCQ	SMSGP	AGSPG	LLNLI	PVDLS	ASLGC	VVGVI	GSQCG
	••					•		•

	60		70		80	
N. crassa EAS	ASVKC	CKDDV	TNTGN	SFLII	NAANC	VA
N. tetrasperma	ASVKC	CKDDV	TNTGN	SFLII	NAANC	VA
N. toroi	ASVKC	CKDGV	TNTGN	SFLII	NAANC	VA
N. intermedia	ASVKC	CKDDV	TNTGN	SFLII	NAANC	VA
N. discreta	ASVKC	CKDDV	TNTGN	SFLII	NAANC	VA
N. sitophila	ASVKC	CKDDV	TNTGN	SFLII	NAANC	VA
	•	•			•	

In Figure 23 an alignment of the amino acid sequences predicted to arise from the *eas* genes detected in the conidiating *Neurospora* species is depicted. **Key:** species-specific differences in the amino acid sequences are highlighted in red text. The leader sequence known for EAS is shown in italics. A predicted cleavage site for a secretory leader sequence is indicated by the grey triangle. The black triangle indicates the position of the alternate cleavage site that produces isoforms IIa and IIb. The amino acid sequence of these isoforms is highlighted in green. The amino acid sequence of isoforms Ia and Ib is includes the green isoform II sequence and the three amino acids highlighted in blue. Black circles highlight the position of cysteine residues.

3.3.2.1 EAS FROM *N. SITOPHILA*.

The mass spectrometry measurements revealed that *N. sitophila* EAS undergoes a different pattern of post-translational modifications. Firstly, the ESI/MS derived mass of *N. sitophila* EAS isoform Ia indicated that it arose from a post-translational cleavage at the $Arg_{(-1)}$-Ala_1 peptide bond. As discussed above, this modification is common to the other conidiating species. I was unable to isolate any species equivalent to isoform Ib from *N. sitophila* rodlet extracts (see section 3.3.1.1). Secondly, two pairs of isoforms (four isoforms in total) co-eluted in the RP-HPLC fraction collected between the 25th and 28th minute of the experiment (see Figure

22B, this peak normally yields EAS isoforms IIa and IIb when N. crassa rodlet extracts are applied to the column). In each pair, one member carried an undetermined 16 Da addition. Hence these new isoforms were designated IIa, IIb, IIIa, and IIIb in Table 9.

TABLE 9: ESI/MS MASS MEASUREMENTS ON *NEUROSPORA* EAS EXTRACTS.

ISOFORM I.

Species	Predicted Mass (Da) Isoform I	Observed Mass (Da) Isoform Ia	Observed Mass (Da) Isoform Ib	Mass Difference Between Isoforms (Da)
***N. crassa* StA**	*8178.26*	*8180.4*	*8195.0*	*14.6*
N. crassa Sta	*8178.26*	*8179.0*	*8195.0*	*16.0*
N. discreta	*8205.29*	*8207.0*	*8224.0*	*17.0*
N. intermedia	*8178.26*	*8180.0*	*8193.0*	*13.0*
N. tetrasperma	*8178.26*	*8177.0*	*8193.0*	*16.0*
N. sitophila	*8210.25*	*8209.0*	—	—

ISOFORM II.

Species	Predicted Mass (Da) Isoform II	Observed Mass (Da) Isoform IIa	Observed Mass (Da) Isoform IIb	Mass Difference Between Isoforms (Da)
***N. crassa* StA**	*7904.98*	*7908.0*	*7925.9*	*17.9*
N. crassa Sta	*7904.98*	*7906.0*	*7922.2*	*16.2*
N. discreta	*7904.98*	*7906.0*	*7923.0*	*17.0*
N. intermedia	*7904.98*	*7907.0*	*7924.0*	*17.0*
N. tetrasperma	*7904.98*	*7904.0*	*7920.0*	*16.0*
N. sitophila	*7936.97*	*7934.0*	*7950.0*	*16.0*

N. SITOPHILA ISOFORM III.

Species	Predicted Mass (Da) Isoform III	Observed Mass (Da) Isoform IIIa	Observed Mass (Da) Isoform IIIb	Mass Difference Between Isoforms (Da)
N. sitophila	*7637.85*	*7632.0*	*7648.0*	*16.0*

The predicted mass of each isoform with the experimental values are compared in Table 9. Mass predictions were calculated using the predicted translation of the *eas* genes detected in the conidiating species. The prediction includes the assumption that the same post-translational modifications known in EAS (described in Figure 23) from *N. crassa*, including the introduction of four intramolecular disulfide bonds. The "Mass Difference" column lists the difference in mass between the observed mass of the 'a' and 'b' forms of each isoform.

Isoforms IIIa and IIIb were ~300 Da lighter than the prediction based on the DNA sequence of *N. sitophila eas* indicated. DNA-sequencing of *N. sitophila eas* cDNA indicated that the gene's intron is excised as predicted in Figure 21 (see Appendix IIID for cDNA sequence). An explanation was found when the rodlet-extracts from this species were N-terminally sequenced (described in section 2.4.5).

The N-terminal sequencing experiment detected at least two peptides: (1) a "minor species" present in the sample at low concentration and (2) a "major species" which was present at a high concentration. The sequence of the "minor species" matches the predicted product of the *N. sitophila eas* gene *if* the protein is post-translationally cleaved at Thr_3–Ile_4 peptide bond. This is the same the same modification seen *N. crassa eas*. Thus, I have designated the pair of proteins contributing this sequence as isoforms IIa and IIb.

The sequence of the "major species" matches the predicted *N. sitophila eas* gene product if the protein is post-translationally cleaved at Ala_6–Asn_7 peptide bond. Such a modification would produce a pair of proteins 299.12 Da lighter than Isoforms IIa and IIb; this is consistent with the results shown in Table 9.

FIGURE 24: *N. SITOPHILA* EAS N-TERMINAL SEQUENCING RESULTS.

	1 ▼	10		
N. sitophila EAS predicted mature protein sequence	ATTID	ANTCS	IDDYK	P
N-Terminal sequencing results: major species		NT*S	IDDYK	P
N-Terminal sequencing results: minor species	ID	ANT*S	IDD	
		•		

The predicted *N. sitophila* EAS amino acid sequence is aligned in Figure 24 with the sequence derived when the RP-HPLC fraction containing *N. sitophila* EAS isoforms II and III were N-terminally sequenced **Key:** species specific differences in the amino acid sequence (relative to *N. crassa* EAS) of the protein produced by *N. sitophila* are highlighted in red. The EAS leader sequence is shown in italics. The predicted amino acid sequence of *N. sitophila* isoform II is highlighted in green. The amino acid sequence for isoform III (derived by N-Terminal sequencing) is highlighted in purple. The isoform I amino acid sequence includes both the green isoform II sequence and the three amino acids highlighted in blue. The sample was submitted to N-Terminal sequencing without methylating the cysteine residues and [*] indicates the position of a residue, assumed to be cysteine, involved in one of the four intramolecular disulfide bonds.

Compared to *N. crassa eas* the gene, the *N. sitophila eas* gene has different nucleotides at positions 92 and 94 (Figure 21A on page 76). In turn, this alters the identity of two amino-acids $Gly_5 \rightarrow Asp_5$ and $Pro_6 \rightarrow Ala_6$. These differences are close to the site where the signal-peptide is cleaved in *N. crassa* EAS. I suggest that these amino acid differences alter the signal-peptide cleavage site, lowering the efficiency of proteolytic cleavage at the Thr_3–Ile_4 bond while simultaneously permitting the Ala_6–Asn_7 peptide bond to be cleaved. Thus, proteolytic processing of the EAS signal-peptide in *N. sitophila* results in the production of six different isoforms of EAS from a single gene and I have detected five of these in this study.

3.3.2.2 EAS FROM *N. TOROI*.

N. tetrasperma (first described by Shear and Dodge, 1927) and *N. toroi* (first described by Tai, 1935) are so similar that the two species are regarded as synonymous by Perkins *et al.*, 1976). The similarity between the sequences of the ITS/5.8S region and *eas*-genes in each species supports this hypothesis. The *eas* genes from *N. toroi* and *N. tetrasperma* differ by a single nucleotide (see Figure 21A. In the *N. tetrasperma* gene nucleotide 78 = T, while in the *N. toroi* gene nucleotide 78 = C), while the *N. toroi* ITS/5.8S sequence is identical to the *N. tetrasperma* ITS/5.8S sequence (sequences are compared in Appendix IIIC) obtained by Dettman *et al.* (2001). The single nucleotide polymorphism in the *N. toroi eas*-gene is should cause the following amino-acid substitution in the gene's product: $Asp_{64} \rightarrow Gly_{64}$ (see Figure 23). My inability to induce the *N. toroi* isolate to conidiate prohibited any analysis of EAS proteins produced by this strain.

3.4 EAS EXPRESSION IN ACONIDIAL *NEUROSPORA*.

PCR experiments amplified potentially functional versions of *eas* from genomic DNA extracts taken from species of *Neurospora* that are unable to form conidia. In the case of *N. crassa*, the *eas* gene is transcriptionally controlled by both the circadian clock and the conidiation apparatus. Thus, despite these species' inability to produce conidia, their *eas*-genes might still be transcribed (possibly under the control of the circadian-clock?) for another purpose. For instance, there are several examples where hydrophobins are found coating aerial hyphae and other emergent structures (Whiteford and Spanu, 2002).

To test whether EAS is expressed in the aconidial species three experiments were undertaken. Because conidiation could not be induced in *N. toroi* in our hands, this organism was also included in these experiments.

3.4.1 MYCELIUM HYDROPHOBICITY TESTS.

The hydrophobic coating imparted by the film of EAS coating *N. crassa* conidia and conidiophores is hydrophobic enough to support an intact water droplet (Figure 25B). The *N. crassa* mutants lacking this hydrophobic coating and cannot support the water droplet (Figure 25A). This same test was applied to aconidial *Neurospora* cultures to determine whether a hydrophobic coating is present on their aerial hyphae (section 2.3). Briefly, cultures of aconidial *Neurospora* species and *N. toroi* were grown on sucrose-enriched Vogel's N agar medium. The overall hydrophobicity of mycelium from each species was tested by adding of 500 µL of

water to a single point on the surface of the culture. The droplets formed were photographed and the individual results are presented in Appendix IIIE.

FIGURE 25: THE WETTABILITY OF EAS COATED MACROCONIDIA.

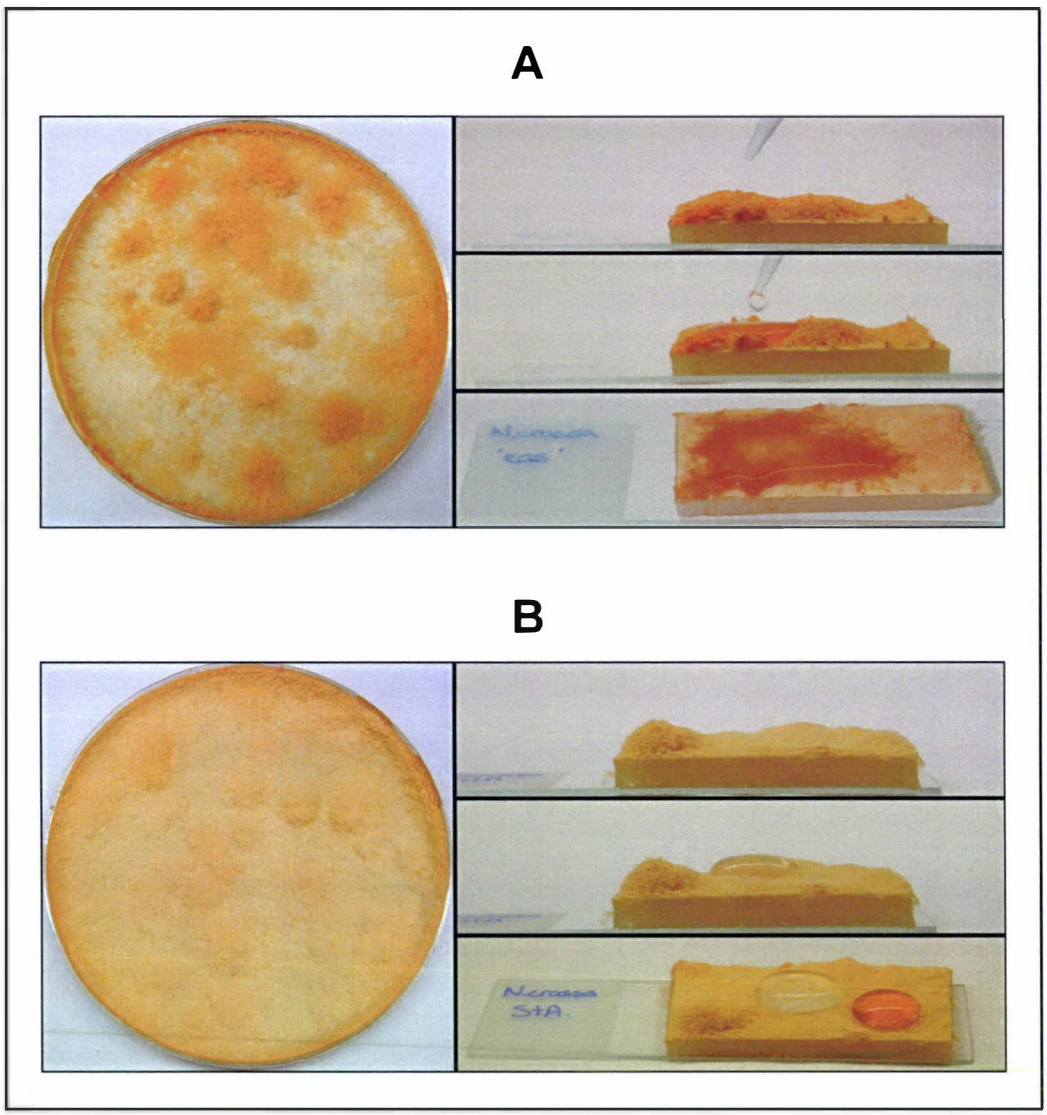

Figure 25 compares photographs of Petri-plates containing conidiating cultures of mutant *N. crassa* strain *eas* (left-hand picture in A) and wild-type *N. crassa* strain STA4 (left-hand picture in B) grown on sucrose-enriched Vogel's N agar. The wettability of these cultures was compared as described in section 2.3 and the result photographed. *N. crassa* strain *eas* do not express EAS and therefore lack the hydrophobic coating imparted by this protein. Water added to the surface of this culture instantly disperses [right-hand sequence in A]. Strains expressing EAS (like *N. crassa* strain STA4) possess a hydrophobic coating that can maintain an intact water droplet at the point of application (Right-hand sequence in Figure 25B).

Mycelial hyphae from every species tested were able to support intact water droplets, presumably because of the presence of an undetermined water-repelling coating. Variations were observed in both the contact angle and shape of the water droplets – both within individual colonies and between different species. However, because there was no way to standardize the surface geometry factors that affect wettability measurements such as roughness, thickness, and porosity (Busscher *et al.*, 1984; Adamson, 1990; Noordmans and Busscher, 1991) no significance has

been attached to the inter-species variations in wettability seen in these experiments.

3.4.2 RP-HPLC Purification of Mycelial Extracts.

To determine whether the hydrophobic coatings detected in the hydrophobicity assay were similar to EAS an attempt was made to extract any hydrophobins associated with the mycelial hyphae.

The hydrophobin extraction method developed by Beever *et al.* (1979) works because EAS is not covalently attached to the surfaces of the cells that express it. The *eas* genes from the aconidial species are similar to *N. crassa eas* and this suggests that their products would not be covalently attached to the cell wall of any cells expressing them. Therefore, the same extraction method developed used to extract conidial hydrophobins was applied to the aconidial species (section 2.4.1).

The culture growth media and incubation conditions were identical to those used for *N. crassa* (section 2.1.1). Extracts were treated with TFA at 0 ºC to disassemble any hydrophobins present then the extracts were fractionated by RP-HPLC (as described in section 2.4.2). A wider mobile-phase gradient was chosen to ensure that any form of EAS expressed by the aconidial species proteins would be detected regardless of any unexpected variations in the amino-acid sequence.

As demonstrated in section 3.3.2 and Figure 22, EAS has a distinct RP-HPLC elution-profile that consists of two peaks (one a doublet) eluting when the mobile phase consists of ~50 %(v/v) acetonitrile. The elution profiles of TFA-soluble protein extracts obtained from the mycelia of each species are compared in Figure 26. The EAS signature-profile is absent from extracts obtained from *N. pannonica* and *N. toroi.* These species possess genes virtually identical to *N. crassa eas* and therefore their products should be identical to *N. crassa* EAS.

If the pattern of intron-splicing and post-translational modifications seen in conidiating species is consistent, aconidial species should express the proteins depicted in Figure 27. The hydropathy profiles for each of these protein is very similar to EAS (Appendix IIIF), so it is anticipated that the 25 differences in the predicted amino acid sequences will have a negligible effect how these proteins elute from the RP-HPLC column.

FIGURE 26: ELUTION PROFILES OF MYCELIUM EXTRACTS.

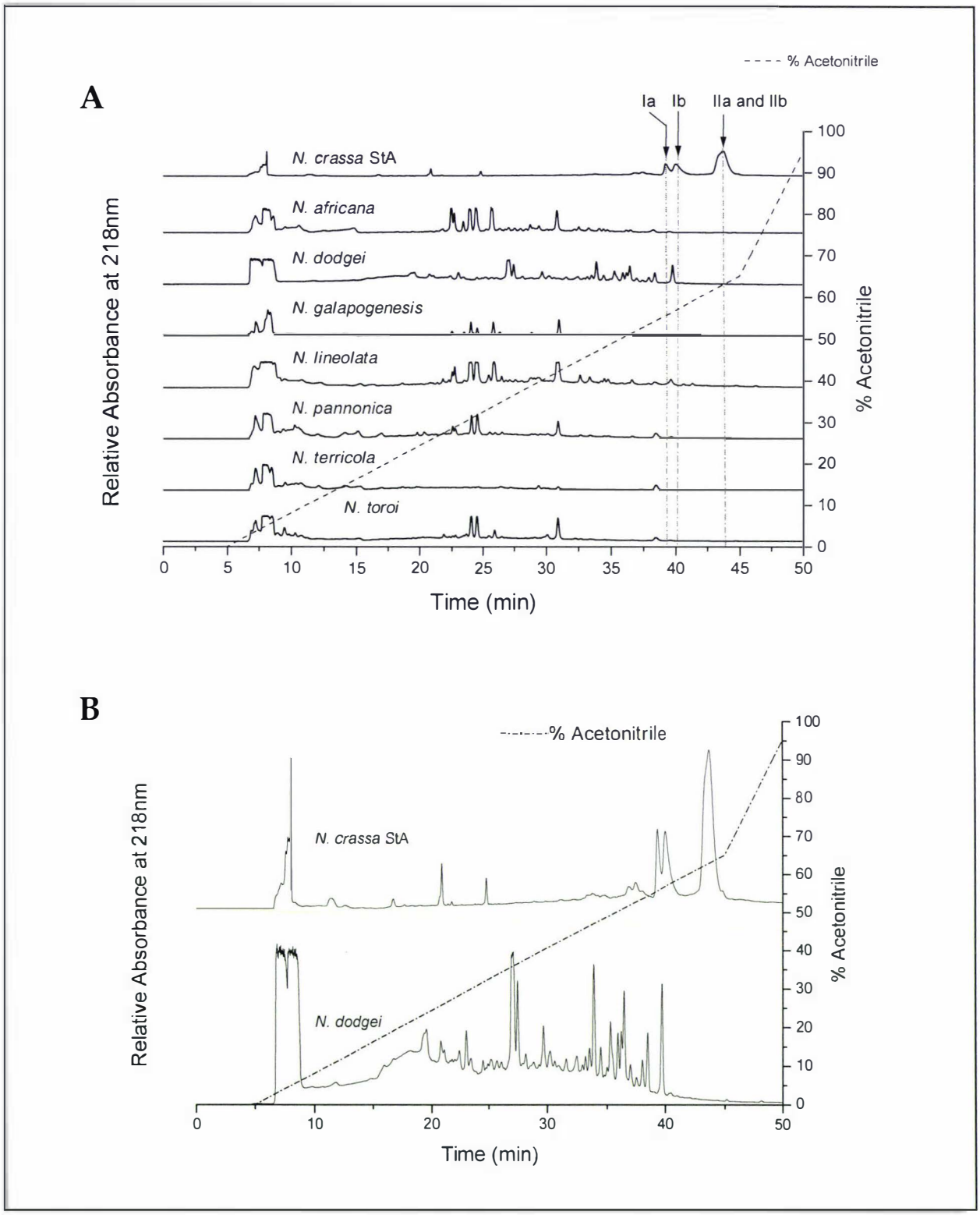

RP-HPLC elution profiles of aconidial *Neurospora* extracts are shown in Figure 26 and compared to the elution profile obtained when purifying *N. crassa* EAS. Grey dotted lines indicate approximate retention times for each isoform of EAS. Figure 26B shows closer view of the comparison between extracts from *N. dodgei* mycelium and EAS. **Note:** The absorbance data for each profile was transformed to a dimensionless scale between 0 and 1. The absorbance datum at apex of isoform IIa and IIb elution peak was determined and all absorbance data were transformed into a fraction of that value. Transformed data greater with a value greater than 1 were given a value of 1.

FIGURE 27: PREDICTED AMINO ACID SEQUENCES FOR THE ACONIDIAL *NEUROSPORA* SPECIES.

	−26		−20		−10 ▼			1 ▼	10	
N. crassa EAS	*M*	*QFTSV*	*FTILA*	*IAMTA*	*AAAPA*	*EVVPR*		ATTIG	PNTCS	IDDYK
N. pannonica	*M*	*QFTSV*	*FTILA*	*IAMTA*	*AAAPA*	*EVVPR*		ATTIG	PNTCS	IDDYK
N. lineolata	*M*	*QFTSV*	*FTILT*	*IAMTA*	*AAAPA*	*EVVAR*		·TTIT	PESCS	IPNYK
N. africana	*M*	*QFTSV*	*FTILT*	*IAMTA*	*AAAPA*	*EVVAR*		·TTIT	PESCS	IPNYK
N. dodgei	*M*	*QFTSV*	*FTILT*	*IAMTA*	*AAAPA*	*EVVAR*		·TTIT	PESCS	IPNYK
N. terricola	*M*	*QFTSV*	*FTILT*	*IAMTA*	*AAAPA*	*EVVAR*		·TTIT	PESCT	IPNYK

	20		30		40		50	
N. crassa EAS	PYCCQ	SMSGP	AGSPG	LLN·L	IPVDL	SASLG	CVVGV	IGSQC
N. pannonica	PYCCQ	SMSGP	AGSPG	LLN·L	IPVDL	SASLG	CVVGV	IGSQC
N. lineolata	PYCCQ	SLSST	GG··G	ILGAL	LGVDL	SATLG	CVVGA	VGGQC
N. africana	PYCCQ	SLSST	GG··G	ILGAL	LGVDL	SATLG	CVVGA	VGGQC
N. dodgei	PYCCQ	SLSST	GG··G	ILGAL	LGVDL	SATLG	CVVGA	VGGQC
N. terricola	PYCCQ	SLSGT	GG··G	LLG·L	LPIDL	SATLG	CVVGV	IGGQC

	60		70		80	
N. crassa EAS	GASVK	CCKDD	VTNTG	NSFLI	INAAN	CVA
N. pannonica	GASVK	CCKDD	VTNTG	NSFLI	INAAN	CVA
N. lineolata	SASVK	CCKSD	ATNTG	NSLIL	INAAN	CVA
N. africana	SASVK	CCKSD	ATNTG	NSLIL	INAAN	CVA
N. dodgei	SASVK	CCKSD	ATNTG	NSLIL	INAAN	CVA
N. terricola	SASVK	CCKSD	VTNTG	NSLII	INAAN	CVA

Figure 27 aligns the predicted amino acid sequences from the *eas* genes identified in aconidial *Neurospora* species. **Key:** specific differences in the amino acid sequences relative to EAS from *N. crassa* are highlighted in red. The leader sequence known for EAS is shown in Italics. A predicted cleaved site for a secretory leader sequence is indicated by the grey triangle. The black triangle indicates the position of the alternate cleavage site that produces isoforms IIa and IIb in EAS. The amino acid sequence of these isoforms is highlighted in green. The amino acid sequence of isoforms Ia and Ib is includes the green isoform II sequence and the three amino acids highlighted in blue. Black circles highlight the position of cysteine residues.

One significant difference exists between the conidial versions of EAS and the predicted sequences of four of the aconidial versions of the protein; the putative signal-peptide protease cleavage site is disrupted by the absence of Ala_1. This could alter the expression of isoform I and II in *N. africana, N. dodgei, N. lineolata,* and *N. terricola* (Figure 27) because, – as discussed previously – changes in the same region were suggested to affect the expression of EAS in *N. sitophila* (section 3.3.2.1).

Minor components in the extracts of *N. africana, N. dodgei, N. lineolata,* and *N. terricola* eluted at a similar stage as EAS (Figure 26). A comparison of elution profiles (absorbance against elution time) collected at 218 nm and 280 nm indicates that unlike any version of EAS, real or predicted, because some of these components strongly absorb strongly UV-light at 280 nm (see Appendix IV). EAS from *N. crassa* exhibits low absorbance of UV-light at 280 nm because it only has two aromatic amino acids: Tyr_{13} and Tyr_{16}. This situation is predicted to persist in the proteins from the aconidial species (Figure 27).

The component of the extract obtained from *N. dodgei* (highlighted in Figure 26B) is not one of these. EAS *could* have been expressed as predicted in at least one of these species, but the sensitivity of this experiment was limited so it is impossible to tell for certain.

These results show that EAS was not expressed in the aconidial mycelial hyphae in a form or in a concentration similar to that seen in the conidial species. The question pertaining to whether the proteins are expressed at all remains open, as does the origin of the hydrophobicity displayed by the mycelium examined in section 3.4.1. To resolve the former question, I undertook experiments to investigate whether the *eas* gene is transcribed in the aconidial species.

3.4.3 The Transcription of *eas* in Aconidial Species.

The transcription of aconidial *eas* genes was examined by Northern blotting analysis and RT-PCR (Sambrook and Russell, 2001). RNA for both of these experiments was extracted from *Neurospora* cultivated as static-liquid cultures under conditions similar to those used in experiments described in sections 3.4.1 and 3.4.2. Northern hybridisation analysis was carried out using the same hybridisation conditions and probe (*eas* DNA sequence) used during Southern hybridisation analysis described in section 2.2.7.2.

The results of Northern analysis are displayed in Figure 28 and show that the probe could only hybridise to mRNA sequences in those lanes containing total RNA extracts from *N. crassa*. These *eas* mRNAs are abundantly expressed in wild-type *N. crassa*: >1% of the whole in the mRNA population (Bell-Pedersen *et al.,* 1992; Sommer *et al.,* 1989). However, in the *N. crassa eas* mutant, transcription of *eas* occurs at levels undetectable by Northern analysis; remember that conidia from this strain lack an effective hydrophobic coating.

Northern blotting is most sensitive when 10 µg of total RNA is used per sample (Sambrook and Russell, 2001; Brown and Mackey, 2002), in the blots depicted in Figure 28 a minimum of 6 µg per lane used. To confirm that this wasn't the reason why I could not detect *eas* transcripts could in the RNA extracts from the aconidial species I analysed these extracts using RP-PCR.

RT-PCR requires less total RNA to detect and amplify rare mRNA sequences, it is more sensitive than Northern blotting analysis (Sambrook and Russell, 2001; Brown and Mackey, 2002).

FIGURE 28: NORTHERN BLOT ANALYSIS OF *EAS* TRANSCRIPTION IN ACONIDIAL *NEUROSPORA*

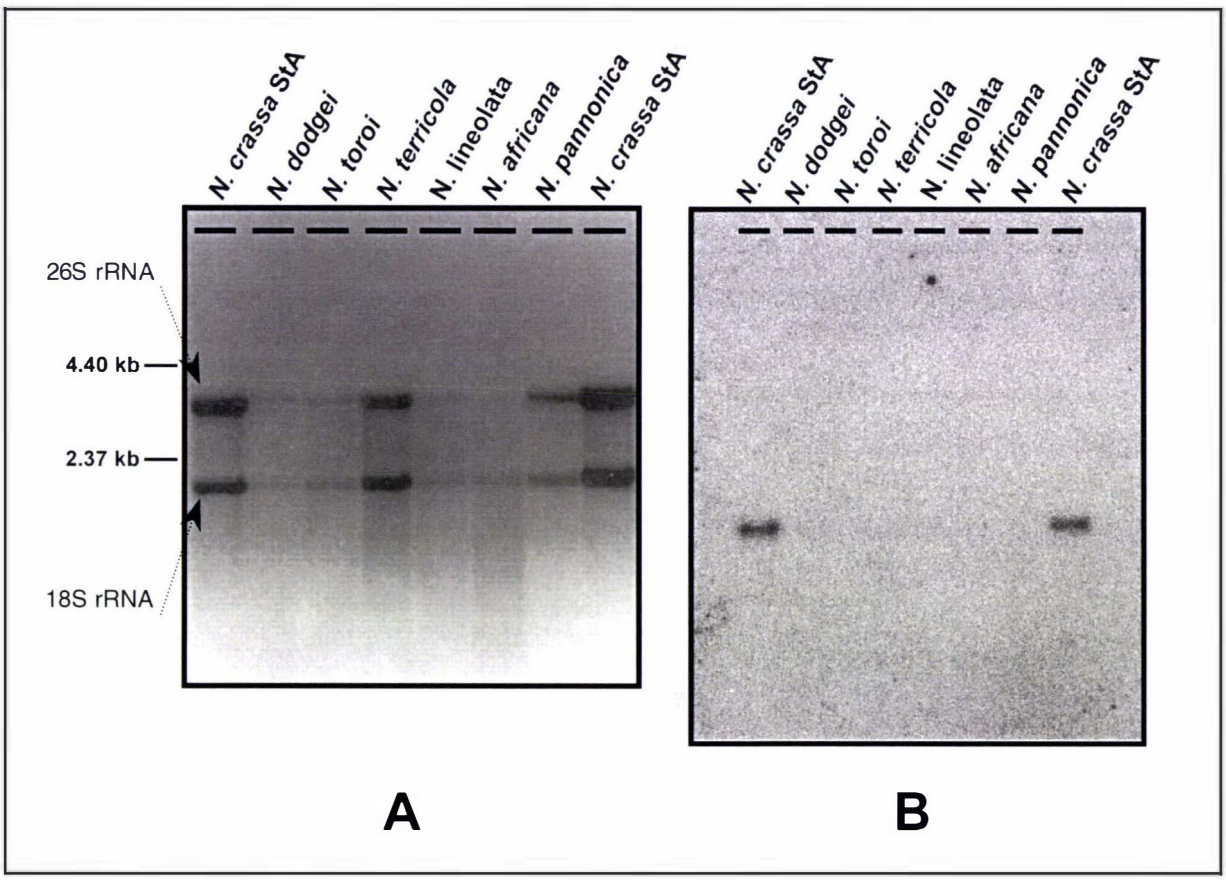

The results of an attempt detect transcription of *eas* in aconidial *Neurospora* using Northern blotting analysis is shown in Figure 28. Figure 28A contains the electrophoretically resolved total RNA extracts from each species prior to being blotted onto the Hybond XL membrane (as described in section 2.2.7.2). Ribosomal RNA bands are as indicated. The spectroscopically determined concentration of total RNA per lane is between 6-10 µg. A DNA *eas*-probe was hybridised to the DNA bound to the Hybond XL membrane (Figure 28B) and the blot was washed with medium stringency to give the result shown. The probe has hybridised to *eas* transcripts, approximately 0.8 kb in size according to Bell-Pedersen *et al.* (1992), in the *N. crassa* total RNA extract which is serving as a positive control.

RT-PCR experiments, repeated three times with two separately extracted sets of total RNA samples, were carried out as described in section 2.2.3.1. The clearest result is presented in Figure 29, while the others are presented in Appendix IIIG.

A product corresponding to the 320 bp *eas* cDNA from *N. crassa* was amplified from *N. toroi* RNA extracts (Figure 29B). A similar (but less obvious) result was obtained in one other replicate of this experiment carried out with a separate RNA extract from *N. toroi*, the result of the third replicate was obscured by a precipitation problem during staining (Appendix IIIG).

The presence of this product in *N. toroi* suggests that the *eas* gene in this species may be functional. Northern analysis is not sensitive enough to detect the transcription of *eas* in *N. crassa* prior to the genes induction by conidiation, blue-light and circadian clock mechanisms (*e.g.* Bell-Pedersen *et al.*, 1992; Sommer *et al.*, 1989). Because I was unable to induce conidiation in *N. toroi* during this experiment,

I cannot conclude that the low concentration of *eas* mRNA in this species is due to a malfunction in the *eas* gene.

FIGURE 29: RT-PCR ANALYSIS OF *EAS* TRANSCRIPTION IN THE ACONIDIAL *NEUROSPORA*

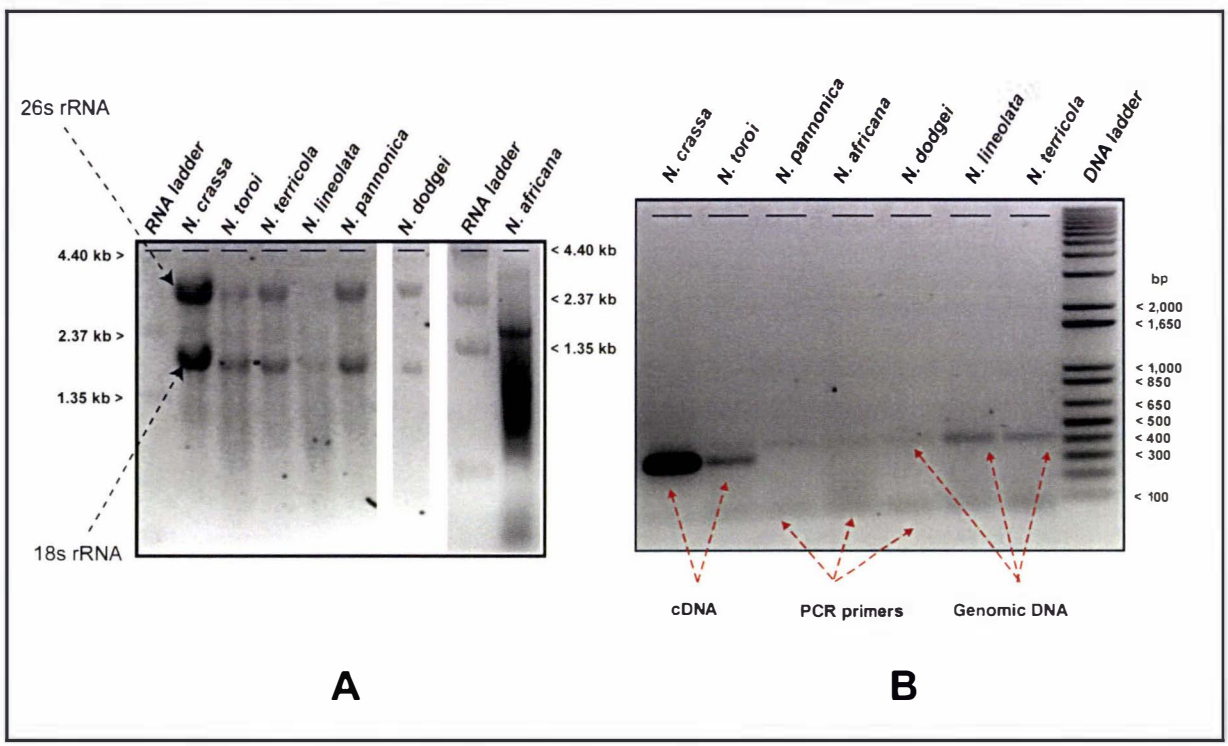

The results from an RT-PCR investigation of *eas* gene-transcription in aconidial *Neurospora* species are reproduced in Figure 29. Figure 29A is a formaldehyde-agarose gel containing the (electrophoretically resolved) total RNA extracts that were used as templates for the 1st strand amplification reaction (described in section 2.2.3.1); the ribosomal RNA bands are also highlighted. The products of the 2nd strand RT-PCR amplification using *eas*-specific primers are shown in Figure 29B. Products corresponding to the 320 bp *eas* cDNA were amplified from *N. crassa* and *N. toroi* total RNA extracts. Bands labelled "Genomic DNA" arose from PCR amplification of residual genomic DNA that contaminated the extracts. These 420 bp bands are the same size as those seen in Figure 20. Bands >100 bp are residual PCR primers remaining from the 2nd strand RT-PCR reaction.

Transcripts could not be detected by RT-PCR in the RNA extracted from the other aconidial species. The 420 bp bands seen in Figure 29B are the same size as the *eas* PCR products obtained from genomic DNA extracts (see Figure 20). They are likely to have arisen from genomic DNA that contaminated the RNA extracts used. Such contamination is normally removed by treating the RNA extracts with DNase I prior to use and because there were no 420 bp bands in the replicate RT-PCR experiments I performed (see Appendix IIIG), I believe that the DNase I used to decontaminate the RNA samples depicted in Figure 29A, was defective.

Taken together, the results of the Northern analysis and RT-PCR clearly indicate that *eas* genes in the aconidial species are inactive under these growth conditions. Consequently, EAS is unlikely to be responsible either for the hydrophobic protein species detected in RP-HPLC or for the hydrophobic properties of the hyphae from the aconidial species.

3.5 Discussion.

3.5.1 EAS in Non-Homothallic *Neurospora*.

The results presented in this chapter confirm the predictions made by Hallett and Beever (1981), specifically that EAS coats the surfaces of macroconidia produced by every non-homothallic *Neurospora* species - including *N. discreta* which was only recognised in 1986 (Perkins and Raju, 1986). In each species, the protein is produced by a single-copy of *eas* that, within the coding region at least, is almost identical to that originally isolated from *N. crassa.* This is unsurprising given the fact that the non-homothallic *Neurospora* species form a single phylogenetic clade. In fact, historically there has been some debate as to whether *N. intermedia* and *N. crassa* are the same species (Dettman *et al.*, 2001).

Figure 30: *cis* Transcriptional Regulatory Elements of *eas*.

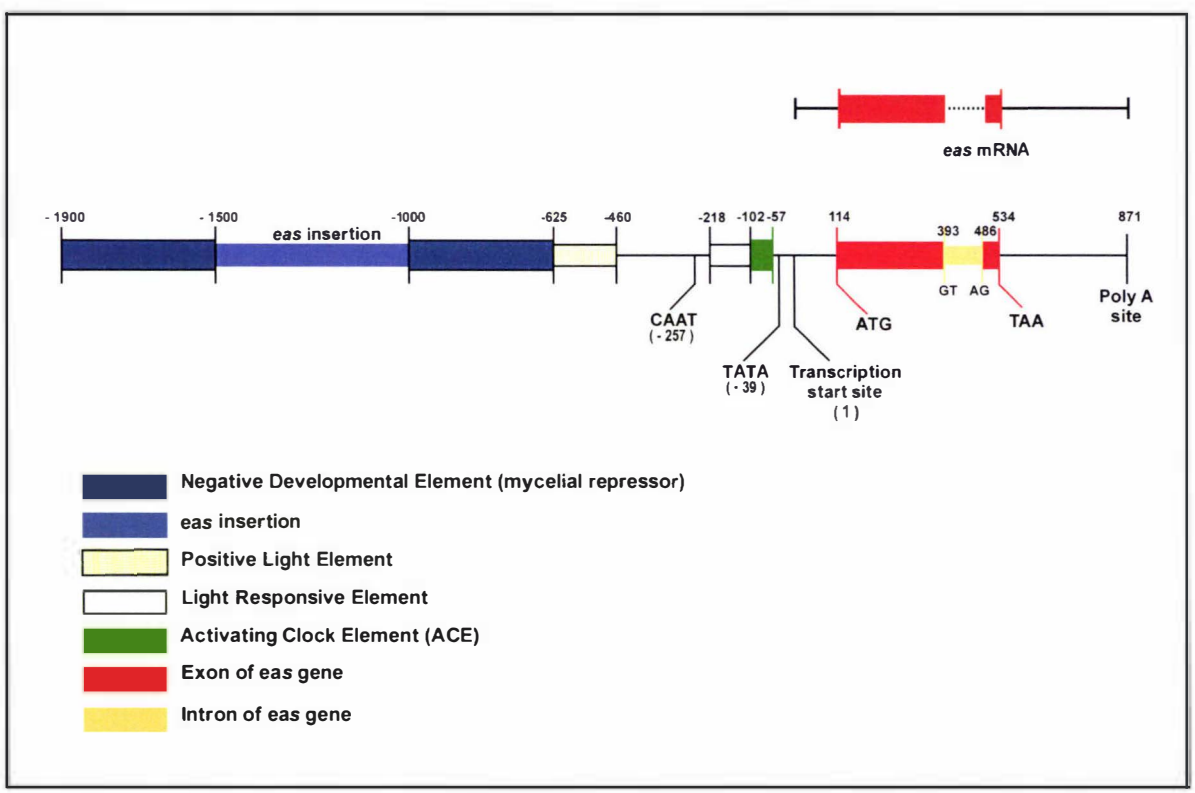

Figure 30 diagrammatically depicts the structure of the *N. crassa eas* gene along with locations of known and suspected *cis*-acting transcription regulatory elements. The smaller (upper) diagram depicts the structure of the *eas* mRNA sequence (the location of the deleted of the intron is shown with a dotted line). **Key:** (1) The light sensitive elements of *eas* were characterised by Sommer *et al.* (1989) and Bell-Pedersen *et al.* (1996). The *light responsive element* affects the kinetics of transcription induced by blue-light, while the *positive light element* proved to be essential for light-induction of expression. These conclusions conflict with an earlier investigation by Kaldenhoff and Russo (1993). (2) The *negative developmental element* is believed to suppress *eas* expression in germinating or mature conidia, ascospores and vegetative mycelium. The action of this repressor is over-ridden or masked when the circadian clock and the exogenous cues trigger transcription of *eas* (Lauter *et al.*, 1992; Bell-Pedersen *et al.*, 1996). (3) Nuclear run-on experiments indicated that *eas* is positively transcriptionally regulated by the circadian clock (Loros and Dunlap, 1991). When the circadian clock triggers conidiation, circadian regulatory elements bind to the *activating clock element* transcriptionally activating *eas* (Bell-Pedersen *et al.*, 1996; Correa and Bell-Pedersen, 2002). (4) The insertion of a part of the *cya-8* gene into *eas* (labelled as "*eas* insertion") causes the *eas*-wettable phenotype in the *N. crassa eas* mutant (Selitrennikoff, 1976; Lauter *et al.*, 1992; Bell-Pedersen *et al.*, 1992).

In *N. crassa*, *eas* is controlled by a complex, multi-layered, transcriptional regulation system whose *cis*-acting components are independent of each other (Arpaia *et al.*,

1993; Bell-Pedersen *et al.,* 1996). Because the gene-amplification strategy used was designed to complement the protein structural studies by identifying regions of conservation within the sequence of EAS, it precluded any investigation of the upstream region where these cis-acting elements are located (Figure 30).

The interplay between the *cis*-acting transcriptional control elements of *eas* has been described in a model posited by Correa and Bell-Pedersen (2002). Their model distinguishes between transcription that is induced by the endogenous circadian clock, and transcription induced in response to signals originating from the exogenous cues that also induce conidiation. Thus, in conditions where nutrients are plentiful, the circadian clock triggers both conidiation and EAS production in order to produce macroconidia in anticipation of each new dawn. The additional regulatory layers exist to boost and to extend the production of macroconidia (and therefore *eas*) upon the receipt of exogenous stress cues such as nutrient limitation and desiccation (Springer, 1993).

The same light-entrained growth regime is sufficient to induce each of the non-homothallic *Neurospora* species to produce EAS *in vitro* (this study and Hallett and Beever, 1981). This fact combined with the close phylogenetic relatedness of these species implies that the systems that regulate *eas* in *N. crassa* are probably common to all conidiating *Neurospora.*

3.5.2 EAS IN HOMOTHALLIC *NEUROSPORA.*

Neurospora macroconidia are thought to serve either as airborne male gametes, or as an efficient method to colonise a substrate rapidly through clonal reproduction, or both. The role EAS plays in these activities appears to be restricted to coating the conidia and the conidiophores because there are no reports of EAS being expressed by *Neurospora* in any circumstance not related to conidiation (Perkins and Turner, 1988; Pandit and Maheshwari, 1996; Bell-Pedersen, 2000; Davis, 2000). Consequently, it is surprising to find the *eas* gene, intact (as far as could be determined), in the aconidiate homothallic species.

This is interesting from both the evolutionary and taxonomic points of view. Cleary the gene is ubiquitous in the genus, suggesting that it predates the evolution of the homothallic species from their (probably) heterothallic ancestor (Pöggeler, 1999). As described in section 1.0.4.2, Dettman *et al.* (2001) strongly argued that members of the *Gelasinospora* genus were so closely related to the homothallic *Neurospora* that the previous criteria for separating the two genera were invalid. This may mean that *eas* is present in species from related genera and that this gene could be useful to

investigators attempting to clarify the taxonomy of the Sordariaceae (Dettman *et al.*, 2001).

It is interesting to note that both aconidiate heterothallic *Gelasinospora* species and of conidiating homothallic *Coniochaeta* and *Cochliobolus* species exist; suggesting that homothallism and conidiation are independent traits (Yun *et al.*, 1999; Raju and Perkins, 2000; Dettman *et al.*, 2001). Thus it is quite possible that conidiating homothallic *Neurospora* exist, but may have been overlooked by Perkins' study which focused only on coloured, conidiating colonies (homothallic *Neurospora* lack carotenoids) (Perkins and Turner, 1988).

I attempted to determine whether *eas* was active and in use in some other capacity by homothallic *Neurospora*. The mycelium of each species was not wettable but I could not extract EAS from them, and nor could I detect transcription of the gene. This strongly suggests that the gene is inactive in these species, especially considering that the RT-PCR technique was sensitive enough to detect the latent transcription of eas in *N. toroi* – which could not be induced to conidiate in my hands.

Given that the gene appears inactive in the homothallic species, the question is what event inactivated these genes and when? The presence of so few mutations in the homothallic versions of *eas* (relative to *N. crassa eas*) indicates that a short time period that has past since these species lost the ability to express *eas*. The number of mutations in the homothallic *eas*-genes is not constant. Comparisons of the sequences obtained in this study show that *N. lineolata eas* is the most divergent gene while *N. pannonica* possesses a version of *eas* identical (as far as could be determined) to the active gene found in *N. intermedia* (Figure 27 and personal communication with Dr. Elena Hilario – Hort Research). Note that the origin of the genomic DNA that yielded the *N. lineolata* and *N. pannonica eas*-genes sequences was confirmed by PCR analysis (section 2.2.3). A ITS/5.8S rRNA sequence was obtained from each extract and compared with those obtained by Dettman *et al.* (2001) (see Appendices IIIA and IIIB for the sequence comparison). Together this evidence suggests that the event that robbed the homothallic species of their ability to express *eas* has occurred multiple times.

When considering how the homothallic genes were inactivated, the inherent redundancy in the complex mechanism that controls *N. crassa eas* expression needs to be considered. The *Negative Developmental Element* (NDE) is responsible for the suppression of *eas* transcription in vegetatively growing mycelium and in both

juvenile and mature conidia. The inability of the *N. crassa eas* mutant to produce EAS is caused by the *cya-8* gene interrupting this strain's NDE. Despite this, latent transcription of *eas* induced by signals from the circadian clock can still be detected in this mutant (see Figure 30; Bell-Pedersen *et al.,* 1992, 1996; Lauter *et al.,* 1992).

In the model proposed by Correa and Bell-Pedersen (2002), each exogenous regulatory cue acts to enhance the basal rhythmic conidiation and thus expression of *eas*. Yet we could not detect latent expression of the gene in the homothallic species. It is possible therefore that the inability of homothallic *Neurospora* to express *eas* may be linked to their inability to conidiate.

It is also possible that the circadian clock is defective in these species. Raju (1981) reported that perithecium development in *N. africana*, *N. dodgei*, *N. galapagosensis,* and *N. lineolata* was drastically reduced when these species are grown in permanent darkness or permanent illumination. Such sensitivity could be caused by a deficiency in circadian clock. Thus, it would be interesting to see if the *activated clock element* (ACE), responsible for the basal rhythmic expression of EAS in seen *N. crassa*, and the transcription factors that bind to it are present in the homothallic species (Bell-Pedersen *et al.,* 1996; Correa and Bell-Pedersen, 2002).

3.6 Summary of Results.

The aim of this investigation was to identify regions of conserved amino-acid sequence that might be vital to the functions of EAS. The results – from the structural perspective – were inconclusive due to the high degree of similarity between the genes and proteins isolated. This degree of similarity is consistent with the evolutionary trends determined in previous phylogenetic studies; the *eas* genes and EAS proteins present in each heterothallic *Neurospora* species are virtually identical because the heterothallic species are closely related. Surprisingly, versions of the gene exist in the homothallic species. Neither the production of the protein nor the transcription of the gene could be detected in these species, leading us to conclude that the gene is inactive despite our inability to pinpoint the genetic reason. Interestingly, the gene is surprisingly well preserved relative to the active forms of *eas* in the non-homothallic species, this despite the absence – in the aconidiate homothallic species – of any selective pressure to resist mutations detrimental to the function of EAS.

The taxonomic and evolutionary implications of these findings are worthy of further investigation and in the discussion, I highlighted some of the questions that might be posed. Unfortunately, answering these questions is beyond the scope of this thesis.

4

HETEROLOGOUS EXPRESSION OF EAS.

4.0 INTRODUCTION.

How does the amino-acid sequence affect the structure and the spontaneous self-assembly of hydrophobins? Answering this question would be simplified if an easy means of expressing modified versions of a hydrophobin could be developed. Such was the aim of the experiments described in this chapter.

Two strategies for expressing hydrophobin proteins have been pursued previously. Firstly, hydrophobins have been expressed in *E. coli* as fusion proteins; this normally has the affect of increasing the stability of the recombinant protein and ensuring that it remains soluble (Bolyard and Sticklen, 1992; Nakari-Setälä *et al.,* 1996). This approach simplifies protein purification but means that the fusion protein must be removed prior to structural studies. It also means that the disulfide bonds can only be formed if the protein is expressed in the bacterial periplasm (Makrides, 1996).

The second approach has been to express the protein either in the native fungal host or in a near relative (e.g. cerato-ulmin: Del Sorbo *et al.,* 2000; HFB1: Askolin *et al.,* 2001; SC3: Scholtmeijer *et al.,* 2002). Nevertheless, the effectiveness of this approach depends on the species of fungi. At least two problems must be overcome in these kinds of experiments:

(1) Hydrophobin null-mutants of the species must be created – the complexity of this task varies between species. For example: the expression of both the native and the modified versions of SC3 in monokaryonic *Schizophyllum commune* worked because the host's other endogenous hydrophobins (SC1, SC4 and SC6) are only expressed when *S. commune* enters its the dikaryonic life stage (Scholtmeijer *et al.,* 2002). By contrast, *Cladosporium fulvum* contains six hydrophobins and at least two of these must be knocked out before a *C. fulvum* can be used as an expression host (Whiteford and Spanu, 2002); the assumption being that *C. fulvum* has only six hydrophobins.

(2) Both the recombinant and the reporter genes must evade the various forms of gene-silencing phenomena which occur in fungi, some of which have only been characterised recently (Schuren and Wessels, 1994; Schuurs *et al.,* 1997; Lugones *et al.,* 1999b; Scholtmeijer *et al.,* 2001). For instance, Lugones *et al.* (1999b) and Scholtmeijer *et al.* (2001) determined that the accumulation of full-length, transcripts was dependent on the presence of an intron in the heterologous gene, as well as the absence of any AT-rich regions. EAS has been successfully expressed in *N. crassa* during promoter and phenotype-

rescue studies (Lauter *et al.,* 1992; Bell-Pedersen *et al.,* 1992; Kaldenhoff and Russo, 1993). However, *N. crassa* is far from the ideal expression host - DNA-mediated transformation in this species is usually ectopic, resulting from non-homologous recombination of circular DNA into the chromosome (Vollmer and Yanofsky, 1986). Current protocols for DNA-mediated transformation in *N. crassa* utilise multinucleate macroconidia that yield low numbers of heterokaryotic transformants (Ebbole and Sachs, 1990; Maheshwari, 1999). Any attempt to purify transformed nuclei via the sexual cycle runs the gauntlet of the *repeat induced point mutation* (RIP) phenomena: a gene-silencing mechanism that acts to inactivate duplicated genes. Additionally, if *N. crassa* was used as a host then the complications arising from the N-terminal processing of EAS (discussed in the previous chapter) could not be easily avoided.

By contrast, the yeast *Pichia pastoris* is an attractive alternative host for expressing hydrophobins. Hydrophobins have never been detected in yeasts and, further, the eukaryotic *P. pastoris* combines ease of manipulation and culturing with the ability to incorporate eukaryotic post-transcriptional modifications such as proteolytic processing, folding, disulfide bond formation, and O- or N-linked glycosylation (Higgins and Cregg, 1998a). In this species, DNA-mediated transformation occurs by homologous recombination, which allows the specific integration of the gene in order to avoid positional gene-silencing effects can occur with ectopically integrated genes (Higgins and Cregg, 1998a).

For these reasons, *P. pastoris* was selected as the host for the eukaryotic expression of EAS. At the same time, the opportunity was taken to express EAS natively in *E. coli.*

4.1 Construction of Expression Vectors.

4.1.1 Constructing a Vector to Express EAS in *P. pastoris.*

In *P. pastoris* heterologous proteins can be expressed either intracellularly or extracellularly (secreted into the media). The latter approach was attractive for two reasons:

(1) EAS is secreted by its natural host *in vivo*, meaning that it is naturally an extracellular protein.

(2) Purifying secreted heterologous proteins from *Pichia* is simplified by the use of defined growth media, and by the fact that *P. pastoris* naturally excretes minimal amounts of protein.

This expression strategy required that the expression vector p9KEASF1 be constructed by ligating the 984 bp (*Sst* I$_{209\ bp}$–*Xho* I$_{1193\ bp}$) and 8,262 bp (*Eco* RI$_{1223\ bp}$–*Sst* I$_{209\ bp}$) arms of the pPIC9K to a 261 bp cDNA (*Xho* I$_{5\ bp}$–*Eco* RI$_{266\ bp}$) encoding EAS isoform I (see Figure 31 and section 2.2.6.5).

FIGURE 31: CREATING THE PP9KEASF1 EXPRESSION VECTOR.

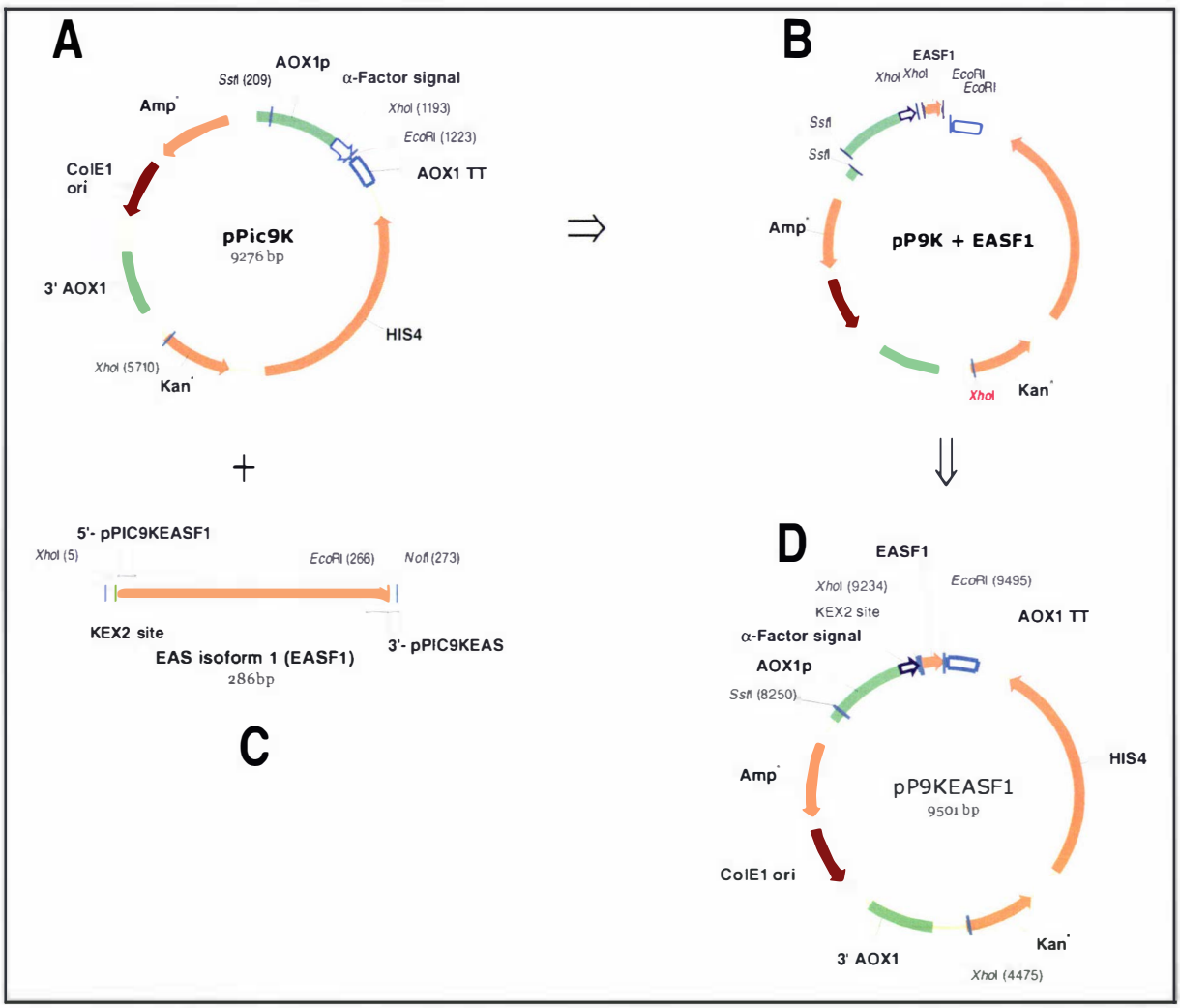

The steps used to create of the pPIC9KEASF1 expression vector are shown in Figure 31. The cDNA encoding the EAS gene was ligated (sequence C inserted is shown here being cloned into plasmid B) into the pPIC9K plasmid (plasmid A). The 3-way ligation strategy described in the text was used to create p9KEASF1 (plasmid D) which was intended to allow the secreted expression of EAS isoform I in *P. pastoris*. **Key to abbreviations:** The expression vector pPIC9K (pP9K) supplied by Invitrogen™ comprises **(1)** an E. coli origin of replication (Col E1) and Ampicillin (Amp^R) resistance genes to aid manipulations in *E. coli*. **(2)** A Kanamycin (Kan^R) resistance gene to confer G418-resistance to *P. pastoris*. **(3)** The *Pichia* histidinol dehydrogenase gene (HIS4) for selection of recombinant *Pichia* strains. **(4)** Three separate portions of the *Pichia* Alcohol oxidase 1 (AOX1) gene. The AOX1 promoter (AOX1p), transcriptional terminator, and polyadenylation-signal regions (AOX1 TT) serve as control elements allowing methanol-inducible expression of the foreign gene. **(5)** The 3' AOX1 and 5' AOX1 (AOX1p) regions of the AOX1 gene direct the targeted homologous recombination of the expression cassette into the *P. pastoris* genome. **(6)** A secretion signal peptide (α-factor signal) along with the protease cleavage site (KEX2) was added to the N-terminus of the recombinant protein to permit its secretion by *P. pastoris*. **(7)** The cDNA encoding the EAS isoform I (EASF1) was synthetised by RT-PCR using the PCR primers 5'-pPIC9KEASF1 and 3'-pPIC9KEAS described in Figure 33. **(8)** In this diagram, the position of nucleotide 1 of the plasmid DNA sequence is located at the top (0°). The locations of restriction enzyme cleavage sites are indicated as a distance (in bp) from this nucleotide.

The pPIC9K plasmid comprises the *Saccharomyces cerevisiae* α-factor secretion leader sequence with an *Xho* I site just 5' to a cleavage site for the protease KEX2 (Figure 31 and Figure 32). This secretion signal must be fused to the N-terminus of

the recombinant protein. The KEX2 cleaves the peptide bond to the C-terminus of the arginine residue in the sequence: Glu-Lys-Arg-↕-X, where "↕" denotes the site of cleavage and X any amino acid other than proline.

FIGURE 32: EASF1 FUSION PROTEIN AND GENE SEQUENCE.

The gene and protein sequences of the AOX1 promoter region and multi-cloning site in pPIC9K and its derivative pPIC9EASF1 are shown in Figure 32. The numbers in the margins refer to the position of each nucleotide in the plasmid sequence as compiled using the Vector NTI 8 program. **Nucleotide colour key**: Nucleotides not contributing to the EAS cDNA sequence are coloured grey. Nucleotides encoding restriction enzyme cleavage sites are underlined. The positions of the PCR primers described in Figure 33 are indicated with horizontal arrows. **Amino acid colour key:** The sequence of EAS isoform I is coloured black, while the sequence of the *S. cerevisiae* α-factor secretion signal peptide is coloured blue. The Kex2 protease cleavage site is coloured red and the site of cleavage is indicated with a downward arrow.

FIGURE 33: PCR PRIMERS USED TO AMPLIFY EAS FOR CLONING INTO PPIC9K.

The PCR oligonucleotide primers used to synthetize EAS cDNA are shown in Figure 33; genetic features that permit plasmids derived from these primers to be used in the pPIC9K *P. pastoris* expression are highlighted. **Key:** Nucleotides and amino acids that don't contribute to either EAS cDNA or the mature EASF1 protein are coloured grey. The amino acid sequence of EAS isoform I is coloured black, while the EAS cDNA nucleotide sequence is coloured. Nucleotides encoding restriction enzyme sites are underlined. Amino acids encoding the Kex2 cleavage site are coloured red, with the site of cleavage indicated with an upward arrow.

A complete cDNA encoding the EAS isoform I was synthesized by RT-PCR (section 2.2.3) using the oligonucleotide primers described in Figure 33. A 5' *Xho* I site and a 3' *Eco*R I site were incorporated into the cDNA to allow it to be inserted near the KEX2 site, with only an alanine residue adjacent to the site of cleavage (Figure 32). Accordingly, the proteolytic removal of the signal peptide fusion should generate a version of the EAS isoform Ia identical to that expressed by *N. crassa.*

Unfortunately, the *Xho* $I_{1193\ bp}$ site is not unique in pPIC9K, so I had to use the three-way ligation protocol described at the outset to construct pPIC9EASF1. This method was successful but inefficient, yielding only two ampicillin-resistant *E. coli* isolates. I used DNA-sequencing to prove that the plasmids these recombinant isolates carried were, in fact, pP9KEASF1. The DNA-sequence of part of the pP9KEASF1 is shown in Figure 32.

4.1.2 Construction of a Vector to Express EAS in *E. coli*.

Strategies for expressing cysteine-rich eukaryotic proteins in *E. coli* usually involve expressing the recombinant protein in the periplasmic space, where the oxidising environment and the presence of certain enzymes both serve to aid protein disulfide-bonds to form. By contrast, the cytoplasm is a reducing environment that contains a larger number of proteases. Novagen® has introduced two *E. coli* strains: AD494 and Origami™ to address the former deficiency. AD494 is deficient in thioredoxin reductase (*trxB*) and Origami™ is deficient in *trxB* and glutathione reductase (*gor*). These enzymes are responsible for maintaining the reducing potential of the cytoplasm - their deletion has aided the formation of disulfide bonds in the recombinant proteins expressed in that compartment. By using these strains, we sought to natively express EAS in the cytoplasm of *E. coli.*

Complementary DNA sequences (cDNAs) encoding both EAS isoforms were ligated into the prokaryotic expression vector pKK223-3 between the *Eco* $RI_{4583\ bp}$ and *Pst* $I_{25\ bp}$ sites to create plasmids called pKKEASF1 and pKKEASF2 (Figure 34). The cDNAs were synthesized by RT-PCR using a 5' PCR primer that incorporated an *Eco*R I restriction site and a start codon (ATG) to the 5' end of the PCR product. The 3' PCR primer added a *Pst* I restriction site to the 3' end (see Figure 35 and section 2.2.3). This design permitted the cDNAs to be incorporated 10 bp downstream of pKK223-3's ribosome binding site, thus enabling the recombinant gene to be controlled by the plasmid's *tac* promoter (Figure 36). The sequence of the pKKEASF1 expression vectors is shown in Figure 36; the sequence of pKKEASF2 lacks the nucleotides encoding the Ala_1–Thr_2–Thr_3 tripeptide in EAS isoform I.

FIGURE 34: CREATING THE PPKK223EAS EXPRESSION VECTORS.

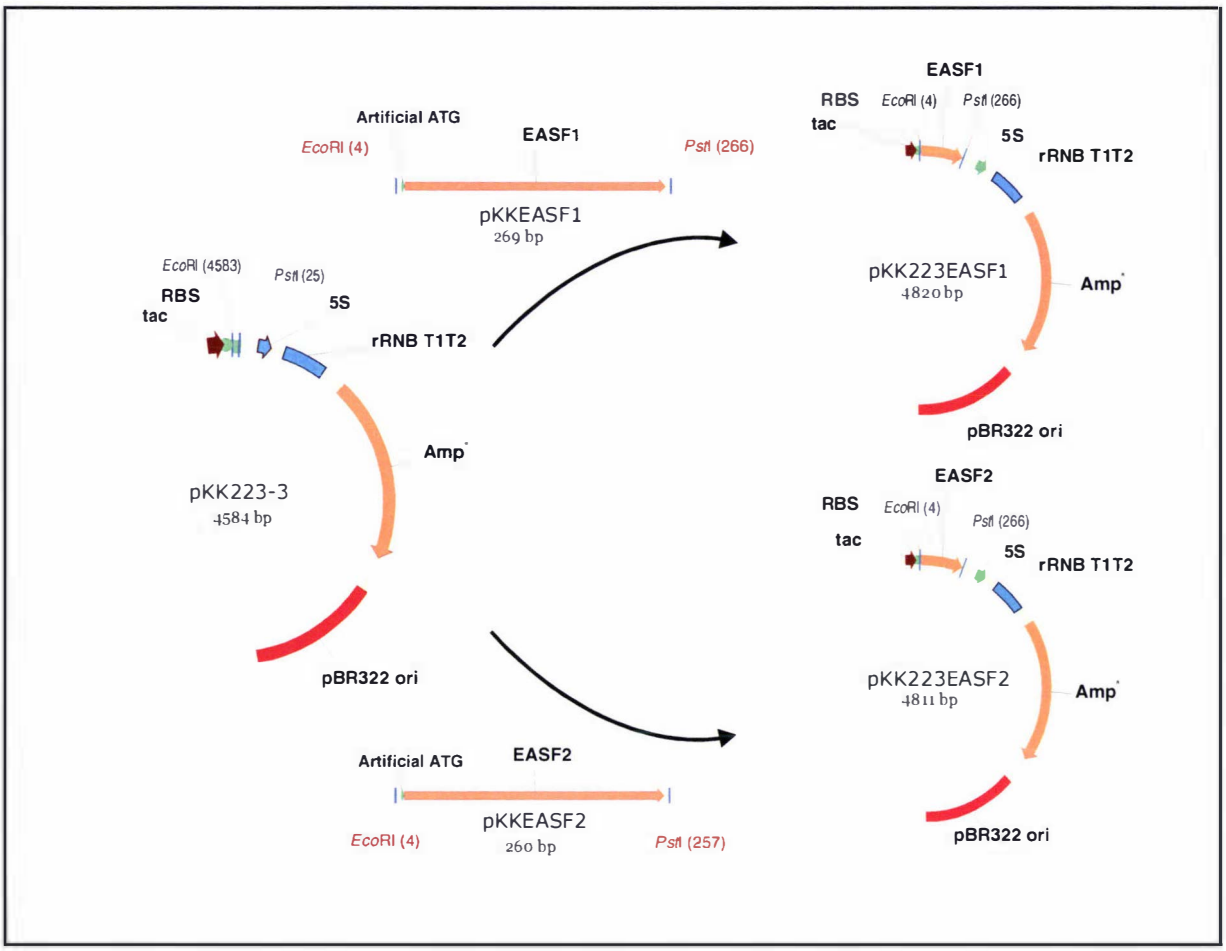

The steps in the creation of the *E. coli* expression vectors pKK223EASF1 and pKK223EASF2 are shown in Figure 34. The cDNA encoding the each EAS isoform was synthesized by RT-PCR using appropriate 5'pKKEAS PCR primers and the 3' PCR primer 3'-pKKEAS (see Figure 35). In this diagram, the position of nucleotide 1 of the plasmid DNA sequence is located at the top (0°). The locations of restriction enzyme cleavage sites are indicated as a distance (in bp) from this nucleotide. **Key to abbreviations:** The expression vector pKK223-3 supplied by AP-Biotech comprises of: **(1)** An E. coli origin of replication (pBR322 ori) ensuring 15-20 copies of the plasmid are produced per cell. The Ampicillin (Amp^R) resistance gene is used as a selectable marker. **(2)** The strong synthetic *tac* transcription promoter including the –35 and –10 regions depicted in Figure 36 precedes the ribosome binding site (RBS) and the multi-cloning site (MCS) incorporating the unique *Eco*R I_{4583} and *Pst* I_{25} restriction sites. **(3)** Part of the *rrnB* operon follows the MCS, including the 5S rRNA region (5S) and the tandem transcription terminators T1 and T2 (rRNB T1T2). **(4)** The pBR322 based origin of replication (pBR322 ori) ensures that between 15-20 copies of the plasmid are produced per cell while the Ampicillin is used as a selectable marker and Ampicillin (Amp^R) resistance genes to assist manipulations in *E. coli*.

FIGURE 35: PCR PRIMERS.

	EcoR I			
5'- pKKEASF1	GGAATTCATG	GCCACCACC	ATCGGCCCC	AAC.....
5'- pKKEASF2	GGAATTCATG	.....	ATCGGCCCC	AACACCTGC
	Start	AlaThrThr	IleGlyPro	AsnThrCys
			PstI	
3'- PKKEAS	GCCAACTGC	GTTGCCTAA	CTGCAGTT	
	AlaAsnCys	ValAla**Stop**		

The design of PCR oligonucleotide primers used to synthetize EAS cDNA for the pKK223EAS series of expression vectors is shown in Figure 35; genetic elements that allow these cDNA to be ligated into the *E. coli* pKK223-3 expression vector are also highlighted. **Key:** Nucleotides and amino acids that don't contribute to either EAS cDNA or the mature EASF1 protein are coloured grey. The amino acid sequences of each isoform of EAS are coloured black, while the EAS cDNA nucleotide sequence is coloured. Nucleotides encoding restriction enzyme sites are underlined.

FIGURE 36: PKKEAS SEQUENCE.

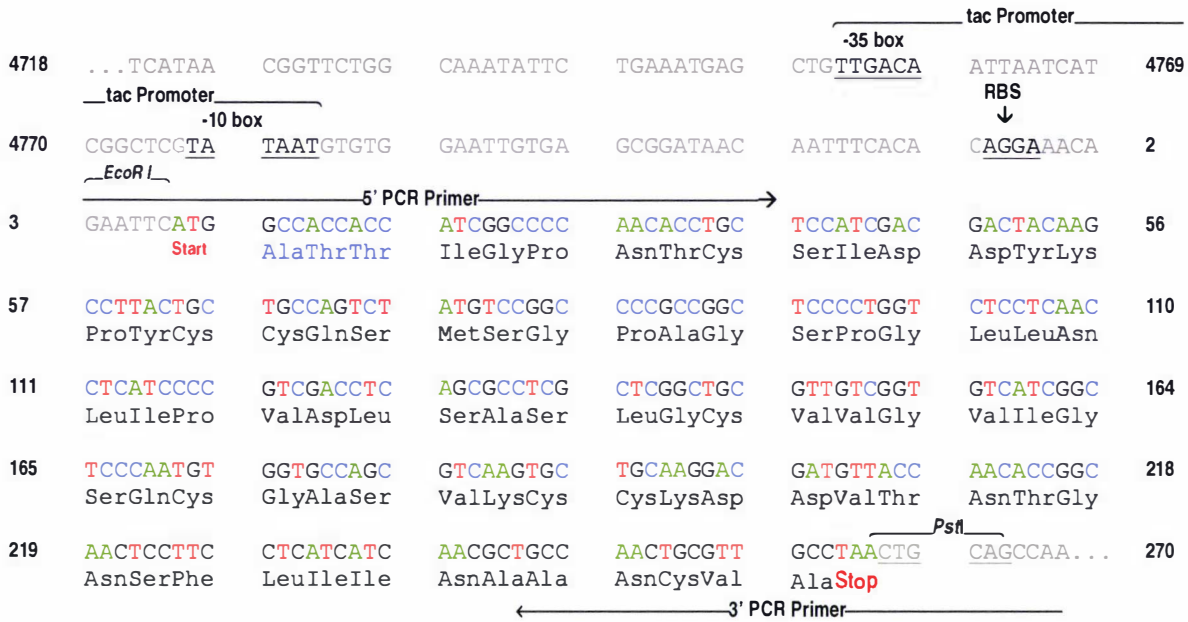

The genetic sequence of the *tac* promoter region and multi-cloning site in pKK223-3 - and its derivative pKKEASF1 - are shown in Figure 36. The numbers in the margins refer to the position of each nucleotide in the pKKEASF1 sequence as compiled using the Vector NTI 8 program. **Nucleotide colour key**: Nucleotides that do not contribute to the EAS cDNA sequence are coloured grey. Key nucleotides of the *tac* promoter (-35 and –10 Pribnow boxes) and the Ribosome binding site are coloured black and underlined. Nucleotides encoding restriction enzyme cleavage sites are underlined. The extent of the *tac* promoter and the positions of the PCR primers, described in Figure 35, are indicated with horizontal arrows. **Amino acid colour key:** The sequence of EAS isoform II is coloured black, while the additional residues added found in EAS isoform I are coloured blue.

4.2 EXPRESSION OF EAS IN *P. PASTORIS*.

4.2.1 GENERATION AND SCREENING RECOMBINANT STRAINS.

In *P. pastoris*, stable transformants are created via homologous recombination between the linear transforming DNA and homologous regions within the genome (Higgins and Cregg, 1998a). *P. pastoris* strains GS115 and SMD1168 (both histidine auxotrophs) were transformed with a version of the pPIC9EASF1 expression vector that had been linearised by digestion with either *Sst* I or *Bgl* II (section 2.2.6.3). Digesting pPIC9EASF1 with *Sst* I ensures that it will be inserted, by a single crossover event, into the 5' region of the endogenous copy of the AOX1 gene.

In *Pichia,* the copy-number of the transfected gene has often been shown to affect the yield of expressed protein. Linearising the plasmid with *Bgl* II can cause the transfected gene to replace the genomic copy of AOX1. This strategy is known to generate a higher proportion of His^+ transformants possessing multiple copies of the inserted gene (Romanos *et al.*, 1998).

The linearised vectors were electro-transformed into the *P. pastoris* strains GS115 and SMD1168 as described in section 2.2.6.3. The latter strain was included because it lacks Proteinase A (a vacuolar aspartyl-protease), and it served to

illustrate the effect of proteolysis – due to cell-lysis during batch-culturing – on the yield of recombinant EAS (Gleeson *et al.,* 1998). This strain has been described as being protease-deficient in the literature. Without Proteinase A, the strain lacks one of the two enzymes (the other being Proteinase B) responsible for activating the majority of vacuole-based proteases (van den Hazel *et al.* 1996; Gleeson *et al.,* 1998). There is no evidence that this genetic modification has any-effect on the activity of the yeast's 26S proteosome.

A total of 832 His^+ *P. pastoris* transformants were obtained and screened to identify their methanol utilisation (Mut) phenotype (Romanos *et al.,* 1998; Invitrogen™, 2002). The transformation often inactivates the endogenous AOX1 gene, generating two classes of His^+ recombinant strains that differing in their ability to metabolise methanol: Mut^+ (methanol utilisation positive) strains are able to metabolise methanol at the same rate as wild type *P. pastoris,* while Mut^S (methanol utilisation slow) cannot. Particular Mut phenotypes have been shown to favour the expression of heterologous proteins; however, this must be determined empirically (Invitrogen™, 2002).

The nine His^+ recombinant strains described in Table 10 were selected as a representative sample of the recombinant population, and then screened for protein expression.

TABLE 10: *P. PASTORIS* RECOMBINANT STRAINS SELECTED FOR SCREENING.

Name	Strain transformed	Expected position of EAS gene in the recombinant genome.	Methanol Utilization Phenotype
4A1	*SMD1168*	*Inserted into the 5' AOX1 region.*	*Mut^+*
4B3	*SMD1168*	*Inserted into the 5' AOX1 region.*	*Mut^+*
4D3	*SMD1168*	*Inserted into the 5' AOX1 region.*	*Mut^+*
9B1	*SMD1168*	*Inserted into the 5' AOX1 region.*	*Mut^+*
10A3	*GS115*	*Replaces the endogenous AOX1 gene.*	*Mut^+*
10A4	*GS115*	*Replaces the endogenous AOX1 gene.*	*Mut^+*
12A1	*GS115*	*Inserted into the 5' AOX1 region.*	*Mut^S*
12A6	*GS115*	*Inserted into the 5' AOX1 region.*	*Mut^S*
12A11	*GS115*	*Inserted into the 5' AOX1 region.*	*Mut^S*

The characteristics of the nine recombinant *P. pastoris* strains screened for the ability to secrete EAS are listed in Table 10. **Note:** strain 9B1 (in Italics) was transformed with the pPIC9K plasmid and was used as a control to check the effect of the expression vector on protein expression.

Bgl II digested genomic DNA from each of the nine recombinant strains was subjected to Southern hybridisation analysis. The results are presented in Figure 37. The *HIS4*-specific probe hybridises with both the defective endogenous *his4* gene inherited from the host strain and with the fragment from pPIC9K containing *HIS4*

(Romanos *et al.*, 1998). In each sample, both bands have a similar intensity, which indicates that a single copy of the expression cassette is present in each recombinant (Romanos *et al.*, 1998).

Isolates 10A3, 10A4, and 10D2 (like the SMD1168 and the GS115 hosts) lack the 6.8 kb band, and therefore cannot contain the expression cassette (Figure 37B). Each of these was transformed with a *Bgl* II digested vector and their reversion to the His^+ phenotype is probably due to *his4* recombining with the plasmid-borne *HIS4* gene (Romanos *et al.*, 1998).

The 9B1 isolate – created by transforming SMD1168 with *Sst* I digested pPIC9K – was used to illustrate the contribution of the plasmid backbone to any protein expression pattern. Isolates 4B3 and 4D3 were transfected with pP9KEASF1. Both isolates contain the *HIS4*-fragment, but the inability of the *eas* probe to hybridise to their DNA indicates that these strains lack the recombinant gene (Figure 37B and C). Figure 37C indicates that only five (4A1, 12A1, 12A6, 12A11 and 12H12) of the selected nine isolates possess the recombinant version of *eas*.

FIGURE 37: SOUTHERN ANALYSIS OF *PICHIA* RECOMBINANTS.

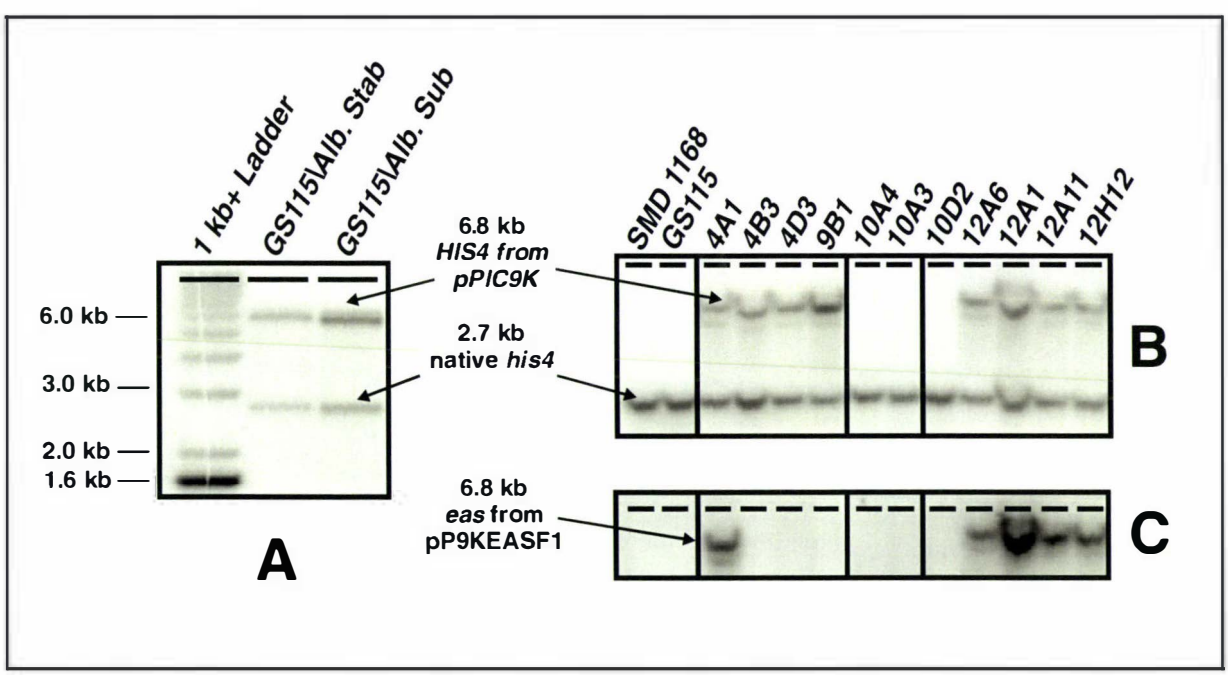

In Figure 37, the Southern analysis of (*Bgl* II-digested) genomic DNA extracted from recombinant *P. pastoris* isolates is shown. The digested DNA extracts shown in membrane A and membrane B were hybridised with a copy of the *P. pastoris HIS4* gene excised from the pPIC9K vector (described in section 2.2.7.1). The same DNA extracts in membrane B were later hybridised with a copy of the *eas* gene(described in section 2.2.7.1), the result of that experiment is shown in membrane C. DNA extracts in membrane A were obtained from *GS115/Alb*, a recombinant *P. pastoris* strain, supplied by Invitrogen™, that was used as a control during these protein secretion assays. When properly induced, this strain secretes Human albumin. A sample of Invitrogen's stab culture of this strain (lane labelled "GS115\Alb. stab") is compared to the subcultured stock (lane labelled "GS115\Alb. sub") used in these experiments.

4.2.2 THE RECOMBINANT *EAS*-GENE IS TRANSCRIBED.

Northern hybridisation analysis was used to assess the transcription of recombinant *eas* in isolates 12H12, 12A1, and 4A1. Total RNA was extracted from methanol-induced cultures during an 84-hour period (section 2.1.2.4). The results, displayed in Figure 38B, show that methanol induction does lead to the accumulation of stable full-length *eas* mRNA (~820 bp) for a period of at least 48 hours in each isolate. Transcripts are accumulated over longer periods in isolates 4A1 (72 h) and 12H12 (84 h). No conclusions should be drawn from the fluctuations in the amounts of *eas* mRNA are evident in Figure 38B; these are likely to be due to a combination of two effects. I neglected to equalise the concentration of total RNA varies between lanes (the intensity of the rRNA bands varies widely in the electrophoresis gel shown in Figure 38A) and this will affect the intensity of the bands in Figure 38B – the fact that *eas* mRNA is present is not in doubt.

FIGURE 38: NORTHERN ANALYSIS OF *PICHIA* RECOMBINANTS.

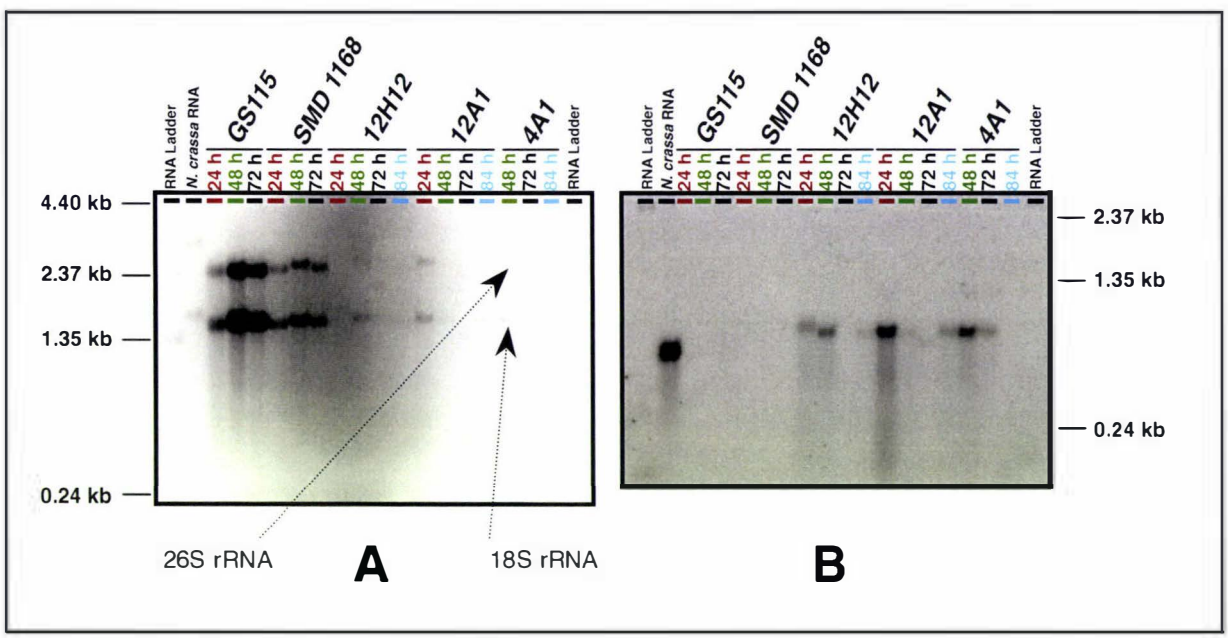

The isolates were screened, using Northern hybridisation analysis, for their ability to transcribe the recombinant *eas* gene. These results are reproduced in Figure 38. Figure 38A shows the electrophoretically separated total RNA extracts from each species prior to being blotted onto a Hybond XL membrane (described in section 2.2.7.2). Figure 38B shows the result of hybridising a radioactive DNA *eas*-probe and medium stringency washing. The probe has hybridised to the native *eas* transcripts (from the total RNA extracted from *N. crassa* to serve as a positive control) and recombinant *eas* transcripts from the three recombinant strains tested. Bell-Pedersen *et al.* 1992 estimated the size of native *N. crassa* eas transcripts to be 0.8 kb in size. The placement of the recombinant *eas* in the p9KEASF1 expression cassette should yield mRNA transcripts of approximately 820 bp in size with a Poly (A) tail adding an additional 60 to 90 bp (Invitrogen™, 2002; McCarthy, 1998).

Note that the level of transcript mRNA is expected to vary in batch-cultured *Pichia* samples. Methanol must be continually added to *Pichia* batch cultures in order to compensate for any methanol consumed as a carbon source, or lost through evaporation. Temporal variations in the addition of methanol can cause fluctuations in the level of induction. This is a recognised drawback of the batch-culture

technique, and optimal heterologous protein in *Pichia* is normally obtained when fermentation culture techniques are used (Tuite *et al.,* 1999).

4.2.3 Screening for Successful Secretion of EAS.

The ability of isolates 12A1, 12A11, and 4A1 to express EAS was analysed by silver staining the proteins resolved by SDS-PAGE. Cell-free media samples from the low density (with a starting OD_{600} of ~ 1), methanol-induced, batch-cultures of each recombinant strain were taken over a five-day period, and then compared with similar samples obtained from strains 9B1, SMD1168, and GS115/Alb that were grown under similar conditions (Figure 39).

Ideally, heterologous proteins secreted by methanol-induced, recombinant *P. pastoris* should accumulate in the culture media to levels equivalent to those seen when human serum albumin is secreted by the GS115/Alb recombinant strain supplied by Invitrogen™ (Figure 39A). Results shown in Figure 39A indicate that none of the recombinants secrete any unique soluble proteins into their culture media.

As recommended in Invitrogen™ (2002), the assay was repeated with denser cultures (starting OD_{600} of ~ 10) to see whether increasing the number of protein-secreting cells increased the yield. This strategy increased the overall protein content in the media of the recombinant cultures, but none of the proteins detected are unique when compared to the proteins expressed by the untransformed SMD1168 strain (Figure 39B).

Pichia cannot utilise methanol under anaerobic conditions, and so throughout these assays cultures were vigorously shaken in baffled flasks to ensure effective aeration. However, even slight agitation can induce EAS to polymerise (Mackay *et al.,* 2001); therefore, there was a possibility that recombinant EAS was present as an insoluble component of cell-free media.

This possibility was investigated by collecting the culture-media's insoluble components by centrifugation and treating them with TFA. Any TFA-soluble components were then examined by RP-HPLC or by SDS-PAGE (described in section 2.4.3). I used SDS-PAGE to compare the insoluble proteins produced by the 12A1 isolate to those produced by GS115 and SMD1168. As Figure 39C clearly demonstrates, 12A1 does produce a protein less than 10 kDa in size, but it is not unique to the recombinant isolate and is also produced by the untransformed host strains (SMD1168 and GS115).

FIGURE 39: ANALYSIS OF PROTEINS SECRETED BY RECOMBINANT *P. PASTORIS* STRAINS.

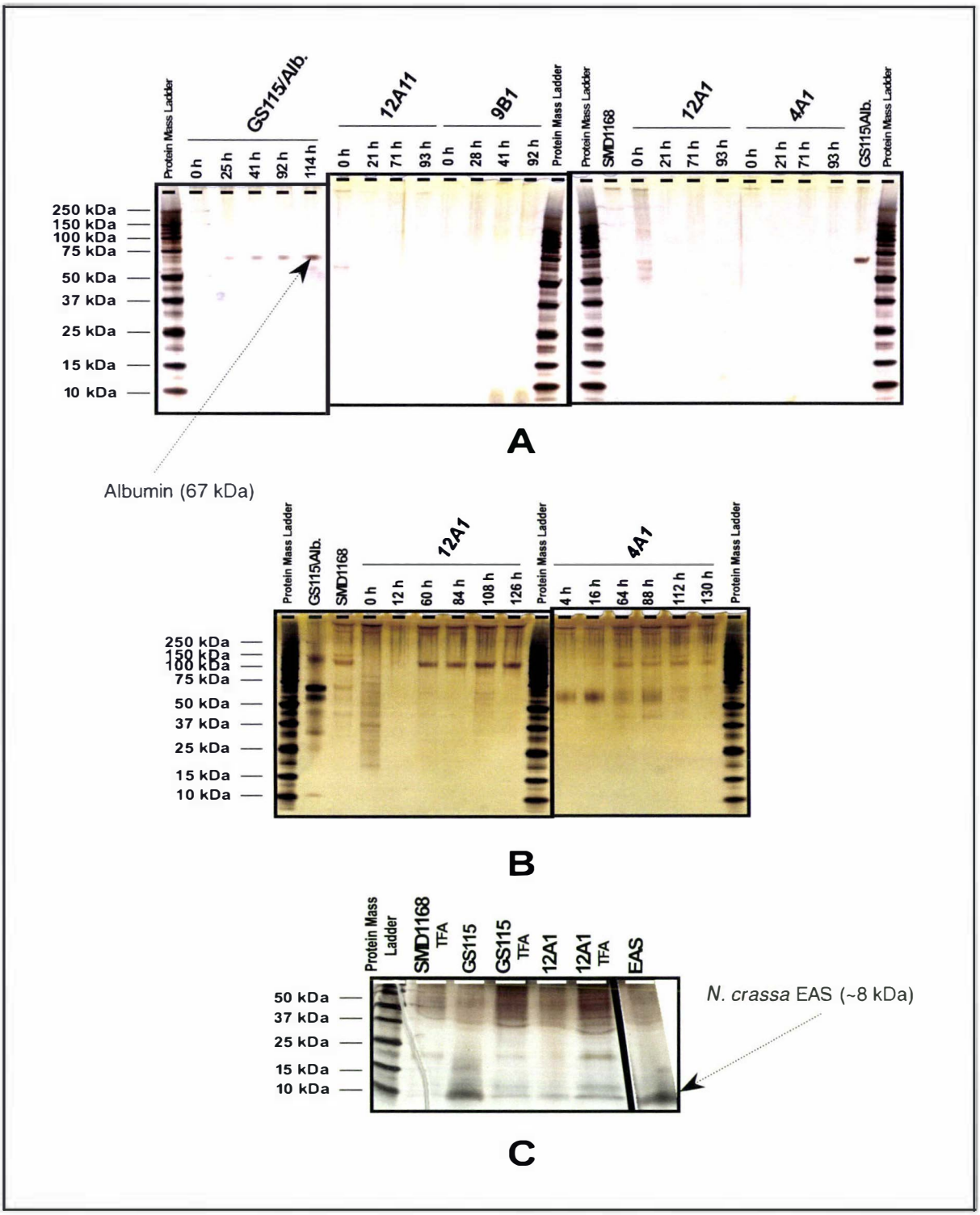

SDS-PAGE analysis was used to screen recombinant *P. pastoris* isolates (4A1, 12A11 and 12A1) and two untransformed strains for their ability to secrete recombinant EAS. The results are shown in Figure 39: **Key: (1)** SMD1168 is an untransformed strain used to illustrate the background secretion. **(2)** 9B1 is a recombinant isolate transformed with pPIC9K to help identify any proteins by elements in the pPIC9K backbone. **(3)** GS115/Alb is an albumin-secreting recombinant strain used to confirm whether protein expression was properly induced in these strains. Samples of the culture media obtained during a 5 day long methanol-induced, batch-culture assay were collected at the times indicated, and 25 µL of each were analysed with a combination of SDS-PAGE and Silver staining (section 2.4.6.2). Figure 39A shows the results obtained with the low cell-density assay (starting culture had a density of OD_{600} ~ 1 prior to the start of this assay) while Figure 39B illustrates the results of the high cell-density assay (starting culture had a density OD_{600} of ~ 10 prior to the start of this assay). SDS-PAGE comparison of proteins present in concentrated growth media is shown in Figure 39C. In this gel, some of samples were prepared from TFA-treated insoluble components of the concentrated growth media (labelled TFA) and while the rest prepared from concentrated the growth media supernatant obtained after the isolates were grown in inducing conditions for 5 days (preparation is described in section 2.4.3.1).

A similar outcome was obtained when extracts from isolates 4A1 and 12A11 were analysed with the same RP-HPLC screening strategy used in section 3.4.2 (procedure described in section 2.4.3, results reproduced in Appendix IV).

The conclusion to be drawn from these experiments is that none of the recombinant isolates are secreting unique sub-ten kilo Dalton proteins into their culture media in sufficient concentration to be detected by the silver-staining technique. Nor was the protein rapidly polymerising as it was secreted. Neither the isolates Mut phenotype nor an increase in the biomass of the induced culture had any detectable effect on the production of recombinant EAS. This means that none of the isolates was able to secrete recombinant EAS at concentrations higher than 2 µg/L of culture (assuming that the sensitivity of silver staining is 5 ng/band) if they were secreting the protein at all.

4.2.4 Screening the Intracellular Protein Fractions.

Figure 40: Analysis of Proteins Produced Internally by Recombinant *P. pastoris*.

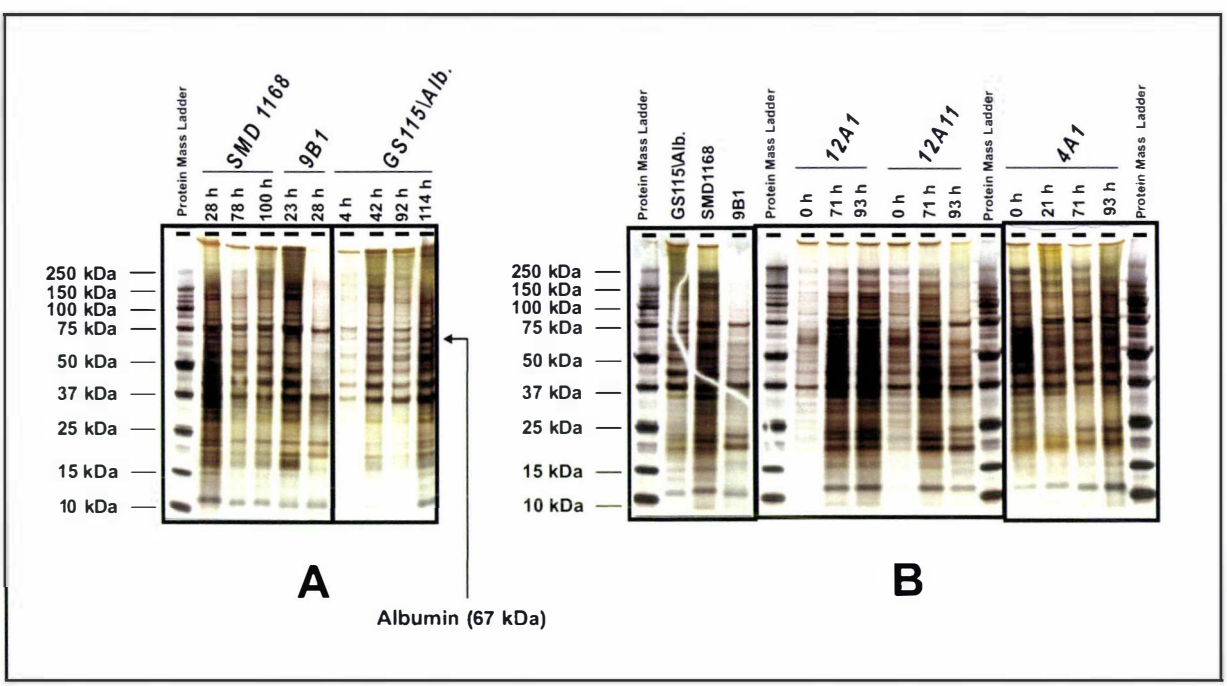

SDS-PAGE analysis of the intracellular protein fractions (cell lysates) of the recombinant isolates is shown in Figure 40. Samples are arranged to show the fluctuation in the internal protein population during the course of a 5-days induced growth. Figure 40A compares the protein populations present in the control strains: **(1)** untransformed SMD1168; **(2)** 9B1 transformed with pPIC9K to illustrate proteins produced by the other components of the expression cassette; **(3)** GS115/Alb, an albumin secreting recombinant strain used in secretion assays to confirm that reliable induction of protein expression occurred. Figure 40B compares the protein populations present in the control strains 4A1, 12A11 and 12A1. Yeast Cells were collected, disrupted and the lysate analysed as described in section 2.4.3.2 and Invitrogen™ (2002).

To determine whether recombinant EAS was accumulating in the cytoplasm of the isolates, the proteins present their cell lysates were examined by SDS-PAGE (section 2.4.3.2). The intracellular accumulation of albumin can be seen in the cell lysates from strain GS115/Alb (Figure 40A), but none of the p9KEASF1 transformed

isolates produce either a unique sub-ten kilodalton (without signal peptide removed) or a unique 17 kDa proteins (with the signal peptide). Each protein produced by the recombinants is also present in the cell lysate samples from the control strains: SMD1168 and 9B1 (Figure 40B).

4.2.5 Discussion – *P. pastoris* Expression.

EAS was not expressed either internally or externally by any of the recombinant *Pichia* isolates tested. This was in spite of their ability to produce full length EAS mRNA when induced with methanol.

Figure 41: Recombinant EAS mRNA Produced by the p9KEASF1 Expression Cassette.

Figure 41 illustrates the nucleotide sequence of recombinant *eas* mRNA (minus the poly (A) tail) that should be produced by isolates transformed with the p9KEASF1 expression cassette. **Key:** pairs of inverted repeats that are capable of base pairing are shaded in blue and grey. Residues that are encoded by rarely used *P. pastoris* codons are coloured. Pink residues are encoded by codons used in less than 10 times per 1000 codons, while dark-red residues are used less than 5 times per 1000 codons (Nakamura *et al.*, 2000). The position of the KEX2 protease site marking the start of the *eas* cDNA is marked with an arrow.

It is unlikely that the expression of EAS was affected by proteolysis while the transfected *Pichia* were cultured or while the protein samples were being extracted. Otherwise EAS would have been expressed by the "protease-deficient" 4A1 isolate.

Had EAS been correctly translated and exported there is good reason to believe that it would have been detected by SDS-PAGE analysis. The p9KEASF1 expression cassette did not contain the optimal KEX2 recognition site. In *S. cerevisiae*, KEX2 mediated cleavage is more efficient if the expressed-protein's cleavage site is followed by Glu-Ala repeats (Invitrogen™, 2002). Nevertheless, this is unlikely to have contributed to the isolates' inability to express EAS, since the Glu-Ala repeats are not necessary for KEX2 activity. Additionally, Sreekrishna *et al.* (1997) noted that the failure to remove the pro-peptide portion of the α-factor secretion signal from the *Brain-derived Neurotrophic Factor* did not affect the ability of the recombinant *P. pastoris* host to secrete the protein.

This suggests either that EAS was not translated properly or that it did not fold correctly and subsequently was degraded by the proteosome.

4.2.5.1 Factors Influencing the Translation of Transgenic EAS.

As currently designed, the p9KEASF1 expression cassette contains three pairs of inverted repeats (Figure 41). Complimentary base pairing between these pairs has the potential to introduce additional stem-loop secondary structures into transcripts of the cassette, but their effect on translation is likely to be trivial in that the resulting stem-loop would possess a thermodynamic stability of only –13.6 kcal.mol^{-1}. The translation apparatus of yeasts has been shown capable of untangling RNA loops with a thermodynamic stability between –28 and -50 kcal.mol^{-1}, depending on the location relative to the start codon (reviewed in Tuite *et al.,* 1999; McCarthy, 1998). The *eas* cDNA sequence contains neither A+T rich regions nor an unflavoured stop codon; moreover, the presence of a guanosine nucleoside immediately after the UAA codon is known to aid efficient translation termination in yeast (reviewed in Sreekrishna *et al.,* 1997; McCarthy, 1998). Thus, these features are unlikely to be responsible for the recombinants' inability to express EAS.

Transcripts containing a number of rare codons or clusters of rare codons are often translated slowly or inefficiently, probably because the cognate tRNA molecules are in short supply. There are reports of transcripts containing rare codons that have adversely affected translation in *E. coli*: the incidents included reading-frame shifts, miss-incorporated amino acids, and the premature termination of translation. A similar state of affairs is expected to exist in yeasts (reviewed in Tuite *et al.,* 1999;

Kane, 1995; Kurland and Gallant, 1996). Optimising both the codon usage and the overall G+C content within a gene so as to suit *P. pastoris* can lead to a major increase (>20 fold) in the yield of expressed recombinant proteins, but the process is laborious (Outchkourov *et al.,* 2002; Sinclair and Choy, 2002; Woo *et al.,* 2002). Twenty-two amino acids in EAS are encoded by codons used infrequently (<1%) in *P. pastoris* genes - most of these are either close to or adjacent to one another (Table 11 and Figure 41). This clustering of rare codons probably has a greater impact than the presence of number of rare codons on their own. Opsin-1 (NOP-1), a 30 kDa (308 residues) *N. crassa* trans-membrane protein, contains twice the number of rare codons (see Table 11), but it was successfully expressed in the *P. pastoris* grown in batch culture yielding 2.2 mg protein/L. The rare codons in the *nop-1* expression cassette appear more evenly distributed than is the case in the *eas* expression cassette (Higgins and Cregg, 1998a; Bieszke *et al.,* 1999).

By using pPIC9K, I was afforded the opportunity to screen for transformants with multiple copies of the p9KEASF1 expression cassette. I choose not to investigate the effect of gene dosage on the expression of EAS because the effects of gene dosage on heterologous protein are unpredictable. In the cases where gene dosage has had a positive effect, the level of expression displayed by isolates with a single copy of the gene was high enough to allow the recombinant protein to be detected by Coommassie® staining. For example, the yield of tetanus-toxin fragment C from single-copy recombinants was 0.33% of the total cell protein (Sreekrishna *et al.,* 1997; Clare *et al.,* 1998). This is not the case with the recombinant isolates generated in this study, hence my decision not to investigate this effect in these isolates.

I believe that future attempts to express EAS in *P. pastoris* would benefit from efforts to optimise the codon usage within the gene and incorporate an epitope-tag at the proteins N-terminus. The latter would permit the use of Western blotting to measure the production of EAS, as well as simplifying trouble-shooting and the optimisation of fermenting conditions. Continuous fermentation reactors permit the *Pichia* growth and protein-induction conditions to be precisely controlled, thus they often deliver greater yields of heterologous protein than do batch-cultures (Higgins and Cregg, 1998a).

If the rare codons from the *eas* cDNA sequence are removed then the amount of EAS produced by recombinant *P. pastoris* isolates should increase. A further yield-increase could be gained by culturing the organisms in a continuous fermentation reactor.

TABLE 11: CODONS USED INFREQUENTLY BY *P. PASTORIS* PRESENT IN EAS CDNA.

CODON BIAS IN *EAS* CDNA.

Rare codons in the cDNA Sequence			Frequency that codon used in genomic genes. (per thousand codons)	
Total	Amino Acid	Codon	*N. crassa*	*P. pastoris*
7	Cysteine	UGC	8.8	4.6
1	Cysteine	UGU	4.6	8.4
6	Glycine	GGC	28.7	8.6
6	Leucine	CUC	27.1	6.9
2	Proline	CCC	22.0	6.9

CODON BIAS IN *NOP-1* CDNA.

Rare codons in the cDNA Sequence			Frequency that codon used in genomic genes. (per thousand codons)	
Total	Amino Acid	Codon	*N. crassa*	*P. pastoris*
8	Alanine	GCG	16.5	3.5
2	Arginine	CGG	8.8	1.9
4	Arginine	CGC	17.6	2.4
2	Cysteine	UGC	8.8	4.6
10	Glycine	GGC	28.7	8.6
6	Histidine	CAC	15.5	8.4
7	Leucine	CUC	27.1	6.9
2	Proline	CCC	22.0	6.9
5	Threonine	ACG	13.1	6.5

Table 11 list codons used by P. pastoris at a frequency of less than 1% that appear in the *eas* and *nop-1* cDNA sequences. Codon usage-frequency data was obtained from Nakamura *et al.* (2000).

4.2.5.2 FACTORS INFLUENCING THE FOLDING OF TRANSGENIC EAS.

As the NOP-1 example discussed above demonstrates, it does not necessarily follow that the presence of rare-codons in a transgenic gene will prevent its translation and eventual expression. Given that the rate of protein folding ($t_{½}$ < 1 second) is much greater that the rate of translation (estimated at between 4-20 amino acids per second) a protein – like a hydrophobin – whose sequence contains regions with rows of hydrophobic amino-acids would be at an increased risk of aggregating while being translated into a hydrophilic environment, the proteosome would then dispose of these miss-folded proteins (Radford, 2000). Presumably, as happens *in vitro*, once the hydrophobin's disulfide bonds had formed the risk of it polymerising would diminish until it encounters an interface (de Vocht *et al.*, 2000).

The role chaperones play in preventing protein miss-folding has been well established (Radford, 2000). There is evidence however that specific chaperones or foldases are required to protect hydrophobins during biosynthesis. Scholtmeijer (2000) attempted to express SC3 and ABH3 in *Aspergillus niger*. She hoped that by growing transgenic isolates in liquid she could supress the expression of organism's native hydrophobins (they are only expressed on air-exposed structures, not submerged ones) while the transgenic SC3 could be secreted into the media. Despite the abundant production SC3 mRNA (20-40% of that seen in the native host -- *S. commune*) only a small amount of each transgenic protein (1% of that produced by *S. commune*) was produced. This was in spite of the fact that SC3 is immune to proteolytic degradation when incubated with *Aspergillus* cultures (Scholtmeijer, 2000). Given the fact some of the transgenic protein was successfully secreted, the implication is that the rest of the protein was degraded intracellularly (Scholtmeijer, 2000), possibly because of aggregation through the lack of the transgenic-host's hydrophobin specific chaperones. Presumably, *Aspergillus* co-expresses its hydrophobin-specific chaperones with its native hydrophobins, thus the appropriate endogenous chaperones were not available to fold transgenic SC3.

It follows that Scholtmeijer's success in expressing SC3 – under the control of promoters from the host's endogenous hydrophobin genes – in *T. reesei* may have been a result of selecting the culture-conditions that triggered the synchronous expression of the endogenous hydrophobin-chaperones and transgenic-SC3 (Scholtmeijer, 2000). If this hypothesis holds then it would explain why *Pichia pastoris* could not express transgenic EAS in its native form.

This hypothesis does not preclude the possibility that yeasts could express transgenic-hydrophobins. Rather that the hydrophobin should be expressed along with an appropriate chaperone or as a fusion protein – where the hydrophobin is linked to a solubility enhancing domain able to increase the protein's solubility. Such strategies have been successful in *E. coli* (Makrides, 1996).

The existence of hydrophobin-specific chaperones has yet to be investigated but the recent completion of both the *Neurospora* and *Aspergillus* genomes should make the task easier (Galagan *et al.* 2003; *Aspergillus* Sequencing Project: Center for Genome Research http://www.broad.mit.edu). A comparison of putative-chaperone proteins from these two species with those from *Saccharomyces cerevisiae* may highlight potential candidates (the *Saccharomyces* Genome Database is located online at http://www.yeastgenome.org). In addition, it might be fruitful to examine the

Neurospora genome for chaperones that are co-expressed with EAS, and as such, may have its transcription regulated by the same circadian rhythm.

It would be interesting to see whether there are any structural or evolutionary relationships between the hydrophobin-specific-chaperones (assuming they exist) and the Hsp104-class of yeast chaperones. These chaperones have been shown to prevent the auto-catalytic aggregation of prion-like proteins in *S. cerevisiae* (Chernoff *et al.*, 1995).

4.3 Expressing EAS in *E. coli*.

4.3.1 Generation and Screening Recombinant Isolates.

Table 12: *E. coli* Recombinants Generated in This Study.

Name	Strain transformed	Transforming Vector.	Antibiotic Resistance in each Strain.
A1	*AD494*	*pKKEASF1*	*Kan^R/Amp^R*
A2	*AD494*	*pKKEASF2*	*Kan^R/Amp^R*
A3	*AD494*	*pKKEASF2*	*Kan^R/Amp^R*
A4	*AD494*	*pKKEASF1*	*Kan^R/Amp^R*
AK	*AD494*	*pKK223-3*	*Kan^R/Amp^R*
AD494		*None*	*Kan^R*
O1	*Origami*	*pKKEASF1*	*Kan^R/Tet^R/Amp^R*
O2	*Origami*	*pKKEASF2*	*Kan^R/Tet^R/Amp^R*
O3	*Origami*	*pKKEASF2*	*Kan^R/Tet^R/Amp^R*
O4	*Origami*	*pKKEASF1*	*Kan^R/Tet^R/Amp^R*
OK	*Origami*	*pKK223-3*	*Kan^R/Tet^R/Amp^R*
Origami		*None*	*Kan^R/Tet^R*
ROTCase	*K-12*	*pKK223-3 + OTCase*	*Amp^R*

The ten recombinant *E. coli* strains screened for the ability to express EAS are described in Table 12. **Key:** strains AK and OK (italicized) were transformed with the pKK223-3 plasmid and were used as a control to check the effect of the expression vector on protein expression. Antibiotic resistant phenotypes listed are Kan^R: Kanamycin resistant Tet^R: tetracycline resistant and Amp^R: Ampicillin resistant. The recombinant ROTCase strain was provided by Dr Matthew Templeton (Hort Research). It consists of an *E. coli* K-12 host transformed with a pKK223-3 based expression vector containing a gene for the encoding the *E. coli* ornithine transcarbamoylase enzyme (Langley *et al.*, 2000).

The expression plasmids pKKEASF1 and pKKEASF2 (whose construction was described in section 4.1.2) were electro-transformed into the *E. coli* host strains AD494 and Origami as described in section 2.2.6.2. From the several thousand recombinants, ten were chosen at random for further analysis (Table 12).

The identity of the plasmid borne by each of these recombinants was confirmed before and after transformation by restriction-mapping combined with the cultivation and plasmid-purification techniques described in sections 2.1.3 and 2.2.6.4. Protein-expression was induced with IPTG, and the cultures were sampled over a period of 9 h (section 2.1.3.3). Samples of recombinant bacteria were lysed in a SDS-PAGE

sample buffer that had been supplemented with reducing (1 M DTT) and chaotrophic (8 M Urea) agents so as to dissolve any inclusion bodies present in the bacterial cytoplasm (section 2.4.4). These cell lysates were then compared by SDS-PAGE. The results of these experiments are presented in Figure 42 and they show that none of the recombinant *E. coli* isolates were able to over-express native EAS in either a soluble or an insoluble form.

FIGURE 42: SCREENING RECOMBINANT *E. COLI* ISOLATES FOR EAS EXPRESSION.

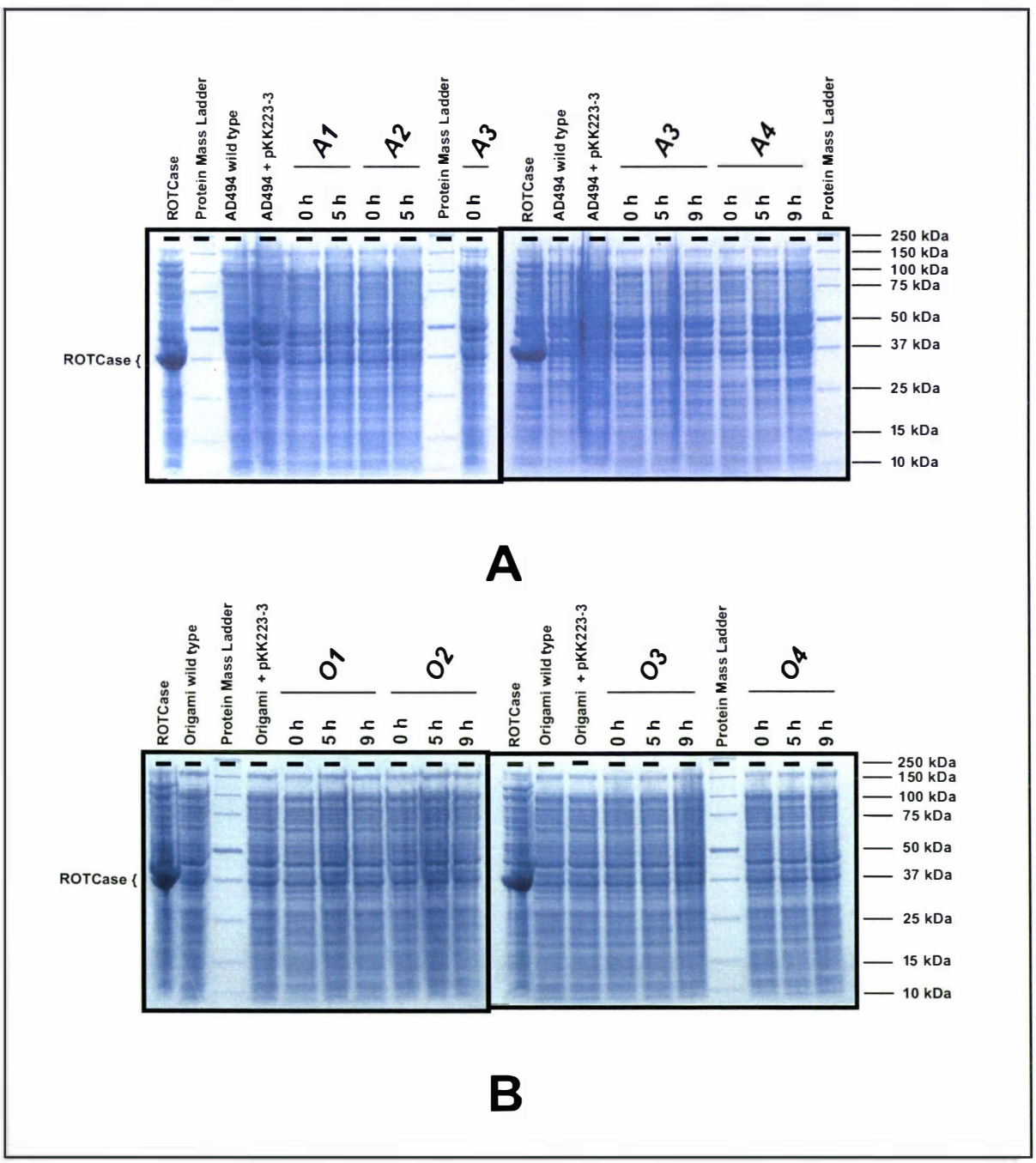

Figure 42 illustrates the result of a SDS-PAGE analysis designed to detect the intracellular, over expression of EAS by the *E. coli* isolates described in Table 12. **Key:** The untransformed Origami (labelled O) and AD494 (Labelled A) strains along with those strains transformed with pKK223-3 (denoted as AK and OK) are included to as controls to demonstrate the proteins produced without the recombinant *eas* gene. The effectiveness of the induction is demonstrated by the accumulation of ROTCase produced by the recombinant strain described in Table 12.

The presence of recombinant ornithine transcarbamoylase (ROTCase) (Figure 42, lane one) proves that the IPTG induction of protein expression in these isolates was effective. The ROTCase enzyme is produced by an *E. coli* K-12 strain (provided by Dr. M. D. Templeton), that had been transformed with a pKK223-3 based expression vector. This modification allows it to express the ROTCase enzyme to levels of 100 mg/L of culture media, illustrating how powerful the synthetic *tac* promoter in pKK223-3 is (Langley *et al.*, 2000).

4.3.2 Discussion - *E. coli* Expression.

Our expression strategy makes it difficult to determine the exact cause of the failure of these strains to over-express EAS. When Nakari-Setälä *et al.* (1996) successfully expressed HFB1 (a class II hydrophobin) in *E. coli*, they did so by fusing the *OmpA* secretion signal and a FLAG epitope to a *hfb1* cDNA that encoding the mature form of the protein. Thus, HFB1 was expressed into the bacterial periplasmic space. This strategy reduced the probability that the protein would be proteolytically degraded while increasing the likelihood that disulfide bonds would form. The *E. coli* periplasm is an oxidising environment containing fewer proteases than the cytoplasm (Makrides, 1996; Baneyx, 1999). The use of the FLAG epitope simplified the screening of recombinant isolates and allowed Nakari-Setälä *et al.* (1996) to purify recombinant HFB1 in a single step using affinity chromatography. Nakari-Setälä *et al.* (1996) do not state how much protein their isolates yielded, nor did they study the activity of the recombinant protein, but they did successfully use their recombinant protein as an adjuvant.

I decided against modifying the N-terminus of recombinant EAS for fear of compromising the unique self-assembly property of hydrophobins, the focal point of our intended site-directed-mutagenesis investigations. There was also a risk that the proclivity of hydrophobins for self-assembly into insoluble films might hamper efforts to remove fusion proteins *in vitro*. Additionally I sought to produce a recombinant version of EAS with a consistent N-terminus to simplify an investigation of the interaction between the pattern of intramolecular disulfide bonds and the spacing of cysteine residues within EAS. Unlike the native version or any recombinant whose N-terminal fusion required proteolytic removal, a natively-expressed version of EAS could have been simply purified as a single isoform. In turn, this would have solved the problems arising from the presence of multiple isoforms in unmodified preparations of EAS – believed to be generated by inaccurate proteolytic cleavage of the endogenous secretion peptide; These contaminating isoforms complicated my

efforts to establishing which pairs of cysteines are linked by intramolecular disulfide-bond (see Chapter 5).

FIGURE 43: CLUSTERING OF RARE CODONS IN PKKEAS EXPRESSION VECTORS.

bp							bp
1	.....AUUG	UGAGCGGAU	AACAAUUUC	ACACAGGAA	ACAGAAUUC	AUGGCCACC StartAlaThr	51
52	ACCAUCGGC ThrIleGly	CCCAACACC ProAsnThr	UGCUCCAUC CysSerIle	GACGACUAC AspAspTyr	AAGCCUUAC LysProTyr	UGCUGCCAG CysCysGln	106
107	UCUAUGUCC SerMetSer	GGCCCCGCC GlyProAla	GGCUCCCCU GlySerPro	GGUCUCCUC GlyLeuLeu	AACCUCAUC AsnLeuIle	CCCGUCGAC ProValAsp	160
151	CUCAGCGCC LeuSerAla	UCGCUCGGC SerLeuGly	UGCGUUGUC CysValVal	GGUGUCAUC GlyValIle	GGCUCCCAA GlySerGln	UGUGGUGCC CysGlyAla	214
201	AGCGUCAAG SerValLys	UGCUGCAAG CysCysLys	GACGAUGUU AspAspVal	ACCAACACC ThrAsnThr	GGCAACUCC GlyAsnSer	UUCCUCAUC PheLeuIle	268
251	AUCAACGCU IleAsnAla	GCCAACUGC AlaAsnCys	GUUGCCUAA ValAlaStop	CUGCAGCCA	AGCUUGGCU	GUUUUGGCG	322
301	GAUGAGAGA	AGAUUUUCA	GCCUGAUAC	AGAUUAAAU	CAGAACGCA	GAAGCGGUC	376
377	UGAUAAAAC	AGAAUUUGC	CUGGCGGCA	GUAGCGCGG	UGGUCCCAC		423

Figure 41 illustrates the nucleotide sequence (minus the poly (A) tail) of recombinant *eas* mRNA predicted to be produced by recombinants transformed with the pKKEASF1 and pKKEASF2 expression cassettes. **Key:** pairs of inverted repeats capable of base pairing are highlighted in blue and grey. Residues encoded by rarely used *E. coli* codons are coloured. Pink residues are encoded by codons used in less that 10 times per 1000 codons. Dark-red residues are used approximately 5 times per 1000 codons or less (Nakamura *et al.*, 2000). Leucines encoding CUC codon (highlighted with green text) occurs with a frequency of 9.9 times per 1000 codons according to Kane (1995). The position of the Kex2 protease site marking the start of the *eas* cDNA is marked with an arrow.

Subsequent studies by Scholtmeijer *et al.* (2002) demonstrated that tri-peptides could be fused to the N-terminus of a class I hydrophobin (SC3) without seriously affecting its ability to self-assemble into an amphipathic film. Thus, I believe it possible to safely add an epitope tag to the N-terminus of the protein and so benefit from a means to detect marginal levels of protein-expression by Western blotting. This would be a prudent strategy for future studies, because it would simplify purification of any modified versions regardless of the effect of the mutagenesis on their activity (reviewed in Hannig and Makrides, 1998; Appelbaum and Shatzman, 1999; Colyer, 1999).

It is likely that the inhibition of EAS production occurred post-transcription. The possibility that some random error in plasmid replication or construction could have introduced a fault that would inhibit transcription (*e.g.* extra nucleotides added between the ribosome binding site and the start codon) can be ruled out because each of the eight recombinants was transformed with a separately constructed plasmid. It is unlikely that an error small enough to go undetected by restriction digest would have occurred in all eight recombinants.

TABLE 13: CODONS USED INFREQUENTLY BY *E. COLI* PRESENT IN *EAS* CDNA.

CODON BIAS IN *EAS* CDNA

cDNA Sequence			Frequency that codon used in genomic genes. (per thousand codons)	
Frequency	Amino Acid	Codon	*N. crassa*	*E. coli*
7	Cysteine	UGC	8.8	6.4
1	Cysteine	UGU	4.5	5.2
5	Leucine	CUC	27.5	11.0 (9.9)
2	Proline	CCC	22.0	5.5
4	Serine	UCC	20.2	7.2 (9.4)
1	Serine	UCG	14.2	8.9 (8.0)

CODON BIAS IN *HFB1* CDNA

cDNA Sequence			Frequency that codon used in genomic genes. (per thousand codons)	
Frequency	Amino Acid	Codon	*T. reesei*	*E. coli*
7	Cysteine	UGC	-	6.4
1	Cysteine	UGU	-	5.2
5	Leucine	CUC	-	11.0 (9.9)
4	Proline	CCC	-	5.5
3	Proline	CCU	-	7.1 (6.6)
1	Serine	UCC	-	7.2 (9.4)

Table 13 lists codons, used by *E. coli* at a frequency of less than 1%, that appear in the *eas* and *hfb1* hydrophobin cDNA sequences. Codon usage frequency data were obtained from Nakamura *et al.* (2000). Frequencies data within parenthesis were obtained from Kane (1995). The codon usage statistics for *T. reesei* are unavailable.

As described in the previous section, the presence of rare codons in heterologous genes that have been translated by *E. coli* has been shown to induce errors during translation and to reduce expression yields (reviewed in Kane, 1995; Makrides, 1996; Baneyx, 1999). The recombinant *eas* cDNA sequence used in this experiment contains 20 rarely used codons that often cluster in close proximity to each other (see Figure 43 and Table 13). In *E. coli,* heterologous genes are often expressed at levels equal to or exceeding highly expressed endogenous genes, and this may place demands on the translation apparatus unmatched to the host's tRNA population. This is the so called "Hungry Codon Syndrome" and it is thought to be a potent inhibitor of heterologous protein-expression (Kurland and Gallant, 1996).

The correlation between rare codons and low expression is not absolute. The number of rare codons in *hfb1* cDNA is similar to the number in *eas,* yet there was

enough HFB1 produced to enable its use as an adjuvant (Nakari-Setälä *et al.*, 1996). Were *E. coli* to be used for another attempt to express EAS, then targeting the expression to the periplasm and incorporating an epitope (i.e. a His-tag or the FLAG epitope) with the N-terminus would be advantageous.

If EAS was successfully expressed in the cytoplasm of *E. coli,* its properties are such that it could be expected to form inclusion bodies. This is another advantage of using fusion-tags when expressing proteins in *E. coli*, proteins fused to them are often expressed in a soluble, and sometimes, in a functional form (Makrides, 1996; Baneyx, 1999). The best example of a fusion protein known to enhance the solubility of recombinant proteins fused to it is NusA in that it was specifically selected from 4,000 *E. coli* proteins as being the one most likely to prevent the formation of inclusion bodies (Harrison, 2000). Novagen have designed a series of vectors (the pET-43.1 and pET-44 expression vectors) that fuse NusA to the N-terminus of the recombinant protein along with domains (e.g. the His-tag) that allow affinity chromatography to be used to purify the recombinant protein.

The Rosetta™ strains of *E. coli* from Novagen are engineered to express the rarest codons – including CCC (proline) which is present in *eas.* Using this strain as a host may negate the need to optimise the codon bias in *eas* cDNA (Novy *et al.*, 2001). These strains of *E. coli* are compatible with the pET vectors described above and if these vectors are used in combination with Novagen's Rosetta-gami™ expression host (combining the traits of the Origami™ and Rosetta™ strains of *E. coli*) it might be possible to cytoplasmically express a version of EAS that is both fully functional (in that its disulfide bonds may have formed) and soluble (because it is fused to NusA). Whether or not it is better to express EAS in the cytoplasmic or periplasmic compartments of *E. coli* can only be established empirically. If another attempt is made to EAS express cytoplasmically then the results obtained from this investigation and experiments described in the literature present a strong argument that the protein can and should be expressed as a fusion protein. Unfortunately, the best combination of fusion-tags and *E. coli* host strains can only be determined empirically.

Alternatively the recombinant version of EAS created in this experiment could have been destroyed by some of the 50 endogenous cytoplasmic proteases known to exist in *E. coli* that are derived from the K-12 strain, such as Origami and AD494 (Makrides, 1996). These proteases are known to efficiently remove abnormal, truncated, or otherwise defective proteins. This might still be the case with EAS, despite the fact that the recombinant version did not violate the "N-end rule"

whereby specific amino-acids (absent in EAS) at the N-terminus of a protein target them for proteolytic destruction (reviewed by Makrides, 1996). The easiest way to avoid this, if another attempt is made to express EAS in *E. coli*, is to express the protein in the periplasm where there the fewer proteases (Makrides, 1996; Baneyx, 1999).

Translational errors due to the presence of rare codons or proteolytic degradation or a combination of both are the most likely reasons for the failure to over-express EAS in the *E. coli* cytoplasm. No other obvious cause presents itself. For instance: the secondary structures introduced when *eas* cDNA was ligated into the pKK223-3 expression cassette are indicated in Figure 43, but appear trivial in that they occur downstream of the start codon and are not stable enough (each less than -13 Kcal mol^{-1}) to interfere with translation.

4.4 Discussion – Other Expression Strategies.

4.4.1 Hydrophobins Expressed in Fungal Hosts.

Recent efforts to develop hydrophobin-based biotechnology have succeeded in producing filamentous fungal hosts that can reliably express hydrophobins such as SC3, ABH1, HFB1, and HFB2.

Filamentous fungi are widely used commercially for industrial-scale protein production. *Trichoderma* and *Aspergillus* species in particular are widely used to produce hydrolysing enzymes (reviewed in Onions, 1981; Keränen and Penttilä, 1995). Excluding laboratories with special interests in these fungi, they are rarely considered for heterologous protein expression (Keränen and Penttilä, 1995). *Saccharomyces cerevisiae*, *P. pastoris,* and *E. coli* are used in preference due to the convenience of using well-characterised expression hosts that are easily cultured and readily commercially available.

Expressing hydrophobins in filamentous fungal hosts had already been proven to work but with only modest yields. Each of the complementation studies used either to confirm the identity of a particular hydrophobin gene or to confirm the functional relatedness of hydrophobins was essentially an exercise in homologous and heterologous protein-expression (*e.g.* Bell-Pedersen *et al.,* 1992; Lauter *et al.,* 1992; Kershaw *et al.,* 1998).

Researchers at the University of Groningen screened *A. niger*, *Schizophyllum commune* and *T. reesei* for their ability express the class I hydrophobins ABH1, ABH3, and SC3 in their native forms. *A. niger* was shown to co-secrete ABH1 and

the proteases that degrade it. SC3 was secreted by *A. niger* but incorrectly glycosylated and ABH3 yields suffered from an uncharacterised inability of *A. niger* to secrete this protein efficiently (Scholtmeijer, 2000). As discussed below homologous and heterologous hydrophobin expression in *S. commune* failed unless the recombinant gene included an intron (Scholtmeijer *et al.,* 2001a). By contrast, the over-expression of both homologous and heterologous hydrophobins has succeeded in *T. reesei*; the latter experiment yielded 60 mg\L of SC3 from a single heterologous gene. This occurred despite the host secreting its endogenous class II hydrophobins (HFB1 and HFB2) into the media (Scholtmeijer, 2000; Askolin *et al.,* 2001). By introducing three copies of the *hfb1* gene into *T. reesei*, Askolin *et al.* (2001) were able to obtain nearly 1.8 g of HFB1 protein from 419 g (dry weight) of mycelium, despite some proteolytic degradation. This indicates that the yields of heterologous hydrophobins that are expressed in this species might increase with gene dosage. Hence, *T. reesei* appears to be an ideal host for the expression of hydrophobins, in that it is able to secrete both classes of hydrophobins. Knock-out mutants that abolish endogenous *T. reesei* hydrophobin production are available, and are inhibited in their vegetative growth (Bailey *et al.,* 2002). Therefore, the chances are good that *T. reesei* could successfully serve as a host for the production of mutagenised proteins.

If not, the obvious alternative is *N. crassa* itself. As stated, EAS has already been successfully expressed on the macroconidia of *eas* mutants, albeit with diminished yields. It is possible to circumvent problems that are presented by the RIP-induced gene-silencing by using uninucleate microconidia (reviewed by Maheshwari, 1999). The microconidia must be carefully handled if they are to germinate, but the benefits from using microconidia in these experiments would include having *N. crassa* handle disulfide-bond formation, folding, and secretion of the mutated variants of a *N. crassa* protein. If the transgenic EAS can be expressed on the host's macroconidia, the current purification method would suffice for extracting and purifying the transgenic protein. The alternative is to use liquid-culture methods and allow the protein to be secreted into the culture media. This strategy risks exposing the transgenic protein to the host's extracellular proteases as Asgeirsdóttir *et al.* found out. Asgeirsdóttir *et al.* expressed ABH1 in *A. niger* only to have the transgenic hydrophobin degraded by the host's extracellular enzymes (Asgeirsdóttir *et al.*, 1999).

If this strategy is adopted then the lesson learnt by Scholtmeijer *et al.* (2001b) in attempting to express SC3 cDNA in *S. commune* should be heeded. Their finding

that *S. commune* mRNA metabolism is dependent on the presence of a spliceable intron agrees with similar findings in *Usilago maydis* and *Podospora anserina* (Onel *et al.,* 1995; Sachs, 1998; Scholtmeijer *et al.,* 2001; Le Hir *et al.,* 2003). The presence of introns in the genes of higher eukaryotes is known to affect many stages of mRNA metabolism including initial transcription, polyadenylation, nuclear export, translation and mRNA decay (Le Hir *et al.,* 2003). Judging by the success of heterologous cDNA expression in the *Saccharomyces cerevisiae*, in *P. pastoris,* and in *T. reesei,* then these species may be the exception within lower eukaryotes rather than the rule.

4.5 Summary of Results.

Two attempts were made to express EAS in its native form. The aim was to create a system that would enable modified versions of EAS to be easily developed and expressed.

(1) A commercially developed eukaryotic expression system based on the yeast *P. pastoris* was selected because it had been successfully used to express other eukaryotic proteins. It also has the ability to secrete recombinant proteins into its protein-free culture media.

We successfully generated and isolated *P. pastoris* recombinants that contained the pPIC9K (pPIC9EASF1) based plasmid into which I had ligated a cDNA sequence encoding the Ia isoform of EAS fused to the α-factor secretion signal peptide. While, Northern hybridisation analysis confirmed that these isolates could be induced to transcribe the EAS cDNA signal, the presence of the recombinant protein could not be detected in any of the intra- or extracellular protein samples obtained from the recombinant isolates.

I proposed that the expression of recombinant EAS was adversely affected by the clusters of rarely used codons in the cDNA sequence or by the lack of chaperones capable of sequestering the newly translated protein until its disulfide bonds had formed.

(2) An attempt was made to cytoplasmically express native-EAS in two strains of *E. coli* (AD494 and Origami). These are strains of *E. coli* in which disulfide bond formation can occur (albeit randomly) within the cytoplasm. While, the successful expression of the ROTCase enzyme in a control experiment indicated that the induction conditions were sufficient to induce strong expression of the recombinant genes in the host *E. coli* strains the presence of

the recombinant protein could not be detected in intracellular protein samples extracted from the recombinant isolates.

After analysing the composition of the EAS cDNA sequence I proposed that the expression of recombinant EAS was affected by the presence of several clusters of codons that *E. coli* K-12 based strains rarely use.

While both the hydrophobin expression strategies used in these experiments failed, other laboratories have succeeded in expressing hydrophobins in both fungi and bacteria and in this light, improvements were discussed that should ensure the successful expression of EAS should any future attempts to develop a heterologous expression system for this hydrophobin be made.

5
DISULFIDE MAPPING.

5.0 INTRODUCTION.

5.0.1 EXPERIMENTAL AIM.

EAS has eight cysteine residues separated thus: 8aa-$\mathbf{C_9}$-9aa-$\mathbf{C_{18}}$-$\mathbf{C_{19}}$-26aa-$\mathbf{C_{45}}$-9aa-$\mathbf{C_{54}}$-5aa-$\mathbf{C_{60}}$-$\mathbf{C_{61}}$-19aa-$\mathbf{C_{80}}$-2aa where *n*aa denotes that *n* amino acids (aa) separate each cysteine residue ($\mathbf{C}_n$) whose position in the sequence of EAS is denoted in subscript. Two pieces of evidence suggest that every cysteine in EAS is involved in an intramolecular disulfide bond:

(1) Amino acid analysis of acid-hydrolysed EAS rodlets found only half-cystine residues (Beever *et al.*, 1979). The protein itself was unable to be acetylated with iodoacetamide unless first treated with DTT, implying that the protein contained no free sulfhydryl groups (Personal communication with Dr M. D. Templeton, Hort Research).

(2) De Vries *et al.* (1993) attempted to acetylate the cysteines in SC3 using tritium-tagged iodoacetic acid. They were unable to modify the cysteines in the unreduced form of SC3, but successfully added radioactive acetyl groups to the free cysteine residues in DTT-treated SC3.

Disulfide bonds are expected to be significant determinants of hydrophobin structural organisation (Voet *et al.*, 1999), because they can stabilise the tertiary structures assumed by proteins (Creighton, 1993). As discussed in section 1.3.2, their role in the structures that hydrophobins assume is to stabilise the monomeric form of the protein and to prevent it from prematurely self-assembling in the *absence* of a hydrophobic-hydrophilic interface (de Vocht *et al.*, 2000). Determining which pairs of cysteines are linked by disulfide bonds would also aid structure prediction – a tool that should prove valuable given the complications imposed on structural investigations by the properties of hydrophobin films. However, each hydrophobin has two pairs of adjacent cysteine residues and these were a major barrier for disulfide-mapping investigations because there were no simple methods (proteolytic or chemical) capable of cleaving the peptide bond between adjacent cysteine residues (Wu and Watson, 1997).

Thus, while the location of the disulfide bonds in HFB2 was determined from its crystal structure (Hakanpää *et al.*, 2004), the location of the disulfide bonds in class I hydrophobins – none of which have ever been crystallised – are still unknown. The aim of the experiments described in this chapter was to determine which pairs of cysteine residues in EAS are linked by each of the four intramolecular disulfide bridges.

5.0.2 Introduction to the Methodology of CN-induced Cleavage Mass-Mapping.

Conventional methods used to identify disulfide-linked cysteines first required that the amide bond between the linked cysteines be cleaved, so that the resulting cysteinyl peptides isolated can and identified through sequencing or mass-spectrometric analysis (Smith and Zhou, 1990; Aitken, 1994). Hydrophobins cannot be analysed by these methods because there are no specific reagents capable of cleaving the peptide bond between adjacent cysteine residues. While, there are non-specific reagents that are capable of cleaving this bond, their use requires the simultaneous use of specific reagents and together these regents generate highly complex mass spectrometry data (Smith and Zhou, 1990; Aitken, 1994).

Figure 44: Wu and Watson's Method Applied to Map Disulfide Bonds in RNase A.

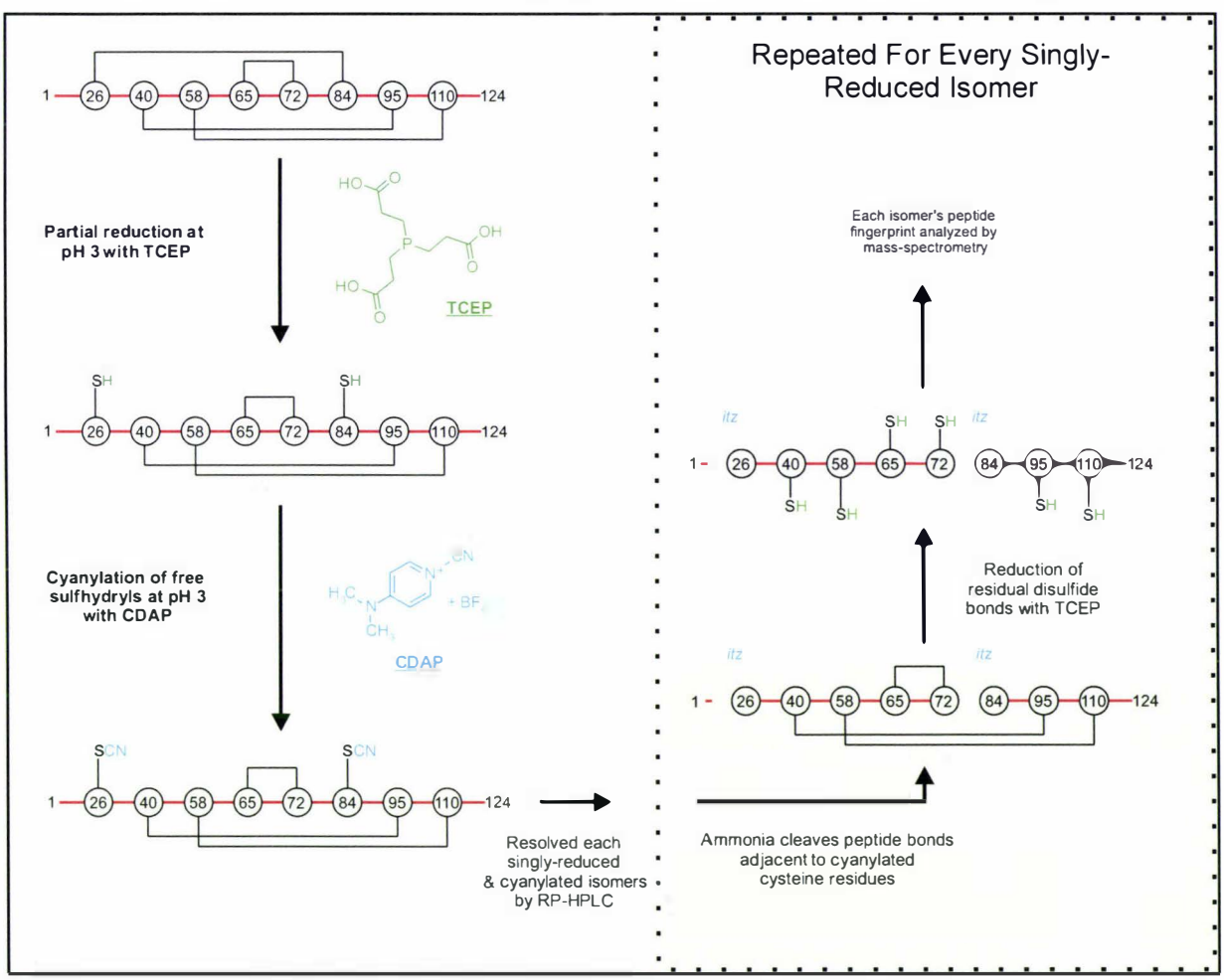

An outline of Wu and Watson's method (using RNase A as an example) is shown in Figure 44. RNase A is a protein with eight cysteine residues linked as shown (Smyth *et al.*, 1963; Avey *et al.*, 1967). It is represented schematically with the red horizontal line depicting the peptide backbone interspersed with circles that represent each of the cysteine residues. The black horizontal lines represent disulfide bonds. In addition to standard chemical nomenclature the following abbreviations are used: TCEP = tris(2-carboxyethyl) phosphine hydrochloride. CDAP = 1-cyano-4-dimethylamino-pyridinium tetrafluoroborate. The symbol itz = iminothiazolidinyl carboxyl residue at the amino termini.

This problem has been addressed by J. T. Watson's laboratory at Michigan State University. They have developed a mapping method capable of dealing with any pattern of cysteine residues, and they have used it successfully to map the disulfide bonds within ferredoxin, the long insulin-like growth factor, ovalbumin, creatine phosphokinase, ribonuclease A, α-lactalbumin and the antimicrobial peptide sillucin from *Rhizomucor pusillus* (Wu *et al.,* 1996; Wu and Watson, 1997, 1998; Yang *et al.,* 1998; Qi *et al.,* 2001). The sillucin example is particularly noteworthy since some of the disulfide-linked cysteine residues are either adjacent to one another or are sterically sheltered or both. Thus, this approach has the potential to resolve the disulfide bonds formed by each pair of adjacent cysteine residues found in all hydrophobins.

An outline of Wu and Watson's method is given in Figure 44 using Bovine pancreatic ribonuclease Type III-A (RNase A) as an example. In the first stage of the protocol, the protein is dissolved in a denaturing dissolved in a buffer solution at pH 3 and then partially reduced by reaction with tris(2-carboxyethyl) phosphine (TCEP) to produce a mixture of partially reduced RNase A isomers and residual intact-RNase A (Burns *et al.,* 1991; Wu and Watson, 1997). The reaction conditions must be empirically optimised in order to ensure that the dominant species in this mixture are isomers of RNase A in which only a single disulfide bond has been cleaved. The reduction reaction is carried out at pH 3 so as to kinetically suppress reactions that scramble the pattern of disulfide bonds. In the second stage, the nascent sulfhydryls on the cysteine residues are cyanylated in acidic conditions (pH 3) by treatment with 1-cyano-4-dimethylamino-pyridinium tetrafluoroborate (CDAP). Then these partially reduced and cyanylated protein isoforms are fractionated by RP-HPLC (Wakselman *et al.,* 1976; Nakagawa *et al.,* 1994; Wu *et al.,* 1996, 1998).

Next, each of the RP-HPLC fractions are analysed by mass spectrometry to determine which contain singly-reduced and cyanylated isomers of RNase A. The mass of the singly-reduced protein will increase by +52 Da if both nascent sulfhydryls are efficiently cyanylated; this is equal to two 26 Da cyanyl groups. Once the correct fractions have been identified, they are treated with aqueous ammonia to specifically cleave the peptide bonds adjacent to the cyanylated cysteines.

A mechanism for this ammonia-catalysed peptide bond cleavage has been proposed and is described in Figure 45; ammonia conducts a nucleophilic attack on the carbonyl to facilitate the cleavage of the peptide bond. If a singly-reduced and cyanylated protein is cleaved in this manner then a pair of 2-iminothiazolidine-4-

carboxyl (itz) peptides and a single α-amidated C-terminal peptide are created. After the volatile ammonia has been removed under vacuum, any residual disulfide bonds that link the peptides are removed with a second treatment of TCEP. The final result is a mixture of separate peptide fragments. The itz-residues are 26 Da heavier than the reduced cysteines they replace, effectively tagging the peptides containing the cysteine residues that had been linked prior to partial reduction. The mass of the fragments can be determined by mass spectrometry, and location of the cysteines involved in a disulfide bond can be related back to the protein's original amino-acid sequence.

FIGURE 45: THE AMMONIA-CATALYSED PEPTIDE BOND CLEAVAGE REACTION.

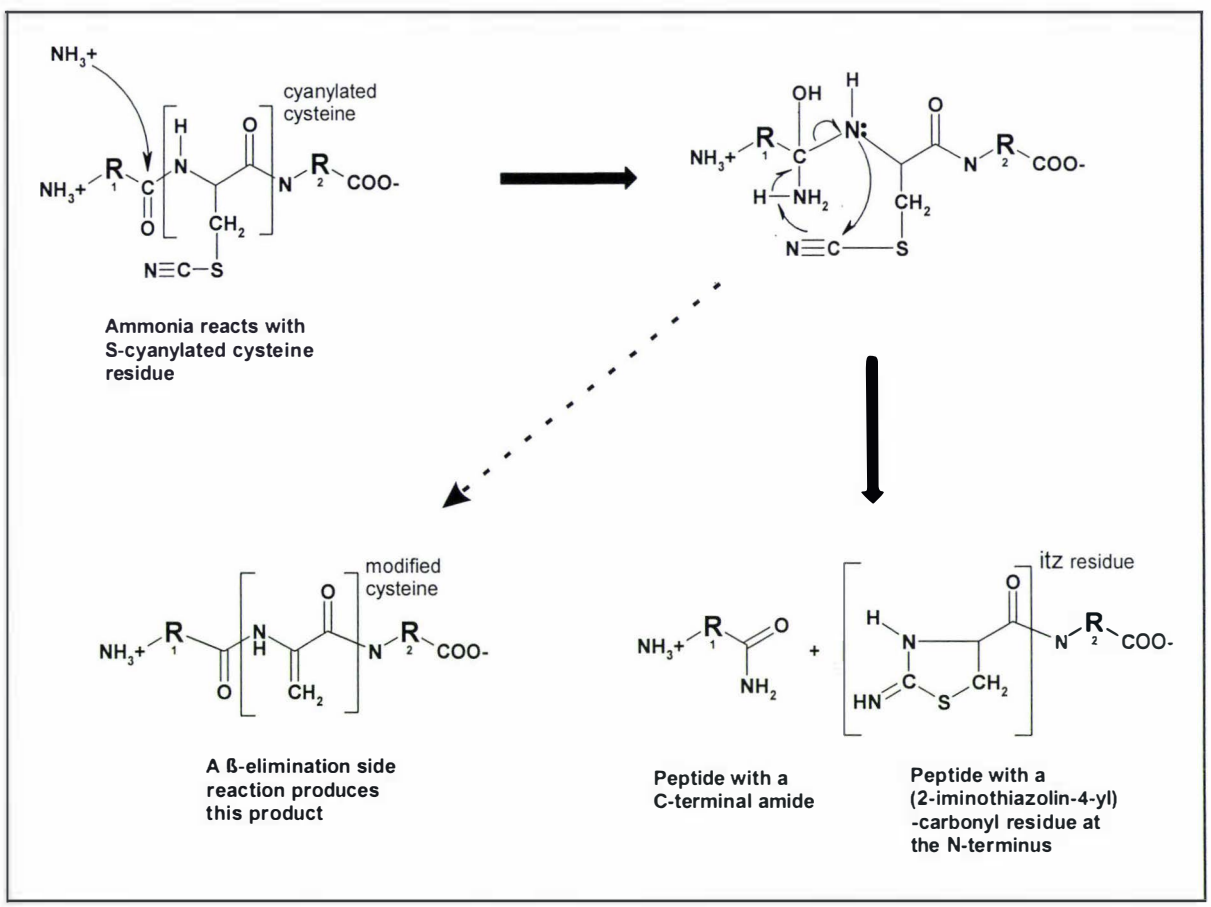

The mechanisms of both the ammonia-catalysed S-cyanylated peptide cleavage and the ß-elimination reaction are shown in Figure 45. This diagram was adapted from Nakagawa *et al.* (1994) and Wu *et al.* (1996 and 1998). **Note:** itz = iminothiazolidinyl carboxyl residue.

5.0.2.1 THE β-ELIMINATION SIDE REACTION.

Wu and Watson recommend that the ammonia-catalysed peptide bond cleavage reaction be carried out under mild alkaline conditions (pH 12). This allows for the efficient, rapid (one hour incubation time in ambient conditions), and selective cleavage of the S-cyanylated proteins. But these conditions also accelerate the rate of a β-elimination side-reaction that removes a hydrogen atom and the SCN-group from the cysteine's α- and β-carbon atoms (respectively), and creates a carbon-

carbon double bond between them. No peptide bonds are broken by this reaction (see Figure 45). As Wu and Watson (1998) demonstrated, for most peptides the cleavage products predominate over the β-elimination product(s).

Thus, up to five different peptide fragments may result from the ammonia-catalysed peptide cleavage in a protein with two cyanylated cysteine residues. Three fragments – two with itz-residues – will result from the ammonia catalysed cleavage and two more may arise from β-elimination reactions that can occur at either of the cyanylated cysteines.

5.0.3 Predicting the Fragment Patterns Likely to Result From the Cleavage of Cyanylated EAS

For EAS, with eight disulfide-linked cysteine residues, there are 105 possible combinations of disulfide-linked cysteine residues[1], but if the partial reduction reaction produces only singly-reduced EAS isomers, then only 28 unique isomers can be obtained. This fact emphasises how crucial the partial reduction step is in Wu and Watson's methodology.

I used the amino acid sequence of EAS (Figure 46) to predict both the structure and molecular mass of the three peptides and of the two β-elimination products that could arise if each of the 28 singly-reduced isomers of EAS was treated with ammonia and TCEP (see section 2.4.7.1). The predicted molecular masses of these five fragments are reported in Figure 47; the structures of these peptides are presented in Appendix VA.

The data in Figure 47 is arranged to demonstrate how the parent molecule can be identified by mass-spectrometric analysis of the ammonia and TCEP peptide digests. A unique combination of peptides results when each singly-reduced and cyanylated isomer is digested. The simultaneous presence of three or more particular fragments in a digested sample is sufficient to identify the parent isomers, and therefore the location of one of the disulfide bonds.

Figure 46: The Amino Acid Sequence of EAS.

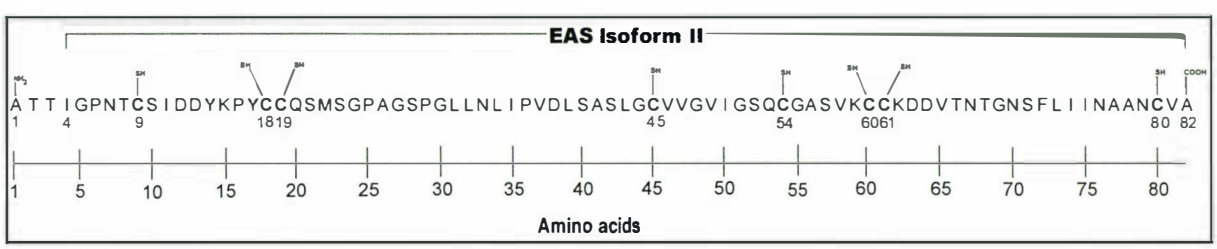

The amino acid sequences of EAS isoforms Ia and IIa are shown in Figure 46.

[1] For the first disulfide bond, eight cysteines may be arranged into seven unique disulfide-linked pairs . For the second bond, the six remaining cysteines can be combined in five different ways and so on. 7 x 5 x 3 x 1 = 105.

FIGURE 47: MOLECULAR MASS OF THE FRAGMENTS PREDICTED TO RESULT FROM THE CLEAVAGE OF EAS ISOFORM I CHAINS AT THE SITES OF THE DESIGNATED CYSTEINE PAIRS.

	Cysteine pairs: (Cys_x-Cys_y)	Ala_1–$X_{(x-1)}$ (Da)	itz_x–$X_{(y-1)}$ (Da)	itz_y–Ala_{82} (Da)	Ala_1-(βCys_x)-$X_{(y-1)}$ (Da)	itz_x–(βCys_y)–Ala_{82} (Da)
1	Cys_9-Cys_{18}	772.88 (788.88)	1127.25 (1143.25)	6370.44 (6386.44)	1824.01 (1840.01)	7421.57 (7437.57)
2	Cys_9-Cys_{19}	772.88 (788.88)	1230.39 (1246.39)	6267.30 (6283.30)	1927.15 (1943.15)	7421.57 (7437.57)
3	Cys_9-Cys_{45}	772.88 (788.88)	3697.27 (3713.27)	3800.42 (3816.42)	4394.03 (4410.03)	7421.57 (7437.57)
4	Cys_9-Cys_{54}	772.88 (788.88)	4541.28 (4557.28)	2957.40 (2973.40)	5237.05 (5253.05)	7421.57 (7437.57)
5	Cys_9-Cys_{60}	772.88 (788.88)	5086.94 (5102.94)	2411.74 (2427.74)	5782.72 (5798.72)	7421.57 (7437.57)
6	Cys_9-Cys_{61}	772.88 (788.88)	5189.12 (5205.12)	2308.59 (2324.59)	5885.86 (5901.86)	7421.57 (7437.57)
7	Cys_9-Cys_{80}	772.88 (788.88)	7181.23 (7197.33)	316.38 (332.38)	7878.07 (7894.07)	7421.57 (7437.57)
8	Cys_{18}-Cys_{19}	1857.10 (1873.10)	145.18 (161.18)	6267.30 (6283.30)	1927.15 (1943.15)	6336.36 (6352.36)
9	Cys_{18}-Cys_{45}	1857.10 (1873.10)	2612.06 (2628.06)	3800.42 (3816.42)	4394.03 (4410.03)	6336.36 (6352.36)
10	Cys_{18}-Cys_{54}	1857.10 (1873.10)	3454.10 (3470.10)	2957.40 (2973.40)	5237.05 (5253.05)	6336.36 (6352.36)
11	Cys_{18}-Cys_{60}	1857.10 (1873.10)	4000.77 (4016.77)	2411.74 (2427.74)	5782.72 (5798.72)	6336.36 (6352.36)
12	Cys_{18}-Cys_{61}	1857.10 (1873.10)	4103.91 (4119.91)	2308.59 (2324.59)	5885.86 (5901.86)	6336.36 (6352.36)
13	Cys_{18}-Cys_{80}	1857.10 (1873.10)	6097.09 (6113.09)	316.38 (332.38)	7878.07 (7894.07)	6336.36 (6352.36)
14	Cys_{19}-Cys_{45}	1961.23 (1977.23)	2508.92 (2524.92)	3800.42 (3816.42)	4394.03 (4410.03)	6233.22 (6249.22)
15	Cys_{19}-Cys_{54}	1961.23 (1977.23)	3351.94 (3367.92)	2957.40 (2973.40)	5237.05 (5253.05)	6233.22 (6249.22)
16	Cys_{19}-Cys_{60}	1961.23 (1977.23)	3897.60 (3913.60)	2411.74 (2427.74)	5782.72 (5798.72)	6233.22 (6249.22)
17	Cys_{19}-Cys_{61}	1961.23 (1977.23)	4000.75 (4016.75)	2308.59 (2324.59)	5885.86 (5901.86)	6233.22 (6249.22)
18	Cys_{19}-Cys_{80}	1961.23 (1977.23)	5993.94 (6009.94)	316.38 (332.38)	7878.07 (7894.07)	6233.22 (6249.22)
19	Cys_{45}-Cys_{54}	4428.13 (4444.13)	885.06 (901.06)	2957.40 (2973.40)	5237.05 (5253.05)	3766.34 (3782.34)
20	Cys_{45}-Cys_{60}	4428.13 (4444.13)	1430.72 (1446.72)	2411.74 (2427.74)	5782.72 (5798.72)	3766.34 (3782.34)
21	Cys_{45}-Cys_{61}	4428.13 (4444.13)	1533.87 (1549.87)	2308.59 (2324.59)	5885.86 (5901.86)	3766.34 (3782.34)
22	Cys_{45}-Cys_{80}	4428.13 (4444.13)	3527.06 (3543.06)	316.38 (332.38)	7878.07 (7894.07)	3766.34 (3782.34)
23	Cys_{54}-Cys_{60}	5270.15 (5286.15)	587.70 (603.70)	2411.74 (2427.74)	5782.72 (5798.72)	2923.32 (2939.32)
24	Cys_{54}-Cys_{61}	5270.15 (5286.15)	690.85 (706.85)	2308.59 (2324.59)	5885.86 (5901.86)	2923.32 (2939.32)
25	Cys_{54}-Cys_{80}	5270.15 (5286.15)	2684.04 (2700.04)	316.38 (332.38)	7878.07 (7894.07)	2923.32 (2939.32)
26	Cys_{60}-Cys_{61}	5815.81 (5831.81)	145.18 (161.18)	2308.59 (2324.59)	5885.86 (5901.86)	2377.66 (2393.66)
27	Cys_{60}-Cys_{80}	5815.81 (5831.81)	2138.38 (2154.38)	316.38 (332.38)	7878.07 (7894.07)	2377.66 (2393.66)
28	Cys_{61}-Cys_{80}	5919.94 (5925.94)	2035.24 (2051.24)	316.38 (332.38)	7878.07 (7894.07)	2274.51 (2290.51)

Figure 47 shows the tabulated m/z values for peptide fragments and β-elimination products predicted to arise if any of the 28 unique, singly-reduced and cyanylated species of EAS isoform Ia were digested with ammonia. Values in brackets refer to the mass of fragments formed from EAS isoform Ib. **Key:** Cys_x-Cys_y designates the disulfide bond that is reduced in the singly-reduced and cyanylated species. Ala_1–(X_{x-1}), itz_x–X_{y-1}, and itz_y–Ala_{82}, designates the S-cyanyl cleavage products. Ala_1–(βCys_x)–X_{y-1} and itz_x–(βCys_y)–Ala_{82} designate the β-elimination products that could result. βCys_x and βCys_y refer to the position of the cysteine modified by the β-elimination reaction. X = any amino acid residue, subscript symbols refer to the position of designated singly-reduced and cyanylated cysteine residues. The symbol itz = iminothiazolidinyl carboxyl residue. The chemical structures of each fragment β-elimination product are given in Appendix VA.

5.1 CONTROL EXPERIMENTS USING RNASE A.

The reduction, cyanylation and cleavage reactions performed on RNase A by Wu and Watson (1997) yielded all but one of the peptide-fragments they predicted would result, thereby confirming the pattern of linked-cysteines previously determined for RNase A by Spackman *et al.* (1960) (see Figure 48 and Table 14).

Prior to analysing EAS by this method, I repeated Wu and Watson's experiments with RNase A to eliminate the uncertainties that might arise from attempting to chemically analysis a protein as chemically resistant as EAS using oxidation-sensitive reagents.

FIGURE 48: THE AMINO ACID SEQUENCE AND DISULFIDE MAP OF RNASE A.

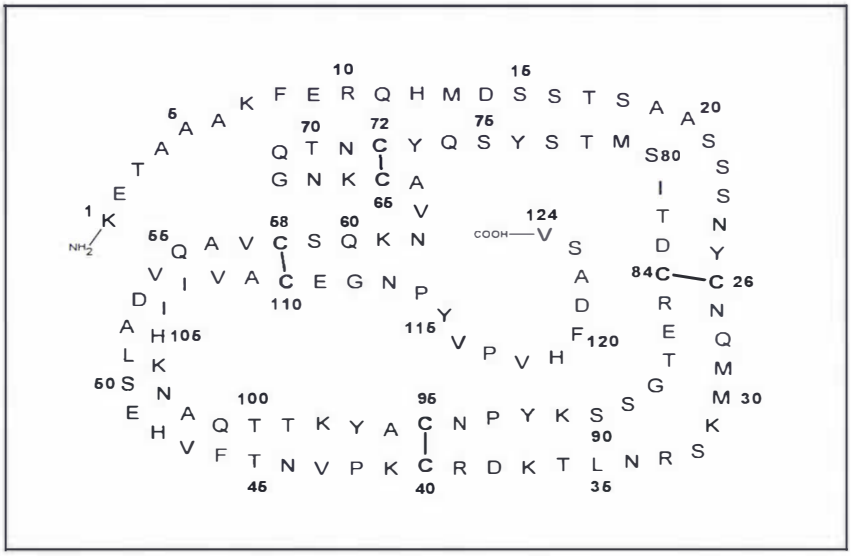

Figure 48 depicts the amino acid sequence and disulfide map of RNase A as determined by Hirs *et al.* (1960), Smyth *et al.* (1963) and confirmed by Wu and Watson (1997). RNase Type IIIA is a molecule consisting of a single chain of 124 amino acids with a molecular mass of 13,680 Da (Smyth *et al.*, 1963). The diagram was adapted from Avey *et al.* (1967).

TABLE 14: M/Z VALUES FOR THE FRAGMENTS OF SINGLY-REDUCED, CYANYLATED RNASE A, CLEAVED AT THE SITES OF THE DESIGNATED CYSTEINE PAIRS (WU AND WATSON, 1997).

Open Cys_{26}-Cys_{84}		Open Cys_{65}-Cys_{72}	
Fragment	**Molecular mass (Da)**	**Fragment**	**Molecular mass (Da)**
Lys_1-Tyr_{25}	2,705.3 (2,701.8#)	Lys_1-Ala_{64}	7,083.8 (7,076.2)
itz_{26}-Asp_{83}	6,548.5	itz_{65}-Asn_{71}	789.8*
itz_{84}-Val_{124}	4,527.4 (4,519.3)	itz_{72}-Val_{124}	5907.7 (5,901.4#)
Lys_1-(βCys_{26})-Asp_{83}	9,176.7	Lys_1-(βCys_{65})-Asn_{71}	7,790.0
itz_{26}-(βCys_{84})- Val_{124}	10,998.6	itz_{65}-(βCys_{72})-Val_{124}	6,618.3
Open Cys_{58}-Cys_{110}		**Open Cys_{40}-Cys_{95}**	
Fragment	**Molecular mass (Da)**	**Fragment**	**Molecular mass (Da)**
Lys_1-Val_{57}	6,351.1 (6,344.2)	Lys_1-Arg_{39}	4,414.4 (4,405.4)
itz_{58}-Ala_{109}	5,766.8 (5,758.8)	itz_{40}-Asn_{94}	6,061.2 (6,053.5)
itz_{110}-Val_{124}	1,659.8 (1,655.5)	itz_{95}-Val_{124}	3,303.7 (3,297.6)
Lys_1-(βCys_{58})-Ala_{109}	12,039.6	Lys_1-(βCys_{40})-Asn_{94}	10,399.5*
itz_{58}-(βCys_{110})-Val_{124}	7,349.1*	itz_{40}-(βCys_{95})-Val_{124}	9,293.4

Table 14 lists the peptides detected by MALDI-TOF/MS after singly-reduced and cyanylated forms of RNase A were subjected to ammonia-catalysed peptide cleavage (Wu and Watson, 1997). **Note:** [*] identifies those fragments that Wu and Watson, (1997) did not detect, the predicted m/z ratio is reported in their place. The symbol itz = iminothiazolidinyl carboxyl residue, βCys denotes that a cysteine residue has been modified by a β-elimination reaction. Bracketed values belong to ions observed during ESI/MS analysis of RNase A performed during this investigation. [#] denotes that these ions were seen in more than one RP-HPLC fractions containing cyanylated RNase A peptides.

FIGURE 49: THE ELUTION PROFILE REDUCED AND CYANYLATED RNASE TYPE III-A.

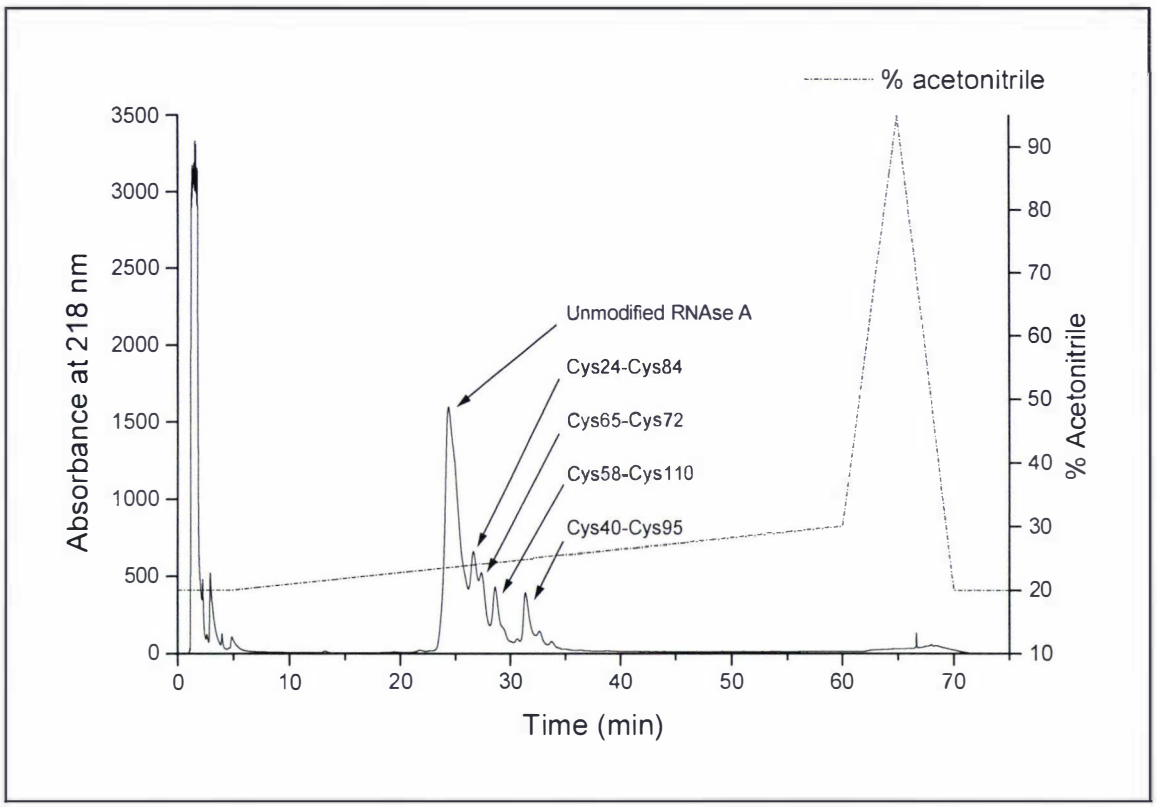

Figure 49 illustrates the elution profile obtained from RP-HPLC purification (section 2.4.7) of reduced and cyanylated RNase A.

As described in section 2.4.7, 1 mg of pure RNase A was dissolved in an aqueous buffer solution containing a chaotrophic agent (6 M guanidine HCl in 0.1 M citrate buffer, pH 3) to completely denature the protein. Then the RNase A was partially-reduced and cyanylated before the derivatised RNase A isomers were resolved by RP-HPLC. The reduced and cyanylated isomers recognised by Wu and Watson (1997) were identified in the RP-HPLC fractions I collected despite the modifications I made to their original protocol (Figure 49).

Each RP-HPLC fraction was treated first with 1 M NH_4OH and then 0.1 M TCEP (as described in section 2.4.7) to cleave the peptide bonds adjacent to the cyanylated cysteine residues and remove any disulfide bonds that remain. Mass-spectrometric analysis of these mixtures identified, in each, the peptide fragments that Wu and Watson predicted would result (Figures 50 and 51).

I analysed peptide mixtures made from the RNase A isomers using both Matrix Assisted Laser Desorption/Ionisation time-of-flight mass spectrometry (MALDI-TOF/MS) and Electrospray Ionisation mass spectrometry with liquid chromatography (LC-ESI/MS). I wanted to that both techniques were compatible with Wu and Watson's protocol in case the range of peptides generated from EAS was too wide to be accurately detected using just MALDI-TOF/MS.

FIGURE 50: LC-ESI/MS ANALYSIS OF TWO OF THE PEPTIDE MIXTURES PRODUCED BY THE DIGESTION OF CYANYLATED RNASE A.

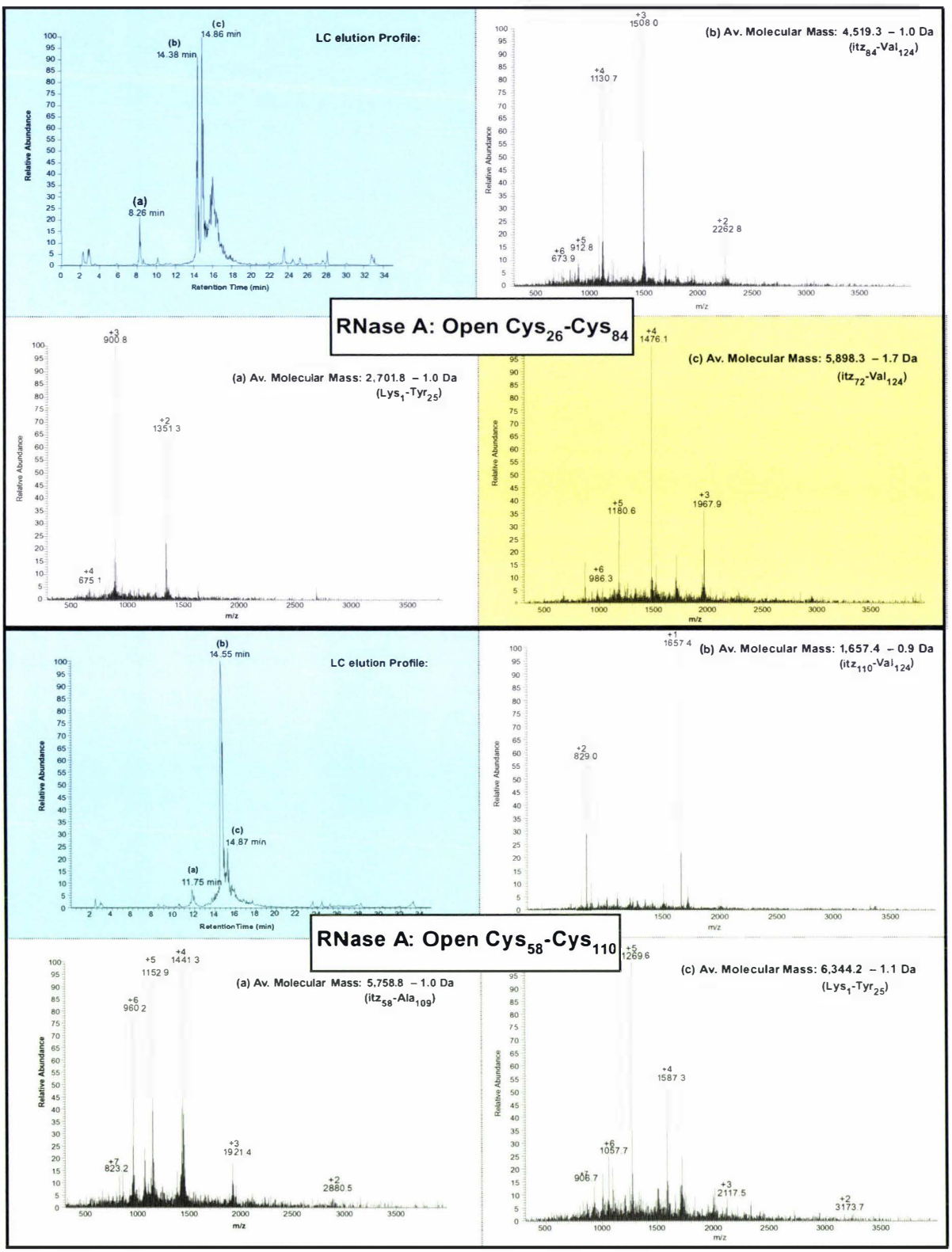

Figure 50 summarises the results of mass-spectrometric analysis of the peptide mixtures obtained from the chemically-digested, cyanylated, isomers of RNase A that are indicated in the central panels. **Key:** each mixture was resolved by HPLC (panels showing the elution profiles have a blue background) then analysed by ESI/MS. The ions within the elution profile peaks labelled (a), (b), and (c) were analysed and the mass-spectrometric result is reproduced in the panels with a white or yellow background. The mass and the identity of the peptide are reported in the panel inset into each spectrum. The molecular mass was calculated using the de-convolution algorithms included with the Finnagin Xcalibur software (version 1.3). The spectra of ions of the peptides that are predicted to occur in a specific mixture have a white background. The spectrum of a peptide contaminating one of the samples has been given a yellow background.

FIGURE 51: MALDI-TOF/MS ANALYSIS OF TWO OF THE PEPTIDE MIXTURES PRODUCED BY THE DIGESTION OF CYANYLATED RNASE A.

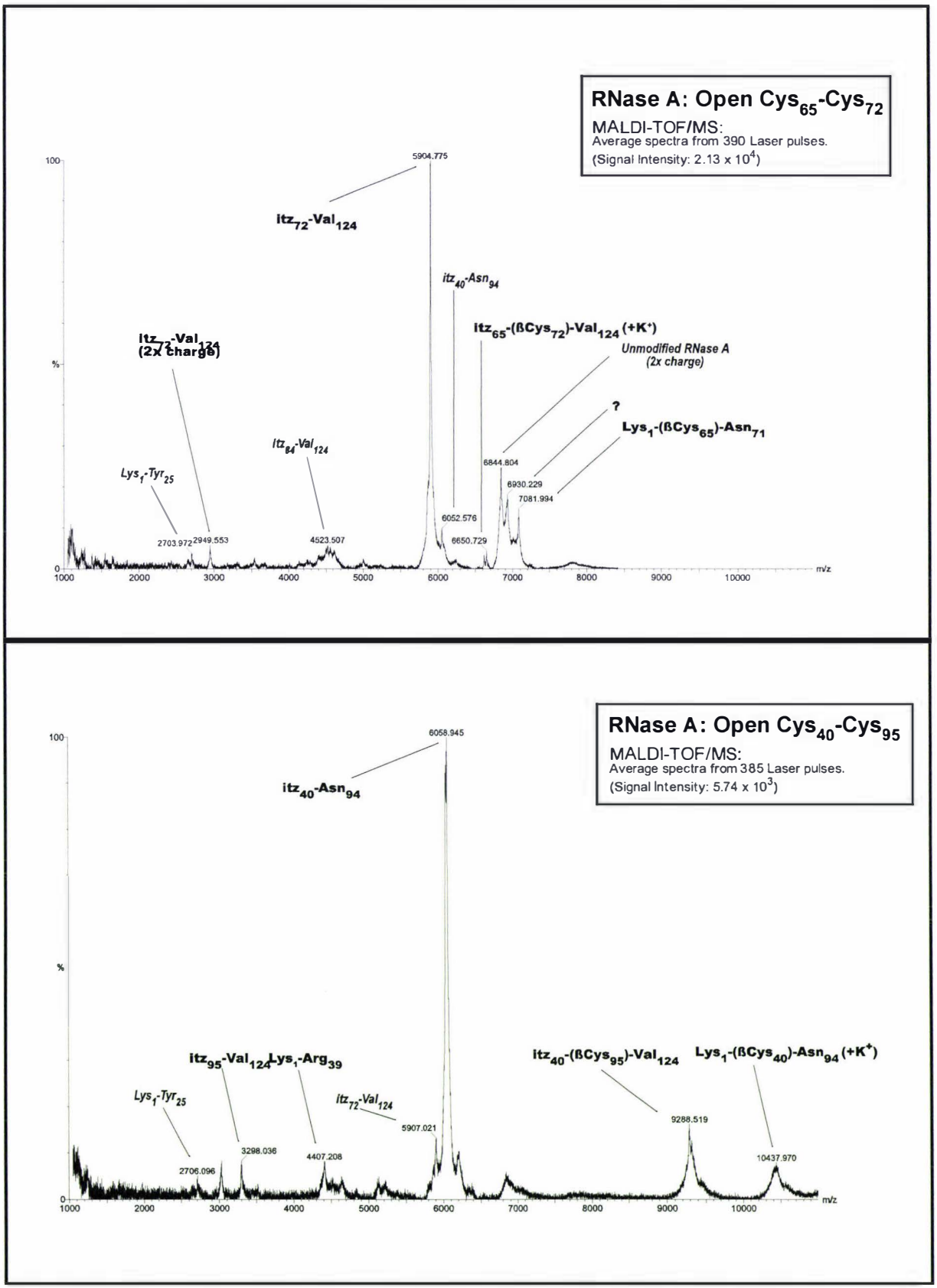

Figure 51 reproduces the results of MALDI-TOF mass-spectrometric analysis of the peptide mixtures derived from chemically-digested cyanylated isomers of RNase A. The two results are divided between the upper and lower panels, A box in each indicates the isomer analysed and the number of samples (number of laser pulses) used to generate each averaged spectra. The mass and the identity for each peptide are reported - contaminating peptides derived from a different RNase A isomers are indicated in italics.

Despite the my inability to completely resolve each of the cyanylated RNase A isomers using RP-HPLC, the specificity of the ammonia-catalysed peptide cleavage reaction allowed each of the peptide species to be identified despite the presence of other peptides derived from RNase A isomers that contaminated each of the RP-HPLC fractions (Figures 50 and 51). By successfully repeating Wu and Watson's RNase A experiments, I proved that I could successfully analyse proteins by this method using the equipment and reagents available to me.

5.2 Disulfide Mass Mapping of EAS

5.2.1 Optimizing the Reduction, Cyanylation and Purification of Derivatised EAS Isomers.

5.2.1.1 Selection of Cyanylation Reaction Conditions.

During these investigations, I used essentially the same protocol to cyanylate EAS. In each case, between 4.7 mM and 9.4 mM of CDAP – equivalent to a 20-fold molar excess over the concentration of cysteine residues present in EAS (eight times the molar concentration of EAS) – was added immediately after the reduction reaction had run its course and it was allowed to react for 30-40 min at 25 °C. CDAP selectively and completely cyanylates sulfhydryls in mild acidic conditions (pH 3 – pH 5), and therefore is compatible with the reaction conditions selected for partial reduction of EAS (Wu and Watson 1997, 1998).

Alternative reagents and conditions were considered for the cyanylation step in this experiment.

Reagents: there are two cyanylating agents currently commercially available: 2-nitro-5-thiocyanobenzoic acid (NTCB) and CDAP. When Wu *et al.* (1996) used NTCB to fully cyanylate the nascent sulfhydryls in Spinach ferredoxin they had to raise the pH of the reaction solution to pH 8, at the risk of promoting disulfide bond scrambling. This is the principal advantage of CDAP; the protein can be maintained in acidic conditions – which are kinetically unfavourable for thiol exchange - throughout the entire procedure.

Reaction conditions: Barbirz *et al.* (1999) observed that CDAP incompletely cyanylated nascent sulfhydryls if the pH of the reaction solution was below pH 4. However, Barbirz *et al.* (1999) omitted the chaotrophic agent from their reactions, introducing the possibility that their results reflect a difference in structural steric hindrance through the pH range tested. The advantages of using guanidine hydrochloride are two-fold:

(1) EAS would have been prevented from aggregating or polymerising during the 45 minute procedure.

(2) While EAS is mostly unstructured in solution, Mackay *et al.* (2001) reported the presence of β-sheet secondary structure near five of the eight cysteine residues. Wu and Watson's strategy depends on each disulfide bond being broken at a comparable rate so that singly-reduced species are produced. Thus, the protein must be denatured prior to any reaction in order to prevent the reducing agent from being sterically hindered (Wu and Watson, 1997).

5.2.1.2 Selecting the Partial Reduction Reaction Conditions.

De Vocht *et al.* (2000) determined that every cysteine in SC3 (after it had been dissolved in a denaturing buffer), could be reduced if it was incubated with a 2-fold excess (over the concentration of disulfide bonds) of DTT for 30 min at 37 °C. It is important to note that De Vocht *et al.* (2000) also used nearly 10-fold more protein per reaction than did Wu and Watson (1997) while investigating RNase A and α-lactalbumin (0.071 μM SC3 versus 0.01 μM of either RNase A or α-lactalbumin). De Vocht's reaction parameters provided a starting point for experiments that were aimed at empirically determining the optimum reaction conditions required to partially reduce EAS with TCEP (A detailed description of these experiments is provided in section 2.4.7.1.) In summary, experiments were conducted to determine the effect on the partial reduction of EAS of varying the reaction temperature (11 °C or 25 °C), or the stoichiometric ratio of TCEP to EAS (between 0.5 μmol and 5 μmol of TCEP to 0.13 μmol of EAS per reaction), or the pH of the reaction solution (pH 3 or pH 5).

For first experiments, the total volume of each reaction was maintained at 1 mL, and after both the reduction and the cyanylation reactions were complete, the solution was diluted and de-salted by applying it to a PD-10 disposable de-salting column (Amersham®) and eluting the protein component with Milli-Q®-water. This eluant was concentrated by lyophilisation and dissolved in an aqueous solution of 30 %(v/v) acetonitrile and 0.1 %(v/v) TFA before each of the cyanylated EAS isomers was resolved by RP-HPLC. The yield of reduced and cyanylated EAS from this protocol was poor, and the HPLC protocol was ineffective at resolving the individual EAS isomers (Figure 52A).

Nevertheless, I was able to analyse these protein fractions by mass-spectrometry and determined that using 10-fold excess of TCEP (reacted pH 3 for 15 min at 25 °C) over the disulfide bond content was sufficient to produce singly-reduced

isoforms of EAS (see Figure 52B and C, the exact reaction details are given in Table 15).

TABLE 15: PROTOCOLS FOR THE REDUCTION AND CYANYLATION OF EAS.

BEST INITIAL PROTOCOL - (TO BE PURIFIED WITH THE JUPITER 250 MM X 4.6 MM COLUMN).

Chemical	Amount per Reaction	(µmol)	(mM)	Reaction Conditions	
				Reaction Volume	1 mL
EAS	1 mg/mL	0.126	0.126	pH	3.0
1 M TCEP	5 µL	5	4.96	Reaction Temperature	25 °C
1 M CDAP	20 µL	20	19.51	Reaction Time: (reduction/cyanylation)	15 min/30min

FINAL OPTIMISED PROTOCOL - (TO BE PURIFIED WITH THE µRPC C2/C18 ST 4.6/100 COLUMN).

Chemical	Amount per Reaction	(µmol)	(mM)	Reaction Conditions	
				Reaction Volume	105 µL (with TCEP).
EAS	1 mg/100 µL	0.126	1.25	pH	3.0
1 M TCEP	5 µL	5	49.6	Reaction Temperature	11 °C
1 M CDAP	20 µL	20	160	Reaction Time: (reduction/cyanylation)	15 min/30min

Note that in Table 15, **Reaction volume** refers to the amount of reaction buffer (6 M guanidine hydrochloride in 0.1 M citrate buffer at pH 3.0) used to dissolve EAS. The volumes of 1 M TCEP and 1 M CDAP solutions were added in addition to this; therefore the concentration (**mM**) column represents the final concentration of each component at the time it was added to the reaction. For reasons outlined in section 5.2.1.3, the isomers generated by the "best initial protocol" were fractionated using the the Jupiter™ 250 mm x 4.6 mm column and the RP-HPLC gradient described by Figure 14, while the isomers generated with the "final optimised protocol" were fractionated using the Amersham® µRPC C2/C18 ST 4.6/100 column and the RP-HPLC gradient described by Figure 15. More detailed descriptions of the reaction and purification protocols are given in 2.4.7.1 while the RP-HPLC columns are described in Table 4.

5.2.1.3 THE OPTIMISED PURIFICATION PROTOCOL.

Kinter and Sherman (2000a) have observed that the amount of sample lost by irreversible adsorption to container surfaces can be minimised by reducing the number of times the sample is handled. The purification protocols described above incorporate a de-salting step designed to remove guanidine hydrochloride from the solution before it was applied to a Jupiter™ 250 mm x 4.6 mm RP-HPLC column (see section 2.4.7.1). Accordingly, I found that by replacing the Jupiter column with an Amersham® µRPC C2/C18 RP-HPLC column the protein-yield from the purification process improved.

The µRPC C2/C18 column is designed for peptide-mapping and (according to the manufacturer) it is resistant to high concentrations of chaotrophic salts. Using this column enabled me to combine the de-salting and RP-HPLC steps of the protocol described above. To use the column this way I had to reduce the total volume of the partial-reduction and cyanylation reactions to ensure that the entire reaction solution could be applied and fractionated in a single RP-HPLC experiment. This had the effect of increasing the concentration of the reactants, but did not alter the stoichiometry of the reaction (see Table 15 and section 2.4.7.1).

The extent to which these changes improved the yield of derivatised EAS isomers is demonstrated by the RP-HPLC elution-profile reproduced in Figure 52D; there is a clear increase in the intensity of the absorbance (at 218 nm) for peaks containing the reduced and cyanylated isomers of EAS.

However, despite the fact that I varied the solvent gradients and the solvent flow rates, I was unable to optimise the RP-HPLC protocol to the point where the peak resolution was sufficient to completely resolve each of the reduced and cyanylated EAS isomers. The best RP-HPLC result is depicted in Figure 52D, and it clearly indicates that the analysis of chemically-digested fractions resolved with this RP-HPLC protocol will be complicated by the presence of peptides from other reduced and cyanylated isomers of EAS.

Hitherto unseen peaks appeared in the elution profile after the protocol was modified to consolidate the de-salting and RP-HPLC steps. To identify these peaks, the RP-HPLC fractions indicated in Figure 53A were collected, resolved by SDS-PAGE and silver-stained (see Figure 53B) to detect any proteinaceous components.

It is clear from the result that the fractions collected during the hydrophilic phase of the solvent gradient (between 0 min and ~15 min) contain no protein and are probably adducts of reagents TCEP and CDAP. This conclusion is supported by the fact that peaks with similar intensity and retention times were seen when a mixture of TCEP and CDAP dissolved in the denaturing buffer were resolved by RP-HPLC (data not shown). The molecular mass of the protein components within the fractions collected during the hydrophobic phase of the gradient (between ~16 min and 40 min) suggest that each is derived from EAS (Figure 53B).

5.2.1.4 Mass-Spectrometric Analysis of Peptide Fragments.

Unfortunately, one of the consequences of the steps taken to reduce the number of times the derivatised products were handled was to increase the concentration of reagents in the reduction and cyanylation reactions 10-fold (Table 15). This caused the yield of doubly reduced and cyanylated EAS isomers to increase (see MALDI-TOF/MS results reproduced in Appendix VB). I found I could counter this effect by lowering the temperature of the reduction reaction from 25 ºC to 11 ºC (see final optimised protocol in Table 15), MALDI-TOF/MS analysis of the RP-HPLC fractions indicated that this change ensured that the reduction reaction once again produces predominately singly-reduced and cyanylated isomers (Figure 54).

FIGURE 52: OPTIMISING THE PURIFICATION OF SINGLY-REDUCED CYANYLATED EAS.

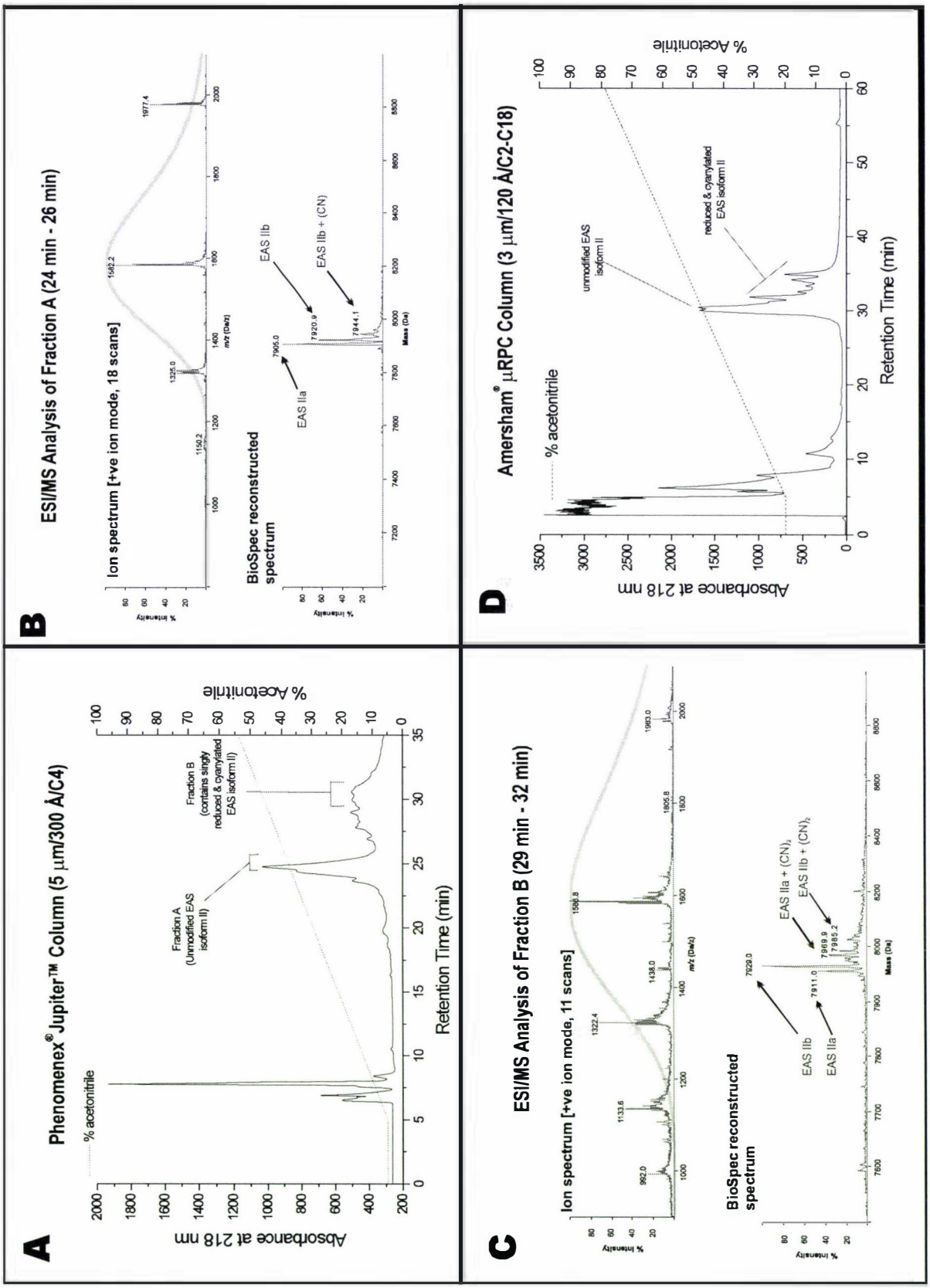

Figure 52A depicts the RP-HPLC elution profile from a preliminary experiment investigating the conditions necessary to singly reduce and cyanylate EAS (see text for details). The protein fractions indicated in Figure 52A were sent for ESI/MS analysis to MasSpec Services (see section 2.4.5) for ESI/MS analysis (shown in Figure 52B and C) which confirmed that singly-reduced and cyanylated isomers had been formed. Steps were taken to improve the initial RP-HPLC purification protocol. Figure 52D depicts the elution profile from the optimized RP-HPLC protocol (see section 2.4.7.1).

FIGURE 53: SDS-PAGE ANALYSIS OF REDUCED AND CYANYLATED ISOMERS.

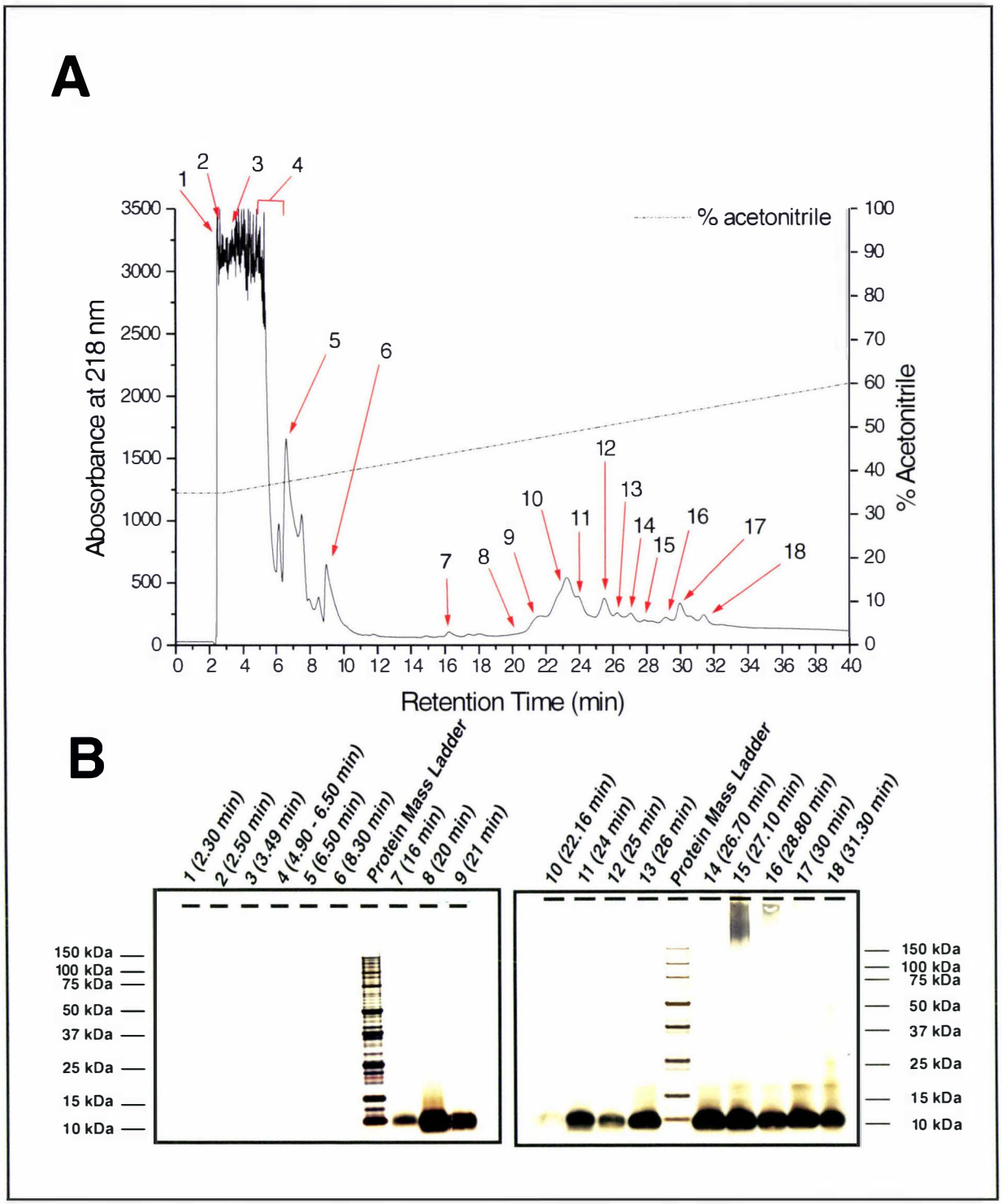

Figure 53A shows the typical elution profile obtained when the optimised RP-HPLC protocol used to purify derivatised EAS isomers from the reduction and cyanylating reaction mixture. In Figure 53B, the RP-HPLC fractions indicated in Figure 53A are shown after they were resolved by SDS-PAGE and the proteins in them stained with silver (see section 2.4.6).

FIGURE 54: THE OPTIMISED DERIVATISATION AND PURIFICATION OF SINGLY-REDUCED EAS

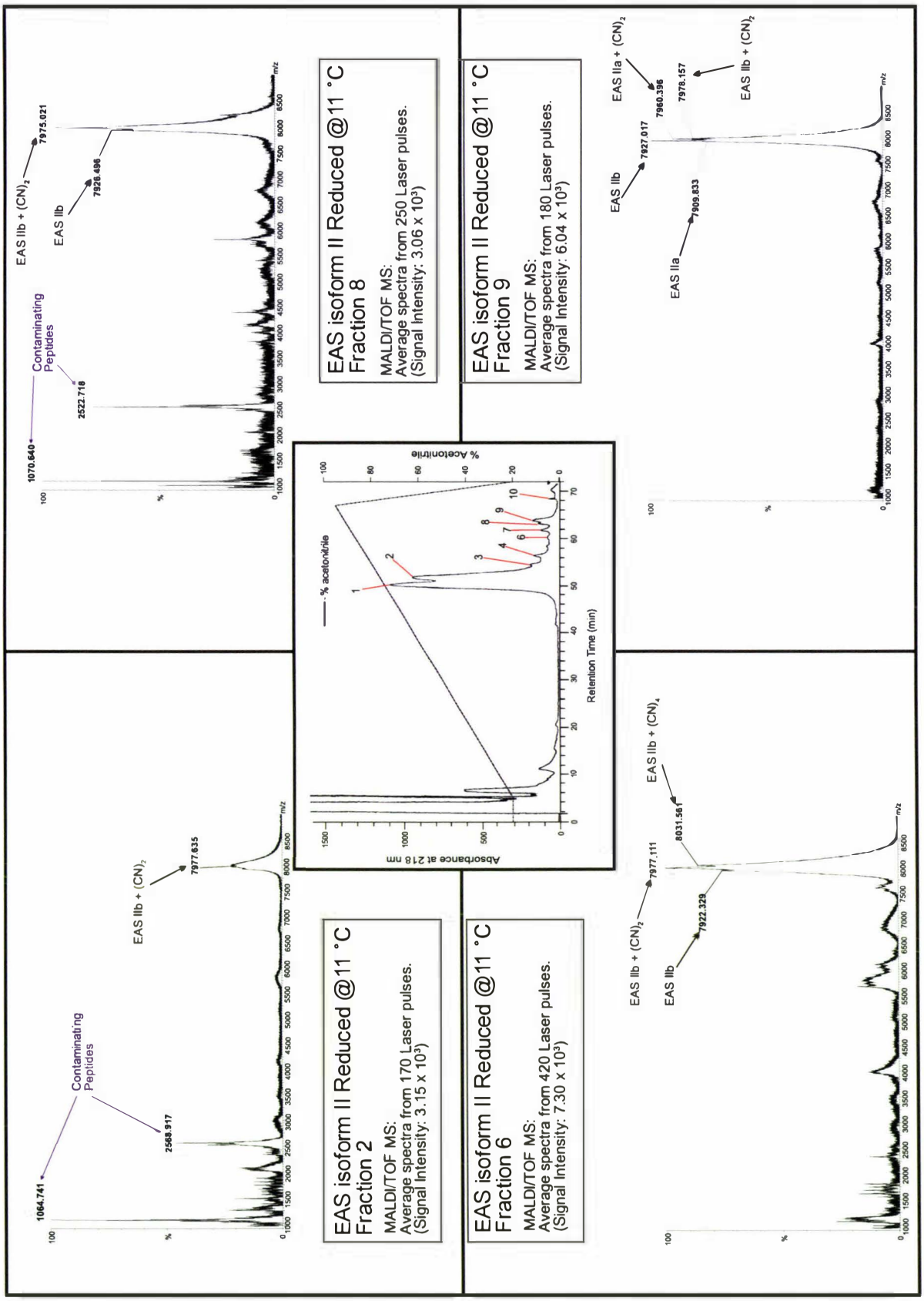

The central panel in Figure 54 reproduces the elution profile obtained by the RP-HPLC fractionation of the derivatised isomers of EAS isoform II; these isomers were derivatised using the optimised protocol described in Table 15. The surrounding panels summarise the MALDI-TOF mass-spectrometric analysis of each of the fractions resolved by RP-HPLC. MALDI-TOF mass spectrometry was used to determine whether these fractions contained any singly-reduced and cyanylated isomers of EAS isoform II (see section 2.4.7.1).

I could not quantitate the yield of derivatised EAS in each RP-HPLC fraction because the amount of protein present was insufficient to permit accurate measurements to be made. After the RP-HPLC fractions had been lyophilised, was hardly enough derivatised EAS to allow it to be seen, let alone be weighed or measured with a protein quantitation assay (Walker, 1996). Despite this, the sensitivity of MALDI-TOF/MS is such that as long as I used the entire RP-HPLC fraction when evaluate the peptide-cleavage reactions and subsequent digestion reactions by mass-spectrometry I was able to obtain a result (Carr and Annan, 1997).

5.2.2 Mapping the Disulfide Bonds in EAS.

I prepared reduced and cyanylated samples of EAS isoforms Ia and Ib using the optimised protocol described in Table 15. After fractionating the derivatised isomers of each isoform with the RP-HPLC protocol described in section 5.2.1.3, I digested them with ammonium hydroxide and TCEP as described in section 2.4.7.1. I analysed the peptide mixtures that resulted from these treatments by MALDI-TOF mass spectrometry (the analysis was conducted in the positive-ion, linear-mode of operation) The analysis of peptide mixtures obtained from isoform Ia are presented in Figure 55, while those obtained from isoform Ib are presented in Figure 56.

The mass resolution of the MALDI-TOF mass-spectrometric analysis presented in Figures 55 and 56 is insufficient to resolve the individual components of the ion cluster represented by each peak in these figures (the FWHM[2] mass resolution is <100 for every peak) (Kinter and Sherman, 2000b). This is an unavoidable consequence of having to perform MALDI-TOF/MS in linear-mode so that the widest possible range of peptide fragments could be detected. The mass resolution of linear-mode is limited to ~600 for peptides, and it decreases as the size (m/z-ratio) of the ions increases (Carr and Annan, 1997). This low-resolution problem is exacerbated by the concentration of the peptide-analytes being so low, which in turn, is due to the small amount of the derivatised parent-molecule available.

Despite these difficulties, the disulfide bridges in EAS can be consistently identified based on the average m/z-value for each of the molecular ion peaks seen in Figures 55 and 56. The ions detected in Figures 55 and 56 are cross-referenced with the peptide fingerprints expected when the disulfide bonds between Cys_9-Cys_{60} (green), Cys_{18}-Cys_{54} (red), Cys_{19}-Cys_{45} (blue), and Cys_{61}-Cys_{80} (black) are broken (see Table 16). The ions associated with each fingerprint are colour coded in both the figures

[2]Full-width, half-maximum (FWHM) definition of mass resolution = [m/z value] ÷ [peak-width (Δm/z) at half the hieght of the peak] (Kinter and Sherman, 2000b).

and the table to aid in identifying the patterns: the colour-code for each fingerprint is indicated in brackets above. Peptide fragments from isomers that are doubly reduced and do not correspond with these bonds are coloured grey in Figure 55 and Figure 56.

In theory, for a disulfide bridge to be assigned the entire pattern of five peptides and β-elimination products unique to a derivatised isomer must be detected in the mass spectra of the peptide-products derived from a single RP-HPLC-purified isomer. In practise one or more of the cleavage and β-elimination products may not be detected (discussed below), and the RP-HPLC fractions used were contaminated with co-eluting derivatised EAS isomers. Therefore, the pattern of disulfide bonds denoted in Figures 55 and 56 was assigned according to two conditions:

(1) that three or more of the peptides predicted to arise from a particular reduced and cyanylated EAS isomer were present in the same mass spectra;

(2) that one of the peptide-ions seen was unique to that isomer's particular pattern of peptides (such peptides are shaded grey in Table 16).

Table 16 demonstrates how the pattern of disulfide bonds denoted in Figures 55 and 56 exceeds these minimum criteria: in the case of each derivatised isomer identified in Table 16, least three of the five peptides (including the unique cleavage product) are present in single mass-spectra obtained during two separate experiments. The fact that these results are consistent over two separate experiments on two separate isoforms of EAS suggests that the results are reproducible and that the pattern of disulfide linkages is identical in all EAS isoforms.

In assigning identities to the peaks in Figures 55 and 56, I have allowed for the production of metastable ion-decay products; such as are produced when the MALDI-TOF/MS laser is used at its highest energy settings (Kinter and Sherman, 2000c). I was forced to use the laser at close to its highest power in order to detect the larger ions in these samples. Some of the ions were assigned as photochemical adducts with the matrix (similar to those seen in experiments performed on sillucin by Qi *et al.,* 2001) and adducts with cations whose presence was expected given that, unlike the samples in Figure 54, these were not purified by RP-HPLC prior to mass-spectrometric analysis.

FIGURE 55: MAP OF DISULFIDE BRIDGES IN EAS ISOFORM IA

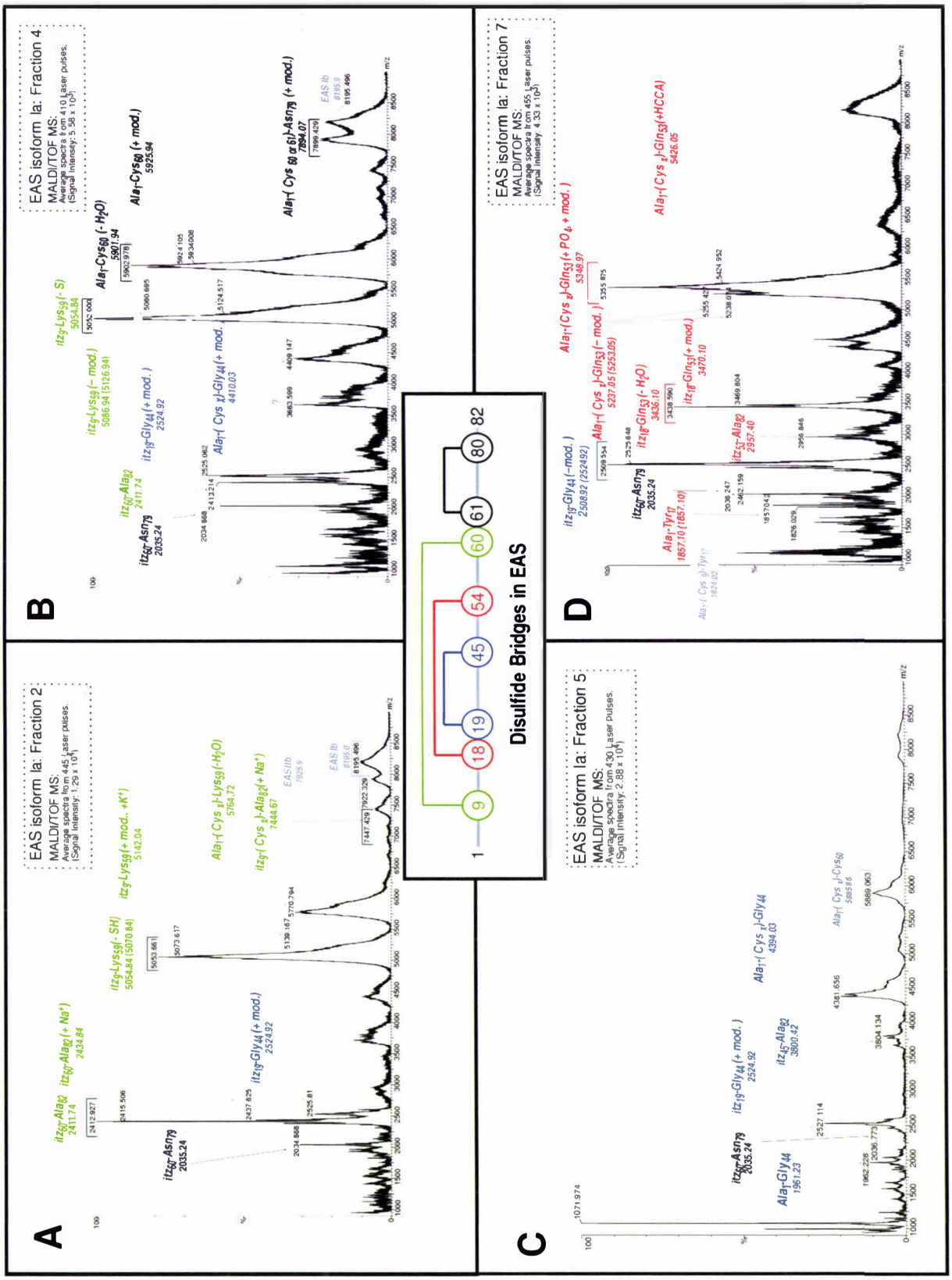

The central panel of Figure 55 shows a map of the disulfide bridges in EAS deduced using the mass mapping method. The surrounding panels reproduce the results of the mass-spectrometric analysis carried out on the chemically digested, singly-reduced and cyanylated isomers of EAS isoform Ia. **Key:** The identity of each ion is indicated and the labels are colour coded to identify fragments arising from the digestion of isomers in which the disulfide bridge - with the same colour in the central panel - has been broken and the cysteines cyanylated. Each ion is identified using the nomenclature established in Figure 46. Adducts/decay products are identified thus: **[-S/H_2O]** = loss of sulfur atom or water (dehydration), **[+K/Na/PO_4]** = a cation adduct, **[+HCCA]** = photochemical adduct with matrix, **[+ mod.]** indicates that a 16 Da post-translational modification is present in this fragment.

FIGURE 56: MAP OF DISULFIDE BRIDGES IN EAS ISOFORM IB.

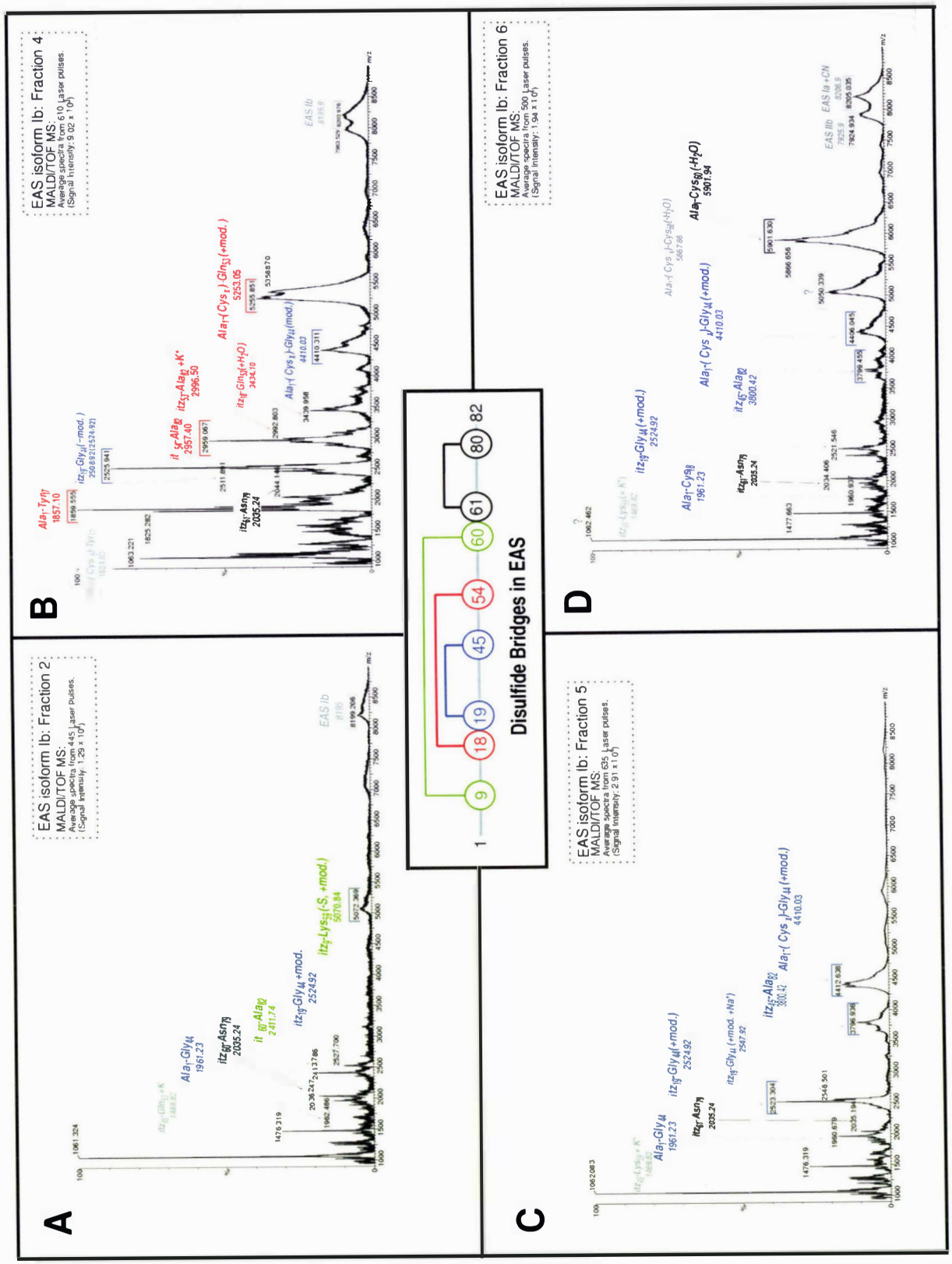

The central panel of Figure 56 shows a map of the disulfide bridges in EAS deduced using the mass mapping method. The surrounding panels reproduce the results of the mass-spectrometric analysis carried out on the chemically digested, singly-reduced and cyanylated isomers of EAS isoform Ib. **Key:** The identity of each ion is indicated and the labels are colour coded to identify fragments arising from the digestion of isomers in which the disulfide bridge - with the same colour in the central panel - has been broken and the cysteines cyanylated. Each ion is identified using the nomenclature established in Figure 46. Adducts/decay products are identified thus: **[-S/H_2O]** = loss of sulfur atom or water (dehydration), **[+K/Na/PO_4]** = a cation adduct, **[+HCCA]** = photochemical adduct with matrix, **[+ mod.]** indicates that a 16 Da post-translational modification is present in this fragment.

TABLE 16: M/Z VALUES FOR THE FRAGMENTS OF SINGLY-REDUCED, CYANYLATED EAS, CLEAVED AT THE SITES OF THE DESIGNATED CYSTEINE PAIRS.

Open Cys_9-Cys_{60}				Open Cys_{18}-Cys_{54}			
Fragment	Predicted mass (Da)	MS result EAS Ia	EAS Ib	Fragment	Predicted mass (Da)	MS result EAS Ia	EAS Ib
Ala_1-Thr_8	772.88 (788.88)	N.D.	N.D.	Ala_1-Tyr_{17}	1857.10 (1873.10)	54D	55B
itz_9-Lys_{59}	5086.94 (5102.12)	54A[1,2]	55A[1,2]	Itz_{18}-Gln_{53}	3454.10 (3470.10)	54D[1,2]	55B[1]
itz_{60}-Ala_{82}	2411.74 (2427.74)	54A[1,2]	55A	Itz_{54}-Ala_{82}	2957.40 (2973.40)	54D	55B[1]
Ala_1-(βCys_9)Lys_{59}	5782.72 (5798.72)	54A[1]	N.D.	Ala_1-(βCys_{18})Gln_{53}	5237.05 (5253.05)	54D[1,2]	55B[1,2]
itz_9-(βCys_{60})Ala_{82}	7421.57 (7437.57)	54A[1]	N.D.	Itz_{18}-(βCys_{54})Ala_{82}	6336.36 (6352.36)	N.D.	N.D.
Open Cys_{19}-Cys_{45}				**Open Cys_{61}-Cys_{80}**			
Fragment	Predicted mass (Da)	MS result EAS Ia	EAS Ib	Fragment	Predicted mass (Da)	MS result EAS Ia	EAS Ib
Ala_1-Cys_{18}	1961.23 (1977.23)	N.D.	N.D.	Ala_1-Cys_{60}	5919.94 (5925.94)	54B[1,2]	55D[1]
itz_{19}-Gly_{44}	2508.92 (2524.92)	54C	55C[2]	Itz_{61}-Asn_{79}	2035.24 (2051.24)	54B	55D
itz_{45}-Ala_{82}	3800.42 (3816.42)	54C	55C	Itz_{80}-Ala_{82}	316.38 (322.38)	N.D.	N.D.
Ala_1-(βCys_{19})Gly_{44}	4394.03 (4410.03)	54C	55C[2]	Ala_1-(βCys_{61})Asn_{79}	7878.07 (7894.07)	54B[2]	N.D.
Itz_{19}-(βCys_{45})Ala_{82}	6233.22 (6249.22)	N.D.	N.D.	Itz_{61}-(βCys_{80})Ala_{82}	2274.51 (2290.51)	N.D.	N.D.

Singly-reduced and cyanylated isomers of EAS isoforms Ia and Ib were fractionated by RP-HPLC and then chemically digested to yield peptide mixtures for MALDI-TOF mass-spectrometric analysis. Table 16 summarises the mass-spectrometric analysis of each peptide mixture, identified by the panel (A, B, C, or D) in either Figure 55 (labelled 54) or Figure 56 (labelled 54) in which the raw result is reproduced. Table 16 lists the identity and predicted mass for each ion (established in Figure 46) along with the panels bearing the mass spectra in which that ion and at least two other ions from that isomers fragment fingerprint are present. The presence or absence of each ion is tabulated here to demonstrate how many fragments of the predicted pattern were detected. **Key:** The symbol **[54A]** denotes that the designated peptide was detected in the mass spectra reproduced in Figure 55A and so on. The colour coding of fragment patterns is consistent with that used in Figure 55 and Figure 56. The number [[1]] denotes that this peptide ion was carrying a cation adduct or some metastable decay product. The number [[2]] denotes that the peptide ion was carrying the 16 Da post translational modification that gives rise to EAS isoforms Ib and IIb. Shaded entries denote peptides that are unique to a particular predicted fragment pattern. N.D. = not detected. The symbol itz = iminothiazolidinyl carboxyl residue, βCys denotes a cysteine residue modified by a β-elimination reaction. Bracketed values denote the predicted mass of the peptide ion it is carrying the 16 Da post translational modification that gives rise to EAS isoforms Ib and IIb.

Some of the peptide-products of the predicted to arise after cleavage were not detected in the experiments described above. This is thought to be due to a combination of ion suppression and to the detection limits intrinsic to MALDI-TOF/MS (Carr and Annan, 1997). Ion suppression occurs when salts or other highly ionisable species in the sample interfere with the ionisation of the analyte, and prevents the mass spectrometer detecting the ion (Carr and Annan, 1997).

The suppression of ions corresponding to the Ala_1-Cys_{18} peptide was likely caused by the presence of salts that were not removed by the de-salting treatment used as the MALDI-TOF samples were prepared (see section 2.4.7.1 and Beavis and Chait, 1990). When a more stringent de-salting technique (passage through Millipore® Ziptip® μ-C18 pipette tips) was used to prepare another sample derived from EAS isoform II, the equivalent ion (Ile_4-Cys_{18}) was detected by MALDI-TOF/MS analysis.

The sub 1 kDa peptide ions (the Ala_1-Tyr_9 and itz_{80}-Ala_{82} peptides) that should have been generated with this protocol could not be detected because I had to set the MALDI-TOF/MS device to ignore ions with an m/z <1 kDa. This step was taken to prevent matrix-derived ions from swamping the mass spectra. Analysis of MALDI-TOF samples that contained no protein, demonstrated that most of the sub 1 kDa ions were derived from the either matrix or non protein reagents in the final reduction solution (data not shown).

Investigations by Wu and Watson (1998) showed that the yields of β-elimination products should be reduced when ammonia is used to induce digest the cyanylated peptides (ammonia has a smaller proton affinity than the alternate: the hydroxyl ion from sodium hydroxide). This may explain why the β-elimination products itz_{61}-(βCys_{80})-Ala_{82}, itz_{19}-(βCys_{45})-Ala_{82}, and itz_{18}-(βCys_{54})-Ala_{82} could not be detected.

Wu and Watson (1998) also noted that the amino acids to the N-terminal side of the cyanylated cysteine could adversely influence the yield from the peptide cleavage reaction. They suggested that the bulky or rigid side-chains on amino acids like proline and tyrosine could sterically hinder each of the two consecutive nucleophilic attacks required to cleave the peptide bond. First, ammonia must be unimpeded in its attack on the scissile carbonyl atom; second, the SCN-group that must be correctly oriented before it can participate in the second nucleophilic attack made by the activated amide of the cyanylated cysteine (Figure 45). This explains why the Ala_1-(βCys_{18})-Gln_{53} β-elimination product was so abundant; Tyr_{17} lies adjacent to the cyanylated Cys_{18} (see Figure 46).

In the mass spectra presented in Figure 56B, both forms of the itz_{19}-Gly_{44} ion, (with and without the 16 Da post-translational modification that gives rise to EAS isoforms Ib and IIb) have been detected. This is the smallest peptide fragment detected with this modification. Larger ions containing this segment of EAS have also been identified as carrying the post-translational modification (see ions with the "+mod." suffix in Figures 54 and 55). This implies that the amino-acid(s) carrying the modification are in this region of EAS. Unfortunately, there are five lysines, three prolines, and five serine residues in this region, any of which could have been post-translationally modified by either methylation (lysine) or hydroxylation (serine and proline). The only way to identify the modified residue(s) would be to sequence the itz_{19}-Gly_{44} by tandem mass spectroscopy or N-terminal sequencing.

5.3 Discussion.

5.3.1 Identifying the 16 Da Post Translational Modification.

The Cys_{19}-Gly_{44} peptide could be generated by oxidising every cysteine in EAS with performic acid, then cleaving the adjacent peptide bonds with endopeptidase Asp-N (EC 3.4.24.33) – a metallo-enzyme isolated from a mutant of *Pseudomonas fragi* that is able to hydrolyze the peptide bonds on the N-terminal side of aspartic and cysteic (oxidised cysteine) acids (Hagmann *et al.,* 1995).

A more attractive alternative would be to modify the partial reduction method described above in order to *fully* reduce and cyanylate the protein prior to chemical digestion with ammonia. This would generate nine peptides, one being itz_{19}-Gly_{44}. Unfortunately, I was unable to fully reduce EAS using TCEP, despite varying the stoichiometry of the reagents, the temperature, and pH. However, de Vocht *et al.* (2000) successfully reduced SC3 using DTT in alkaline denaturing conditions that are compatible with NTCB (another cyanylating agent). Using DTT and NTCB in concert should allow sufficient itz_{19}-Gly_{44} to be produced to enable protein sequencing to identify the modified residue in EAS isoforms Ib and IIb.

5.3.2 Improving the Mapping Protocol.

The product yield of the derivatising reactions was poor, given that a milligram of hydrophobin was consumed. There are several hydrophobins (e.g. cerato-ulmin: Richards and Takai, 1973; SC3: Wösten *et al.* 1993) that can be purified in milligram quantities or more. Therefore, this technique described in this chapter could be applied without modification to support the hypothesis that the disulfide pattern established for EAS and HFB2 is common to class I and class II hydrophobins.

However, improving the mapping protocol would enable it to be used to analyse other cysteine-rich proteins as well as newer – less well-characterised – hydrophobins. The most obvious application of an improved mapping protocol would be to analyse the putative hydrophobin domains of CFTH1 and CPPH1, this task would be made simpler if less hydrophobin was needed for mapping. The reason is that each domain would have to be isolated and purified (assuming that only intra-domain disulfide bonds are present) in milligram amounts using the current method. Therefore, it would be useful to devote some space to discussing ways by which this protocol could be improved.

Clearly, the chemical reaction that limits the amount of derivatised protein available for analysis is the partial reduction step, but before this reaction can be improved, the RP-HPLC protocol used to separate the derivatised isomers from each other

needs improvement. If this were possible, then the effect of varying the chemical parameters of the partial reaction (duration, temperature, pH, or stoichiometry) could be sensibly assessed.

5.3.2.1 Improving the RP-HPLC Protocol.

The biggest improvements in the protocol could potentially, come from using a different RP-HPLC column and raising the pH of the solvents. The resolution of RP-HPLC depends on the efficiency (related to the chemical properties of the solvent), selectivity, and binding capacity of the column (AP-Biotech, 1999).

The effect of systematically altering the chemical properties of the mobile phases was not investigated, even though the silica-based matrix in the Amersham® µRPC ST 4.6/100 column allows it to withstand solvents buffered between pH 2 - 7 (as per manufacturer's specifications). I persisted with the water/acetonitrile-gradient (with 0.1 %(v/v) TFA as an ion pairing agent to ensure a pH <3.5) because cyanylating the protein shouldn't have introduced any new ionisable groups and I did not expect that altering the pH of the mobile phase would have improved the ability of RP-HPLC to resolve these isomers. However, any incompletely cyanylated isomers would have more ionisable groups and these species might be better resolved if the pH of the mobile phase was altered. Replacing TFA as the ion-pairing agent with triethylamine (or even reducing the concentration of TFA) should raise the pH of the solvent (AP-Biotech, 1999; Henzel and Stults, 2001) without the need to introduce an ionic buffering-agent that could interfere with the pH of later reactions (Wu and Watson, 1997).

The Amersham® µRPC ST 4.6/100 column was selected mainly for its resistance to 6 M guanidine hydrochloride. However, given the hydrophobicity of EAS the protocol might be improved if a column with a more hydrophilic solid-phase was used. Amersham® recommends that columns with a C8 ligand be used when purifying hydrophobic proteins (AP-Biotech, 1999). In theory, using such a column affords the opportunity to improve both the relative retention of each species and the efficiency of sample recovery because the hydrophilic ligand should bind the hydrophobin less strongly (Henzel and Stults, 2001).

Researchers at the University of Groningen did not succeed in applying Wu and Watson's method to SC3. Poor resolution during HPLC purification prevented them from properly resolving the partially reduced products (de Vocht, 2001). This result implies that it may not be possible to completely resolve partially-reduced and cyanylated hydrophobins.

5.3.2.2 Improving the Efficiency of Sample Recovery.

The yields of derivatised protein might have been improved if siliconised plastic ware (tubes, pipette tips *etc.*) was used. The siliconising treatment is thought to reducing the number of surface sites to which the sample can adsorb and thus reduces the amount of sample lost through surface adsorption during purification and subsequent concentration steps (Kinter and Sherman, 2000a).

Reducing the number of steps required to analyse the sample by mass spectrometry is another way by which the efficiency of sample recovery might be improved in this protocol. Preparing a sample for analysis by LC-ESI/MS requires fewer sample-preparation steps than MALDI-TOF/MS. Directly after the final TCEP reaction, the sample can be applied to the LC column, and any peptides in the sample can be fractionated and analysed – as they are eluted – by mass spectrometry.

5.3.2.3 Improving MALDI-TOF/MS Analysis.

The greatest advantage with MALDI-TOF/MS is that the technique produces very few multiply-charged ions. This greatly simplifies the interpretation of mass spectra derived from the poorly-resolved, mixed samples analysed in the experiments described above. Nevertheless, the best quality MALDI-TOF/MS results are obtained from salt-free samples (Carr and Annan, 1997; Kinter and Sherman, 2000a).

To generate salt-free samples from Wu and Watson's method requires that the residual TCEP and guanidine be removed from the digested hydrophobins prior to MALDI-TOF mass spectrometry. Xu *et al.* (2003) reviewed a number of "non-specific, on-probe clean-up steps" designed to de-salt the sample during or after it has been prepared for MALDI-TOF/MS. The techniques include the use of membranes bound to the MALDI-TOF sample plate that are designed to specifically adsorb protein (*e.g.* Zaluzec *et al.,* 1994). This is compatible with the micro-scale analysis method developed by Wu *et al.* (1996) for a related protein cyanylation/mass-analysis strategy. In essence, the protein is bound to a Nylon membrane mounted on a MALDI-TOF sample plate. The protein is chemically derivatised, de-salted, and prepared for MALDI-TOF/MS analysis *in situ.* Unfortunately, with Wu and Watson's disulfide mapping protocol, only the steps after RP-HPLC fractionation of the derivatised proteins are compatible with this micro-scale technique, but if used it would reduce the number of times the analyte is handled.

The mass resolution achieved with the linear mode MALDI-TOF/MS analysis was another limitation in this study. Using internal standards or "time-lag focusing" techniques could improve the mass-resolution of this device in linear mode (Carr and Annan, 1997). If the yield of the derivatising reactions could be increased then both the signal-to-noise ratio and the mass-resolution in the MALDI-TOF spectra would increase, as was seen when a ~0.01 µg of unmodified EAS isoform II was analysed with this technique (data not shown).

Alternatively, the part of the analysis could be performed in reflectron (reflector) mode. This technique significantly increases the achievable mass-resolution of MALDI-TOF devices (Carr and Annan, 1997). Unfortunately, the increased mass-resolution comes at the cost of decreased sensitivity (personal communication with David Lun, technical officer, Institute of Fundamental Sciences, Massey University). When the M@ldi™ LR mass spectrometer was used to analyse these samples in reflectron mode, the spectrometer was unable to detect ions larger than ~3000 Da/z from digested RNase A samples (data not shown). Nevertheless, a MALDI-TOF instrument operated in reflectron mode could still be used to obtain monoisotopic masses for the smaller ions derived from a hydrophobin treated according to Wu and Watson's method.

5.3.2.4 LC-ESI/MS Analysis.

LC-ESI/MS offers several advantages over MALDI-TOF/MS. The liquid-chromatography step de-salts the sample and resolves the peptides prior to applying them to the electrospray source. In this way, problems that are encountered with MALDI-TOF/MS (that is, either signal suppression or the improper co-crystallisation of sample and matrix) are eliminated. The invention of nanospray ionisation technology has increased the sensitivity of the technique so that as little as an attomole (10^{-18} moles) of analyte can be detected. The LC-ESI/MS technique can detect ions smaller than 1,000 Da, whereas with MALDI-TOF/MS these were swamped by ions derived from the matrix (Carr and Annan, 1997; Kinter and Sherman, 2000c).

The one clear disadvantage with LC-ESI/MS is that it produces multiply-charged ions, making it necessary to use software to de-convolute the mass spectra derived from the peptide digests. I found I was unable to satisfactorily de-convolute mass spectra that were derived from digested and undigested preparations. It appeared as if the sample was too complex for the de-convolution algorithms to analyse properly (data not shown), and so MALDI-TOF/MS had to be used when analysing EAS.

5.4 SUMMARY OF RESULTS.

A technique developed by Wu and Watson (1997), was successfully adapted to for use on the hydrophobin EAS. Difficulties imposed by an inability to completely purify each set of derivatised-ion species prior to mass spectrometric analysis were partly overcome, and it was repeatedly demonstrated that the following cysteines in EAS are linked by disulfide bonds: Cys_9-Cys_{60}, Cys_{18}-Cys_{54}, Cys_{19}-Cys_{45}, and Cys_{61}-Cys_{80}.

6

ATOMIC FORCE MICROSCOPIC STUDIES ON EAS.

6.0 INTRODUCTION.

6.0.1 MICROSCOPIC INVESTIGATIONS OF THE STRUCTURE OF HYDROPHOBIN POLYMERS.

Obtaining high-resolution structural information about hydrophobin fibrils with conventional techniques has proved difficult. Despite the many challenges, researchers using low-resolution techniques have enjoyed some success imaging dense hydrophobin films on the surfaces of conidia. Researchers have established that class I hydrophobin films consist of bundles of unbranched rodlets or fibrils (see section 1.3.6).

Dempsey and Beever (1979) determined that the individual EAS rodlet fibrils had a width of 10-11 nm. Using a negative-staining technique, they observed a darkly-stained region – nearly one third of the fibril's width – in the centre of the fibril. This implies that the region where the stain accumulated was hollow. They found that the length of the rodlets varied between 47 nm and 220 nm, and that up to four rodlets were bundled together into fascicles which themselves had widths between 22 nm and 99 nm (Hallett and Beever, 1981). Unfortunately, more recent attempts to examine EAS rodlets using transmission electron microscopy (TEM) and carbon-shadowing have been hampered by difficulties in securely adsorbing the hydrophobin to TEM sample-grids (personal communication with Dr. Matthew Templeton and Paul Sutherland, Hort Research).

It is possible therefore, that another technique – atomic force (AF) microscopy – might yield more information. Sertsou (1997) performed a preliminary examination of EAS films using Tapping™ mode AF-microscopy in ambient conditions. He determined that suitable films of EAS rodlets could be prepared on mica substrates using the "drop and spread" sample preparation technique (Morris *et al.*, 1998). He placed 20 µL drop of an aqueous solution containing between 5 ng/mL and 40 ng/mL of EAS, on to the surface of mica and allowed the water to evaporate. Unfortunately, it is likely that Sertsou under-estimated the true concentration of his solution by a factor of 1,000 (see discussion in section 2.5.3).

The length of the rodlets that Sertsou observed on the surface of the mica depended on the concentration of EAS in the droplet. When Sertsou decreased the concentration of EAS in the droplets the length of the rodlets increased from an average 91 nm at 40 ng/mL to an average 221 nm at 5 ng/mL. At concentrations greater than 40 ng/mL the film took on a more granular appearance. Sertsou also measured the width of the rodlets at 25 nm ± 3 nm, but did not allow for the probe-

broadening effect on this measurement (the phenomenon of 'probe-broadening' is explained below). This is why his results do not match those of Beever *et al.* (Dempsey and Beever, 1979; Hallett and Beever, 1981; Sertsou, 1997).

FIGURE 57: ABH1 (HYPA) FROM *A. BISPORUS* (GUNNING *ET AL.*, 1998)

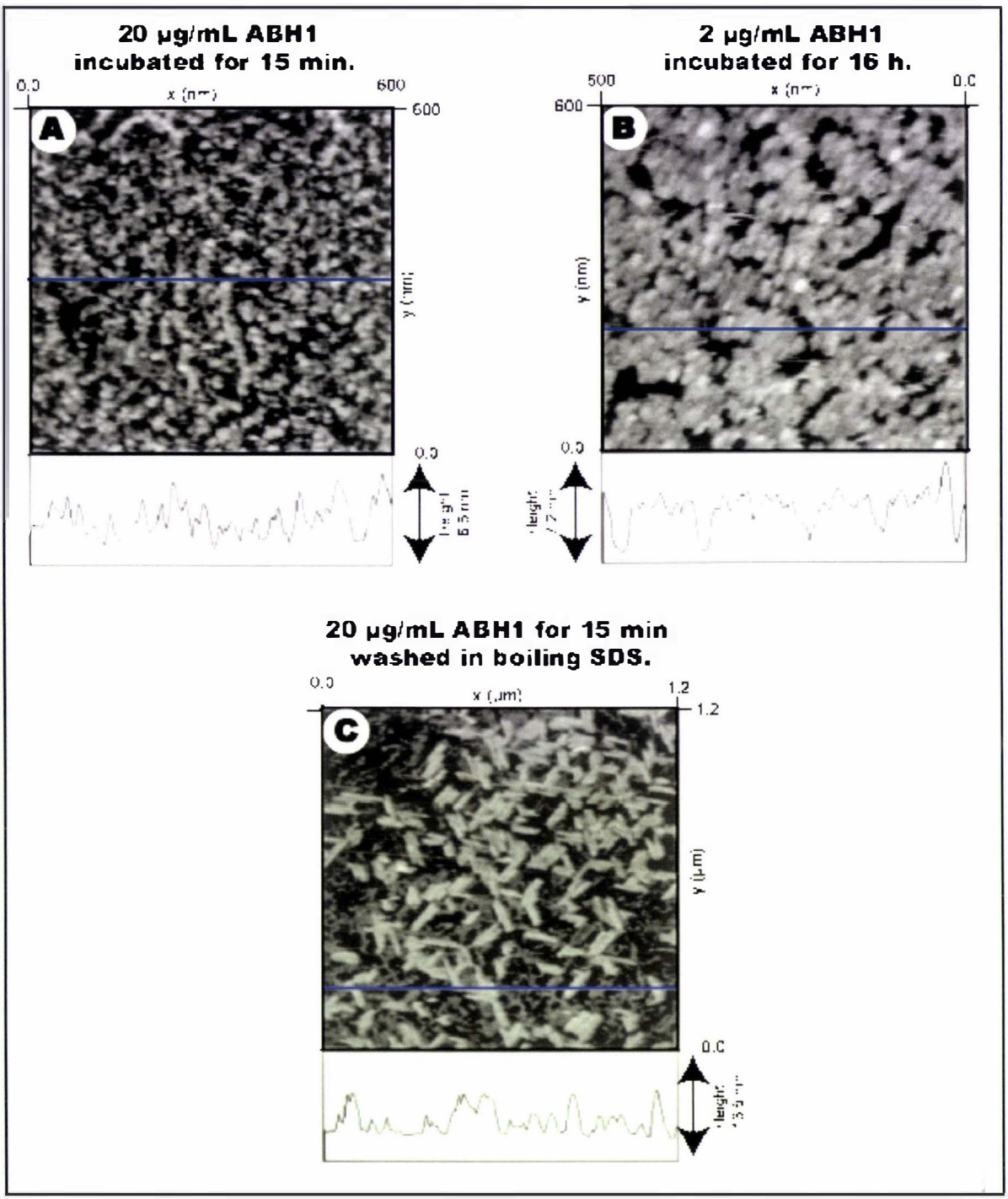

Figure 57 show three the atomic force micrographs that Gunning *et al.* (1998, pages 121-125) obtained while examining the films that ABH1 formed on graphite. Figure 57A shows the film formed after the graphite had been submerged in a 20 µg/mL aqueous solution of ABH1 for 15 minutes at 25 °C. Figure 57B shows the film formed after the graphite had been submerged in a 2 µg/mL aqueous solution of ABH1 for 6 hours at 25 °C. Figure 57C shows the effect of incubating the film formed in Figure 57A in 2 %(v/v) SDS at 100 °C for 10 minutes. The blue line illustrates the path of the height profile below each image. AF-microscopy was carried out in *n*-butanol using contact mode AFM.

The amphipathic nature of hydrophobin films allows them to reverse the wettability of surfaces they adsorb to (evidence reviewed in Wösten and de Vocht, 2000). If the hydrophobin self-assembles on a hydrophilic surface, the hydrophobin film exposes its hydrophobic face to the air. Conversely, when self-assembling on a hydrophobic surface the hydrophilic side is orientated towards the air while the hydrophobic face contacts the surface (Lugones *et al.*, 1996, 1998, 1999a; Wösten *et al.*, 1993, 1995; Sertsou, 1997; de Vocht *et al.*, 1998). If enough hydrophobin is present in solution then an additional layer of the hydrophobin may form on the hydrophilic surface afforded by the first layer. This bi-layer can be removed if the specimen is incubated in 2 %(v/v) SDS at 100 ºC for 10 minutes (van der Vegt *et al.*, 1996; Gunning *et al.*, 1998).

The microscopic investigations described above only studied the hydrophobic face of EAS rodlets. Three pieces of evidence suggest that when a hydrophobin self-assembles on a hydrophobic surface, the structure of the film's air-exposed surface may be different:

(1) X-ray photoelectron spectroscopic measurements performed by Wösten *et al.* (1994c) showed that the hydrophobic and hydrophilic faces of SC3 films formed *in vitro* had different atomic compositions.

(2) Wang *et al.* (2002) and de Vocht *et al.* (1998, 2002) showed that when SC3 self-assembles, the structure of the polymeric form transits through two intermediate states. Soluble SC3 assembles into an α-helix-rich form (also called the α-helical-state) which changes into an amorphous β-sheet-rich form (also called the β-sheet-transition-state) and then into the familiar rodlet-form that is rich in β-sheet secondary-structures. De Vocht *et al.* (2002) showed that the transformation into the rodlet-form could be arrested at the α-helical-state if SC3 self-assembled on the surface of a hydrophobic solid; boiling such a specimen in 2 %(v/v) SDS permitted the self-assembly process to continue until the rodlet-form has been reached. Electron micrographs indicate that SC3 in the β-sheet-transition-state forms an amorphous film, and that the transition to the rodlet-form takes more than six hours (de Vocht *et al.*, 2002).

(3) Gunning *et al.* (1998) used AF-microscopic techniques to examine the films formed on graphite by ABH1 (HypA). The structures seen in these films ranged between un-ordered spherical-structures (Figure 57A) and an ordered 3.6 nm thick film consisting of short rod-like structures (Figure 57B) – the actual composition of these films depended on the concentration of the ABH1

solution. When a specimen, similar to the one depicted Figure 57A, was washed in 2 %(v/v) SDS at 100 ºC for 10 minutes, the amount of protein adsorbed to the graphite decreased. However, Gunning *et al.* detected a significant number of 6 nm high rod-like structures that appeared to have adsorbed to what remained of the underlying protein layer (Figure 57C). Gunning *et al.* believed that these molecules had re-adsorbed to the original protein monolayer during the treatment with the hot detergent. De Vocht *et al.* (2002) believe that this result supports their own findings, namely that the polymerisation process is arrested at the α-helical-state when the hydrophobin adsorbs to a hydrophobic surface and can only be re-started if the specimen is washed in hot SDS. However Gunning *et al.* also saw these rod-shaped molecules in untreated specimens (Gunning *et al.*, 1998).

To summarise: only Gunning *et al.* (1998) have imaged what can unambiguously called the hydrophilic face of a polymeric hydrophobin film, and *their* results did not agree with the electron microscopic results obtained by Wösten *et al.* (1993) and de Vocht *et al.* (2002). The latter allowed a 2 µg/mL solution of SC3 to polymerise at the air/water interface then attempted to "pick-up" the self-assembled film with a hydrophobic (carbon-coated) TEM-specimen-mount. No rodlet-film could be detected until the SC3 had been allowed to polymerise for an extended period (16 hours). Periods less than this yielded a "featureless film." Gunning *et al.* only detected long rodlet molecules when concentrated films were deposited on graphite or when a pre-existing film was washed with hot SDS. It is unclear whether these differences between hydrophobin films formed on hydrophobic substrates were due to the biochemical differences between SC3 and ABH1 (SC3 is glycosylated), or the methods used to prepare the samples, or both.

6.0.2 Experimental Aim.

The aim of the experiments conducted in this chapter was then to better characterise both the hydrophobic and hydrophilic face of polymeric EAS films using AF-microscopy. Sertsou (1997) had already shown that the hydrophobic face of polymeric EAS could be imaged using Tapping™ mode AF-microscopy after the film had self-assembled and adsorbed to mica (a hydrophilic substrate), and we wished to build on his success.

In addition, we wanted to develop a method to reproducibly form single-layered, hydrophilic, films on EAS, and then investigate the surfaces of this film using AF-microscopy.

6.0.3 Introduction to Atomic Force Microscopy.

The following is intended as a brief introduction to the procedures, nomenclature, strengths, and weaknesses of AF-microscopy. For a more comprehensive introduction the reader is referred to either Morris *et al.* (1999) or Jena and Hörber (2002).

AF-microscopy is a technique that produces an image by "feeling" the surface with a sharp tip. This arrangement allows the AFM to examine specimens that have been immersed in fluid as well as those in ambient conditions. Unlike electron microscopy, there is no requirement to stain AFM specimens to enable the AFM to detect them. AFM images are obtained by measuring the changes in the magnitude of the interaction between the AFM probe (also called a tip) and the specimen's surface as it passes beneath the probe. With this design, the AFM cannot only gather topographical information about the specimen's surface but also information regarding its texture and composition. In fact, if the probe has been chemically functionalised, the general chemical nature of a surface can be examined at high resolution (see review by Noy *et al.,* 1997).

AFM specimens need to be secured or adsorbed to solid supports (called "substrates"). AFM tips are typically less than 3 μm tall (Figure 59A), and are mounted on a flexible platform – called a cantilever – that deflects when the AFM tip encounters the surface-features of a specimen. The AFM uses a laser to measure this deflection thereby gathering spatial data used in the images; the same information is used by a feedback-loop that attempts to keep the tip in constant controlled contact with the surface of the specimen.

If the specimen has surface-features taller than the probe, they can collide with the actual cantilever during imaging, thereby interfering with the microscope's ability to contour the surface of the specimen. Even with moderately rough specimens, the edges of tall features scanned with the AFM tip will appear as mirror images of the side-walls of the tip (Figure 59B). The resolution of the AFM is limited by this "probe-broadening" which affects every the image of specimen to a certain degree.

Probe broadening can be minimised, but not done away with, and for most AFM work the results obtained must be interpreted in the light of this probe-broadening effect. Minimisation of the effect can be obtained by selecting flat substrates when preparing flat specimens, or by embedding rough or tall specimens in a supporting matrix with a flat surface or by selecting probes with a higher probe aspect-ratio. Despite this, AFM images of bacterial membrane proteins with a lateral resolution

better than 1 nm have been obtained (e.g. Scheuring *et al.*, 1999). As Müller and Engel (2002) explain: *"Although suppliers specify AFM tip radii of 10 -50 nm... the AFM tips employed most likely had a single nanometre-sized asperity protruding sufficiently to contour the finest surfaces."*

During the experiments described in this chapter, I made use of two of the many different operating modes available with modern AFMs. The most basic method of collecting images is to use the "contact" or "DC" mode, wherein the tip is in constant contact with the specimen during scanning (See Figure 58A and Morris *et al.*, 1999).

FIGURE 58: THE OPERATING PRINCIPLES OF AFM.

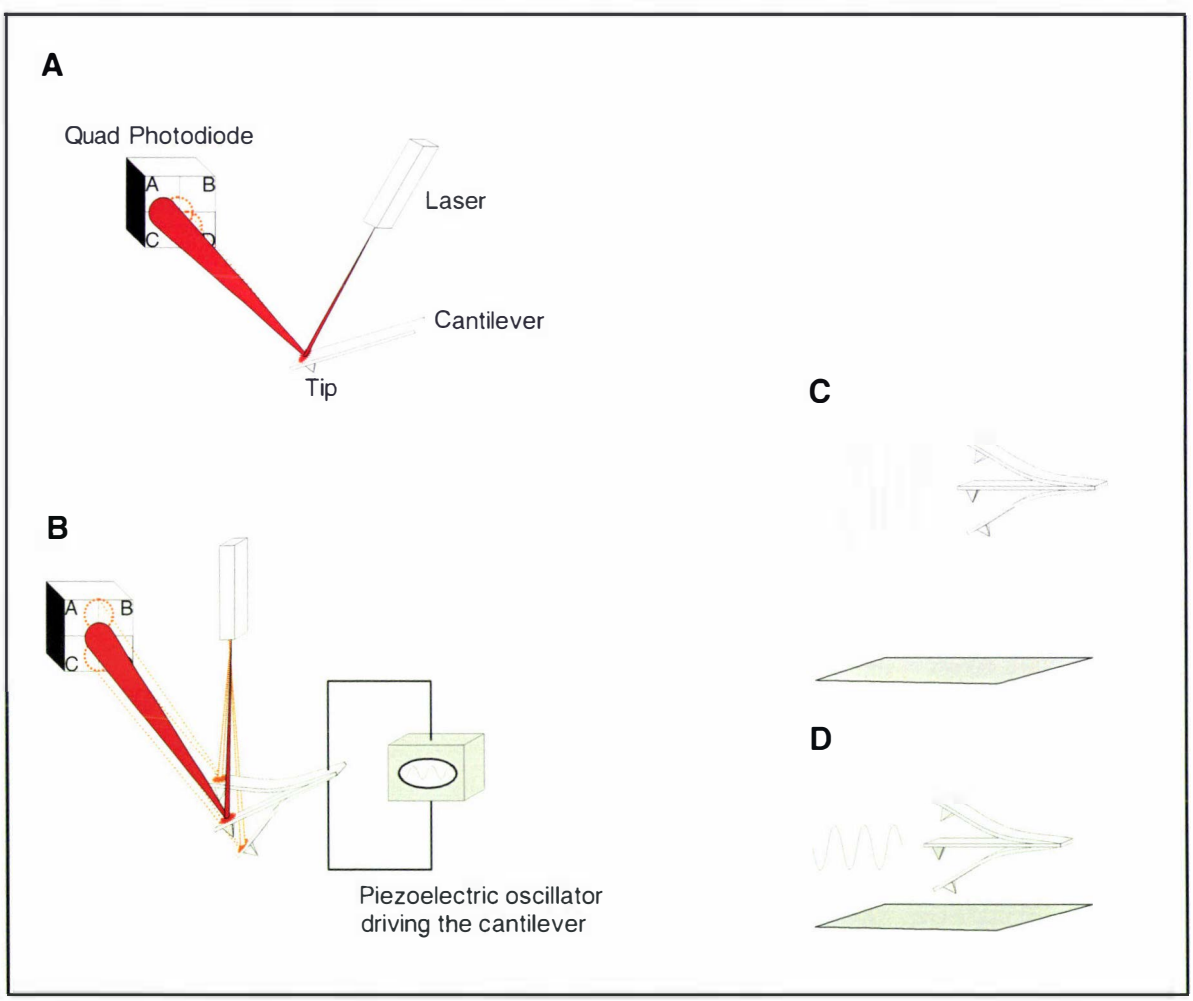

Figure 58 summarizes the operating principles of the Atomic Force Microscope (AFM). AFMs use a sharpened silicon nitrite tip mounted on a flexible cantilever to sense the topography of a surface when tip is raster scanned across the specimen. The AFMs used in this study used optical detection to track the movement of the tip. (Figure 58A) A laser beam focused on the reflective upper surface of the cantilever is redirected onto the face of a photodiode. The photodiode is split into four sections to enable the lateral twisting and vertical deflections of the cantilever to be differentiated. The sample is mounted on a piezoelectric scanner capable of precise movements in the three orthogonal directions (x, y, and z). A feedback loop monitors the tip deflection and sends the appropriate drive signals to the piezoelectric scanner to ensure that the tip maintains and either a constant deflection or a constant height above the sample. The movements of the piezoelectonic scanner are recorded and used to present a topographical image of the specimen. The principle of contact mode AFM is essentially as shown in Figure 58A. Figure 58B, C and D explain the principle of Tapping™ or AC mode. In order to reduce the forces applied to the specimen when it in ambient conditions a piezoelectric oscillator is used to excite the cantilever at a frequency slightly below its resonance frequency. The amplitude of the cantilevers oscillations are monitored with the same optical detection equipment described by Figure 58A. As the tip approaches the sample it comes into intermittent contact with it and the amplitude of the cantilevers oscillation changes. The feedback loop can then compensate by lowering the sample away from the tip and the record of such movements forms the basis for a topographical image of the specimen. The diagrams were adapted from Morris *et al.*, 1999.

FIGURE 59: DIMENSIONS OF AFM TIPS AND IMAGE ARTIFACTS CAUSED BY CONVOLUTION.

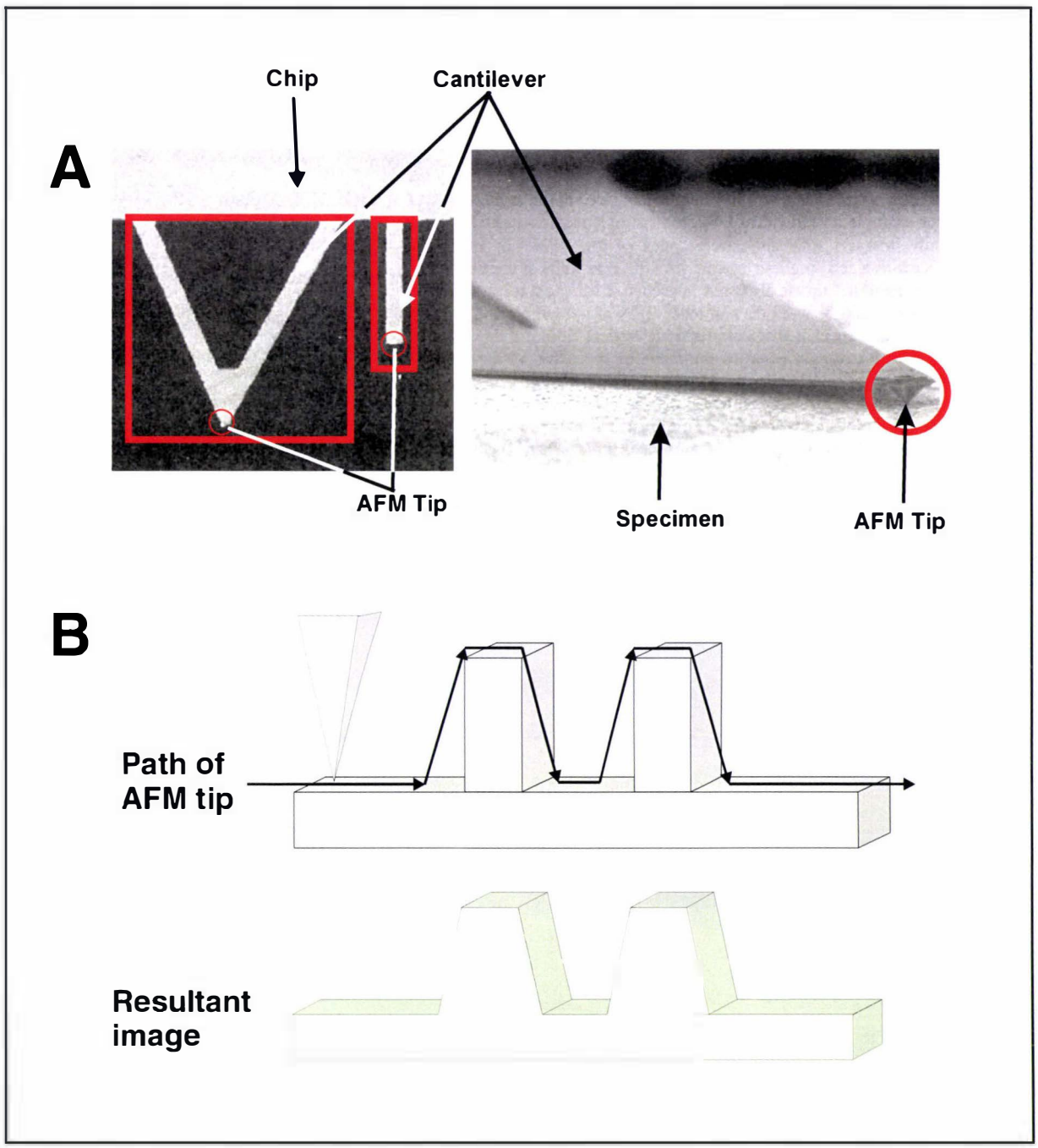

Figure 59A shows a scanning electron micrograph of AFM cantilevers and the tips attached to them. "V" shaped cantilevers in these images are 200 µm in length (The photographs are from Morris *et al.*, 1999 pages 10 and 62). The AFM cantilever and probe assemblies are mounted on block-shaped "chips" which serve as "carry-handles" for the probe assembly because they are large enough to be picked up and manipulated with fine forceps. The AFM tips (also called probes) are mounted on the leading edge of a flexible cantilever (the objects within the red-squares) which can have one of two basic geometries: "springboard" (right) or "V" shaped (left). The actual tip (the objects inside the red circles) is normally less than 3 µm tall.

Convolution induced image artifacts are intrinsic problems in atomic force microscopy - the diagram in Figure 59B shows why. The AFM tip is not infinitely sharp, so every image of an object is smeared out by the profile of the tip. This "probe-broadening" or "tip-convolution" limits the maximum resolution of the AFM. The degree of convolution depends on the tip-geometry and tip-height. The effect can be minimised by selecting sharp tips with high aspect ratios and imaging low-lying specimens on flat substrates. Otherwise, as depicted, images of the edges of tall features will look like a mirror image of the side-walls of the tip rather than the feature itself.

Capillary and adhesive forces associated with water-vapour condensing to form a capillary meniscus between the specimen and tip mean that contact-mode imaging, if performed in ambient conditions, can damage soft biological samples. Tapping™

or "AC" mode was invented to circumvent this problem by bringing the tip into intermittent contact with the sample thereby reducing the forces transmitted to the specimen during scanning (see Figures 58B, 58C, 58D; Humphris and Miles, 2002).

Tapping™ mode AFM brings the tip into contact with the sample at the end of its downward movement, so reducing (in ambient conditions) the contact time and the frictional forces applied to the sample relative to contact-mode. In situations where the lateral forces applied to the sample are irrelevant (*e.g.*, when the sample is hard) or can be eliminated, Tapping™ mode cannot match the spatial resolution of contact-mode. While Tapping™ mode reduces the lateral forces applied to the sample during imaging, a vertical compressing force is still applied (albeit intermittently) during imaging.

The adverse affects of water-vapour on imaging can be eliminated if both tip and sample are submerged in fluid. The imaging fluids can be organic or aqueous in nature; some commonly used organic-imaging fluids include ethanol and propanol. However, organic imaging-fluids must selected with care because they may not remain inert with respect to the specimen, for instance propanol has been shown capable of stiffening gelatine films (Radmacher *et al.*, 1995). If the fluid is aqueous, then electrostatic charges are introduced to any ionisable groups on the surfaces of the specimen and the silicon-nitride AFM probe. The quality of AF-microscopy in fluid depends mainly on the long-range electrostatic double-layer interactions between the probe and the sample (Müller *et al.*, 1999). These interactions can be attractive or repulsive depending on the pH of the sample and the pKa of the ionisable side-chains of amino acids on the surface of the protein (Müller *et al.*, 1999).

Andres Engel and colleagues at the University of Basel have developed a method of screening these interactions by adjusting the electrolyte concentration and pH of the fluid-imaging environment so that the tip-sample electrostatic interactions are favourable for obtaining images with sub-nanometre *vertical* resolution (reviewed in Müller and Engel, 2002). In theory, the adjustments they made to the concentration of electrolytes in the imaging buffer allowed the AFM tip to "surf" on a cushion of long-ranged electrostatic repulsive forces, thus enabling any small asperities to contour the fragile details of the surface. Had the electrolyte concentration had not been tuned in this way, the pressure that the asperity exerted on the specimen during scanning would have distorted the specimen and reduced the resolution of the image (Müller and Engel, 2002).

Note that Müller *et al.* were able to prepare their specimens as flat films with individual molecules arranged in regular, close-packed arrays. The flat nature of such specimens ensures that the effect of probe-broadening (Figure 59) was minimised since the side-walls of the probe did not touch the specimen. Therefore, if the contours in the specimen are deep enough to accommodate more than the very apex of the AFM tip, optimising the electrolyte concentration in the imaging buffer will not contribute significantly to the lateral resolution of the AFM. This particular problem is being addressed by the development of spike-shaped probes that have a tip radius <1 nm and a very high aspect ratio (Wong *et al.* 1998; Cheung *et al.*, 2000; MikroMasch® catalogue: http://www.spmtips.com).

6.1 Subtrates Suitable for AFM Studies on EAS.

6.1.1.1 Choosing a Hydrophobic Support.

Some of the experiments performed to investigate the hydrophilic properties of SC3 have exclusively used Teflon® as a hydrophobic support for the hydrophobin.

However, unpolished Teflon® is an unsuitable substrate for AFM experiments since the surface features random undulations exceeding 1 µm in depth (Figure 60). Examinations of EAS films deposited on unpolished Teflon® using AFM were frustrated by both probe-broadening and by difficulties keeping the probe in controlled contact with the specimen (Smolic, 1997).

So with the assistance of Steven Strover (Department of Chemical and Materials Engineering, The University of Auckland, NZ), I experimented with a variety of abrasive films and cutting compounds in an attempt to polish the Teflon® surface flat. As the AFM images in Figure 60 demonstrate we did succeeded in reducing the average height of the surface features, but unfortunately these surfaces were still too rough to allow accurate AFM imaging of rodlets, which are just 10 nm in diameter (Figure 60).

We turned next to highly ordered pyrolytic graphite (HOPG), which is a popular non-polar hydrophobic substrate for AFM studies. It has a layered polycrystalline structure that can be cleaved (see section 0) to reveal a fresh, chemically inert surface with atomically flat steps only 0.2-0.3 nm (several atomic layers) in height (according to the manufacturer's description). Success with HOPG was not assured however. Clemmer and Beebe (1991) did note that artifacts – with the appearance of biological molecules – could be generated when HOPG is cleaved (see Figure 61).

FIGURE 60: QUALITATIVE ASSESSMENT OF THE ROUGHNESS OF PTFE TEFLON®.

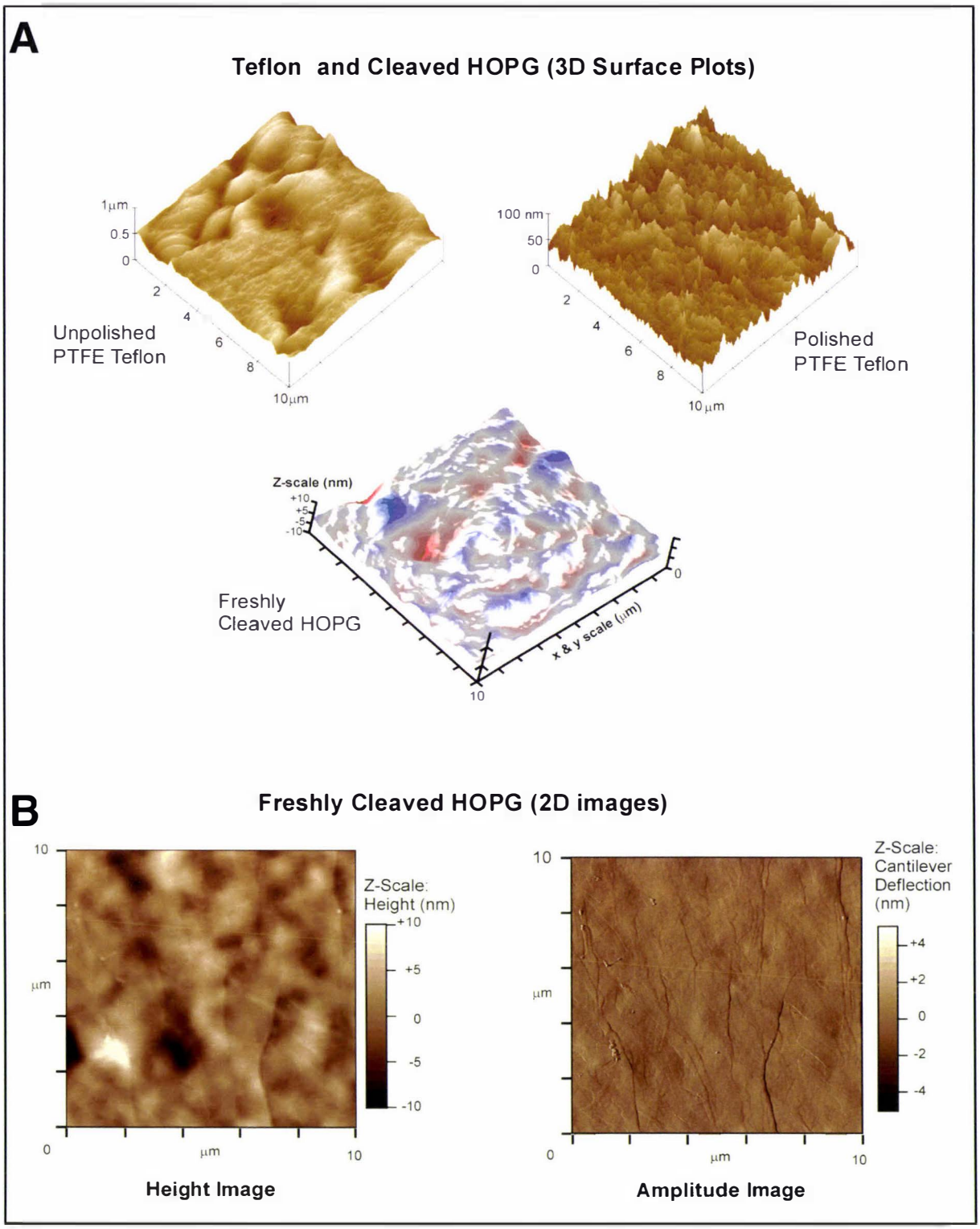

Three, 3-dimensional recreations of the surfaces of unpolished (left) and polished (right) PTFE Teflon® and freshly cleaved HOPG (middle panel) are shown in Figure 60A. Surface data was collected in ambient conditions in contact mode using the NanoScope® IIIa device equipped with a AS-130 "J" scanner and a Veeco® NP20 probe. The surface of freshly cleaved HOPG was examined in ambient conditions using a MFP3D-IO device with an Olympus® AC240TS probe in AC mode and the results are shown in Figure 60B. In the left panel the height of the features on the HOPG surface is shown. In the right panel the change in the amplitude of the cantilevers oscillations as the tip encounters features on the surface of HOPG is shown. See section 2.5 for a full description of AFM instrumentation.

However, Clemmer and Beebe's results were obtained with a scanning tunnelling microscope, which is unable to differentiate between materials having different

densities or surface chemistry (Clemmer and Beebe, 1991). The same is not true however for the AFMs used in this study. In Tapping™ mode, as the oscillating probe approaches a surface, the amplitude, and phase of the oscillation relative to the driver-signal changes. The extent of the phase-angle change is thought to be related to the physical properties of a material, permitting phase-contrast AF-microscopy to differentiate between different materials that make up a composite specimen (Chernoff, 1996; Noy *et al.*, 1998). Artifacts composed of graphite can be expected to be harder and less deformable than a soft biological film like EAS, which can even be scraped off the surface with judicious manipulation of the set-point-voltage, and scan-rate settings (see Figure 61C).

FIGURE 61: ARTIFACTS ON CLEAVED HOPG.

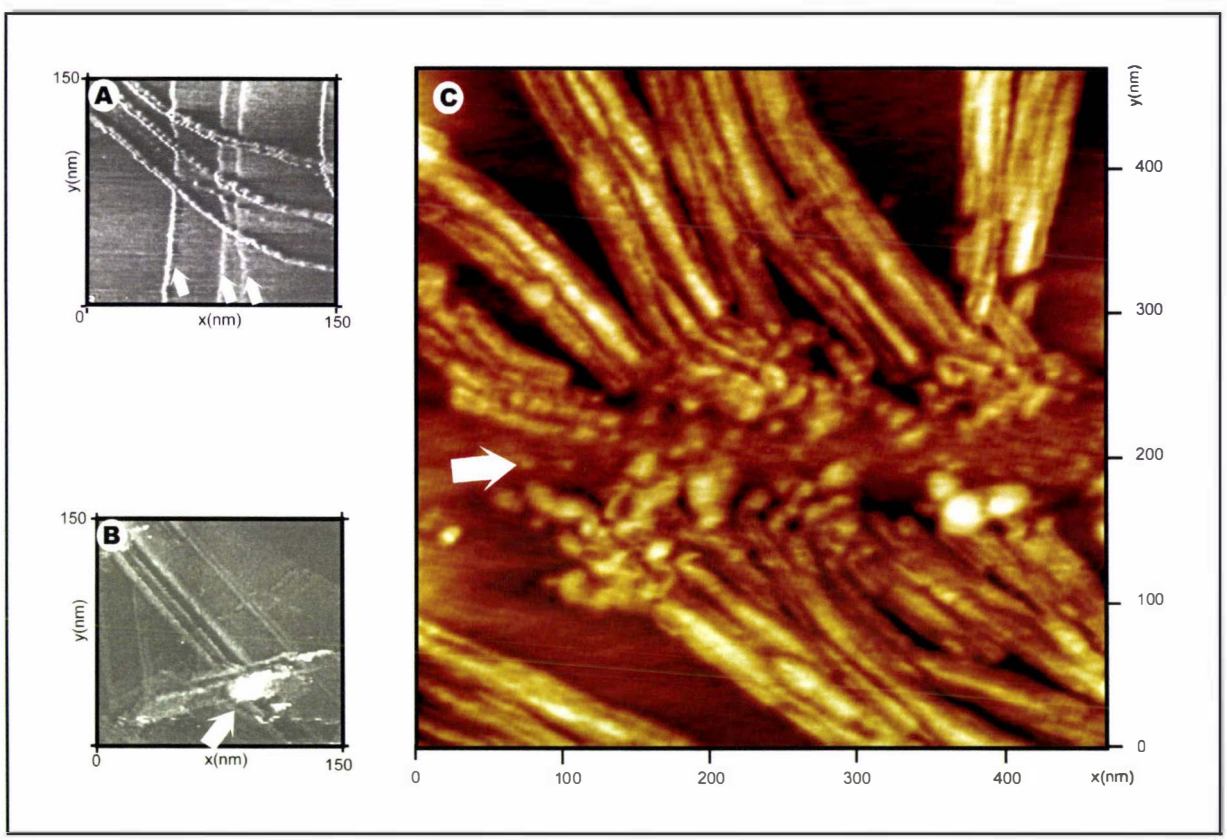

Figure 61A and B depict scanning tunnelling micrographs obtained by Clemmer and Beebe (1991, pages 640-642) showing the artifacts that can be generated on HOPG. Both images measure 150 x 150 x 0.5 nm (x, y, z). Figure 61A shows the edge of the atomically flat steps (arrowed) and three cylindrical shaped artifacts. Figure 61B shows more cylindrical artefacts along with amorphous associated with flakes of HOPG generated during cleavage (arrowed). Figure 61C shows rodlets of EAS (extracted from *N. crassa* strain Sta) deposited on mica (as a 20 µL droplet from a 10 µg/mL solution as described in section 2.5.3) and imaged by Tapping™ mode AFM. By adjusting the set point voltage and scan rate the AFM probe can apply sufficient vertical and lateral force be to disrupt soft biological samples (indicated by arrow). Image C was acquired in Tapping mode using a NanoScope® IIIa device equipped with AS-130 "J" scanner and a Veeco®TESP probe (see section 2.5). The x- and y- axis scales of Figures 61A, 61B and 61C are identical.

Phase-contrast imaging and physically disrupting the sample are two methods by which the AFM can be used to differentiate between rodlets made of protein and graphite fibres that look similar. Of the two techniques, the latter provides a more stringent proof of the rodlet's nature, but it can also blunt or contaminate the tip.

Thus, I selected HOPG as the hydrophobic substrate because it provided a hydrophobic surface that was flat and I relied on the phase-contrast technique to allow me to differentiate between the structures in the protein film and any graphite artefact. I considered this sufficient because the films were normally imaged after having been washed in boiling detergent solutions to remove any loosely adhering protein and I expected that this treatment would have also removed any loosely attached graphite particles as well.

6.1.1.2 Choosing a Hydrophilic Support.

Muscovite mica was selected as the hydrophilic substrate because it is a cheap, widely available, and chemically-inert material that is easily cleaved to provide an atomically flat substrate; also, Sertsou (1997) used muscovite mica when he succeeded in imaged EAS rodlets with the AFM.

Muscovite mica is a potassium aluminium silicate hydroxide fluoride mineral consisting of tetrahedral sheets of $(Si, Al)_2O_5$ ionically linked by a central layer of $Al_2(OH)_2$. The net negative charge of the basal oxygens between these sheets is balanced by an intervening layer of hexagonally coordinated potassium ions cations. These crystalline layers can be easily separated along cleavage planes (see section 0) that are atomically flat over several hundreds of square-microns (Bailey, 1984). After cleavage, the negative aluminosilicate lattice charge ensures that surface of the mica is covered by potassium ions, (0.6 K^+ ions per nm^2), but in air, the surface charge on mica is nil: the cations are completely neutralized by the negative aluminosilicate lattice charge (Gaines and Tabor, 1956). However when mica is immersed in water, some of the potassium ions dissociate from the surface and wetted mica has a net negative surface charge at neutral pH (Pashley, 1981).

It is this net negative charge can pose problems if the AFM experiments are to be conducted in liquid. It is known that some biomolecules (*e.g.* DNA) do not adsorb too strongly to untreated mica. The result is that when such a biomolecule is examined in an aqueous solution, the molecule can desorb from the mica surface making it impossible for the AFM to collect an image (reviewed by Morris *et al.*, 1999).

6.2 Imaging the Hydrophobic Side of EAS Films.

EAS is a cell wall protein expressed on air-exposed surfaces of its fungal host and I thought it prudent to observe EAS in its natural – ambient – environment because this would permit me to detect whether the ionic imaging-buffer altered the polymer's

structure in any way. With this in mind, the initial AFM investigations were conducted in ambient conditions.

6.2.1 Each EAS Isoform Can Form Rodlets.

Many of the investigations conducted on EAS were carried out using one or more of the protein's different isoforms (*e.g.* protein sequencing of EAS isoform II: Templeton *et al.*, 1995; the structural studies on isoform Ib: Mackay *et al.*, 2001; disulfide mapping of isoforms Ia and Ib: Chapter 5). Therefore, it was necessary to confirm that each EAS isoform has the ability to self-assemble into rodlet films – independent of the other isoforms. Accordingly, specimens of rodlet-films formed by each isoform of EAS were examined by Tapping™ mode AFM. The images obtained were published in Mackay *et al.* (2001) and have been reproduced in Figure 62; they confirm that each EAS isoform can indeed form rodlets.

6.2.2 Protofibrils.

Having chosen a hydrophilic substrate and using a modified version of Sertsou's sample preparation method (described in sections 0 and 2.5.3) I proceeded to examine hydrophobic side of EAS films adsorbed to mica.

Solutions with more than 10 µg/mL of EAS produced dense rodlet-films that completely coated the area of mica to which they were applied, while 5 µg/mL solutions produced rodlet-films sparse enough to allow areas of the underlying mica to be seen between groups of rodlets (Figure 63A). When examined, these areas appeared to be populated by smaller spherical structures arranged in an irregular honeycomb-like pattern suggesting that the underlying hexagonal crystal-structure of mica has influenced the molecules adsorption (see Figure 63A-D).

At the edge of the zone where the hydrophobin solution was deposited fewer rodlets are present, while these spherical structures abound (Figure 63C and D). The height of these structures was 1.30 ± 0.05 nm (The actual statistics were: sample size (n) = 50; the sample mean ($\bar{x}$) = 1.30 nm; the standard error of $\bar{x}$ (SE$\bar{x}$) = 0.046 nm).

Taller, more elongated structures are seen alongside EAS rodlets in in Figure 65A (highlighted with a black arrow). These structures have a height of 2.25 ± 0.07 nm (n = 30; $\bar{x}$ = 2.25 nm; SE$\bar{x}$ = 0.073) and an average width estimated at 17.02 ± 1.00 nm (n = 20; $\bar{x}$ = 17.02 nm; SE$\bar{x}$ = 1.00 nm; the widths were measured at half the height of the structures to help mitigate the effect of probe broadening).

FIGURE 62: RODLET FILMS FORMED BY EACH RP-HPLC ISOFORM OF EAS.

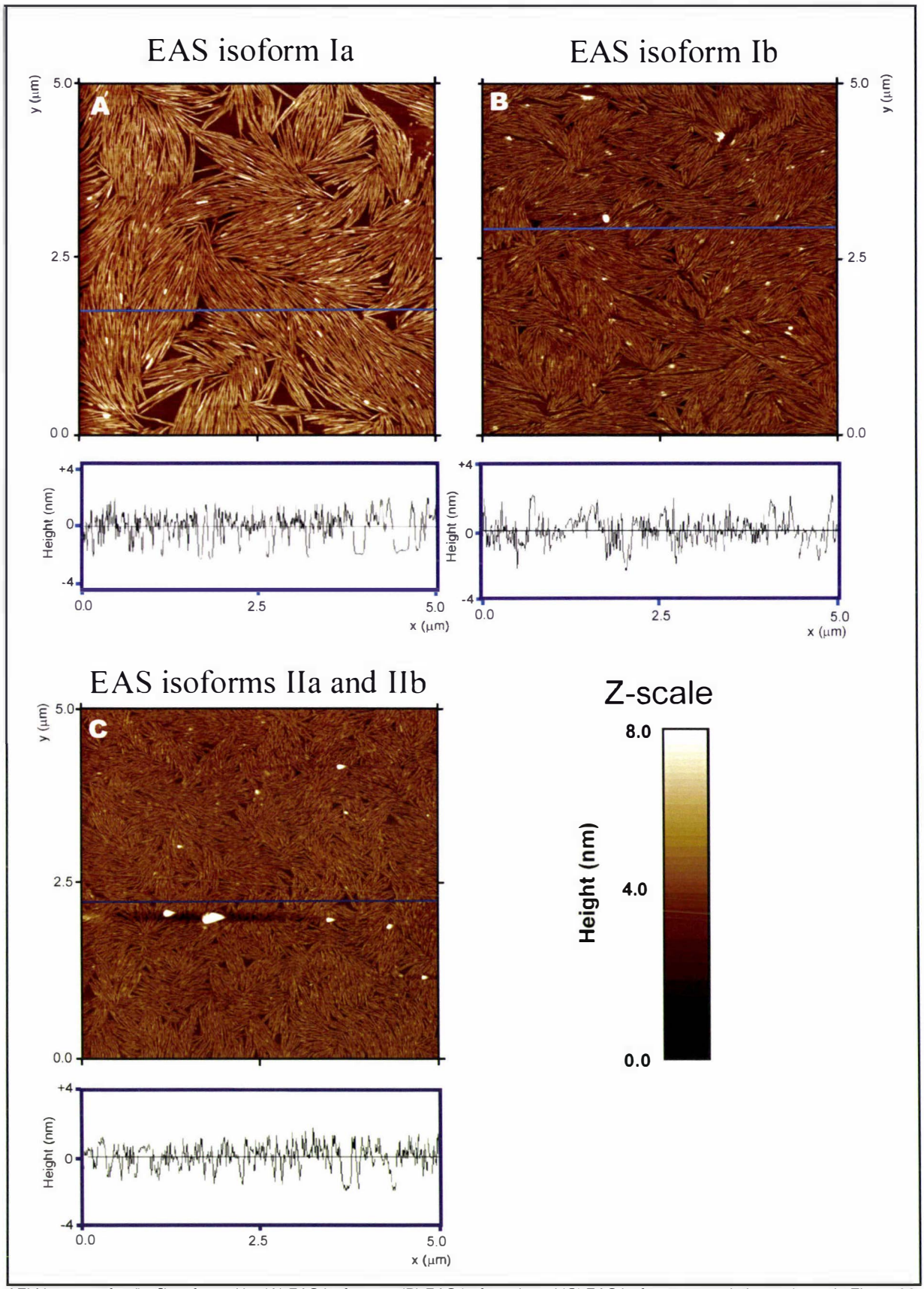

AFM images of rodlet films formed by (A) EAS isoform Ia, (B) EAS isoform Ib and (C) EAS isoforms IIa and IIb are shown in Figure 62. The Z-scale for the images is shown in the lower right panel. The blue line illustrates the path of the height profile below each image. Specimens were prepared on mica was as described in section 2.5.3 from 10 µg/mL aqueous solution of each EAS isoform. The films were examined in ambient conditions in Tapping mode™ using a NanoScope® IIIa device in equipped a TESP probe (see section 2.5.1).

FIGURE 63: PROTOFILAMENTS FORMED BY EAS ISOFORM II.

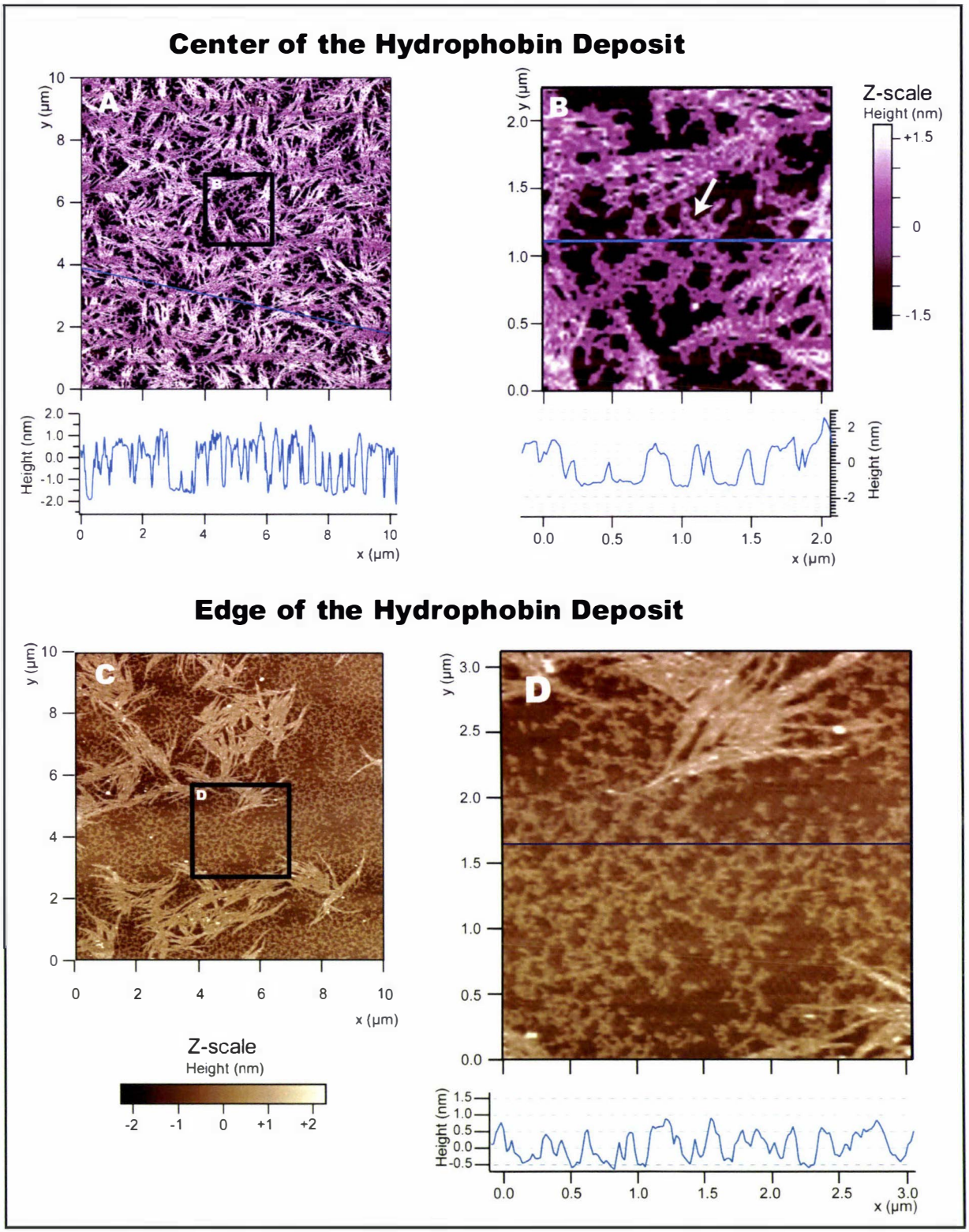

AFM images of rodlet films formed by EAS isoform II are shown in Figure 63. In Figure 63A, at the centre of the film deposited on mica, short globular protofilaments ~2 nm in height, arranged in rings are seen between the taller (~3.5 nm) rodlets. An expanded view of the area indicated with the black square is presented in Figure 63B. A portion of the outer edge of the region where the droplet was applied to mica is presented in Figure 63C. The protofilaments from the area encompassed by the black square are shown in greater magnification in Figure 63D. The height-scale for each pair of images (A, B and C, D) is adjacent to the right-hand image of each pair. Note that Figure 63B and Figure 63D have identical x- and y-axis scales. The blue lines in each image illustrate the path of the height profiles presented below some images. Specimens were prepared on mica was as described in section 2.5.3 from aqueous 5 µg/mL solutions of EAS. The films were examined in ambient conditions in AC mode using a MFP3D-IO device equipped an Olympus® AC240TS probe (see section 2.5.1).

I suggest that the spherical structures in Figure 65A are emergent protofibrils in the process of elongating or coalescing into rodlets, while those in Figure 65C are protofibrils in a more advanced stage of their development into fibrils.

In support of this interpretation, we might recall that spherical or globular protein structures have been observed in previous structural investigations of hydrophobins and amyloid fibrils. Gunning *et al.* (1998) investigated the structures that ABH1 (HYPA) formed while self-assembling on HOPG when the graphite was immersed in an aqueous solution of ABH1. At high concentrations (20 µg/mL), ABH1 formed a monolayer of randomly orientated globular protein structures. When the concentration was lowered, the monolayer was denser, more organised and the globular structures appeared to be arranged end-to-end into short rods approximately 80 nm in length (Gunning *et al.,* 1998).

The assembly of amyloid fibrils has been observed using time-lapse AFM imaging. These experiments show that the protofibrils that go on to form the mature amyloid fibrils begin as spherical or "dot" structures that either elongate or coalesce into rod-shaped protofibrils (Goldsbury *et al.,* 1999; Harper *et al.,* 1999; Stolz *et al.*,. 2000). When the protofibrils formed by the Human amylin (hA) polypeptide assemble, they begin as spherical shaped oligomers - 2.3 ± 1.9 nm in height and 23 ± 14 nm in length - consisting of ~16 hA molecules. Later they grow to be 6 nm in height before they begin to elongate into the familiar fibril shape (Green *et al.*, 2004).

An alternative explanation to that I have suggested is that the spherical structures are formed by the aggregation of hydrophobin molecules in solution prior to their adsorption. The hydrophobins SC3, HFB1, and HFB2 are known to form multimeric aggregates in solution (Martin *et al.,* 2000; Torkkeli *et al.,* 2002; Paananen *et al.,* 2003; Stroud *et al.,* 2003). When Martin *et al.* (2000) investigated the structure of these aggregates, formed when aqueous SC3 solutions between 2-20 µg/mL were vortexed prior to deposition on mica, and determined they formed globular shaped structures with a superficial resemblance to those in Figure 63.

However, in my opinion there are two compelling reasons to conclude that it is unlikely these spherical deposits are multimeric aggregates formed in solution and adsorbed to the surface of mica:

(1) Mackay *et al.* (2001) did not detect any multimeric forms of EAS in solution unless the solutions were shaken. In this experiment, samples were prepared without vortexing and were immediately applied to the mica.

(2) Were aggregates forming in these solutions then the concentration of amorphous deposits should be proportional to the concentration of EAS in the deposition solution and they should be evenly distributed across the zone where EAS adsorbed to mica. It is clear from Figure 63 that this is not the case.

6.2.3 Central Cleft in the Mature Fibrils of EAS.

Theoretically, amyloid fibrils consist of bundles of protofibrils that may or may not have a helical twist (section 1.3.6). There is good reason to believe that the rodlets formed by SC3 and EAS have a similar structure.

"Tracks" (arrowed) that mark the boundaries between the bundled protofibrils that make up the rodlets can be seen in the AFM image of a SC3 rodlet film obtained by de Vocht (2001) (Figure 64A.) De Vocht, citing precedents from amyloid research (*e.g.* Jiménenz *et al.*, 1999), suggests that this cleft is actually the boundary between protofibrils that are bundled together to form each rodlet. The contact mode AFM images obtained by de Vocht show SC3 rodlets that are ~11 nm wide (but the effect of probe broadening was not taken into account), ~5 nm in height and consist of 2-3 protofilaments (each 2-3 nm wide) lying parallel to one another. The measured height of these molecules ("thickness" in de Vocht's words) should be accurate because de Vocht obtained his data using contact mode AFM under ethanol – this imaging-environment presumably suppresses the double-layer electrostatic forces between tip and specimen without modifying the specimen.

Using Tapping™ mode AFM, I examined EAS rodlets for any fine structural details that could be detected in ambient conditions. The images collected are presented in Figures 64 and 65 and represent rodlet films deposited onto mica from solutions containing between 5 and 10 µg/mL of EAS. Like SC3, the presence of a central cleft is evident in EAS rodlets. The results of transmission electron microscopy and AF-microscopy experiments support this interpretation:

(1) An unpublished TEM micrograph of negatively stained EAS rodlets obtained from Dr M. D. Templeton and Paul Sutherland is shown in Figure 64D. The outline of the boundary between each pair of protofibrils that form the rodlets can just be made out (arrowed). This agrees with Dempsey and Beever's (1979) suggestion that the rodlets are hollow. If the protofibrils were cylindrical then the boundary between them would appear to an AFM (in the process of collecting height-data) as a valley with steep-walls.

FIGURE 64: THE CENTRAL CLEFT IN EAS RODLETS.

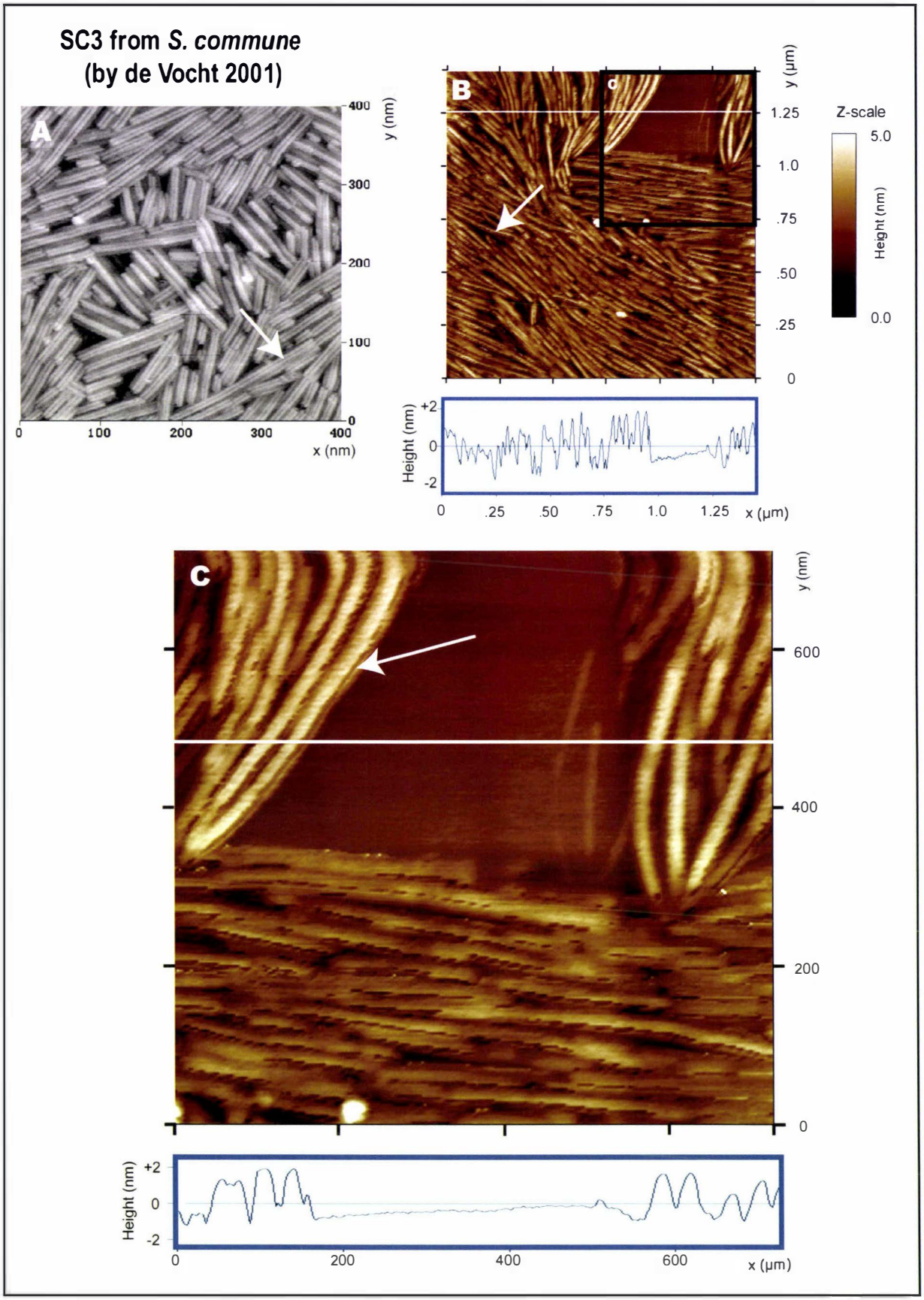

Figure 64 continues onto the next page. (Note that Figures 64B and 64C were collected in Tapping™ mode using a NanoScope IIIa equipped with a TESP probe (section 2.5.1). These specimens were prepared on mica was as described in section 2.5.3 from 20 µL droplet of an aqueous 10 µg/mL solution of EAS.)

FIGURE 64 (CONTINUED): THE CENTRAL CLEFT IN EAS RODLETS.

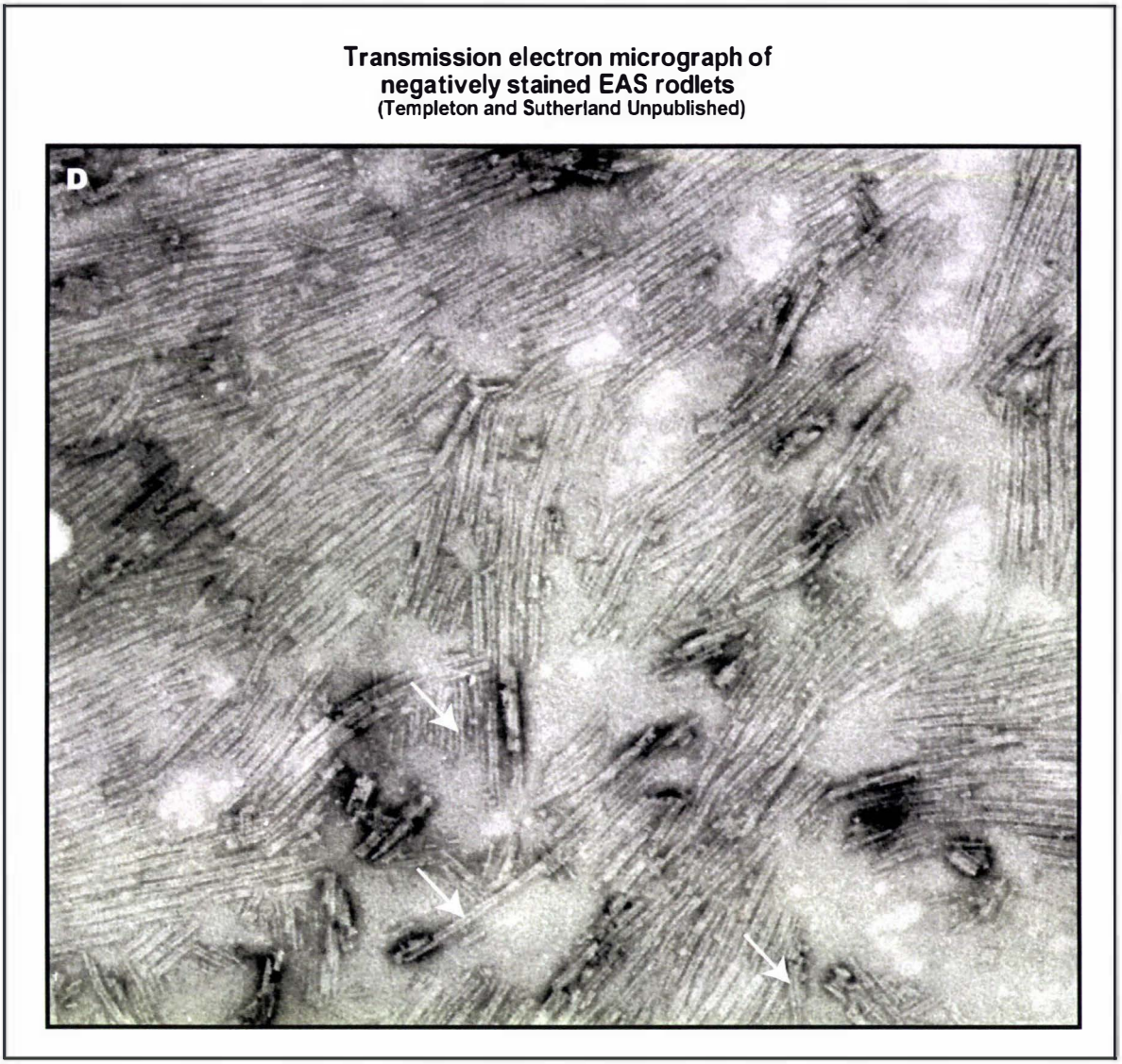

Figure 64A shows an AFM image of the rodlets formed by SC3. This image was obtained by de Vocht (2001, page 70). Figures 64B and 64C are AFM images of EAS rodlets adsorbed to mica and imaged in ambient conditions. These images highlight the cleft (highlighted in both images by white arrows) that spans the length of the rodlets. The cleft is thought to be the boundary between the rodlet's protofibrils. The area encompassed by the black square in Figure 64B is shown in greater magnification in Figure 64C. Note that Figure 64A and Figure 64C have identical x- and y-axis scales. Figure 64D shows a transmission electron micrograph of negatively stained EAS rodlets (Templeton and Sutherland, unpublished results); a white arrows are used in this image to highlight some of the rodlets whose central regions have been stained more darkly than their outer regions, probably because this area is hollow as Dempsey and Beever (1979) have suggested.

(2) The micrographs shown in Figures 64B, 64C, 65 and 66 depict the height-data collected while scanning the surface of EAS rodlet-films adsorbed to mica. Clefts (highlighted with arrows in Figures 64, 65 and 66) can be clearly seen spanning the entire length of those rodlets lying perpendicular to the direction of the AFM scan (from left to right). A closer look at the clefts is provided in Figure 66; phase-contrast data obtained while collecting the image in Figure 65A are reproduced in Figures 65B and 65D. Where the cleft appears on the rodlets in Figure 65C, a dark line is seen in Figure 65D and it depicts a sharp change in the phase of the driven and driver frequencies.

FIGURE 65: THE CENTRAL CLEFT IN EAS RODLETS.

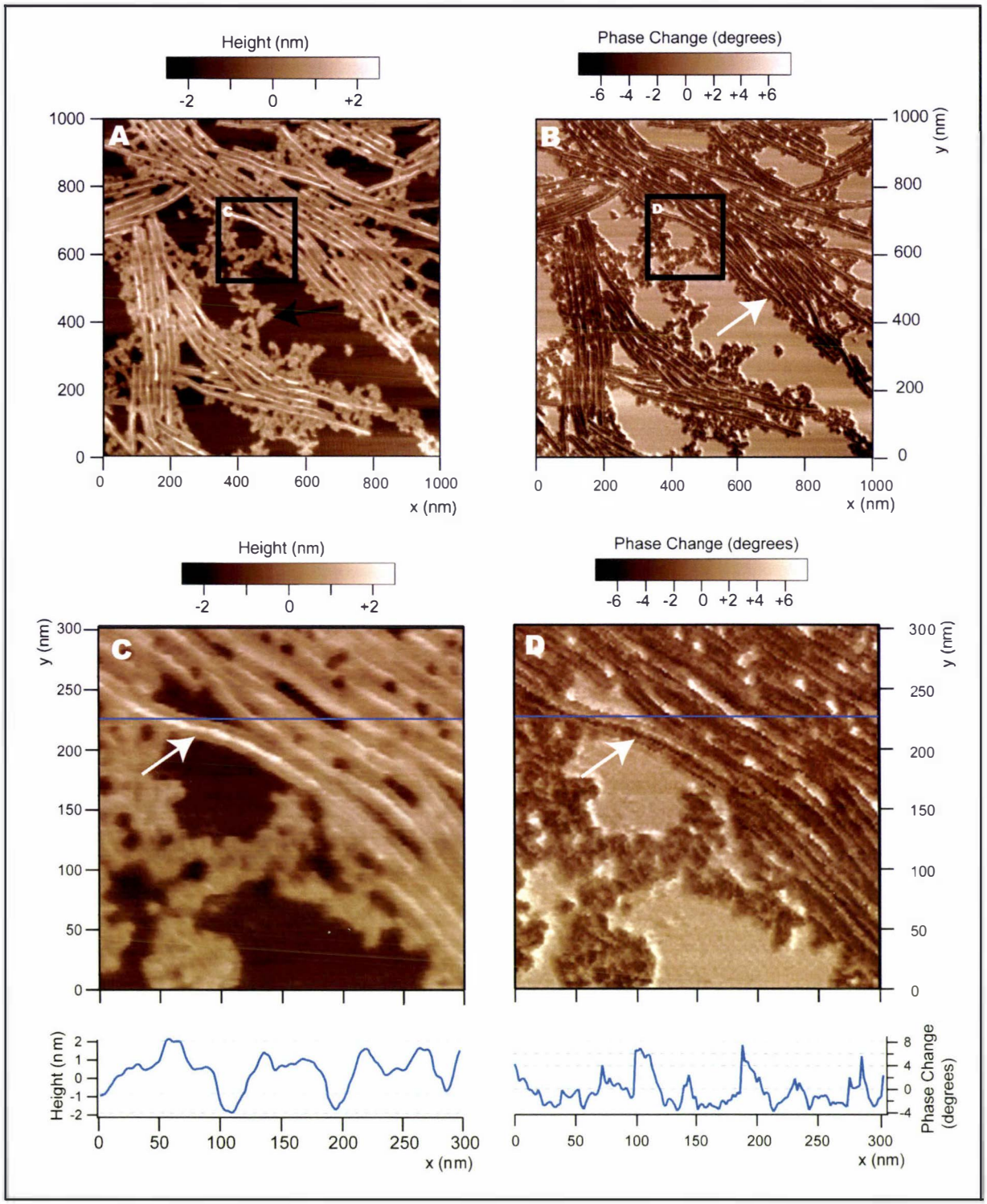

Figures 65A and 65C are AFM images depicting the dimensions of EAS rodlets and their centrally located cleft. Figures 65B and 65D display the phase change of the oscillating probe as it collected the height data presented in Figure 65A. The central cleft in each rodlet (white arrows) is darker than the rest of the rodlet representing a complete change in the density of the rodlet in that region. In Figures 65A and 65C, clefts (white arrows) marking the boundaries between the bundled protofibrils that make up the rodlets can be seen. Immature protofibrils (black arrow in Figure 65A) are also present in these films. The areas encompassed by the black squares in Figures 65A and B are shown in greater magnification in Figures 65C and D respectively. The blue lines in each image illustrate the path of the height profiles presented below some images. The specimen depicted in Figures 65A-65D was prepared from 20 µL of a 5 µg/mL solution of EAS deposited on mica. The images were collected with in AC mode using a MFP3D-IO device equipped a Olympus® AC240TS probe (see sections 2.5.1 and 2.5.3).

FIGURE 66: THE CENTRAL CLEFT IN EAS RODLETS.

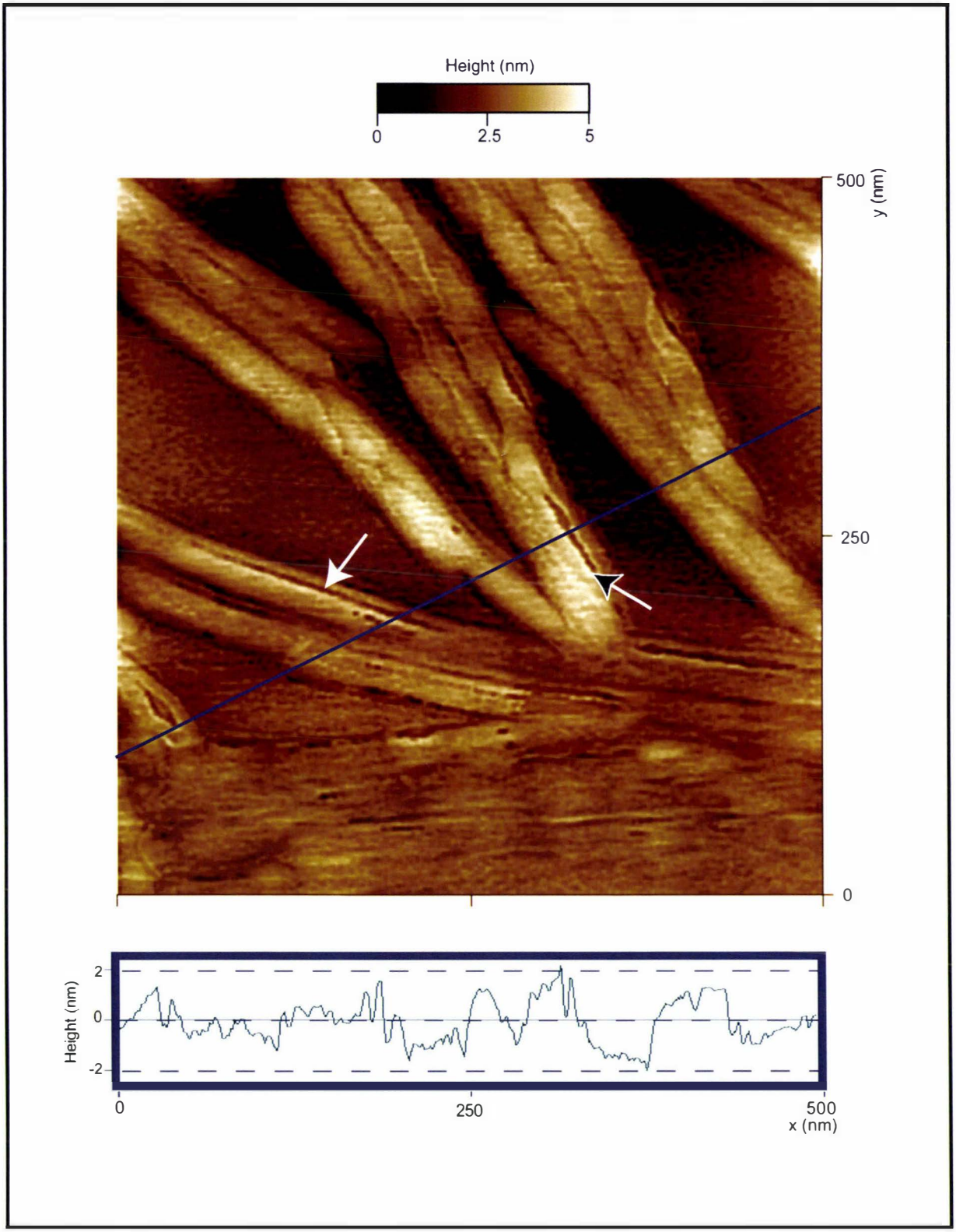

Figure 66 is an AFM image depicting the dimensions of EAS rodlets and their centrally located cleft. Clefts can be clearly seen (highlighted with a white arrow) in the central portion of some rodlets. The data presented here is consistent with the rodlets being formed from a pair of protofibrils arranged parallel to one another assuming that the clefts are actually the boundaries between the bundled protofibrils. There are some rodlets in which the cleft does not follow the rodlet's apex or disappears completely (black arrow). This would occur if the rodlet or rodlet-bundle had taken on a helical twist, as has happened to some of the fascicles depicted in the scanning electron micrograph shown in Figure 4A, page 16.

The film in Figure 66 is formed on mica from a from a 20 µL deposit of a 10 µg/mL solution and was collected in Tapping™ mode using a NanoScope IIIa equipped a TESP probe (see section 2.5.1).

FIGURE 67: THE AFFECT OF HALVING THE SETPOINT.

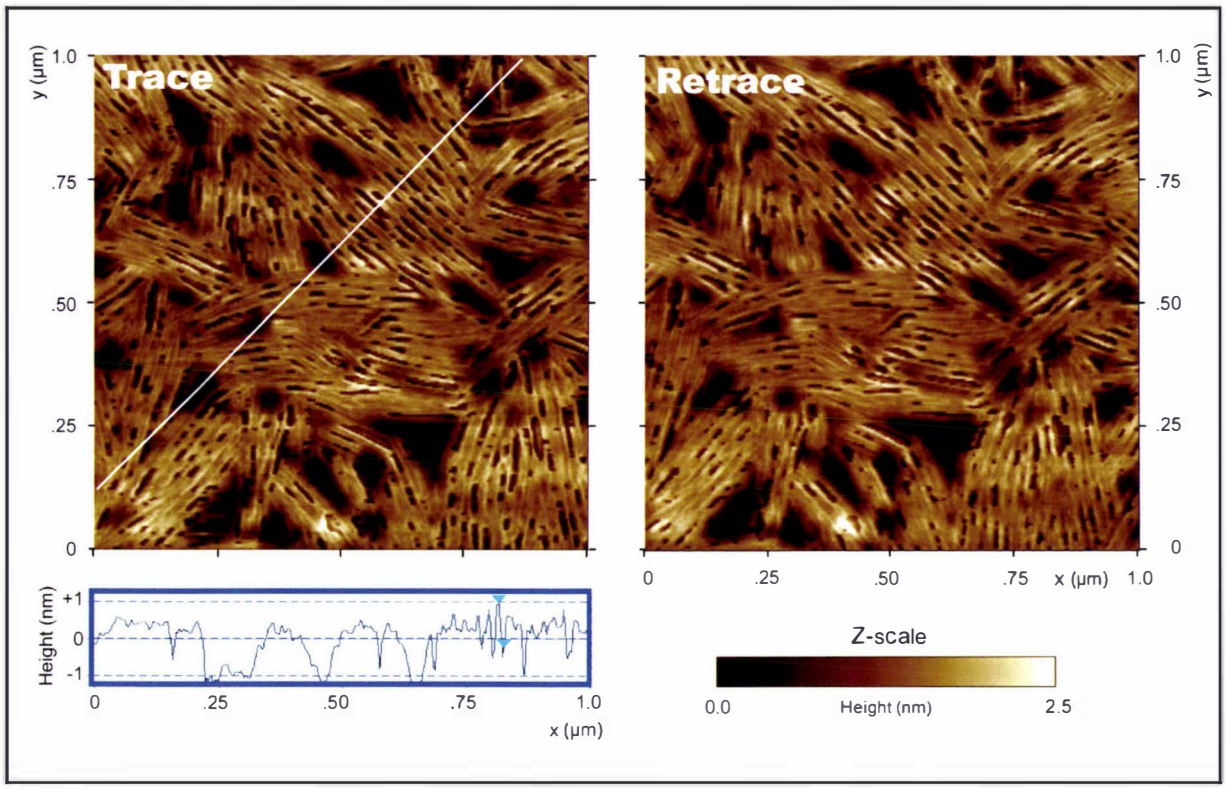

The Tapping mode atomic force micrograph shown in Figure 67 demonstrates the effect of increasing the force applied (by halving the set point) vertically on the specimen during imaging. The central cleft becomes wider than in previously images (*e.g.* Figure 65) probably because the protofibril components of the rodlets are being forced further apart. The images are of the same part of an EAS film deposited on mica. The Image labelled "Trace" was scanned from left to right, the image labelled "retrace" was scanned on the return sweep (right to left). Together they demonstrate that despite the force applied, the rodlets remain intact because no deterioration is seen between sweeps. The films were prepared by deposited a 20 µL droplet from a 5 µg/mL stock solution on mica (section 2.5.3).

FIGURE 68: THE EFFECT OF PROBE BROADENING ON IMAGES OF HYDROPHOBIN RODLETS.

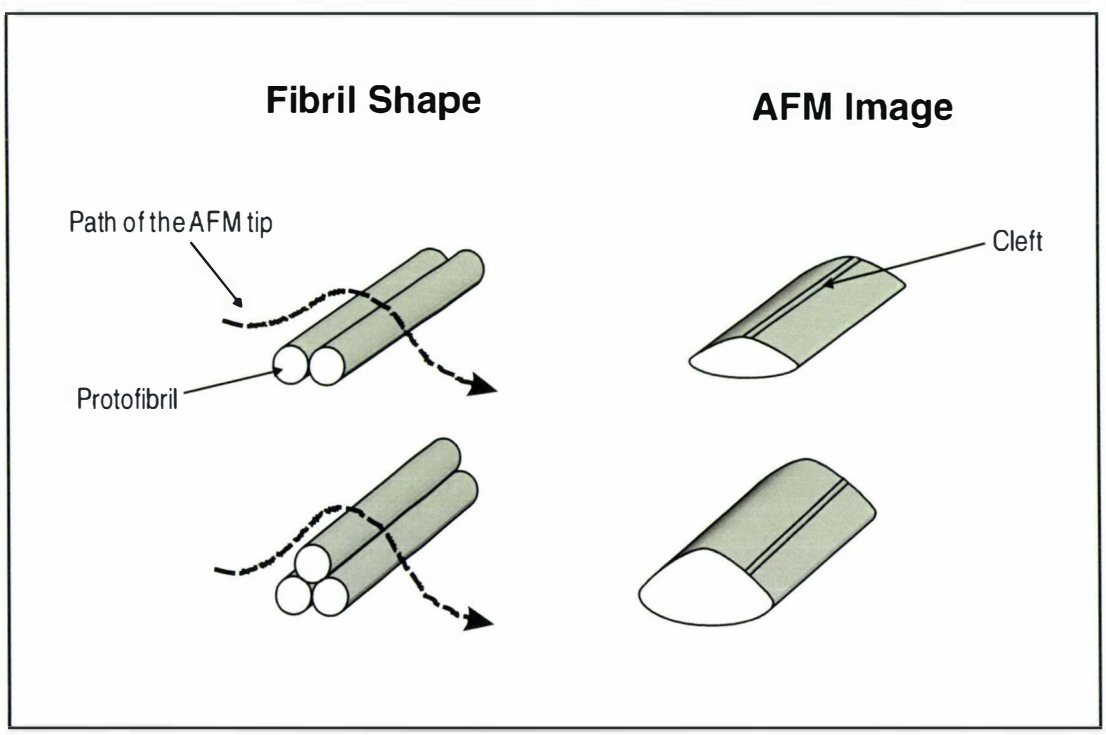

The diagram in Figure 68 is shows how the shape of the AFM probe contributes to the image of some samples. The effect, called probe broadening varies according to the sharpness of the AFM probe used.

The rodlets in Figures 65C and 66 have clefts with a mean width of 7 nm and 11 nm respectively (see Table 17). Like the other width-measurements, these too are affected by probe-broadening. Nevertheless, the variation in mean widths is more likely to be caused by variations in the set-point voltage applied during imaging. In Tapping™ mode, the closer the set-point (measured in volts) is to the maximum cantilever oscillation amplitude (also measured in volts), the lower the amount of force applied to the specimen (Digital Instruments, 1997). Therefore, the ratio of the set-point and maximum cantilever oscillation amplitude is a qualitative guide to the amount of force applied to the specimen during imaging. As demonstrated in Table 17, as the ratio of the set-point and maximum drive amplitude voltages becomes smaller, the apparent height of the rodlets decreases, the width of the cleft increases, and the depth to which the probe penetrates the cleft increases. The effect is clearly visible if the images in Figure 67 are compared with those in Figures 64, 65 and 66.

TABLE 17: SET-POINT VOLTAGES USED DURING IMAGING.

AFM Image (Figure)	AFM	Maximum Drive Amplitude.	Set-point	Ratio	Mean Rodlet Height (nm)	Mean Cleft Width (nm)	Mean Cleft Depth (nm)
66	*Nan*	*0.5 V*	*0.41 V*	*0.83*	*2.76 ± 0.09 (n=20)*	*10.96 ± 4.47 (n=20)*	*1.19 ± 0.57 (n=20)*
65	*MFP*	*1 V*	*0.80 V*	*0.80*	*3.3 ± 0.1 (n=30)*	*Too Small*	*Too Small*
64	*Nan*	*1.7 V*	*0.52 V*	*0.30*	*2.31 ± 0.09 (n=30)*	*7.14 ± 0.35 (n=22)*	*1.0 ± 0.07 (n=21)*
67	*Nan*	*10 V*	*0.20 V*	*0.02*	*1.88 ± 0.05 (n=30)*	*16.96 ± 4.18 (n=31)*	*1.33 ± 0.05 (n=30)*

The dimensions of EAS rodlets and their clefts are tabulated in Table 17 to compare them to the ratio of the set-point voltage: maximum amplitude voltage settings used during imaging. In Tapping mode™, the closer the setpoint voltage is to the maximum cantilever oscillation amplitude (measured in volts), the lower the amount of force applied to the specimen.

Key: The images in question are identified by the number of the figure they are presented in. The AFM used to collect the image is identified as either MFP (MFP3D-IO device used in AC mode and equipped with an Olympus® AC240TS probe) and Nan (NanoScope IIIa device used in Tapping™ mode and equipped with a Veeco® TESP probe). Ratio = the Set-point setting/Maximum Drive Amplitude setting. The sample mean ($\bar{x}$), standard error of the sample mean ($SE_{\bar{x}}$) and number of samples per dimension (n) is reported in this table as follows: $\bar{x} \pm SE_{\bar{x}}(n)$. The clefts seen in the rodlets displayed in Figure 66A, 66B and 66C were too small to accurately measure with the sectional analysis software (see section 2.5.5).

These effects are consistent with the protofibrils within each rodlet being compressed and possibly separated as the force applied by the probe increases. This treatment apparently does not damage the rodlets because images collected during the trace (left to right) and retrace (right to left) scans of the probe are the same (Figure 67). If damage was occurring then these images should be different and the image-resolution could be expected to deteriorate as debris began to

adhere to the probe – this was not observed even after the same are viewed in Figure 67 was repeatedly scanned (data not shown).

Unfortunately Tapping™ mode AFM carried out in ambient conditions lacks the ability to resolve the individual protofilaments within each rodlet in as much detail as is apparent in the contact-mode images obtained by de Vocht (2001). However, the presence of the cleft and its behaviour when compressed suggests that protofibrils are present but that the probe broadening effect prevents them from being clearly delineated as suggested by Figure 68.

The data presented here is consistent with the rodlets being formed from a pair of protofibrils arranged parallel to one another – the fibril might also have a helical twist. The cleft does not follow the rodlet's apex or disappears completely (Figure 66) in some rodlets. This would occur if the rodlet or rodlet-bundle had taken on a super-helical twist, and, this is exactly what is seen in the scanning electron micrograph shown in Figure 4A (Page 16). The image shows carbon-shadowed replicas of bundles of EAS rodlets on the surface of a *N. crassa* macroconidium; some of the bundles have a distinct left-hand twist (Beever and Dempsey, 1978).

Rodlets with clefts running along their flanks are also evident in Figures 64C and 66. The position of the cleft on the flank of a rodlet could imply either that the rodlet has twisted and is propped up against an elevated surface (e.g. another rodlet) or that three protofibrils arranged as shown in Figure 68 make up some of the rodlets.

Finally, some finer surface features can be seen on the side-walls of some of the rodlets in Figure 66. Such fine structure is not seen on the side-walls of rodlets in that or any other image, therefore it is probably an artifact; most likely, a blend of the surface features from the probe's side-walls and the rodlet itself.

As discussed in the introduction to this chapter, the highest resolution AF-microscopy studies on protein specimens in general have always been conducted in fluid. The next logical step in the AF-microscopic investigation of the EAS films then would be to image EAS in fluid, and in so doing collect accurate data on the dimensions of the rodlets and their surface features.

6.2.4 Imaging Hydrophobins Under Fluid.

The experiments described in this section were limited because the available AFM most suitable for high resolution imaging (the NanoScope® IIIe) suffered a major electrical fault that was only repaired just prior to this thesis being submitted.

Unlike the NanoScope® IIIe device, the remaining functional AFM (the MFP3D-IO) has a large piezo-electronic scanner (10 mm^2 lateral range, 16 µm vertical range) that could not fit any of the available acoustic shrouds, meaning that the device cannot be shielded from the effect of acoustic vibrations. In addition, smaller scanners deflect through a smaller distance per volt; therefore, any electrical-noise-induced piezo movement will be smaller in a small scanner. These effects combine to generate far more noise in images collected by the MFP3D-IO microscope. For instance, compare the number of random lines in Figures 65C and 74B with the number of random lines in Figure 66; Figure 66 was collected in Tapping™ mode with an acoustically shielded a NanoScope IIIa device equipped with the AS-130 "J" scanner (125 μm^2 lateral range, 5.0 µm vertical range). Therefore, of the two microscopes, the NanoScope IIIe is better at examining small specimens (such as the hydrophobin rodlet) at high-resolutions. The AFM experiments I was able to carry out under fluid using the MFP3D-IO are described below.

6.2.4.1 EAS Does Not Desorb From Mica When Imaged in Fluid.

Figure 69: The Effect of Water on EAS Adsorbed to Mica.

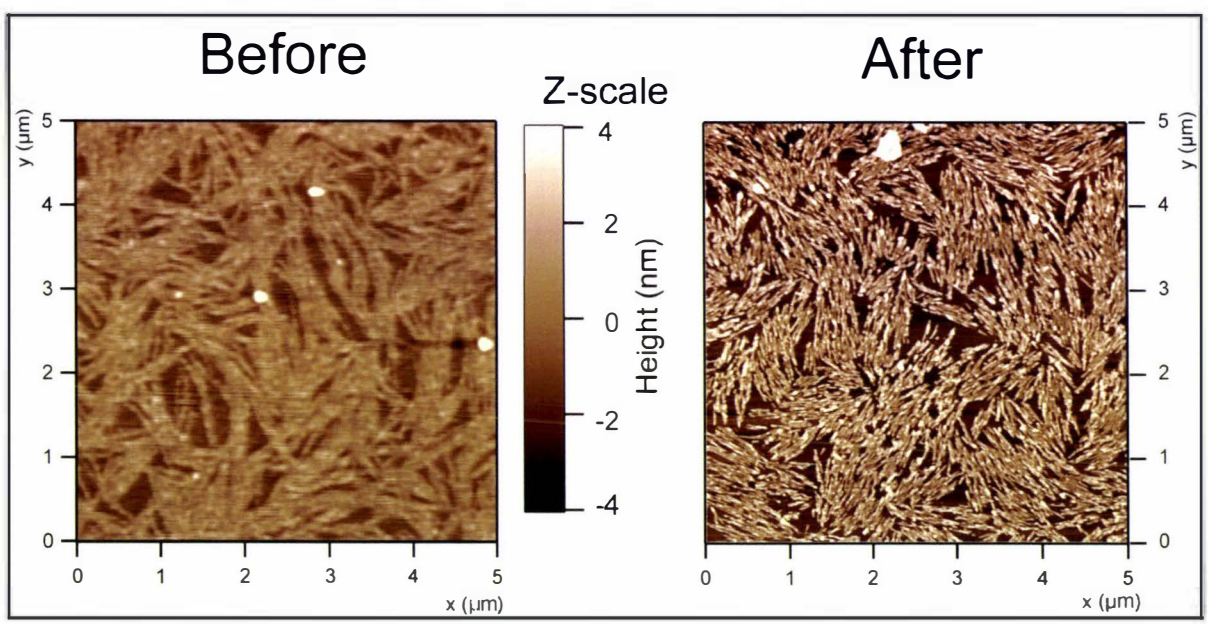

Figure 69 shows two Tapping™ mode AFM images of a polymeric EAS film deposited on mica as a 20 µL droplet from a 5 µg/mL stock solution (method described in section 2.5.3). The sample was imaged before (left) and after (right) the substrate was rinsed with 10 mL of filtered Milli-Q® water delivered from a syringe fitted with a 0.22 µm Millipore® GSWP type filter and a 25 gauge needle. The sample was dried under a stream of CO_2 before the image on the left was acquired. Imaging was performed in AC mode in ambient conditions using a MFP3D-IO AFM and a different Olympus® AC240TS probe for each image (see section 2.5).

Although SC3 adsorbed to mica has been imaged in ethanol using an AFM, SC3 (unlike EAS) has glycosylated residues that are thought to improve its ability to adhere to hydrophilic surfaces (see section 1.1.2; de Vocht *et al.*, 1998; van Wetter *et al.*, 2000a). Therefore, I conducted a simple experiment in fluid to confirm that

EAS adsorbs to untreated mica strongly enough not to be displaced while being examined with an AFM.

A specimen was prepared on mica (see section 2.5.3) and imaged before and after being rinsed with 10 mL of filtered Milli-Q® water. The water was delivered from a syringe fitted with a 0.22 µm Millipore® GSWP type filter and a 25 gauge needle, and the sample was dried under a stream of CO_2. Tapping™ mode AFM was used to confirm that the rodlets were intact and undamaged (see Figure 69). The result, seen in Figure 69 was conclusive. (Although the rodlets in Figure 69 appear different, the increase in sharpness of second image can be attributed to the use of a new Olympus® AC240TS probe to examine the specimen after rinsing.)

6.2.4.2 Images of EAS Submerged in Milli-Q® water.

Unfortunately, Tapping™ mode AF-microscopy in ambient conditions is not conducive to the accurate measurement of the dimensions of a protein specimen (See Table 17). Yet accurate measurements of the height of EAS rodlets are required to accompany SEM measurements of their width (Dempsey and Beever, 1979). Together, these dimensions would confirm whether the rodlets are shaped like a cylinder with a circular cross section – as implied by electron microscopy (Dempsey and Beever, 1979 and Figure 64D) – or a cylinder with an elliptical cross section (*e.g.* Figure 68) as implied by AF-microscopy experiments described above.

Accordingly, I imaged an EAS film adsorbed to mica, submerged in Milli-Q® water using the MFP3D-IO device equipped with an Olympus® Biolever (see sections 2.5.1.1 and 2.5.4). The results are reproduced in Figure 70.

The low spring-constants of the Biolever probes enabled the forces applied to the sample to be kept to ~40 pN. Normally, the force applied to a protein by the AFM probe must exceed 100 pN before a protein specimen is deformed (data reviewed by Müller *et al*, 1998b, 1999). The force applied by the tip was also sufficient to overcome any repulsive interaction between the gold-coated tip and EAS film (measured at 0.90 pN) implying that the tip was actually in contact with the surface during this experiment. In these conditions the mean height of the rodlets was calculated to be 4.7 ± 0.14 nm (n = 17; $\bar{x}$= 4.73 nm; SE$\bar{x}$= 0.14 nm). Evidently then EAS rodlets at least twice as wide at ~11 nm (Dempsey and Beever, 1979) as they are high, which agrees with the idea that rodlets are formed from cylindrical pairs of parallel protofibrils.

Spherical structures were also seen between the rodlets on one part of Figure 70B. These were assumed to be emergent protofibrils similar to those seen in Figure 63;

the mean height of these molecules was calculated to be 2.6 ± 0.31 nm (n = 9; $\bar{x}$ = 2.63 nm; SE$\bar{x}$ = 0.31 nm).

FIGURE 70: AFM IMAGES OF EAS ADSORBED TO MICA WHILE SUBMERGED IN WATER.

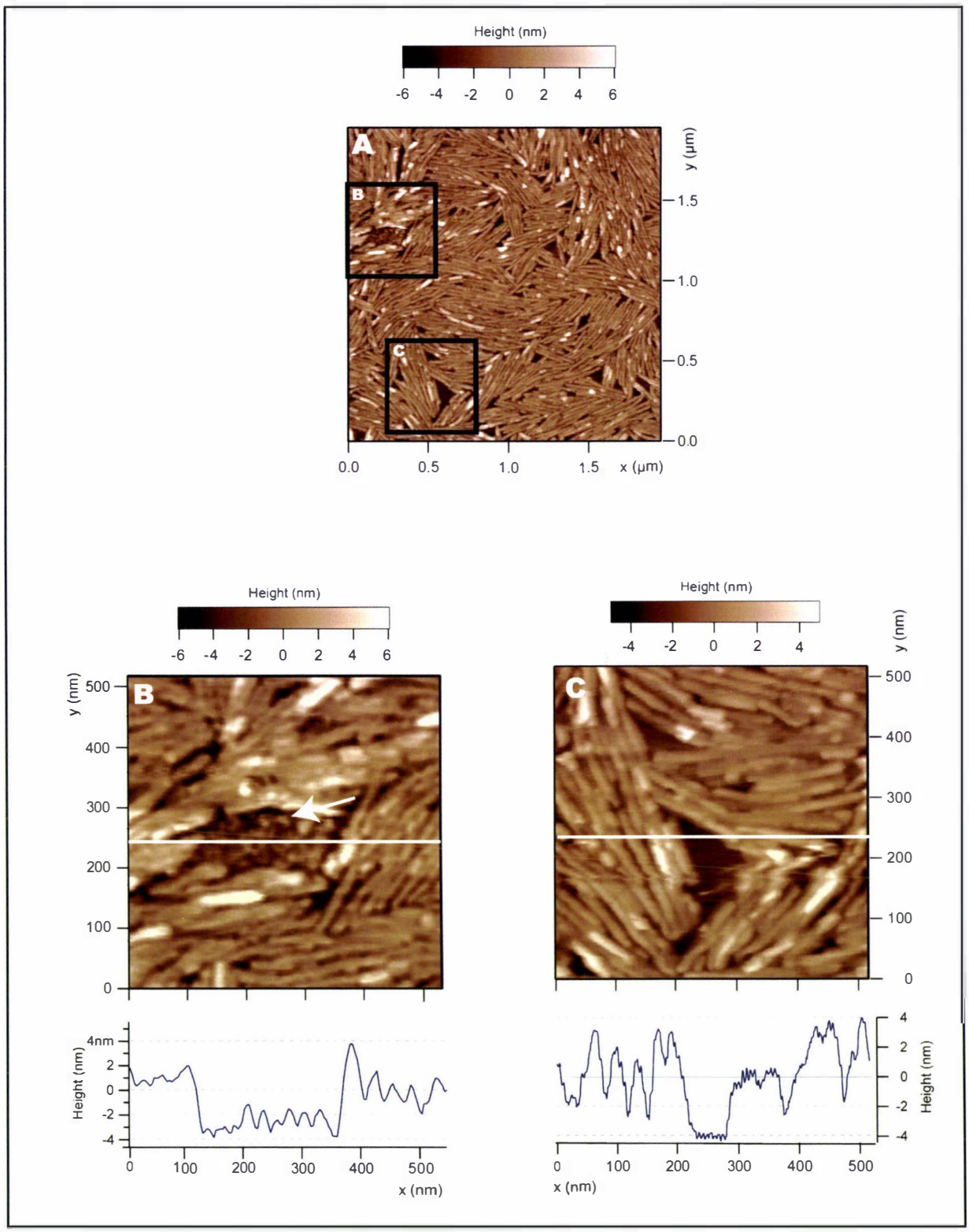

Figure 70A, B and C are AF-micrographs of an EAS film EAS film deposited on mica as a 20 µL droplet from a 5 µg/mL stock solution (method described in section 2.5.3) and imaged in Milli-Q® water using a MFP3D-IO device equipped with an Olympus® Biolever AFM probe. The areas encompassed by the black squares in Figure 70A are magnified in Figure 70B and C as indicated. The arrow Figure 70C highlights the presence of globular structures similar to those described in section 6.2.2. The white lines in images C and D illustrate the path of the height profiles presented below these images.

6.2.4.3 Optimising the Fluid Imaging Conditions for EAS.

A third experiment was carried out to determine which imaging buffer could modulate the electrostatic repulsion between a silicon nitrite tip and an EAS film so as to permit the AFM to image the surface of EAS rodlets at the highest resolution possible. These experiments are described in section 2.5.6 and the results are reproduced in Appendix VI. As explained above, an unfortunate equipment failure curtailed any further AF-microscopic investigation of EAS films under fluid.

6.3 Imaging the Hydrophilic Side of EAS Films.

The goal of the experiments described below was to examine the types of polymeric films that EAS forms as it self-assembles on HOPG.

There was also an emphasis on finding the conditions under which rodlets – comparable to rodlets seen on mica – would form. The results of these are presented in sections 6.3.1 and 6.3.2. All of the images presented in these sections were collected in AC mode using a MFP3D-IO device equipped with an Olympus AC240TS probe; the same set-point voltage (0.80 V) and drive amplitude (1 V) was used in each instance. This means that height measurements obtained in these experiments are comparable because roughly the same force has been applied to the samples in each experiment. The height of structures present in these films are compared in Table 18.

6.3.1 Films formed by the "Drop and Spread" technique.

EAS films were prepared on HOPG by the "drop and spread" technique identical to that used to prepared EAS films on mica substrates: twenty-microlitres droplets of aqueous solutions containing 50 µg/mL, 10 µg/mL, 5 µg/mL, and 0.5 µg/mL of EAS were applied to freshly cleaved HOPG and allowed to dry overnight (see section 2.5.3). The hydrophobic HOPG surface prevented the droplet from spreading on the surface (see Figure 71) and thus these films were concentrated in a small part of the substrate.

Recall that bi-layers of hydrophobin may form when the protein self-assembles on hydrophobic surfaces, but washing the substrate with hot SDS removes the weakly adsorbed protein, leaving a monolayered film exposing its hydrophobic face to the atmosphere (Wösten *et al.,* 1994a, 1995; van der Vegt *et al.,* 1996). So it was understandable that the multi-layered films were formed from the 50 µg/mL, 10 µg/mL, and 5 µg/mL (Figure 72A and Figure 73A).

TABLE 18: THE HEIGHT OF SURFACE FEATURES DETECTED BY AF-MICROSCOPY

Figure	Height of Surface Features (nm)				
	Rodlets	Short Rodlets	Spherical Protofibrils	Elongated Protofibrils	Amorphous monolayer
57A-C	*~3.0*	*3.4*	*1.7 - 3.9*	-	-
63A-D	*Not measured*	-	*1.30 ± 0.05 (n=50)*	-	-
65C	*3.3 ± 0.1 (n=30)*	-	-	*2.25 ± 0.07 (n=30)*	-
72B	-	*2.82 ± 0.19 (n=30)*	-	-	-
73B	-	-	-	*2.36 ± 0.15 (n=18)*	*Not measured*
74A	-	-	*1.84 ± 0.18 (n=15)*	*1.84 ± 0.18 (n=15)*	-
75C	*2.64 ± 0.12 (n=30)*	-	*Not measured*	*Not measured*	-
76C	*2.81 ± 0.10 (n=24)*	-	-	*0.92 ± 0.03 (n=5)*	-

The dimensions of EAS rodlets and other structures seen in films deposited on mica and HOPG are tabulated in Table 18. Each of the films described here have been imaged using the MFP3D-IO device used in AC mode and equipped with an Olympus® AC240TS probe. The images in question are identified by the number of the figure they are presented in. The sample mean ($\bar{x}$), standard error of the sample mean (SE.$\bar{x}$) and number of samples per dimension (n) is reported in this table as follows: $\bar{x}$ ± SE.$\bar{x}$(n). The absence of a particular type of molecule (rodlet, short rodlet, protofibril *etc.*) from a film is indicated with a hyphen. The term "Not measured" indicates that that type of molecule was present in the film, but it couldn't be measured accurately using the sectional analysis software (see section 2.5.5).

FIGURE 71: 100 µL WATER DROPLETS ON FRESHLY CLEAVED MICA AND HOPG.

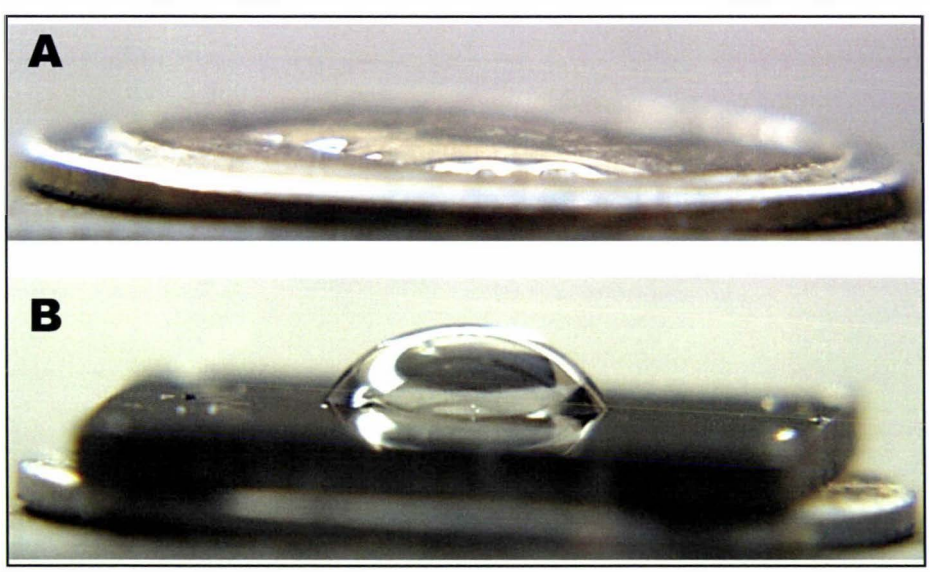

In the digital photograph depicted in Figure 71, a 100 µL droplet of Milli-Q water was deposited on freshly cleaved mica (panel A) or HOPG (Panel B). The mica and HOPG were prepared as described in section 0 and then photographed using the method described in section 2.3.

After the film formed by the 10 µg/mL of EAS solution was washed with hot SDS in order to remove any weakly adsorbed hydrophobin (see section 2.5.3), a thin layer of spherical molecules still remained (Figure 72B). There are three reasons to suggest that these molecules are actually short rodlets:

(1) These molecules are 1.5 times the size of those seen in films adsorbed to mica (2.8 nm compared to 1.3 nm) in Figure 63B, which means they are

approximately the same height as the mature rodlets seen in the mica-films (see Figure 64C and Table 18).

(2) Sertsou (1997) observed similar looking molecules in EAS films adsorbed to mica after 20 µL aliquots of the most concentrated EAS solution assayed were deposited on the mica (Note that Sertsou reported this as being a 100 ng/mL aqueous EAS solution. The discrepancy between Sertsou's sample-preparation techniques and my own is discussed in section 2.5.3). The rodlets that Sertsou observed were shorter, presumably because the process by which rodlets form is arrested when the elongating rodlet encounters an obstacle of similar size that it cannot extend through. The majority of rodlets in films adsorbed to mica seem to have elongated until they collide with other rodlets, they do not bend or extend around the obstruction (e.g. rodlets seen in Figures 64 and 65). Logically, the number of rodlets in a film would be proportional to the number of nucleation events; the rate of nucleation events was shown by de Vocht (2001) to be proportional to the concentration of hydrophobin in a solution. This is important because the concentration of hydrophobin molecules at the interface between water and HOPG will clearly be higher than it would be at the interface between water and mica because, as Figure 71 clearly shows, the latter interface will be larger in area.

(3) These molecules are unlikely to be artifacts produced by the cleavage of graphite since they have remained attached to the surface after the entire substrate was immersed in boiling SDS for 10 minutes (see section 2.5.3).

As the concentration of the hydrophobin solutions applied to the HOPG decreased so too did the size of the bi-layered film. The areas highlighted with the white arrow in Figure 73B are regions where a second layer of protein, approximately 5 nm thick, has been deposited on the layer (whose thickness could not be assessed) indicated by the red arrow. Rodlet-like molecules can also be seen (indicated by the black arrows). When this specimen was washed with hot SDS most of the upper layer of protein was removed while the lower layer appeared undamaged. Curiously the number of rodlet-like molecules increased substantially as de Vocht *et al.* (2000) would predict they should (they believed that the hot SDS treatment aids rodlets to self-assemble on hydrophobic solids). The height of these molecules (2.36 ± 0.15 nm) is intermediate between the height of mature rodlets (~ 3 nm under these AF-microscopy conditions) and for this reason, I have deemed them to be protofibrils (Table 18).

FIGURE 72: 10 µg/mL EAS DEPOSITED ON HOPG BY THE DROP AND SPREAD METHOD.

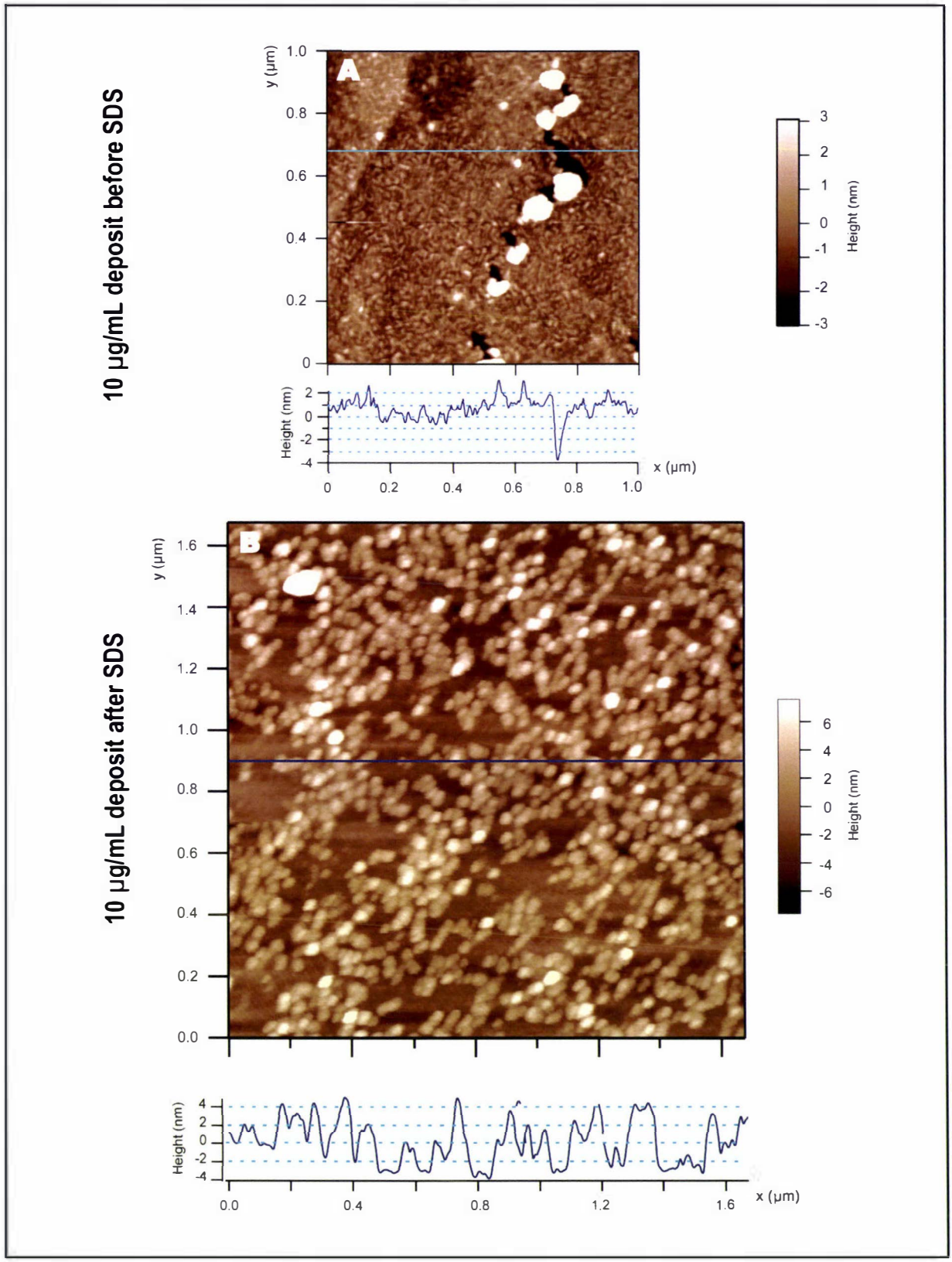

Figure 72 depicts the films formed on HOPG by drying down a 20 µL aliquot of a 10 µg/mL aqueous solution of EAS. Figure 72B depicts the film in Figure 72A after it was washed in hot 2 %(v/v) SDS as described in section 2.5.3. The spherical molecules in Panel B have a mean height of 2.82 ± 0.19 nm (n = 20; $\bar{x}$ = 2.82 nm; SE$\bar{x}$ = 0.19 nm). The blue line Figure 72B in illustrates the path of the height profile below each image. All images were collected in AC mode in ambient conditions using an MFP3D-IO device equipped with an Olympus® AC240TS probe. Note that the zero height of the height scale accompanying each image is different. Prior to the SDS treatment the AFM probe could not have encountered the surface of the graphite therefore the thickness of the protein coating in Figure 72A will be greater than the accompanying height scale suggests.

FIGURE 73: 5 µg/mL EAS DEPOSITED ON HOPG BY THE DROP AND SPREAD METHOD.

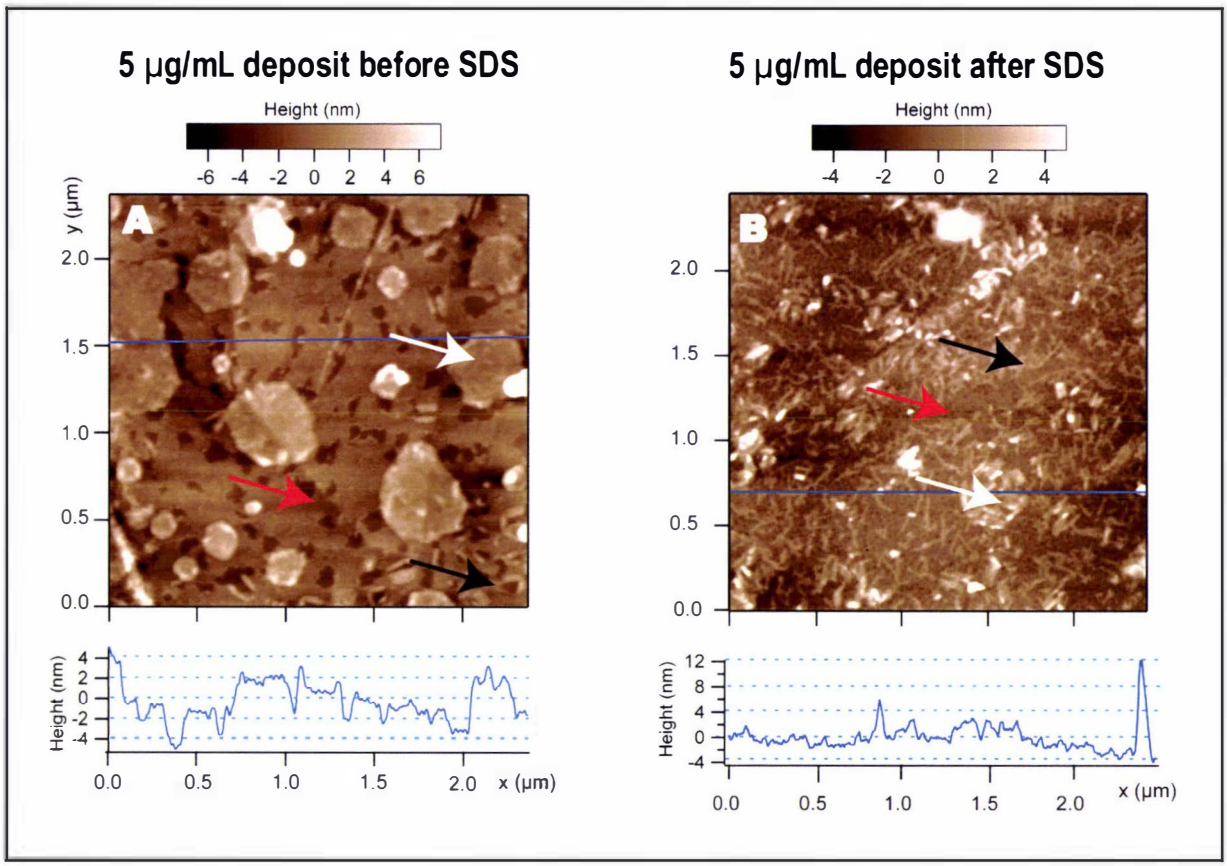

Figure 73 depicts the films formed on HOPG by drying down a 20 µL aliquot of a 5 µg/mL aqueous solution of EAS. Figure 73B depicts the film in Figure 73A after it was washed in hot 2 %(v/v) SDS as described in section 2.5.3.

Key: Black arrows in Figures 73 A and B draw attention to rodlet like molecules which have a mean height 2.36 ± 0.15 nm (n = 18; $\bar{x}$ = 2.36 nm; SE$\bar{x}$ = 0.15 nm). The white arrows highlight the rodlet bearing plateaus that may be part of an EAS bi-layer. The mean height of these plateaus is 5.17 ± 0.20 nm (n = 15; $\bar{x}$ = 5.17 nm; SE$\bar{x}$ = 0.20 nm). The red arrows highlight the amorphous layer of protein believed to be adsorbed directly to the HOPG surface. The mean thickness of this layer could not be measured. The blue lines in each image illustrate the path of the height profile below each image. All images were collected in AC mode in ambient conditions using an MFP3D-IO device equipped with an Olympus® AC240TS probe.

The weakest solution of EAS (0.5 µg/mL) did not yield a multi-layered protein film (Figure 74). Instead, a loose network of spherical and rodlet-like molecules – all of which were ~1.84 nm in height – was detected (Table 18). The fact that the phase-contrast image (Figure 74C) shows these molecules in a lighter shade than the background demonstrates that these molecules are unlikely to be artifacts of the type described by Clemmer and Beebe (1991).

Without observing EAS assembling on HOPG in real time (see section 6.4.3), unambiguously identifying these molecules will prove difficult. They are about two-thirds the height of EAS rodlets imaged under similar conditions and thus could be protofibrils in the process of forming mature rodlets. This process may have been arrested when the evaporation of the solvent robbed them of the mobility required to completely self-assemble. Interestingly, some of the images obtained by Gunning *et al.* (1998) also showed spherical molecules seeming to align bead-like into linear molecules similar to those in Figure 74B (see Figure 57A).

6.3.2 Films formed by Submerging HOPG in EAS Solutions.

A survey of the films formed when HOPG was submerged in aqueous EAS solutions was carried out as described in 2.5.3. Aqueous solutions containing 5 µg/mL, 1 µg/mL and 0.5 µg/mL of EAS were prepared in which freshly cleaved HOPG substrates were incubated for either 12 or 24 hours.

When HOPG was incubated in solutions containing >0.5 µg/mL of EAS for 24 hours it formed multi-layered films similar that seen in Figure 72A.

Figure 74: 0.5 µg/mL EAS Deposited on HOPG by the Drop and Spread Method.

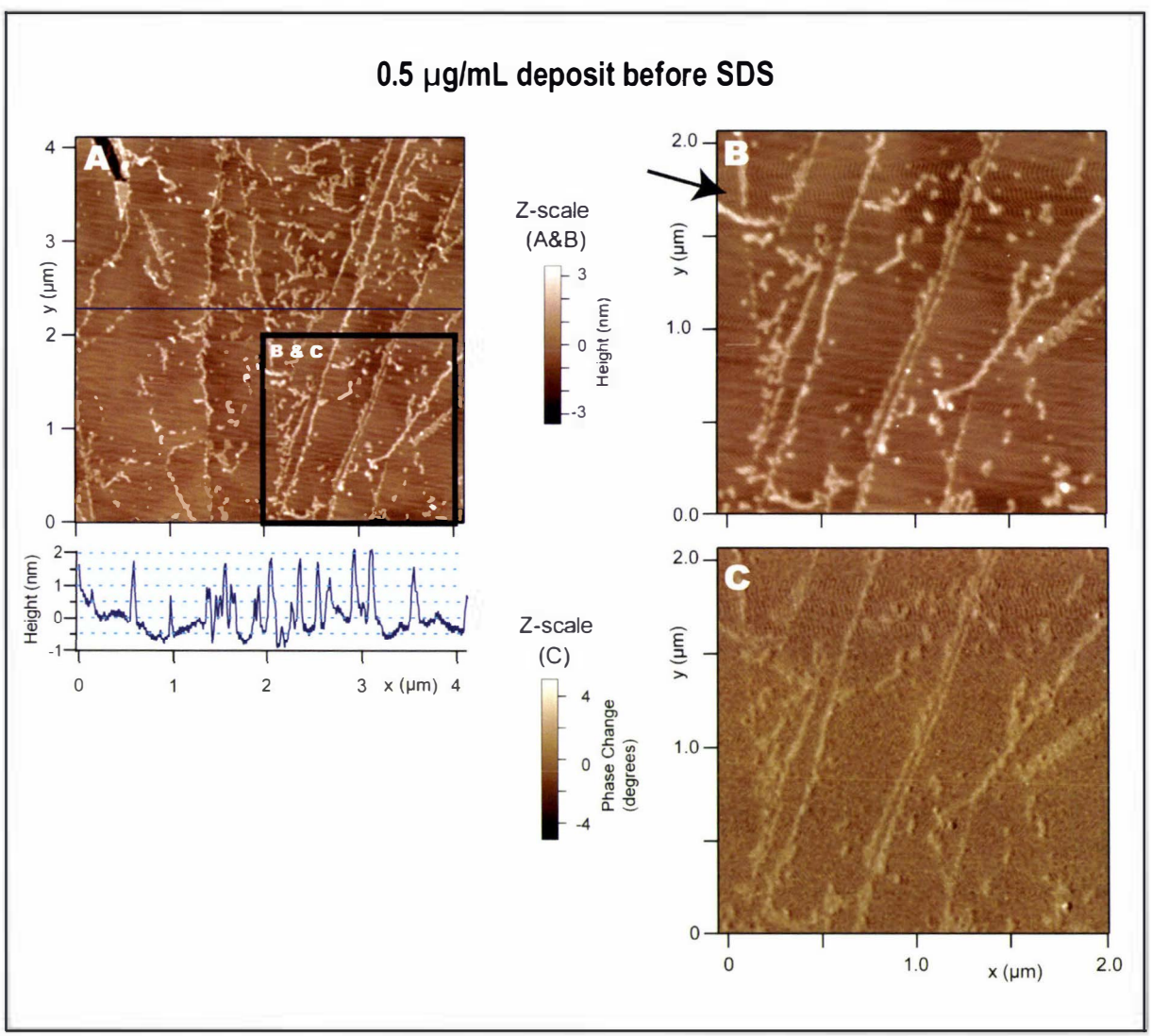

Figure 74 depicts the films formed on HOPG by drying down a 20 µL aliquot of a 0.5 µg/mL aqueous solution of EAS. The area encompassed by the black square in Figure 74A has been magnified in Figures 74B and C. Note that Figure 74C depicts the phase contrast data collected simultaneously to the height data presented in Figure 74B.

Key: The blue line in Figure 74A illustrates the path of the height profile below each image. The rodlet-like molecules in Figure 74B have a mean height of 1.84 ± 0.18 nm (n = 15; $\bar{x}$ = 1.84 nm; SE$\bar{x}$ = 0.18 nm).The black arrow in Figure 74B highlights the elevated signal-to-noise ratio of the MFP3D-IO device by calling attention to the dark diagonal lines. These are believed to be due to background electrical noise in this AFM. All images were collected in AC mode in ambient conditions using an MFP3D-IO device equipped with an Olympus® AC240TS probe.

FIGURE 75: HOPG SUBMERGED IN 1 µg/mL EAS SOLUTIONS.

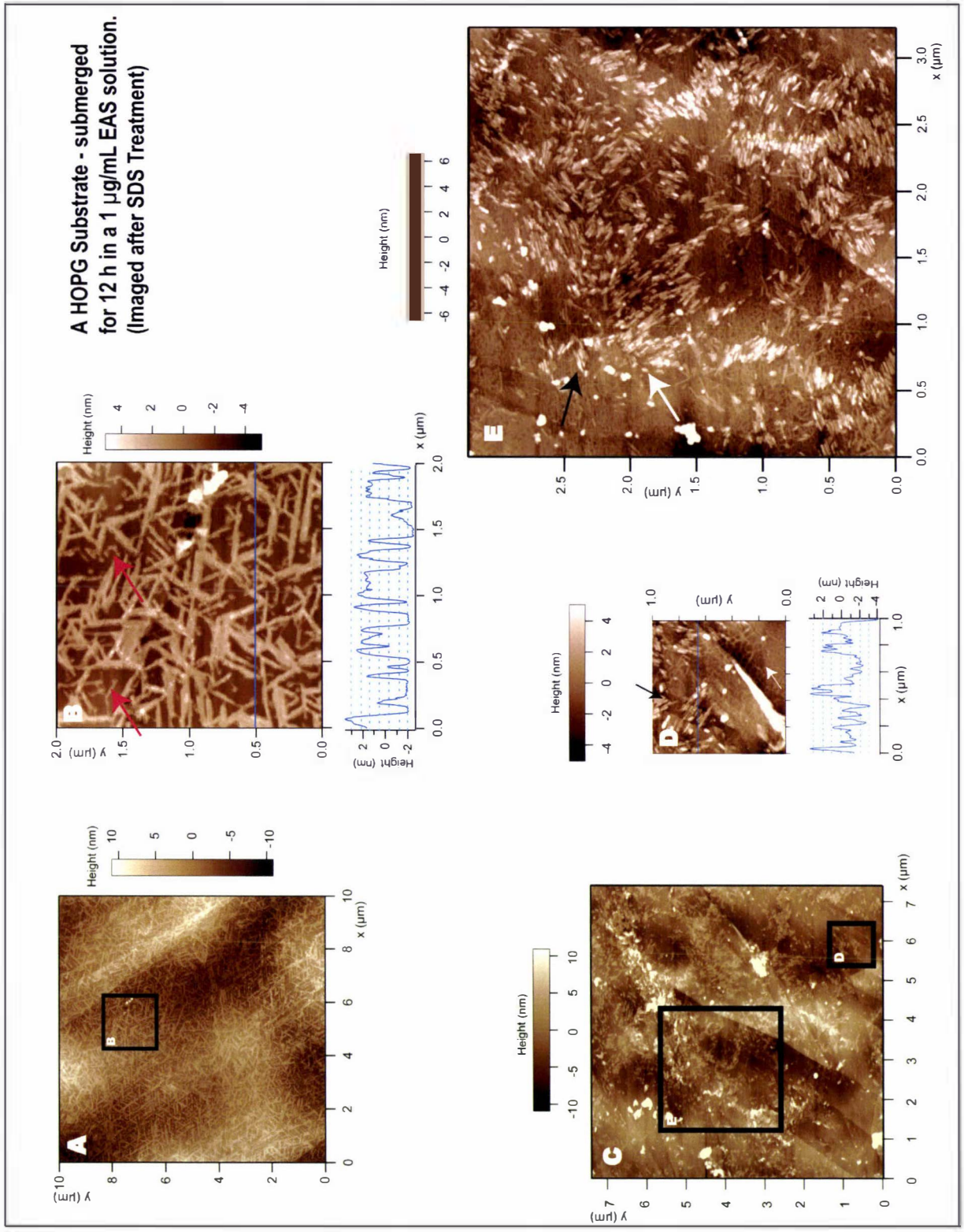

Figure 75 depicts different areas of the film formed on a single, freshly-cleaved HOPG substrate when it was immersed in a 1.0 µg/mL aqueous solution of EAS for 12 hours. Prior to these images being collected, the substrate was washed with hot SDS as described in section 2.5.3. The area encompassed by the black square in Figures 75A and 75B are magnified in Figures 75C, 75D and 75E. In Figure 75B the red arrows highlight some spherically-shaped and short-thin molecules that are seen between the larger interlaced fibrils.

Figures 75B, 75D and 75E depict an area of the film where rodlets (black arrows) were seen to form on top of the fibrous film (white arrows) seen in Figures 75A and 75C.

The mean height of the fibres seen in Figures 75A and 75C is 2.64 nm ± 0.12 nm (n = 30; $\bar{x}$ = 2.64 nm; SE$\bar{x}$ = 0.12 nm). The blue line in some images illustrates the path of the height profile below each image. All images were collected in AC mode in ambient conditions using an MFP3D-IO device equipped with an Olympus® AC240TS probe.

FIGURE 76: EAS RODLETS ON HOPG.

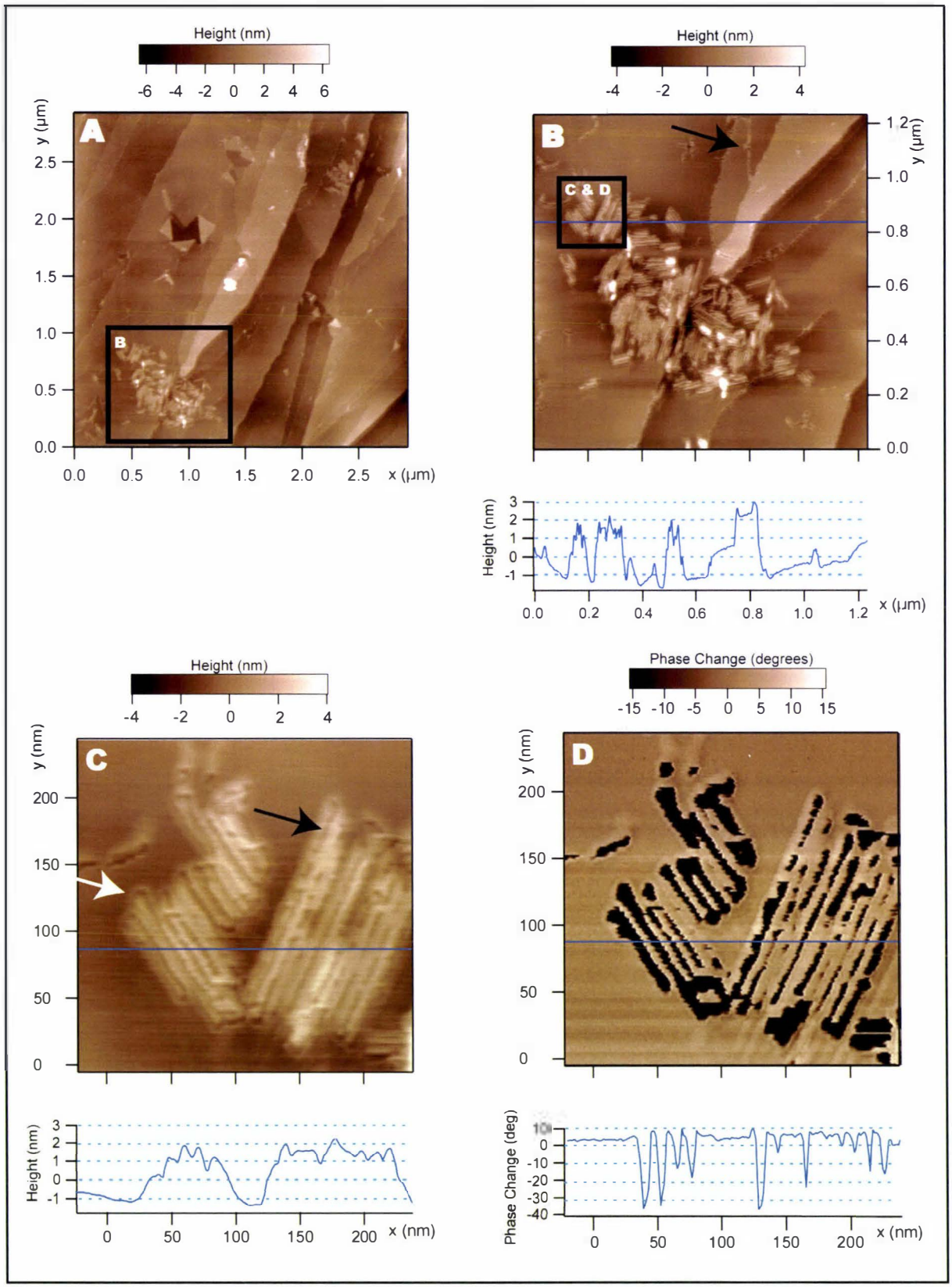

Figure 76 depicts rodlets formed in one region of a freshly-cleaved HOPG substrate when it was immersed in a 0.5 µg/mL aqueous solution of EAS for 12 hours. Prior to these images being collected, the substrate was washed with hot SDS as described in section 2.5.3. The areas encompassed by the black squares are magnified in the panels indicated. Panel D depicts the phase contrast data collected simultaneously to the height data presented in Panel C. The mean height of the fibres seen in Figure 76 is 2.81 ± 0.10 nm (n = 24; $\bar{x}$ = 2.81 nm; SE$\bar{x}$ = 0.10 nm). The blue line illustrates the path of the height profile below each image. The black arrow in Panel B highlights the presence of thinner rodlets lining the edges of the "steps" in the HOPG substrate. All images were collected in AC mode in ambient conditions using an MFP3D-IO device equipped with an Olympus® AC240TS probe.

By comparison, the 0.5 µg/mL solution formed monolayered film 1.64 nm thick. The resolution of the AFM images of this film was insufficient to allow the shape of molecules within it to be clearly identified, but the molecules appeared to be similar to those in Figure 57B. A few rodlet-like molecules ~1.7 nm in height were seen on the surface of the amorphous film (data not shown).

After 12 hours of incubation, rodlet molecules over 2.6 nm in height were detected in films formed from the 1 µg/mL and 0.5 µg/mL solutions. Each specimen was washed in hot SDS prior to imaging in order to ensure that only the hydrophilic side of EAS films was being imaged. The film formed by 1 µg/mL solution contained an extensive network (Figures 75A and 75C) of flattened rodlet-like molecules with a mean height of 2.64 ± 0.12 nm – between the network's interlaced fibres some spherically-shaped and short-thin molecules are also seen (highlighted with red arrows in Figure 75C). In discrete regions of the same specimen, bundles of more cylindrical rodlet molecules (near the black arrow in Figures 75D and 75E) were seen adsorbed on top of the network of flattened rodlets (near the white arrow Figures 72D and 72E).

The manner in which these rodlets were bundled hampered an attempt to measure the height of individual molecules using the AFM's sectional analysis software.

By contrast, the film formed by 0.5 µg/mL film yielded bundles of molecules I have designated as being rodlets because their mean height (2.81 ± 0.10 nm) and shape was similar to rodlets adsorbed to mica when these were imaged under similar conditions (Figures 65A, 76B). A pair of dark parallel lines running longitudinally along the upper surface of these rodlets (highlighted by a black arrow in Figure 76C). These appear to be a pair of clefts and this conclusion is supported by the phase contrast image which implies that area in Figure 76C where the clefts are seen contains a void (Figure 76D).

A pair of clefts with the juxtaposition suggested by Figure 76C implies that these rodlets consist of three protofibrils in the triangular arrangement suggested by Figure 68. The image in Figure 76C also implies that the crowning rodlet is shorter than the pair of rodlets on which it sits, because the clefts appear to be joined as by a curved cleft that is located at the termini of some of the rodlets (highlighted by a white arrow in Figure 76C). Longer thinner molecules – 0.92 ± 0.03 nm in height – lining the edge of the steps in the graphite were also visible (highlighted by a black arrow in Figure 76B) – their size is similar to other protofibrils that have been detected (Table 18).

6.4 DISCUSSION.

It was unfortunate that an electrical fault in the AFM best suited to imaging small sample areas prevented the films being closely examined in fluid. Had this been possible, then many of the novel molecules and surface features that were detected in ambient conditions could have been unambiguously identified with AFM techniques like time-lapse imaging, and chemical force microscopy – each of which can only be conducted in a liquid environment (see section 6.4.3).

That said there are at least two reasons why hydrophobins should be imaged in air as part of any AF-microscopic investigation of their structure:

(1) Hydrophobins are naturally exposed to the air in their role as fungal cell-wall proteins. They are believed to self-assemble on or near the exterior surface of the cell wall and if they are exposed to fluid, it is normally composed of rainwater rather than an organic or an electrolyte-bearing fluid (Wösten and Willey, 2000).

(2) While AF-microscopy in fluid is a better environment for imaging soft samples (see section 6.0.3), there are problems associated with it that must be countered with carefully designed control experiments. One set of control experiments seeks to differentiate between structural features that are naturally present on the surface of the substrate and sample and those that have arisen out of the presence of the imaging fluid. If possible, such experiments should be conducted in air because a sample may become contaminated may or even desorb while it is being imaged in fluid (see comments made by Paananen *et al.*, 2003). In such experiments, the sample must remain stably attached to the substrate for long periods. For example, the experiment cannot begin until each of the sample, probe, probe-holder, and imaging fluid reach thermal equilibrium (Kindt *et al.* recommend that samples be allowed to stand for 30 minutes or more – which introduces more problems if the imaging fluid is volatile) in order to prevent micro-convention currents from buffeting the tip during imaging (Kindt *et al.*, 2002).

Thus, there is normally a 30-minute delay before the AFM operator can even discover if the sample has been affected by the imaging buffer.

6.4.1 THE HYDROPHOBIN FILMS ON MICA .

As was discussed in sections 6.2.2 and 6.2.3, the presence of (putative) protofibrils-molecules near mature rodlets, and the presence of a central cleft in those rodlets both support the idea that hydrophobins are comprised of the same structural

elements as amyloid proteins and that they polymerise in the same manner. Nevertheless, the true nature of both the cleft and the protofibrils remains to be confirmed:

(1) If the spherical and short rod-like molecules seen in Figures 63, 64, and 65 are protofibrils then they should elongate to form mature rodlets and this process can be observed in real time using the AFM (see below).

(2) I proposed in section 6.2.3, that the rodlet's central cleft (seen in Figures 64, 65, and 66) was the boundary between two adjacent protofibrils of equal length. While this conclusion is certainly consistent with data gained by other researchers it should be possible to confirm for the case presented here if the AFM experiments could be repeated in fluid. Results presented in Appendix VI imply that a silicon-nitrite tip immersed in a buffer consisting of 50 mM KCl and 10 mM MOPS at pH 7.0 should be able to contour the surface of the rodlet without deforming it. Therefore, if these imaging conditions are used, the AFM should more clearly reveal the protofibrils in the rodlet's substructure than was the case with the ambient imaging-conditions favoured for here.

6.4.2 The Hydrophobin on HOPG.

One of the stated goals of the HOPG experiments was to determine the conditions under which true hydrophobin rodlets could be formed.

Several fibril-like forms have been detected in this study. According to an ad-hoc comparison of height measurements, I have identified these variously as rodlets, protofibrils, and amorphous films. The true nature of these molecules could be identified if the self-assembly process was observed using time-lapse AF-microscopy. This experiment should be performed in tandem with chemical force microscopy experiments (see below) that are designed to prove that the amphipathic films have exposed their hydrophilic side to the probe.

Nevertheless, the rodlets seen in Figure 76 are clearly related to the rodlets seen in the films adsorbed to mica. Not only are they the same size, but they *are* bundled together and a series of clefts within each rodlet *is* evident. Results presented in this chapter suggest that the number of protofibrils per rodlet may be limited to either two or three. This is a tentative hypothesis because I have only examined two combinations of film and interface in these experiments. The number of protofibrils per rodlet may depend in the individual hydrophobin or even on the nature of interface and environmental-conditions encountered.

For reasons discussed in section 6.4.3 (below), the HOPG specimens were pre-treated with hot SDS because this was the only method available to ensure that the hydrophilic face of EAS polymers was being presented for examination. However, according to the mechanism of self-assembly proposed by de Vocht *et al.* (1998, 2000, and discussed in section 1.3.5) this treatment could have triggered the final stage in the formation of EAS rodlets. The SDS treatment may have caused an additional protein layer – consisting of bundled rodlets – to form on the monolayered protein film seen in Figure 75. Because I cannot be certain that these rodlets were present prior to the SDS treatment, the experiments described in this chapter are not ideal for evaluating the model proposed by de Vocht *et al.* Researchers seeking to evaluate that model with AF-microscopy would have to devise ways of locating and identifying particular regions of the HOPG/EAS specimen before and after the SDS treatment. For instance, it may be possible to use Asylum Research's MicroAngelo™ Nanolithography system, which is built into the MFP3D-IO device, in order to score the HOPG surface prior to depositing the hydrophobin. If could be successfully accomplished, it should then be possible to monitoring the manner in which films form on graphite submerged in a 0.5 µg/mL solution of EAS for about 12 hours before and after (but not during) being washed in boiling SDS.

Finally, previous hydrophobin specimens have been prepared on hydrophobic substrates by one of two methods: (1) submerging the surface in an aqueous solution of the hydrophobin (*e.g.* Wösten *et al.*, 1994b, 1995; Lugones *et al.*, 1996, 1999a; Gunning *et al.*, 1998; de Vocht *et al.*, 2002) and (2) the "drop and spread" technique where an aqueous solution is applied on to a hydrophobic surface and the solvent is allowed to evaporate (Wösten *et al.*, 1993, 1994a; Wösten and de Vocht, 2000 and Figure 64A). The results obtained from specimens prepared by these techniques have been mixed (section 6.0.1).

Films prepared by both methods were examined as described in section 6.3. The experiments clearly showed that the morphology of the hydrophilic side of hydrophobin films depends on the concentration of the hydrophobin solution and the method by which the films are allowed to form on graphite. This show that some caution needs to be applied when interpreting electron micrographs of hydrophobin films prepared on Formvar or carbon-coated surfaces. These have previously shown rodlet-films but were prepared by the "drop and spread" technique (Wösten *et al.*, 1993, 1994a; Wösten and de Vocht, 2000 and Figure 64A) which, as our experiments showed, permitted bi-layers of hydrophobin to form unless hydrophobin solutions of 0.5 µg/mL were used.

When rodlets adsorb on mica, it is believed that they form at the air-water interface and settle on mica after the water has evaporated: Wösten *et al.* (1995) demonstrated that there must be a hydrophobicity sharp gradient between the materials at the interface before a hydrophobin can self-assemble between them.

The question is how is the rodlet film actually formed? Have the rodlets seen to have been formed on hydrophobic electron-microscope grids formed at the solid-water interface or, instead, has an additional rodlet-film formed at the air-water interface and then settled on top (and thus obscured) any film forming at the solid-water interface? If the latter has occurred, than the hydrophobic face of the amphipathic film is being exposed.

6.4.3 Further Experiments.

Atomic force microscopy is a versatile tool that compliments other ultra-structural imaging techniques like electron microscopy. So far atomic force microscopes have only been used to image hydrophobin polymeric films (*e.g.* Gunning et al. 1998; de Vocht *et al.*, 1998, 2000; Martin *et al.*, 2000; Mackay *et al.*, 2001; Paananen *et al.*, 2003; Hakanpää *et al.* 2004), but as discussed below this is only one of several AFM techniques that could be applied.

(a) **Spike-Shaped Probes:** Conventional AFM probes are large compared to the rodlets they were required to image in the experiments described in this chapter. The Veeco® TESP and Olympus® AC240TS Tapping mode probes used have a pyramidal geometry that limits the maximum tip radius to 5-10 nm. While these probes often have asperities that permit surface features less than 1 nm in width to be seen, the rest of the tip's surface must still be supported by the sample (Müller and Engel, 2002) – it is this additional bulk that contributes to an excessive amount of probe-broadening which gets worse as the contours in the sample become deeper. This is because the probes (which are normally pyramid-shaped) have a width of 5-10 nm at their apex only, the width increases to several microns at the point where the probe is mounted to the cantilever. However, this situation is changing; it should soon be possible to image hydrophobin rodlets with tips just one-tenth of their estimated 11 nm width!

Tapping™-mode probes with nearly vertical side-walls and 1 nm tip radii have become commercially available (*e.g.* Veeco®'s Focused Ion Beam Machined Silicon Probes or Mikromasch®'s Hi'Res series of probes). At the same time, it is now possible to mount carbon nanotubes with sub-nanometer radii and

vertical side-walls onto silicon nitrite probes (Wong *et al.*, 1998; Cheung *et al.*, 2000). These two advances finally provide the AFM with a means to probe deep trenches such as the boundary between protofibrils in hydrophobin rodlets.

If probes with near vertical side-walls and 1 nm tips are used, then the contribution from the probe-broadening effect will be 10-fold reduced - for cylindrical samples like the hydrophobin rodlet, probes such as these should dramatically increase the accuracy of imaging and of the dimension-measurements obtained from them. It should then be possible to determine whether a single rodlet is formed from two or three protofibrils and how these protofibrils are arranged.

(b) **Langmuir Troughs:** Surfactant molecules have often been studied with the aid of a Langmuir trough. The Langmuir trough is a shallow rectangular PTFE Teflon® trough with moveable Teflon® barriers that not only enables researchers to monitor the surface tension of a liquid but also to manipulate the packing of amphipathic films that form on the surface of liquid contained within the trough (Morris *et al.*, 1999). To my knowledge nobody has attempted to see if the self-assembly of class I hydrophobin films can be controlled using this device (note that Paananen *et al.*, 2003 have examined HFB1 and HFB2 films formed using this technique). Obviously, the PTFE Teflon® must be treated to prevent the hydrophobin from adsorbing to the walls, rather than at the air-liquid interface (pre-treated with hydrophobin perhaps?). The moveable barriers might permit close or loosely packed films to be formed on the surface of the liquid. Were a standing wave able to be induced in the liquid contained by the trough (perhaps through the use of mechanical dippers or a fan) it might be possible to reduce the randomness in the orientation of rodlets within the film. DNA molecules have reportedly been induced to adsorb to mica substrates in relatively straight lines by blowing a unidirectional stream continually over the substrate's surface (Li *et al.*, 1998). Such films could then be transferred to any planar surface by Langmuir-Blodgett techniques (reviewed in Morris *et al.*, 1999).

There are several advantages to be gained from generating close-packed films of linear rodlets. The first is that these are the conditions exploited by used by Müller *et al.* when they obtain nanometer-resolution images of bacterial membrane proteins (reviewed in Müller *et al.* 1998b). The regularity of these films also allow more advanced noise-filtering algorithms and image-

enhancement techniques – based on averaging sub-units from a uniform object – to be employed to further reduce any background noise in the data and improve the clarity of high resolution images (*e.g.* Scheuring *et al.*, 1999; Paananen *et al.*, 2003).

(c) **Time-Lapse Imaging:** The AFM has previously been used to monitor the self-assembly of amyloid and F-actin protein fibres in real time (reviewed by Stolz *et al.*, 2000). Performing these experiments and comparing the results when mica or HOPG are used as substrates, would enable many of the features seen during the investigations described above and by Gunning *et al.*, (1998) to be identified correctly. Other questions relating to the dynamics of hydrophobin self-assembly might be answered: Do the rodlets elongate from one or both ends? What determines the rodlet's length and directionality, do they continue to elongate until they strike some obstacle? Is the number of protofibrils per rodlet limited? How do rodlets come to be bundled together into fascicles? Does assembly begin with the formation of spherical particles that grow to a certain thickness and then elongate as happens with the human amylin protein (Green *et al.*, 2004)? What do the α-helix-rich and ß-sheet-rich transition states detected by de Vocht *et al.* (1998, 2000) look like and how do they assemble?

Unfortunately monitoring the assembly of hydrophobins by time-lapse imaging is not likely to be trivial. While I was able to confirm that the hydrophobin could self-assemble while mounted on the AFM the time-scale involved was in excess of 12 hours (data not shown). Such experiments require that the investigator manually adjust the set-point voltage during imaging to compensate for drift in the system settings that would eventually see the probe crash into the sample if left unchecked. More experiments are required to see whether increasing the concentration of the EAS solution also increases the rate of rodlet formation without affecting the quality of the AF-microscopy. Other investigators have increased the rate of polymerisation of amyloid proteins by the addition of preformed seed molecules (e.g. Green *et al.*, 2004). It is not clear whether this will work with hydrophobins, all that has been established is that in the absence of a hydrophobic/hydrophilic interface hydrophobin self-assembly could not be initiated by the addition of preformed rodlets (de Vocht, 2001).

If time-lapse imaging of hydrophobin-assembly is possible then it could be a powerful tool in combination with site-directed mutagenesis (assuming enough

structural data about the positions of individual amino-acids within the rodlets forthcoming) to enable the self-assembly of wild-type and mutagenized hydrophobins to be compared. Such experiments might shed light on structural questions such as why the number of protofibrils per rodlets appears limited to between two and three (as was suggested in experiments described in this chapter).

(d) Chemical-Force Microscopy and Force Measurements: It is possible to covalently-modify both silicon nitrite probes and carbon nanotubes so that a molecule bearing a particular chemical group is expressed at their apex (Cheung *et al.*, 2000 and review by Noy *et al.*, 1997). Assuming the cantilever to which such probes are attached has a low spring-constant, the interaction between the chemical at the tip of the probe and the surface of the specimen over which it is scanned should induce some lateral twisting in the cantilever as the chemical probe is alternately attracted to and repulsed by regions in a chemically heterogeneous sample. This twisting motion can be detected by the AFM and the results graphically displayed to yield a chemical force micrograph – literally a map of specimen's chemically distinct regions (Noy *et al.*, 1997). This technique would allow a researcher to confirm which side of the hydrophobin film has been exposed to the AFM. This is important because contact angle measurements are likely to be influenced by contact with the underlying substrate – a consequence of the unevenly distributed films that result when specimens are prepared with low-concentrations of hydrophobin. This limitation must be accepted in order to obtain the best imaging conditions (i.e. monolayered films with easily accessible rodlets).

Chemical-force microscopy and force measurements could allow the surface of the hydrophobin rodlet to be surveyed for hydrophobic or hydrophilic interactions with sharp, high-aspect ratio tips expressing methyl or hydroxyl groups. This is how Dufrêne (2000) established, at a microscopic level, that the exterior surfaces of *Phanerochaete chrysosporium* spores were hydrophilic. By this method, any broad chemical heterogeneity in the rodlet's surface might be mapped, albeit with low spatial resolution.

Recently Olympus® brought the gold-coated Biolever AFM probe into commercial production. The availability of a gold-coated AFM probe with a low spring-constant (despite its metallic coating) means that chemical force microscopy can be performed by any laboratory with an AFM. This is because the protocols used to chemically functionalise AFM probes rely on covalently

bonding mercapto-alkane molecules to a gold-coated probe (Noy *et al.*, 1997). Unfortunately, coating conventional silicon-nitrite tips requires specialised equipment that is not commonly available even to well-equipped electron microscopy laboratories. This was the major impediment to my attempts to confirm whether the hydrophobic or hydrophilic side of the EAS films was being imaged. This was the reason that I choose to image SDS-treated HOPG/EAS specimens: if the film had adsorbed strongly enough to HOPG to resist boiling SDS then according to Wösten *et al.* (1995) the hydrophobic side must be facing the substrate leaving the hydrophilic side facing the AFM probe.

The ability of the AFM to measure forces applied to a sample may also enable the tensile strength of the rodlets to be measured. The effects of shear-forces or external-fields on hydrophobin polymerisation could also be investigated by this method.

(e) **Imaging *N. crassa* Macroconidia:** The AFM also has the potential to image the rodlets expressed to the exterior surface of *N. crassa* macroconidia at a higher resolution than that achieved by Beever and Dempsey (1979). The reason is that the actual surface, not a carbon shadowed replica, could be imaged if Millipore® Isopore polycarbonate membranes were used, the macroconidia could be mechanically trapped and immobilized on a surface suitable for AFM imaging (Kansas and Ikai, 1995). Dufrêne *et al.* have used this technique successfully to examine *Phanerochaete chrysosporium* spores (Dufrêne *et al.*, 1999; Dufrêne, 2000). Repeating this experiment with *N. crassa* macroconidia would enable the dimensions and structure of a hydrophobin film formed *in vivo* to be compared to the dimensions and structure of the TFA-treated films formed *in vitro*.

6.5 Summary of Results.

AF-microscopy was used to gain a better understanding of the shape and composition of the polymeric structures that form when EAS self-assembles on hydrophobic or hydrophilic solid surfaces:

(1) Each of the isoforms of EAS purified from *N. crassa* was tested, and each was found capable of independently forming rodlets.

(2) One or more clefts were detected in the rodlets that comprise EAS films adsorbed to both mica and – under certain conditions – to graphite. Evidence presented previously was considered alongside results collected in this study

and together they indicate that these clefts represent the boundary between the adjacent cylindrical protofibril molecules that comprise these rodlets.

At the same time, smaller, shorter molecules with either a spherical or an oval shape were also observed to be present in the thinner hydrophobin films. In keeping with current data that shows that class I hydrophobins are functional amyloids it was suggested that many of these molecules are elongating protofibrils.

(3) The conditions under which the highest resolution AFM images of EAS rodlets might be obtained have been suggested, along with other AFM experiments that should confirm the true nature of the molecules that have been putatively identified as protofibrils in this study.

(4) The morphology of the polymeric molecules within films formed as a class I hydrophobin self-assembles on a hydrophobic solid was examined. Many of the structures had been seen previously in a little-known study by Gunning *et al.* (1998),

(5) Finally, and significantly, for the first time a procedure for preparing hydrophobin specimens that will permit the hydrophilic side of true EAS rodlets to be unambiguously examined was developed.

7
GENERAL CONCLUSIONS.

7.0 SUMMARY: HYDROPHOBIN RESEARCH.

Hydrophobins are small proteins secreted by filamentous fungi to coat the air-exposed surfaces of various structures that are formed by these fungi. The individual functions of each hydrophobin are normally related to their ability to form amphipathic polymer-films (see reviews by Wessels, 1997; Wösten, 2001; Whiteford and Spanu, 2002). Although the proteins share similar hydropathy patterns, and eight conserved cysteine-residues, the amino-acid sequences of hydrophobin proteins are not homologous. Despite this, the class I hydrophobins can partially substitute for one another (Kershaw *et al.,* 1998; van Wetter *et al.,* 2000a; Whiteford and Spanu, 2002).

If a hydrophobic-hydrophilic interface is present and the concentration of hydrophobin in solution is above the critical value, then the protein will spontaneously self-assemble into an insoluble, chemically-resistant film (Wessels, 1997; de Vocht, 2001). Class I hydrophobin films are composed of bundles of 10 nm wide polymeric fibres called rodlets (Wessels, 1997). The ultrastructure of these fibres has yet to be examined at high-resolution, but they do contain a significant amount of β-sheet structure; further, their reactions with the dyes Congo Red and Thioflavin T suggest that rodlets have a structure similar to the amyloid fibril (Mackay *et al.,* 2001; Butko *et al.,* 2001; de Vocht, 2001).

By contrast, the class II films are believed to consist of a two-dimensional crystalline array of monomeric hydrophobin molecules. The monomer molecules are thought to orientate themselves so that their hydrophobic "patch" is buried in the hydrophobic side of the interface (Wessels, 1997; Wösten and de Vocht, 2000; Paananen *et al.,* 2003; Hakanpää *et al.,* 2004).

The monomeric form of HFB2 has a single-domain globular-shaped structure that includes one α-helix and four anti-parallel β-hairpin loops. The β-hairpin loops contain a number of hydrophobic amino-acid residues and together they form the flattened hydrophobic patch that is responsible for the amphipathic properties of HFB2. The disulfide bonds in HFB2 are arranged to maintain this structural arrangement: disulfide bonds link the arms of individual β-hairpin loops and the remaining disulfides bonds connect each β-hairpin loop to distal regions of the molecule (Hakanpää *et al.,* 2004).

The monomeric structure of the class I hydrophobin has yet to be solved, although EAS monomers have been shown to be relatively unstructured with a small amount of β-sheet structure localised around the regions containing the cysteines (Mackay

et al., 2001). Curiously, SC3 is known to contain a greater proportion of α-helix and β-sheet secondary structure, but this might be explained by the fact that SC3 forms multimeric structures in solution (de Vocht, 2001). The arrangement of disulfide bonds in any class I hydrophobin has yet to be determined (Mackay *et al.,* 2001; Hakanpää *et al.,* 2004).

While hydrophobins are interesting because they play important roles in fungal development and pathogenesis, the potential exists to develop a large number of medical and biotechnical applications that could exploit the hydrophobin's unique physical properties (Wessels, 1997; Scholtmeijer *et al.*, 2001). Hydrophobins are highly surface-active molecules that have the ability to bind strongly to hydrophobic and hydrophilic surfaces, and to reverse that surface's wettability (Wösten *et al.,* 1993; Wösten *et al.,* 1994a; de Vocht *et al.,* 1998; Lugones *et al.,* 1996, 1998, 1999a; Wösten and de Vocht, 2000). It was shown recently that hydrophobins could retain these properties even when fused to other proteins. This result opens the door to the development of hydrophobin-based biosensors, protective coatings, surfactants and various medical or diagnostic technologies (Scholtmeijer *et al.,* 2002; Linder *et al.,* 2001; Nakari-Setälä *et al.,* 2002).

Studies using site-directed mutagenesis techniques are one means of investigating both the ultrastructure of hydrophobins polymers and the mechanism by which they self-assemble; this information would greatly simplify the process of developing hydrophobin-based technologies. But, before such studies could commence, the conserved regions within a hydrophobin's protein sequence have to be identified – perhaps by investigating the genes and proteins produced by closely-related fungal species (Chapter 3) – and then a heterologous system for hydrophobin expression has to be developed to enable mutagenised hydrophobins to be produced for further study (Chapter 4).

Solving the monomeric structure of class I hydrophobins would help to determine how hydrophobins self-assemble. Such a structure might explain the amphipathic nature of the class I hydrophobins, as was the case with HFB2 (Hakanpää *et al.,* 2004); it might also help to explain some of the biophysical differences between class I and class II hydrophobins. Unfortunately, none of the class I hydrophobins has ever been crystallised, so their structure has to be elucidated from models built from NMR spectra and disulfide-bond mapping experiments (Chapter 5).

Because the polymeric structure of class I hydrophobins cannot be studied with crystallographic techniques, they must be studied at lower resolution techniques like

electron microscopy and atomic force microscopy. The advantage of studying these films with the AFM (Chapter 6) is that the surface of the film can be examined directly which should enable the sub-structure of hydrophobin rodlets to be better characterised. The principal aim of such studies is to confirm that hydrophobin rodlets composed of protofibrils similar to those found in amyloid fibrils (Wetzel, 2002; Sipe and Cohen, 2000; Dobson, 1999, 2001).

The aim of the experiments described in this thesis was to contribute to our understanding of the structure and function of hydrophobins. The class I hydrophobin EAS (which is a product of the gene *eas*) coats macroconidia that has been produced by the model ascomycete *Neurospora crassa* (Davis, 2000), making this species an ideal subject for structural studies on hydrophobins.

7.1 Conclusions: EAS Homologues in Other Species of *Neurospora*.

The experiments described in Chapter 3 aimed to identify key conserved amino acids that are vital to the structure and self-assembly of EAS. Unfortunately, the original aim of these experiments could not be achieved because the genes and proteins isolated from each *Neurospora* species were virtually identical. This is consistent with the evolutionary trend determined in previous phylogenetic studies (Dettman *et al.,* 2001); the *eas* genes and EAS proteins present in the heterothallic *Neurospora* species were virtually identical because the heterothallic species are closely related.

Surprisingly, versions of *eas* were discovered in the aconidiate homothallic *Neurospora* species. However, I was unable to detect either the transcription of gene or the production of protein. This implies that the gene is inactive in these species, but I was unable to pinpoint the reason why. This is the first report of the existence of (putatively) inactive hydrophobin genes – probably because hydrophobins are normally uncovered by during gene-expression studies (see Appendix I).

In the light of the phylogenetic results presented by Dettman *et al.* (2001), my results also suggest that members of the Sordariaceae apart from *Neurospora* may possess *eas*. Thus, if the survey described in Chapter 3 were repeated with a wider sample of Sordariaceae species, then the chances are higher that conserved amino acids within EAS might be revealed. At the same time, it would be advantageous to include more strains of *Neurospora*, especially the more diverse strains isolated by

Perkins' laboratory (Perkins *et al.,* 1976; Perkins and Turner, 1988; Turner *et al.,* 2001), in order to see how the sequence of *eas* varies within a species.

With regard to the versions of *eas* from the homothallic *Neurospora* species, it is interesting that this inactive gene is well conserved relative to the active forms of *eas* in the non-homothallic species. This is despite the fact that these species are aconidiate, and therefore lack the selective pressures required to resist mutations that are detrimental to the function of EAS – a protein that acts to protect conidia. Given that *N. crassa* has evolved a complex *cis*-acting mechanism to control the expression of *eas*, the question is why is this gene not expressed in the homothallic *Neurospora*? Are the other mechanisms used to control *eas* in *N. crassa* (including the circadian clock) defective or absent in the homothallic *Neurospora*? Answering this question might reveal some insights into the function of the eukaryotic circadian clock – such insights would build on previous circadian clock investigations that focused on the action of *eas* in *N. crassa* (*e.g.* Bell-Pedersen *et al.,* 1996; Correa and Bell-Pedersen, 2002).

The first step in any analysis of the genetic elements that control *eas* in *Neurospora* would be to revise the gene-amplification strategy we pursued in Chapter 3. The task of designing PCR-primers homologous to regions upstream of *eas* in recent times been simplified by the availability of genomic DNA data available from the *N. crassa* database (Galagan *et al.,* 2003). The PCR-amplified sequence derived with primers by this method would enable researchers to confirm the presence of the rudimentary eukaryotic transcriptional elements (TATA- and CAAT- boxes, start codon *etc.*) that either were obscured by or were undetectable with the PCR-primers used here.

7.2 Conclusions: Heterologous Expression of EAS.

The experiments described in Chapter 4 were designed to create a heterologous expression system for natively expressing EAS. We chose to express EAS in *P. pastoris* and *E. coli* strains because neither species expresses endogenous hydrophobins, while both have successfully expressed a wide variety of transgenic proteins.

I was successful in isolating recombinant *P. pastoris* and *E. coli* isolates that contained the plasmid-vector that incorporated an EAS-encoding cDNA sequence. However, upon examining these isolates I did not detect any expression of recombinant EAS. This was in spite of the fact that the *Pichia* isolates were actively transcribing the *eas* cDNA. In each case, I suggested two hypotheses that would

explain this. The first is that the *eas* cDNA sequence that I used contained clusters of codons that are rarely used by either host. The presence of rare-codons has been known to cause serious reduction in the yields of expressed proteins. Alternatively, these heterologous hosts may not have been capable of correctly processing EAS, possibly because they lack chaperones capable of sequestering the protein until the disulfide bonds have formed. This hypothesis subsumes the existence of hydrophobin-specific chaperones.

These results are useful from the point of view that heterologous protein-expression is an immature technology that lacks any means to predict which combination of host and vector will produce a properly folded and active form of a protein like EAS. Instead, different host and vector combinations need to be screened until the protein is successfully expressed. Observe for example, Scholtmeijer's approach to heterologously expressing SC3 (Scholtmeijer, 2000). Experiments described in Chapter 4 have uncovered two hydrophobin protein-expression strategies that do not work. However, there are now additional techniques (including more sophisticated vectors and host strains) by which *P. pastoris* and *E. coli* could be made to express recombinant EAS. There are good reasons for continuing to develop a hydrophobin expression system with these species; they are easy to manipulate genetically, and are easily cultured (Makrides, 1996; Higgins and Cregg, 1998b). Alternately, fungal species could be used to express recombinant hydrophobins. This strategy has the advantage of building on the successes of other researchers who were able to express recombinant forms of SC3 and HFB1 in *S. commune* and *T. reesei* (Scholtmeijer *et al.,* 2002; Linder *et al.,* 2001; Nakari-Setälä *et al.,* 2002).

7.3 Conclusions: Disulfide Mapping.

The cysteine residues in EAS are linked as follows by disulfide bonds: Cys_9-Cys_{60}, Cys_{18}-Cys_{54}, Cys_{19}-Cys_{45}, and Cys_{61}-Cys_{80}. This is the first time that the pairing of the disulfide bonds in a class I hydrophobin has been deduced.

An identical arrangement of the disulfide bonds exists in the class II hydrophobin HFB2 (Hakanpää *et al.,* 2004). This implies that the arrangement of disulfide bonds is not the primary cause for the structural and physical differences that exist between the polymeric forms of class I and class II hydrophobins. It also suggests that the arrangement of disulfide bonds within the hydrophobin proteins is uniform, with the first cysteine in the sequence linked to the sixth, the second to the fifth, the third to the fourth and the seventh cysteine linked to the eighth.

Now that Wu and Watson's technique has been adapted for use with a hydrophobin (Wu and Watson, 1997), this assumption can be tested. It would be interesting to apply this method to deducing the disulfide linkages in cerato-ulmin to see if Yaguchi *et al.* (1993) were correct in their assignment. Cerato-ulmin is the only hydrophobin proven to have toxic properties, (albeit species-specific toxicity) and it is possible that this toxicity could be due in part to the unique disulfide pattern determined by Yaguchi *et al.* (1993).

Accurate disulfide maps will increase the resolution of computer-modelling experiments used to deduce the structure of class I hydrophobins. Indeed these results will allow us to generate a structure for EAS based on NMR spectra collected by Dr Joel Mackay and colleagues. Such models will allow the structure of EAS and HFB2 to be compared and the comparison will be insightful. Hakanpää *et al.* (2004) believe that the arrangement of the intramolecular disulfide bonds locks the molecule into a rigid, amphipathic globular structure both in solution and at the hydrophobic interface. The disulfide bonds also stabilise the β-hairpins that form the hydrophobic patch that gives HFB2 its amphipathic properties (Hakanpää *et al.*, 2004). Does the same arrangement of β-sheet structure exist in EAS? The structural model of EAS we are assembling will provide an answer to this question, and may reveal the origin of the differences in the physical properties of Class I and II hydrophobins.

The disulfide-mapping technique developed for EAS could be used to map the disulfide bridges in other hydrophobins including recombinant hydrophobins, cerato-ulmin, and the putative "multi-domain" hydrophobins CFTH1 and CPPH1 (Arntz and Tudzynski, 1997; de Vries *et al.,* 1999; Mey, G., Correia, T., Oeser, B., Garre, V. and Tudzynski, P., unpublished results).

However, the sensitivity of the assay should be improved because, at present, milligram amounts of hydrophobin must be expended in each experiment. The simplest way to address this problem is to decrease the amount of analyte lost through surface adsorption during each of the reaction and purification steps. As described in Chapter 5, combining the de-salting and RP-HPLC did increase the amount of sample that was recovered from these steps, and it is likely that even more might be recovered if siliconised plastic-ware was used for every manipulation (Kinter and Sherman, 2000a). Using a RP-HPLC column with a hydrophilic ligand should increase the efficiency of sample recovery still further, because the hydrophilic ligand should bind the hydrophobin less strongly (AP-Biotech, 1999; Henzel and Stults, 2001).

While the mass spectra of MALDI-TOF/MS is easier to interpret than is the spectra derived from LC-ESI/MS, the fact that the latter is compatible with in-line chromatographic purification suggests that it is better suited to separating the digested derivatised-hydrophobin isomers, which in turn gives more accurate mass-measurements (Carr and Annan, 1997; Kinter and Sherman, 2000a, 2000b, 2000c). Thus, the sensitivity of the assay could be improved if LC-ESI/MS were used instead of MALDI-TOF/MS analysis. If necessary, the latter could still be used to first to identify which isomers are present before LC-ESI/MS is used to obtain accurate mass measurements of each peptide in the digests.

7.4 Conclusions: Atomic Force Microscopic Studies on EAS.

The disulfide mass mapping experiments described in Chapter 5 and the structural research performed by Mackay *et al.* (2001) both relied on purified forms of EAS isoforms Ia and Ib. I examined the films formed by both of these isoforms and by EAS isoform II, and confirmed that each film was essentially identical. This shows that each isoform of EAS can independently form rodlets, suggesting that the conclusions drawn from the experiments described in Chapter 5 and by Mackay *et al.* (2001) should apply to other rodlet-forming hydrophobins, including every isoform of EAS.

The atomic force microscopy experiments I performed also lent weight to the argument that the rodlets formed by class I hydrophobin film consist of two or three smaller protofibrils:

(1) AFM measurements performed under fluid demonstrate that EAS rodlets themselves are twice as wide as they are tall, which is consistent with the TEM data (Beever and Dempsey, 1978, 1979; Hallett and Beever, 1981) – implying that they are formed from at least two protofibrils of equal-length, lying adjacent to one another.

(2) The simultaneous presence of rodlets and smaller (shorter) fibril-like and spherical molecules in films adsorbed to both mica and HOPG are reminiscent of nucleating and elongating protofibrils detected during time-lapse AFM experiments on amyloid proteins (Goldsbury *et al.,* 1999; Harper *et al.,* 1999; Stolz *et al.*,. 2000; Green *et al.*, 2004). This supports the hypothesis that hydrophobin self-assembly is similar to amyloid fibril formation (de Vocht, 2001).

I conducted a survey that aimed to characterise the types of films that EAS forms when it self-assembles on HOPG. This investigation showed that the morphology of EAS polymers within these films varied according to the concentration of EAS used to prepare each specimen.

Many of the structures had been detected previously by Gunning *et al.* (1998) In keeping with current data that shows that class I hydrophobins are functional amyloids, my experiments implied that many of the polymeric molecules seen were, in fact, EAS protofibrils in the process of elongating.

Finally, and significantly, I developed a procedure that will permit microscopic examination of the hydrophilic side of EAS rodlets.

7.5 Future Work.

Thus far, only low-resolution techniques have been used to examine the structure of hydrophobin rodlets. The fruits of these studies include the discovery that class I hydrophobin polymers are functional amyloids with a substructure similar to the amyloid fibril (de Vocht, 2001; Butko *et al.*, 2001; Mackay *et al.*, 2001). It seems that hydrophobin rodlets are composed of protofibrils, which in turn are composed of monomers with a high level of β-sheet secondary structure (de Vocht *et al.*, 1998, 2002; Butko *et al.*, 2001, Mackay *et al.*, 2001). A model describing the process of self-assembly – which has itself been found to be nucleation dependent – has been proposed (de Vocht, 2001; de Vocht *et al.*, 1998, 2002; Wang *et al.*, 2002). The crystal structure of HFB2 provides a point of reference that should improve the interpretation of the low-resolution data and structure-prediction experiments (Hakanpää *et al.*, 2004).

Other techniques might prove useful:

(1). De Vocht (2001) mentioned the results of a series of unpublished experiments which showed that adding detergents (SDS or Tween-20) or amphipols to SC3 solutions - or even chemically modifying SC3 to increase its surface charge - could prevent SC3 from aggregating in solution, even when it was present in high concentrations. This technique should aid NMR spectroscopic studies that have previously been hampered by hydrophobins' propensity to aggregate in solution: Mackay *et al.* (2001) were unable to use EAS isoform II in their experiments for this reason. Fortunately, EAS isoform Ib did not aggregate and Mackay *et al.* were able to complete their NMR examination of the monomeric form of EAS.

(2). Hydrophobin films have yet to be examined by cryo-electron microscopy. In this technique, low-dose electron microscopy is carried out on cryogenically frozen biomolecules in order to gain information about the molecule in its hydrated state (Mankin and Serpell, 2002). The biomolecule does not need to be crystallised or stained prior to imaging, and the technique does less damage to the specimen than does conventional electron microscopy (Unger, 2001; Frank, 2002; Mankin and Serpell, 2002). Structural information is obtained either directly from the micrograph or by three-dimensional reconstructions based on the data obtained during the experiment (Frank, 2002; Mankin and Serpell, 2002).

The spatial resolution of the technique is currently limited to between 4 and 10 Å but, unlike conventional electron microscopy techniques, the molecule is examined in its natural state (more or less) which lessens the possibility that the molecule may have been distorted during preparation (Unger, 2001; Frank, 2002). The technique has been used in successful examinations of amyloid fibrils (*e.g.* Jimémez *et al.*, 1999; Serpell and Smith, 2000) and so should be appropriate for examining hydrophobin rodlets.

(3). Scanning-transmission-electron-microscopy (STEM) has been used to obtain mass-distribution-maps of single biomolecules (see reviews by Müller and Engel, 1998a, 2001). From such a map, the mass-per-unit-length of a biomolecule can be calculated. If this technique were applied to hydrophobin rodlets it should reveal how many of the hydrophobin monomer-units are packed into a unit-length of an individual rodlet and possibly give some inkling as to how they are arranged.

The various polymeric forms detected in the experiments described in this chapter could be examined by STEM and compared with the transition states proposed by de Vocht *et al.* (1998, 2002).

One of the prerequisites of mass-distribution-mapping is that separate individual biomolecules need to be examined, so the sample preparation techniques presented here may well require further modifications before the structures detected using AF-microscopy could be examined by STEM (personal communication with Dr Shirley Müller, M. E. Müller Institute for Microscopy, University of Basel, Basel, Switzerland).

(4). Only one hydrophobic surface was examined in this study. Hydrophobin films have been examined on a variety of hydrophobic surfaces including: HOPG

(used here), colloidal Teflon® particles, Formvar coated grids, and siliconised glass slides. Each surface has a different surface chemistry that might individually affect the manner in which hydrophobins self-assemble on them (Wösten *et al.*, 1995; de Vocht *et al.*, 2000). While macroscopic measurements certainly suggest that there are no differences between the hydrophobin films formed on each substrate, microscopic examination should ensue to ensure that the structure of the hydrophobin-films components *is* actually the same in each case.

References.

Adamson, A. W. (**1990**) "Chapter XIII - Wetting, Flotation, and Detergency." **In:** *Physical Chemistry of Surfaces. 5th Edition. (pp.493-524).* John Wiley & Sons Inc.: New York, Chichester, Brisbane, Toronto, Singapore,

Aitken, A. (**1994**). "Chapter 38: Analysis of Cysteine Residues and Disulfide Bonds." **In:** *Basic Protein and Peptide Protocols (pp. 351-360).* J. M. Walker (Ed.), Humana Press: Totowa, New Jersey.

Altschul, S. F., Gish, W., Miller, W., Myers, E. W., and Lipman, D. J. (**1990**). "Basic local alignment search tool." *Journal of Molecular Biology,* **215**, 403-410.

Altschul, S. F., Madden, T. L., Schaffer, A. A., Zhang, J., Zhang, Z., Miller, W., and Lipman, D. J. (**1997**). "Gapped BLAST and PSI-BLAST: a new generation of protein database search programs." *Nucleic Acids Research*, **25**, 3389-3402.

AP-Biotech. (**1999**). "Reversed Phase Chromatography - Principles and Methods." Amersham Pharmacia Biotech AB: Uppsala, Sweden.

Ando, A., Harada, A., Miura, K. and Tamai, Y. (**2001**) "A gene encoding a hydrophobin, fvh1, is specifically expressed after the induction of fruiting in the edible mushroom *Flammulina velutipes.*" *Current Genetics*, **39** (3), 190-197.

Appelbaum, E. R. and Shatzman, A. R. (**1999**). "Prokaryotic *in vivo* expression systems." **In:** *Protein Expression - A Practical Approach (pp. 169-200).* S. J. Higgins and B. D. Hames (Ed.), Oxford University Press: Oxford, NY. USA.

Arntz, C., and Tudzynski, P. (**1997**) "Identification of genes induced in alkaloid-producing cultures of *Claviceps* sp." *Current Genetics*, **31** (4), 357-360.

Aronson, A. I. and Fitz-James, P. (**1976**). "Structure and morphogenesis of the bacterial spore coat." *Bacteriological Reviews*, **40**, 360-402.

Arpaia, G., Loros, J. J., Dunlap, J. C., Morelli, G., and Macino, G. (**1993**). The interplay of light and the circadian clock. Independent dual regulation of clock-controlled gene *ccg-2* (*eas*). *Plant Physiology*, **102**, 1299-1305.

Asgeirsdóttir, S. A. (**1994**) "PhD Thesis: Proteins involved in the emergent growth of *Schizophyllum commune.*" Wiskunde en Natuurwetenschappen (Mathematics and Natural Sciences), Rijkuniversiteit Groningen (University of Groningen), Groningen, Netherlands.

Asgeirsdóttir, S. A., Halsall, J. R., and Casselton, L. A. (**1997**) "Expression of two closely linked hydrophobin genes of *Coprinus cinereus* is monokaryon-specific and down-regulated by the oid-1 mutation." *Fungal Genetics and Biology*, **22,** 54-63.

Asgeirsdóttir, S. A., Scholtmeijer., K. and Wessels, J. G. (**1998**). "Identification of three differentially expressed hydrophobins in *Pleurotus ostreatus* (oyster mushroom)." *Microbiology*, **144**, (Pt 11), 2961-2969.

Asgeirsdóttir, S. A., de Vries, O. M., and Wessels, J. G. H. (**1999**). "A Sandwiched-Culture Technique for Evaluation of Heterologous Protein Production in a Filamentous Fungus." *Applied and Environmental Microbiology*, **65,** (5), 2250–2252.

Askolin, S., Nakari-Setälä, T., and Tenkanen, M. (**2001**). "Overproduction, purification, and characterization of the *Trichoderma reesei* hydrophobin HFBI." *Applied Microbiology and Biotechnology*, **57**, 124-30.

Avey, H. P., Boles, M. O., Carlisle, C. H., Evans, S. A., Morris, S. J., Palmer, R. A., Woolhouse, B. A., and Shall, S. (**1967**). "Structure of Ribonuclease." *Nature*, **213**, 557-562.

Bailey, M. J., Askolin, S., Hörhammer, N., Tenkanen, M., Linder, M., Penttilä, M., and Nakari-Setälä, T. (**2002**). "Process technological effects of deletion and amplification of hydrophobins I and II in transformants of *Trichoderma reesei.*" *Applied Microbiology and Biotechnology*, **58**, 721-727.

Bailey, S. W. (**1984**). "*Micas.*" Mineralogical Society of America; Washington, D.C, USA.

Baneyx, F. (**1999**). "Recombinant protein expression in *Escherichia coli.*" *Current Opinion in Biotechnology*, **10**, 411-421.

Barbirz, S., Happersberger, H. P., Przybylski, M., and Glocker, M. O. (**1999**). "Selective cyanylation of cysteinyl residues as an approach for the mass-spectrometric determination of protein structures." *European Journal of Mass Spectrometry*, **5**, 123-131.

Beatty, N. P., Smith, M. L., and Glass, N. L. (**1994**). "Molecular characterization of mating-type loci in selected homothallic species of *Neurospora, Gelasinospora,* and *Anixella.*" *Mycological Research*, **98**, 1309-1316.

Beavis, R. C., and Chait, B. T. (**1990**). "High-Accuracy Molecular Mass Determination of Proteins Using Matrix-Assisted Laser Desorption Mass Spectrometry." *Analytical Chemistry*, **62**, 1836-1840.

Beckerman, J. L., and Ebbole, D. J. (**1996**). "MPG1, a gene encoding a fungal hydrophobin of *Magnaporthe grisea,* is involved in surface recognition." *Molecular Plant-Microbe Interactions*, **9**, 450-6.

Beever, R. E., and Dempsey, G. P. (**1978**) "Function of rodlets on the surface of fungal spores." *Nature*, **272** (5654), 608-610.

Beever, R. E., Redgwell, R. J., and Dempsey, G. P. (**1979**). "Purification and chemical characterization of the rodlet layer of *Neurospora crassa* conidia." *Journal of Bacteriology,* **140**, 1063-1070.

Bell-Pedersen, D. (**2000**) "Understanding circadian rhythmicity in *Neurospora crassa:* from behaviour to genes and back again" *Fungal Genetics and Biology*, **29** (1), 1-18.

Bell-Pedersen, D., Dunlap, J. C. and Loros, J. J. (**1992**) "The *Neurospora* circadian clock-controlled gene, *ccg-2*, is allelic to *eas* and encodes a fungal hydrophobin required for formation of the conidial rodlet layer" *Genes and Development*, **6** (12A), 2382-2394.

Bell-Pedersen, D., Dunlap, J. C., and Loros, J. J. (**1996**) "Distinct *cis*-acting elements mediate clock, light, and developmental regulation of the *Neurospora crassa eas (ccg-2)* gene." *Molecular and Cellular Biology*, **16** (2), 513-521.

Bell-Pedersen, D., Lewis, Z. A., Loros, J. J., and Dunlap, J. C. (**2001**) "The *Neurospora* circadian clock regulates a transcription factor that controls rhythmic expression of the output *eas (ccg-2)* gene." *Molecular Microbiology*, **41** (4), 897-909.

Benson, D. A., Karsch-Mizachi, I., Lipman, D. J., Ostell, J., Rapp, B. A. and Wheeler, D. L. (**2002**). "GenBank." *Nucleic Acids Research*, **30**, 17-20.

Bidochka, M. J., St-Leger, R. J., Joshi, L., and Roberts, D. W. (**1995**). "The rodlet layer from aerial and submerged conidia of the entomopathogenic fungus *Beauveria bassiana* contains hydrophobin." *Mycological Research*, **99**, 403-406.

Bidochka, M. J., De Koning, J., and St Leger, R. J. (**2001**) "Analysis of a genomic clone of hydrophobin *(ssgA)* from the entomopathogenic fungus *Metarhizium anisopliae*." *Mycological Research*, **105** (3), 360-364.

Bieszke, J. A., Spudich, E. N., Scott, K. L., Borkovich, K. A., and Spudich, J. L. (1999). "A eukaryotic protein, NOP-1, binds retinal to form an archaeal rhodopsin-like photochemically reactive pigment." *Biochemistry*, **38**, 14138-14145.

Bohlmann, R. (1996) "*Dissertation: Isolierung und Charakterisierung von filamentspezifisch exprimierten Genen aus Ustilago maydis. (Isolation and experimental characterisation of filament-specific genes from Ustilago maydis).*" Institut für Genetik und Mikrobiologie (Institute of Genetics and Microbiology), Universitat Munchen (University of Munich), Munich, Germany.

Bolyard, M. G., and Sticklen, M. B. (1992). "Expression of a modified Dutch elm disease toxin in *Escherichia coli." Molecular Plant-Microbe Interactions*, **5**, 520-524.

Bowden, C. G., Hintz, W. E., Jeng, R., Hubbes, M., and Horgen, P. A. (1994) "Isolation and characterization of the cerato-ulmin toxin gene of the Dutch elm disease pathogen, *Ophiostoma ulmi.*" *Current Genetics*, **25** (4), 323-329.

Bowden, C. G., Smalley, E., Guries, R. P., Hubbes, M., Temple, B., and Horgen, P. A. (1996) "Lack of association between cerato-ulmin production and virulence in *Ophiostoma novo-ulmi.*" *Molecular Plant-Microbe Interactions*, **9** (7), 556-564.

Braithwaite, K. S., Irwin, J. A. G., and Manners J. M. (1990). "Restriction fragment length polymorphisms in *Colletotrichum gloeosporioides* infecting *Stylosanthes* spp. in Australia." *Mycological Research*, **94**, 1129-1137.

Brasier, C. M., Kirk, S. A., and Tegli, S. (1995). "Naturally occurring non cerato-ulmin producing mutants of *Ophiostoma novo-ulmi* are pathogenic but lack aerial mycelium." *Mycological Research*, **99**, 436-440.

Brown, T., and Mackey, K. (2002). "Unit 4.9: Analysis of RNA by Northern and Slot Blot Hybridisation." **In:** *Current Protocols in Molecular Biology*. F. M. Ausube, B. Roger, Kingston R. E.; Moore, D. D. Moore, J. G. Seidman, and K. Struhl (Ed.), John Wiley & Sons, Inc.; Hoboken, New Jersey.

Bruns, T. D., White, T. J., and Taylor, J. W. (1991). "Fungal molecular systematics." *Annual Review of Ecology and Systematics*, **22**:525-564.

Bruns, T. D., Vilgalys, R., Barns, S. M., Gonzalez, D., Hibbett, D. S. , Lane, D. J., Simon, L., Stickel, S., Szaro, T. M., Weisburg, W. G., and Sogin, M. L. (1993). "Evolutionary relationships within the fungi: analysis of nuclear small subunit rRNA sequences." *Molecular Phylogenetics and Evolution*, **1**:231-241.

Burns, J. A., Butler, J. C., Moran, J., and Whitesides, G. M. (1991). "Selective Reduction of Disulfides by Tris(2-carboxyethyl) phosphine." *Journal of Organic Chemistry*, **56**, 2648-2650.

Busscher, H. J., Van Pelt, A. W. J., De Boer, P., De Jong, H. P., and Arends, J. (1984). "The effect of surface roughening of polymers on measured contact angles of liquids." *Colloids and Surfaces*, **9**, 319-331.

Butko, P., Buford, J. P., Goodwin, J. S., Stroud, P. A., McCormick, C. L., and Cannon, G. C. (2001). "Spectroscopic evidence for amyloid-like interfacial self-assembly of hydrophobin Sc3." *Biochemical and biophysical research communications*, **280**, 212-215.

Carpenter, C. E., Müller, R. J., Kazmierczak, P., Zhang, L., Villialon, D. K., and van Alfen, N. K. (1992) "Effect of a Virus on Accumulation of a Tissue-Specific Cell-Surface Protein of the Fungus *Cryphonectria (Endothia) parasitica*" *Molecular Plant-Microbe Interactions*, **4** (6), 55-61.

Carr, S. A., and Annan, R. S. (**1997**). "Unit 10.21: Overview of Peptide and Protein Analysis by Mass Spectrometry." **In:** *Current Protocols in Molecular Biology (pp. 10.21.1-10.21.27).* F. M. Ausubel, R. Brent, R. E. Kingston, D. D. Moore, J. G. Seidman, J. G. Smith, and K. Struhl (Ed.), John Wiley and Sons Inc.: Hoboken, New Jersey.

Chernoff, D. A. (**1996**). "Phase Imaging: What, How and Why." *Nanovations: Digital Instruments*, **3**, 6-9.

Chernoff, Y. O., Lindquist, S. L., Ono, B., Inge-Vechtomov, S. G., and Liebman, S. W. (**1995**). "Role of the chaperone protein Hsp104 in propagation of the yeast prion-like factor [psi+]" *Science*, **268**, 880-884.

Cheung, C. L., Hafner, J. H., and Lieber, C. M. (**2000**). "Carbon nanotube atomic force microscopy tips: Direct growth by chemical vapor deposition and application to high-resolution imaging." *Proceedings of the National Academy of Sciences of the United States of America*, **97**, (8), 3809-3813.

Church, G. M., and Gilbert, W. (**1984**). "Genomic Sequencing." *Proceedings of the National Academy of Sciences of the United States of America,* **81**, 1991-1995.

Claessen, D., Wösten, H., van Keulen, G., Faber, O. G., Alves, A. M., Meijer, W. G., and Dijkhuizen, L. (**2002**). "Two novel homologous proteins of *Streptomyces coelicolor* and *Streptomyces lividans* are involved in the formation of the rodlet layer and mediate attachment to a hydrophobic surface." *Molecular Microbiology*, **44**, 1483-1492.

Claessen, D., Rink, R., de Jong, W., Siebring, J., de Vreugd, P., Boersma, F. G. H., Dijkhuizen, L., and Wösten, H. A. B. (**2003**). "A novel class of secreted hydrophobic proteins is involved in aerial hyphae formation in *Streptomyces coelicolor* by forming amyloid-like fibrils." *Genes and Development*, **17**, 1714-1726.

Clare, J., Sreekrishna, K., and Romanos, M. (**1998**). "Chapter 13 - Expression of the Tetanus Toxin Fragment C." **In:** *Pichia Protocols (pp. 193-208).* D. R. Higgins and J. M. Cregg (Ed.), Humana Press: Totowa, New Jersey.

Clemmer, C. R., and Beebe, T. P. J. (**1991**). "Graphite: A Mimic for DNA and Other Biomolecules in Scanning Tunnelling Microscope Studies." *Science*, **251**, 640-642.

Collén, A., Penttilä, M., Stålbrand H, Tjerneld F., and Veide, A. (**2001**). "Extraction of endoglucanase I (Ce17B) fusion proteins from *Trichoderma reesei* culture filtrate in a poly(ethylene glycol)-phosphate aqueous two-phase system." *Journal of Chromatography A*, **943**, 55-62.

Collén, A., Persson, J., Linder, M., Nakari-Setälä, T., Penttilä, M., Tjerneld, F., and Sivars U. (**2002**). "A novel two-step extraction method with detergent/polymer systems for primary recovery of the fusion protein endoglucanase I-hydrophobin I." *Biochimica et Biophysica Acta*, **1569**, 139-150.

Colyer, J. (**1999**). "Monitoring Protein Expression." **In:** *Protein Expression - A Practical Approach (pp. 225-265).* S. J. Higgins and B. D. Hames (Ed.), Oxford University Press: Oxford, NY. USA.

Corpet, F. (**1988**). "Multiple sequence alignment with hierarchical clustering." *Nucleic Acids Research*, **16**, 10881-10890.

Corran, P. H. (**1998**). "Reverse-phase chromatography of proteins." **In:** *HPLC of Macromolecules - A Practical Approach (pp. 93-140).* R. W. A. Oliver (Ed.), Oxford University Press Inc.: Oxford, New York.

Correa, A., and Bell-Pedersen, D. (**2002**). "Distinct signalling pathways from the circadian clock participate in regulation of rhythmic conidiospore development in *Neurospora crassa." Eukaryotic Cell*, **1**, 273-280.

Cregg, J. M. and Russell, D. W. (**1998**). Transformation. **In:** *Pichia Protocols (pp. 27-39).* D. R. Higgins and J. M. Cregg (Ed.), Humana Press: Totowa, New Jersey.

Creighton, T. E. (**1993**). "*Proteins: Structures and Molecular Properties. 2nd Edition."* W. H. Freeman and Company, New York.

Davis, R. H. (**2000**). "*Neurospora Contributions of a Model Organism*." Oxford University Press Inc. New York.

Dayhoff, M. O., Schwartz, R. M., and Orcutt, B. C. (**1979**). "*Atlas of Protein and Sequence Structure*." National Biomedical Research Foundation, Washington D.C.; USA.

de Groot, P. W., Schaap, P. J., Sonnenberg, A. S., Visser, J., and Van Griensven, L. J. (**1996**) "The *Agaricus bisporus* hypA gene encodes a hydrophobin and specifically accumulates in peel tissue of mushroom caps during fruit body development." *Journal of Molecular Biology*, **257** (5), 1008-1018.

de Groot, P. W., Roeven, R. T., van Griensven, L. J., Visser, J., and Schaap, P. J. (**1999**) "Different temporal and spatial expression of two hydrophobin-encoding genes of the edible mushroom *Agaricus bisporus*." *Microbiology*, **145 (Pt 5),** 1105-1113.

de Vocht, M. L. (**2001**) "PhD Thesis: Structural changes that accompany the self-assembly of hydrophobins." Wiskunde en Natuurwetenschappen (Mathematics and Natural Sciences), Rijkuniversiteit Groningen (University of Groningen), Groningen, The Netherlands.

de Vocht, M. L., Scholtmeijer, K., van der Vegte, E. W., de Vries, O. M., Sonveaux, N., Wösten, H. A., Ruysschaert, J. M., Hadziloannou, G., Wessels, J. G., and Robillard, G. T. (**1998**) "Structural characterization of the hydrophobin SC3, as a monomer and after self-assembly at hydrophobic/hydrophilic interfaces." *Biophysical Journal*, **74** (4), 2059-2068.

de Vocht, M. L., Reviakine, I., Wösten, H. A., Brisson, A., Wessels, J. G., and Robillard, G. T. (**2000**). "Structural and functional role of the disulfide bridges in the hydrophobin SC3." *Journal of Biological Chemistry*, **275**, 28428-28432.

de Vocht, M. L., Reviakine, I., Ulrich, W. P., Bergsma-Schutter, W., Wösten, H. A., Vogel, H., Brisson, A., Wessels, J. G., and Robillard, G. T. (**2002**). "Self-assembly of the hydrophobin SC3 proceeds via two structural intermediates." *Protein Science*, **11**, 1199-1205.

de Vries, O. M. H., Fekkes, M. P., Wösten, H. A. B., and Wessels, J. G. H. (**1993**) "Insoluble hydrophobin complexes in the walls of *Schizophyllum commune* and other filamentous fungi." *Archives of Microbiology*, **159,** 330-335.

de Vries, O. M., Moore, S., Arntz, C., Wessels, J. G. and Tudzynski, P. (**1999**) "Identification and characterization of a tri-partite hydrophobin from *Claviceps fusiformis.* A novel type of class II hydrophobin." *European Journal of Biochemistry*, **262** (2), 377-385.

Del Sorbo, G. F., Scala, F., Parrella, G., Lorito, M., Comparini, C., Ruocco, M., and Scala, A. (**2000**) "Functional expression of the gene cu, encoding the phytotoxic hydrophobin cerato-ulmin, enables *Ophiostoma quercus,* a non pathogen on elm, to cause symptoms of Dutch elm disease" *Molecular Plant-Microbe Interactions*, **13** (1), 43-53.

Dempsey, G. P., and Beever, R. E. (**1979**). "Electron microscopy of the rodlet layer of *Neurospora crassa* conidia." *Journal of Bacteriology*, **140**, 1050-1062.

Dettman, J. R., Harbinski, F. M., and Taylor, J. W. (**2001**). "Ascospore morphology is a poor predictor of the phylogenetic relationships of *Neurospora* and *Gelasinospora." Fungal Genetics and Biology*, **31**, 49-61.

Difco® Laboratories (**1984**). "Difco® Manual - Dehydrated Culture Media and Reagents for Microbiology. 10th Edition." Difco Laboratories®: Detroit, USA.

Digital Instruments. (**1997**). "NanoScope® Command Reference Manual, Version 4.31, Rev. B." Digital Instruments Inc. Santa Barbara, CA, USA.

Dobson, C. M. (**1999**). "Protein misfolding, evolution and disease." *Trends in Biochemical Science*, **24**, 329-332.

Dobson, C. M. (**2001**). "The structural basis of protein folding and its links with human disease." *Philosophical transactions of the Royal Society of London. Series B, Biological sciences*, **356**, 133-145.

Dodge, B. O. (**1927**). "Nuclear phenomena associated with heterothallism and homothallism in the ascomycete *Neurospora." Journal of Agricultural Research*, **35**, 289-305.

Dorsey, J. G., and Cooper, W. T. (**1994**). "Retention Mechanisms of Bonded-Phase Liquid Chromatography." *Analytical Chemistry*, **66**, 857A-867A.

Dufrêne, Y. F. (**2000**). "Direct Characterization of the Physicochemical Properties of Fungal Spores Using Functionalized AFM Probes." *Biophysical Journal* **78**, 3286-3291.

Dufrêne, Y. F., Boonaert, C. J. P., Gerin, P. A., Asther, M., and Rouxhet, P. G. (**1999**). "Direct Probing of the Surface Ultrastructure and Molecular Interactions of Dormant and Germinating Spores of *Phanerochaete chrysosporium*." *Journal of Bacteriology*, **181**, (17) 5350-5354.

Duplessis, S., Sorin, C., Voiblet, C., Palin, B., Martin, F., and Tagu, D. (**2001**) "Cloning and expression analysis of a new hydrophobin cDNA from the ectomycorrhizal basidiomycete *Pisolithus*." *Current Genetics*, **39** (5-6), 335-339.

Ebbole, D., and Sachs, M. S. (**1990**). "A rapid and simple method for isolation of *Neurospora crassa* homokaryons using microconidia." *Fungal Genetics Newsletter*, **37**.

Ebbole, D. J. (**1997**) "Hydrophobins and fungal infection of plants and animals." *Trends in Microbiology*, **5** (10), 405-408.

Eberle, J., and Russo, V. E. (**1992**) "*Neurospora crassa* blue-light-inducible gene *bli-7* encodes a short hydrophobic protein." *DNA sequence: the journal of DNA sequencing and mapping.*, **3** (3), 131-141.

Edelmann, S. E., and Staben, C. (**1994**). "A Statistical Analysis of Sequence Features within Genes from *Neurospora crassa." Experimental Mycology*, **18**, 70-81.

Engebrecht, J., Brent, R., and Kaderbhai, M. A. (**1992**). *Unit 1.6: Minipreps of Plasmid DNA.* **In:** *Current Protocols in Molecular Biology (pp. 1.6.1-1.6.10).* F. M. Ausubel, R., Brent, R. E., Kingston, D. D., Moore, J. G., Seidman, J. G., Smith, and K. Struhl (Ed.), John Wiley and Sons Inc.: Hoboken, New Jersey.

Frederick, L., Uecker, F. A., and Benjamin, C. R. (**1969**). "A new species of *Neurospora* from the soil of West Pakistan." *Mycologia*, **61**, 1077-1084.

Frank, J. (**2002**). "Single-Particle Imaging of Macromolecules by Cryo-Electron Microscopy." *Annual Review of Biophysics and Biomolecular Structure*, **31**, 303-319.

Gaines, G., and Tabor, D. (**1956**). "Surface adhesion and elastic properties of mica." *Nature*, **178**, 1304-1305.

Galagan, J. E., Calvo, S. E., Borkovich, K. A., Selker, E. U., Read, N. D., Jaffe, D., FitzHugh, W., Ma, L. J., Smirnov, S., Purcell, S., Rehman, B., Elkins, T., Engels R., Wang, S., Nielsen, C. B., Butler, J., Endrizzi, M., Qui, D., Ianakiev, P., Bell-Pedersen, D., Nelson, M. A., Werner-Washburne, M., Selitrennikoff, C. P., Kinsey, J. A., Braun, E. L., Zelter, A., Schulte, U., Kothe, G. O., Jedd, G., Mewes, W., Staben, C., Marcotte, E., Greenberg, D., Roy, A., Foley, K., Naylor, J., Stange-Thomann, N., Barrett, R., Gnerre, S., Kamal, M., Kamvysselis, M., Mauceli, E., Bielke, C., Rudd S., Frishman, D., Krystofova, S., Rasmussen, C., Metzenberg, R. L., Perkins, D. D., Kroken, S., Cogoni, C., Macino G., Catcheside D., Li W., Pratt R. J., Osmani S. A., DeSouza C. P., Glass, L., Orbach, M. J., Berglund, J. A., Voelker, R., Yarden, O., Plamann, M., Seiler, S., Dunlap, J., Radford, A., Aramayo, R., Natvig, D. O., Alex, L. A, Mannhaupt, G., Ebbole, D. J., Freitag, M., Paulsen, I., Sachs, M. S., Lander, E. S., Nusbaum, C., and Birren, B. (**2003**). "The genome sequence of the filamentous fungus *Neurospora crassa." Nature*, **422**, 859-868.

Geiser, D. M., Frisvad, J. C., and Taylor, J. W. (**1998**) "Evolutionary relationships in *Aspergillus* section *Fumigati* inferred from partial ß-tubulin and hydrophobin DNA sequences." *Mycologia*, **90** (5), 831-845.

Gerin, P. A., Asther, M., Sleytr, U. B., and Rouxhet, P. G. (**1994**). "Detection of rodlets in the outer wall region of conidiospores of *Phanerochaete chrysosporium." Canadian Journal of Microbiology* **40**, 412-416.

Getz, E. B., Xiao, M., Chakrabarty, T., Cooke, R., and Selvin, P. R. (**1999**). "A Comparison between the Sulfhydryl Reductants Tris(2-carboxyethyl) phosphine and Dithiothreitol for Use in Protein Biochemistry." *Analytical Biochemistry*, **273**, 73-80.

Girardin, H., Paris, S., Rault, J., Bellon-Fontaine, M. N., and Latge, J. P. (**1999**) "The role of the rodlet structure on the physicochemical properties of *Aspergillus* conidia." *Letters in Applied Microbiology*, **29** (6), 364-369.

Glass, N. L., Metzenberg, R. L., and Raju, N. B. (**1990**). "Homothallic Sordariaceae from nature: the absence of strains containing only *a* mating-type sequence." *Experimental Mycology*, **14**, 247-289.

Gleeson, M. A. G., White, C. E., Meininger, D. P., and Komives, E. A. (**1998**). "Generation of Protease-Deficient Strains and Their Use in Heterologous Protein Expression." **In:** *Pichia Protocols (pp. 81-94).* D. R. Higgins and J. M. Cregg (Ed.), Humana Press: Totowa, New Jersey.

Goldsbury, C., Joerg Kistler, J., Ueli Aebi, U., Arvinte, T., and Cooper, G. J. S. (**1999**). "Watching amyloid fibrils grow by time-lapse atomic force microscopy." *Journal of Molecular Biology,* **285**, 33-39.

Gorman, P. M. and Chakrabartty, A. (**2001**). "Alzheimer ß-amyloid peptides: structures of amyloid fibrils and alternate aggregation products." *Biopolymers*, **60**, 381-394.

Green, J. D., Goldsbury, C., Kistler, J., Cooper, G. S., Aebi, U. (**2004**). "Human amylin oligomer growth and fibril elongation define two distinct phases in amyloid formation." *Journal of Biological Chemistry*, **In Press.**

Gunning, A. P., De Groot, P. W. J., Visser, J., and Morris, V. J. (**1998**). "Atomic Force Microscopy of a Hydrophobin Protein from the Edible Mushroom *Agaricus bisporus*." *Journal of Colloid Interface Science*, **201**, 118-126.

Guttman, A., Nelson, R. J., and Cooke, N. (**1992**). "Prediction of migration behaviour of oligonucleotides in capillary gel electrophoresis." *Journal of Chromatography*, **593**, (1-2) 297-303.

Hagmann, M. L., Guess, U., Fischer, S., and Kresse, G. B. (**1995**). "Peptidyl-Asp metalloendopeptidase." *Methods in Enzymology*, **248**, 782-787.

Hakanpää, J., Paananen, A., Askolin, S., Nakari-Setälä, T., Parkkinen, T., Penttilä, M., Linder, M. B. and Rouvinen, J. (**2004**). "Atomic resolution structure of the HFBII hydrophobin: a self-assembling amphiphile." *Journal of Biological Chemistry*, **279**, 534-539.

Hallett, I. C., and Beever, R. E. (**1981**). "Rodlets of the Surface of *Neurospora* Conidia." *Transcripts of the British Mycological Society*, **77**, 662-666.

Hamada, W., and Spanu, P. D., (**1998**) "Co-suppression of the hydrophobin gene HCf-1 is correlated with antisense RNA biosynthesis in *Cladosporium fulvum.*" *Molecular and General Genetics*, **259** (6), 630-638.

Han, J. C., and Han, G. Y. (**1994**). "A Procedure for Quantitative Determination of Tris(2-carboxyethyl) phosphine, an Odourless Reducing Agent More Stable and Effective That Dithiothreitol." *Analytical Biochemistry*, **220**, 5-10.

Hannig, G. and Makrides, S. C. (**1998**). "Strategies for optimizing heterologous protein expression in *Escherichia coli*." *Trends in Biotechnology*, **16**, 54-59.

Harper, J. D., Wong, S. S., Lieber, C. M., and Lansbury, P. T. J. (**1999**). "Assembly of Aß amyloid protofibrils: an *in vitro* model for a possible early event in Alzheimer's disease." *Biochemistry*, **38**, 8972-8980.

Harrison, R. G. (**2000**). "Expression of soluble heterologous proteins via fusion with NusA protein." *in**Nova**tions - The Newsletter of Novagen Inc.*, **11**, 4-7.

Heinz, W. F., and Hoh, J. H. (**1999**). "Relative Surface Charge Density Mapping with the Atomic Force Microscope." *in**Nova**tions*, **11**, 4-7.

Henzel, W. J., and Stults, J. T. (**2001**). "Unit 10.14: Reversed-Phase Isolation of Peptides." **In:** *Current Protocols in Molecular Biology (pp. 10.14.1-10.14.17).* F. M. Ausubel, R. Brent, R. E. Kingston, D. D. Moore, J. G. Seidman, J. G. Smith, and K. Struhl (Ed.), John Wiley & Sons Inc.: Hoboken, New Jersey.

Higgins, D. R., and Cregg, J. M. (**1998a**). "Introduction to *Pichia pastoris*." **In:** *Pichia Protocols. (pp. 1-16).* D. R. Higgins and J. M. Cregg (Ed.) Humana Press Inc.: Totowa NJ.

Higgins, D. R., and Cregg, J. M. (Ed.) (**1998b**). "*Pichia Protocols - Methods in Molecular Biology Volume 103.*" Humana Press Totowa, New Jersey.

Hirs, C. H. W., Moore, S., and Stein, W. H. (**1960**). "The Sequence of the Amino Acid Residues in Performic Acid-oxidized Ribonuclease." *Journal of Biological Chemistry*, **235**, 633-647.

Hoffman, C. S., and Winston, F. (**1987**). "A ten-minute DNA preparation from yeast efficiently releases autonomous plasmids for transformation of *Escherichia coli.*" *Gene*, **57**, 267-272.

Holt, S. C., and Leadbetter, E. R. (**1969**). "Comparative Ultrastructure of Selected Aerobic Spore-forming Bacteria: a Freeze-Etching Study." *Bacteriological Reviews*, **33**, 346-378.

Honneger, R. (**1991**). "Functional aspects of the lichen symbiosis." *Annual Review of Plant Physiology and Plant Molecular Biology*, **42**, 553-578.

Humphris, A. D. L., and Miles, M. J. (**2002**). "Chapter 16: Developments in Dynamic Force Microscopy and Spectroscopy." **In:** *Atomic Force Microscopy in Cell Biology (pp. 337-355).* B. P. Jena and J. K. H. Hörber (Ed.), Academic Press: London.

Hutter, J. L., and Bechhoefer, J. (**1993**). "Calibration of atomic-force microscope tips." *Review of Scientific Instruments*, **64**, 1868-1873.

Iconomidou, V. A., Vriend, G., and Hamodrakas, S. J. (**2000**). "Amyloids protect the silk moth oocyte and embryo." *FEBS Letters*, **479**, 141-145.

Invitrogen™. (**2000**). "*NuPAGE® Novex high performance pre-cast gels: Bis-Tris Gel Instruction Booklet.*" Invitrogen™ Corporation, Carlsbad, CA.

Invitrogen™. (**2002**). "*Instruction Manual: Multi-copy Pichia Expression Kit - Version F.*" Invitrogen Corporation, Carlsbad, CA.

Janssen, M. L., van Leeuwen, M. B. M., Scholtmeijer, K., van Kooten, T. G., Dijkhuizen, L., and Wösten, H. A. B. (**2002**) "Coating with genetic engineered hydrophobin promotes growth of fibroblasts on a hydrophobic solid." *Biomaterials*, **23**, 4847-4854.

Janssen, M. L., van Leeuwen, M. B. M., van Kooten, T. G., de Vries, J., Dijkhuizen, L., and Wösten, H. A. B. (**2004**) "Coating with genetic engineered hydrophobin promotes growth of fibroblasts on a hydrophobic solid." *Biomaterials*, **25**, 2731-2739.

Jena, B. P., and Hörber, J. K. H. (Ed.) (**2002**) "*Atomic Force Microscopy in Cell Biology.*" Academic Press, London.

Jiménez, J. L., Guijarro, J. I., Orlova, E., Zurdo, J., Dobson, C. M., Sunde, M., and Saibil, H. R. (**1999**) "Cryo-electron microscopy structure of an SH3 amyloid fibril and model of the molecular packing." *The EMBO Journal*, **18**, (4), 815-821.

Jiménez, J. L., Nettleton, E. J., Bouchard, M., Robinson, C. V., Dobson, C. M., and Saibil, H. R. (**2002**). "The protofilament structure of insulin amyloid fibrils." *Proceedings of the National Academy of Sciences of the United States of America,* **99**, 9196-9201.

Kaldenhoff, R., and Russo, V. E. (**1993**). "Promoter analysis of the *bli-7leas* gene." *Current Genetics*, **24**, 394-9.

Kane, J. F. (**1995**). "Effects of rare codon clusters on high-level expression of heterologous proteins in *Escherichia coli.*" *Current Opinion in Biotechnology*, **6**, 494-500.

Kansas, S., and Ikai, A. (**1995**). "A method for anchoring round shaped cells for atomic force microscope imaging." *Biophysical Journal*, **68**, 1678-1680.

Keränen, S., and Penttilä M. (**1995**). "Production of recombinant proteins in the filamentous fungus *Trichoderma reesei.*" *Current Opinion in Biotechnology*, **6** (5), 534-537.

Kershaw, M. J., and Talbot, N. J. (**1998**). "Hydrophobins and repellents: proteins with fundamental roles in fungal morphogenesis." *Fungal Genetics and Biology*, **23**, 18-33.

Kershaw, M. J., Wakley, G., and Talbot, N. J. (**1998**). "Complementation of the mpg1 mutant phenotype in *Magnaporthe grisea* reveals functional relationships between fungal hydrophobins." *The EMBO Journal*, **17**, 3838-49.

Kim, S., Ahn, I. P., and Lee, Y. H. (**2001**) "Analysis of genes expressed during rice-*Magnaporthe grisea* interactions" *Molecular Plant-Microbe Interactions*, **14** (11), 1340-1346.

Kindt, J. H., Sitko, J. C., Pietrasanta, L. I., Oroudjev, E., Becker N., Viani, M. B., and Hansma, H. G. (2002) "Chapter 10: Methods for Biological Probe Microscopy in Aqueous Fluids." **In:** *Atomic Force Microscopy in Cell Biology (pp. 214-230).* B. P. Jena and J. K. H. Hörber (Ed.), Academic Press: London.

Kinter, M., and Sherman, N. E. (**2000a**). "Chapter 6: The preparation of protein digests for mass-spectrometric sequencing experiments." **In:** *Protein Sequencing and Identification Using Tandem Mass Spectrometry (pp. 147-165).* Wiley-Interscience Inc.: New York.

Kinter, M., and Sherman, N. E. (**2000b**). "Chapter 3: Mass analysers." **In:** *Protein Sequencing and Identification Using Tandem Mass Spectrometry (pp. 29-63).* Wiley-Interscience Inc.: New York.

Kinter, M., and Sherman, N. E. (**2000c**). "Chapter 7: Mass-spectrometric analysis of Tryptic digests." **In:** *Protein Sequencing and Identification Using Tandem Mass Spectrometry (pp. 166-206).* Wiley-Interscience Inc.: New York. (c)

Kowalewski, T., and Holtzman, D. M. (**1999**). "*In situ* atomic force microscopy study of Alzheimer's ß-amyloid peptide on different substrates: new insights into mechanism of ß-sheet formation." *Proceedings of the National Academy of Sciences of the United States of America*, **96**, 3688-3693.

Krug, J. C., and Khan, R. S. (**1991**). "A New Homothallic Species of Neurospora from Hungary." *Mycologia*, **83**, 829-832.

Kurland, C., and Gallant, J. (**1996**). "Errors of heterologous protein expression." *Current Opinion in Biotechnology*, **7**, 489-493.

Kyte, J., and Doolittle, R. F. (**1982**). "A simple method for displaying the hydropathic character of a protein." *Journal of Molecular Biology*, **157**, 105-132.

Langley, D. B., Templeton, M. D., Fields, B. A., Mitchell, R. E., and Collyer, C. A. (**2000**). "Mechanism of inactivation of ornithine transcarbamoylase by *N* delta-(*N* - Sulfodiaminophosphinyl)-L-ornithine, a true transition state analogue? Crystal structure and implications for catalytic mechanism." *Journal of Biochemistry*, **275**, 20012-20019.

Larraya, L. M., Perez, G., Peñas, M. M., Baars, J. J., Mikosch, T. S., Pisabarro, A. G., and Ramirez, L. (**1999**) "Molecular karyotype of the white rot fungus *Pleurotus ostreatus*." *Applied and Environmental Microbiology*, **65** (8), 3413-3417.

Lauter, F. R., and Russo, V. E. (**1991**) "Blue light induction of conidiation-specific genes in *Neurospora crassa*." *Nucleic Acids Research,* **19** (24), 6883-6886.

Lauter, F. R., Russo, V. E. and Yanofsky, C. (**1992**) "Developmental and light regulation of *eas,* the structural gene for the rodlet protein of *Neurospora*." *Genes and Development*, **6** (12A), 2373-2381.

Le Hir, H., Nott, A., and Moore, M. J. (**2003**). "How introns influence and enhance eukaryotic gene expression." *Trends in Biochemical Science*, **28**, 215-220.

Li, J., Bai, C., Wang, C., Zhu, C., Lin, Z., Li, Q., and Cao, E. (**1998**). "A convenient method of aligning large DNA molecules on bare mica surfaces for atomic force microscopy." *Nucleic Acids Research*, **26**, (20), 4785-4786.

Linder, M., Selber, K., Nakari-Setälä, T., Qiao, M., Kula, M. R., and Penttilä, M. (**2001**). "The Hydrophobins HFBI and HFBII from *Trichoderma reesei* Showing Efficient Interactions with Non-ionic Surfactants in Aqueous Two-Phase Systems." *Biomacromolecules*, **2**, 511-517.

Lora, J. M., de la Cruz, J., Benitez, T., Llobell, A., and Pintor-Toro, J. A. (**1994**) "A putative catabolite-repressed cell wall protein from the mycoparasitic fungus *Trichoderma harzianum*." *Molecular and General Genetics*, **242** (4), 461-466.

Lora, J. M., Pintor-Toro, J. A., Benítez, T., and Romero, L. C. (**1995**) "Qid3 protein links plant bimodular proteins with fungal hydrophobins." *Molecular Microbiology*, **18** (2), 380-382.

Loros, J. J., and Dunlap, J. C. (**1991**). "*Neurospora crassa* clock-controlled genes are regulated at the level of transcription." *Molecular Cell Biology,* **11**, 558-563.

Loros, J. J., Denome, S. A., and Dunlap, J. C. (**1989**). "Molecular cloning of genes under control of the circadian clock in *Neurospora." Science*, **243**, 385-388.

Lowry, R. J., Durkee, T. L., and Sussman, A. S. (**1967**). "Ultrastructural studies of microconidium formation in *Neurospora crassa." Journal of Bacteriology*, **94,** 1757–1763.

Lugones, L. G., Bosscher, J. S., Scholtmeyer, K., de Vries, O. M., and Wessels, J. G. (**1996**) "An abundant hydrophobin (ABH1) forms hydrophobic rodlet layers in *Agaricus bisporus* fruiting bodies." *Microbiology*, **142 (Pt 5),** 1321-1329.

Lugones, L. G., Wösten, H. A., and Wessels, J. G. (**1998**) "A hydrophobin (ABH3) specifically secreted by vegetatively growing hyphae of *Agaricus bisporus* (common white button mushroom)." *Microbiology*, **144 (Pt 8),** 2345-2353.

Lugones, L. G., Wösten, H. A. B., Birkenkamp, K. U., Sjollema, K. A., Zagers, J., and Wessels, J. G. H. (**1999a**) "Hydrophobins line air channels in fruiting bodies of *Schizophyllum commune* and *Agaricus bisporus*." *Mycological Research*, **103** (5), 635-640.

Lugones, L. G., Scholtmeijer, K., Klootwijk, R., and Wessels, J. G. (**1999b**). "Introns are necessary for mRNA accumulation in *Schizophyllum commune." Molecular Microbiology*, **32**, 681-9.

Mackay, J., Matthews, J. M., Winefield, R. D., Mackay, L. G., Haverkamp, R. G., and Templeton, M. D. (**2001**). "The hydrophobin EAS is largely unstructured in solution and functions by forming amyloid-like structures." *Structure (Cambridge)*, **9**, 83-91.

Maddelein, M. L., Dos Reis, S., Duvezin-Caubet, S., Coulary-Salin, B., and Saupe, S. J. (**2002**). "Amyloid aggregates of the HET-s prion protein are infectious." *Proceedings of the National Academy of Sciences of the United States of America*, **99**, 7402-7407.

Maheshwari, R. (**1999**). "Microconidia of *Neurospora crassa." Fungal Genetics and Biology*, **26**, 1-18.

Mahoney, D. P., Huang, L. H., and Backus, M. P. (**1969**). "New homothallic *Neurospora* from tropical soils." *Mycologia*, **61**, 242-272.

Makin, O. S., and Serpell, L. C. (**2002**). "Examining the structure of the mature amyloid fibril." *Biochemical Society Transactions*, **30**, (4), 521-525.

Makrides, S. C. (**1996**). "Strategies for achieving high-level expression of genes in *Escherichia coli." Microbiological Reviews*, **60**, 512-538.

Mankel, A., Krause, K., and Kothe, E. (**2002**) "Identification of a hydrophobin gene that is developmentally regulated in the ectomycorrhizal fungus *Tricholoma terreum*." *Applied and Environmental Microbiology,* **68** (3), 1408-1413.

Martin, G. G., Cannon, G. C., and McCormick, C. L. (**2000**). "Sc3p hydrophobin organization in aqueous media and assembly onto surfaces as mediated by the associated polysaccharide schizophyllan." *Biomacromolecules*, **1**, 49-60.

McCabe, P. M. and Van Alfen, N. K. (**1999**) "Secretion of cryparin, a fungal hydrophobin." *Applied and Environmental Microbiology*, **65** (12), 5431-5435.

McCarthy, J. E. G. (**1998**). "Post-transcriptional Control of Gene Expression in Yeast." *Microbiology and Molecular Biology Reviews*, **62**, 1492-1553.

Metzenberg, R. L. and Ahlgren, S. K. (**1971**). "Structural and regulatory control of aryl sulfatase in *Neurospora*." *Genetics*, **68**, 369-381.

Morris, V. J., Kirby, A. R., and Gunning, A. P. (**1999**). "*Atomic Force Microscopy for Biologists*." Imperial College Press: London.

Müller, D. J., and Engel, A. (**2002**). "Chapter 13: Conformations, Flexibility, and Interactions Observed on Individual Membrane Proteins by Atomic Force Microscopy." **In:** *Atomic Force Microscopy in Cell Biology (pp. 258-300).* B. P. Jena and J. K. H. Hörber (Ed.) Academic Press: London.

Müller, S. A., and Engel, A. (**1998a**). "Mass measurement in the Scanning Transmission Electron Microscope: A powerful Tool for Studying Membrane Proteins." *Journal of Structural Biology,* **121**, 219-230.

Müller, D. J., Fotiadis, D., and Engel, A. (**1998b**). "Mapping flexible protein domains at subnanometer resolution with the atomic force microscope." *FEBS Letters,* **430**, 105-111.

Müller, S. A., and Engel, A. (**2001**). "Structure and mass analysis by scanning transmission electron microscopy." *Micron*, **32**, 21-31.

Müller, D. J., Fotiadis, D., Scheuring, S., Müller, S. A., and Engel, A. (**1999**). "Electrostatically Balanced Subnanometre Imaging of Biological Specimens by Atomic Force Microscope." *Biophysical Journal*, **76**, 1101-1111.

Muñoz, G. A., Agosin, E., Cotoras, M., San Marin, R., and Volpe, D. (**1995**) "Comparison of aerial and submerged spore properties for *Trichoderma hazianum*." *FEMS Microbiology Letters*, **125** (1), 63-70.

Muñoz, G., Nakari-Setälä, T., Agosin, E., and Penttilä, M. (**1997**) "Hydrophobin gene srh1, expressed during sporulation of the biocontrol agent Trichoderma harzianum." *Current Genetics*, **32** (3), 225-230.

Murray, N. E., and Perkins, D. D. (**1963**). "Stanford *Neurospora* Methods." *Neurospora Newsletter*, **4**, 21-25.

Nakagawa, S., Tamakashi, Y., Hamana, T., Kawase, M., Taketomi, S., Ishibashi, Y., Nishimura, O., and Fukuda, T. (**1994**). "Chemical Cleavage of Recombinant Fusion Proteins to Yield Peptide Amides." *Journal of the American Chemical Society*, **116**, 5513-5514.

Nakamura, Y., Gojobori, T., and Ikemura, T. (**2000**). "Codon usage tabulated from the international DNA sequence databases: status for the year 2000." *Nucleic Acids Research*, **28,** (1), 292.

Nakari-Setälä, T., Aro, N., Kalkkinen, N., Alatalo, E., and Penttilä, M. (**1996**) "Genetic and biochemical characterization of the *Trichoderma reesei* hydrophobin HFBI." *European Journal of Biochemistry*, **235** (1-2), 248-255.

Nakari-Setälä, T., Aro, N., Ilmén, M., Muñoz, G., Kalkkinen, N., and Penttilä, M. (**1997**) "Differential expression of the vegetative and spore-bound hydrophobins of *Trichoderma reesei* — cloning and characterization of the hfb2 gene." *European Journal of Biochemistry*, **248** (2), 415-423.

Nakari-Setälä, T., Azeredo, J., Henriques, M., Oliveira, R., Teixeira, J., Linder, M., and Penttilä, M. (**2002**). "Expression of a fungal hydrophobin in the *Saccharomyces cerevisiae* cell wall: effect on cell surface properties and immobilization." *Applied and Environmental Microbiology*, **68**, 3385-3391.

Natvig, D. O., Jackson, D. A., and Taylor, J. W. (**1987**). "Random Fragment Hybridisation Analysis of Evolution in the Genus *Neurospora:* The Status of Four-Spored Strains." *Evolution*, **4**, 1003-1021.

Nelson, P. E., Novak, R. O., and Backus, M. P. (**1964**). "A new species of *Neurospora* from soil." *Mycologia*, **56**, 384-392.

Ng, W. L., Ng, T. P., and Kwan, H. S. (**2000**) "Cloning and characterization of two hydrophobin genes differentially expressed during fruit body development in *Lentinula edodes*." *FEMS Microbiology Letters*, **185** (2), 139-145.

Nielsen, P. S., Clark, A. J., Oliver, R. P., Huber, M., and Spanu, P. D. (**2001**) "HCf-6, a novel class II hydrophobin from *Cladosporium fulvum*." *Microbiological Research*, **156** (1), 59-63.

Noordmans, J. and Busscher, H. J. (**1991**). "The influence of droplet volume and contact angle on liquid surface tension measurements by axisymmetric drop shape analysis-profile (ADSA-P)." *Colloids and Surfaces*, **58**, 239-249.

Novy, R., Drott, D., Yaeger, K., and Mierendorf, R. (**2001**). "Overcoming the codon bias of *E. coli* for enhanced protein expression." *in**Nova**tions - The Newsletter of Novagen Inc.*, **12**, 1-3.

Noy, A., Vezenov, D. M., and Lieber, C. M. (**1997**). "Chemical Force Microscopy." *Annual Review of Materials Science*, **27**, 381-421.

Noy, A., Sanders, C. H., Vezenov, D. V., Wong, S. S., and Lieber, C. M. (**1998**). "Chemically-Sensitive Imaging in Tapping Mode by Chemical Force Microscopy: Relationship between Phase Lag and Adhesion." *Langmuir*, **14**, 1508-1511.

Onel, K., Thelen, M. P., Ferguson, D. O., Bennett, R. L., and Holloman, W. K. (**1995**). "Mutation avoidance and DNA repair proficiency in Ustilago maydis are differentially lost with progressive truncation of the REC1 gene product." *Molecular and Cellular Biology*, **15**, (10), 5329-5338

Onions, A. H. S., Allsopp, D., and Eggins, H. O. W. (**1981**). "Industrial Uses of Fungi." **In:** *Smith's Introduction to Industrial Mycology. 7th Edition (pp. 347-361).* Edward Arnold Ltd.: London.

Outchkourov, N. S., Stiekema, W. J., and Jongsma, M. A. (**2002**). "Optimization of the expression of equistatin in *Pichia pastoris*." *Protein Expression and Purification*, **24**, 18-24.

Paananen, A., Vuorimaa, E., Torkkeli, M., Penttilä, M., Kauranen, M., Ikkala, O., Lemmetyinen, H., Serimaa, R., and Linder, M. B. (**2003**). "Structural hierarchy in molecular films of two class II hydrophobins." *Biochemistry*, **42**, 5253-5258.

Page, R. D. (**1996**). "TreeView: an application to display phylogenetic trees on personal computers." *Computer Applications in the Biological Sciences*, **12**, 357-358.

Palomo, J. M., Peñas, M. M., Fernández-Lorente, G., Mateo, C., Pisabarro, A. G., Fernández-Lafuente, R., Ramirez, L., and Guisán, J. M. (**2003**). "Solid-phase handling of hydrophobins: immobilized hydrophobins as a new tool to study lipases." *Biomacromolecules*, **4**, 204-210.

Pandit, A., and Maheshwari, R. (**1996**). "Life-history of *Neurospora intermedia* in a sugar cane field." *Journal of Bioscience and Bioengineering*, **21**, 57-79.

Paris, S., Debeaupuis, J. P., Crameri, R., Carey, M., Charles, F., Prevost, M. C., Schmitt, C., Philippe, B., and Latge, J. P. (**2003**) "Conidial hydrophobins of *Aspergillus fumigatus*." *Applied and Environmental Microbiology*, **69** (3), 1581-1588.

Parta, M., Chang, Y., Rulong, S., Pinto-DaSilva, P., and Kwon-Chung, K. J. (**1994**) "HYP1, a hydrophobin gene from *Aspergillus fumigatus,* complements the rodletless phenotype in *Aspergillus nidulans*." *Infection and Immunity*, **62** (10), 4389-4395.

Pashley, R. M. (**1981**). "Hydration forces between mica surfaces in Li^+, Na^+, Na^+ and Cs^+ electrolyte solutions: a correlation of double layer and hydration forces with surface cation exchange properties." *Journal of Colloid Interface Science*, **83**, 531-546.

Peñas, M. M., Asgeirsdóttir, S. A., Lasa, I., Culiañez-Macià, F. A., Pisabarro, A. G., Wessels, J. G., and Ramírez, L. (**1998**) "Identification, characterization, and In situ detection of a fruit-body-specific hydrophobin of *Pleurotus ostreatus*." *Applied and Environmental Microbiology*, **64,** 4028-4034.

Peñas, M. M., Rust, B., Larraya, L. M., Ramirez, L., and Pisabarro, A. G. (**2002**) "Differentially regulated, vegetative-mycelium-specific hydrophobins of the edible basidiomycete *Pleurotus ostreatus*." *Applied and Environmental Microbiology*, **68** (8), 3891-3898.

Perkins, D. D. (**1977**). "Details for preparing silica gel stocks." *Neurospora Newsletter*, **24**, 16.

Perkins, D. D. and Davis, R. H. (**2000**). "Evidence for safety of *Neurospora* for Academic and Commercial Uses." *Applied and Environmental Microbiology*, **66**, 5107-5109.

Perkins, D. D., and Raju, N. B. (**1986**). "*Neurospora discreta,* a new heterothallic species defined by its crossing behaviour." *Experimental Mycology*, **10**, 323-338.

Perkins, D. D., and Turner, B. C. (**1988**). "*Neurospora* from Natural Populations: Towards the Population Biology of a Haploid Eukaryote." *Experimental Mycology*, **12**, 19-131.

Perkins, D. D., Turner, B. C., and Barry, E. G. (**1976**). "Strains of *Neurospora* collected from nature." *Evolution*, **30**, 281-313.

Pickersgill, R. W. (**2003**). "A primordial structure underlying amyloid." *Structure*, **11**, 137-138.

Pierce®. (**2003**). "Instructions: TCEP.HCl. Number 20490 (0647.1)." Pierce® Biotechnology Inc.**:** Rockford, IL, USA.

Pöggeler, S. (**1999**). "Phylogenetic relationships between mating-type sequences from homothallic and heterothallic ascomycetes." *Current Genetics*, **36**, 222-231.

Qi, J., Wu, J., Somkuti, G. A., and Watson, J. T. (**2001**). "Determination of the disulfide structure of sillucin, a highly knotted, cysteine-rich peptide, by cyanylation/cleavage mass mapping." *Biochemistry*, **40**, 4531-4538.

Radford, S. (**2000**). "Protein folding: progress made and promises ahead." *Trends in Biochemical Sciences*, **25,** (12), 611-618.

Radmacher, M., Fritz, M., and Hansma, P. K. (**1995**). "Imaging Soft Samples with the Atomic Force Microscope: Gelatin in Water and Propanol." *Biophysical Journal*, **69**, 264-270.

Raju, N. B. (**1981**). "Fungal Genetics Newsletter." *Neurospora Newsletter*, **28**, 16-17.

Raju, N. B. (**1992**). "Functional heterothallism resulting from homokaryotic conidia and ascospores in *Neurospora tetrasperma*." *Mycological Research*, **96**, 103-116.

Raju, N. B., and Perkins, D. D. (**1994**). "Diverse programs of ascus development in pseudohomothallic species of *Neurospora, Gelasinospora,* and *Podospora.*" *Developmental Genetics*, **15**, 104-108.

Raju, N. B., and Perkins, D. D. (**2000**). "Programmed Ascospore Death in the Homothallic Ascomycete *Coniochaeta tetraspora*." *Fungal Genetics and Biology*, **30**, 213-221.

Ramirez-Alvarado, M., Merkel, J. S., and Regan, L. (**2000**). "A systematic exploration of the influence of protein stability on amyloid formation *in vitro.*" *Proceedings of the National Academy of Sciences of the United States of America* **97**, 8979-8984.

Randall, T. A., and Metzenberg, R. L. (**1995**). "Species-specific and mating type-specific DNA regions adjacent to mating type idiomorphs in the genus *Neurospora.*" *Genetics*, **141**, 119-136.

Richards, W. C. (**1993**). "Cerato-ulmin: A Unique Wilt Toxin of Instrumental Significance in the Development of Dutch Elm Disease." **In:** *Dutch elm disease Research, Cellular and Molecular Approaches (pp. 89-151).* M. B. Sticklen and J. L. Sherald, (Ed.), Springer Verlag: New York.

Richards, W. C. and Takai, S. (**1973**) "Novel technique for isolating microstructures present in shake cultures of the fungus *Catalysts ulmi.*" *Applied Microbiology*, **26** 443-444.

Romanos, M., Scorer, C., Sreekrishna, K., and Clare, J. (**1998**). "The Generation of Multicopy Recombinant Strains." **In:** *Pichia Protocols (pp. 73-80).* D. R. Higgins and J. M. Cregg (Ed.), Humana Press: Totowa, New Jersey.

Sachs, M. S. (**1998**). "Posttranscriptional Control of Gene Expression in Filamentous Fungi." *Fungal Genetics and Biology*, **23**, 117-125.

Sambrook, J., and Russell, D. W. (**2001**). "*Molecular Cloning: A Laboratory Manual.*" Cold Spring Harbor Laboratory Press. Cold Spring Harbor, New York.

Santos, C., and Labarere, J. (**1999**) "Aa-Pri2, a single-copy gene from *Agrocybe aegerita,* specifically expressed during fruiting initiation, encodes a hydrophobin with a leucine-zipper domain." *Current Genetics*, **35** (5), 564-70.

Sasse, J., and Gallagher, S. R. (**2000**). "Unit 10.6: Detection of Proteins." **In:** *Current Protocols in Molecular Biology (pp. 10.6.1-10.6.13).* F. M. Ausube, B. Roger, Kingston R. E.; Moore, D. D. Moore, J. G. Seidman, K. Struhl (Ed.), John Wiley & Sons, Inc.: Hoboken, New Jersey.

Scherrer, S., De Vries, O. M., Dudler, R., Wessels, J. G., and Honegger, R., (**2000**) "Interfacial self-assembly of fungal hydrophobins of the lichen-forming ascomycetes *Xanthoria parietina* and *X. ectaneoides.*" *Fungal Genetics and Biology*, **30** (1), 81-93.

Scherrer, S., Haisch, A., and Honegger, R. (**2002**) "Characterization and expression of *XPH1,* the hydrophobin gene of the lichen-forming ascomycete *Xanthoria parietina*." *New Phytologist*, **154,** 175-184.

Scheuring, S., Ringler, P., Borgnia, M., Stahlberg, H., Müller, D. J., Agre, P., and Engel, A. (**1999**). "High resolution AFM topographs of the *Escherichia coli* water channel aquaporin Z." *The EMBO Journal*, **18**, (18), 4981-4987.

Schladitz, C., Euridice, E. P., Hermel, H., and Möhwald, H. (**1999**). "Amyloid-ß-sheet formation at the air-water interface." *Biophysical Journal*, **77**, 3305-3310.

Schmitt, M. E., Brown, T. A., and Trumpower B. L. (**1990**). "A rapid and simple method for preparation of RNA from *Saccharomyces cerevisiae*." *Nucleic Acids Research*, **18**, 3091-3092.

Scholtmeijer, K. (**2000**) "PhD Thesis: Expression and Engineering of Hydrophobin Genes." Wiskunde en Natuurwetenschappen (Mathematics and Natural Sciences), Rijksuniversiteit Groningen (University of Groningen), Groningen, The Netherlands.

Scholtmeijer, K., Wessels, J. G., and Wösten, H. A. (2001a). "Fungal hydrophobins in medical and technical applications." *Applied Microbiology and Biotechnology*, 56, 1-8.

Scholtmeijer, K., Wösten, H. A., Springer, J., and Wessels, J. G. (**2001b**). "Effect of introns and AT-rich sequences on expression of the bacterial hygromycin B resistance gene in the basidiomycete *Schizophyllum commune*." *Applied and Environmental Microbiology,* **67**, 481-483.

Scholtmeijer, K., Janssen, M. I., Gerssen, B., de Vocht, M. L., van Leeuwen, B. M., van Kooten, T. G., Wösten, H. A., and Wessels, J. G. (**2002**). "Surface modifications created by using engineered hydrophobins." *Applied and Environmental Microbiology,* **68**, 1367-1373.

Schuren, F. H., and Wessels, J. G. (**1994**). "Highly-efficient transformation of the homobasidiomycete *Schizophyllum commune* to phleomycin resistance." *Current Genetics*, **26**, 179-183.

Schuren, F. H., and Wessels, J. G. (**1990**) "Two genes specifically expressed in fruiting dikaryons of *Schizophyllum commune:* homologies with a gene not regulated by mating-type genes." *Gene*, **90** (2), 199-205.

Schuurs, T. A., Schaeffer, E. A., and Wessels, J. G. (**1997**). "Homology-dependent silencing of the SC3 gene in *Schizophyllum commune*." *Genetics*, **147**, 589-96.

Segers, G. C., and Nuss, D. L. (**2003**) "Constitutively activated G alpha negatively regulates virulence, reproduction and hydrophobin gene expression in the chestnut blight fungus *Cryphonectria parasitica*." *Fungal Genetics and Biology*, **38** (2), 198-208.

Segers, G. C., Hamada, W., Oliver, R. P., and Spanu, P. D. (**1999**) "Isolation and characterisation of five different hydrophobin-encoding cDNAs from the fungal tomato pathogen *Cladosporium fulvum*." *Molecular and General Genetics*, **261** (4-5), 644-52.

Seidman, C. E., Struhl, K. and Sheen, J. (**1992**). "Unit 1.8: Introduction of Plasmid DNA into Cells." **In:** *Current Protocols in Molecular Biology (pp. 1.8.1-1.8.8).* F. M. Ausubel, R. Brent, R. E. Kingston, D. D. Moore, J. G. Seidman, J. G. Smith, and K. Struhl (Ed.) Greene Publishing Associates and Wiley-Interscience: New York, Chichester, Brisbane, Toronto, Singapore.

Selitrennikoff, C. P. (**1976**) "Easily-*wettable,* a new mutant." *Neurospora Newsletter*, **23,** 23.

Serpell, L. C., and Smith, J. M. (**2000**). "Direct Visualisation of the ß-Sheet Structure of Synthetic Alzheimer's Amyloid." *Journal of Molecular Biology*, **299**, (1), 225-231.

Sertsou, G. (**1997**) "Fourth Year Project Report: The formation and structure of films produced from *Neurospora crassa* rodlet proteins." Department of Chemicals and Materials Engineering, The University of Auckland, Auckland, New Zealand.

Shear, C. L., and Dodge, B. O. (**1927**). "Life histories and heterothallism of the red bread-mold fungi of the *Monilia sitophila* group." *Journal of Agricultural Research*, **34**, 1019-1042.

Sinclair, G., and Choy, F. Y. (**2002**). "Synonymous codon usage bias and the expression of human glucocerebrosidase in the methylotrophic yeast, *Pichia pastoris*." *Protein Expression and Purification*, **26**, 96-105.

Sipe, J. D., and Cohen, A. S. (**2000**). "Review: history of the amyloid fibril." *Journal of Structural Biology*, **130**, 88-98.

Skupski, M. P., Jackson, D. A., and Natvig, D. O. (**1997**). "Phylogenetic Analysis of Heterothallic *Neurospora* Species." *Fungal Genetics and Biology*, **21**, 623-633.

Smith, D. L., and Zhou, Z. (**1990**). "Strategies for Locating Disulfide Bonds in Proteins." *Methods in Enzymology*, **193**, 374-389.

Smolic, T. (**1997**) "Fourth Year Project Report: Microstructure of Hydrophobin Rodlets from *Neurospora crassa.*" Department of Chemicals and Materials Engineering, The University of Auckland, Auckland, New Zealand.

Smyth, D., Stein, W. H., and Moore, S. (**1963**). "The Sequence of Amino Acid in Bovine Pancreatic Ribonuclease: Revisions and Confirmations." *The Journal of Biological Chemistry*, **238**, 227-233.

Soanes, D. M., Kershaw, M. J., Cooley, R. N., and Talbot, N. J. (**2002**) "Regulation of the *MPG1* Hydrophobin gene in the Rice Blast Fungus *Magnaporthe grisea*." *Molecular Plant-Microbe Interactions*, **15** (12), 1253-1267.

Sommer, T., Chambers, J. A., Eberle, J., Lauter, F. R., and Russo, V. E. (**1989**). "Fast light-regulated genes of *Neurospora crassa*." *Nucleic Acids Research*, **17**, 5713-5723.

Spackman, D. H., Stein, W. H., and Moore, S. (**1960**). "The Disulfide Bonds of Ribonuclease." *Journal of Biological Chemistry*, **235**, 648-659.

Spanu, P., (**1997**) "HCF-1, a hydrophobin from the tomato pathogen *Cladosporium fulvum*." *Gene*, **193** (1), 89-96.

Springer, M. L. (**1993**). "Genetic control of fungal differentiation: the three sporulation pathways of *Neurospora crassa*." *Bioessays*, **15**, 365-374.

Springer, M. L. and Yanofsky, C. (**1992**). "Expression of *con* in *Neurospora crassa*." *Genes and Development*, **6**, 1052–1057.

Sreekrishna, K., Brankamp, R. G., Kropp, K. E., Blankenship, D. T., Tsay, J. T., Smith, P. L., Wierschke, J. D., Subramaniam, A., and Birkenberger, L. A. (**1997**). "Strategies for optimal synthesis and secretion of heterologous proteins in the methylotrophic yeast *Pichia pastoris*." *Gene*, **190**, 55-53.

St Leger, R. J., Staples, R. C., and Roberts, D. W. (**1992**) "Cloning and regulatory analysis of starvation-stress gene, ssgA, encoding a hydrophobin-like protein from the entomopathogenic fungus, *Metarhizium anisopliae*." *Gene*, **120** (1), 119-124.

St Leger, R. J., Joshi, L., and Roberts, D. (**1998**) "Ambient pH is a major determinant in the expression of cuticle-degrading enzymes and hydrophobin by *Metarhizium anisopliae*." *Applied and Environmental Microbiology*, **64** (2), 709-13.

Staden, R., Beal, K. F., and Bonfield, J. K. (**1999**). "The Staden Package, 1998. Computer Methods in Molecular Biology." **In:** *Bioinformatics Methods and Protocols (pp. 115-130).* S. Misener and S. A. Krawetz (Ed.), The Humana Press Inc.: Totowa, NJ 07512, USA.

Staples, R. C. (**2001**) "A hydrophobin aids water-mediated dispersal of *Cladosporium* conidia" *Trends in Plant Science*, **6** (8), 343-344.

Stolz, M., Stoffler, D., Aebi, U., and Goldsbury, C. (**2000**) "Monitoring biomolecular interactions by time-lapse atomic force microscopy." *Journal of Stuctural Biology,* **131** (3), 171-180.

Stringer, M. A. and Timberlake, W.E. (**1995**) "dewA encodes a fungal hydrophobin component of the *Aspergillus* spore wall" *Molecular Microbiology."* **16** (1), 33-44.

Stringer, M. A., Dean, R. A., Sewall, T. C., and Timberlake, W. E. (**1991**) "Rodletless, a new *Aspergillus* developmental mutant induced by directed gene inactivation." *Genes and Development*, **5** (7), 1161-1171.

Stroud, P. A., Goodwin, J. S., Butko, P., Cannon, G. C., and McCormick, C. L. (**2003**). "Experimental Evidence for Multiple Assembled States of Sc3 from *Schizophyllum commune.*" *Biomacromolecules*, **4**, 956-967.

Svircev, A. M., Jeng, R. S., and Hubbes, M. (**1987**) "Detection of Cerato-Ulmin on Aggressive Isolates of *Ophiostoma ulmi* by Immunocytochemistry and Scanning Electron Microscopy." *Phytopathology*, **78** (3), 322-327.

Tagu, D., Nasse, B., and Martin, F. (**1996**) "Cloning and characterization of hydrophobins-encoding cDNAs from the ectomycorrhizal basidiomycete *Pisolithus tinctorius.*" *Gene*, **168** (1), 93-97.

Tagu, D., De Bellis, R., Balestrini, R., De Vries, O. M. H., Piccoli, G., Stocchis, V., Bonfante, P., and Martin, F. (**2001**) "Immunolocalization of hydrophobin HYDPt-1 from the ectomycorrhizal basidiomycete *Pisolithus tinctorius* during colonization of *Eucalyptus globulus* roots." *New Phytologist*, **149,** 127-135.

Tagu, D., Marmeisse, R., Baillet, Y., Riviere, S., Palin, B., Bernardini, F., Mereau, A., Gay, G., Balestrini, R., Bonfante, P., and Martin, F. (**2002**) "Hydrophobins in ectomycorrhizas: heterologous transcription of the *Pisolithus* HydPt-1 gene in yeast and *Hebeloma cylindrosporum.*" *European Journal of Histochemistry*, **46** (1), 23-29.

Tai, F. L. (**1935**). "Two new species of *Neurospora*." *Mycologia*, **27**, 328-330.

Takai, S. (**1974**). "Pathogenicity and cerato-ulmin production in *Ceratocystis ulmi.*" *Nature*, **252**, 124-6.

Takai, S., and Hiratsuka, Y. (**1980**) "Accumulation of the material containing the toxin cerato-ulmin on the hyphal surface of *Ceratocystis ulmi.*" *Canadian Journal of Botany*, **58,** 658-662.

Takai, S., and Richards, W. C. (**1978**) "Cerato-ulmin, a wilting toxin of *Ceratocystis ulmi:* isolation and some properties of cerato-ulmin from the culture of *C. ulmi.*" *Phytopathologische Zeitschrift*, **91,** 129-146.

Takai, S. (**1974**) "Pathogenicity and cerato-ulmin production in *Ceratocystis ulmi.*" *Nature*, **252** (5479), 124-126.

Takai, S., Richards, W. C., Davies, Y. P., Hiratsuka, Y., and Krywienczyk, J. (**1980**) "Evidence for the presence of the toxin Cerato-ulmin in the head fluid of *Ceratocystis ulmi.*" *Canadian Journal of Botany*, **58,** 669-675.

Takai, S., Richards, W. C., and Stevenson, K. J. (**1983**) "Evidence for the involvement of cerato-ulmin, the *Ceratocystis ulmi* toxin, in the development of Dutch elm disease." *Physiological Plant Pathology*, **23,** 275-280.

Talbot, N. J., Ebbole, D. J., and Hamer, J. E. (**1993**) "Identification and characterization of MPG1, a gene involved in pathogenicity from the rice blast fungus *Magnaporthe grisea.*" *Plant Cell*, **5** (11), 1575-1590.

Talbot, N. J., Kershaw, M. J., Wakely, G. E., de Vries, O. M. H., Wessels, J. G. H., and Hamer, J. E. (**1996**) "MPG1 Encodes a Fungal Hydrophobin Involved in Surface Interactions during Infection-Related Development of *Magnaporthe grisea.*" *The Plant Cell*, **8,** 985-999.

Taylor, J. W. and Natvig, D. O. (**1989**). "Mitochondrial DNA and evolution of heterothallic and pseudohomothallic *Neurospora* species." *Mycological Research*, **93**, 257-272.

Taylor, J. W., Jacobson, D. J., Kroken, S., Kasuga, T., Geiser, D. M., Hibbett, D. S., and Fisher, M. C. (**2000**). "Phylogenetic species recognition and species concepts in fungi." *Fungal Genetics and Biology*, **31**, 21-32.

Temple, B. and Horgen, P. A. (**2000**). "Biological roles fro cerato-ulmin, a hydrophobin secreted by the elm pathogens, *Ophiostoma ulmi* and *O. novo-ulmi.*" *Mycologia*, **92**, 1-9.

Temple, B., Horgen, P. A., Bernier, L., and Hintz, W. E. (**1997**) "Cerato-ulmin, a hydrophobin secreted by the causal agents of Dutch elm disease, is a parasitic fitness factor." *Fungal Genetics and Biology*, **22** (1), 39-53.

Templeton, M. D., Rikkerink, E. H. A., and Beever, R. E. (**1994**). "Small cysteine-rich proteins and recognition in fungal-plant interactions." *Molecular Plant-Microbe Interactions*, **7**, 320-325.

Templeton, M., Greenwood, D. R., and Beever, R. E. (**1995**). "Solubilization of *Neurospora crassa* rodlet proteins and identification of the predominant protein as the proteolytically processed eas (ccg-2) gene product." *Experimental Mycology*, **19**, 166-9.

Thau, N., Monod, M., Crestani, B., Rolland, C., Tronchin, G., Latge, J. P., and Paris, S. (**1994**) "Rodletless mutants of *Aspergillus fumigatus." Infection and Immunity*, **62** (10), 4380-4388.

Thompson, J. D., Gibson, T. J., Plewniak, F., Jeanmougin, F., and Higgins, D. G. (**1997**). "The CLUSTAL X windows interface: flexible strategies for multiple sequence alignment aided by quality analysis tools." *Nucleic Acids Research*, **25**, 4876-4882.

Tillotson, R. D., Wösten, H. A. B., Richter, M., and Willey, J. M. (**1998**). "A surface active protein involved in aerial hyphae formation in the filamentous fungus *Schizophillum commune* restores the capacity of a bald mutant of the filamentous bacterium *Streptomyces coelicolor* to erect aerial structures." *Molecular Microbiology*, **30** (3), 595-602.

Torkkeli, M., Serimaa, R., Ikkala, O., and Linder, M. (**2002**). "Aggregation and Self-Assembly of Hydrophobins from *Trichoderma reesei:* Low Resolution Structural Models." *Biophysical Journal*, **83**, 2240-2247.

Trembley, M. L., Ringli, C., and Honegger, R. (**2002a**) "Hydrophobins *DGH1, DGH2,* and *DGH3* in the lichen-forming basidiomycete *Dictyonema glabratum.*" *Fungal Genetics and Biology*, **35** (3), 247-259.

Trembley, M. L., Ringli, C., and Honegger, R. (**2002b**) "Differential expression of hydrophobins *DGH1, DGH2* and *DGH3* and immunolocalization of *DGH1* in strata of the lichenized basidiocarp of *Dictyonema glabratum.*" *New Phytologist,* **154** (1), 185-195.

Tucker, S. L., and Talbot, N. J. (**2001**). "Surface attachment and pre-penetration stage development by plant pathogenic fungi." *Annual Review of Phytopathology*, **39**, 385-417.

Tuite, M. F., Clare, J. J., and Romanos, M. A. (**1999**). "Expressing cloned genes in the yeasts *Saccharomyces cerevisiae* and *Pichia pastoris.*" **In:** *Protein Expression - A Practical Approach (pp. 61-100).* S. J. Higgins and B. D. Hames (Ed.), Oxford University Press: Oxford, NY. USA.

Turian, G. (**1964**). "Synthetic Conidiogenous Media for *Neurospora crassa.*" *Nature*, **202**, 1240.

Turner, B. C., Perkins, D. D., and Fairfield, A. (**2001**). "*Neurospora* from Natural Populations: A Global Study." *Fungal Genetics and Biology*, **32**, 67-92.

Unger, V. M. (**2001**). "Electron cryomicroscopy methods." *Current Opinion in Structural Biology*, **11**, (5), 548-554.

van der Hazel, H. B., Kielland-Brandt, M. C., and Winther, J. R. (**1996**). "Review: Biosynthesis and Function of Yeast Vacuolar Proteases." *Yeast*, **12**, 1-16.

van der Vegt, W., van der Mei, H. C., Wösten, H. A., Wessels, J. G., and Busscher, H. J. (**1996**). "A comparison of the surface activity of the fungal hydrophobin SC3p with those of other proteins." *Biophysical Chemistry*, **57**, 253-260.

van Wetter, M. A., Schuren, F. H. J., Schuurs, T. A., and Wessels, J. G. H., (**1996**) "Targeted mutation of the SC3 hydrophobin gene of *Schizophyllum commune.*" *FEMS Microbiological Letters*, **140,** 265-269.

van Wetter, M. A., Wösten, H. A., and Wessels, J. G. (**2000a**) "SC3 and SC4 hydrophobins have distinct roles in formation of aerial structures in dikaryons of *Schizophyllum commune.*" *Molecular Microbiology*, **36** (1), 201-210.

van Wetter, M. A., Wösten, H. A., Sietsma, J. H., and Wessels, J. G. (**2000b**) "Hydrophobin gene expression affects hyphal wall composition in *Schizophyllum commune.*" *Fungal Genetics and Biology*, **31** (2), 99-104.

Voet, D., Voet, J. G., and Pratt, C. W. (**1999**). "*Fundamentals of Biochemistry.*" John Wiley & Sons, Inc.; New York, Chichester, Weinhem, Brisbane, Singapore, Toronto.

Vogel, H. J. (**1964**). "Distribution of lysine pathways among fungi: Evolutionary implications." *The American Naturalist,* **XCVIII**, 435-446.

Vollmer, S. J. and Yanofsky, C. (**1986**). "Efficient cloning of genes of *Neurospora crassa.*" *Proceedings of the National Academy of Sciences of the United States of America*, **83**, 4869-4873.

von Arx, J. A. (**1981**). "*The Genera of Fungi Sporulating in Pure Culture. 3rd Edition.*" J.Cramer: Vaduz, Liechtenstein.

Vorm, O., Roepstorff, P., and Mann, M. (**1994**). "Improved Resolution and Very High Sensitivity in MALDI-TOF of Matrix Surfaces Made by Fast Evaporation." *Analytical Chemistry*, **66**, 3281-3287.

Wakselman, M., and Guibe-Jambel, E. (**1976**). "1-Cyano-4-dimethylamino-pyridinium salts: New water-soluble reagents for the cyanylation of protein sulphydryl groups." *Journal of the Chemical Society. Chemical Communications*, 21-22.

Walker, J. M. (Ed.) (**1996**) "*The Protein Protocols Handbook*." Humana Press Inc. Totowa, New Jersey.

Walters, D., Cleveland, J., Thomson, N. H., Hansma, P. K., Wendman, M. A., Gurley, G., and Elings, V. (**1996**). "Short Cantilevers for Atomic Force Microscopy." *Review of Scientific Instruments*, **67**, 3583-3590.

Wang, X., de Vocht, M. L., de Jonge, J., Poolman, B., and Robillard, G. T. (**2002**). "Structural changes and molecular interactions of hydrophobin SC3 in solution and on a hydrophobic surface." *Protein Science*, **11**, 1172-1181.

Weeks, D. P., Beerman, N., and Griffith, O. M. (**1986**). "A small-scale five-hour procedure for isolating multiple samples of CsCl-purified DNA: application to isolations from mammalian, insect, higher plant, algal, yeast, and bacterial sources." *Analytical Biochemistry*, **152**, 309-314.

Wessels, J. G. (**1987**) "Mating-type genes and the control of expression of fruiting genes in basidiomycetes." *Antonie Van Leeuwenhoek*, **53** (5), 307-316.

Wessels, J. G. H. (**1994**). Development regulation of fungal cell wall formation. *Annual Review of Phytopathology*, **32**, 413-437.

Wessels, J. G. (**1996**). "Fungal Hydrophobins: Proteins that function at an interface." *Trends in Plant Sciences*, **1**, 9-15.

Wessels, J. G. (**1997**). "Hydrophobins: proteins that change the nature of the fungal surface." *Advances in Microbial Physiology*, **38**, 1-45.

Wessels, J. G. H., Mulder G. H., and Springer, J. (**1987**) "Expression of dikaryon-specific and non-specific mRNAs of *Schizophyllum commune* in relation to environmental conditions and fruiting." *Journal of General Microbiology*, **133,** 2557-2561.

Wessels, J. G. H., Asgeirsdóttir, S. A., Birkenkamp, K. U., de Vries, O. M. H., Lugones, L. G., Scheer, J. M. J., Schuren, F. H. J., Schuurs, T. A., van Wetter, M. A. and Wösten, H. A. B. (**1995**) "Genetic regulation of emergent growth in *Schizophyllum commune.*" *Canadian Journal of Botany*, **73,** S273-S281.

Wetzel, R. (**2002**). "Ideas of order for amyloid fibril structure." *Structure*, **10**, 1031-1036.

White, T. J., Bruns, T., Lee, S., and Taylor, J. (**1990**). "Amplification and Direct Sequencing of Fungal Ribosomal RNA Genes for Phylogenetics." **In:** *PCR Protocols: A Guide to Methods and Applications.* Academic Press, Inc.: San Diego.

Whiteford, J. R., and Spanu, P. D. (**2001**) "The hydrophobin HCf-1 of *Cladosporium fulvum* is required for efficient water-mediated dispersal of conidia" *Fungal Genetics and Biology*, **32** (3), 159-168.

Whiteford, J. R., and Spanu, P. D. (**2002**). "Hydrophobins and the interaction between fungi and plants." *Molecular Plant Pathology*, **3**, 391-400.

Wickner, R. B. (**1994**). "[URE3] as an altered URE2 protein: evidence for a prion analogue in *Saccharomyces cerevisiae*." *Science*, **264**, 566-569.

Wild, C. J., and Seber, G. A. F. (**1993**). "Introduction to Probability and Statistics." Department of Mathematics and Statistics, The University of Auckland: Auckland, New Zealand.

Wildermuth, H. (**1972a**). "Morphological characteristics of *Streptomyces glaucescens* and *S. acrimycini,* two streptomycetes with 'hairy' spores." *Archiv für Mikrobiologie*, **81**, 321-332.

Wildermuth, H. (**1972b**). "The surface structure of spores and aerial hyphae in *Streptomyces viridochomogenes*." *Archiv für Mikrobiologie*, **81**, 301-320.

Wildermuth, H., Wehrli, E., and Horne, R. W. (**1971**). "The surface structure of spores and aerial mycelium in *Streptomyces coelicolor*." *Journal of Ultrastructural Research*, **35**, 168-180.

Wong, S. S., Harper, J. D., Lansbury, P. T. Jr., and Lieber, C. M. (**1998**). "Carbon Nanotube Tips: High-Resolution Probes for Imaging Biological Systems." *Journal of the American Chemical Society*, **120** (3), 603-604.

Woo, J. H., Liu, Y. Y., Mathias, A., Stavrou, S., Wang, Z., Thompson, J., and Neville, D. M. J. (**2002**). "Gene optimization is necessary to express a bivalent anti-human anti-T cell immunotoxin in *Pichia pastoris*." *Protein Expression and Purification*, **25**, 270-282.

Wösten, H. A. (**2001**) "Hydrophobins: multipurpose proteins." *Annual Review of Microbiology*, **55,** 625-646.

Wösten, H., and de Vocht, M. L. (**2000**). "Hydrophobins, the fungal coat unravelled." *Biochimica et Biophysica Acta*, **1469**, 79-86.

Wösten, H. A. B., and Wessels, J. G. H. (**1997**). "Hydrophobins, from molecular structure to multiple functions in fungal development." *Mycoscience*, **38**, 363-374.

Wösten, H. A. B., and Willey, J. M. (**2000**). "Surface-active proteins enable microbial aerial hyphae to grow into the air." *Microbiology*, **146**, 767-773.

Wösten, H. A. B., Ruardy, T. G., van der Mei, H. C., Busscher, H. J. and Wessels J. G. H. (**1995**). "Interfacial self-assembly of a *Schizophyllum commune* hydrophobin into an insoluble amphipathic membrane depends on surface hydrophobicity." *Colloids and Surfaces B: Biointerfaces*, **5**, 189-195.

Wösten, H. A. B., de Vries, O. M. H., and Wessels, J. G. H. (**1993**) "Interfacial self-assembly of a fungal hydrophobin into a hydrophobic rodlet layer." *The Plant Cell*, **5,** 1567-1574.

Wösten, H. A., Asgeirsdóttir, S. A., Krook, J. H., Drenth, J. H., and Wessels, J. G. (**1994a**) "The fungal hydrophobin Sc3p self-assembles at the surface of aerial hyphae as a protein membrane constituting the hydrophobic rodlet layer." *European Journal of Cell Biology*, **63,** 122-129.

Wösten, H. A., Schuren, F. H., and Wessels, J. G. (**1994b**) "Interfacial self-assembly of a hydrophobin into an amphipathic protein membrane mediates fungal attachment to hydrophobic surfaces." *The EMBO Journal*, **13** (24), 5848-5854.

Wösten, H., de Vries, O. M., van der Mei, H. C., Busscher, H. J., and Wessels, J. G. (**1994c**). "Atomic composition of the hydrophobic and hydrophilic membrane sides of self-assembled SC3p hydrophobin." *Journal of Bacteriology*, **176**, 7085-7086.

Wösten, H. A., van Wetter, M. A., Lugones, L. G., van der Mei, H. C., Busscher, H. J., and Wessels, J. G. (**1999a**) "How a fungus escapes the water to grow into the air." *Current Biology*, **9** (2), 85-88.

Wösten, H. A. B., Richter, M., and Willey, J. M. (**1999b**). "Structural Proteins Involved in Emergence of Microbial Aerial Hyphae." *Fungal Genetics and Biology*, **27**, 153-160.

Wu, J., and Watson, J. T. (**1997**). "A novel methodology for assignment of disulfide bond pairings in proteins." *Protein Science*, **6**, 319-398.

Wu, J., and Watson, J. (**1998**). "Optimization of the cleavage reaction for cyanylated cysteinyl proteins for efficient and simplified mass mapping." *Analytical Biochemistry*, **258**, 268-276.

Wu, J., Gage, D. A., and Watson, J. T. (**1996**)."A Strategy to Locate Cysteine Residues in Proteins by Specific Chemical Cleavage Followed by Matrix-Assisted Laser Desorption/Ionisation Time-of-Flight Mass Spectrometry." *Analytical Biochemistry*, **235**, 161-174.

Xu, Y., Bruening, M. L., and Watson, J. T. (**2003**). "Non-specific, on-probe cleanup methods for MALDI-MS samples." *Mass Spectrometry Reviews*, **22**, 429-440.

Yaguchi, M., Pusztai-Carey, M., Roy, C., Surewicz, W. K., Carey, P. R., Stevenson, K. J., Richards, W. C., and Takai, S. (**1993**)." Amino-acid sequence and spectroscopic studies of Dutch elm disease toxin, cerato-ulmin." **In:** *Dutch elm disease Research, Cellular and Molecular Approaches (pp. 152-170).* M. B. Sticklen and J. L. Sherald (Ed.), Springer Verlag: New York.

Yang, Y., Wu, J., and Watson, J. T. (**1998**). "Disulfide Mass Mapping in Proteins Containing Adjacent Cysteines is Possible with Cyanylation/Cleavage Methodology." *Journal of the American Chemical Society*, **120**, 5834-5835.

Yun, S., Berbee, M. L., Yoder, O. C. and Turgeon, B. G. (**1999**). "Evolution of the fungal self-fertile reproductive life style from self-sterile ancestors." *Proceedings of the National Academy of Sciences of the United States of America*, **96**, 5592-5597.

Zaluzec, E. J., Gage, D. A., Allison, J. and Watson J. T. (**1994**). "Direct Matrix-Assisted Laser Desorption Ionisation Mass-spectrometric Analysis of Proteins Immobilized on Nylon-Based Membranes." *Journal of the American Society for Mass Spectrometry*, **5**, 230-237.

Zhang, L., Villalon, D., Sun, Y., Kazmierczak, P. and van Alfen, N. K. (**1994**) "Virus-associated down-regulation of the gene encoding cryparin, an abundant cell-surface protein from the chestnut blight fungus, *Cryphonectria parasitica*." *Gene*, **139** (1), 59-64.

Zhou, C., Yang, Y., and Jong, A. Y. (**1990**). "Mini-prep in ten minutes." *Biotechniques*, **8**, 172-173.

APPENDICES.

APPENDIX I — HYDROPHOBINS: RESEARCH SUMMARY

HYDROPHOBINS DISCOVERED IN FILAMENTOUS FUNGI

Species	Name	Expression details	Proposed Function
Agaricus bisporus	ABH1/ hypA	Coats the air channels and external surfaces of dikaryon fruiting bodies (Lugones *et al.* 1996, de Groot *et al.* 1996, Lugones *et al.* 1999.)	Provides a hydrophobic coating to the surface of fruiting bodies, and maintains air channels in dikaryon (Lugones *et al.* 1996, de Groot *et al.* 1996, Lugones *et al.* 1999.)
Agaricus bisporus	ABH2/ hypC	Discovered independently by Lugones *et al.* (1996) and de Groot *et al.* (1996), ABH2/hypC is expressed at low levels alongside ABH1/hypA.. *ABH2/hypC* is located 2.5 Kbp downstream of *ABH1/hyp A* and may have arisen through gene duplication.	
Agaricus bisporus	ABH3	Secreted into the medium *in vitro* (de Vries *et al.* 1993, Lugones *et al.* 1998) and forms a hydrophobic coating on aerial mycelium of homokaryotic organisms (Lugones *et al.* 1998.)	May contribute to attaching hyphae to substrates, aiding the exploitation of lignocellulose substrates (Lugones *et al.* 1998.)
Agaricus bisporus	hypB	Expressed strongly during early mushroom development and thereafter only in the stipe (stalk) of the mushroom (de Groot *et al.* 1999.)	Thought to contribute to the tissue differentiation that occurs during fruit body (mushroom) formation. It may also maintain air channels (de Groot *et al.* 1999.)
Agrocybe aegerita	Aapri-2	Protein is expressed during basidiocarp formation and contains a putative Leucine zipper domain (Santos and Labarere 1999.)	
Aspergillus (Emericella) nidulans	DewA	Hydrophobic conidial surface coating thought to aid dispersal. Girardin *et al.* (1999) detected a marked decrease in hydrophobicity of the conidia when this gene was disrupted. Cellular expression occurs after sterigmata derivation and was immunolocalised on mature spores only (Stringer and Timberlake 1995.)	
Aspergillus Asp.	RODA	RodA is expressed during sterigma- and spore differentiation in *Emericella* (*Aspergillus*) *nidulans*. The protein is present as a hydrophobic conidial surface coating. Deletion of the gene causes easily wettable phenotype (Stringer *et al.* 1991, Stringer and Timberlake 1995.) Presence of the rodA gene in other members of *Aspergillus* section *Fumagati* confirmed by Geiser *et al.* (1998).	Thought to aid conidia dispersal and possibly protecting conidia from the host's phagocytic cells (Stringer *et al.* 1991, Stringer and Timberlake 1995, Paris *et al.* 2003.)

Species	Name	Expression details	Proposed Function
Aspergillus fumigatus	RODB	Present in the conidial outer wall but not necessary for rodlet formation, RodA- mutants show any rodlets on their conidia. Expressed in *Asp. nidulans* dewA mutants but not secreted (Paris *et al*. 2003.)	
Cladosprium fulvum	HCf1	Expression increases during sporulation (Spanu 1997, Segers *et al*. 1999.) The protein is the principle hydrophobic element on the conidial surface (Hamada and Spanu 1998, Whiteford and Spanu 2001, Staples 2001.)	Thought to aid water-mediated conidia dispersal (Hamada and Spanu 1998, Whiteford and Spanu 2001, Staples 2001.)
Cladosprium fulvum	HCf2	Expression increases during sporulation and decreases during carbon and nitrogen starvation (Segers *et al.* 1999.)	
Cladosprium fulvum	HCf3	HCf-3 expression increases during sporulation and decreases during carbon and nitrogen starvation (Segers *et al*. 1999.)	
Cladosprium fulvum	HCf4	HCf-4 expression increases during sporulation. The predicted mature form of HCf4 is 210 amino acids long. Its N-terminal domain contains a segment of 100 mainly hydrophilic amino acids of which 10 are predicted to occur in the N-terminal domain of the mature protein. This region shows no homology to the G/N rich N-termini of Qid3 or CFTH1 (Segers *et al.* 1999.)	
Cladosprium fulvum	HCf5	HCf-5 expression increases during sporulation and increases during nitrogen starvation (Segers *et al*. 1999.)	
Cladosprium fulvum	HCf6	HCf-6 expression halts during sporulation, Rich N-terminal GN-repeat may be cell wall anchor (Nielsen *et al.* 2001.)	
Claviceps fusiformis	CFTH1/ or cpa3	Mature protein is not glycosylated and contains 3 complete class II hydrophobin domains separated by Rich GN-repeats appear to confer considerable alpha helical structure (Arntz and Tudzynski 1997, de Vries *et al*. 1999.) Proposed that the GN-rich regions may be cell wall anchor Nielsen *et al*. (2001). CFTH1 is expressed in the mucilaginous coat surrounding submerged hyphae and as a discrete layer on aerial hyphae (de Vries *et al*. 1999.)	Proposed to aid formation of aerial hyphae (de Vries *et al*. 1999.)
Coprinus cinereus	COH1	Expressed in vegetative monokaryonic cells coating aerial hyphae as well as being excreted into culture media. Strains unable to express both COH1 and COH2 cannot form aerial hyphae (Asgeirsdóttir *et al.* 1997.)	

Species	Name	Expression details	Proposed Function
Coprinus cinereus	COH2	Expressed in vegetative monokaryonic cells only, strains unable to express both COH1 and COH2 cannot form aerial hyphae (Asgeirsdóttir *et al.* 1997.)	
Cryphonectria (Endothia) parasitica	Cryparin (CRP)	Expressed during fruiting body formation post infection (Carpenter *et al.* 1992, Zhang *et al.* 1994, McCabe and Van Alfen 1999). CRP is found coating the surface of fruiting bodies, the mature-form of CRP has lectin-like properties but the secreted mature-version is not glycosylated but the transient pro-protein is (McCabe and van Alfen 1999.) Possibly regulated by the G-protein *cpg*-1 (Segers and Nuss 2003.)	
Dictyonema glabratum	DICH1	DICH1 is present in a hydrophobic rodlet-patterned layer lining the cell walls of hyphae within the lichens air-cavities (Trembley *et al.* 2002a, Trembley *et al.* 2002b.)	Maintenance of air spaces in lichen thalli and canalisation of solutes in the apoplasts (Trembley *et al.* 2002b.)
Dictyonema glabratum	DICH2	DICH2 is expressed by hyphae present in the photobiont layer and lower stratum of the lichen, a rodlet-patterned layer known to contain DICH1 lines hyphal cell walls in this region (Trembley *et al.* 2002a, Trembley *et al.* 2002b). A total hydrophobin extract from this rodlet layer was able to re-polymerise into a rodlet film *in vitro* (Trembley *et al.* 2002b.)	Maintenance of air spaces in lichen thalli and canalisation of solutes in the apoplasts (Trembley *et al.* 2002b.)
Dictyonema glabratum	DICH3	DICH3 is expressed by hyphae in the boundary layer of the symbiotic compartment, a rodlet-patterned layer lines hyphal cell walls in this region (Trembley *et al.* 2002a, Trembley *et al.* 2002b.)	Maintenance of air spaces in lichen thalli and canalisation of solutes in the apoplasts Trembley *et al.* 2002b.
Flammulina velutipes	FVH1	Expressed during fruiting body development (Ando *et al.* 2001.)	May help to initiating fruiting body development (Ando *et al.* 2001.)
Lentinula edodes	Le.HYD1	Strongly expressed in the primordium and to a lesser extent in mature fruiting body (Ng *et al.* 2000.)	Suggested to line air channels in fruiting body (Ng *et al.* 2000.)
Lentinula edodes	Le.HYD2	Strongly expressed in the primordium and to a lesser extent in mature fruiting body (Ng *et al.* 2000.)	May aid mycelial attachment to substrates (Ng *et al.* 2000.)
Magnaporthe grisea	MPG1	Expressed during pathogenesis and axenic culture (Talbot *et al.* 1993.) Expression of MPG1 under the dual control of genes regulating appressorium development and nitrogen metabolism (Soanes *et al.* 2002.)	(1) A primer for allowing structures to adhere to the leaf surface (Talbot *et al.* 1993.) (2) Signalling component of appressorium differentiation and or Conidiogenesis (Talbot *et al.* 1996.)
Magnaporthe grisea	MPH1	Expressed *in planta* only (Kim *et al.* 2001.)	

Species	Name	Expression details	Proposed Function
Metarhizium anisopliae	SSGA	Expressed during appressorium development (St Leger *et al.* 1992, St Leger *et al.* 1998, and Bidochka *et al.* 2001).	Adhesion to host cuticle (St Leger *et al.* 1998, Ebbole 1997.)
Neurospora crassa	EAS	Expression controlled by the circadian clock, environmental cues and conidiation (Lauter and Russo 1991, Eberle and Russo 1992, Bell-Pedersen *et al.* 1992, Lauter *et al.* 1992, Bell-Pedersen *et al.* 1996, Bell-Pedersen 2000, and Bell-Pedersen *et al.* 2001.) The protein forms a hydrophobic film on macroconidia whose deletion leads to the easily wettable phenotype (Selitrennikoff 1976, Beever and Dempsey 1978.)	Aids in the dispersal of macroconidia (Beever and Dempsey 1978).
Ophiostoma ulmi	cerato-ulmin	Protein is secreted constitutively being found in culture media (Richards and Takai 1973, Takai 1974, Takai and Richards 1978), the host tissues (Takai *et al.* 1983) and on aerial hyphae and sporulating structures of surface cultures (Takai *et al.* 1980, Takai and Hiratsuka 1980, Svircev *et al.* 1987.) If the gene is deleted the fungi produces fewer aerial hyphae with a less hydrophobic surface (Bowden *et al.* 1996.)	(1) Wilt Toxin (Takai 1974, Takai *et al.* 1983). Contrast with: Deletion of *cu* has no effect on pathogenicity of *O. ulmi* (Bowden *et al.* 1996.) Expression of transgenic cerato-ulmin made *O. quercus* pathogenic on Elm trees (Del Sorbo *et al.* 2000.) (2) Aids in the formation of aerial hyphae (Bowden *et al.* 1994.) (3) Hydrophobic coating on conidiospores (Bowden *et al.* 1996.) (4) Adhesion to insect bodies (Temple *et al.* 1997.)
Pisolithus tinctorius	HydPt-1	Expressed only *in planta* on symbiotic tissues and associated with aerial and vegetative hyphae (Tagu *et al.* 1996, Tagu *et al.* 2001, Tagu *et al.* 2002.)	
Pisolithus tinctorius	HydPt-2	Expressed only *in planta* on symbiotic tissues and associated with aerial hyphae (Tagu *et al.* 1996.)	
Pisolithus tinctorius	HydPt-3	Secreted into culture media. Expression up-regulated during the formation of ectomycorrhizae but unaffected by nutrient concentration (Duplessis *et al.* 2001.)	
Pleurotus ostreatus	FBH1	Expression detected only in fruiting bodies, though not in the gill tissue (Peñas *et al.* 1998.)	
Pleurotus ostreatus	POH1	Expressed in the fruiting bodies (Asgeirsdóttir *et al.* 1998.)	
Pleurotus ostreatus	POH2	Mature POH2 is glycosylated and expressed dikaryotic and monokaryonic vegetative mycelium. It is secreted into the culture and is immunolocalised in the interhyphal mucilage and on the cell wells of aerial hyphae (Asgeirsdóttir *et al.* 1998.) Not expressed in the var. *florida* strain (Peñas *et al.* 2002.) Co-purified POH2 and POH3 form rodlets (Asgeirsdóttir *et al.* 1998.)	POH2 and POH3 or both coat aerial hyphae aiding in their formation and hydrophobicity (Asgeirsdóttir *et al.* 1998.)

Species	Name	Expression details	Proposed Function
Pleurotus ostreatus	POH3	Expressed dikaryotic and monokaryonic vegetative mycelium and secreted into media *in vitro* (Asgeirsdóttir *et al.* 1998), but not fruiting bodies Peñas *et al.* (2002). Co-purified POH2 and POH3 form rodlets (Asgeirsdóttir *et al.* 1998.)	POH2 and POH3 or both coat aerial hyphae aiding in their formation and hydrophobicity (Asgeirsdóttir *et al.* 1998.)
Pleurotus ostreatus	VMH1	Expressed in dikaryotic and monokaryonic vegetative mycelium (Larraya *et al.* 1999, Peñas *et al.* 2002.)	
Pleurotus ostreatus	VMH2	Expressed in dikaryotic and monokaryonic vegetative mycelium (Peñas *et al.* 2002.)	
Pleurotus ostreatus	VMH3	Mature VMH3 is glycosylated and expressed in vegetative mycelium and fruiting bodies (Larraya *et al.* 1999, Peñas *et al.* 2002.)	Allows hyphae to adhere to hydrophobic surfaces (Peñas *et al.* 2002.)
Schizophyllum commune	Sc1	Expressed in fruiting dikaryon only (Schuren and Wessels 1990.)	
Schizophyllum commune	SC3	It is highly expressed during emergent growth in both mono- and dikaryon being secreted into liquid media and found coating aerial hyphae. Irrespective of culture conditions SC3 is expressed after 2-3 days of growth (Wessels 1987, Wessels *et al.* 1987, Schuren and Wessels 1990, de Vocht *et al.* 1998.) SC3 is glycosylated. Removal of the mannose residues from SC3 caused a slight drop in hydrophilicity of the hydrophilic side of assembled SC3 (but not the surface activity) and weakened the proteins ability to bind to hydrophilic surfaces (de Vocht *et al.* 1998.)	(1) Coats aerial hyphae aiding in their formation and hydrophobicity (Wösten *et al.* 1993, Wösten *et al.* 1994a, Wösten *et al.* 1999, van Wetter *et al.* 1996.) (2) Allows hyphae to adhere to hydrophobic surfaces (Wösten *et al.* 1994b, van Wetter *et al.* 2000a.) (3) Is involved in cell wall synthesis (van Wetter *et al.* 2000b.)
Schizophyllum commune	Sc4	Expressed in the fruiting dikaryon only (Schuren and Wessels 1990, van Wetter *et al.* 2000a).	Coats the air- channels of fruiting bodies to prevent water-logging (van Wetter *et al.* 2000a.)
Schizophyllum commune	Sc6	Expressed in fruiting dikaryon only (Wessels *et al.* 1995.)	
Trichoderma harzianum	QID3	Highly expressed in chitin-containing media (Lora *et al.* 1994.)	Contributes to the hydrophobicity of the cell and may be involved in cell to cell or cell to substrate attachment (Lora *et al.* 1994, Lora *et al.* 1995.)
Trichoderma harzianum	SRH1	Expression increased during sporulation and nutrient limiting conditions (Muñoz *et al.* 1997), it is secreted into liquid media and coats dry spores (Muñoz *et al.* 1995.)	Confers hydrophobic coating to spores (Muñoz *et al.* 1995.)
Trichoderma reesei	HFB1	Expressed on cell wall and glucose-containing culture medium (Nakari-Setälä *et al.* 1996.)	

Species	Name	Expression details	Proposed Function
Trichoderma reesei	HFB2	Expressed on spores and secreted into culture medium when. Expression is induced by light, nutrient starvation and conidiation (Nakari-Setälä *et al.* 1997.).	
Tricholoma terreum	Hyd1	10 fold increase in Hyd1 expression occurs when grown symbiotically with Pine species (Mankel *et al.* 2002.)	Coating the symbiotic tissues and aerial hyphae (Mankel *et al.* 2002).
Xanthoria ectaneoides	XEH1	The fungal and algae cell walls in the thalline interior of this lichen are lined with a hydrophobic rodlet-patterned layer. From this symbiotically grown mycobiont, Scherrer *et al.* (2000) identified and characterised this hydrophobin gene. A putative Leucine zipper domain was also identified in the gene-product.	Maintenance of air spaces in lichen thalli and canalisation of solutes in the apoplasts (Scherrer *et al.* 2000).
Xanthoria parietina	XPH1	The fungal and algae cell walls in the thalline interior of this lichen are lined with a hydrophobic rodlet-patterned layer. From this symbiotically grown mycobiont, Scherrer *et al.* (2000) identified and characterised this hydrophobin gene. A putative Leucine zipper domain was also identified in the gene-product. XPH1 is not expressed in the aposymbiotically cultured mycobiont, but highly expressed when growing symbiotically (Scherrer *et al.* 2002.)	Maintenance of air spaces in lichen thalli and canalisation of solutes in the apoplasts (Scherrer *et al.* 2000, Scherrer *et al.* 2002.)

HYDROPHOBINS FROM ASCOMYCETES

Species	Ecological niche/Description	Hydrophobin Name	GenBank Ref #	Reference
Aspergillus fumigatus	Opportunistic human pathogen	HYP1/RODA (fum.)	L25258/UO6121	Parta *et al.* (1994), Thau *et al.* (1994)
Aspergillus fumigatus (and possibly Asp. nidulans)	Opportunistic human pathogen	RODB	AY057385	Paris *et al.* (2003)
Aspergillus section Fumigati (incl. Neosartorya sp. and Emericella nidulans)	Opportunistic human pathogen(s)	RODA (nid.)	M61113, with partial gene sequences AF057331—AF057350	Stringer *et al.* (1991), Geiser *et al.* (1998)
Cladosprium fulvum	Plant pathogen (tomatoes)	HCf1	X98578	Spanu (1997)
Cladosprium fulvum	Plant pathogen (tomatoes)	HCf2	AJ133700	Segers *et al.* (1999)
Cladosprium fulvum	Plant pathogen (tomatoes)	HCf3	AJ133701	Segers *et al.* (1999)
Cladosprium fulvum	Plant pathogen (tomatoes)	HCf4	AJ133702	Segers *et al.* (1999)
Cladosprium fulvum	Plant pathogen (tomatoes)	HCf5	AJ133703	Segers *et al.* (1999)
Cladosprium fulvum	Plant pathogen (tomatoes)	HCf6	AJ251294	Nielsen *et al.* (2001)
Claviceps fusiformis	Plant pathogen (grass sp.) & ergot alkaloid producer	CFTH1/cpa3	AJ133774	de Vries *et al.* (1999), Arntz and Tudzynski (1997)
Claviceps purpurea	Plant pathogen (grass sp.) & ergot alkaloid producer	CPPH1	AJ418045	Mey, G., Correia, T., Oeser, B., Garre, V. and Tudzynski, P. unpublished results
Emericella (Aspergillus) nidulans	Saprophyte	DewA	U07935	Stringer and Timberlake (1995)
Endothia (Cryphonectria) parasitica	Plant pathogen (Chestnut trees)	Cryparin (CRP)	L09559	Zhang *et al.* (1994), Carpenter *et al.* (1992)
Magnaporthe grisea	Pathogens (rice & grass sp.)	MPG1	L20685	Talbot *et al.* (1993)
Magnaporthe grisea	Pathogens (rice & grass sp.)	MPH1	AF126872	Kim *et al.* (2001)
Metarhizium anisopliae	Insect pathogen.	SSGA	M85281	St Leger *et al.* (1992), Bidochka *et al.* (2001)
Neurospora crassa	Saprophyte	EAS	X67339	Bell-Pedersen *et al.* (1992) Lauter *et al.* (1992)

Species	Ecological niche/Description	Hydrophobin Name	GenBank Ref #	Reference
Ophiostoma ulmi	Pathogen (Elm trees)	cerato-ulmin	U00963	Bowden *et al.* (1994)
Trichoderma harzianum	Fungus pathogen	QID3	X71913	Lora *et al.* (1994)
Trichoderma harzianum	Fungus pathogen	SRH1	Y11841	Muñoz *et al.* (1997), Muñoz *et al.* (1995)
Trichoderma reesei	Cellulo-lytic fungus	HFB1	Z68124	Nakari-Setälä *et al.* (1996)
Trichoderma reesei	Cellulo-lytic fungus	HFB2	Y11894	Nakari-Setälä *et al.* (1997)

HYDROPHOBINS FROM BASIDIOMYCETES

Species	Ecological niche/Description	Hydrophobin Name	GenBank Ref #	Reference
Agaricus bisporus	Edible mushroom	ABH1/hypA	X89242/X90818	Lugones *et al.* (1996), de Groot *et al.* (1996)
Agaricus bisporus	Edible mushroom	ABH2/hypC	X92860/X90818	Lugones *et al.* (1996), de Groot *et al.* (1996)
Agaricus bisporus	Edible mushroom	ABH3	Y14601	Lugones *et al.* (1998)
Agaricus bisporus	Edible mushroom	hypB	Y15940	de Groot *et al.* (1999)
Agrocybe aegerita (possibly *Agr. chaxingu* too.)	Edible mushroom	Aapri-2	AF081493	Santos and Labarere (1999)
Coprinus cinereus	Inky cap mushroom	COH1	Y10627	Asgeirsdóttir *et al.* (1997)
Coprinus cinereus	Inky cap mushroom	COH2	Y10628	Asgeirsdóttir *et al.* (1997)
Dictyonema glabratum	Mycobiont	DICH1	AJ320544	Trembley *et al.* (2002a)
Dictyonema glabratum	Mycobiont	DICH2	AJ320545	Trembley *et al.* (2002a)
Dictyonema glabratum	Mycobiont	DICH3	AJ320546	Trembley *et al.* (2002a)
Flammulina velutipes	Temperate white-rot fungus	FVH1	AB026721	Ando *et al.* (2001)
Lentinula edodes	Edible mushroom	Le.HYD1	AF217807	Ng *et al.* (2000)

Species	Ecological niche/Description	Hydrophobin Name	GenBank Ref #	Reference
Lentinula edodes	Edible mushroom	Le.HYD2	AF217808	Ng *et al.* (2000)
Pisolithus tinctorius	Ectomycorrhyza (Eucalyptus sp.)	HydPt-1	U29605	Tagu *et al.* (1996)
Pisolithus tinctorius	Ectomycorrhyza (Eucalyptus sp.)	HydPt-2	U29606	Tagu *et al.* (1996)
Pisolithus tinctorius	Ectomycorrhyza (Eucalyptus sp.)	HydPt-3	AF097516	Duplessis *et al.* (2001)
Pleurotus ostreatus	Edible mushroom	FBH1	AJ004883	Peñas *et al.* (1998)
Pleurotus ostreatus	Edible mushroom	POH1	Y14656	Asgeirsdóttir *et al.* (1998)
Pleurotus ostreatus	Edible mushroom	POH2	Y14657	Asgeirsdóttir *et al.* (1998)
Pleurotus ostreatus	Edible mushroom	POH3	Y16881	Asgeirsdóttir *et al.* (1998)
Pleurotus ostreatus	Edible mushroom	VMH1	AJ238147	Larraya *et al.* (1999), Peñas *et al.* (2002)
Pleurotus ostreatus	Edible mushroom	VMH2	AJ420974	Peñas *et al.* (2002)
Pleurotus ostreatus	Edible mushroom	VMH3	AJ238148	Larraya *et al.* (1999), Peñas *et al.* (2002)
Schizophyllum commune	Bracket fungus	Sc1	JU0321	Schuren and Wessels (1990)
Schizophyllum commune	Bracket fungus	SC3	M32329	Schuren and Wessels (1990), de Vocht *et al.* (1998)
Schizophyllum commune	Bracket fungus	Sc4	M32330	Schuren and Wessels (1990)
Schizophyllum commune	Bracket fungus	Sc6	AJ007504	Wessels *et al.* (1995)
Tricholoma terreum	Ectomycorrhyza (Pine and Spruce)	Hyd1	AY048578	Mankel *et al.* (2002)
Ustilago maydis	Fungal pathogen (maize and teosinte)	HUM2	Sequence not deposited. Protein sequence published in Wösten (2001)	Bohlmann (1996)
Xanthoria ectaneoides	Mycobiont of a leaf-like Lichen	XEH1	AJ250793	Scherrer *et al.* (2000)
Xanthoria parietina	Mycobiont of a leaf-like Lichen	XPH1	AJ250794	Scherrer *et al.* (2000)

APPENDIX II – PICHIA GROWTH MEDIA COMPONENTS.

YNB (YEAST NITROGEN BASE) DERIVED MEDIA.

BMD, BMG, and BMM media are derivatives of a standard media formulation called yeast nitrogen base (Invitrogen™, 2002). Normally these are made using a commercially prepared lyophilised concentrate of YNB, to avoid this a I modified the formulae for YNB without amino acids (Difco® Laboratories, 1984) to create a liquid concentrate form of YNB that could substitute for the lyophilised preparation. This modified formula is given below.

Concentrated stock solutions were created for the every other constituent in BMD, BMG, and BMM besides YNB. These solutions were sterilised and stored at 4 ºC until use. BMD, BMG, and BMM media were freshly made prior to use by diluting the constituents in sterile Milli-Q® water as required. When solid media was required, the media constituents were diluted in a hot, autoclave-sterilised, aqueous solution of 2% (w/v) Difco® Bacteriological Agar and dispensed into Petri-dishes to cool. The procedure used to create the stock solutions and these media are given below.

1000X YNB TRACE ELEMENTS SOLUTION (1000X TE).

To create a YNB trace elements stock solution these compounds were dissolved in 800 mL of Milli-Q® water: 500 mg Boric Acid, 40 mg $CuSO_4.5H_2O_{(s)}$, 100 mg $KI_{(s)}$, 200 mg $FeCl_3.6H_2O_{(s)}$, 400 mg $MnSO_4.4H_2O_{(s)}$, 200 mg $Na_2MoO_4.2H_2O_{(s)}$, 400 mg $ZnSO_4.7H_2O_{(s)}$. The volume of the solution adjusted to 1000 mL with Milli-Q® water and then sterilised by autoclaving and stored at 4 ºC.

100X YNB SALTS SOLUTION (100X SS).

To create an YNB salts stock solution these compounds were dissolved in 800 mL of Milli-Q® water: 10 g $KH_2PO_{4(s)}$, 5 g $MgSO_4.4H_2O_{(s)}$, 1 g NaCl, 1 g $CaCl_2.2H_2O_{(s)}$. The volume of the solution adjusted to 1000 mL with Milli-Q® water and then sterilised by filtration prior to storage in a darkened bottle at 4ºC.

1000X YNB VITAMINS SOLUTION (1000X VS).

To create a YNB vitamins stock solution these compounds were dissolved in 800 mL of Milli-Q® water: 2 mg Biotin, 400 mg Calcium Pantothenate, 2 mg Folic-Acid, 2 g Inositol, 400 mg Niacin, 200 mg Pyridoxine Hydrochloride, 200 mg Riboflavin, 400 mg Thiamine Hydrochloride. The volume of the solution adjusted to

1000 mL with Milli-Q® water and then sterilised by filtration and stored in a darkened bottle at 4 °C.

1 M POTASSIUM PHOSPHATE BUFFER PH 6.0.(1 M PPB).

To create a 1 M potassium phosphate buffer stock solution, 132 mL of a 1 M $K_2HPO_{4(aq)}$ solution and 868 mL of a 1 M $KH_2PO_{4(aq)}$ solution were combined. 10 M $KOH_{(aq)}$ or 10 M phosphoric acid were added as necessary to achieve pH 6. The solution was sterilised by autoclaving and stored at 4 °C.

BIOTIN, HISTIDINE METHANOL, GLYCEROL AND DEXTROSE STOCK SOLUTIONS.

Individual stock solutions consisting of biotin (500x BS), histidine (100x HS), methanol (10x MS), glycerol (10x GS) and dextrose solutions (10x DS) were made using Milli-Q® water as described in Invitrogen™ (2002). Each stock solution was sterilised by filtration (Glycerol stock-solutions were autoclaved) and stored at 4°C until use.

BUFFERED MINIMAL MEDIA PLUS DEXTROSE MEDIA (BMD).

BMD media was made by diluting 700 mL of sterilised Milli-Q® water or 2% (w/v) aqueous Difco® Bacteriological Agar solution: 1 mL of 1000x VS, 1 mL of 1000x TE, 10 mL of 100x SS, 100 mL of 1 M PPB, 2 mL of 500x BS, 100 mL of 10x DS. If *Pichia* strains GS115 or SMD1168 were being cultivated, 10 mL of 100x HS was also added. The volume of the solution was adjusted to 1000 mL with sterile Milli-Q® water prior to storage at room temperature until use. Solutions more than 5 days old were discarded.

BUFFERED MINIMAL MEDIA PLUS METHANOL MEDIA (BMM).

BMM was prepared in an identical manner to BMD except that the Dextrose solution (10x DS) was substituted for 100 mL of 10X MS.

BUFFERED MINIMAL MEDIA PLUS GLYCEROL MEDIA (BMG).

BMG was prepared in an identical manner to BMD except that the Dextrose solution (10x DS) was substituted for 10 mL of 10x GS.

APPENDIX III – SUPPLEMENTARY DATA FOR CHAPTER 3.

APPENDIX IIIA.

N. LINEOLATA ITS/5.8S RRNA SEQUENCE ALIGNMENT.

						bp
GenBank AF388924	GGTGAACAGC	GGAGGGATCA	TTACAGAGTT	GCAAAACTCC	CACAAACCAT	50
N. lineolata	GGTGAACAGC	GGAGGGATCA	TTACAGAGTT	GCAAAACTCC	CACAAACCAT	50
GenBank AF388924	CGCGAATCTT	ACCCGTACGG	TTGCCTCGGC	GCTGGCGGTC	CGGAAGGCCC	100
N. lineolata	CGCGAATCTT	ACCCGTACGG	TTGCCTCGGC	GCTGGCGGTC	CGGAAGGCCC	100
GenBank AF388924	TCGGGCCCCC	CGGATCCTCG	GGTCTCCCGC	TCGCGGGAGG	CTGCCCGCCG	150
N. lineolata	TCGGGCCCCC	CGGATCCTCG	GGTCTCCCGC	TCGCGGGAGG	CTGCCCGCCG	150
GenBank AF388924	GAGCGCCGAA	ACCAAACTCT	TGATATTTTA	TGTCTCTCTG	AGTAAACTTT	200
N. lineolata	GAGCGCCGAA	ACCAAACTCT	TGATATTTTA	TGTCTCTCTG	AGTAAACTTT	200
GenBank AF388924	TAAATAAGTC	AAAACTTTCA	ACAACGGATC	TCTTGGTTCT	GGCATCGATG	250
N. lineolata	TAAATAAGTC	AAAACTTTCA	ACAACGGATC	TCTTGGTTCT	GGCATCGATG	250
GenBank AF388924	AAGAACGCAG	CGAAATGCGA	TAAGTAATGT	GAATTGCAGA	ATTCAGTGAA	300
N. lineolata	AAGAACGCAG	CGAAATGCGA	TAAGTAATGT	GAATTGCAGA	ATTCAGTGAA	300
GenBank AF388924	TCATCGAATC	TTTGAACGCA	CATTGCGCCC	GCCAGTATTC	TGGCGGGCAT	350
N. lineolata	TCATCGAATC	TTTGAACGCA	CATTGCGCCC	GCCAGTATTC	TGGCGGGCAT	350
GenBank AF388924	GCCTGTTCGA	GCGTCATTTC	AACCATCAAG	CTCTGCTTGC	GTTGGGGATC	400
N. lineolata	GCCTGTTCGA	GCGTCATTTC	AACCATCAAG	CTCTGCTTGC	GTTGGGGATC	400
GenBank AF388924	CGCGGCTGCC	CGCGGTCCCT	CAAAAACAGT	GGCGGGCTCG	CTAGTCACAC	450
N. lineolata	CGCGGCTGCC	CGCGGTCCCT	CAAAAACAGT	GGCGGGCTCG	CTAGTCACAC	450
GenBank AF388924	CGAGCGTAGT	AACTCTACAT	CGCTATGGTC	GTGCGGCGGG	TTCTTGCCGT	500
N. lineolata	CGAGCGTAGT	AACTCTACAT	CGCTATGGTC	GTGCGGCGGG	TTCTTGCCGT	500
GenBank AF388924	AAAACCCCCC	CAATTTTTAA	GGTTGACCTC	GAATCAGGTA	GGAATACCCG	550
N. lineolata	AAAACCCCCC	CAATTTTTAA	GGTTGACCTC	GAATCAG---	----------	537
GenBank AF388924	CTGAACTTAA					560
N. lineolata	----------					

To confirm the purity *N. lineolata* genomic DNA extracts an ITS/5.8S rRNA sequence was PCR amplified that extract. It is shown here aligned with published the *N. lineolata* ITS/5.8S rRNA sequence (GenBank accession number AF388924) obtained by Dettman *et al.* (2001). Numbers in right-hand margin refer to length of sequence in bp.

APPENDIX IIIB.

N. PANNONICA ITS/5.8S RRNA SEQUENCE ALIGNMENT.

						bp
GenBank AF388925	GGTGAACCAG	CGGAGGGATC	ATTACAGAGT	TGCAAAACTC	CCACAAACCA	50
N. pannonica	GGTGAACCAG	CGGAGGGATC	ATTACAGAGT	TGCAAAACTC	CCACAAACCA	50
GenBank AF388925	TCGCGAATCT	TACCCGTACG	GTTGCCTCGG	CGCTGGCGGT	CCGGAAGGCC	100
N. pannonica	TCGCGAATCT	TACCCGTACG	GTTGCCTCGG	CGCTGGCGGT	CCGGAA·GCC	99
GenBank AF388925	CTCGGGCCCC	CCGGATCCTC	GGGTCTCCCG	CTCGCGGGAG	GCTGCCCGCC	150
N. pannonica	CTCGGGCCCC	CCGGATCCTC	GGGTCTCCCG	CTCGCGGGA·	GCTGCCCGCC	148
GenBank AF388925	GGAGTGCCGA	AACCAAACTC	TTGATATTTT	ATGTCTCTCT	GAGTAAACTT	200
N. pannonica	GGAGTGCCGA	AACCAAACTC	TTGATATTTT	ATGTCTCTCT	GAGTAAACTT	198
GenBank AF388925	TTAAATAAGT	CAAAACTTTC	AACAACGGAT	CTCTTGGTTC	TGGCATCGAT	250
N. pannonica	TTAAATAAGT	CAAAACTTTC	AACAACGGAT	CTCTTGGTTC	TGGCATCGAT	248
GenBank AF388925	GAAGAACGCA	GCGAAATGCG	ATAAGTAATG	TGAATTGCAG	AATTCAGTGA	300
N. pannonica	GAAGAACGCA	GCGAAATGCG	ATAAGTAATG	TGAATTGCAG	AATTCAGTGA	298
GenBank AF388925	ATCATCGAAT	CTTTGAACGC	ACATTGCGCT	CGCCAGTATT	CTGGCGAGCA	350
N. pannonica	ATCATCGAAT	CTTTGAACGC	ACATTGCGCT	CGCCAGTATT	CTGGCGAGCA	348
GenBank AF388925	TGCCTGTTCG	AGCGTCATTT	CAACCATCAA	GCTCTGCTTG	CGTTGGGGAT	400
N. pannonica	TGCCTGTTCG	AGCGTCATTT	CAACCATCAA	GCTCTGCTTG	CGTTGGGGAT	398
GenBank AF388925	CCGCGGCTGC	CCGCGGTCCC	TCAAAAACAG	TGGCGGGCTC	GCTAGTCACA	450
N. pannonica	CCGCGGCTGC	CCGCGGTCCC	TCAAAAACAG	TGGCGGGCTC	GCTAGTCACA	448
GenBank AF388925	CCGAGCGTAG	TAACTCTACA	TCGCTATGGT	CGTGCGGCGG	GTTCTTGCCG	500
N. pannonica	CCGAGCGTAG	TAACTCTACA	TCGCTATGGT	CGTGCGGCGG	GTTCTTGCCG	498
GenBank AF388925	TAAAACCCCC	CAATTTCTAA	GGTTGACCTC	GGATCAGGTA	GGAATACCCG	550
N. pannonica	TAAAACCCCC	CAATTTCTAA	GGTTGACCTC	GGATCAGGTA	GGAATACCCG	548
GenBank AF388925	CTGAACTTAA					560
N. pannonica	CTGAACTTAA					558

To confirm the identity of *N. pannonica* genomic DNA extract, an ITS/5.8S rRNA sequence was PCR amplified from it. That sequence is shown here aligned with published the *N. pannonica* ITS/5.8S rRNA sequence (GenBank accession number AF388925) obtained by Dettman *et al.* (2001). Numbers in right-hand margin refer to length of sequence in bp.

APPENDIX IIIC.

N. TOROI AND *N. TETRASPERMA* ITS/5.8S RRNA SEQUENCES COMPARED.

						bp
GenBank AF388929	GGTGAACCAG	CGGAGGGATC	ATTACAGAGT	TGCAAAACTC	CCACAAACCA	50
N. toroi	GGTGAACCAG	CGGAGGGATC	ATTACAGAGT	TGCAAAACTC	CCACAAACCA	50
GenBank AF388929	TCGCGAATCT	TACCCGTACG	GTTGCCTCGG	CGCTGGCGGT	CCGGAAAGGC	100
N. toroi	TCGCGAATCT	TACCCGTACG	GTTGCCTCGG	CGCTGGCGGT	CCGGAAAGGC	100
GenBank AF388929	CCTCGGGCCC	TCCCGGATCC	TCGGGTCTCC	CGCTCGCGGG	AGGCTGCCCG	150
N. toroi	CCTCGGGCCC	TCCCGGATCC	TCGGGTCTCC	CGCTCGCGGG	AGGCTGCCCG	150
GenBank AF388929	CCGGAGTGCC	GAAACTAAAC	TCTTGATATT	TTATGTCTCT	CTGAGTAAAC	200
N. toroi	CCGGAGTGCC	GAAACTAAAC	TCTTGATATT	TTATGTCTCT	CTGAGTAAAC	200
GenBank AF388929	TTTTAAATAA	GTCAAAACTT	TCAACAACGG	ATCTCTTGGT	TCTGGCATCG	250
N. toroi	TTTTAAATAA	GTCAAAACTT	TCAACAACGG	ATCTCTTGGT	TCTGGCATCG	250
GenBank AF388929	ATGAAGAACG	CAGCGAAATG	CGATAAGTAA	TGTGAATTGC	AGAATTCAGT	300
N. toroi	ATGAAGAACG	CAGCGAAATG	CGATAAGTAA	TGTGAATTGC	AGAATTCAGT	300
GenBank AF388929	GAATCATCGA	ATCTTTGAAC	GCACATTGCG	CTCGCCAGTA	TTCTGGCGAG	350
N. toroi	GAATCATCGA	ATCTTTGAAC	GCACATTGCG	CTCGCCAGTA	TTCTGGCGAG	350
GenBank AF388929	CATGCCTGTT	CGAGCGTCAT	TTCAACCATC	AAGCTCTGCT	TGCGTTGGGG	400
N. toroi	CATGCCTGTT	CGAGCGTCAT	TTCAACCATC	AAGCTCTGCT	TGCGTTGGGG	400
GenBank AF388929	ATCCGCGGCT	GCCCGCGGTC	CCTCAAAATC	AGTGGCGGGC	TCGCTAGTCA	450
N. toroi	ATCCGCGGCT	GCCCGCGGTC	CCTCAAAATC	AGTGGCGGGC	TCGCTAGTCA	450
GenBank AF388929	CACCGAGCGT	AGTAACTCTA	CATCGCTATG	GTCGTGCGGC	GGGTTCTTGC	500
N. toroi	CACCGAGCGT	AGTAACTCTA	CATCGCTATG	GTCGTGCGGC	GGGTTCTTGC	500
GenBank AF388929	CGTAAAACCC	CCCATTTCTA	AGGTTGACCT	CGGATCAGGT	AGGAATACCC	550
N. toroi	CGTAAAACCC	CCCATTTCTA	AGGTTGACCT	CGGATCAGGT	AGGAATACCC	550
GenBank AF388929	GCTGAACTTA	A				561
N. toroi	GCTGAACTTA	A				561

The aligned DNA sequences above confirm that *N. toroi* is synonymous with *N. tetrasperma*. Genomic DNA was extracted from *N. toroi* and an ITS/5.8S rRNA sequence was PCR amplified that extract. The sequence is shown aligned with published the *N. tetrasperma* ITS/5.8S rRNA sequence (GenBank accession number AF388929) obtained by Dettman *et al.*, (2001). Numbers in right-hand margin refer to length of sequence in bp.

APPENDIX IIID.

CDNA SEQUENCING OF *EAS* FROM *N. SITOPHILA*.

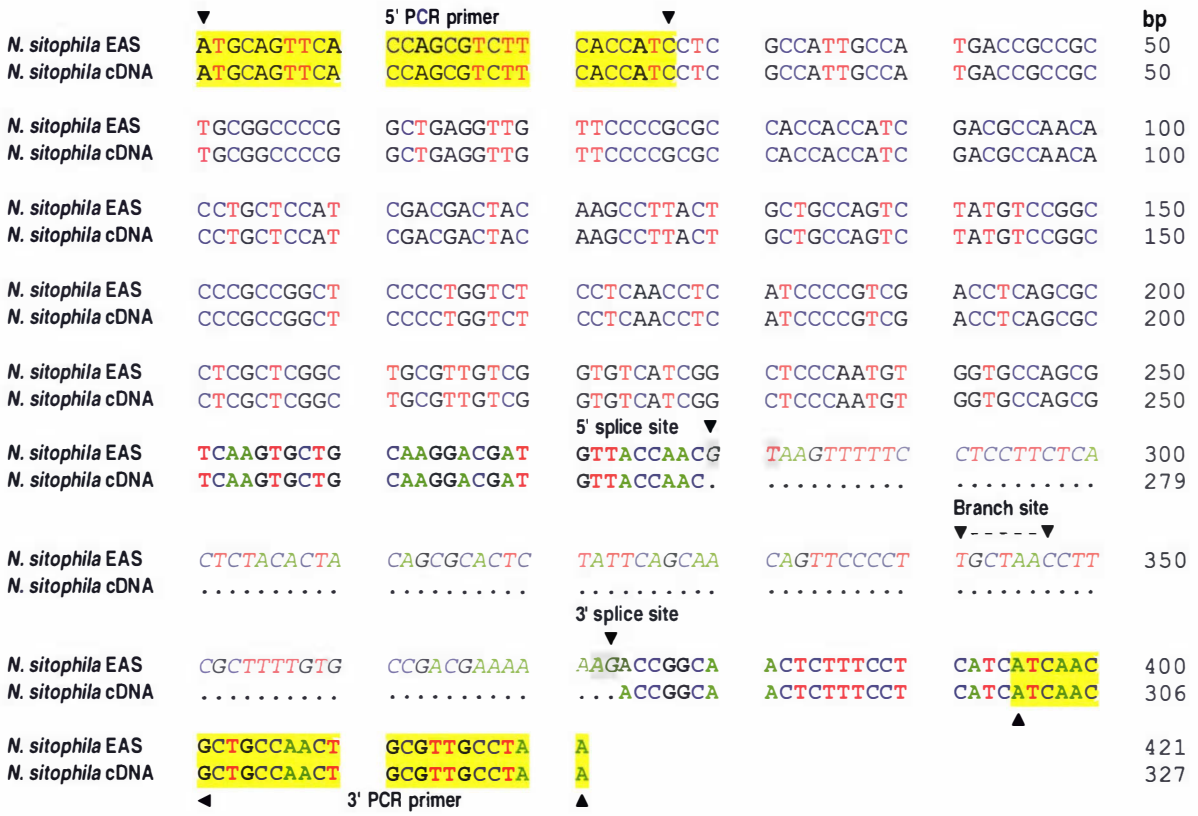

The sequences of the cDNA and endogenous *eas* genes from *N. sitophila* are aligned in this diagram. Positions of the PCR primers used to amplify the sequence as described in section 2.2.3 are shown with a yellow background. The putative intron splice sites in the gene are shown with a grey background. As can be seen from this comparison with cDNA, the intron is spliced from the gene as predicted.

APPENDIX IIIE.

MYCELIUM HYDROPHOBICITY TEST RESULTS.

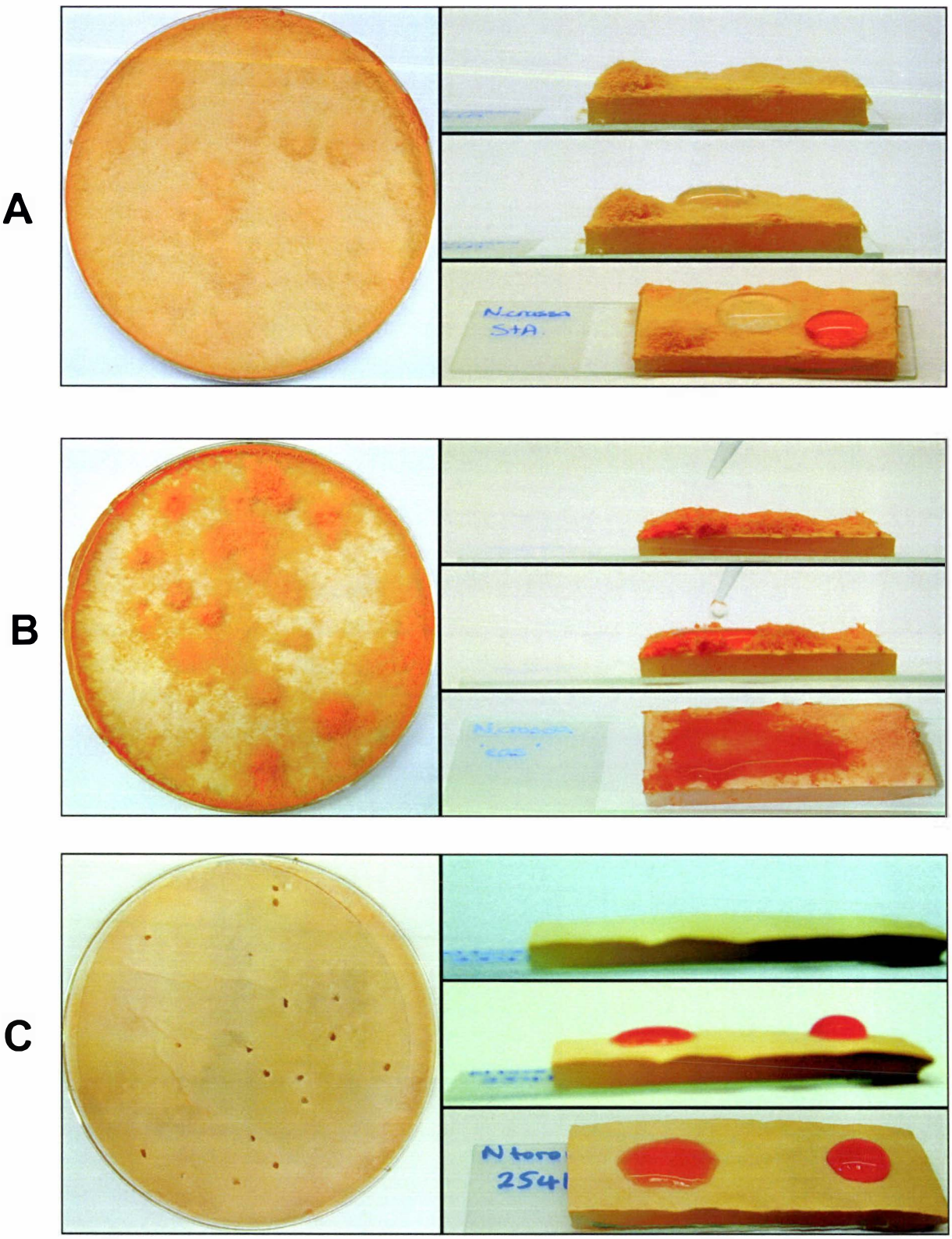

Petri-plates containing conidiating cultures of (A) wild-type *N. crassa* strain STA4 (B) mutant *N. crassa* strain *eas* and (C) *N. toroi* photographed growing on sucrose-enriched Vogel's N agar. The sequences of images on the right-hand side show the results of a qualitative wettability assay described in section 2.3 on each sample. These results are discussed in section 3.4.1

MYCELIUM HYDROPHOBICITY TEST RESULTS CONTINUED…

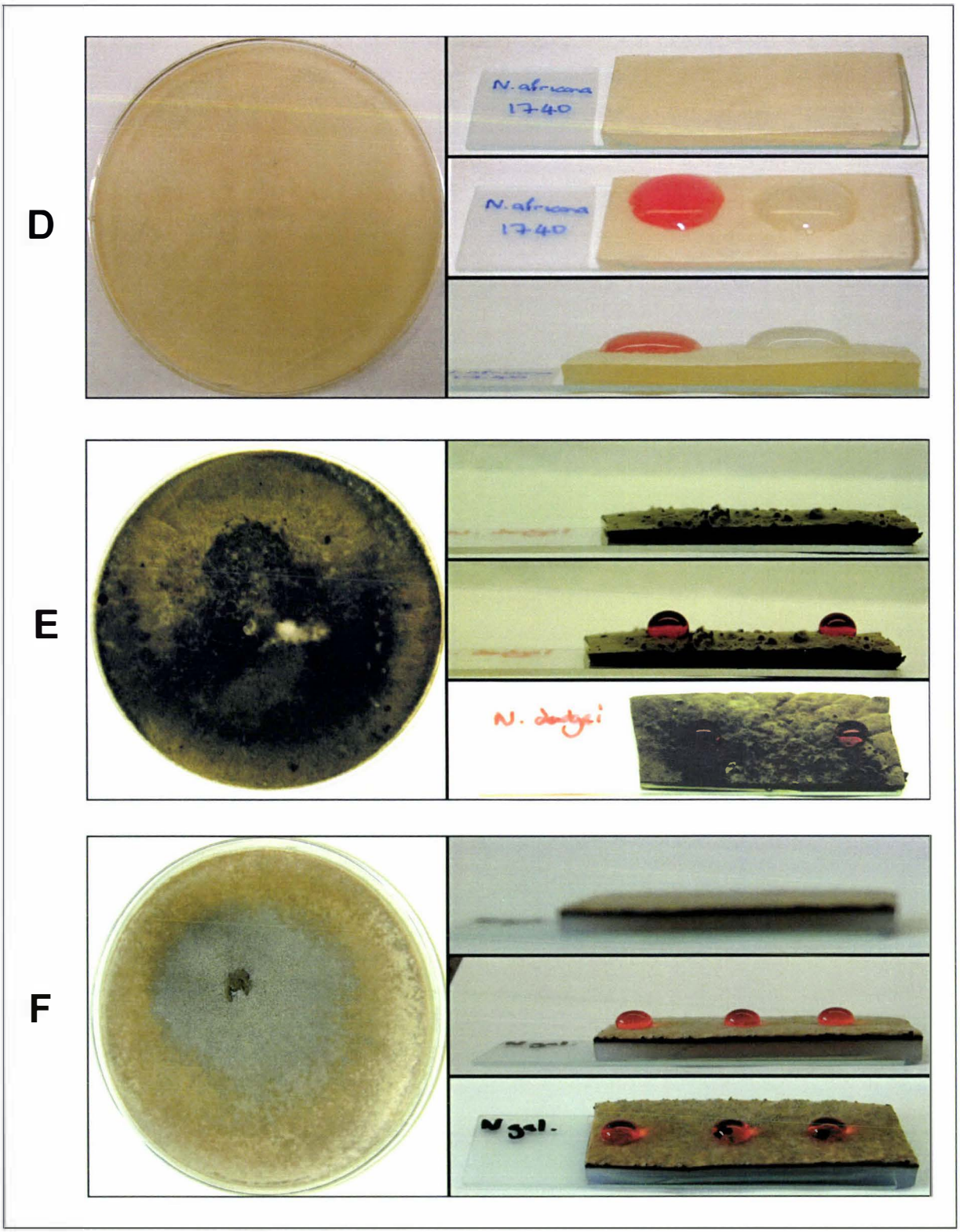

Petri-plates containing conidiating cultures of (D) *N. africana*, (E) *N. dodgei*, and (F) *N. galapagosensis* photographed growing on sucrose-enriched Vogel's N agar. The sequences of images on the right-hand side show the results of a qualitative wettability assay described in section 2.3 on each sample. These results are discussed in section 3.4.1.

MYCELIUM HYDROPHOBICITY TEST RESULTS CONTINUED...

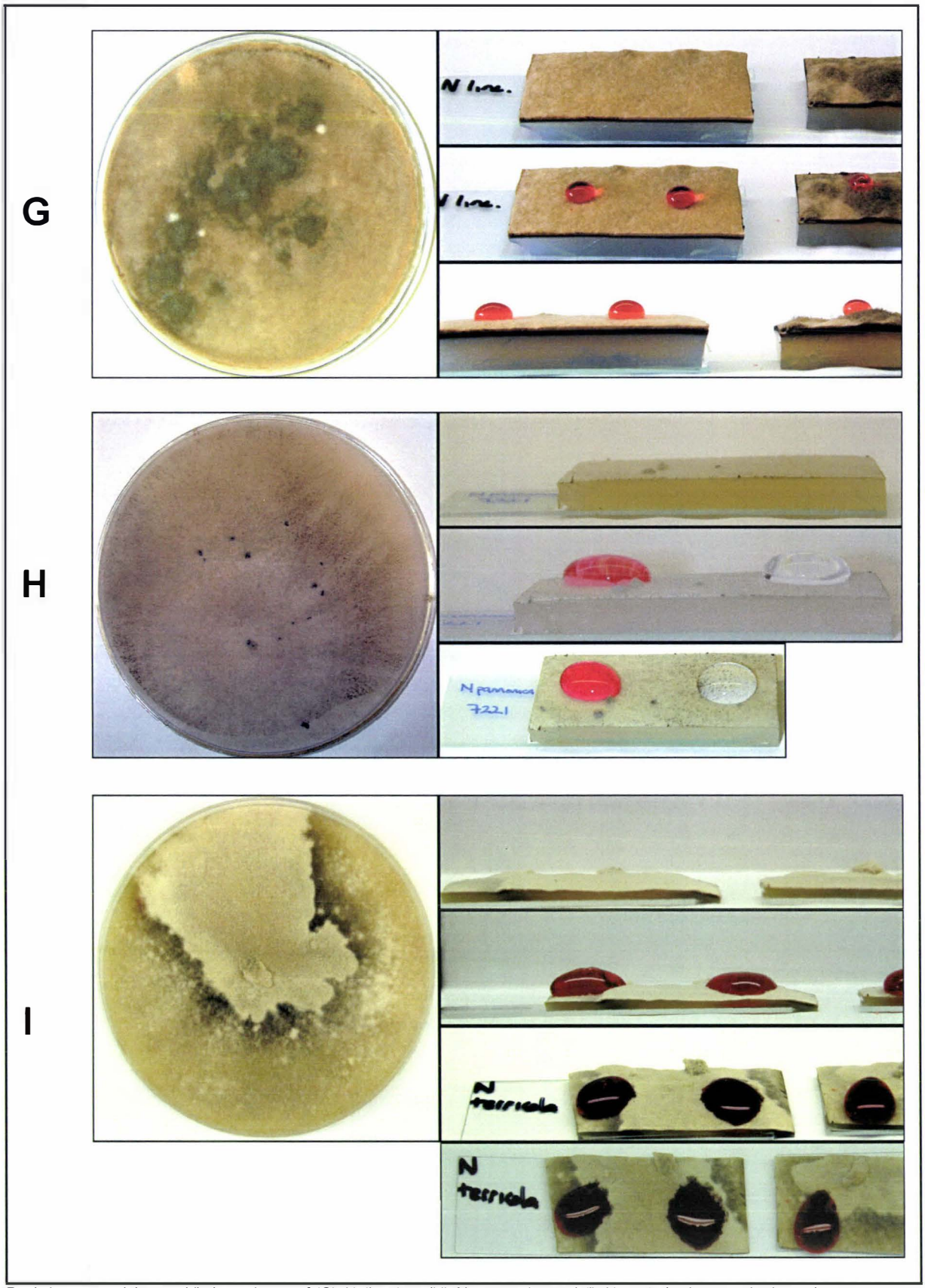

Petri-plates containing conidiating cultures of (G) *N. lineolata*, (H) *N. pannonica* and (I) *N. terricola* photographed growing on sucrose-enriched Vogel's N agar. The sequences of images on the right-hand side show the results of a qualitative wettability assay described in section 2.3 on each sample. Lowest left-hand image of (I) shows the effect of letting the liquid sit on distinct areas of *N. terricola* mycelium for ~5 min. These results are discussed in section 3.4.1.

APPENDIX IIIF.

HYDROPHATHY PLOTS.

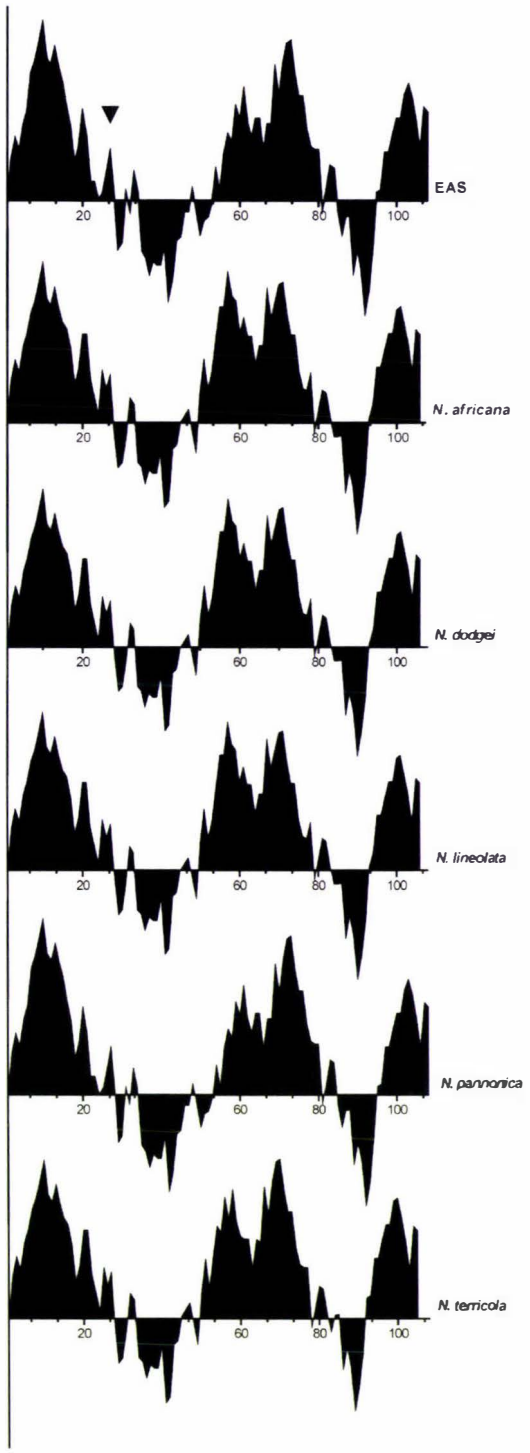

The hydropathy patterns of the proteins predicted to arise from *eas* genes found in non-conidial *Neurospora* species (see section 3.4). These patterns are aligned for comparison to show their similarity with the actual pattern derived from EAS (top pattern). Hydropathy patterns were determined using the parameters of Kyte and Doolittle (1982). This system assigns an arbitrary value for the side-chain of each amino acid in a protein sequence. A positive value is given to hydrophobic side-chains, negative to hydrophilic and these values are plotted against the Y-axis. The position of the amino acid in the sequence is plotted against the X-axis. The arrow indicates the approximate position of the N-terminus of the isoforms of EAS.

APPENDIX IIIG.

RT-PCR DETECTION OF *EAS* MRNA #1.

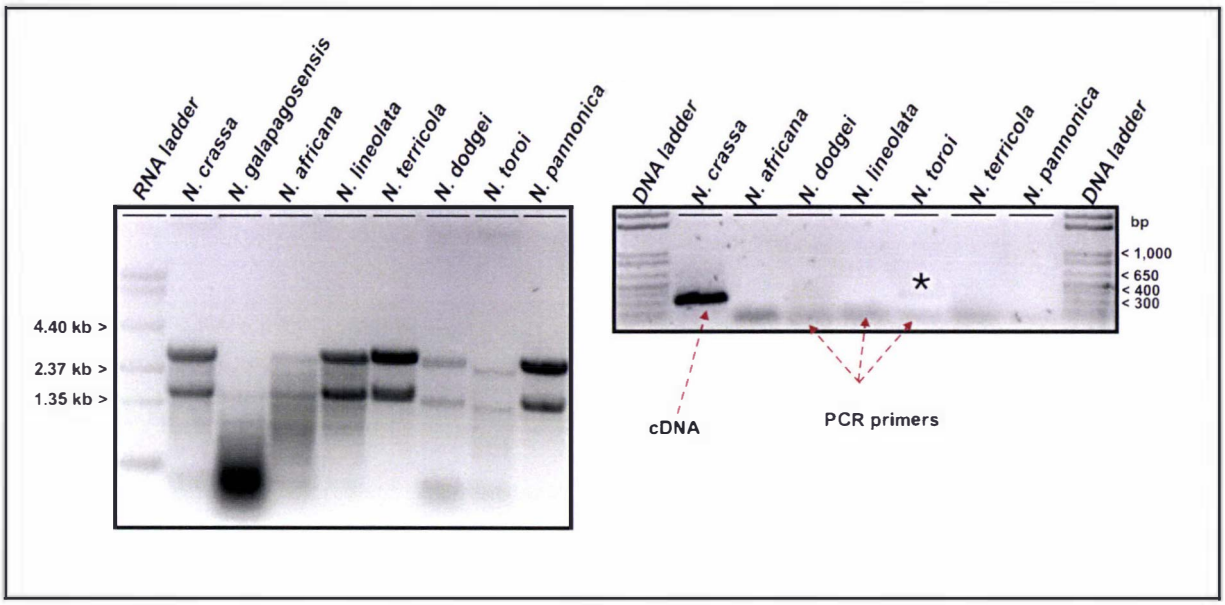

Upper Panel: The results of an attempt detect transcription of *eas* genes in aconidiate *Neurospora* species by RT-PCR amplification. The left image shows the electrophoretically separated total RNA extracts from each species used as templates for the 1st strand amplification reaction (as described in section 2.2.3.1). Right image: electrophoretically separated products of the second strand RT-PCR amplification using *eas* specific primers. Products corresponding to 320 bp *eas* cDNA were amplified from *N. crassa* and *N. toroi* total RNA extracts. Asterisk indicates the position of the 320 bp product from the *N. toroi* sample. Bands less that 100 bp in size are residual PCR primers remaining from the 2nd strand RT-PCR reaction.

RT-PCR DETECTION OF *EAS* MRNA #2

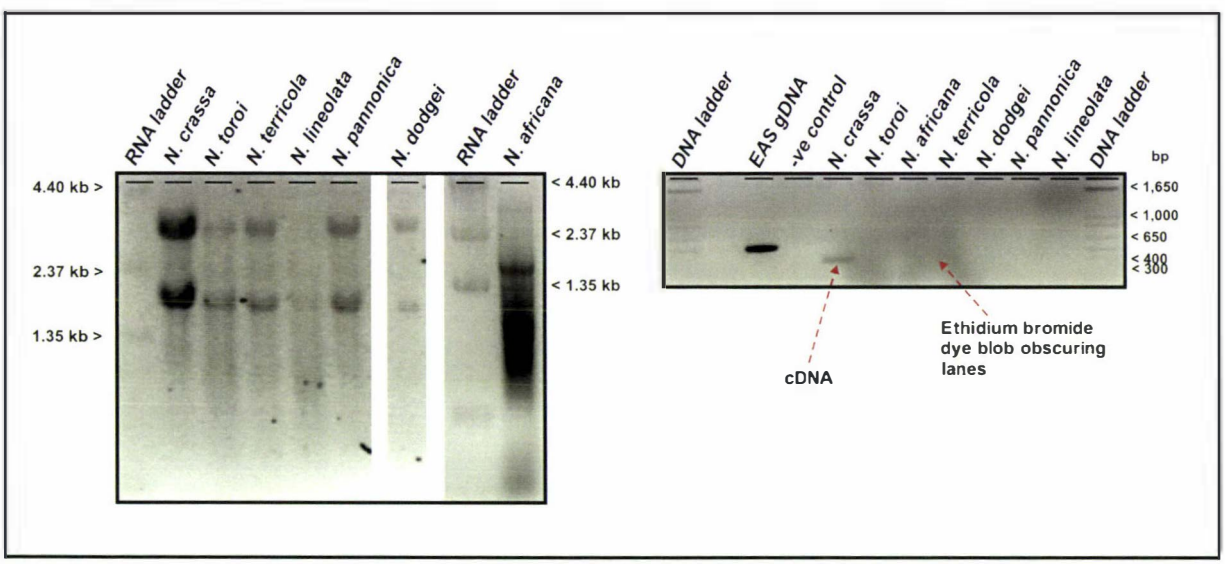

Lower Panel: The results of an attempt detect transcription of *eas* genes in aconidial *Neurospora* species by RT-PCR amplification. The left image shows the electrophoretically separated total RNA extracts from each species used as templates for the 1st strand amplification reaction (as described in section 2.2.3.1). Right image: electrophoretically separated products of the second strand RT-PCR amplification using *eas* specific primers. Products corresponding to 320 bp *eas* cDNA were amplified from *N. crassa.* Results of the second strand reaction are obscured in some lanes by a dye blob seen after staining with ethidium bromide. Note however that the 420 bp products seen in Figure 29 are absent. This is further evidence those bands were caused by chance amplification of genomic DNA contaminating the template.

APPENDIX IV – SUPPLEMENTARY DATA FOR CHAPTER 4.

RP-HPLC ELUTION PROFILES: TFA SOLUBLE COMPONENTS OF RECOMBINANT *PICHIA* GROWTH MEDIA.

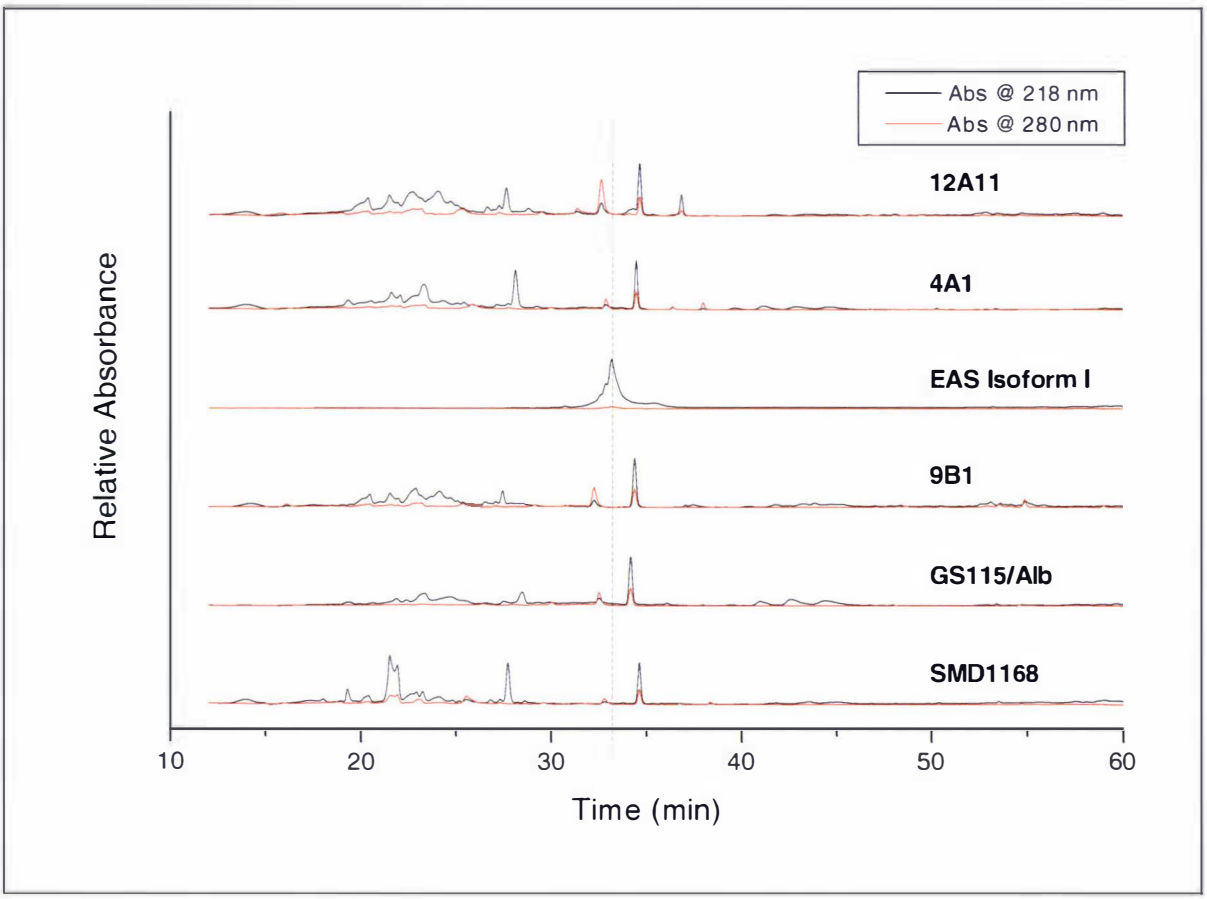

Appendix IV: RP-HPLC elution profiles of TFA soluble extracts from the growth media of recombinant *P. pastoris* strains are compared to the elution profile of wild-type EAS isoforms Ia and Ib obtained from (section 4.1.1, p 99). The grey dotted line indicates approximate retention times for these isoforms **Note:** The absorbance data for each profile was transformed to a dimensionless scale between 0 and 1. The largest absorbance datum in the 218 nm profiles for each sample was determined and the absorbance data in both 218 nm and 280 nm profiles was transformed into a fraction of that value.

The proteins responsible for the unique peaks in the elution profiles of the TFA-soluble extracts from recombinant *Pichia* growth media are unlikely to be the recombinant EAS they are strains. The figure compares the relative absorbance of UV-light at 218 nm and 280 nm for each fractionated sample. EAS absorbs 280 nm UV-light weakly (compare the absorbance at 218 nm) because it contains only one aromatic amino acid (Tyr_{16}) residue). This is not the case for the TFA-soluble compounds eluted from the growth media extracts thus these are unlikely to be due to the recombinant EAS protein.

APPENDIX V – SUPPLEMENTARY DATA FOR CHAPTER 5.

APPENDIX VA.
PREDICTED PEPTIDE STRUCTURES RESULTING FROM THE AMMONIA CATALYSED CLEAVAGE OF REDUCED AND S-CYANYLATED EAS ISOFORMS.

(A1) EAS SEQUENCE AND REACTION MECHANISM.

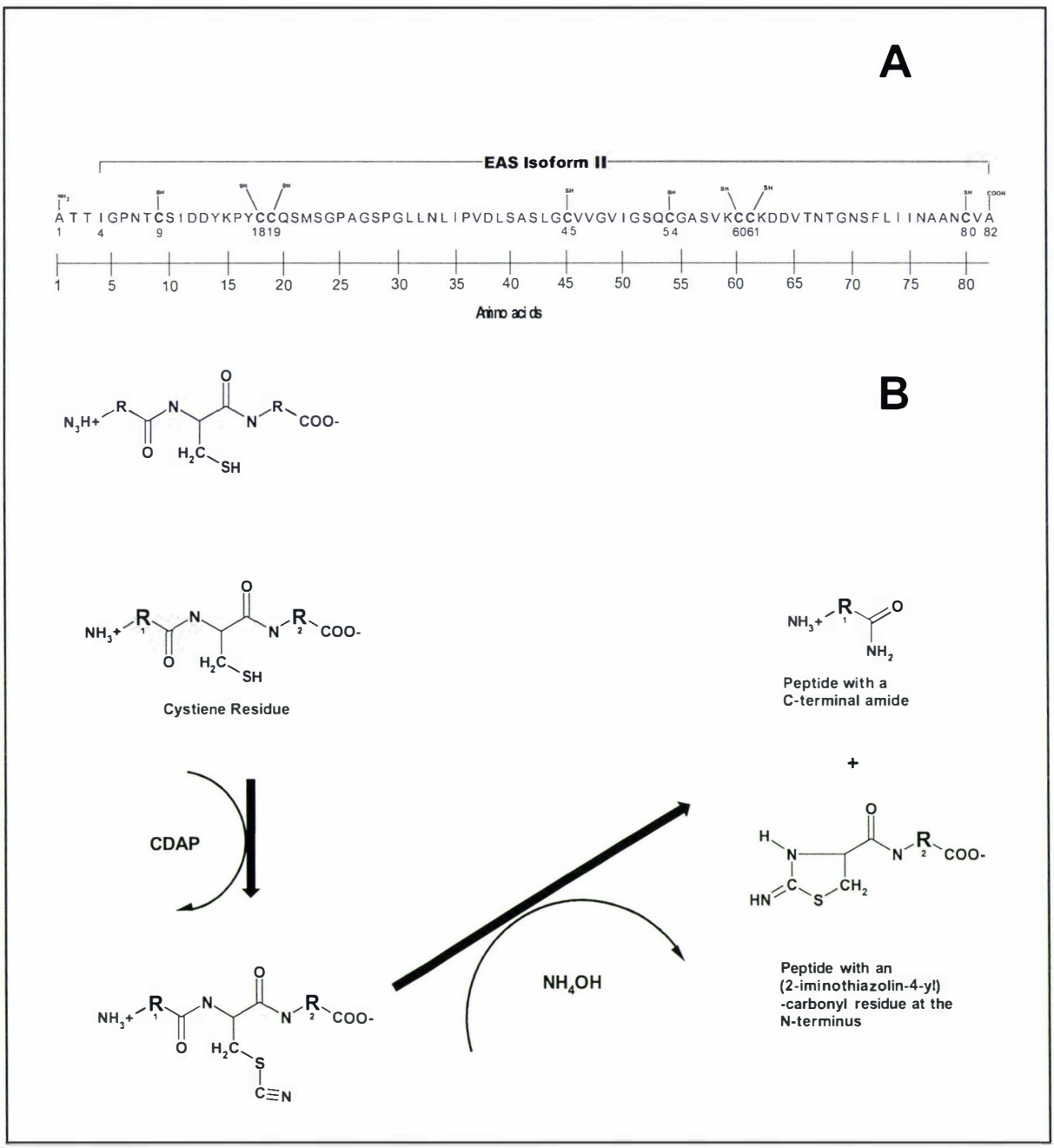

A: Amino acid sequence of EAS isoforms I and II. B: In the disulfide-mapping protocol proposed by Wu and Watson (1997), nascent sulfhydryl groups on the cysteine residues are cyanylated in acidic conditions by 1-cyano-4-dimethylamino-pyridinium tetrafluoroborate (CDAP). The addition of ammonia catalyses the cleavage of the peptide bond adjacent to the S-cyanylated residue resulting in one peptide with a C-terminal amide and another with the S-cyanylated cysteine residue replaced with an (2-iminothiazonlin-4-yl)-carbonyl residue (Nakagawa *et al.*, 1994; Wu *et al.*, 1996; Wu and Watson, 1998).

(A2) The Structures and m/z values Resulting From the Cleavage of EAS Proteins at the Designated Cysteine Pairs.

Cys9-Cys18

Isoform Ia(b)		Isoform II a(b)
772.86 (788.86) Da	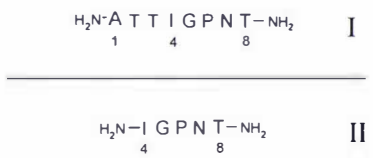	499.57 (515.57) Da
1127.25 (1143.25) Da		1127.25 (1143.25) Da
6370.44 (6386.44) Da	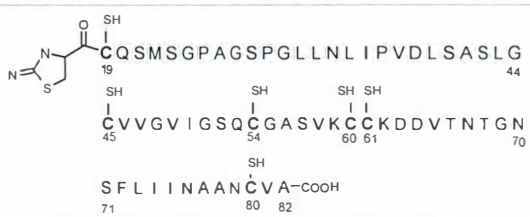	6370.44 (6386.44) Da

Cys9-Cys19

Isoform Ia(b)		Isoform II a(b)
772.86 (788.86) Da	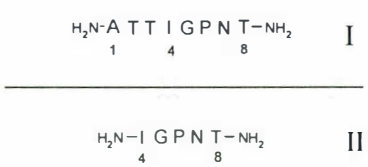	499.57 (515.57) Da
1230.39 (1246.39) Da	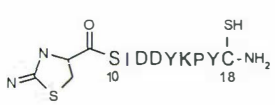	1230.39 (1246.39) Da
6267.30 (6283.30) Da		6267.30 (6283.30) Da

The structure of fragments unique to the cleavage of EAS isoform I or II are indicated by I or II respectively. The m/z values of peptides resulting from isoform Ib and IIb are bracketed.

(A3) The Structures and m/z values Resulting From the Cleavage of EAS Proteins at the Designated Cysteine Pairs.

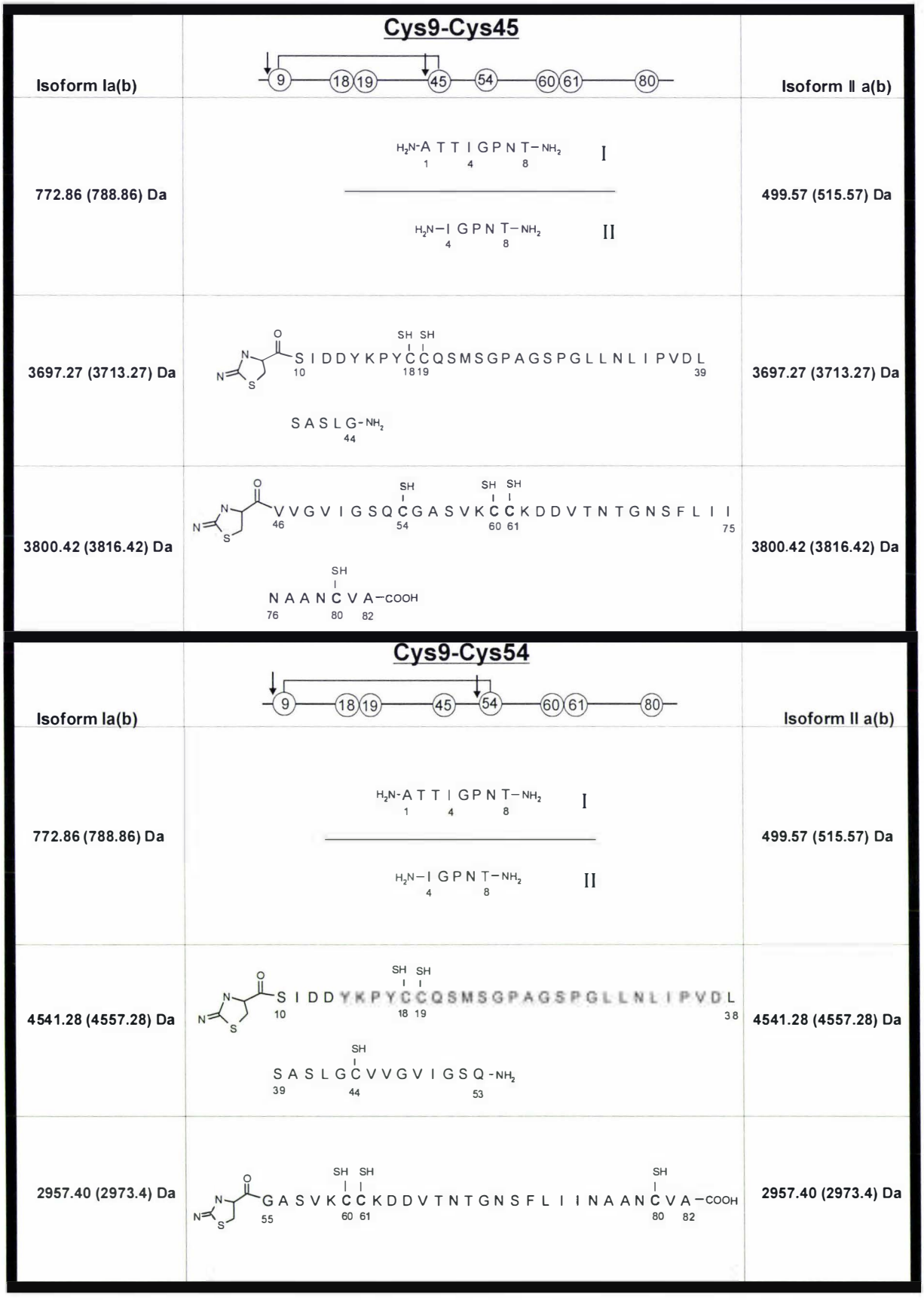

The structure of fragments unique to the cleavage of EAS isoform I or II are indicated by I or II respectively. The m/z values of peptides resulting from isoform Ib and IIb are bracketed.

(A4) The Structures and m/z values Resulting From the Cleavage of EAS Proteins at the Designated Cysteine Pairs.

Cys9-Cys60

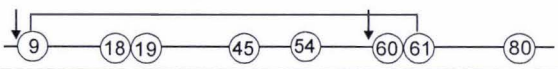

Isoform Ia(b)		Isoform II a(b)
772.86 (788.86) Da	H_2N-A T T I G P N T-NH_2 (I) ——— H_2N-I G P N T-NH_2 (II)	499.57 (515.57) Da
5086.94 (5086.94) Da	S I D D Y K P Y C C Q S M S G P A G S P G L L N L I P V D L 10 18 19 39 S A S L G C V V G V I G S Q C G A S V K-NH_2 45 54 59	5086.94 (5086.94) Da
2411.74 (3427.74) Da	C K D D V T N T G N S F L I I N A A N C V A-COOH 61 80 82	2411.74 (3427.74) Da

Cys9-Cys61

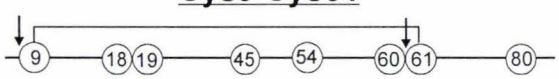

Isoform Ia(b)		Isoform II a(b)
772.86 (788.86) Da	H_2N-A T T I G P N T-NH_2 (I) ——— H_2N-I G P N T-NH_2 (II)	499.57 (515.57) Da
5189.12 (5205.12) Da	S I D D Y K P Y C C Q S M S G P A G S P G L L N L I P V D L 10 18 19 39 S A S L G C V V G V I G S Q C G A S V K C-NH_2 62	5189.12 (5205.12) Da
2308.59 (2324.59) Da	K D D V T N T G N S F L I I N A A N C V A-COOH 62 80 82	2308.59 (2324.59) Da

The structure of fragments unique to the cleavage of EAS isoform I or II are indicated by I or II respectively. The m/z values of peptides resulting from isoform Ib and IIb are bracketed.

(A5) The Structures and m/z values Resulting From the Cleavage of EAS Proteins at the Designated Cysteine Pairs.

Cys9-Cys80

Isoform Ia(b)		Isoform II a(b)
772.86 (788.86) Da		499.57 (515.57) Da
7181.33 (7197.33) Da	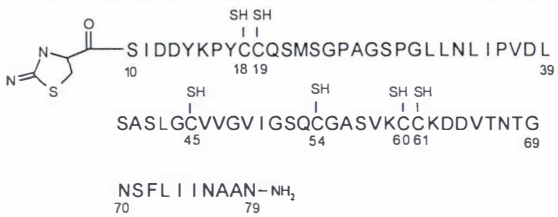	7181.33 (7197.33) Da
316.38 (334.38) Da	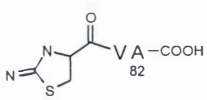	316.38 (334.38) Da

Cys18-Cys19

Isoform Ia(b)		Isoform II a(b)
1857.08 (1873.08) Da		1583.79 (1599.79) Da
145.18 (145.18) Da	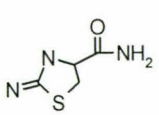	145.18 (145.18) Da
6267.30 (6283.30) Da		6267.30 (6283.30) Da

The structure of fragments unique to the cleavage of EAS isoform I or II are indicated by I or II respectively. The m/z values of peptides resulting from isoform Ib and IIb are bracketed.

(A6) The Structures and m/z values Resulting From the Cleavage of EAS Proteins at the Designated Cysteine Pairs.

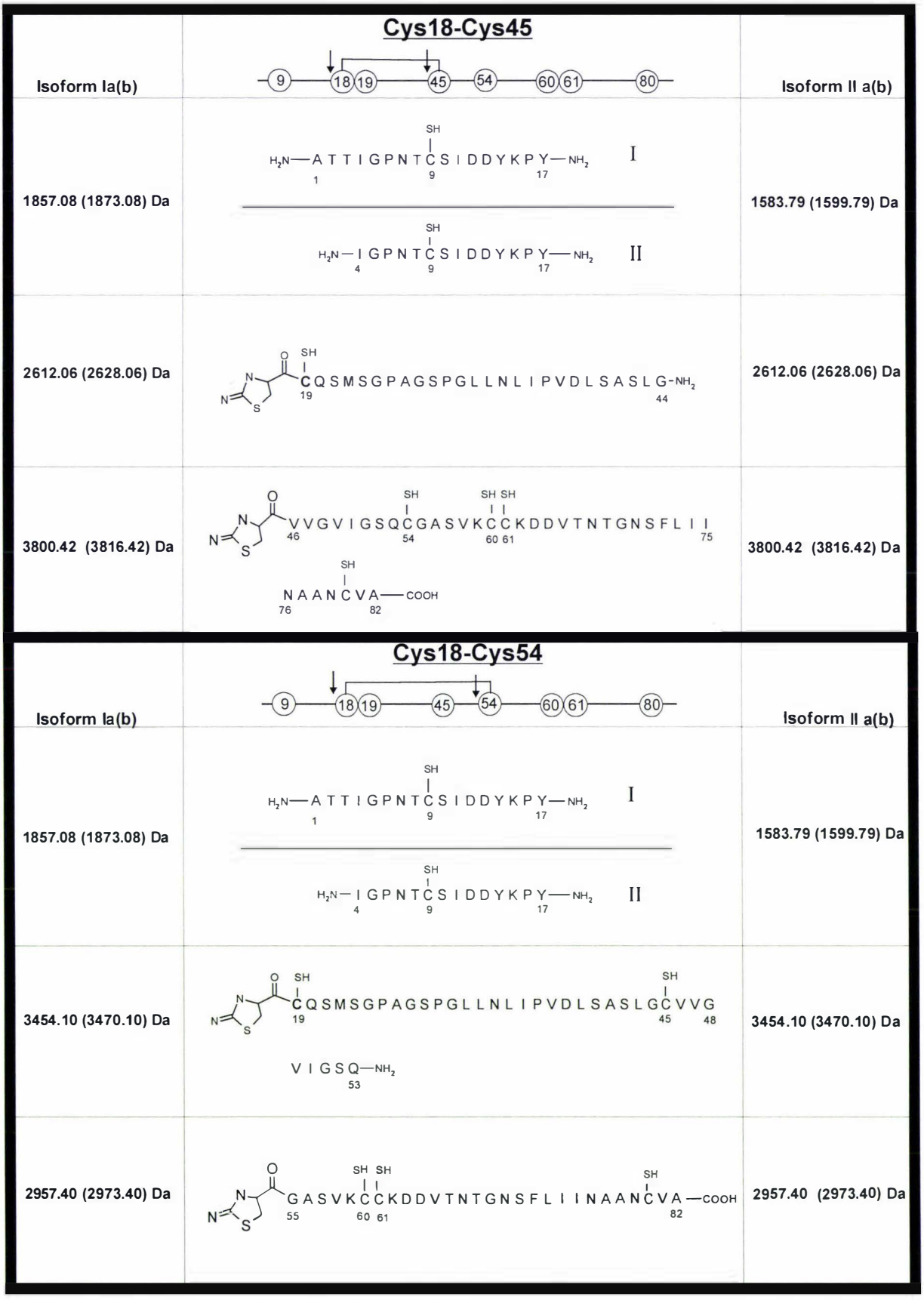

The structure of fragments unique to the cleavage of EAS isoform I or II are indicated by I or II respectively. The m/z values of peptides resulting from isoform Ib and IIb are bracketed.

(A7) The Structures and m/z values Resulting From the Cleavage of EAS Proteins at the Designated Cysteine Pairs.

Isoform Ia(b)	**Cys18-Cys60** 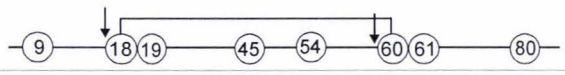	Isoform II a(b)
1857.08 (1873.08) Da		1583.79 (1599.79) Da
4000.77 (4016.77) Da	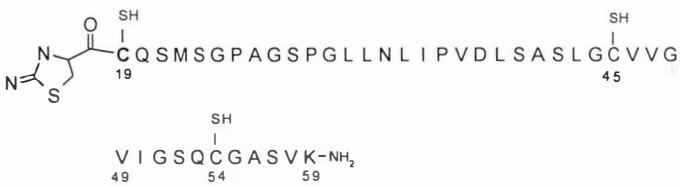	4000.77 (4016.77) Da
2411.74 (2427.74) Da		2411.74 (2427.74) Da

Isoform Ia(b)	**Cys18-Cys61** 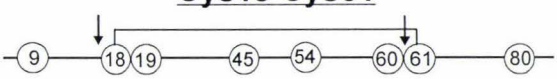	Isoform II a(b)
1857.08 (1873.08) Da	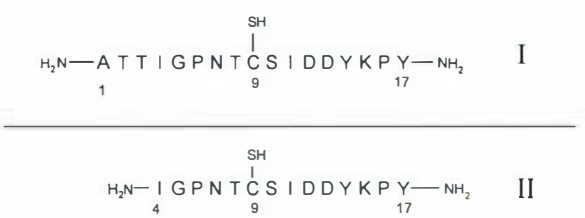	1583.79 (1599.79) Da
4103.91 (4119.91) Da	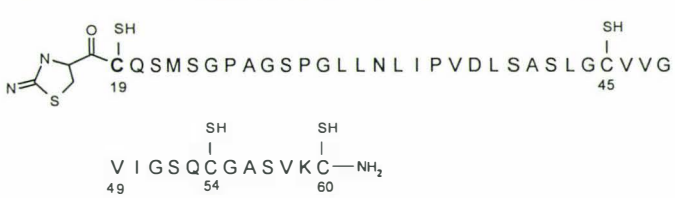	4103.91 (4119.91) Da
2308.59 (2324.59) Da		2308.59 (2324.59) Da

The structure of fragments unique to the cleavage of EAS isoform I or II are indicated by I or II respectively. The m/z values of peptides resulting from isoform Ib and IIb are bracketed.

(A8) The Structures and m/z values Resulting From the Cleavage of EAS Proteins at the Designated Cysteine Pairs.

Isoform Ia(b)	Cys18-Cys80	Isoform II a(b)
	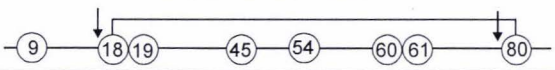	
1857.08 (1873.08) Da		1583.79 (1599.79) Da
6097.09 (6113.09) Da	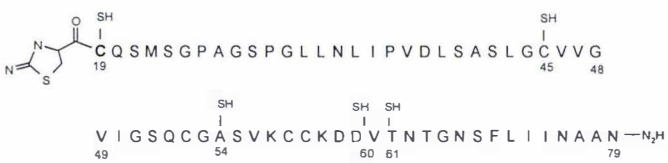	6097.09 (6113.09) Da
316.38 (334.38) Da	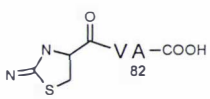	316.38 (334.38) Da

Isoform Ia(b)	Cys19-Cys45	Isoform II a(b)
	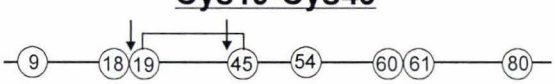	
1961.21 (1977.21) Da	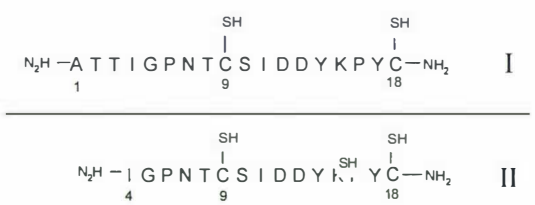	1687.92 (1703.92) Da
2508.92 (2524.92) Da		2508.92 (2524.92) Da
3800.42 (3816.42) Da	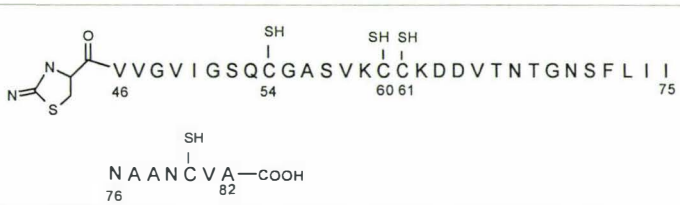	3800.42 (3816.42) Da

The structure of fragments unique to the cleavage of EAS isoform I or II are indicated by I or II respectively. The m/z values of peptides resulting from isoform Ib and IIb are bracketed.

(A9) The Structures and m/z values Resulting From the Cleavage of EAS Proteins at the Designated Cysteine Pairs.

Isoform Ia(b)	Cys19-Cys54	Isoform II a(b)
	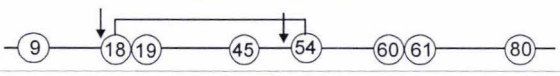	
1961.21 (1977.21) Da		1687.92 (1703.92) Da
3351.94 (3367.94) Da		3351.94 (3367.94) Da
2957.40 (2973.40) Da		2957.40 (2973.40) Da

Isoform Ia(b)	Cys19-Cys60	Isoform II a(b)
	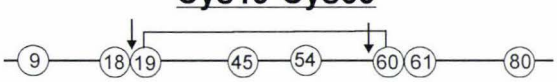	
1961.21 (1977.21) Da	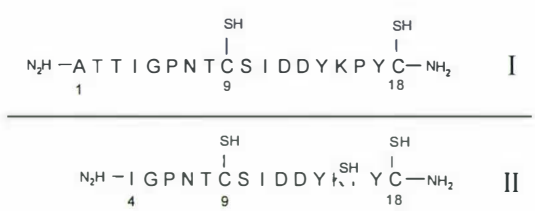	1687.92 (1703.92) Da
3897.60 (3913.60) Da		3897.60 (3913.60) Da
2411.74 (2411.74) Da		2411.74 (2411.74) Da

The structure of fragments unique to the cleavage of EAS isoform I or II are indicated by I or II respectively. The m/z values of peptides resulting from isoform Ib and IIb are bracketed.

(A10) The Structures and m/z values Resulting From the Cleavage of EAS Proteins at the Designated Cysteine Pairs.

<table>
<tr><td>Isoform Ia(b)</td><td>Cys19-Cys61
 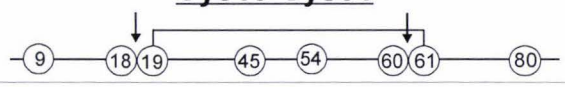 </td><td>Isoform II a(b)</td></tr>
<tr><td>1961.21 (1977.21) Da</td><td> 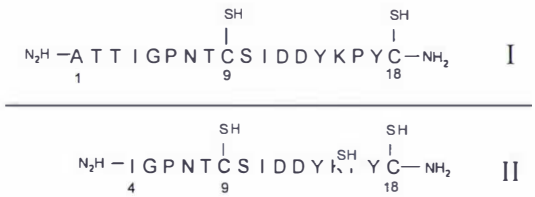 </td><td>1687.92 (1703.92) Da</td></tr>
<tr><td>4000.75 (4016.75) Da</td><td> 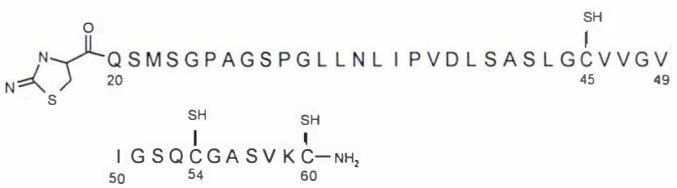 </td><td>4000.75 (4016.75) Da</td></tr>
<tr><td>2308.59 (2324.59) Da</td><td>  </td><td>2308.59 (2324.59) Da</td></tr>
<tr><td>Isoform Ia(b)</td><td>Cys19-Cys80
 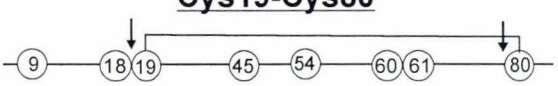 </td><td>Isoform II a(b)</td></tr>
<tr><td>1961.21 (1977.21) Da</td><td> 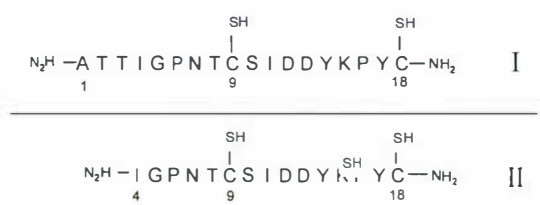 </td><td>1687.92 (1703.92) Da</td></tr>
<tr><td>5993.94 (6009.94) Da</td><td> 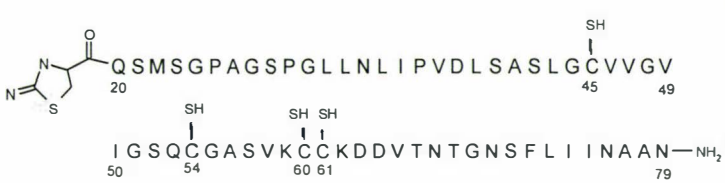 </td><td>5993.94 (6009.94) Da</td></tr>
<tr><td>316.38 (334.38) Da</td><td> 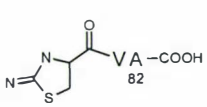 </td><td>316.38 (332.38) Da</td></tr>
</table>

The structure of fragments unique to the cleavage of EAS isoform I or II are indicated by I or II respectively. The m/z values of peptides resulting from isoform Ib and IIb are bracketed.

(A11) The Structures and m/z values Resulting From the Cleavage of EAS Proteins at the Designated Cysteine Pairs.

Isoform Ia(b)	Cys45-Cys54	Isoform II a(b)
	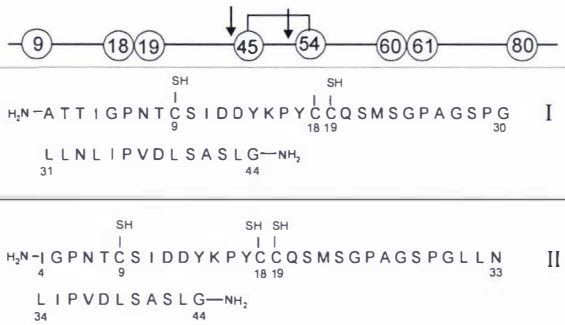	
4428.11 (4444.11) Da		4154.82 (4170.82) Da
885.06 (901.06) Da		885.06 (901.06) Da
2957.40 (2973.40) Da		2957.40 (2973.40) Da

Isoform Ia(b)	Cys45-Cys60	Isoform II a(b)
	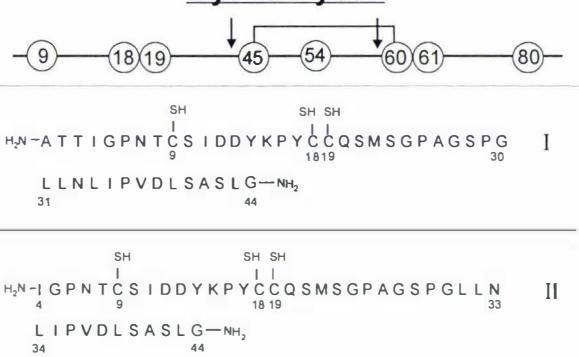	
4428.11 (4444.11) Da		4154.82 (4170.82) Da
1430.72 (1446.72) Da		1430.72 (1446.72) Da
2411.74 (2411.74) Da		2411.74 (2411.74) Da

The structure of fragments unique to the cleavage of EAS isoform I or II are indicated by I or II respectively. The m/z values of peptides resulting from isoform Ib and IIb are bracketed.

(A12) The Structures and m/z values Resulting From the Cleavage of EAS Proteins at the Designated Cysteine Pairs.

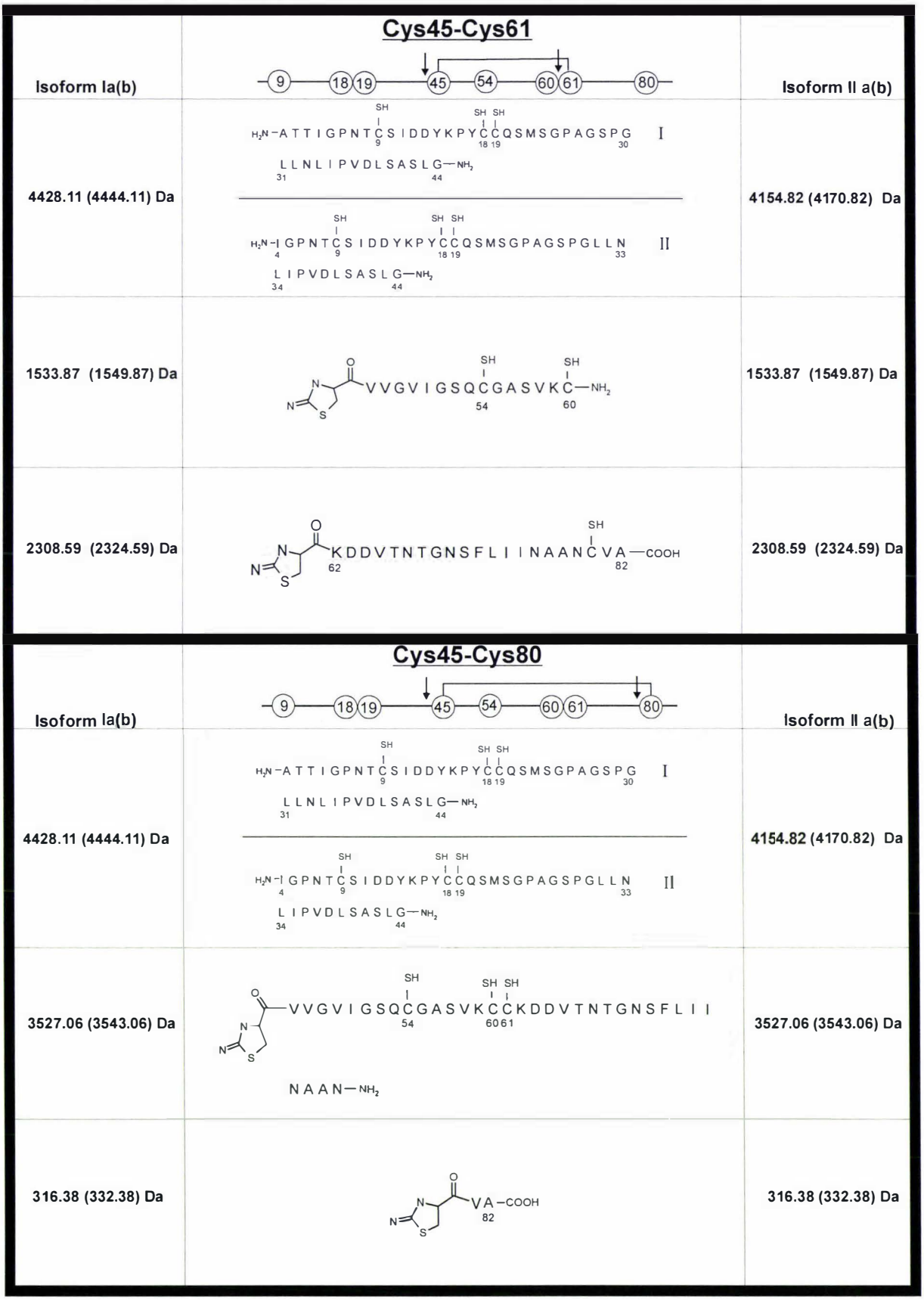

The structure of fragments unique to the cleavage of EAS isoform I or II are indicated by I or II respectively. The m/z values of peptides resulting from isoform Ib and IIb are bracketed.

(A13) The Structures and m/z values Resulting From the Cleavage of EAS Proteins at the Designated Cysteine Pairs..

Cys54-Cys60

Isoform Ia(b)		Isoform II a(b)
5270.13 (5286.13) Da		4996.84 (5012.84) Da
587.70 (603.70) Da	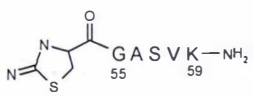	587.70 (603.70) Da
2411.74 (2427.74) Da		2411.74 (2427.74) Da

Cys54-Cys61

Isoform Ia(b)		Isoform II a(b)
5270.13 (5286.13) Da	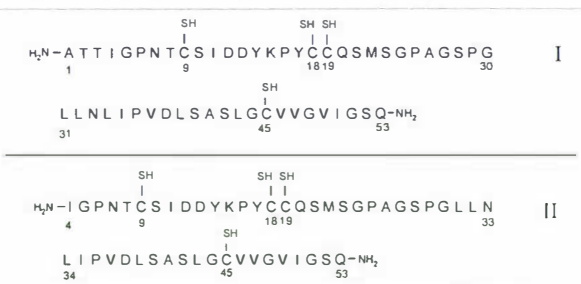	4996.84 (5012.84) Da
690.85 (706.85) Da	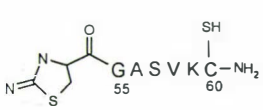	690.85 (706.85) Da
2308.59 (2324.59) Da		2308.59 (2324.59) Da

The structure of fragments unique to the cleavage of EAS isoform I or II are indicated by I or II respectively. The m/z values of peptides resulting from isoform Ib and IIb are bracketed.

(A14) The Structures and m/z values Resulting From the Cleavage of EAS Proteins at the Designated Cysteine Pairs.

Cys54-Cys60

Isoform Ia(b)		Isoform II a(b)
5270.13 (5286.13) Da		4996.84 (5012.84) Da
2684.04 (2700.04) Da		2684.04 (2700.04) Da
316.38 (334.38) Da	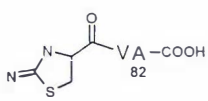	316.38 (334.38) Da

Cys60-Cys61

Isoform Ia(b)		Isoform II a(b)
5815.79 (5831.79) Da	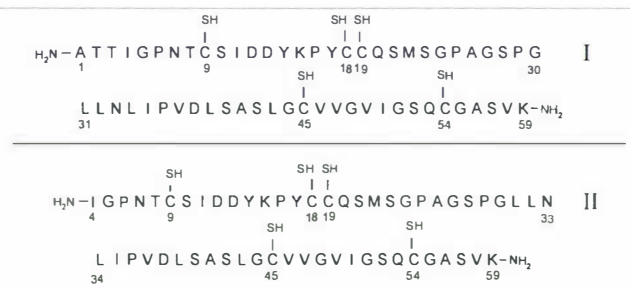	5542.5 (5558.5) Da
145.18 (145.18) Da	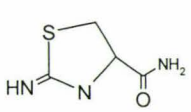	145.18 (145.18) Da
2308.59 (2324.59) Da		2308.59 (2324.59) Da

The structure of fragments unique to the cleavage of EAS isoform I or II are indicated by I or II respectively. The m/z values of peptides resulting from isoform Ib and IIb are bracketed.

(A15) The Structures and m/z values Resulting From the Cleavage of EAS Proteins at the Designated Cysteine Pairs.

Cys60-Cys80

Isoform Ia(b)		Isoform II a(b)
5815.79 (5831.79) Da		5542.50 (5558.50) Da
2138.38 (2154.38) Da		2138.38 (2154.38) Da
316.38 (332.38) Da	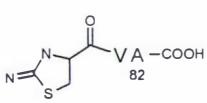	316.38 (332.38) Da

Cys61-Cys80

Isoform Ia(b)		Isoform II a(b)
5919.29 (5935.29) Da		5646.63 (5662.63) Da
2035.24 (2051.24) Da		2035.24 (2051.24) Da
316.38 (332.38) Da	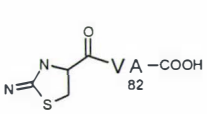	316.38 (332.38) Da

The structure of fragments unique to the cleavage of EAS isoform I or II are indicated by I or II respectively. The m/z values of peptides resulting from isoform Ib and IIb are bracketed.

(A16) The Structures and m/z Values Resulting from β-elimination Reactions.

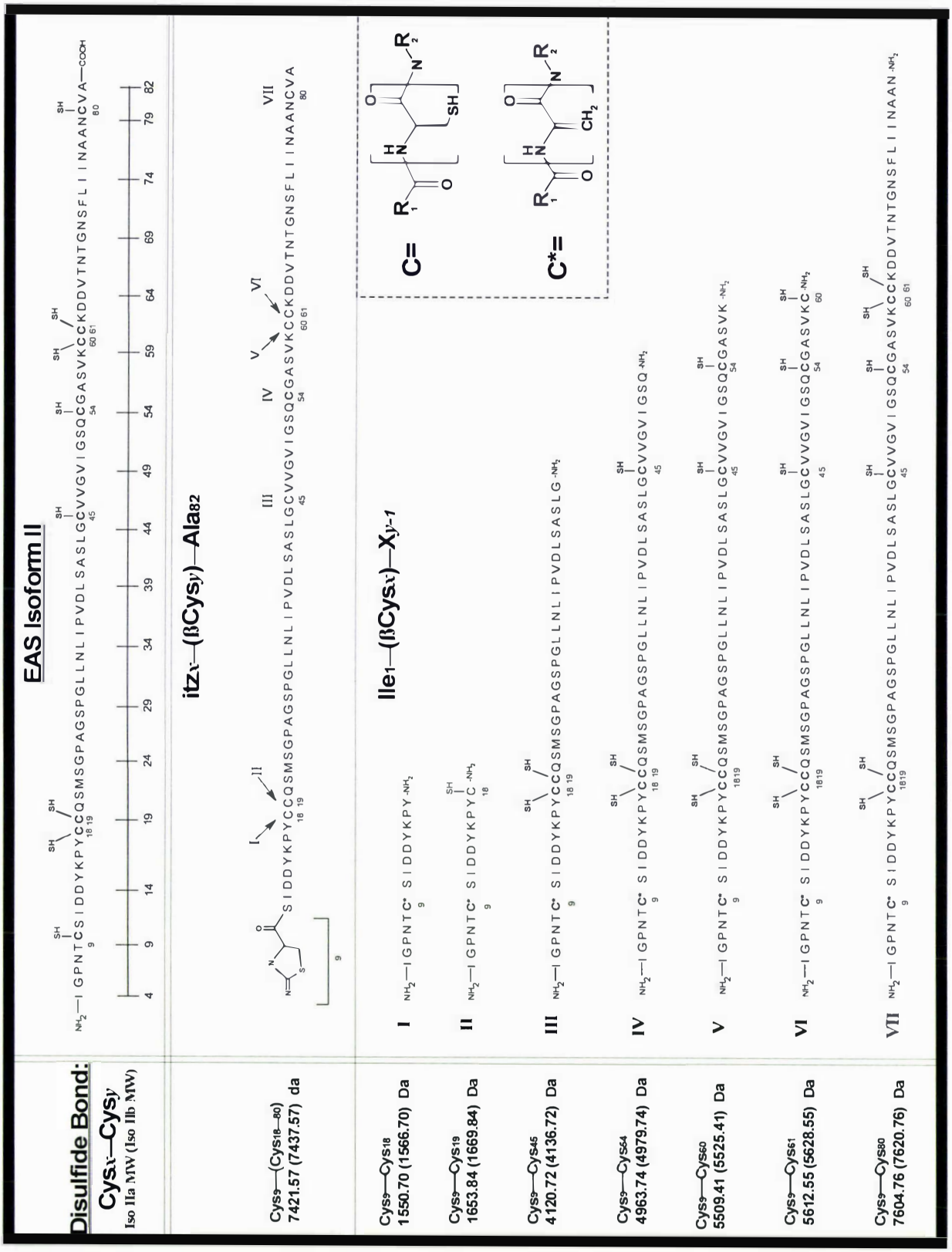

The β-elimination can occur at either cyanylated cysteine residue and removes the SCN-group leaving the peptide bond intact (See inset. Modified residues are designated C* or are assigned a roman numeral). Thus a pairs of peptides may result. One will have an N-terminal iminothiazolidinyl carboxyl residue, the other a C-terminal amide (if NH_4OH is used). The sequence of each peptide depends on the original disulfide linkages because only linked cysteines are cyanylated in this experiment. The pairs of peptides that are predicted to result from β-elimination are indicated with roman numerals. The different iminothiazolidinyl carboxyl terminated peptides have the same molecular mass but the position of the modified cysteine in each case is indicated by Roman numeral that corresponds to the amide terminated peptide that will form when the designated pairs of cysteines are linked.

(A17) The Structures and m/z Values Resulting from β-elimination Reactions.

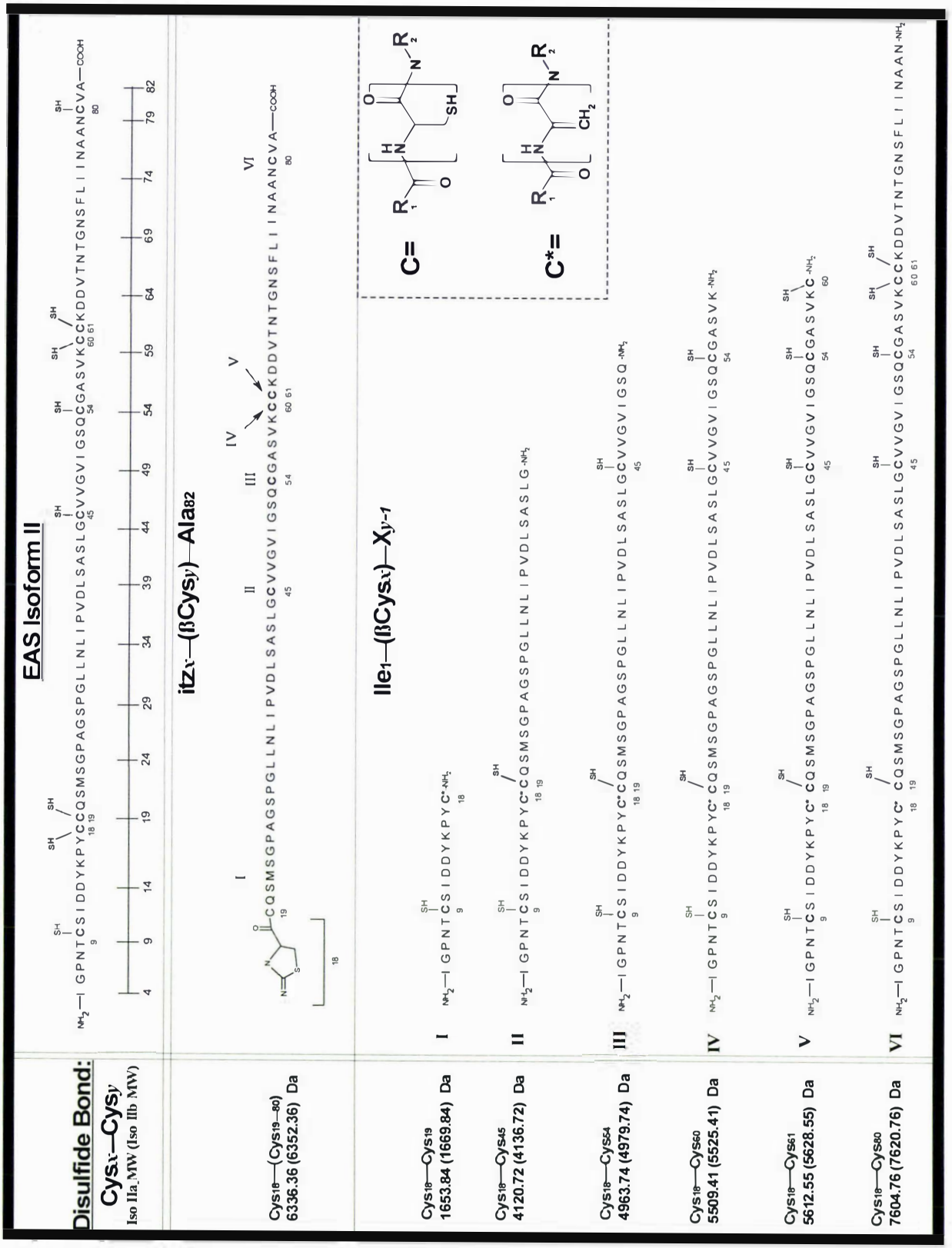

The β-elimination can occur at either cyanylated cysteine residue and removes the SCN-group leaving the peptide bond intact (See inset. Modified residues are designated C* or are assigned a roman numeral). Thus a pairs of peptides may result. One will have an N-terminal iminothiazolidinyl carboxyl residue, the other a C-terminal amide (if NH_4OH is used). The sequence of each peptide depends on the original disulfide linkages because only linked cysteines are cyanylated in this experiment. The pairs of peptides that are predicted to result from β-elimination are indicated with roman numerals. The different iminothiazolidinyl carboxyl terminated peptides have the same molecular mass but the position of the modified cysteine in each case is indicated by Roman numeral that corresponds to the amide terminated peptide that will form when the designated pairs of cysteines are linked.

(A18) THE STRUCTURES AND M/Z VALUES RESULTING FROM β-ELIMINATION REACTIONS.

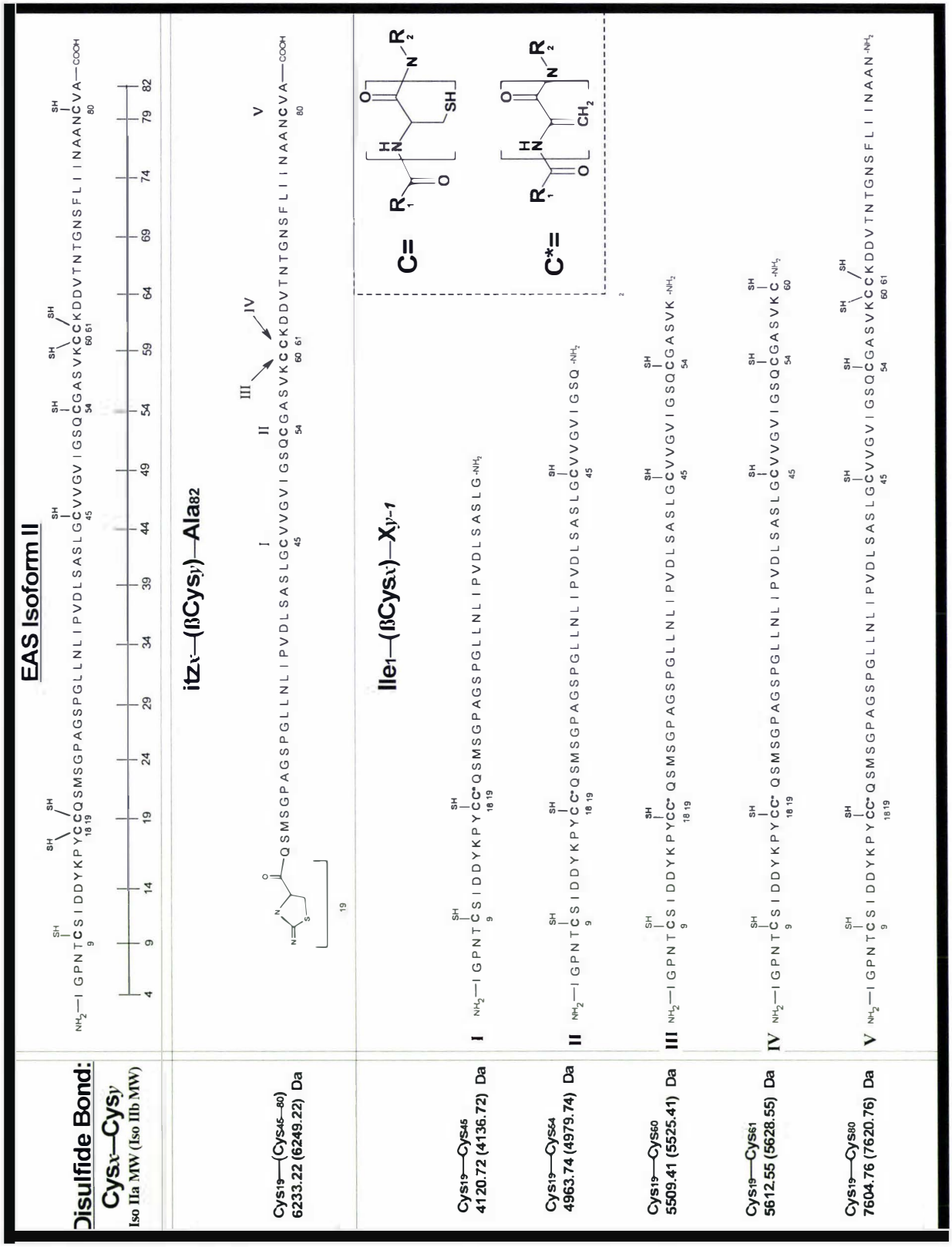

The β-elimination can occur at either cyanylated cysteine residue and removes the SCN-group leaving the peptide bond intact (See inset. Modified residues are designated C* or are assigned a roman numeral). Thus a pairs of peptides may result. One will have an N-terminal iminothiazolidinyl carboxyl residue, the other a C-terminal amide (if NH_4OH is used). The sequence of each peptide depends on the original disulfide linkages because only linked cysteines are cyanylated in this experiment. The pairs of peptides that are predicted to result from β-elimination are indicated with roman numerals. The different iminothiazolidinyl carboxyl terminated peptides have the same molecular mass but the position of the modified cysteine in each case is indicated by Roman numeral that corresponds to the amide terminated peptide that will form when the designated pairs of cysteines are linked.

(A19) THE STRUCTURES AND M/Z VALUES RESULTING FROM β-ELIMINATION REACTIONS.

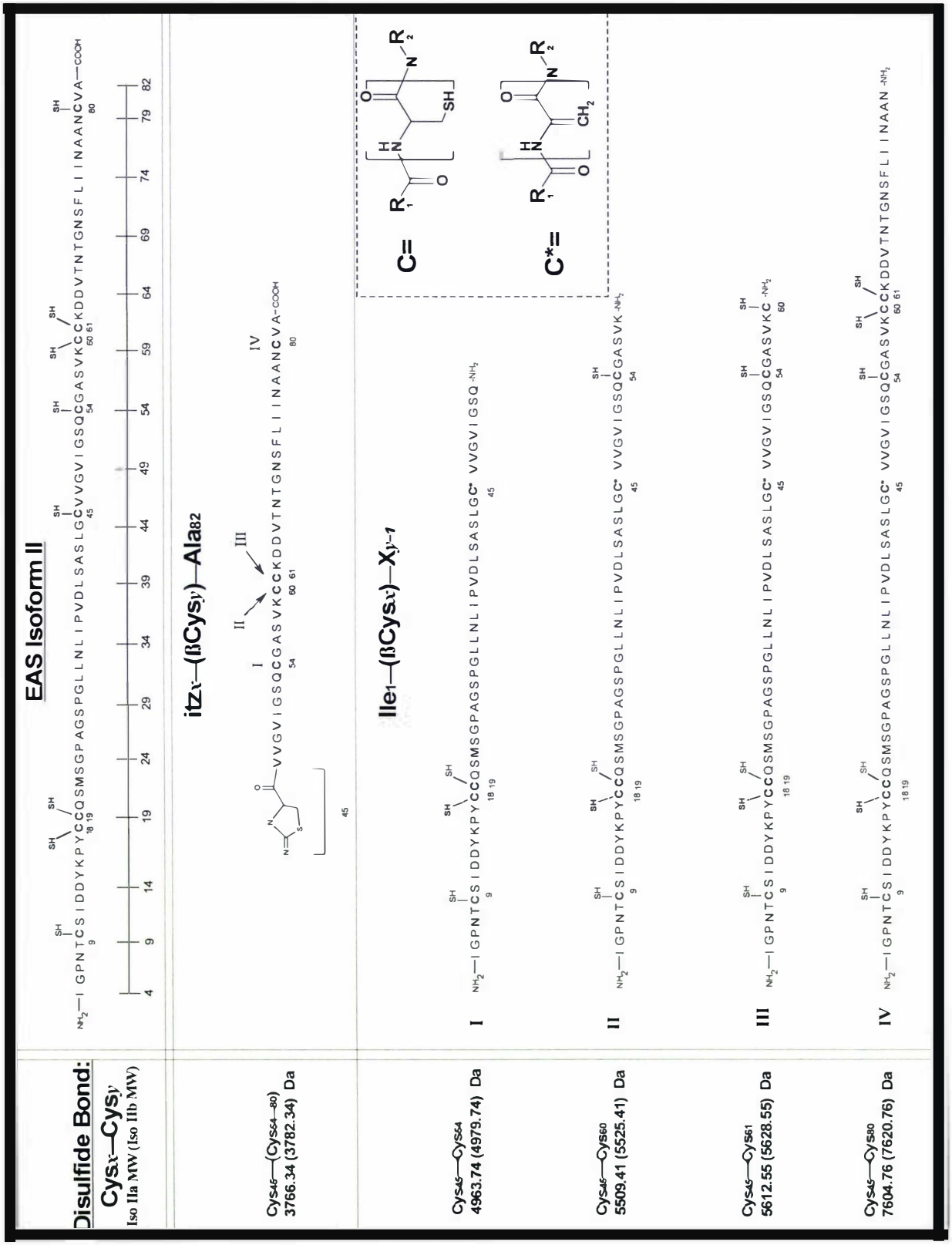

The β-elimination can occur at either cyanylated cysteine residue and removes the SCN-group leaving the peptide bond intact (See inset. Modified residues are designated C* or are assigned a roman numeral). Thus a pairs of peptides may result. One will have an N-terminal iminothiazolidinyl carboxyl residue, the other a C-terminal amide (if NH_4OH is used). The sequence of each peptide depends on the original disulfide linkages because only linked cysteines are cyanylated in this experiment. The pairs of peptides that are predicted to result from β-elimination are indicated with roman numerals. The different iminothiazolidinyl carboxyl terminated peptides have the same molecular mass but the position of the modified cysteine in each case is indicated by Roman numeral that corresponds to the amide terminated peptide that will form when the designated pairs of cysteines are linked.

(A20) THE STRUCTURES AND M/Z VALUES RESULTING FROM β-ELIMINATION REACTIONS.

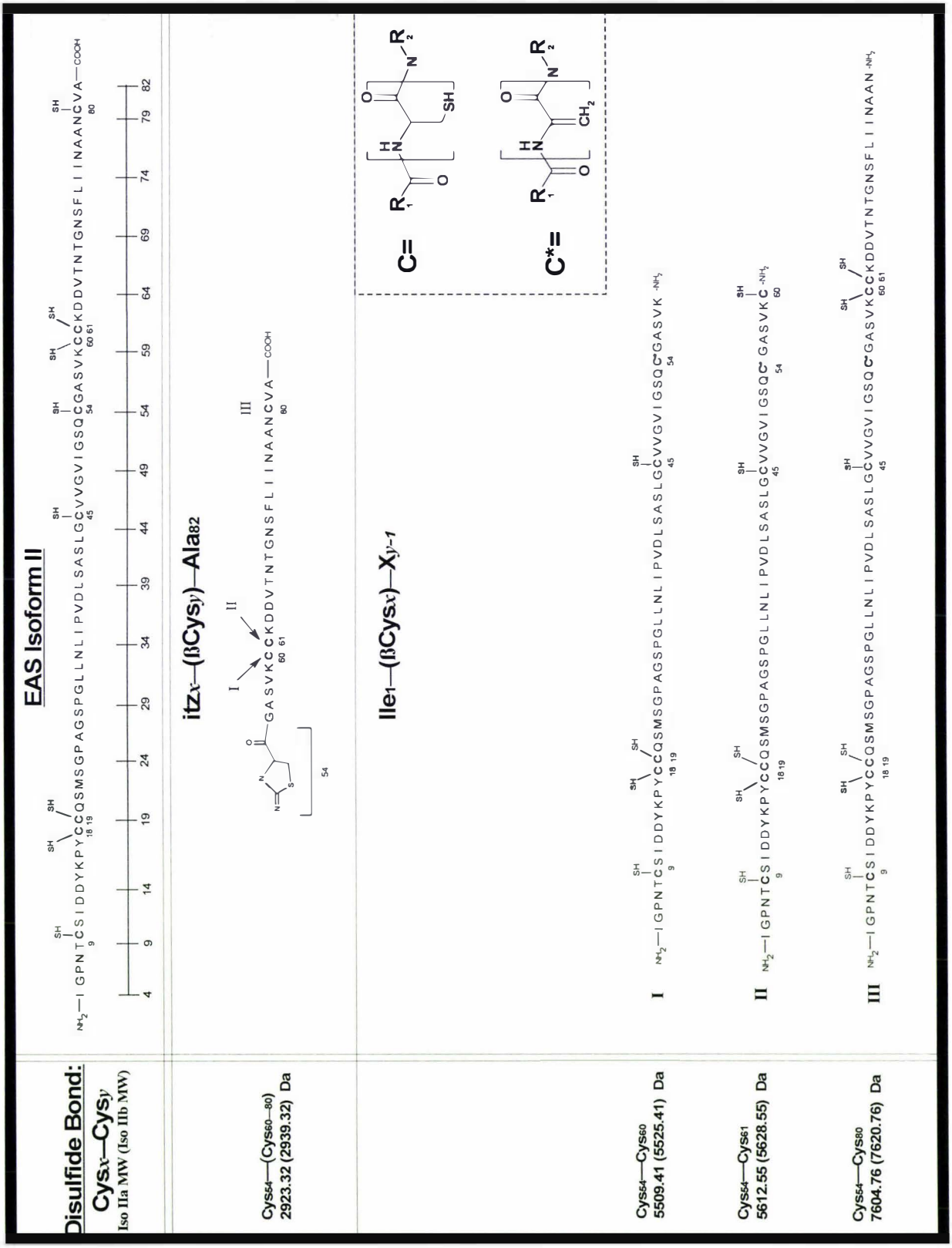

The β-elimination can occur at either cyanylated cysteine residue and removes the SCN-group leaving the peptide bond intact (See inset. Modified residues are designated C* or are assigned a roman numeral). Thus a pairs of peptides may result. One will have an N-terminal iminothiazolidinyl carboxyl residue, the other a C-terminal amide (if NH_4OH is used). The sequence of each peptide depends on the original disulfide linkages because only linked cysteines are cyanylated in this experiment. The pairs of peptides that are predicted to result from β-elimination are indicated with roman numerals. The different iminothiazolidinyl carboxyl terminated peptides have the same molecular mass but the position of the modified cysteine in each case is indicated by Roman numeral that corresponds to the amide terminated peptide that will form when the designated pairs of cysteines are linked.

(A21) THE STRUCTURES AND M/Z VALUES RESULTING FROM β-ELIMINATION REACTIONS.

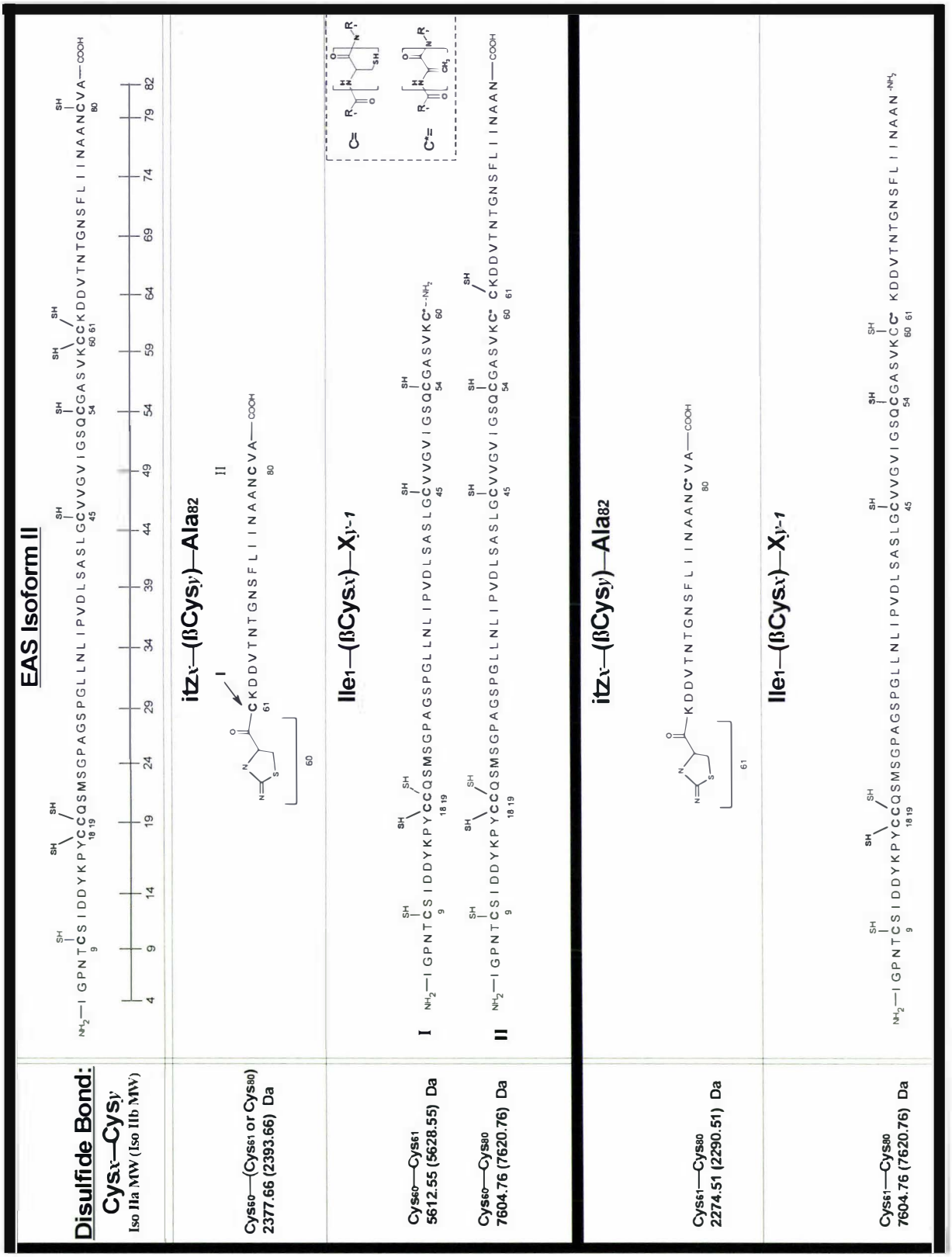

The β-elimination can occur at either cyanylated cysteine residue and removes the SCN-group leaving the peptide bond intact (See inset. Modified residues are designated C* or are assigned a roman numeral). Thus a pairs of peptides may result. One will have an N-terminal iminothiazolidinyl carboxyl residue, the other a C-terminal amide (if NH_4OH is used). The sequence of each peptide depends on the original disulfide linkages because only linked cysteines are cyanylated in this experiment. The pairs of peptides that are predicted to result from β-elimination are indicated with roman numerals. The different iminothiazolidinyl carboxyl terminated peptides have the same molecular mass but the position of the modified cysteine in each case is indicated by Roman numeral that corresponds to the amide terminated peptide that will form when the designated pairs of cysteines are linked.

APPENDIX VB.

OPTIMISING THE DERIVATISATION AND PURIFICATION OF SINGLY-REDUCED EAS.

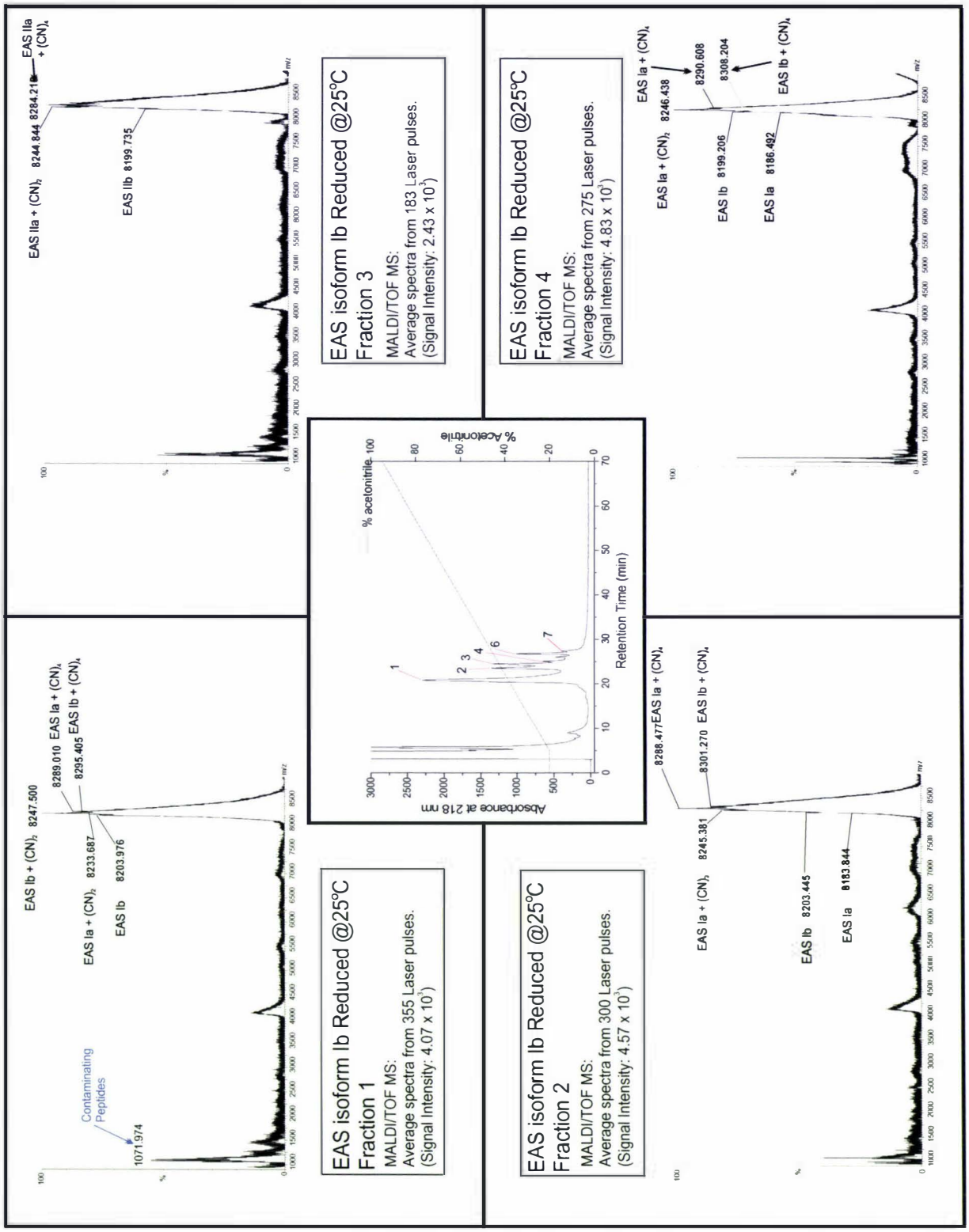

Central Panel: RP-HPLC elution profile (see section 2.4.7.1) depicting the fractionation of singly-reduced, cyanylated isomers of EAS isoform Ib derivatised using a modified version "Best Initial Protocol" described in Table 15. For reasons discussed in section 5.2.1, in the derivatising reactions tested here, the final reaction volume was reduced to 102 µL and between 1 µL of 1 M TCEP added instead of 5 µL. The other panels show the fractions collected during the RP-HPLC run after they had been analysed by MALDI-TOF/MS (see section 2.4.7.1). The results of that analysis showed that these reaction conditions produced more doubly reduced and cyanylating isomers of EAS than are produced in a protocol where the reagents were less concentrated (see Figure 54 and section 5.2.1).

APPENDIX VI – SUPPLEMENTARY DATA FOR CHAPTER 6.

OPTIMIZING THE AFM IMAGING BUFFER FOR EAS.

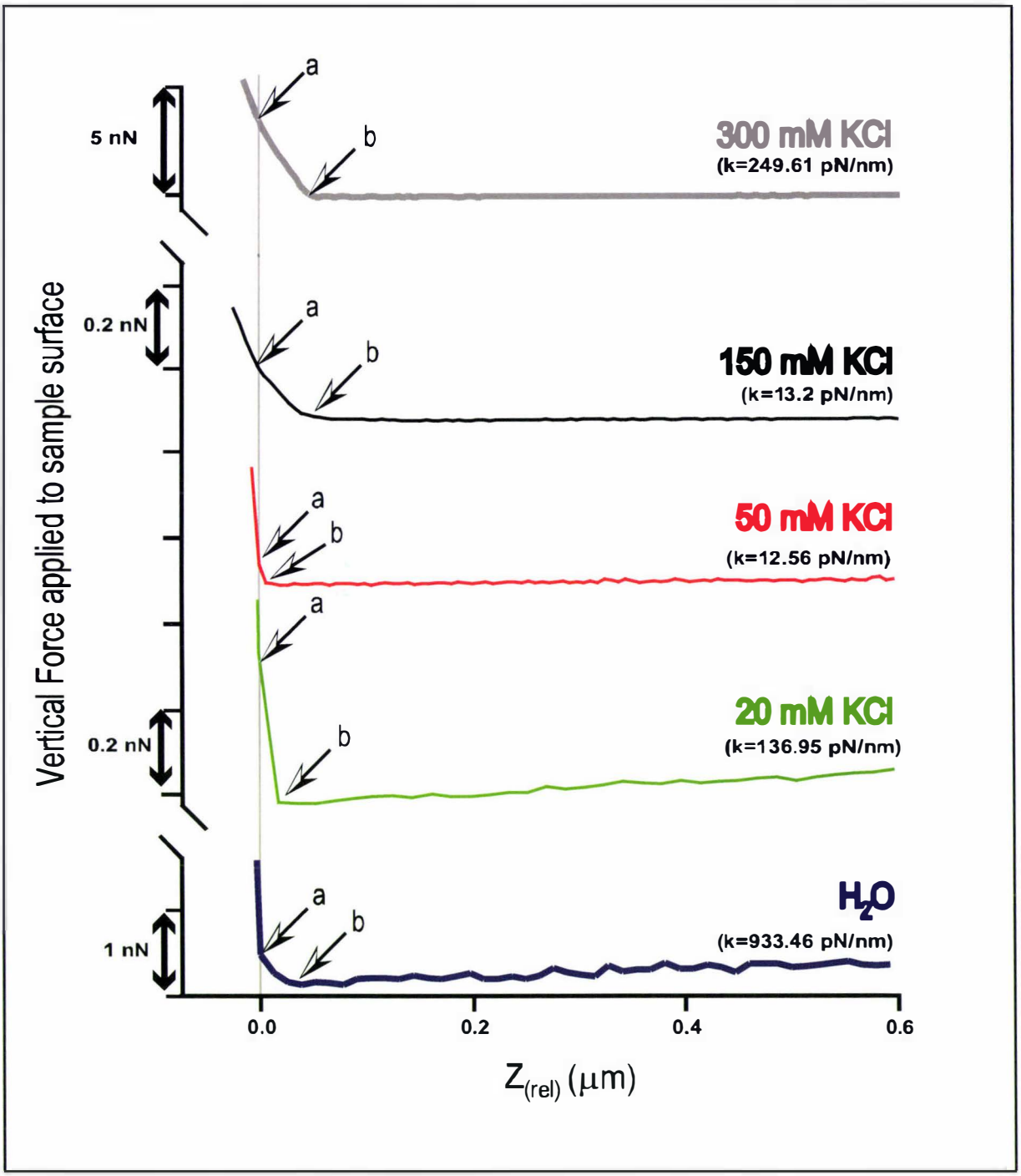

The figure above compares the extension portions of force distance curves collected to measure the ability of the five different aqueous fluids to reduce the double-layer electrostatic repulsive forces between an EAS rodlet film and a Veeco® NP20 Silicon nitrite AFM probe. Arrows indicate **(a)** the point where the tip is in physical contact with the sample and **(b)** the point at which the electrostatic repulsion begins between tip and sample. The spring constant (k) for the probes used in these experiments are indicated in the diagram.

Müller *et al* (1999) developed a method for optimising the composition of imaging buffers to mask the double-layer electrostatic repulsion between the AFM tip and the

sample. In essence the deflection response of the AFM cantilever is monitored as the tip is pushed towards a sample submerged in a variety of different fluids. The data is plotted as a force distance curve (force versus z_{rel}) to reveal both (1) the point at which the electrostatic repulsion begins between tip and sample and (2) the point where the tip is in physical contact with the sample. This is the point when the cantilever's deflection shows a linear response to being pushed against the sample. These points should coincide if the imaging buffer completely neutralises the repulsive forces between sample and tip. Müller *et al.* suggest that a small repulsive interaction is necessary to support the bulk of the tip during imaging, allowing any asperity at the apex of the tip to map the contours in the surface without destroying it. However this force must be ≤100 pN to prevent the tip from deforming the sample (data reviewed by Müller *et al*, 1998b, 1999). Obviously if the magnitude of the electrostatic repulsion between the tip and the sample exceeds this value, the tip will not be in contact with the sample (Müller *et al*, 1999).

I tested four aqueous buffers and Milli-Q® water for their ability to compensate for the electrostatic repulsive interaction between the hydrophobic surface of EAS rodlets and a Veeco® NP20 probes during AF-microscopy. The buffers contained KCl at one of four concentrations (20 mM, 50 mM KCl, 150 mM, 300 mM) and MOPS (10 mM, pH 7.0) as a buffering agent. The experiment was performed as described in section 2.5.6.1. The results of these experiments (presented on the previous page), and show that the is a net electrostatic repulsion between the tips and the hydrophobic face of EAS. The force required to overcome this force and bring the tip in contact with the sample ranged between ~90 pN (in the 50 mM KCl buffer) and ~7 nN (in the 300 mM KCl buffer). Clearly then the 50 mM KCl buffer will assist with high resolution AFM-imaging using silicon-nitrite tips.

APPENDIX VII – CONSUMABLES AND EQUIPMENT SUPPLIERS.

Brand Name	Manufacturer	Local distributor
AnalR®	*VWR International, Poole, UK.*	*Merck Ltd. Palmerston North, NZ.*
ABI	*Applera Corporation, Norwalk, CT. USA.*	*Applied Biosystems, Soresby, Victoria Australia.*
ABI Prism®	*Applera Corporation, Norwalk, CT. USA.*	*Applied Biosystems, Soresby, Victoria Australia.*
Accelrys®	*Accelrys Inc. San Diego, CA, USA.*	
Acrodisc®	*Pall Corporation, Ann Arbor, USA.*	*Pall Life Sciences, Sydney, Australia.*
Agilent®	*Agilent Technologies Deutschland GmbH, Waldbronn, Germany.*	
Airpure®	*Email Westinghouse Pty Ltd. NSW, Australia.*	*Medic Scientific, Lower Hutt NZ.*
Amersham®	*Amersham® Biosciences Uppsala, Sweden.*	*Amersham® Biosciences NZ Ltd. Auckland, NZ.*
AP-Biotech	*Amersham® Pharmacia Biotech AB, Uppsala, Sweden.*	*Amersham® Biosciences NZ Ltd. Auckland, NZ.*
Axygen®	*Axygen Scientific Inc. Union City, CA, USA.*	*Biolab Ltd. Auckland, NZ.*
BDH®	*VWR International, Poole, UK.*	*Merck Ltd. Palmerston North, NZ.*
Bacto®	*BD Diagnostic Systems, Sparks, MD, USA.*	*Fort Richard Auckland NZ.*
BigDye™	*Applera Corporation, Norwalk, CT. USA.*	*Applied Biosystems, Soresby, Victoria Australia.*
BioLab®	*Biolab Limited, Auckland, NZ.*	*Biolab Limited, Auckland, NZ.*
Bio-Rad®	*Bio-Rad Laboratories, Hercules, CA, USA.*	*Bio-Rad Laboratories Pty Ltd. Auckland NZ.*
Blast®	*National Institutes of Health, Bethesda, Maryland, USA.*	*http://www.ncbi.nlm.nih.gov/BLAST/*
Calbiochem®	*Calbiochem, San Diego; USA.*	*Merck Ltd. Palmerston North, NZ.*
Cell-Porator®	*Invitrogen™, Carlsbad, CA, USA.*	*Invitrogen™ NZ Ltd. Auckland, NZ.*
Concert™	*Promega Corporation, Madison, WI, USA.*	*Dade Behring Diagnostics Ltd. Auckland, NZ.*
Coommassie®	*Imperial Chemical Industries PLC. London, UK.*	*Sigma Chemical Company.*
Corel®	*Corel Corporation, Ottawa, Canada.*	*Harvey Norman Ltd. Auckland NZ.*
Difco®	*BD Diagnostic Systems, Sparks, MD, USA.*	*Fort Richard Auckland NZ.*
DYEnamic™	*Amersham® Biosciences Uppsala, Sweden.*	*Amersham Biosciences NZ Ltd. Auckland, NZ.*
Eppendorf®	*Eppendorf AG, Hamburg, Germany.*	*Biolab Ltd. Auckland, NZ.*
Finnigan LCQ™ Deca	*Thermo Finnigan, San Jose, CA, USA.*	
Finnigan Surveyor®	*Thermo Finnigan, San Jose, CA, USA.*	

Brand Name	Manufacturer	Local distributor
Gallenkamp®	*Sanyo Gallenkamp PLC, Loughborough UK.*	*Global Science & Technology Ltd. Auckland, NZ.*
GelmanSciences	*Pall Corporation, Ann Arbor, USA.*	*Pall Life Sciences, Sydney, Australia*
Gel-Pak®	*Gel-Pak LLC, Hayward, CA, USA.*	
GenBank®	*National Institutes of Health, Bethesda, Maryland, USA.*	***http://www.ncbi.nlm.nih.gov***
Genius®	*Techne Inc. Princeton, NJ, USA.*	*John Morris Scientific Ltd. Auckland, NZ*
Gene-Pulser®	*Bio-Rad Laboratories, Hercules, CA, USA.*	*Bio-Rad Laboratories Pty Ltd. Auckland NZ.*
GibcoBRL®	*Invitrogen™, Carlsbad, CA, USA.*	*Invitrogen™ NZ Ltd. Auckland, NZ.*
Hewlett Packard (Scientific Instruments)	*Agilent Technologies Deutschland GmbH, Waldbronn, Germany.*	
Hybond™	*Amersham Biosciences Uppsala, Sweden.*	*Amersham Biosciences NZ Ltd. Auckland, NZ.*
InforMax®	*InforMax Inc. Bethesda, MD, USA.*	
Invitrogen™	*Invitrogen™ Carlsbad, CA, USA.*	*Invitrogen™ NZ Ltd. Auckland, NZ*
Jupiter™	*Phenomenex Inc. Torrance, CA, USA.*	*Phenomenex NZ Ltd. Auckland, NZ.*
Li-cor®	*Li-cor Inc. Lincoln, NE, USA.*	*John Morris Scientific Ltd. Auckland, NZ.*
M@ldi™	*Waters Corporation, Milford, MA, USA.*	*Alphatech Systems Ltd. Auckland, NZ.*
MDL®	*MDL® Information Systems Ltd. San Leandro, CA, USA.*	
Micromass Systems	*Waters Corporation, Milford, MA, USA.*	*Alphatech Systems Ltd. Auckland, NZ.*
Millipore®	*Millipore Corp. Massachusetts, USA*	*Biolab Ltd. Auckland, NZ.*
MikroMasch®	*MikroMasch Eesti OU. Tallinn, Estonia.*	*Online retailer (2003):* ***http://www.spmtips.com***
Molecular Dynamics®.	*Amersham Biosciences Uppsala, Sweden.*	*Amersham Biosciences NZ Ltd. Auckland, NZ.*
nano-K®	*Minus K® Technology, Inglewood, CA. USA.*	
NEB®	*New England Biolabs Inc. Beverly, CA, USA.*	*Biolab Ltd. Auckland, NZ.*
Nikon®	*Nikon Instruments Inc., Melville, NY, USA.*	
Novagen®	*Novagen Inc. Madison, WI, USA.*	*Merck Ltd. Palmerston North, NZ.*
Novex®	*Invitrogen™, Carlsbad, CA, USA.*	*Invitrogen™ NZ Ltd. Auckland, NZ.*
NT-MDT®	*NT-MDT Co. Moscow, Russia.*	*Online retailer (2003): http://www.ntmdt.ru*
Nuaire™	*Nuaire Inc. Plymouth, MN, USA.*	*Medic Scientific, Lower Hutt NZ.*
NuPAGE®	*Invitrogen™, Carlsbad, CA, USA.*	*Invitrogen™ NZ Ltd. Auckland, NZ.*
Olympus®	*Olympus Optical Company Ltd. Tokyo, Japan.*	
pGEM-T® / pGEM-Teasy®	*Promega Corporation, Madison, WI, USA.*	*Dade Behring Diagnostics Ltd. Auckland, NZ.*
Phenomenex®	*Phenomenex Inc. Torrance, CA.*	*Phenomenex NZ Ltd. Auckland, NZ.*
Phosphor Imaging™	*Amersham Biosciences Uppsala, Sweden.*	*Amersham Biosciences NZ Ltd. Auckland, NZ.*
Photoshop®	*Adobe Systems Inc. San Jose, CA USA.*	*Any NZ based computer software retailer.*

Brand Name	Manufacturer	Local distributor
Pierce®	*Pierce Chemical Company. Rockford, IL, USA.*	*Global Science & Technology Ltd. Auckland, NZ.*
Promega®	*Promega Corporation, Madison, WI, USA.*	*Dade Behring Diagnostics Ltd. Auckland, NZ.*
PYE	*PYE Ltd. Cambridge, UK. Company bought out in by Philips in 1976.*	*Instrumentation manufactured by PYE Ltd. no longer available.*
Qiagen®	*Qiagen Pty Inc. Valencia, CA, USA.*	*Qiagen Pty Ltd. Victoria, Australia.*
QIAquick®	*Qiagen Pty Inc. Valencia, CA, USA.*	*Qiagen Pty Ltd. Victoria, Australia.*
Rediprime™	*Amersham Biosciences, Uppsala, Sweden.*	*Amersham Biosciences NZ Ltd. Auckland, NZ.*
RNeasy®	*Qiagen Pty Inc. Valencia, CA, USA.*	*Qiagen Pty Ltd. Victoria, Australia.*
Roche®	*Roche Diagnostics GmbH, Mannerhiem, Germany.*	*Roche Diagnostics NZ Ltd. Auckland, NZ.*
ScanMaker™	*MicroTek International, Inc. Hsinchu, Taiwan.*	*Any NZ-based computer hardware retailer.*
Selleys®	*Selleys Pty. Ltd. Padstow, N.S.W. Australia.*	*Any NZ-based hardware retailer.*
Sellotape®	*HENKEL Consumer Adhesives, Hertfordshire, UK.*	*Any NZ-based stationary retailer.*
Sigma-Aldrich®	*Sigma-Aldrich Corporation. St Louis, MO, USA.*	*Sigma-Aldrich Pty Ltd. NSW, Australia*
SPI Supplies®	*SPI Supplies/Structure Probe, Inc., West Chester PA, USA.*	*Global Science & Technology Ltd. Auckland, NZ*
Sorvall®	*Kendro Laboratory Products. Asheville NC USA.*	*Kendro Laboratory Products. Auckland NZ.*
Storm®	*Amersham Biosciences Uppsala, Sweden.*	*Amersham Biosciences NZ Ltd. Auckland, NZ.*
Stratagene®	*Stratagene. La Jolla, CA. USA.*	*Global Science & Technology Ltd. Auckland, NZ.*
SuperScript™	*Invitrogen™, Carlsbad, CA, USA.*	*Invitrogen™ NZ Ltd. Auckland, NZ.*
Techne®	*Techne Inc. Princeton, NJ, USA.*	*John Morris Scientific Ltd. Auckland, NZ.*
Teflon®	*E.I du Pont de Nemours and Company. Wilmington, DE, USA.*	
UltraPURE™	*Invitrogen, Carlsbad, CA, USA.*	*Invitrogen NZ Ltd. Auckland, NZ.*
Uvettes®	*Eppendorf AG, Hamburg, Germany.*	*Biolab Ltd. Auckland, NZ.*
VirTis™	*The VirTis Company, Gardiner NY USA.*	*Global Science & Technology Ltd. Auckland, NZ/*
Xcalibur®	*Thermo Finnigan, San Jose, CA, USA.*	
Xcell SureLock™	*Invitrogen™, Carlsbad, CA, USA.*	*Invitrogen™ NZ Ltd. Auckland, NZ/*
Veeco® Instruments	*Veeco Instruments Inc. Woodbury, NY. USA.*	*Group Scientific Pty. Ltd., Adelaide, SA, Australia.*
VirTis™	*The VirTis Company, Gardiner NY USA.*	*Global Science & Technology Ltd. Auckland, NZ.*
WaveMetrics™	*WaveMetrics, Inc. Oswego, OR, USA.*	
ZipTip®	*Millipore Corp. Massachusetts, USA.*	*Biolab Ltd. Auckland, NZ.*

APPENDIX VIII – LISTS OF ABBREVIATIONS.

ABBREVIATED INSTITUTE AND COMPANY NAMES.

AP-Biotech	*Amersham Pharmacia Biotech AB, Uppsala, Sweden.*
FGSC	*Fungal Genetics Stock Centre, Department of Microbiology, University of Kansas Medical Center, Kansas City, KS, USA.*
GenBank®	*National Institutes of Health, Bethesda, Maryland, USA (http://www.ncbi.nlm.nih.gov).*
Hort Research	*The Horticulture and Food Research Institute of New Zealand Ltd. Mt Albert Research Center, Auckland NZ.*
Landcare Research	*Manaaki-Whenua Landcare Research, Mt Albert Research Center, Auckland NZ.*
MIT	*Massachusetts Institute of Technology, Massachusetts, USA.*
NCBI	*National Center for Biotechnology Information, Bethesda, MD, USA.*
NIH	*US Department of Health and Human Services, National Institutes of Health, Bethesda, MD, USA.*
NLM	*US National Library of Medicine, Bethesda, MD, USA.*
WI-CGR	*The Center for Genome Research, Whitehead Institute for Biomedical Research, Massachusetts Institute of Technology, Cambridge, MA, USA.*

CHEMICALS AND SOLUTIONS

Buffer Solutions	
AE	*Acetate, EDTA buffer.*
FA	*Formaldehyde agarose (denaturing gel-solution for RNA electrophoresis).*
SSC	*Sodium hydroxide, trisodium citrate buffer.*
TAE	*Tris, acetate acid, EDTA, buffer.*
TE	*Tris, EDTA, buffer.*
Chemicals	
BCA	*bicinchoninic acid.*
BSA	*Bovine serum albumin.*
Biotin	*D-Biotin (Vitamin B7).*
Bis-Tris	*Bis[2-hydoxyethyl]iminotris(hydroxymethyl)methane.*
CDAP	*1-Cyano-4-dimethylaminopyridinium tetrafluoroborate.*
DEPC	*Diethyl pyrocarbonate.*
DTT	*Dithiothreitol.*
EDTA	*ethylene diamine tetra-acetic acid.*
G418	*Geneticin® disulfate salt. (An aminoglycoside toxic to a wide range of cell types).*
Glucose	*D-Glucose.*
Glycerol	*1,2,3-Propanetriol.*
HCCA	*α-Cyano-4-hydroxycinnamic acid (matrix used in MALDI-TOF/MS experiments).*
HEPES	*N-(2-Hydroxyethyl)piperazine-N'-(2-ethanesulfonic acid).*

CHEMICALS AND SOLUTIONS

Chemicals	
IPTG	*Isopropyl-β-D-thiogalactopyranoside.*
itz residue	*2-Iminothiazolidine-4-carboxyl residue (a chemically modified cysteine residue).*
LDS	*Lithium dodecyl sulfate (denaturing detergent used in protein electrophoresis).*
MES	*2-(N-morpholino)ethanesulfonic acid.*
MilliQ®-water	*Water purified with the Milli-Q PF-plus water purification system (Millipore®).*
MOPS	*3-(N-morpholino)propanesulfonic acid.*
Peptone	*Bacto® Peptone (a source of amino acids in growth media).*
PMSF	*Phenylmethylsulfonyl fluoride. (protease inhibitor).*
RNase A	*Bovine Pancreatic ribonuclease Type III-A.*
SDS	*Sodium dodecyl sulfate.*
Sorbitol	*D-Sorbitol (D-Glucitol).*
Teflon®	*Trade name for a polymer material made from polytetrafluoroethylene (PTFE).*
TCEP	*Tris(2-carboxyethyl)phosphine hydrochloride.*
TFA	*Trifluoroacetic acid.*
Tris	*Tris(hydroxymethyl)-aminomethane.*
Tris-HCl	*Tris solution, pH adjusted with HCl.*
Tryptone	*Pancreatic digest of casein (a source of amino acids in growth media).*
X-gal	*5-Bromo-4-chloro-3-indolyl β-D-galactopyranoside.*
Yeast Extract	*Autolysed yeast cell extract (growth media vitamin and amino acid supplement).*
Media	
1 M PPB	*1 M Potassium phosphate buffer pH 6.0 (a component of Pichia growth media).*
10x DS	*10x Dextrose solution (a component of Pichia growth media).*
10x GS	*10x Glycerol solution (a component of Pichia growth media).*
10x MS	*10x Methanol solution (a component of Pichia growth media).*
100x HS	*100x Histidine solution (a component of Pichia growth media).*
100x SS	*100x YNB salts solution (a component of Pichia growth media).*
500x BS	*500x Biotin solution (a component of Pichia growth media).*
1000x TE	*1000x YNB trace elements Solution (a component of Pichia growth media).*
1000x VS	*1000x YNB vitamins solution (a component of Pichia growth media).*
BMD	*Buffered minimal media plus dextrose (a Pichia growth medium).*
BMG	*Buffered minimal media plus glycerol (a Pichia growth medium).*
BMM	*Buffered minimal media plus methanol (a Pichia growth medium).*
LB	*Luria-Bertani broth or Lennox broth (an E. coli growth medium).*
SOC medium	*An E. coli growth medium.*
YNB	*Yeast nitrogen base with ammonium sulphate without amino acids.*
YPD	*Yeast extract peptone dextrose (a Pichia growth medium).*

Genes, Proteins and Genetic Elements

AOX1/AOX1	*Alcohol oxidase 1 gene/protein.*
cDNA	*Complementary DNA.*
Col E1	*E. coli origin of replication.*
dsDNA	*Double stranded DNA.*
eas/EAS	*Easily wettable. A hydrophobin gene/protein.*
EST	*Expressed sequence tag.*
His^+/His^-	*Pichia phenotype: his4 gene functional(+)/non-functional(-).*
His4	*Native Pichia pastoris histidinol dehydrogenase gene.*
HIS4	*Plasmid borne histidinol dehydrogenase gene complementary to his4.*
ITS	*Internal transcribed spacer region of nuclear rRNA genes.*
mat A/mat a	*Mating-type loci. The sexual determinant genetic elements in Neurospora.*
mRNA	*Messanger RNA.*
Mut^S/Mut^+/Mut^-	*Pichia phenotype: Methanol utilisation slow(s)/normal(+)/absent(-).*
p (as prefix)	*Denotes a plasmid.*
RIP	*Repeat Induced Polymorphism.*
ROTCase	*Recombinant ornithine transcarbamoylase.*
rRNA	*Ribosomal RNA.*
ssDNA	*Single stranded DNA.*
UTR	*Untranslated region.*
Enzymes	
DNase	*Deoxyribonuclease.*
EC 3.4.24.33.	*IUBMB Enzyme Nomenclature that specifically identifies endopeptidase Asp-N.*
Phosphatase	*Orthophosphoric-monoester phosphohydrolase (alkaline optimum).*
RNase	*Ribonuclease.*
SAP	*Shrimp Alkaline Phosphatase.*
T4 DNA Ligase	*Polydeoxyribonucleotide Synthase from T4-phage.*

Methods, Techniques and Equipment

AFM	*Atomic force microscopy.*
ATR-FTIR	*Attenuated total reflection Fourier transform infrared spectroscopy.*
CD	*Circular dichroism.*
ESI/MS	*Liquid chromatography with electrospray ionisation mass spectrometry.*
HPLC	*High performance liquid chromatography.*
Laser	*Light amplification by stimulated emission of radiation.*
LC–ESI/MS	*Liquid chromatography with electrospray ionisation mass spectrometry.*
MALDI-TOF/MS	*Matrix-assisted laser desorption/ionisation time-of-flight mass spectrometry.*
NMR	*Nuclear magnetic resonance.*
PAGE	*Polyacrlyamide gel electrophoresis.*
PCR	*Polymerase chain reaction.*

METHODS, TECHNIQUES AND EQUIPMENT

RP-HPLC	*Reverse-phase high performance liquid chromatography*
RT-PCR	*Reverse transcription polymerase chain reaction.*
SDS-PAGE	*Sodium dodecyl sulfate – polyacrlyamide gel electrophoresis.*
SEM	*Scanning electron microscopy.*
SPM	*Scanning probe microscopy.*
TEM	*Transmission electron microscopy.*
UV	*Ultraviolet (spectroscopy).*

NON S.I.-UNITS USED IN THIS WORK.

Centrifuge and Spectrophotometer Settings	
g	*Acceleration of gravity (units for relative centrifugal force).*
OD_{260}	*Optical density (subscript indicates wavelength (nm) used during measurement).*
rpm	*Revolutions per minute (rotor speed).*
Concentration	
%(v/v)	*Percent concentration; volume of solute (mL)/volume of solvent (100mL).*
%(w/v)	*Percent concentration; weight of solute (g)/volume of solvent (100mL).*
M	*Molarity (moles per litre).*
U	*Units of enzyme.*
nx	*Denotes magnitude of concentration. If n=5 then 5x=5 times stronger than standard (1x).*
Genetic Size/Distance	
bp	*Base pair(s).*
kbp	*Kilo base pair(s).*
kb	*Kilo base(s).*
Molecular Mass	
Da	*Dalton(s) or atomic mass unit(s) 1 Da = 1/12 mass of a ^{12}C atom.*
kDa	*Kilo Dalton(s).*
Da/z	*Daltons per fundamental units of charge (z).*
m/z	*The mass-to-charge ratio for ions detected by mass spectrometry. Units = Da/z.*
Pressure	
bar	*A unit of pressure (equal to a million dynes per square centimetre).*
Time	
h	*Hour(s).*
min	*Minute(s).*
Liquid volume	
L	*Litre(s).*

STATISTICAL SYMBOLS

n	*Sample size.*
$\bar{x}$	*Sample mean.*
$SE\bar{x}$	*Standard error of the sample mean* (s_x / n^{-2})
s_x	*Sample standard deviation.*

PHRASES

OHP	*Over head projector.*